Burial diagenesis, organic maturation and tectonic loading in the French subalpine chains, S.E. France

Moss, Stephen James

Burial Diagenesis, Organic Maturation and Tectonic Loading in the French Subalpine Chains, S.E. France.

Stephen James Moss.

A thesis submitted to the University of Durham for the degree of Doctor of Philosophy.

Department of Geological Sciences.

September, 1992.

Burial diagenesis, Organic Maturation and Tectonic Loading in the French Subalpine Chains, S.E. France.

Abstract.

The French Subalpine Chains of southeastern France lie on the western edge of the Western Alps. The area is the foreland fold/thrust belt to the main orogenic hinterland to the east. The Mesozoic and Cenozoic geological history of the area is typical of many foreland regions, with a former gently subsiding passive margin altered to a destructive margin through compressional tectonics and ocean closure.

This thesis details the results of a case study into particular aspects of the sedimentology and basin history of the Subalpine Chains fold/thrust belt. The two main aspects to this thesis are burial diagenesis and the causes of palaeo-temperature variation within the fold/thrust belt.

A principal aim of this research was to document the burial diagenetic history of the mid-Cretaceous rudist-bearing 'Urgonian' limestone. Similar Cretaceous rudist platform limestones elsewhere in the world are good reservoir rocks. Often their good porosity is due to the selective dissolution associated with the bi-mineralic rudist shells. Although later cement precipitation often has modified this. Regional dolomitization of platform carbonates has also been known for a long time to increase the reservoir potential of such sediments. In the Urgonian, fabric selective secondary porosity, equant burial cements and dolomitization are important components of the platform's diagenetic history. The petrography and geochemistry of rudist shells, the equant calcite cements responsible for occluding the majority of porosity and replacive dolomitization within the basal section of the Urgonian platform are described. On the basis of the field, petrographic and geochemical data, a diagenetic model for the Urgonian is proposed.

The second principal aim was to study the regional variations in maximum burial temperatures and depths. To this end several palaeo-thermal indices were studied (clay minerals, vitrinite reflectance and spore fluorescence) and the thermal history of the region is modelled using a PC-based modelling package (Basinmod). Regional trends in thermal indices are presented and quite clearly indicate an along strike (of the foreland fold/thrust belt) variation in burial temperatures, with a less important across strike trend. A simple thermal history model is used to estimate the maximum depths of burial of specific locations and the results compared to measured values of maturity. Both the modelling and field relationships suggest that major overthrust sheets emplaced only in the northern part of the study area are the principal cause of the greater depth of burial of that part of the Subalpine Chains. The causes of thermal perturbations in fold/thrust belts are discussed.

A final third part of this thesis details the results of a pilot study of the geochemistry of syn-tectonic veins. The petrography and outcrop nature of these veins indicate that cyclic hydraulic fracturing (the so-called "crack-seal mechanism") was very important in producing fractures within the rocks during Alpine deformation. These were healed by calcite cements, the stable isotope composition of which indicates the significance of water/wall rock interaction and the temperature of the precipitating fluids on the isotopic composition of the precipitate. Taken as a whole the geochemistry strongly suggests that syn-tectonic fluid flow was highly channelised.

Declaration.

The contents of this thesis is the original work of the author and has not previously been published for a degree at this or any other university. The work of other people is acknowledged by reference.

Steve Moss, BSc,
Department of Geological Sciences,
University of Durham.

Copyright.

Thesis dedication.

This thesis is dedicated to my mother and her sister, Norah, for their unfailing support and care over the years.

Acknowledgements.

-Firstly I must thank my mother and Norah, who through their support, encouragement and advice have made so much possible. I will always be indebted to them both.

-Maurice Tucker is thanked for many discussions and much advice during this project. His time and effort is gratefully appreciated, particularly with proof reading. Even though I'm not sure whether Maurice understood my Darlington sense of humour (or lack of it) all the time, I'm sure Department cheese and wine parties will never be the same for our Maurice. Maurice's family (Vivianne, Ashley and Zoe) also deserve a mention for their good food, good company and free windsurfing lessons.

-I am particularly grateful to Dave Asberry for all his help and advice with everything from field expenses to car radios. In particular for not being upset about the damage to his garden wall or the department photocopier!

-Ron Hardy is acknowledged for his numerous encounters with *"the machine that time forgot"* (Durham's XRD), certain parts of this thesis would not of been possible without his endeavours.

-Peter Greenwood and Hilary Sloane (NIGL, Keyworth) contributed much in time and effort to smooth running of the isotopic analysis of samples for this study. Baruch Spiro (also NIGL) is also thanked for several discussions concerning isotope geochemistry and diagenesis.

-Dr. J.M. Jones (NRG, Newcastle) is thanked for his advice on organic maturation. Mrs Summerbell (also NRG) is thanked for helping to prepare many of the polished blocks used in this study.

-Rob Butler (Leeds) is thanked for numerous discussions on Subalpine geology both in and out of the field.

-Rachel Flanagan and Jane Morris are thanked for performing several TOC analyses. Rachel also deserves a big thank you for all her help (proof reading, typing, *etc*) and encouragement during the final few weeks of torment.

-Gerald Roberts and Dave Hunt (the original Urgonian twins, sorry brothers) are thanked for all their advice and sarcasm, especially during that formative (and informative!) first year in Durham. Dave's denim jacket deserves a mention for its services to keeping the streets of Durham clean.

-Dick Swarbrick is thanked for the free use of his computer, office and several stimulating conversations concerning many aspects of geology. Likewise, Hugh Sinclair is also thanked for several dicussions on Alpine geology and his interest in the project.

-Cherry Walker (Miss Microsoft) deserves a special mention for her encyclopedic-knowledge of 'Windows' and many discussions on life in general in the New Inn.

-All the technicians at Durham have helped me during my time at Durham and I gratefully acknowledge all of them. In particular I would like to thank Karen Atkinson, Alan Carr, Carole Blair, Lynne Gilchrist, George Randall and Ron Lambert for their help.

-Doug Forbes is acknowledged for not complaining when he realised he wasn't going to get on the room's computer whilst I was writing. Cheers Doug!

-Jon Booler is thanked for staying out of the country whilst this thesis was written.

-Gazza, Marky, Parky, Mikey, Paul (Wiskies) and Andy are thanked for their accompaniment on numerous (usually fruitless) sorties into enemy territory (up the hill and round the Castle) on a Friday night.

-Robert Hall (UCL) is thanked for his help and advice over the years, and especially for introducing me to Alpine geology.

-The UCL posse are thanked for providing a free bed 'n' breakfast service in London for me and many hospitality beers over the years.
-Hubert Arnaud and Annie Arnaud-Vanneau (Grenoble) are thanked for showing me around the Urgonian of the Grenoble region and their interest in the project.
-Several other european geologists are also thanked for supplying imformation and/or discussions on related topics. They are: Christian Beck; Martin Burkhard; Jean-François Deconinck, Doris Goy-Eggenberger; Bernard Loup; John Ramsay; Roland Schegg; Guenter Trabold; and François Villars.

Cheers!

Contents

Chapter 1 Introduction and thesis outline.

1.1 Introduction.

For many decades mountain belts have been a major area of geological research not only because of the variety of geological structures exposed there but also because of the various sedimentary and mineral deposits associated with them. The Western Alps is no exception to this and many fundamental ideas concerning a variety of aspects of geology have been derived from research into the Alps.

The Subalpine Chains lie on the most western edge of the Western Alps and is the foreland fold/thrust belt to the main orogenic hinterland to the east. The Mesozoic and Cenozoic geological history of the area is typical of many foreland regions, with a former gently subsided continental passive margin altered to a foreland basin through compressional tectonics and ocean closure.

This thesis details the results of a case study into particular aspects of the sedimentology and basin history of the Subalpine Chains fold/thrust belt. The two main aspects to this thesis are burial diagenesis and the causes of palaeo-temperature variation within the fold/thrust belt.

A principal aim of this research was to document the burial diagenetic history of the mid-Cretaceous rudist-bearing 'Urgonian' limestone. Similar Cretaceous rudist platform limestones elsewhere in the world are good reservoir rocks (e.g. the Stuart City trend, Gulf Coast, Texas, Prezbindowski, 1985; Poza Rica trend, Mexico, Enos, 1988). Often their good porosity is due to the selective dissolution associated with the bi-mineralic rudist shells. Regional dolomitization of platform carbonates has also been known for a long time to increase the reservoir potential of such sediments. The basal section of the Urgonian platform has been replaced by a variable thickness of mosaic dolomite.The petrography and geochemistry of rudist shells, the equant calcite cements responsible for occluding the majority of porosity and replacive dolomitization within the basal section of the Urgonian platform are described. On the basis of the field, petrographic and geochemical data, a diagenetic model for the Urgonian is proposed.

The second principal aim was to study the regional variations in maximum burial temperatures and depths. To this end several palaeo-thermal indices were used (clay minerals, vitrinite reflectance and spore fluorescence) and the thermal history of the region is modelled using a PC-based modelling package (Basinmod). Regional trends in thermal indices are presented and quite clearly indicate an along strike (of the foreland fold/thrust belt) variation in burial temperatures. Both the modelling and field relationships suggest that major overthrust sheets emplaced only in the northern part of the study area are the principal cause of the greater depth of burial of that part of the Subalpine Chains.

A final aim of this research was to carry out a pilot study of the geochemistry of syn-tectonic veins. The petrography and outcrop nature of these veins indicate that cyclic hydraulic fracturing (the so-called "crack-seal mechanism", Ramsay, 1980) was very important in producing fractures within the rocks during Alpine deformation. These were healed by calcite cements, the stable isotope composition of which indicates the significance of water/wall rock interaction and the temperature of the precipitating fluids on the isotopic composition of the precipitate.

1.2 Thesis outline.

Chapter 2.

This chapter introduces the regional geology of the area. Firstly the geodynamic evolution of the Western Alps from passive margin to compressional fold/thrust belt is reviewed. Then the more detailed aspects of the Mesozoic and Tertiary sediments of Subalpine Chains are discussed and finally the structural geology of the area is described.

Chapter 3.

Here the mid-Cretaceous Urgonian carbonate platform is introduced in terms of its depositional setting, characteristic facies and facies arrangement. A generalised paragenetic sequence for the platform is presented and within the framework provided by this the diagenesis of the platform is described from field relationships and petrography. In particular, three main features of the Urgonian are described: 1) the stabilization of the bi-mineralic shells of rudists; 2) the precipitation of shallow burial equant calcite cements and 3) shallow burial dolomitization.

Chapter 4.

This chapter details the results of stable isotope and trace element analysis of the diagenetic features described in Chapter 3. Both the isotopic and trace element composition of these features is used to infer possible fluid sources involved in the various aspects of diagenesis of the Urgonian. A synthesis of the data presented in these two chapters culminates in the presentation of a diagenetic model for the Urgonian, which is related to basin scale events such as eustatic and/or tectonic-induced exposure of the platform.

Chapter 5.

In this chapter the results of a pilot study of the field relationships, petrography and geochemistry of veins and their calcite vein fills are described. Both field relationships and the petrography of the veins indicate a syn-tectonic origin for the veins and show the importance of hydraulic fracturing. The stable isotopic geochemistry of these veins is difficult to interpret in isolation, but when grouped together a strong isovariant trend (with

respect to carbon) is seen and this shows the effects of temperature on the fluids responsible for the precipitation of the vein fills.

Chapter 6.

Chapter 6 details the composition of clay mineral assemblages within one particular lower Cretaceous mudstone unit, the aim being to infer any possible differences in the burial and thermal history within the Subalpine Chains from the nature of the clay mineral assemblages. From the differences in the presence of illite and chlorite and changes in the composition of the mixed-layer illite/smectite within this mudstone it is suggested that the north-east part of the fold/thrust belt has experienced greater burial temperatures through deeper burial.

Chapter 7.

The results and interpretations of a study of the levels of organic maturity of Mesozoic and Tertiary sediments from the Subalpine Chains are presented in this chapter. Vitrinite reflectance measurements (along with estimates of spore fluorescent colours) are used to estimate peak palaeotemperatures within the Subalpine Chains. The results support the interpretations of the previous chapter, that the north-east part of the fold/thrust belt has experienced greater burial depths and temperatures. Potential hydrocarbon source rocks are discussed from the point of view of their total organic carbon content, kerogen type and maturity.

Chapter 8.

Chapter 8 discusses the controls on subsurface temperature and in particular various aspects of thermal and subsidence histories of foreland areas. A simple thermal history for the Subalpine Chains is used to model the thermal history of the area using a PC-based modelling package. The assumptions and criteria used in the selection of values for key parameters such as geothermal gradient are discussed. Comparison of calculated maturity to measured maturity (Chapter 7) suggests that the model is a first order representation of the thermal history of the Subalpine Chains. The modelling suggests that the north-east part of the chain must have experienced up to around 5km greater depth of burial than the south-western part to account for the palaeotemperatures indicated by the thermal indices described in Chapters 6 and 7.

Chapter 9.

The main conclusions to the chapters and the thesis as a whole are presented in this chapter.

Chapter 2 Regional Geology of the Subalpine Chains, S.E. France.

2.1 Introduction.

The northern French Subalpine Chains are a roughly NE-SW trending mountain belt, located in the southeast corner of France. It is part of the external Western Alps and is a classic example of a foreland fold/thrust belt.

This chapter introduces the structural geology and Mesozoic and Tertiary stratigraphy and sedimentology of the Subalpine Chains. The Mesozoic evolution of the present day Subalpine Chains began in the Triassic and continued until the late Cretaceous. Rifting associated with the opening of the Tethyan oceanic region in the Jurassic led to the formation of a passive margin on the southern edge of the European continent. Sedimentation, dominantly of carbonates on platforms and also in equivalent basinal areas, continued through the Jurassic and Cretaceous aided by thermal subsidence of the margin.

In the upper Cretaceous the outer extremities of the passive margin to the east and southeast began to experience compressional tectonics, as the leading edge of the Adria/north African continent began to move northward in response to a change in the plate motion vectors. This was the beginning of the Alpine orogeny. Foredeep flexure and related compressional deformation did not reach the area of the Subalpine Chains until much later, in the upper Eocene and Miocene. Prior to foredeep flexure the area had been subaerially exposed and eroded. Part of this exposure was related to uplift due to the formation of the Rhône/Bresse Graben.

Following the deposition of flysch and molasse sediments and thrusting and faulting associated with the final stages of the Alpine orogeny, the area was uplifted to its present position.

2.2 Location of the Subalpine Chains.

The Subalpine Chains are a series of massifs (named on Fig. 2.1) located in the southeastern corner of France. The area studied extends from the Vercors massif to the south of the city of Grenoble to the Haut-Giffre massif on the French-Swiss border.

The Subalpine Chains represent the most westerly portion of the Western Alps mountain belt. To the west are the low lying plains of the Bas-Dauphine region and to the northwest, the gentle hills of the Jura and the Swiss molasse basin. This region is often referred to as the peri-Alpine area. Beyond the plains of the Bas-Dauphine
to the west is the Massif Central. To the east are the much higher mountains of the Dauphine, Savoy and Italian Alps (including Mont Blanc).

The Subalpine Chains on their eastern edge are bounded by the External crystalline basement Massifs, Belledonne, Mont Blanc and Aiguilles Rouge (the small area of

basement rocks to the northwest of Mont Blanc on Fig. 2.1). These massifs are morphologically separated from the Subalpine Chains by the 'sillon subalpin'.

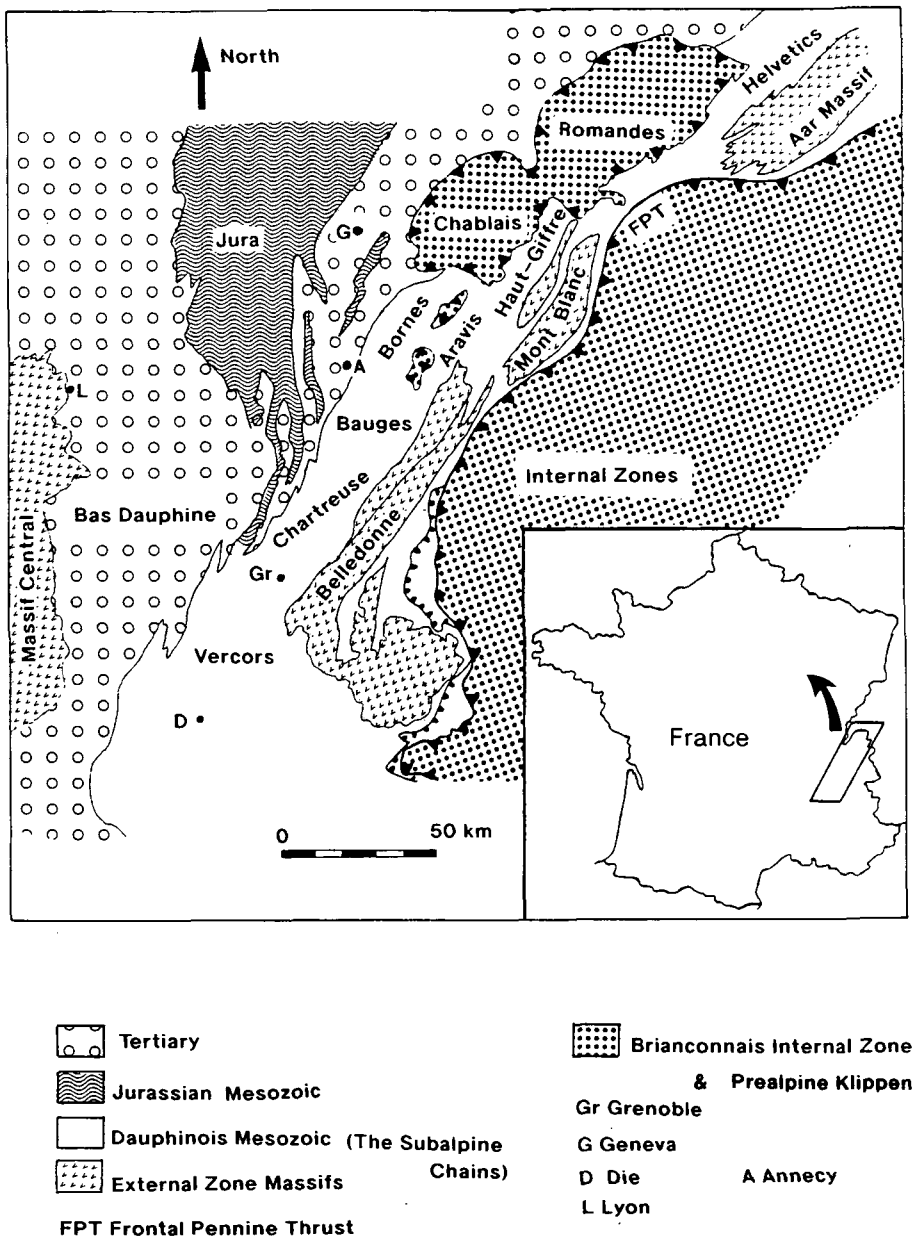

Fig. 2.1 Location of the Subalpine Chains in the southeastern corner of France and a simplified geological map of the area.

2.3 Mesozoic basin evolution of the Western Alps.

2.3.1 Palaeogeography of the Western Alps.

The Subalpine Chains are part of what is referred to as the External Zone, which is the most craton-ward and least deformed part of the former European passive margin to Ligurian Tethys (see Figs 2.2a and 2.2b). The External zone is bounded to the east by the

Internal Zone; this was the distal, sediment-starved part of the passive margin. The two zones are delimited by the Frontal Pennine Thrust (see Fig. 2.1). The Internal Zone comprises rocks from the Penninic and Austroalpine palaeogeographic domains (see Figs 2.2a and 2.2b) which contain the remnants of the Ligurian Tethys ocean and the Adria/African plate margins (as discussed in Dewey, 1973; Debelmas et al., 1983; Lemoine et al., 1986; Butler, 1989a).

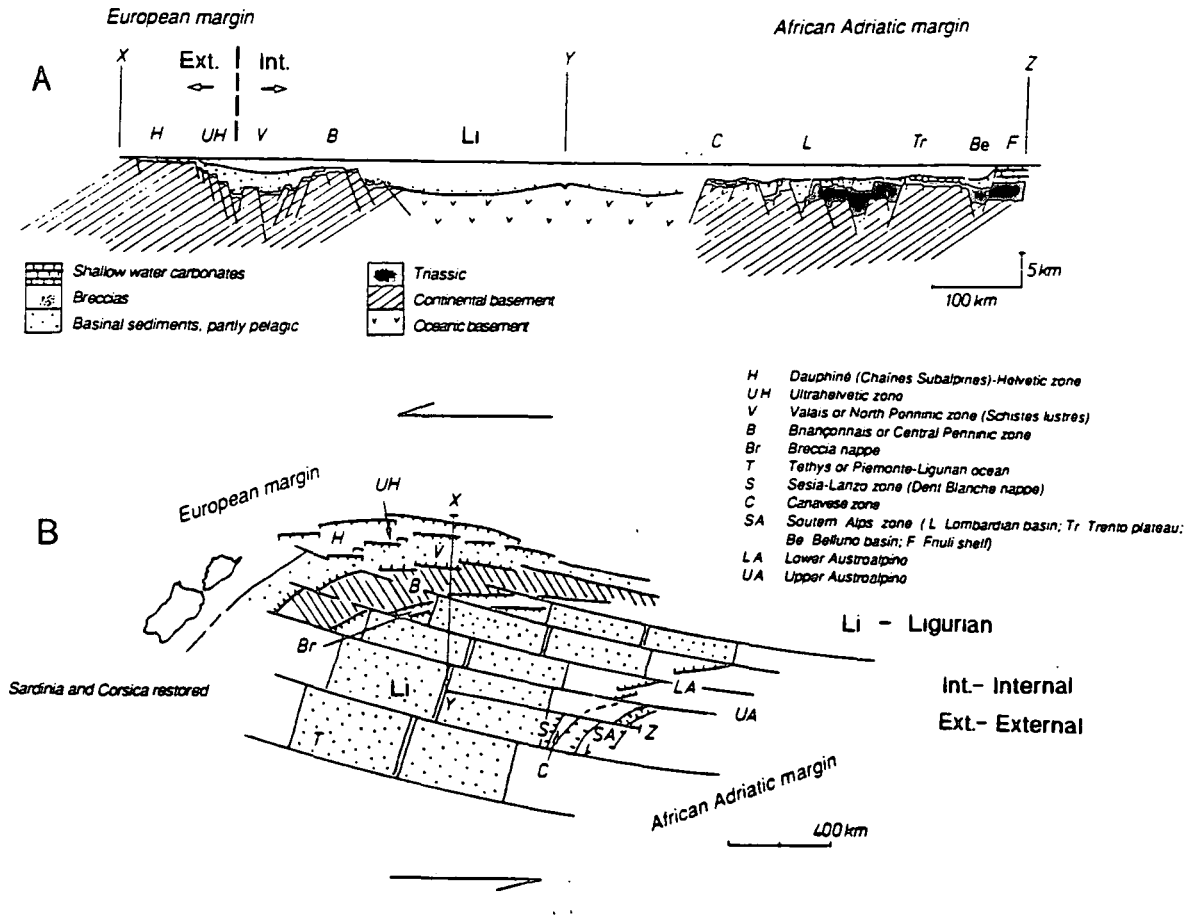

Fig. 2.2a Schematic section of Ligurian Tethys and its margins in the upper Jurassic. Internal and external areas are indicated for the European margin. Fig. 2.2b Palaeogeography of Ligurian Tethys in the upper Jurassic. From Coward & Dietrich (1989).

The External Zone is also divisible into discrete palaeogeographic domains, the Jura/Bas-Dauphine platform, the Dauphinois/Helvetic basin and the Provençal platform (see section 2.4). These domains are separated by major NNW-SSE trending lineaments, such as the Isère-Cevennes and Durance faults (see section 2.4.1 and Fig. 2.7a). The Dauphinois basin (to the south of the present Vercors region) was cut by the more highly subsident east-west trending Vocontian Basin (see Figs 2.7b and 2.10).

The External Basement massifs (see Fig. 2.1) are composed of pre-Triassic sediments and Variscan (and older) high grade gneisses and granitoids. The pre-Triassic sediments include Stephanian aged coals, which are locally of economic importance (see

Chapter 7), deposited during the final stages of the Variscan orogeny in NNW-SSE trending pull-apart basins (Blès et al., 1989). Major Variscan strike slip faults exerted a marked control upon the dip-slip extensional structures associated with the Jurassic and Cretaceous extension (Blès et al., 1989; Roure et al., 1992) and later during Tertiary compressional tectonics (see section 2.6.2).

2.3.2 Post Carboniferous sedimentation.

Prior to the Triassic the area was peneplained and the topography produced during the Variscan orogeny levelled off. Across the European margin sedimentation began with Triassic continental sands directly above the erosion surface followed by shallow-water carbonates and evaporites. This succession can be seen as remnant autochthonous patches on the flanks of the basement massifs and in boreholes in the Subalpine Chains (e.g. Michel & Caillon, 1957; Charollais & Jamet, 1990, Huggenberger & Wildi, 1991). The initial siliciclastic sedimentation was followed by Triassic to Cretaceous aged sediments. This sedimentary sequence is generally starved of siliciclastic input (particularly the External Zone) and as such is predominantly composed of basinal argillaceous limestones and equivalent carbonate platform limestones

The development and subsequent demise of the European passive margin can be divided into three tectono-stratigraphic periods: 1) Triassic, to mid-Jurassic pre-oceanic rifting; 2) mid- to late- Jurassic rifting and Cretaceous thermal subsidence and 3) late Cretaceous onset of basin inversion and Tertiary compression. This is shown in Fig. 2.3.

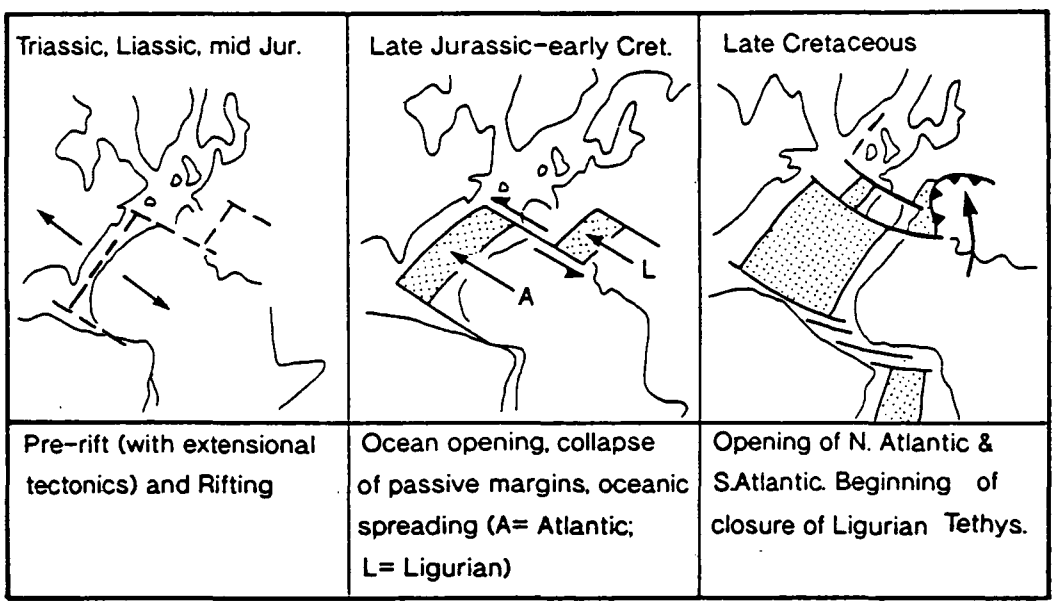

Fig. 2.3 The three main tectono-stratigraphic stages in the development of Ligurian Tethys. From Lemoine et al. (1986).

2.3.3 Late Triassic to mid-Jurassic pre-oceanic rifting.

During the Triassic and Hettangian gentle, undifferentiated subsidence occurred across the area of the future passive margin. The intercalation of alkaline volcanics within the sedimentary succession during this period suggests this early stage of continental

extension was coupled to the initial stages of opening of the Atlantic (Lemoine et al., 1986; Lemoine & Trümpy, 1987; Graciansky & Lemoine, 1988; see Fig. 2.3). Sedimentation passed up from the continental and shallow-marine sands to a shallow-marine carbonate platform and associated evaporites (Curnelle & Dubois, 1986). In the early to middle Jurassic subsidence became highly differentiated across the passive margin and was accommodated by the formation of tilted fault blocks within the External Zone of the passive margin. These faults formed along several major lineaments (i.e. the Isère and Durance faults; see Fig. 2.7a and section 2.4.1), producing fault blocks up to several 10's km wide and generally downthrowing to the east. These structures are well preserved in the Belledonne-Taillefer Massif (Lemoine et al., 1986). Sedimentation was strongly controlled by the tectonics due to the basin and shoal topography it produced, with the uplifted crests of blocks sub-aerially exposed or the sites of shallow-water deposition of crinoidal sand bodies. Within the half-grabens deeper-water pelagic and hemipelagic sediments are intercalated with gravity deposits derived from the footwall (e.g. Col d'Ornon; see Fig. 2.4; Lemoine et al., 1986; Lemoine & Trümpy, 1987). A marked acceleration in the rate of tectonic subsidence in the External Zone in the Toarcian and Aalenian caused the drowning of both 'unstable' basinal areas and 'stable' platform as (Arnaud, 1988; Roux et al., 1988; Rudkiewicz, 1988). At the same time the Briançonnais domain of the Internal Zone was subaerially exposed or under very shallow-water (see Fig. 2.5; Roux et al., 1988).

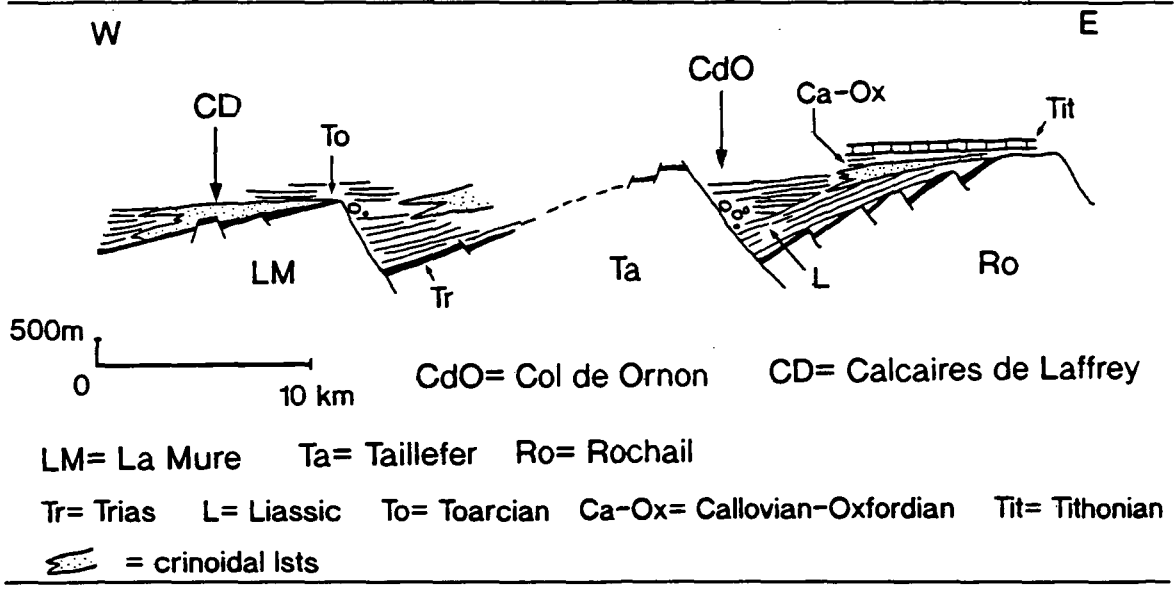

Fig. 2.4 Late Jurassic reconstruction of three tilted fault block structures in the external crystalline basement massifs (LM, Ta and Ro) to the east of Grenoble. Note the gravity deposits in the hanging-wall at Col d'Ornon. Re-drawn from Lemoine & Trümpy (1987).

2.3.4 Mid- to late Jurassic rifting and Cretaceous thermal subsidence.

During the late middle Jurassic to early late Jurassic major palaeogeographic changes occurred with the onset of sea floor spreading in the Ligurian palaeogeographic domain (see Figs 2.2a and 2.2b) and formation of oceanic crust upon which deep water sediments (radiolarian cherts) were deposited. The subsidence associated with this event

was strongly differentiated across the margin, being concentrated in the distal Briançonnais and Piemont domains of the Internal Zones (which are adjacent to the Ligurian domain; see Figs 2.2a & 2.2b).

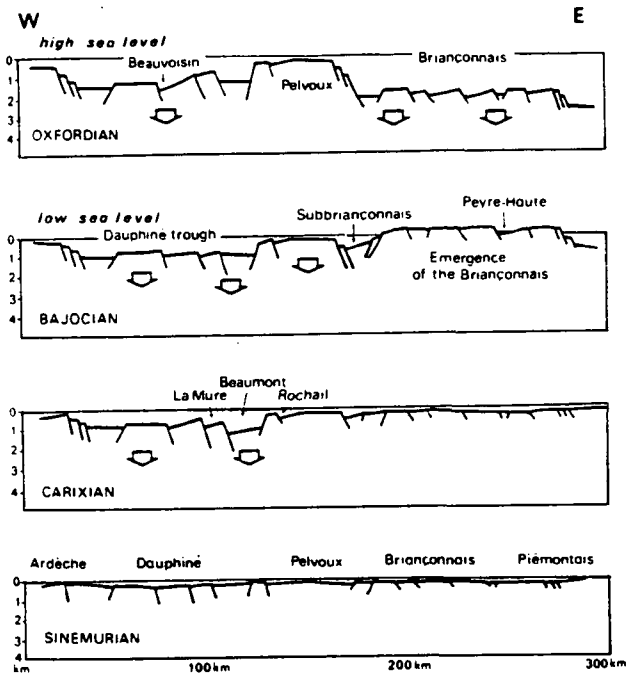

Fig. 2.5 Reconstruction of the bathymetric evolution of the European Tethyan margin across the French Alps, during the Jurassic. From Roux et al. (1988).

Within the External Zone shallow-water sedimentation was restricted to the stable domains of the Bas-Dauphine and Provençal platforms. Throughout the rest of the External and Internal Zones hemipelagic and pelagic sediments were deposited. Within the External Zone this period corresponded to a marked increase in sedimentation rates (the 'Oxfordian crisis' of Arnaud, 1988).

Following the onset of oceanic spreading in the Ligurian domain, thermal subsidence of the margin occurred, during which the margin gently subsided. The supply of detrital sediment to the margin was greatly reduced, reflecting the relative tectonic quiescence at this time. The post-rift break-up unconformity is usually interpreted to be marked by the base of widespread Tithonian platform limestones, which blanket the tilted fault blocks (Lemoine et al., 1986; Lemoine & Trümpy, 1987; see Fig. 2.4). However, the possible effects of increased carbonate production rates and/or eustatic effects should also be considered in this situation.

Within the External Zone shallow-water platform sedimentation during the Tithonian-Berriasian was restricted to the stable platforms bordering the Dauphinois/Helvetic basin (Arnaud-Vanneau et al., 1987; Detraz & Steinhauser, 1988;

Detraz, 1989). This suggests that the lineament which forms the western margin of the Dauphinois basin (see Figs 2.2a, 2.2b and 2.7a) still possessed a marked topography inherited from earlier rifting and/or was still actively moving (as suggested by Detraz & Steinhauser, 1988; Detraz, 1989; Villars, 1992). During this period predominantly pelagic and hemipelagic sediments were deposited in the Dauphinois basin.

Shallow-water sedimentation did cross the Isère lineament and extended into the Dauphinois basin for a considerable distance in the Barremian-Aptian. During this period the Urgonian carbonate platform was deposited (see Chapter 3). This period is marked by an abrupt increase in the rate of sedimentation (the 'Barremian crisis' of Arnaud, 1988). This abruptly ended in the upper Aptian with a return to deeper water sedimentation and lower rates of sedimentation.

2.3.5 Late Cretaceous and Tertiary of basin inversion and compression tectonics.

In the mid-late Cretaceous a major reorganization of the relative plate motion vectors between the European and African plates resulted from the northward propagation of rifting in the south Atlantic (see Fig. 2.3). The anti-clockwise rotation of Africa eventually led to the closure of Ligurian Tethys (Lemoine et al., 1986; Lemoine & Trümpy, 1987). The first indication of this plate reorganization was a renewal of detrital sedimentation over much of the external domain and compressional tectonics in some localities (e.g. Dèvoluy and Provençe, Debelmas & Kerchkove, 1980; Debelmas, 1983; Arnaud-Vanneau et al., 1987, see also Fig. 2.9). These structures are dated as pre-Senonian (Siddans, 1979) and the phase of deformation often referred to as the Pyrenean-Provençal event.

Closure of the Ligurian ocean and continental collision between the already deformed margins of Europe and Adria/North Africa occurred during the late Cretaceous and Tertiary (Lemoine et al., 1986; Lemoine & Trümpy, 1987; Coward & Dietrich, 1989). This produced the main phase of Alpine deformation with the emplacement of the Austroalpine nappes (containing rock-units of the deformed margin of Adria/Africa) onto European continental crust (see Fig.2.3).

During the late Cretaceous and early Tertiary the Dauphinois basin was emergent. Possibly partially due to the onset of compressional tectonics with the change in plate motion vectors and partially due to uplift related to the Rhône-Bresse graben in the early Palaeogene (Bergerat et al., 1990).

In the upper Palaeogene and Neogene rapid subsidence due to foredeep formation (Karner & Watts, 1983) and compressional tectonics (manifested by the formation of folds and thrusts) affected the Dauphinois/Helvetic basin. Deposition was dominated by a gradual return to siliciclastic sedimentation, which diachronously migrated from the Internal Zone to the External Zone as the foredeep migrated toward the west and northwest (see Fig. 2.6) (Homewood, 1983; Homewood et al., 1986; Mugnier & Menard, 1986; Guellec et al., 1990; Mugnier et al., 1990). The style of sedimentation changed from

Nummulite carbonate banks deposited with the inception of the foredeep, to deeper water volcaniclastic turbidites (classically referred to as flysch; Homewood & Lateltin, 1988). The latter are succeeded by shallow marine and continental sands and conglomerates (the molasse sequence; Homewood & Lateltin, 1988). Tertiary sedimentation and ages of the sediments are variable through the region of Dauphinois/Helvetic basin (see Fig. 2.11 and Chapter 8 of this thesis).

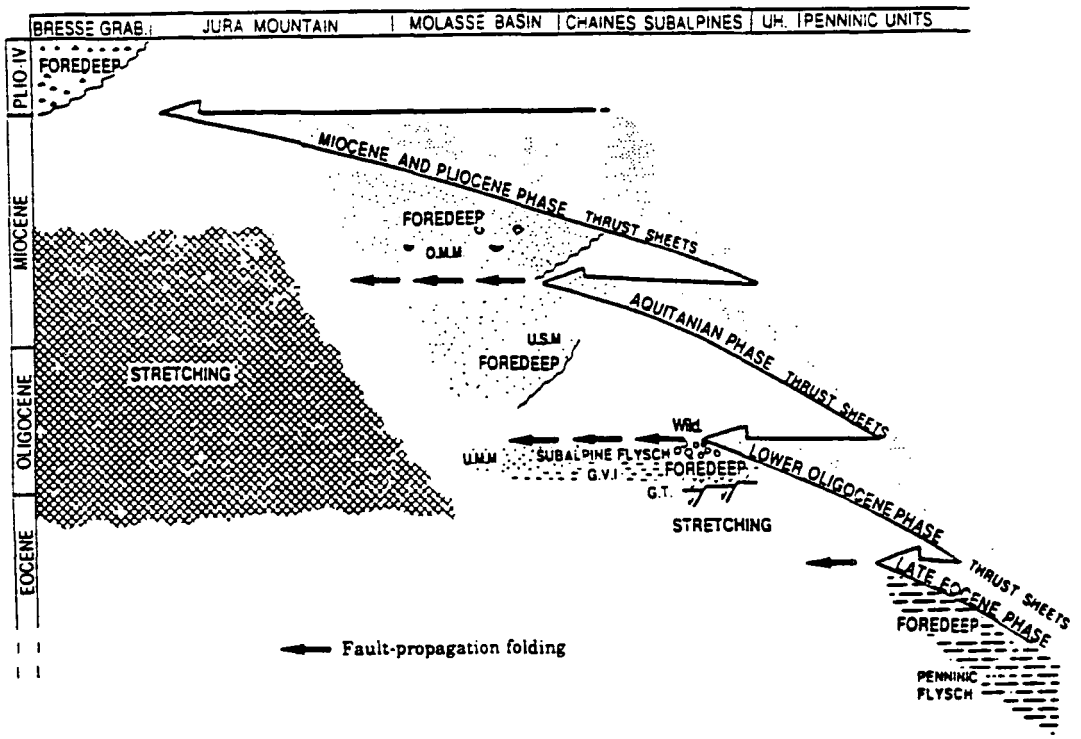

Fig. 2.6 Timing of foredeep migration along a section running roughly northwest to southeast through the western Alps in the Jura and Mont Blanc (the same section line as in Fig. 2.16). Bresse grab.= Bresse graben; UH=UltraHelvetic, GT=Taveyannaz ssts; GVI= Val d'Illiez ssts; OMM= Upper Marine Molasse; USM= Lower Freshwater Molasse; UMM= Lower Marine Molasse; Wild.= wildflysch. From Guellec et al. (1990).

Final deformation in the Subalpine Chains occurred in the late Miocene (Mugnier et al., 1990), although it did continue in the Jura till the Pliocene. Following the closure of the Ligurian ocean thermal re-equilibration of the crust led to isostatic re-bounding. This, together with the erosive power of the Pleistocene glaciations, shaped the present-day Subalpine Chains and provided the generally good exposure.

2.4 The Dauphinois/Helvetic shelf.

Having introduced the general basin evolution of the Western Alps and in particular the External Zone this section provides more detail on the Mesozoic sedimentology and stratigraphy of the Subalpine Chains.

2.4.1 Mesozoic structure of the Dauphinois/Helvetic platform.

Fig. 2.7a shows the three main palaeogeographic divisions of the Dauphiois/Helvetic platform. These are clearly bounded by the major lineaments, such as the Isère-Cevennes fault which separates the more highly subsident Dauphinois basin from the more stable platform areas, as shown by the isopachs in Fig. 2.7b.

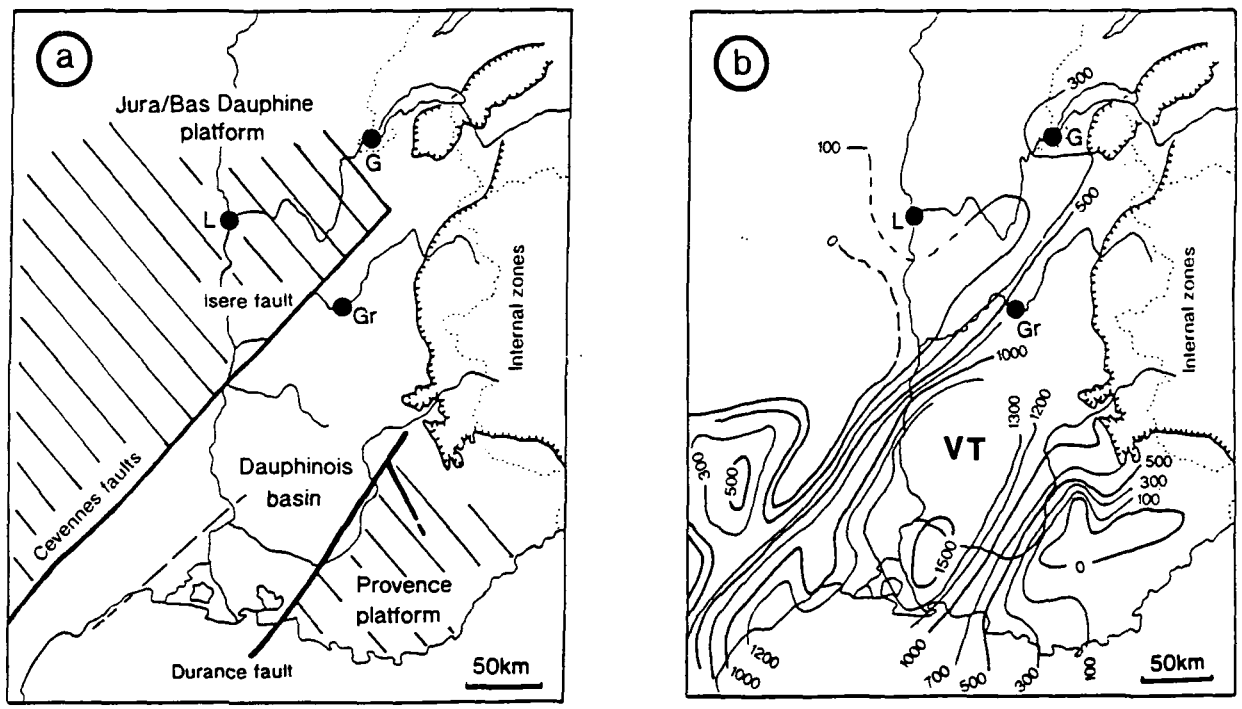

G=Geneva L=Lyon Gr=Grenoble

Fig. 2.7a Main palaeogeographic divisions of the Dauphinois/Helvetic shelf. The hachured areas (Jura/Bas Dauphine and Provence platforms) are the more stable areas. **Fig. 2.7b** Isopachs for the Liassic of the same area as Fig. 2.7a. VT= Vocontian trough. Re-drawn from Arnaud-Vanneau et al., (1987).

In the area of the present day French-Swiss border (the Platé and Haut-Giffre massifs) a graben structured sub-basin existed between the palaeo-highs of the future Aiguilles Rouges and Mont Blanc basement massifs. The former has a very attenuated cover sequence of only a 100m of mid- to upper Jurassic aged sediments. On the Mont Blanc massif the cover sediments are slightly thicker (up to 200 metres) of Triassic to mid-Cretaceous aged sediments (Ayrton, 1980). Both these palaeo-highs are believed to have been bounded by major east throwing normal faults (Lemoine & Trümpy, 1987, see Fig. 2.8). Several hundred metres of lower Jurassic (marly limestones and shales) accumulated in the graben between these two highs, as part of a typical Dauphine succession. The palaeo-highs and graben are important in the Tertiary during the inversion of the passive margin (this is discussed later in section 2.5) and in controlling the structural position of decollement horizons.

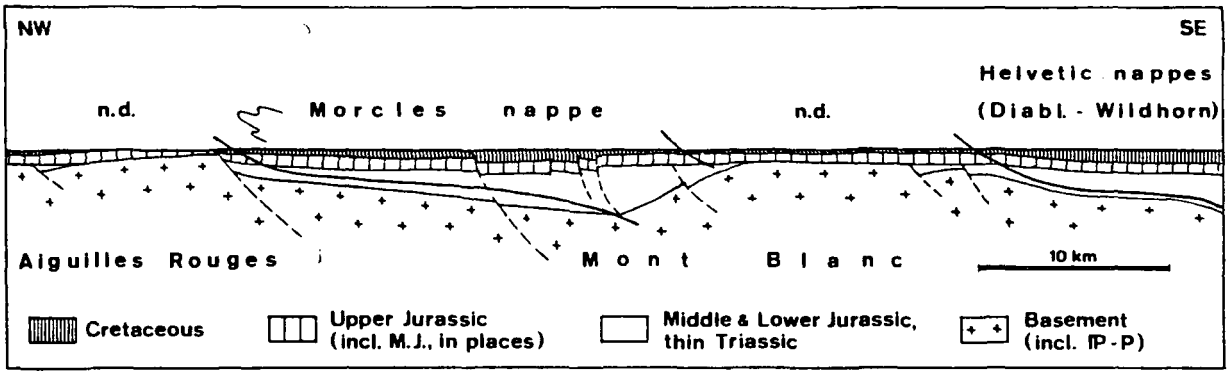

Fig. 2.8 Schematic restoration of the Aiguelles Rouge and Mont Blanc area of the Dauphine/Helvetic shelf, showing the existence of graben structured sub-basin between the future Aiguelles Rouges and Mont Blanc massifs. From Lemoine & Trümpy (1987). N.B. Such restorations are controversial and several alternatives have been offered (Butler, 1985; for example)

2.4.1 Mesozoic sediments and stratigraphy of the Subalpine Chains.

The stratigraphy of the Subalpine Chains is reviewed in Debelmas & Kerchkove (1980), Debrand-Passard et al. (1984) and in numerous other papers and theses. Fig. 2.9 shows a stratigraphic log for the Mesozoic of the Subalpine Chains.

The Mesozoic of the Subalpine Chains is referred to as the Dauphinois Mesozoic and differs in sedimentary facies and thickness from the Mesozoic of the Jura and Briançonnais zones. The Dauphinois Mesozoic is essentially more basinal in character and consists of more deeper water sediments, whereas the Jura Mesozoic succession contains principally shallow-water sediments. The two are in effect divided by the Isère fault lineament (see Fig. 2.7a). The control of this fault lineament on Subalpine and Jura sedimentation can be seen in Fig. 2.10, where particularly in the Lias and upper Jurassic (Malm superior on Fig. 2.10) when the shallow-water facies of the Jura can be seen not to extend beyond the Isére fault.

2.5 Tertiary basin evolution of the Subalpine Chains.

2.5.1 Early Paleogene history of the Subalpine Chains.

During early Paleogene (at least to the Eocene) the Dauphinois/Helvetic shelf was emergent (see Fig. 2.10). Allen et al. (1991) put the timing of initial exposure as between 65-53.5 Ma. The time gap produced by this period of Paleogene exposure varies from SSW to NNE along strike of the Subalpine Chains with a larger chronostratigraphic gap in the south-western massifs of the Chartreuse and Vercors than in the Aravis, Haut-Giffre, *etc.* A WNW to ESE decrease in the duration of the Paleogene exposure has been shown in the North Alpine Foreland Basin of Switzerland; the decrease is such that in the UltraHelevetic units the unconformity is not recognised (Allen et al., 1991; Bachmann & Müller, 1991).

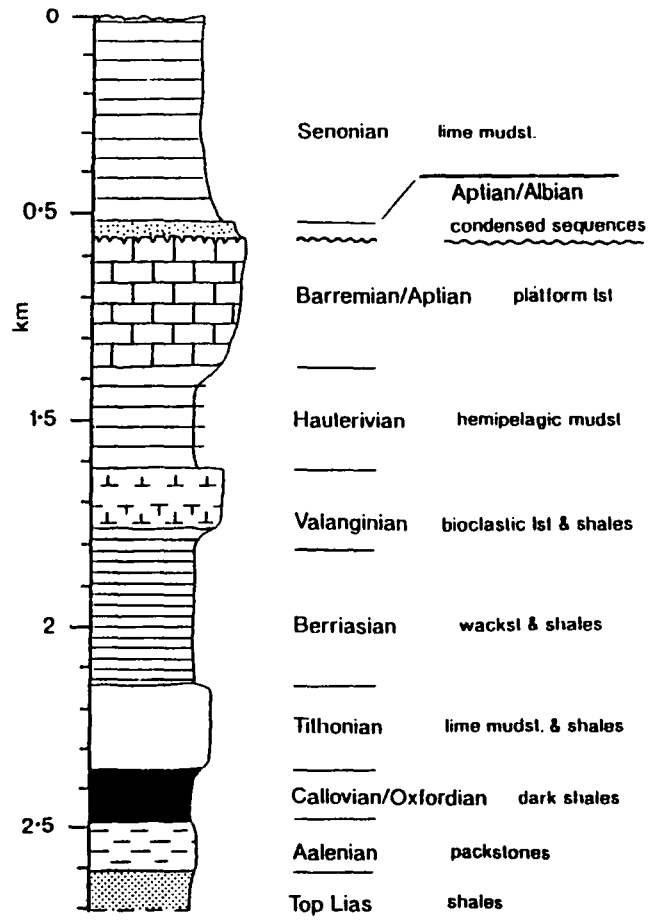

Fig. 2.9 General stratigraphic log for the Mesozoic of the Subalpine Chains.

During this period of exposure, before and during the accumulation of foredeep sediments in the north-east of the chain, localised pockets of thin (maximum thickness 30m) continental clastics and the 'siderolithique' deposits of the Jura and western Bornes were forming (Debrand-Passard et al., 1984; BRGM, 1988; Bachmann & Müller, 1991). Farther to the west in the Rhodanian trough (Rhône valley) lacustrine limestones and evaporites were being precipitated in small fault-controlled basins (Debrand-Passard et al., 1984). The erosion level was deeper to the west, causing the upper Cretaceous to be eroded from the western margins of the Subalpine Chains but remain preserved in the eastern regions of the chain (Villars, 1988; 1992).

Normal faulting, of Paleogene age, has been recognised at several localities within the Subalpine Chains (Pairis & Pairis, 1975; Trümpy, 1980; Debrand-Passard, 1984; Villars, 1986; Doudoux et al., 1987; *Notice explicative* BRGM, 1988; Villars et al., 1988; Welbon, 1988; Butler, 1989b, Chaplet 1989; Bachmann & Müller, 1991). The displacement on these faults is usually low (a few tens of metres) and they are only traceable for several kilometres (Chaplet 1989; Bachmann & Müller, 1991) Some of these faults are syn-sedimentary and contain footwall conglomerates containing material from

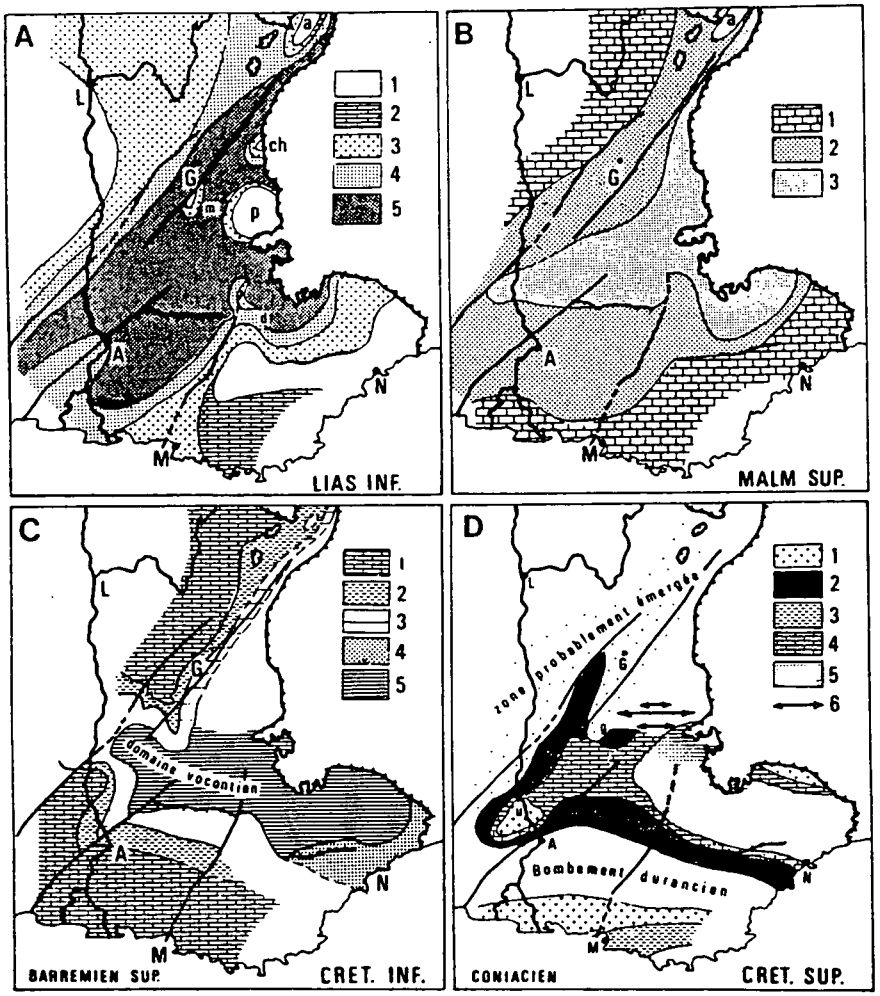

Fig. 2.10 Mesozoic facies distribution maps for; A lower Lias, 1= exposed regions; 2= intertidal-supratidal dolomites; 3= shallow-water bioclastic facies; 4= open marine limestone and shales, average thickness; 5= very thick open marine limestone and shales. B upper Malm, 1= reefal facies (often dolomitized); 2= pelagic facies; 3= very deep water pelagic facies. C lower Cretaceous, 1 and 2 'Urgonian' 1= shelf rudist facies; 2= shelf margin facies; 3= hemipelagic limestone and shales; 4= micritic limestones with glauconite and phosphate; 5= deepwater shales (Vocontian facies *sensu stricto*). D upper Cretaceous, 1= rudist limestones; 2= glauconitic sands; 3= sandy limestones; 4= calcareous sands; 5= limestone and shales; 6= folds. A= Avignon; G= Grenoble; L= Lyon; M= Marseille, N= Nice. Major fault lineaments marked on the map, are from NW to SE; the Cevennes-Isère fault; the Cléry fault; the Nîmes fault and the Durance fault. From Debelmas & Kerchkove (1980).

the earliest foredeep sediments (e.g. the normal fault at La Goenne, southern Aravis massif, Doudoux et al., 1987; Villars et al., 1988; Welbon, 1988). It has been suggested that these faults are part of a transtensional system linked to the formation of the Rhône-Bresse graben to the west during the Oligocene (Butler, 1989b). The east-west oriented extension

responsible for the formation of this graben both in the Jura and Dauphinois basin was associated with reactivation of many of the major NNE-SSW and N-S trending lineaments such as the Isère-Cevennes lineament (Blès et al., 1989). However, many of these faults appear to be due to extension and stretching resulting from the downwarping of the Subalpine Chains associated with foredeep flexure (Homewood et al., 1986; Guellec et al., 1990; Bachmann & Müller, 1991; see Fig. 2.6).

2.5.2 Foredeep flexure and sedimentation.

Foredeep-related flexure commenced in the area of the Subalpine Chains in the Eocene (46 Ma, the age of the oldest sediments in the foredeep; Pairis & Pairis, 1975; Debelmas & Kerchkhove, 1980; Debrand-Passard et al., 1984). However, in Vercors and Chartreuse, foredeep formation occurred much later in the Aquitanian (25 Ma, Nicolet, 1979; Debrand-Passard et al., 1984). The reason for this difference is that the north-east part of the chain (Haut-Giffre, Platé, Aravis, particularly) represents a more internal (and slightly different structured) portion of the former Dauphinois/Helvetic shelf, whereas the south-western part of the chain represents a more external part of the former margin.

Foredeep-related sedimentation in the area of the French Subalpine Chains studied can be divided into two major phases: i) the initial 'flysch' stage and ii) the 'molasse' stage. The flysch stage began in the upper Lutetian (Eocene) and ended in the mid-Chattian (Oligocene) (Homewood & Lateltin, 1988; Lateltin, 1988, see also Fig. 2.6). Sedimentation was predominantly of turbidite sands and shales in basins bordering the active deformation front. The molasse stage ranges from upper Oligocene to roughly Messinian (Miocene). Sedimentation is predominantly from fluvial systems, interrupted by a marine incursion.

The foreland basin siliciclastics of the Western Alps have been described on numerous occasions from palaeontological, stratigraphical and sedimentological points of view. Often this has led to confusion over the stratigraphic relationships around the arc. Given below is a brief summary of the sedimentogical and stratigraphic evolution of the foreland basin. A summary chronostratigraphic chart for the Tertiary is shown in Fig. 2.11.

i) 'Flysch' stage.

The initial foredeep deposits in the north-east part of the chain are classically interpreted to be 'flysch' deposits (Homewood, 1983; Homewood & Lateltin, 1988) formed in front of the advancing Alpine deformation front and are incorporated into the present day Alpine front. The onset of sedimentation saw a diachronous, relatively thin, transgressive, carbonate ramp (the 'calcaire Nummulitique') being deposited within the basin. The Nummulitique is divided into a lower marine unit (upper Lutetian) and an upper marine unit (Priabonian) (Debrand-Passard et al., 1984). These two are divided by a period of emergence during which locally continental, lacustrine and brackish marine sediments were deposited (including the so-called 'couches des Diablerets' or Diableret beds) (Charollais et al., 1980; Debrand-Passard et al., 1984; *Notice explicative* BRGM, 1988).

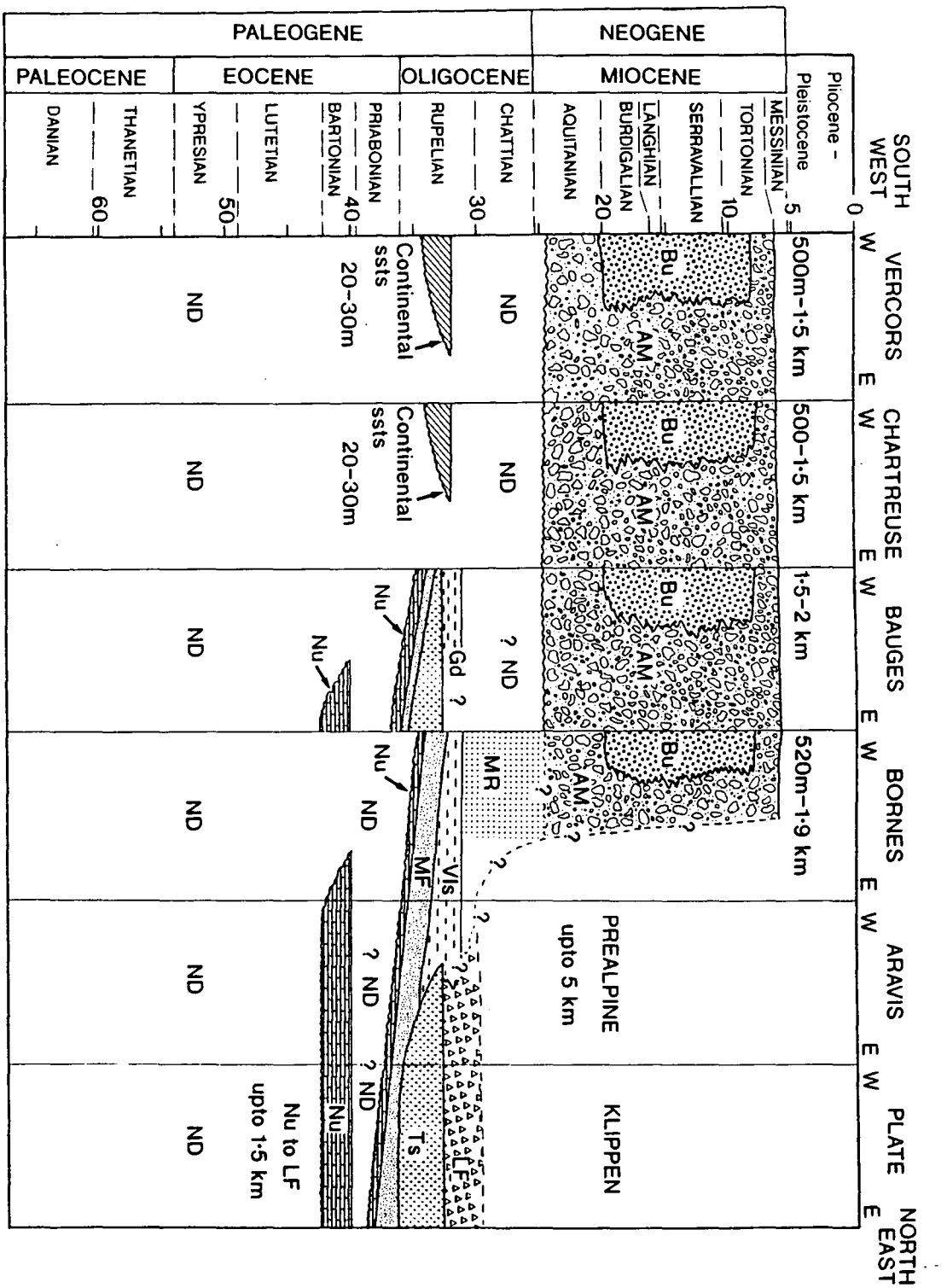

The Nummulitique unit passes up into the deeper-water lower Oligocene aged, pelagic shales ('marnes à Foraminifera' or Globigerina marls as they are also referred to), which are also time transgressive (Lateltin, 1988). Within the Bornes massif the upper 30m or so of these shales is referred to as the 'schistes à Melatta' (or Melatta shales). This

Fig. 2.11 (preceding page). Summary chart of facies and ages for the Tertiary of the Subalpine Chains from SW to NE. Bu= Burdigalian molasse; Am= Alpine molasse; MR= Molasse Rouge; Gd= Gres de Deserts; VIs= Val d'Illiez ssts; Ts= Taveyannaz ssts; MF= Marnes foraminifera; NU= Nummulite lsts. ND= non-deposition. Data from the following sources: Nicolet (1979), Homewood (1983), Debrand-Passard et al. (1984), Mugnier & Menard (1986), Lateltin (1988), Chaplet (1989) and Charollais & Jamet (1990). Timescale from Haq et al. (1987). Diagram originally published in Moss (1992).

horizon contains abundant fish scales and debris and predominantly planktonic foraminifera. Gorin et al. (1989) have shown from the palynofacies and organic geochemistry of these shales that they were deposited in elongate basins formed in the Eocene upon the Helvetic shelf and had restricted circulation due to the effects of tectonism and/or eustasy. These small graben-type basins were equally important for controlling the location, nature and organic content of the older 'couches des Diablerets' (mentioned above). As mentioned in section 2.5.1 Eocene and Oligocene aged normal faulting was quite common within the former area of the Dauphinois/Helvetic shelf.

Deposition of the 'marnes à Foraminifera' was followed by the volcaniclastic turbidites of the Taveyannaz and Val d'Illiez Formations (Lateltin & Muller, 1987; Lateltin, 1988). These are thought to represent two underfilled depositional troughs which paralleled the advancing deformational front. With the slightly older (lower Rupelian) inner, Tavayannaz Formation, the trough was filled with andesitic greywackes derived from contemporaneous volcanoes, located somewhere in the UltraHelvetic zone (Debelmas et al., 1983; Homewood et al., 1986; Lateltin, 1988). Whilst the slightly younger (upper Rupelian to lower Chattian) outer, Val d'Illiez Formation trough was filled mainly by material derived from the advancing Austroalpine and Penninic thrust sheets and is more mudstone rich (micaceous shales) and less andesitic dominated than the Taveyannaz Formation (Lateltin & Muller, 1987; Lateltin, 1988). The inclusion of pebbles of local sedimentary rocks in both the Taveyannaz (Tertiary aged units) and Val d'Illiez (Tertiary and Cretaceous aged units, see Lateltin, 1988) suggests that parts of the Dauphinois/Helvetic shelf were experiencing erosion at this time.

Both these formations pass up into shales with blocks of material of UltraHelvetic origin; these are the Wildflysch or Lenticular Flysch deposits. They are interpreted as olistostromes derived laterally from the 'active' margin of the approaching Penninic and Austroalpine nappes (Debrand-Passard et al., 1984; Homewood et al., 1986; Lateltin, 1988). These olistostromes are the final sedimentary deposits in the eastern Bornes, Aravis, Platé and Haut-Giffre before the emplacement of the Prealpine thrust sheets.

ii) 'Molasse' stage

In the western Bornes (Plateau des Bornes) and Bauges, sedimentation continued, with shallow-marine sands as part of a regressive series. Often called the Lower Freshwater Molasse, these sediments have also been given many more 'local' names such as the Grès

de Deserts or the Molasse rouge. These sediments were deposited in increasingly more continental environments (alluvial fans and braided rivers). It is during this period (in the upper part of the Freshwater Molasse) in the Aquitanian that molasse style deposits began to form in the Vercors, Chartreuse, Bas-Dauphine and Annecy molasse basin (south of Geneva, the Plataeu des Bornes region), with the deposition of the 'Molasse de Lans', the 'conglomerates de Voreppe', the 'Molasse de Lausanne', *etc* (Debrand-Passard et al., 1984).

Close to the Aquitanian-Burdigalian boundary the westerly part of the molasse basin was transgressed, producing a shallow tide- and wave- dominated seaway linking all the way round the mountain front (Allen et al., 1985). This is often referred to as the Upper Marine Molasse (the Lower Marine Molasse are the Taveyannaz and Val d'Illiez sandstones, *etc*, of the flysch stage). West of the Chartreuse these sands are well exposed with large scale cross bedding structures (see Fig. 2.12) and overlie a former rocky shoreline of bored mid-Cretaceous limestone (see Fig. 2.13).

Fig. 2.12 Large scale cross bedding within the shelly sandstones of the Burdigalian molasse at Les Echelles (labelled as EDG on Fig. 2.18a) Hammer approximately 350mm long.

In the mid-Miocene the depositional style reverted to continental sedimentation with proximal alluvial fans feeding river systems. This is referred to as the Upper Freshwater Molasse.

Heavy mineral assemblages and the overall composition of these sands suggest that the predominant source was from the east with the progressive unroofing of the Austroalpine thrust and Penninic units. Heavy mineral assemblages reflect different source

regions (Allen et al., 1985). For example, lawsonite and blue sodic amphibolite within the molasse of the Annecy area are believed to be sourced from the Schistes lustré of the Briançonnais zone (Mange-Rajtzky & Oberhänsli, 1982). Lack of Dauphinois/Helvetic

Fig. 2.13 Clasts of bored Urgonian limestone (U) within the Miocene aged molasse at the western end of the Chailles gorge (see Fig. 2.18a for location). The clasts were identified as Urgonian after thin section inspection of a sample of the conglomerate shown.

material until the Upper Marine Molasse suggest that the Subalpine Chains antiformal stack had not reached the syn-orogenic surface at this time. Within the Upper Marine Molasse and Upper Freshwater Molasse clasts of Dauphinois/Helvetic origin are common (see Fig. 2.13).

The Bas Dauphine and Swiss Molasse basins (collectively referred to as the Peri-Alpine Molasse Basin or 'sillon perialpine') represent the final position of the molasse basin. This migration of the foredeep is shown in Fig. 2.6.

2.6 Present day structure of the Subalpine Chains.

2.6.1 Present day crustal structure of the Western Alps.

The overall geometry of the Western Alps is well constrained, both from geophysics (Perrier, 1980; Bayer et al., 1987) and from structural studies (Debelmas et al. 1983; Ramsay, 1981, 1989; Butler, 1989a). Although it should be mentioned that some aspects of the following description are controversial. In particular, the restoration of the Mont Blanc/Aiguelles Rouges area, the exact nature of the relationship between the

Helvetic nappes and the Subalpine Chains and how they link up and the timing of deformation.

The Western Alps is an area of thickened continental crust as shown by the west to east increase in the depth of the Moho (see Fig. 2.14), this is due to the stacking of several large overthrust sheets (see Fig. 2.15) with the closure of the Ligurian ocean. ECORS-CROP deep seismic data presented in Bayer et al. (1987) and Roure et al. (1990) has confirmed the overall crustal structure of the Alps. This data, with one possible interpretation, are shown in Fig. 2.16a. Several large displacement low-angle thrusts can be inferred from the seismic line which penetrate the mantle and imbricate rocks of different crustal depths. One important thrust is the Alpine sole thrust (this sole thrust is marked on Figs 2.15 and 2.16b); this carries the External Basement Massifs in its hanging wall.

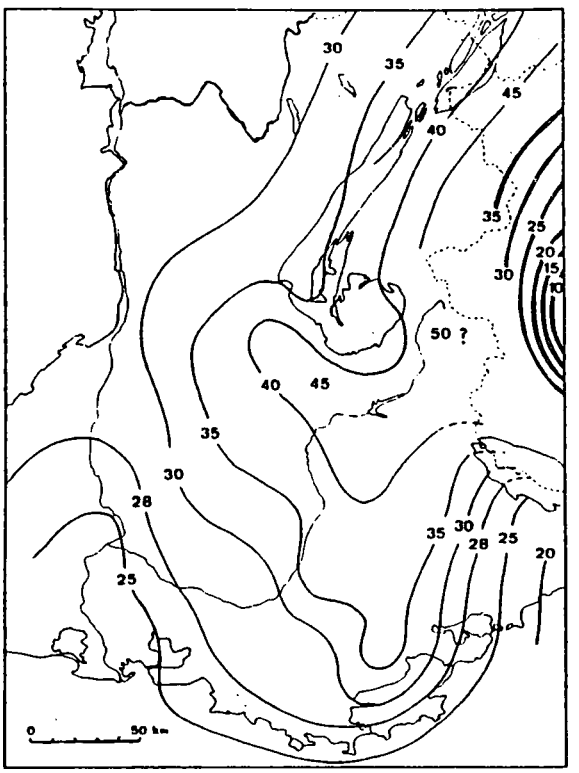

Fig. 2.14 Contour map of the depth to the Moho in the western Alps. Note the eastward increase in crustal thickness. From Perrier (1980).

2.6.2 Present day structure of the Subalpine Chains.

The overall structure of the Subalpine Chains has been interpreted in terms of 'detachment tectonics' (Boyer & Elliot, 1982), with the Mesozoic cover detaching from the pre-Triassic basement. The Alpine sole thrust which carries the basement massifs such as the Belledonne in its hanging wall (see Figs 2.15 and 2.16b) passes into the foreland area underneath the Subalpine Chains as the basal detachment for the Subalpine Chains (Butler, 1989a). Structural style within the Subalpine Chains varies along strike of the fold/thrust belt. The structures in the Subalpine Chains are nearly the western limit of Alpine.

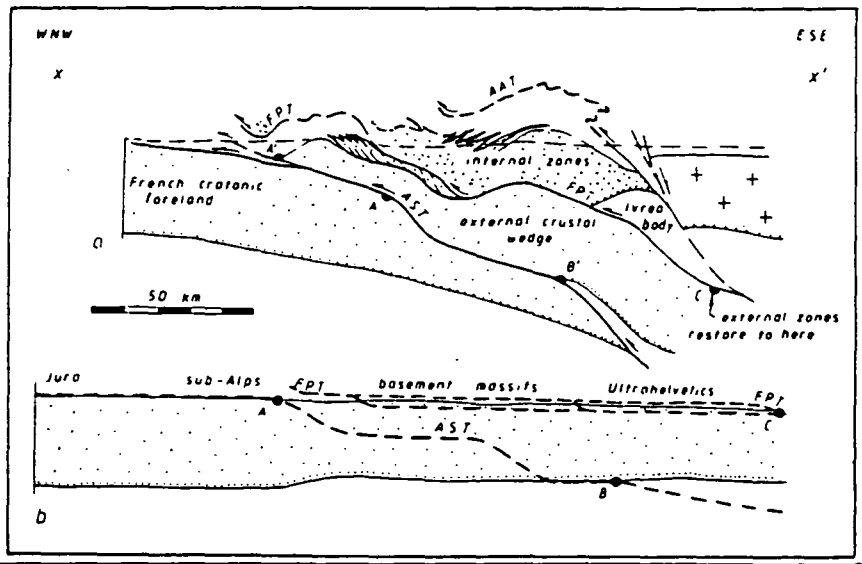

Fig. 2.15 Crustal scale cross-section through the western Alps, showing the stacking of several large overthrust sheets. AST= Alpine sole thrust; FPT= Frontal Pennine thrust. From Butler (1989a).

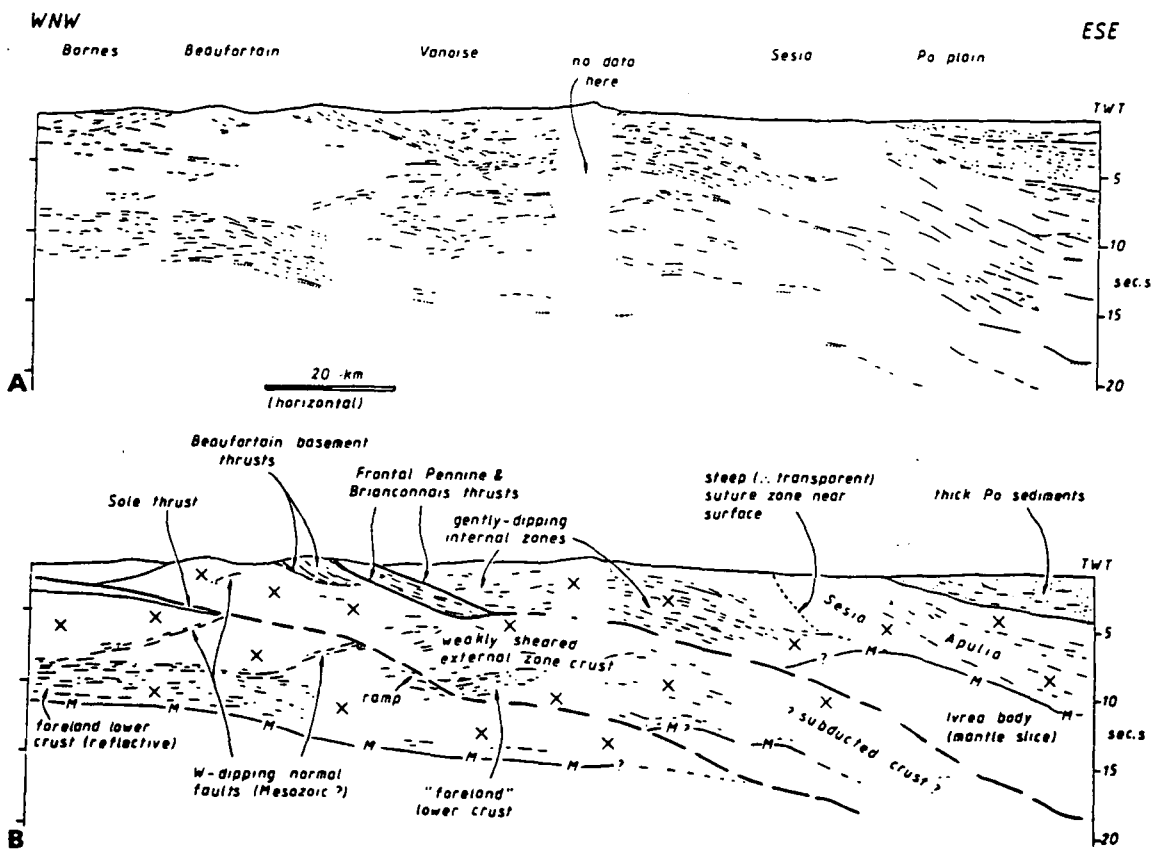

Fig. 2.16a Line drawing of the ECORS-CROP deep seismic profile (time section) through the western Alps.
Fig. 2.16b One interpretation of the data presented in Fig. 2.16a. From Butler (1989b).

deformation. The Jura to the east is the most westerly part of the belt and represents the final stages of deformation (Mugnier et al., 1990).

Tertiary structural development of the Subalpine Chains was strongly controlled by the pre-existing Mesozoic structure. Lineaments such as the Isère-Cevennes lineament and younger Oligocene intrabasinal faults played an important role in the Tertiary structural development of the Subalpine Chains. For example, in the frontal part of the Vercors backthrusting and buttressing structures (upright folds, cleavage and strain intensification) are produced where the leading edge of developing thrusts have run into the Isére fault (Butler, 1989b). Other features seen within the Subalpine Chains produced by the influence of pre-existing structures include overturned and reactivated normal faults, ramps developing ahead of faults and normal faults cut through by thrusts (Subalpine and Alpine examples of these structures are given in Gilchrist et al., 1987; Welbon, 1988; Butler, 1989b). One of the major influences of pre-existing structure, particularly normal faults, is the vertical displacement of easy-slip décollement horizons which may lead to thrust ramp localization (Welbon, 1988; Butler, 1989b). At the Jura thrust front the Triassic easy-slip horizon has been downthrown by normal faults associated with the western edge of the Rhône-Bresse graben (Butler, 1989b).

To avoid a lengthy descriptions of each massifs a geological map is presented for each area along with four cross-sections (see Fig. 2.17c for location). For further information on the geological structure the reader is referred to the following papers: BRGM (1979a, 1979b & 1985), Gidon (1981), Boyer & Elliot, (1982), Doudoux et al., (1982, 1984), Butler et al., 1987, Mugnier et al. (1987), Butler, (1989a, 1989b); Ramsay, (1989), Mugnier et al., (1990) Huggenberger & Wildi (1991), Butler, (1992a), Butler (in press a & b). Several important features are mentioned in the paragraph following these maps.

i) The Vercors.

The geology and structure of the Vercors is shown in Figs 2.17a and 2.17b.

Fig. 2.17c Location of the four cross-sections shown in this section. A= 2.17b; B= 2.18b, C= 2.20b; D= 2.21b. City and town abbreviations as in Fig. 2.1.

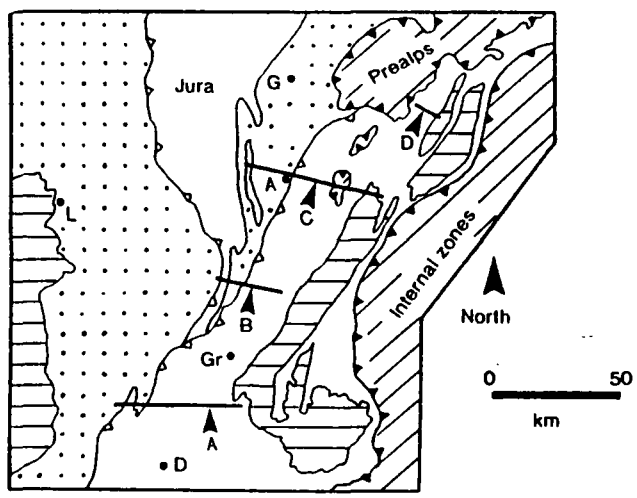

Fig. 2.17a (opposite page). Simplified geological map of the Vercors. Modified from BRGM (1979b). **Fig. 2.17b** Balanced (1) and restored (2) cross-sections through the Vercors. From Butler (1989b).

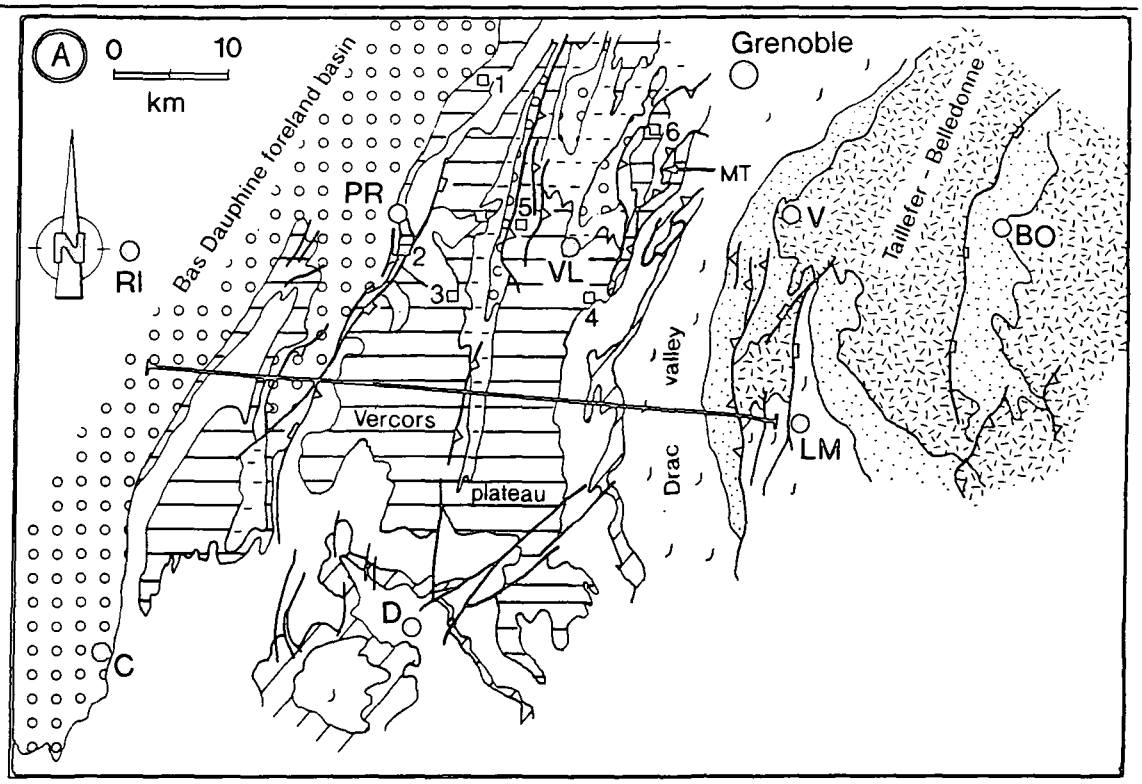

Miocene

Oligocene - mid-Cretaceous

Urgonian

lower Cretaceous

Tithonian

m - u Jurassic

Lias - Trias

Basement

LM - La Mure V - Vizille

RI - Romans-sur- Isere PR - Pont-en-Royans C - Crest D - Die

BO - Bourg d'Oisans VL - Villard-de-Lans MT - Moucherotte thrust

1= Gorge du Nant 2= Petit Goulets 3= Grand Goulets

4= la Grande Moucherolle 5= lower Bourne gorge 7= Moucherotte

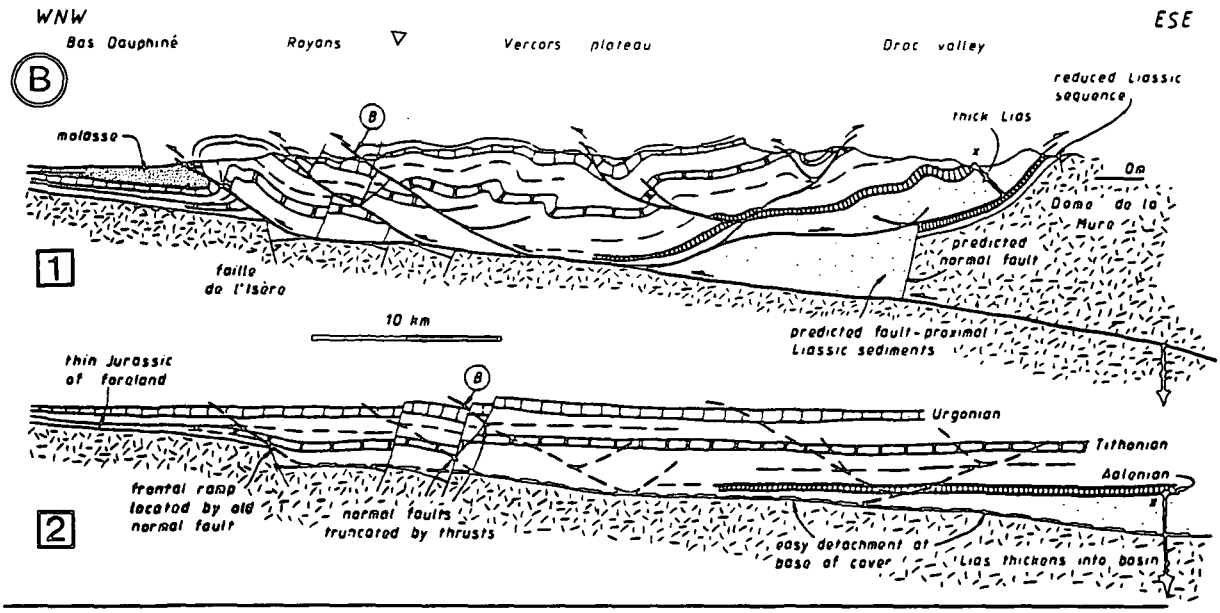

ii) The Chartreuse.

The geology and structure of the Chartreuse is shown in Figs 2.18a and 18b.

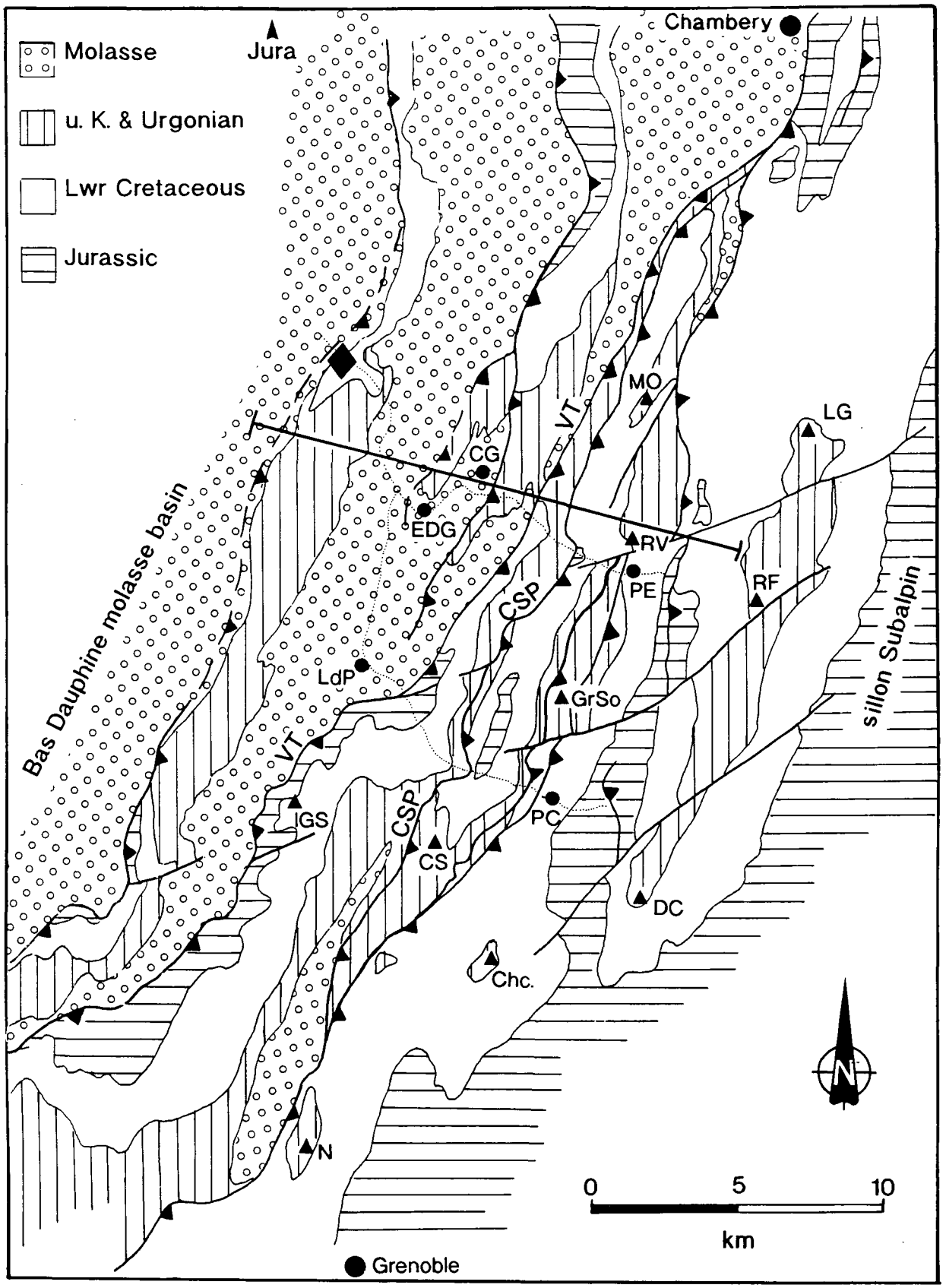

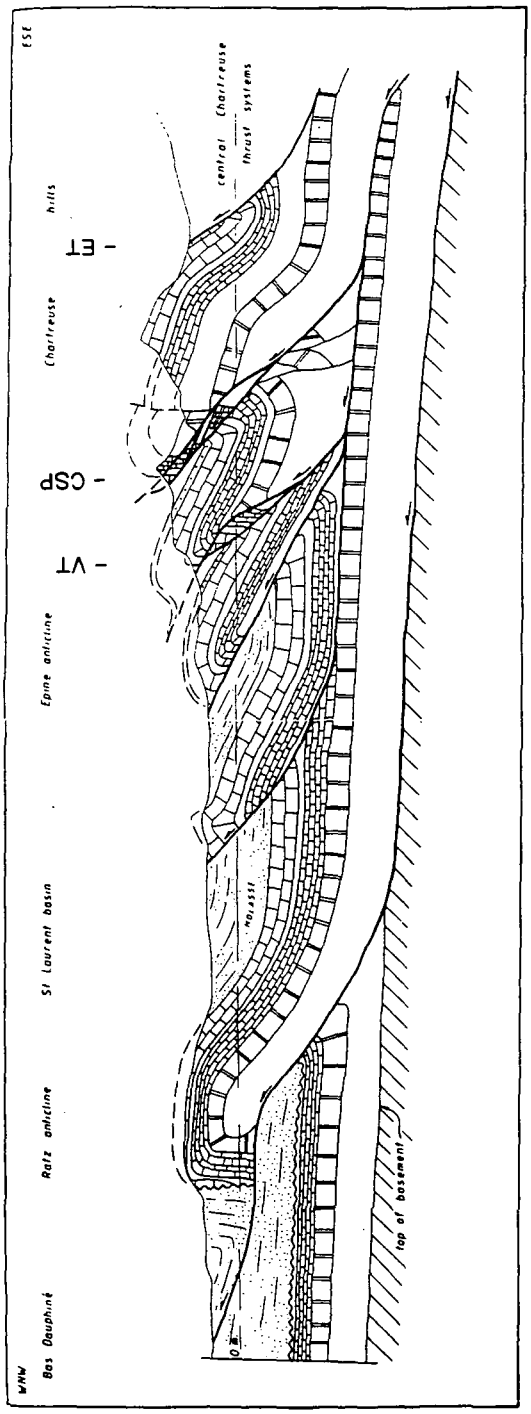

Fig. 2.18a (preceding page). Simplified geological map of the Chartreuse massif. Modified from BRGM 1979b and Butler (1992a). MO= Mt. Outheran; LG= Le Granier; RV= Roche Veyrand; RF= Roche de Fitta; GrSo= Grande Sommet; CS= Charmont Sommet; DC= Dents de Crolles; Chc= Chamchaude; lGS= la Grande Sure; N= le Neron; CG= St. Christophe-sur-Guiers; EDG= Entre-deux-Guiers; PE= St. Pierre-d'Entremont; LdP= St. Laurent-du-Pont; PC= St. Pierre-en-Chartreuse. VT= Voreppe thrust; CSP= *'chevauchement subalpin principalment'* principal Subalpine thrust. Black diamond is the Chailles gorge. Dotted lines are the main rivers. **Fig. 2.18b** Balanced cross-section through the Chartreuse. From Butler (1992a). ET= Entremont thrust; VT and CSP as in Fig. 2.18a.

iii) The Bauges.

The geology and structure of the Bauges is shown in Fig. 2.19.

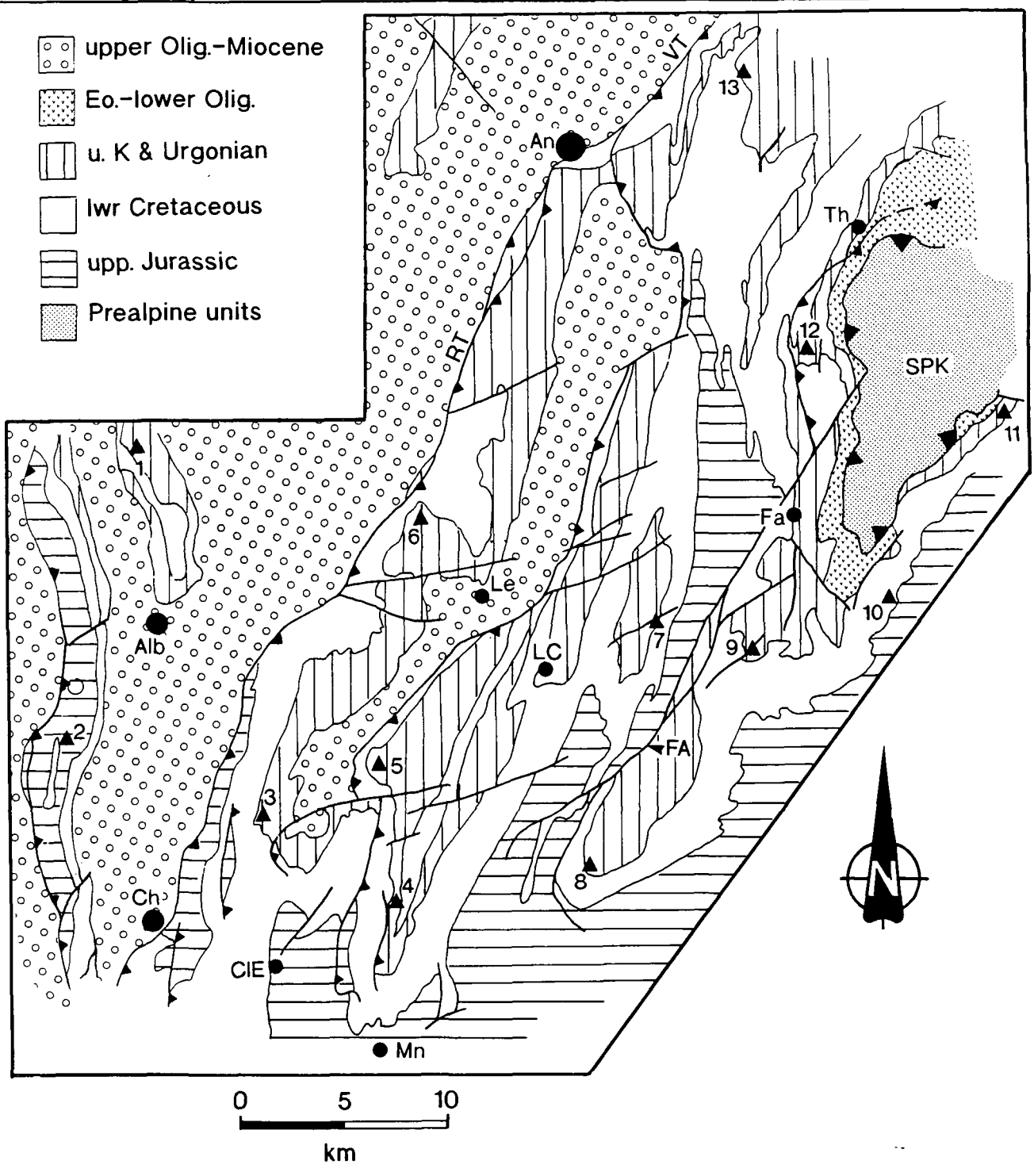

Fig. 2.19 Simplified geological map of the Bauges. Modified from BRGM (1979a; 1979b). 1= Chambotte; 2= Mont du Chat; 3= Croix du Nivolet; 3= Pointe de Galoppaz; 4= Mt. Margeriaz; 5= Mt. de Bange; 6= Mt. Trelod; 8= Dents d'Arclusaz; 9= Pointe de la Sambuy; 10= Dent des Cons; 11= Mt. Charvin; 12= La Tournette; 13= Tête du Parmalan. An= Annecy; AlB= Aix-les-Bains; Ch= Chambéry; ClE= Challes-les-Eaux; Mn= Montmelian; LC= Le Chatelard; Fa= Faverges; Th= Thônes; Le=Lescheraines. SPK= Sulens Prealpine klippen; RT= Revard thrust; VT= Veyrier thrust; FA= Arcalod fault.

iv) The Bornes/Aravis.

The geology and structure of the Bornes/Aravis is shown in Figs 2.20a and 2.20b.

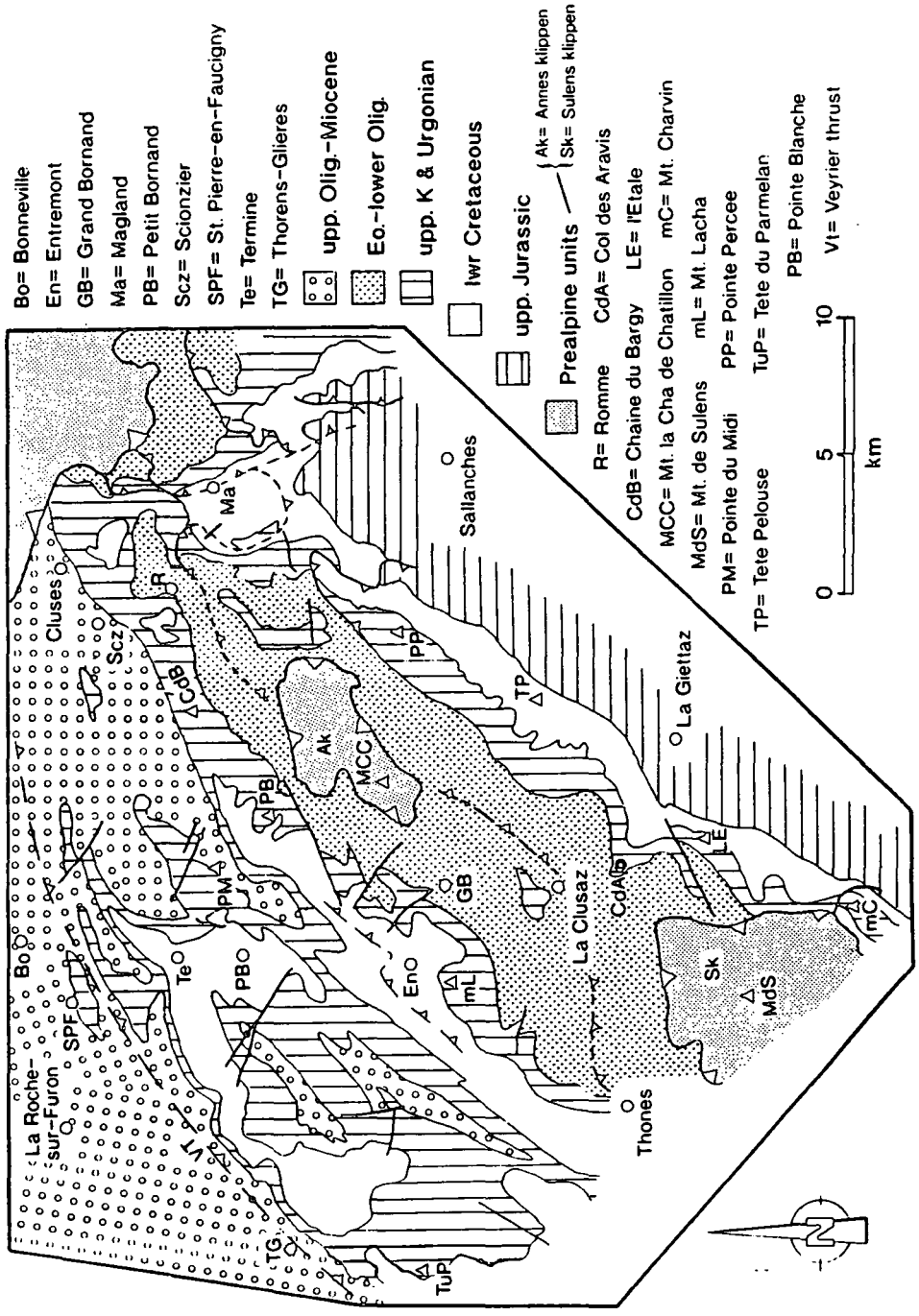

Fig. 2.20a Simplified geological map of the Bornes/Aravis massifs. Modified from BRGM (1979a; 1985; 1988) and Huggenberger & Wildi (1991).

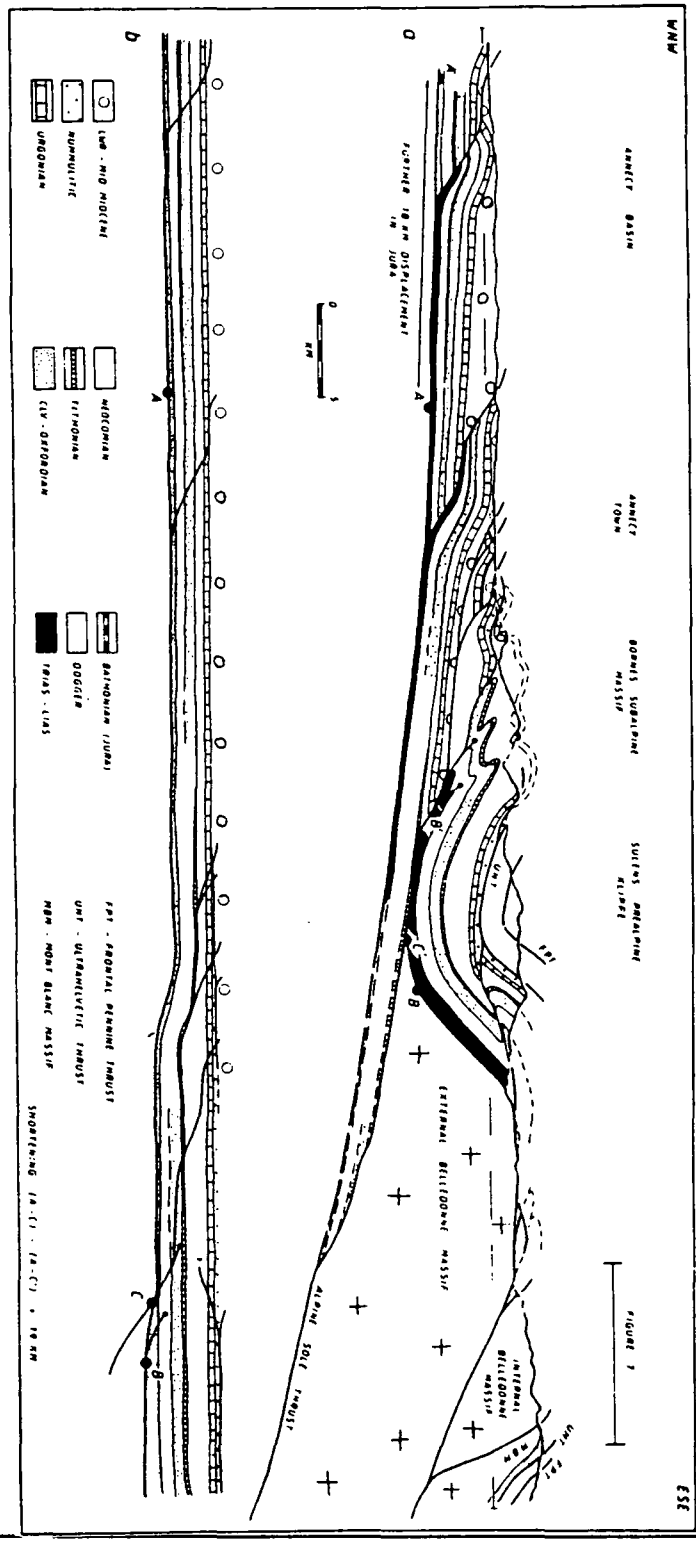

Fig. 2.20b Cross-section through the Bornes/Aravis (see Fig. 2.17c for location of the line of section). From Butler (1989a).

v) The Platé and Haut-Giffre.

The geology and structure of the Platé and Haut-Giffre is shown in Fig. 2.21a and 2.21b.

Fig. 2.21a (opposite page) Simplified geological map of the Platé and Haut-Giffre (after BRGM, 1985; Butler et al., 1987). **Fig. 2.21b** (opposite page) Cross-section through the Haut-Giffre. From Butler et al. (1987).

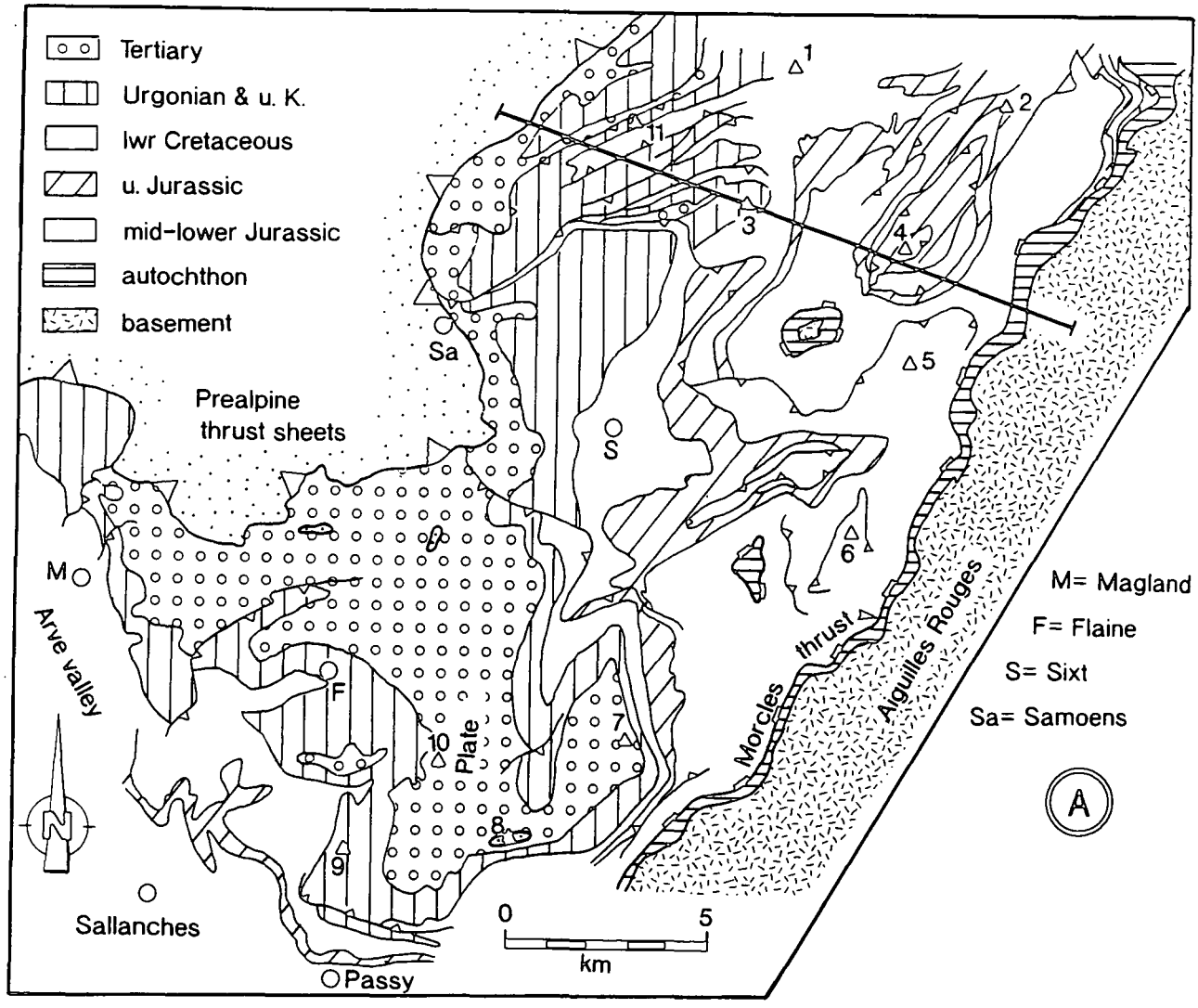

1= Dent de Barme 2= Mont Ruan 3= Pointe de Bellegarde

4= Pic de Tenneverge 5= Pointe de Cavales 6= Le Buet 7= Tete de l'Anne

9= Tete du Colonne 8= Pointe de Plate 10= Grande Platieres 11= Dents d'Oddaz

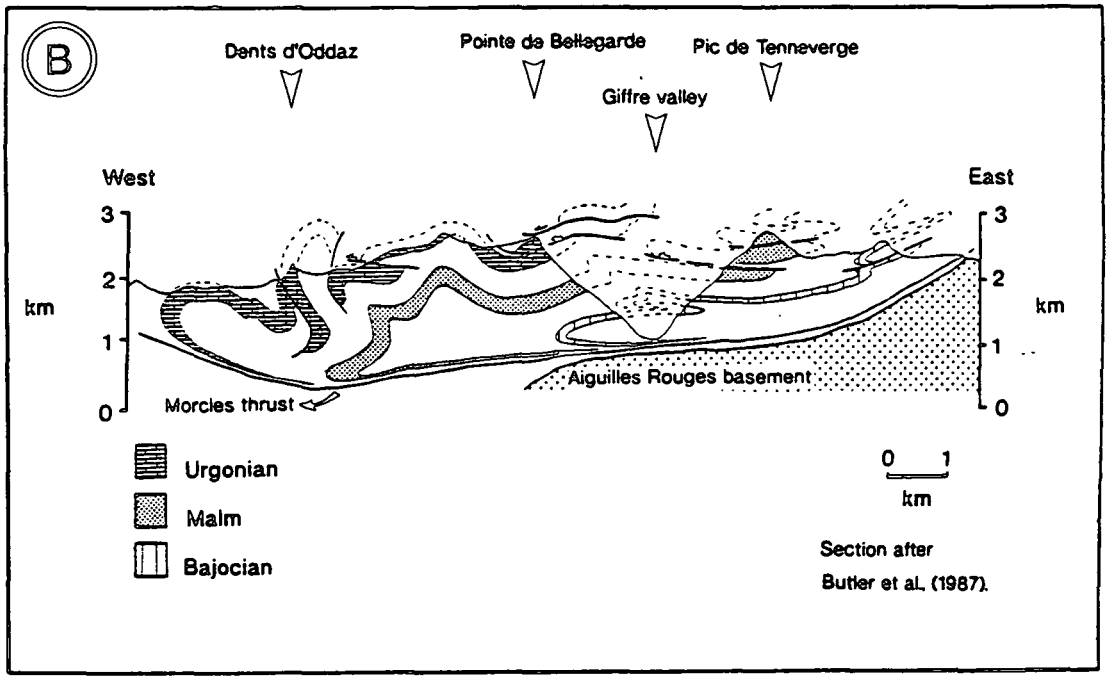

The dominant structural trend of fold axial planes and thrust traces in the Subalpine Chains is NNE-SSW. This, however, changes toward the north-east part of the chain (in the northern Bornes, Platé and Haut-Giffre) where the structural trend is NE-SW. This is reflected in the thrusting directions and fold vergence, both of which swing round from WNW to NW (Ramsay, 1989; Huggenberger & Wildi, 1991; Butler, in press a).

The south-western massifs of the Chartreuse, Vercors and Bauges are characterised by discrete, low displacement thrusts and open asymmetric folds (Butler et al., 1987; Mugnier et al., 1987; see Fig.2.22). The north-eastern part of the Subalpine Chains (the Haut-Giffre, Platé, Aravis and Bornes massifs) represents the southern termination of the Helvetic nappes (Doudoux et al., 1982, 1984; Butler et al., 1987; Ramsay, 1989) and contain recumbent fold structures (see Fig. 2.23b). The Helvetic nappes are three stacked nappe units, which from bottom to top are the Morcles, Diablerets (or Samöens) and Wildhorn (or Sallanches) nappes (shown in Fig. 2.23a). These nappes have their 'root zone' in the 'syncline de Chamonix' (Ayrton, 1980), between the Mont Blanc and Aiguilles Rouges basement massifs, the latter of which, along with its own thin cover sequence, has been overridden by this cover sequence nappe pile (see section 2.4.1 and Fig. 2.8 for one possible reconstruction for the Mesozoic structure of this area). The frontal thrust of the Bornes massif (the Veyrier thrust, marked on Fig. 2.20a) and the Haut-Giffre have been correlated with the Morcles thrust (Doudoux et al., 1982; 1984). However the continuity of the two higher nappes into the area is still debated (compare Ramsay, 1989 with Butler, in press a). The Morcles nappe in Switzerland has an overturned limb (see Ramsay et al., 1983; see Figs 2.23a and 2.23b), which becomes less prominent toward the southwest where thrusting has a greater influence on structural development. The Bornes, Aravis, Platé and Haut-Giffre massifs restore to the east of the Aiguilles Rouges massif and northern tip of the Belledonne massif and are emplaced onto a similar Meosozoic Subalpine sequence below. The western Bauges, Chartreuse and Vercors restore to the west of the basement massifs and directly overlie the basement massif with no attenuated cover; hence they are para-autochthonous. The difference in geometry of thrusting from north to south may suggest a strong control by the Mesozoic structures (see Welbon, 1988, for discussion). For example the increased importance of backthrusting in the Vercors reflects the presence of a down to the west normal fault bounding the Belledonne massif there (see Fig. 2.17b).

The Helvetic nappe pile, prior to its formation, was itself overridden by Ultra-Helvetic and Pennine nappes, containing sediments with affinities to those seen in the Internal zones (Kindler, 1988) and tectonically linked to the Ultra-Helvetic thrust (UHT) and the FPT, both of which are exposed to the east of the Mont Blanc massif (see Fig. 2.1). These more travelled nappes are represented today in the Subalpine Chains by erosional klippe, such as the Sulens, Annes, Chablais and Romandes klippen (see Figs 2.1, 2.20a and 2.21a). Boyer & Elliot (1982) suggested that the UHT and FPT provided the roof thrust for

the Helvetic nappes, forming a duplex structure. Both the UHT and FPT were then re-folded and breached with the formation of the Helvetic nappes (Boyer & Elliot, 1982).

Fig. 2.22 The structure of southwestern corner of the Chartreuse massif, viewed looking north from north from the Tunnel du Mortier (northern Vercors). U= Urgonian; V= Valanginian; b= Berriasian; T= Tithonian (VT and CSP, see Fig. 2.18a). The Tithonian beds defines an open, asymmetric anticline in the hanging wall to VT. Houses (little white dots) for scale.

Estimates for the amount of displacement and shortening in the Vercors and Chartreuse from section balancing suggest a constant 30 km of displacement (Butler, 1989), which is considered to pass down to the Alpine sole thrust beneath the Belledonne massif. In the Vercors the majority of this displacement is taken up by backthrusting, this backthrusting dies out to the northeast. Such that in the Chartreuse the displacement is virtually entirely taken up by foreland directed thrusting. The final few kilometres of displacement pass out into the Jura which branches onto the Subalpine Chains in the vicinity of the Chartreuse front (Mugnier et al., 1987; Butler, 1992a; see Figs 2.17c and 2.18a). Estimates of shortening in the Haut-Giffre and Platé are in the region of 47 km, this figure includes 27 km of shortening within the succession and 20 km needed to restore the succession to the east of the Aiguelles Rouges (Butler, 1985; 1989a).

2.6.3 Dating of tectonism in the Subalpine Chains.

Dating of tectonism is always open to speculation and dates are likely to be estimates at best. Episodes of thrusting can be roughly approximated by using shortening rates within the Alpine arc (Butler, 1989a; 1991) and the dating of the youngest sediments

in footwall localities (Mugnier et al., 1990) to estimate the dates of deformational periods. The absence of units unconformably overstepping thrusts makes dating more speculative.

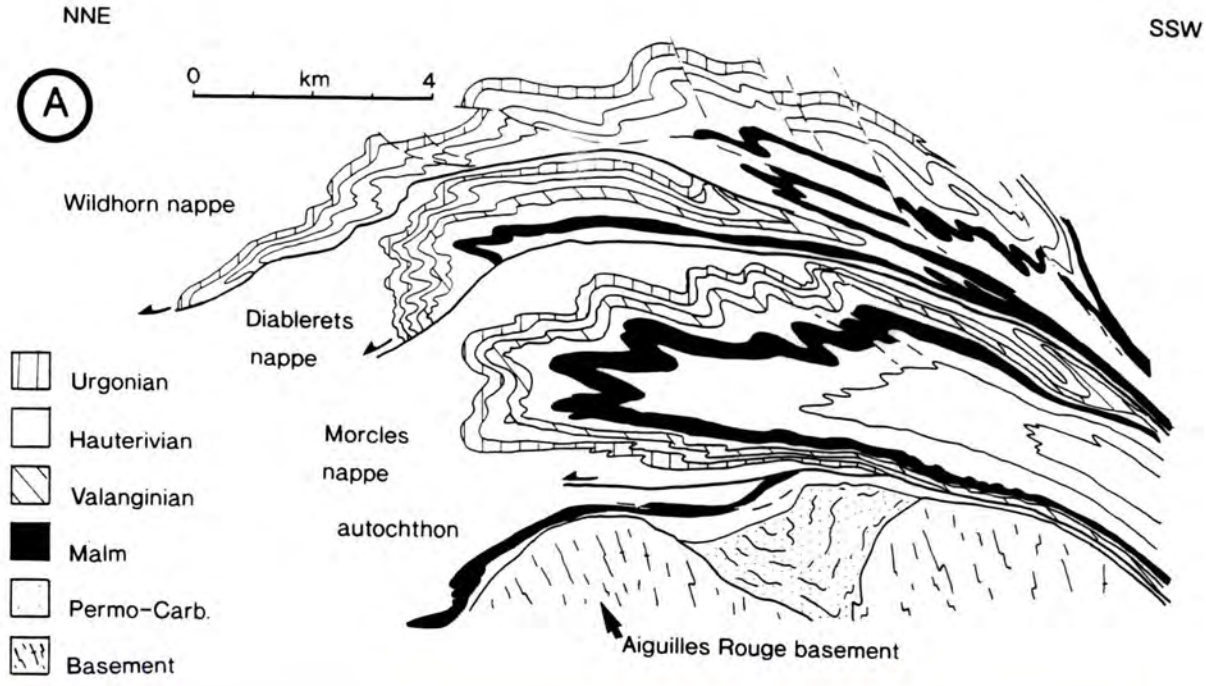

Fig. 2.23a Profile through the Helvetic nappes, showing the three stacked nappe units. From Ramsay (1981). **Fig. 2.23b** A large recumbent fold at the front of the Morcles nappe, in the western cliff face of Dents du Midi (Switzerland). View from Col de Bossetan on the French/Swiss border, looking northeast. The cliff face is approximately 600m high. T= Tertiary; U= Urgonian; lC= lower Cretaceous; Y= younging direction.

For the north-east part of the chain, deformation began during the Oligocene (Burkhard, 1990; Huggenberger & Wildi, 1991; see also Butler, 1989a; 1992b; for a different interpretation), whilst more external areas, such as the south-west part of the chain experienced deformation much later in the Tertiary (mid- to end- Miocene; Burkhard, 1990; Mugnier et al., 1990). Deformation ended in the Late Miocene (see discussion in Burkhard, 1990 and section 2.6.4 below).

2.6.4 Post deformational uplift of the Subalpine Chains.

In the late Miocene, in response to the erosion of the thickened crust (in the hinterland to the east), isostatic uplift of the Subalpine Chains began. Often uplift can be easier to quantify than periods of deformation since techniques such as K-Ar isotope ratios and fission track analysis can be employed (see Mugnier & Menard, 1986; Mugnier et al., 1990; Hurford et al., 1991) Timing of the uplift and exhumation of the external crystalline massifs from fission track and Ar-Ar isotope data (see Mugnier et al. 1990 for references and discussion) can be used to constrain the timing and rate of uplift of the Subalpine Chains to be around 10 Ma. Burkhard & Kalkreuth (1989) used the timing and rate of uplift of the crystalline Aar massif to estimate a starting time for uplift of 12 Ma to 6 Ma respectively for the Kander Valley region of the Swiss Helvetics. Dates of around 12-10 Ma for the starting time of uplift of the Subalpine Chains would seem to be reasonable and are similar to the values suggested by Mugnier & Menard (1986) and by Mugnier et al. (1990), estimated by dating of the uplift and cooling of the external basement massifs, and by Butler (1986; 1991), estimated from shortening rates across the Western Alps. Section 8.5.2 gives a more detailed discussion on the rates and timing of uplift of the Subalpine Chains.

2.7 Conclusions.

1) The Mesozoic development of the Subalpine Chains began in the Triassic and continued through to the late Cretaceous. Sedimentation was principally of platform carbonates and equivalent basinal mudstones

2) The Mesozoic Subalpine Chains were part of the inner (external) region of a former passive continental margin to an oceanic region which formed in the Jurassic and is referred to as the Dauphinois/Helvetic shelf.

3) Basin inversion of this margin occurred in the Eocene to Miocene during the final stages of the Alpine orogeny.

4) Classic fold and overthrust structures developed in response to WNW and NW directed thrusting.

5) Tertiary sedimentation was dominated by syn- and post- orogenic clastics principally derived from the orogenic hinterland to the east.

6) Isostatic uplift occurred in the late Miocene and is responsible for the present elevation of the Subalpine Chains.

Chapter 3 Sedimentology and diagenetic history of the Urgonian carbonate platform.

3.1 Introduction

This chapter and chapter 4 describe the petrography and geochemistry of both original marine components and diagenetic features of a carbonate platform within the framework of a generalised paragenetic sequence for that platform. This sequence is based on the study of several well exposed sections and both standard and cathodoluminescence petrography. This sequence is then related to the burial history of the platform and the pattern of fluid movement.

This chapter introduces the Urgonian carbonate platform in terms of its age, depositional setting and characteristic facies, and presents a generalised diagenetic sequence for the platform, which forms the basis for the description of diagenesis. The petrography of diagenetic features within the Urgonian are described approximately in their order of formation.

3.2 Definition of the Urgonian carbonate platform.

The Urgonian carbonate platform is a mid-Cretaceous (upper Barremian to lower Aptian) platform, typified by rudist bivalve and peloid/foraminifera wackestones and packstones. The Urgonian is spectacularly exposed within the mountains and valleys of the Subalpine Chains. The area of outcrop of the Urgonian within the study area is shown in Fig. 3.1, along with the localities where the Urgonian was studied and sampled in greater detail.

It should be noted that the term Urgonian can be misleading, since it has been used in time, facies and lithostratigraphic contexts since its introduction by Lory in 1846. The term Urgonian has commonly been used in a facies context to describe any limestones containing rudist bivalves (calcaires à rudistes, Masse & Philip, 1981). In this thesis the term Urgonian is defined as upper Barremian-lower Aptian aged platform carbonates of the Jura-Subalpine region and is equivalent to the Urgonian Limestone Formation of Arnaud (1981). In Switzerland the Urgonian is referred to as the Schrattenkalk Formation (Funk, 1988).

3.3 Age of the Urgonian platform.

The age of the Urgonian platform, particularly its basal section, is the subject of an ongoing stratigraphic debate. The Urgonian had been dated as upper-Barremian to lower Aptian in age by Arnaud-Vanneau (1980) and Arnaud (1981) (see Fig. 5 in Jacquin et al., 1991). This dating of the base of the platform was questioned by Clavel et al. (1986; 1987),

Fig. 3.1. (opposite page). Outcrop map of the Urgonian in the Subalpine Chains and location of the sections studied. 1=St. Nazaire en-Royan, 2=Petit Goulets, 3= Grand Goulets, 4= lower Bourne gorge, 4a=upper Bourne gorge, 5=Rencurel, 6=Gorge du Nant, 7=Balcon des Ecouges, 8=Moucherotte, 9=Dents de Crolles, 10=Pas de L'Echelle, 11= Pic de Oeillette, 12=Gorge de Frou, 13=St. Christophe-sur-Guiers, 14=Les Echelles, 15=Mt. Nivolet, 16=Dents d'Arclusaz, 17=Villaret Rouge, 18=Pont de l'Abine. 19=Pointe de la Sambuy, 20=Mt. Trelod, 21=La Tournette, 22=La Clusaz, 23=upper Borne valley, 24=Rumilly (lower Borne valley), 25=northwest Termine road section (both upper and lower roads), 26=Pic de Jallouvre, 27=Col d'Encrenaz, 28=Combe de Tardevant, 29=Pointe Percée, 30=Col de la Fête, 31= Sales, 32=Chambres. Graphic logs for some of these localities are given in Appendix 1.

who proposed that the base of the platform is of upper Hauterivian to lower Barremian age. Two different palaeogeographic models for the development of the platform have been proposed based on these two differing age estimates and they are shown in Figs 3.2a and 3.2b. The differences are slight and have no implications for the results presented in this thesis. The problem of dating of the base of the platform is discussed in Arnaud-Vanneau & Arnaud (1991) and Hunt (1992).

In this thesis the stratigraphy of Arnaud-Vanneau (1980) and Arnaud (1981) is followed, so the dates used for the onset of the platform deposition will be upper Barremian to lower Aptian (115 to 112 Ma; see Jacquin et al.,1991).

3.4 Depositional setting of the Urgonian platform.

The Urgonian platform is the youngest of a series of platforms that developed on the European continental margin to Tethys during the Jurassic-Cretaceous. The palaeogeography of the Subalpine Chains area during the Mesozoic has already been discussed in detail in Chapter 2. Prior to late Barremian times platform development had been restricted in extent to the Jura/Bas Dauphiné area to the northwest and Provençe to the south (see section 2.4.1 and Figs 2.7a, 3.2a and 3.2b). However, in the Barremian-Aptian, a number of factors enabled the installation of a platform around the margin of the Dauphinois/Helvetic/Vocontian basin.

Following a period of hemipelagic ramp sedimentation in the Hauterivian a relative sea level fall in the early Barremian led to emergence of the inner part of this ramp in the Jura, Chartreuse and northern Vercors. A relatively high stand of sea level in the late Barremian following this period of emergence is responsible for the installation of the Urgonian platform within the Dauphinois basin, as a transgressive unit, resting upon strata of lower Hauterivian to lower Barremian age. The gradual filling of the north-western margin of the Dauphinois basin (delimited by the Isère fault line; see Fig. 2.7a and section 2.4.1) from the Berriasian onwards, helped the development of shallow water platform

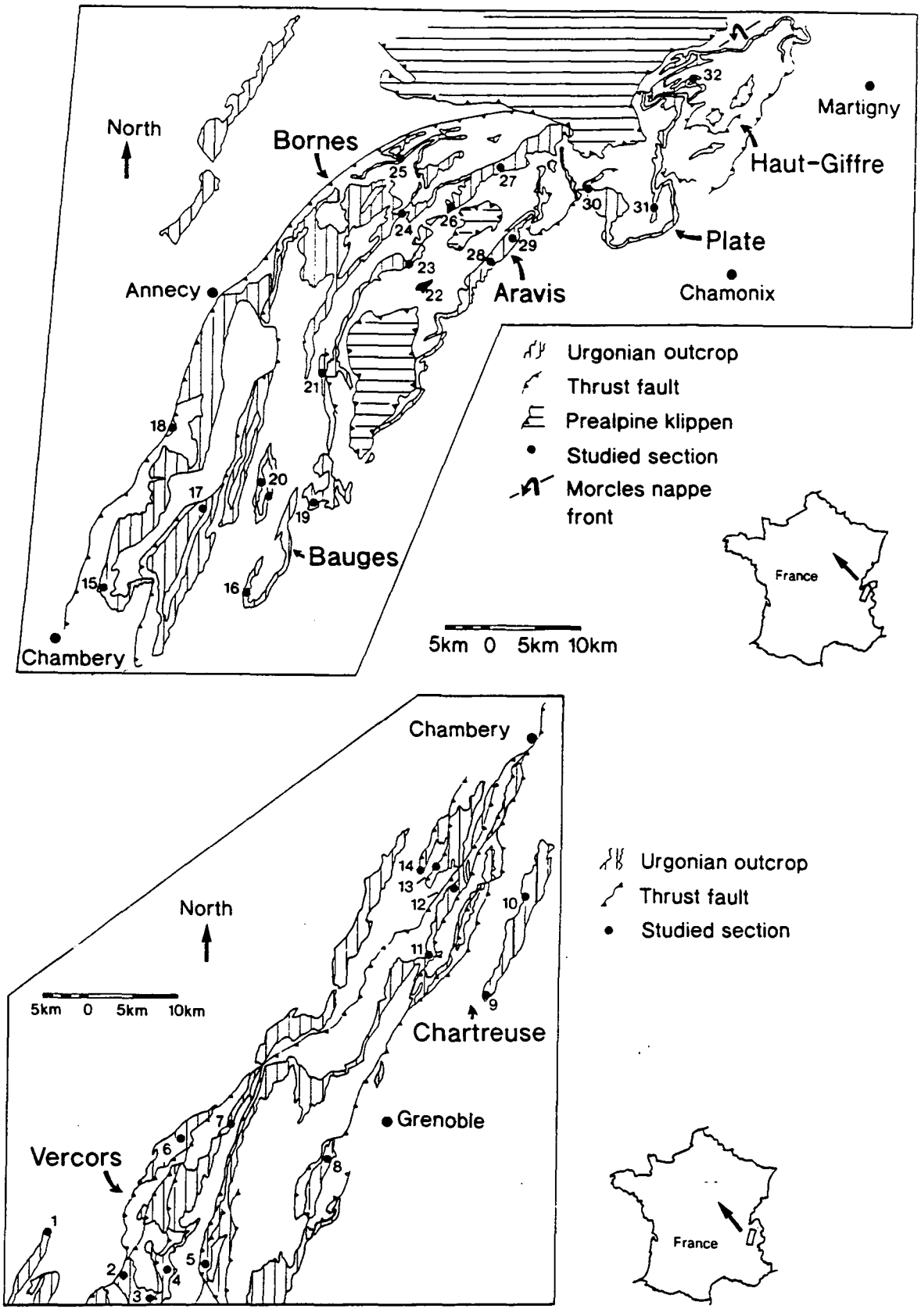
North
Bornes
Martigny
Haut-Giffre
Plate
Aravis
Chamonix
Annecy
Bauges
Chambery
Urgonian outcrop
Thrust fault
Prealpine klippen
Studied section
Morcles nappe front
France
5km 0 5km 10km
Chambery
North
Chartreuse
Grenoble
Vercors
5km 0 5km 10km
Urgonian outcrop
Thrust fault
Studied section
France

sediments in the Jura and the Dauphinois basin. This growth out into the basin of platform carbonates reduced the area of the basin to a smaller east-west trending area of greater subsidence (the Vocontian basin), which opened out to the east and the Ligurian ocean (see Figs 2.7b and 2.10).

Fig.3.2a and **3.2b**. The two palaeogeographic models for the Urgonian from Clavel et al. (1986) (3.2a) and Arnaud-Vanneau & Arnaud (1990) (3.2b).

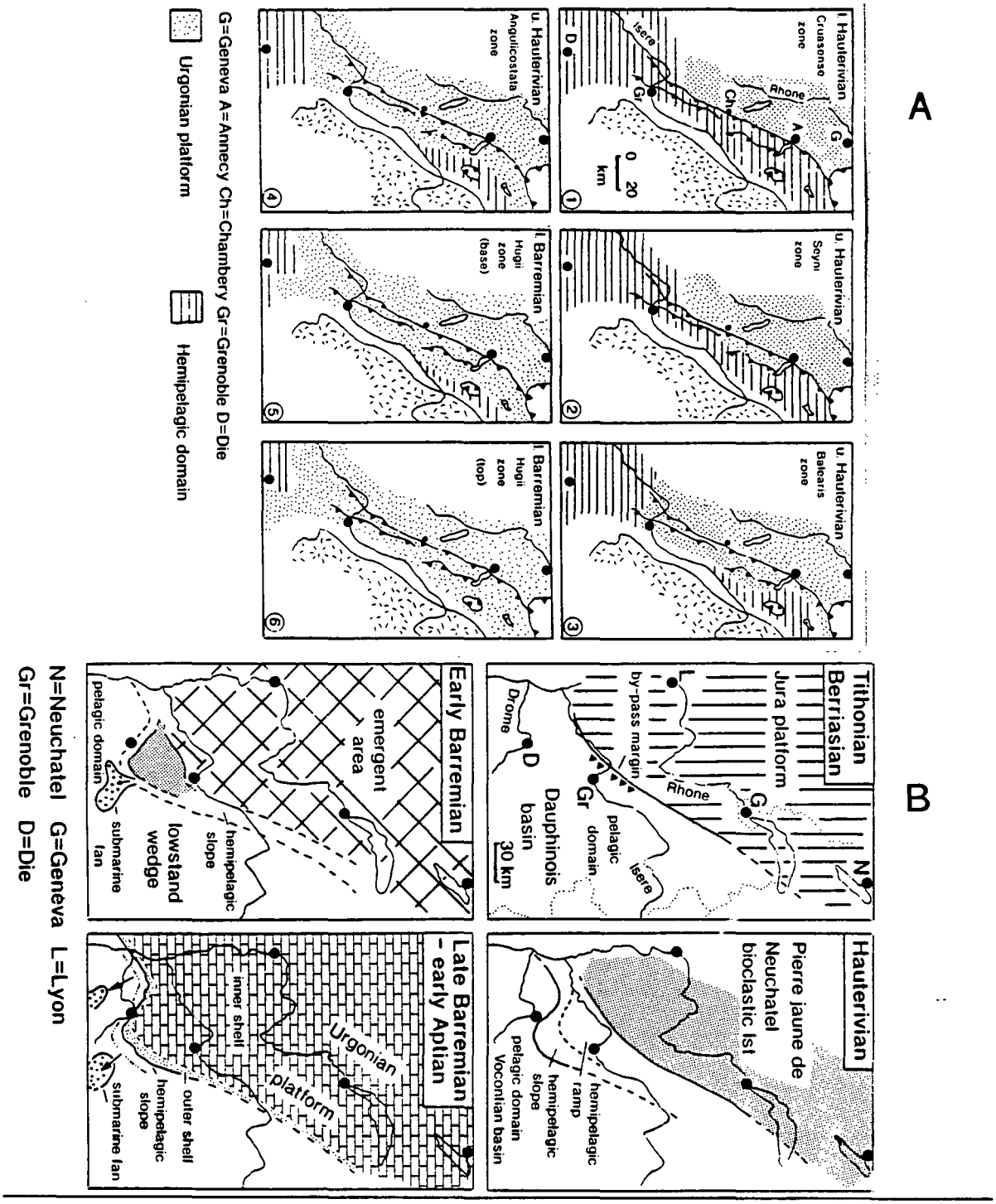

In the lower Aptian a major relative sea level fall led to a period of platform emergence followed by drowning of the platform and deposition of glauconitic open marine mixed siliciclastic/carbonate sediments (Arnaud & Arnaud-Vanneau, 1989; Arnaud-Vanneau & Arnaud, 1991; Jacquin et al., 1991).

3.5 Characteristic facies patterns within the Urgonian

Microfacies organisation within the Urgonian platform is similar to that described by Wilson (1975), as the standard microfacies for shelf-type platforms. In the platform interior, bioclastic packstones and wackestones with rudists and foraminifera are seen. On the platform margin oolitic and oolitic-bioclastic grainstones occur, locally with corals. On the foreslope to the platform, grainstones with rounded bioclastic grains of crinoidal-bryozoan debris pass downslope into basinal wackestones and mudstones and hemipelagic sediments. Within the Urgonian twelve different microfacies have been recognised, ranging from lime mudstones with radiolaria and ammonites to bioclastic grainstones/wackestones with signs of emergence (see Arnaud-Vanneau et al., 1987). The standard microfacies are listed below:-

F0 - wackestones with Radiolaria and Calpionellids.

F1 - wackestones/packstones with sponge spicules.

F2 - packstones with Spatangidae.

F3 - grainstones with rounded echinoderm debris and small foraminifera.

F4 - packstones and grainstones with crinoids and bryozoans.

F5 - grainstones with large rounded bioclasts.

F6 - oolitic grainstones.

F7 - grainstones and boundstones with coralline organisms.

F8 - wackestones, packstones, grainstones with large foraminifera, locally with large rudists.

F9 - wackestones/packstones/grainstones with Miliolidae and rudists.

F10 - packstones/grainstones with oncolites and *Bacinella.*

F11 - mudstones/wackestones with *Pseudotriloculina* and bird's eye fenestrae.

For the sake of convenience other features of emergence can be grouped into the F11 facies, such as vadose cements, keystone vugs, shell dissolution, stromatolitic laminae and root-molds.

Volumetrically, the lagoonal to supratidal facies (F8 to F11 above) are the most important facies upon the platform. These represent the true Urgonian facies, i.e. rudist bearing limestones.

3.5.1.Lateral and vertical facies arrangements within the Urgonian platform.

The lateral arrangement of microfacies is shown in Fig. 3.3. Across the platform the vertical evolution of these facies varies, such that in the Jura and the northern Subalpine area internal platform facies (F7 to F11) may be seen directly above the basal transgressive surface or within a few metres of it. By way of contrast, in the southern Vercors there is a much greater thickness of outer platform facies before the appearance of inner platform facies above. For example rudist wackestone/packstone (internal platform facies, F8 to F9) occurs within eight metres of the base of the Urgonian in the Chambotte section (Chambotte anticline, southern Jura; see Arnaud-Vanneau et al., 1987), whereas in the southern Vercors there are several tens of metres of hemipelagic and outer shelf facies (F0 to F4) before shelf-margin (F5 to F7) and inner platform facies (F8 to F11) are found (Arnaud-Vanneau & Arnaud, 1990; see Fig. 3.4a).

Fig. 3.3. The lateral arrangement of microfacies within the Urgonian of the Vercors and Chartreuse. From Arnaud-Vanneau et al. (1987).

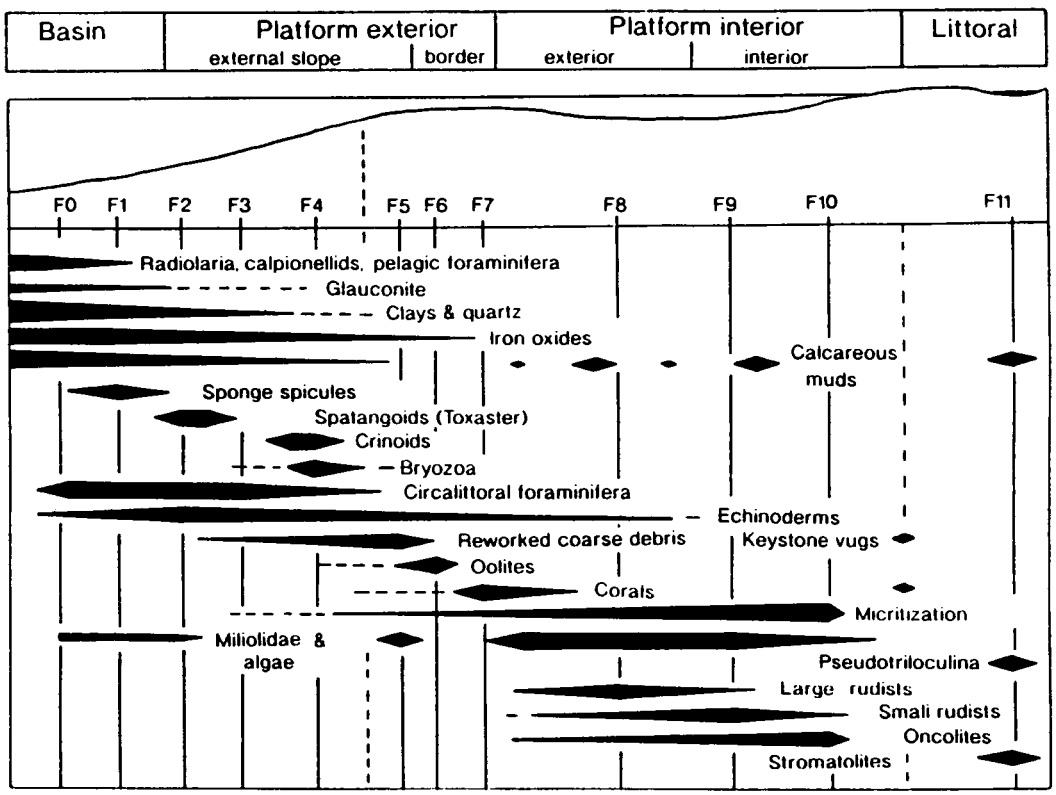

The pure limestone of the Urgonian produces a very clear lithological break from the underlying hemipelagic marly limestones of the Hauterivian and has a distinct vertical succession. The initial deposits of the Urgonian ("séquence d'installation") commonly display, from bottom upwards: (1) marls, commonly containing the irregular echinoid *Toxaster*; (2) wackestones-packstones with small foraminifera in decimetric wavy beds;

and (3) grainstones with bioclasts and/or ooids. These may pass upward either into grainstones with coral fragments, coral reefs or cross-bedded oolitic grainstones. Above these outer platform deposits are the inner platform shallow subtidal bioclastic sediments with rudist shell debris deposited in a low energy shelf-lagoon (true Urgonian facies) and often micritised due to the activity of endolithic microbes. The inner platform sediments are usually arranged in units 4 to 10 m thick, always of a shallowing-upward nature, showing an upward passage from packstones with large and small rudists and a variety of foraminifera to packstones/wackestones with only small rudists and a prevalence of Miliolidae foraminifera. The top of each unit is terminated by either a storm deposit of oncoids, rudist shells or coral fragments (which may be a transgressive lag at the bottom of the next cycle), or the uppermost bed is composed of a wackestone/mudstone with a restricted foraminifera fauna and bird's eye fenestrae or stromatolites.

The Urgonian shelf can be subdivided into a number of component members, which are shallowing upward in nature and separated by surfaces indicative of deepening or of subaerial exposure. Periods of development of open shelf facies across the platform indicate deepening of the water above the platform (a maximum flooding surface in sequence stratigraphy terminology). Brief periods of subaerial exposure across the platform (sequence boundaries) are indicated by the presence of freshwater limestones, incised valley fills, the influx of siliciclastic sediments, pedogenic features, micro-karstic topography and meteoric diagenesis (Arnaud-Vanneau et al., 1987; Hunt, 1992). These features can also be considered in terms of carbonate sequence stratigraphy (Arnaud & Arnaud-Vanneau, 1989; Jacquin et al., 1991; Hunt, 1992; Hunt & Tucker, 1992). Carbonate sequence stratigraphy is considered by Sarg (1988) and Tucker & Wright (1990).Two such sequence stratigraphic schemes for the Urgonian of the northern Vercors and southern Chartreuse are shown in Fig. 3.4b.

Two marly horizons occur within the upper part of the platform; these are referred to as the Lower Orbitolina Beds and the Upper Orbitolina Beds, so-called due to the abundance of Orbitolinid foraminifera, particularly *Palorbitolina*. These two horizons sub-divide the true platform facies into a lower and upper division (lower and upper Urgonian members of Arnaud-Vanneau & Arnaud, 1990). These two horizons reflect substantial trangressive events, produced by relative sea-level rises during the evolution of the platform. The Upper Orbitolina Beds mark the end of the Urgonian platform. Both have been described from the Vercors and Chartreuse massifs (Arnaud-Vanneau et al., 1987; Arnaud-Vanneau & Arnaud, 1990) and from the Bornes and Aravis (Rivano-Garcia, 1978; Chaplet, 1989). A similar Orbitolina horizon from the Bauges is described for the first time in section 3.8.5. The author has also seen a similar Orbitolina rich-horizon in the Urgonian equivalent in the Swiss Helvetics (on the south-western face of Dents du Midi, near the French-Swiss border).

Following the Upper Orbitolina Beds the top of the platform is truncated by a sub-aerial exposure surface, produced by a major Aptian relative sea-level fall (Arnaud-Vanneau & Arnaud, 1990; Jacquin et al., 1991). Immediately above this surface and locally filling karstic dissolution channels formed upon the upper surface of the Urgonian during meteoric diagenesis are the circalittoral glauconitic, bioclastic grainstones (the "Lumachelle" facies), followed by phosphatic condensed units (the "Béton phosphaté" facies) described by Arnaud-Vanneau et al. (1987) and Delamette (1986; 1988). The latter two mark the drowning of the platform and an end to platform sedimentation. These post-Urgonian sediments are regionally variable, for instance the Lumachelle facies is only seen in the more westerly portions of the Subalpine Chains (Delamette, 1986; 1988).

Fig. 3.4a Vertical and lateral arrangement of facies within the Urgonian. From Arnaud-Vanneau et al. (1987). This figure illustrates the rapid development of platform facies (F5 to F11) within the internal regions compared to the margin and external slope where inner platform facies never developed. Note: true reef barriers never developed on the platform margin border. **Fig. 3.4b** (opposite page) Comparison of the sequence stratigraphic schemes of Jaquin et al. (1991) and Hunt (1992) developed for the Urgonian of the northern Vercors and southern Chartreuse. Sb = sequence boundary, mfs = maximum flooding surface, TST = trangressive sequence tract, HST = highstand sequence tract. Figure courtesy of D. Hunt.

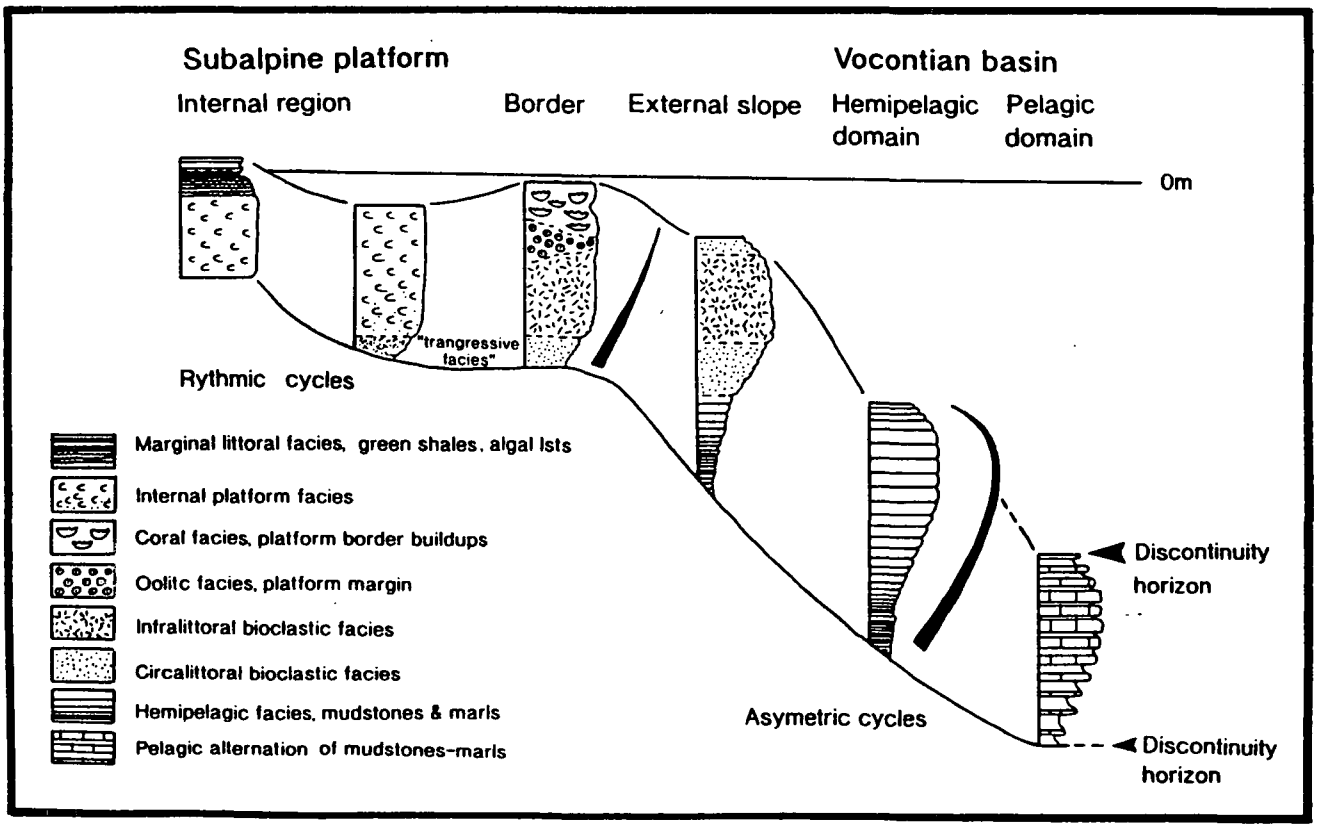

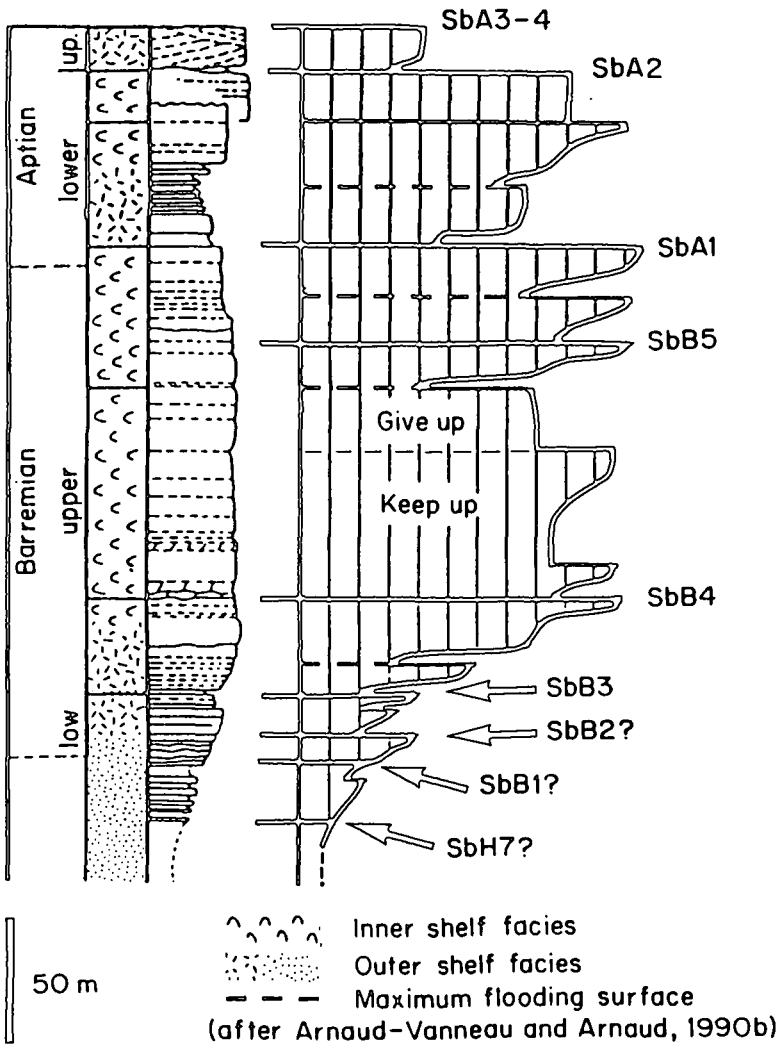

Jaquin et al (1991)

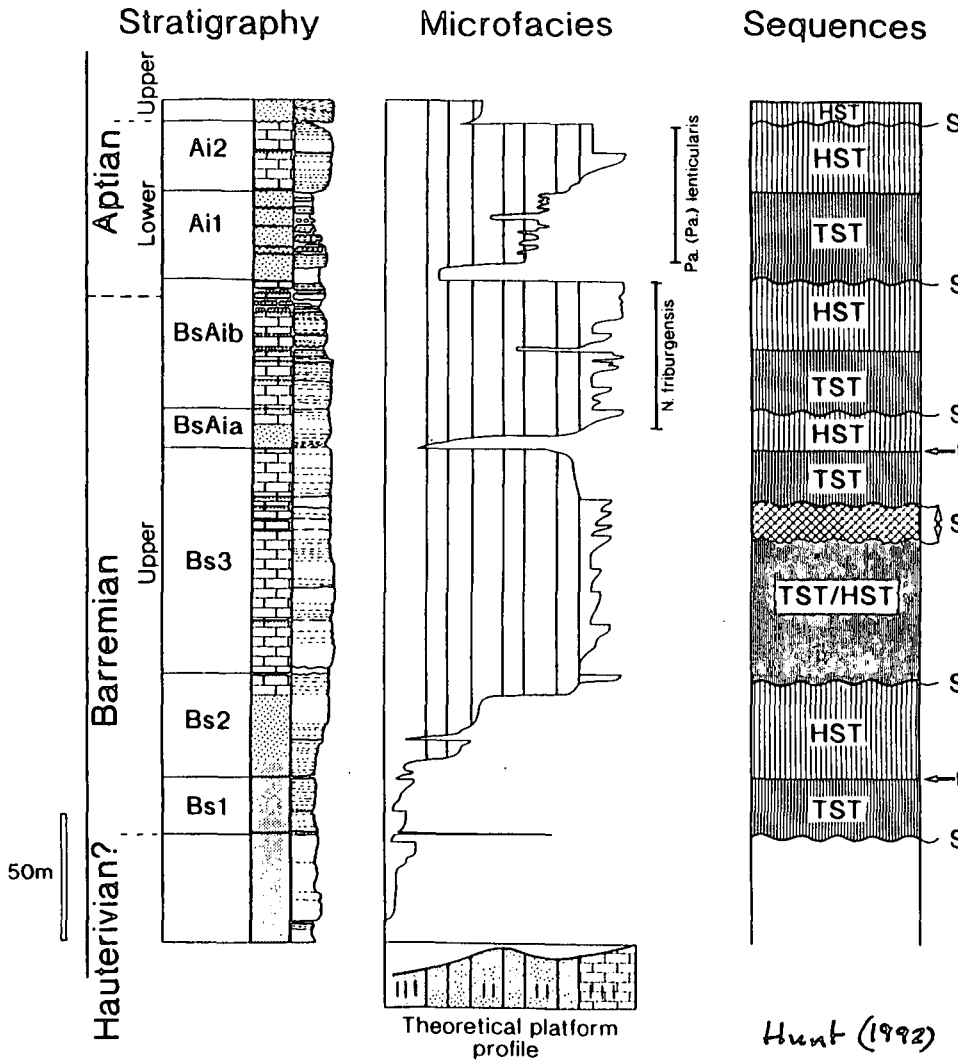

Hunt (1992)

3.6 General diagenetic sequence (paragenesis) within the Urgonian platform.

For the study of diagenesis of sedimentary units one of the most fundamental concepts is the establishment of the relative timing of diagenetic events to produce a paragenetic sequence. The creation of such a sequence, placing phases of cementation and dissolution in a relative time order allows the comparison of different sections for their diagenetic history, assesses the importance of various cement phases, shows periods of porosity modification and provides a framework for analytical work (Wilson et al., 1983; Harris et al., 1985; Bathurst, 1986; Halley, 1987; Moore, 1989). At best a paragenetic sequence can only consist of a generalised statement of the timing of diagenetic events.

Fig. 3.5 (opposite page) General paragenetic sequence for the Urgonian platform. This diagram is discussed in the text.

Since the depositional setting can exert a strong control on the type and amount of early diagenesis within a limestone and in so doing control the nature of later diagenesis of the limestone, paragenetic sequences often involve a fair degree of compromise, as not all diagenetic features may be present in every section of the unit under study. Two recent examples of the depositional setting controlling diagenesis are presented by Minero (1991) and Scholle et al. (1991). Climatic differences may also control early diagenesis and the general paragenetic scheme, as shown by Hird & Tucker (1988) and Wright (1988). Brief periods of emergence and flooding of the platform punctuating 'normal' platform sedimentation brought about by eustatic and/or tectonic induced changes in relative sea-level can also produce variations in the diagenesis. This latter point is discussed from a sequence stratigraphic point of view by Tucker (1992).

Bearing these points in mind a generalised paragenetic sequence is presented for the Urgonian platform (see Fig. 3.5). This sequence is based on the study of over 240 thin sections using both standard petrography and cathodoluminescence (the application of this technique is described in section 3.11.1). It should be noted that for a large platform like the Urgonian part of the platform may be undergoing marine phreatic diagenesis, whereas another part of the platform could be experiencing exposure and meteoric diagenesis (see Fig. 3.3); this applies particularly to the F11 facies (emergence facies). In view of the geographic extent of the area studied and the area of the platform exposed after uplift and erosion, only the shelf-margin (F5 to F7) to shelf-lagoon facies (F8 to F11) of the Urgonian were examined.

The relative timing of the diagenetic stages (shown in Fig. 3.5) through which the platform has passed is controlled by biostratigraphic dating of succeeding deposits (i.e. ammonites in the upper Aptian/Albian, Delamette, 1986, 1988), from field relationships

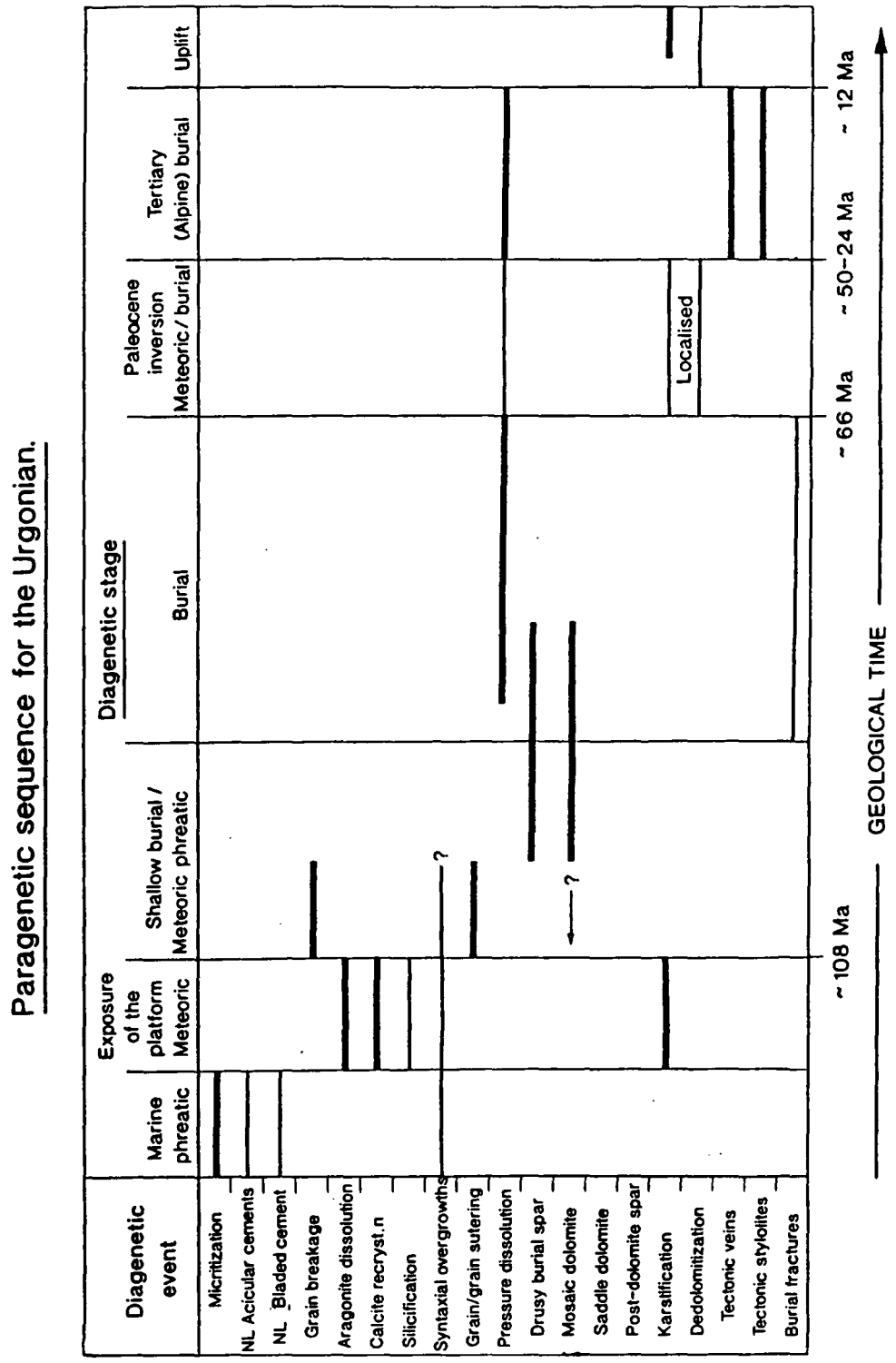

and from petrography (see section 3.11.1). The occurrence of micritization and marine cementation is controlled by the facies and the geographic position of the sediments on the platform, such as lagoonal rudist packstones versus platform bio-oolitic grainstones. Following this, a major relative sea level fall in the late Aptian (above the Upper Orbitolina

Beds), exposure of the platform, led to the dissolution of aragonite allochems, recrystallization of calcite and the formation of a micro-karst on top of the platform. Shallow burial, after drowning of the platform in the late Albian, produced the breakage of some grains and irregular-shaped fractures. Subsequently these pores and fractures were filled by a drusy calcite spar, which may show a zoning under CL in its earliest part. After this phase of cementation the platform was essentially lithified; continued burial led to the formation of a variety of pressure dissolution features. Extensive (but variable in thickness) replacement dolomitization of the basal section of the platform is inferred to have occurred at this time, possibly nucleating on and overprinting earlier dolomite cements.

A period of inversion in the Paleocene, (see section 2.5.1), locally produced karstification and dedolomitization. Then in the Eocene to Miocene (depending on which part of the Subalpine Chains the locality is in, see Chapters 2 and 8, Fig. 8.6, and Moss, 1992) foredeep formation due to thrust loading during the Alpine orogeny led to renewed and in some cases burial and the formation of tectonic features. Finally uplift occurred in the late Miocene producing the present day exposure of the Urgonian within the Subalpine Chains. The burial history of the Urgonian is discussed again in Chapter 4. The burial history of the Subalpine Chains as a whole and the geodynamic evolution of the chain is discussed in Chapter 8 and in Moss (1992).

In the following sections the petrography of each of the major diagenetic features of the platform (shown in Fig. 3.5) is described and interpreted in approximately their order of formation.

3.7 Micritization of Urgonian marine components.

Micritization within the Urgonian occurs in two forms, as micritic envelopes and completely micritised grains.

Within the marine realm many grains may have been altered to micrite by the activity of endolithic algae and microbes (micritization). This was apparently a common phenomenon upon the Urgonian platform (particularly the shelf-lagoon facies) with the shells of foraminifera often completely micritised. In many cases this makes identification of the origin of the grains impossible. Micritization of grains can be seen in Figs. 3.6, 3.7a, 3.9, 3.11a, 3.11b, 3.17c, 3.20b, 3.22b, 3.23b.

Micritization is typical of the platform top/ lagoonal sediments which often did not experience any other form of marine diagenesis. In these sediments micritization was promoted by the protected nature of the environment and the relatively slow rate of sedimentation on the platform top. This environment has been referred to as a 'stagnant marine phreatic' environment (Longman, 1980).

The shells of larger bioclasts, such as rudist bivalves, often have micritised shell walls. Both inner (former body chamber walls) and outer walls of the shells display these.

The formation of micritic envelopes would have been controlled by the same factors as micritization of smaller bioclastic grains (such as foraminifera) as mentioned above. Occasionally the micritic envelope can be seen to be associated with borings in to the shell wall, as shown in Fig. 3.6.

Fig .3.6 Photomicrograph of micritised envelopes enclosing a rudist bivalve shell grain. Small borings into the shell wall can also be seen (arrowed). Field of view= 2mm. 200/90, Vercors.

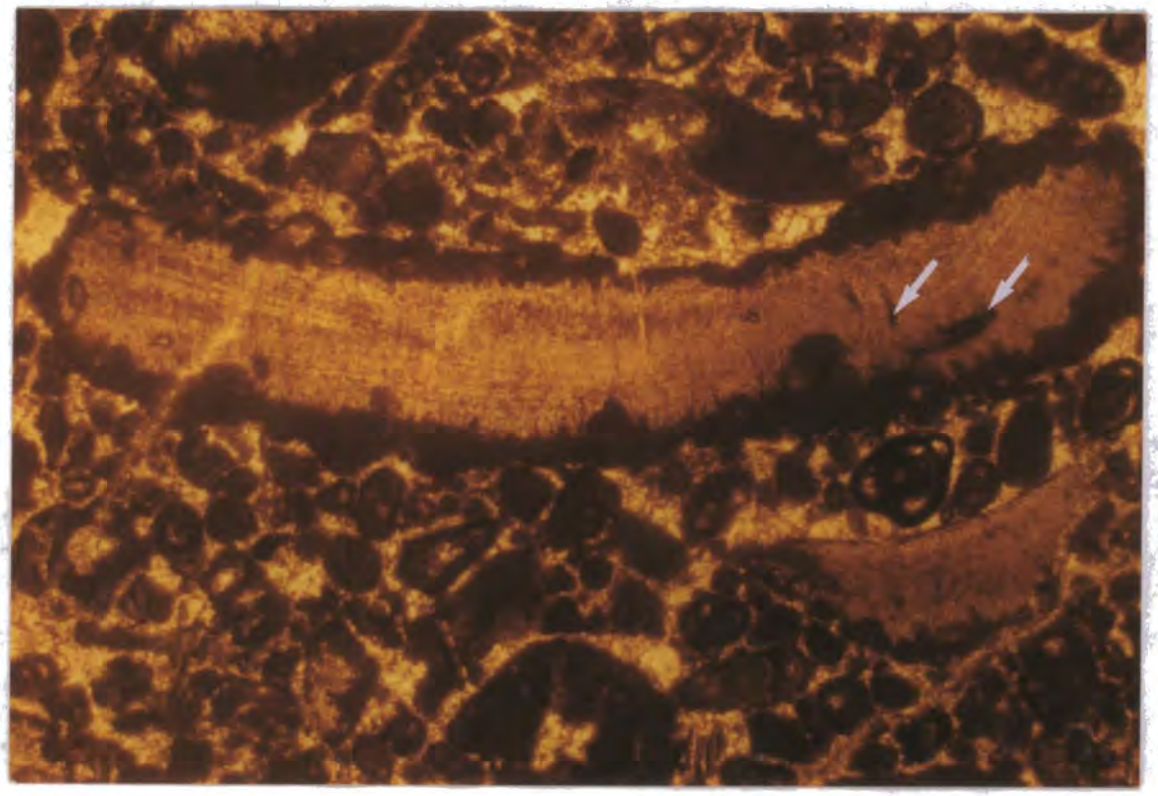

3.8 Marine cements.

In both modern and ancient limestones marine cements appear to be rare, except in specific environments suitable for their formation (e.g. reefs) (James & Choquette, 1983). Within the Urgonian this would also appear to be true in the majority of cases, as they only occur in certain facies, typically those of the shelf-margin or those associated with transgressive events.

Common features of marine cements are: (1) they are usually the first cement generation; (2) they usually form continuous and even thickness (isopachous) rims around the grains; (3) they are commonly fibrous; (4) they may be cut by borings; (5) they may be associated with internal sediments; (6) the crystals are non-ferroan and non-luminescent; and (7) they may occur within intraclasts (Bathurst, 1975; James & Choquette, 1983).

Four different types of marine cement are seen within the Urgonian. Each is described individually along with the common location of that cement type within the Urgonian succession.

3.8.1 Acicular isopachous cements.

These occur in the shelf-lagoon facies lining the substrates surrounding both primary intergranular porosity and fenestral porosity, which is typical of peritidal carbonates (see Fig. 3.7a). They consist of delicate, needle-like crystals which are much longer than they are broad (i.e. a large length:width ratio; see Fig. 3.7b). They are often rich in inclusions and non-luminescent. They are never present within areas of skeletal dissolution (see section 3.9.2), although this has clearly occurred within some of the sections where this cement is present (see Fig. 3.7c). Often they are only visible within the first crystals of the next cement generation.

Aragonite marine cements with a comparable morphology to these have been described by Pierson & Shinn (1985) from Pleistocene limestones of the Bahamas (see their figure 8c and 8d), where the cements were precipitated both in the marine phreatic and intertidal zones. In modern supratidal-intertidal zones acicular aragonite is the most common cement type (Tucker & Wright, 1990, page 323). However, the good preservation suggests that they would have been precipitated as calcite originally.

Fig. 3.7a Acicular isopachous cements lining fenestral porosity. Field of view= 1.5mm. **Fig. 3.7b** (opposite page) Close-up view of acicular marine cements. Field of view= 0.17mm. **Fig. 3.7c** (opposite page) Acicular isopachous cements lining fenestral porosity (on the left) but not bio-moldic porosity (labelled SP, on the right). Field of view=0.7mm. Sample 58/89, Chartreuse.

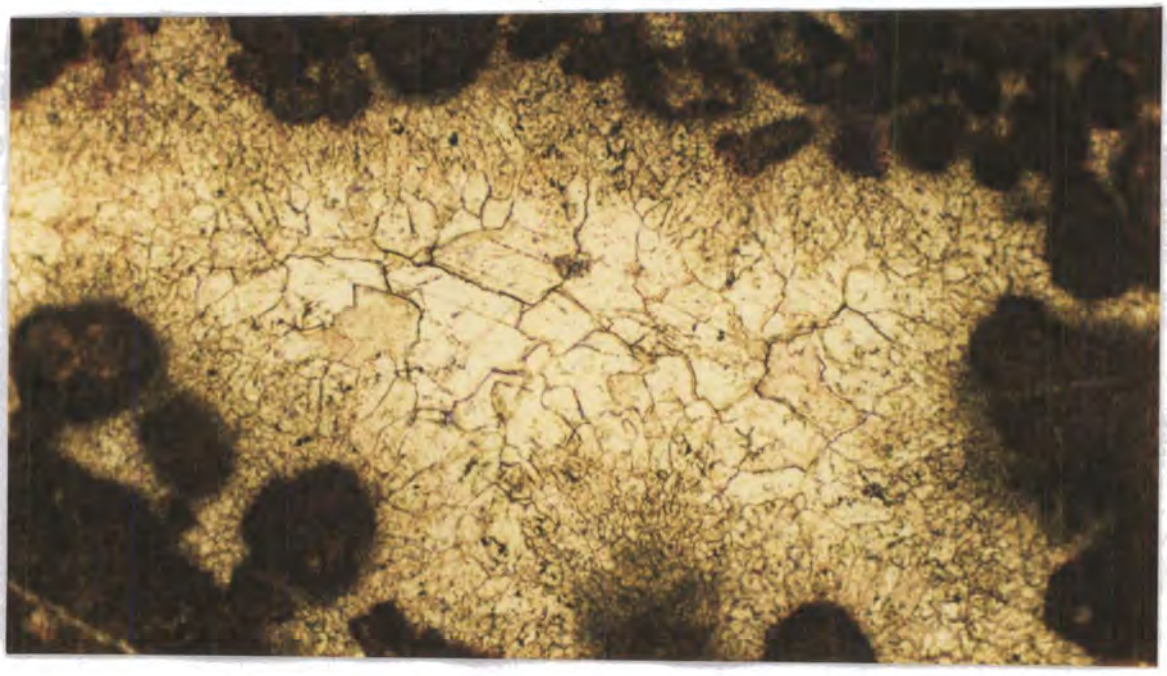

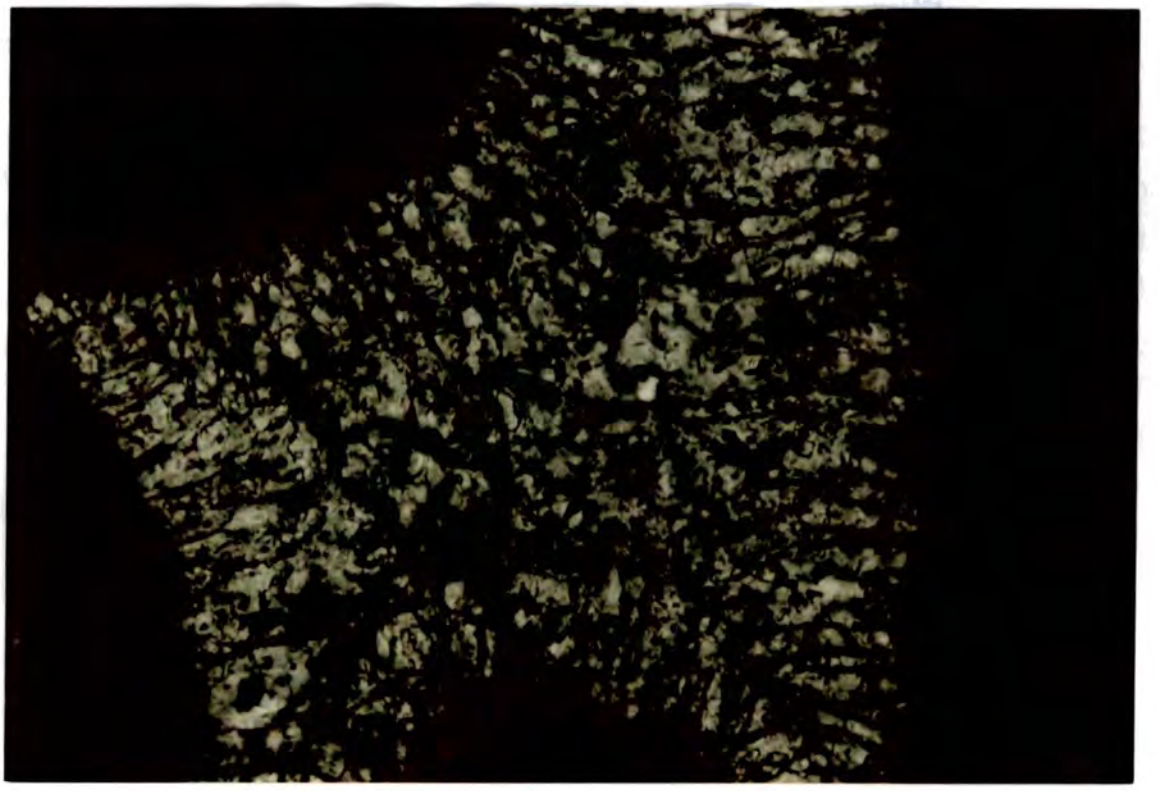

Fig. 3.7b

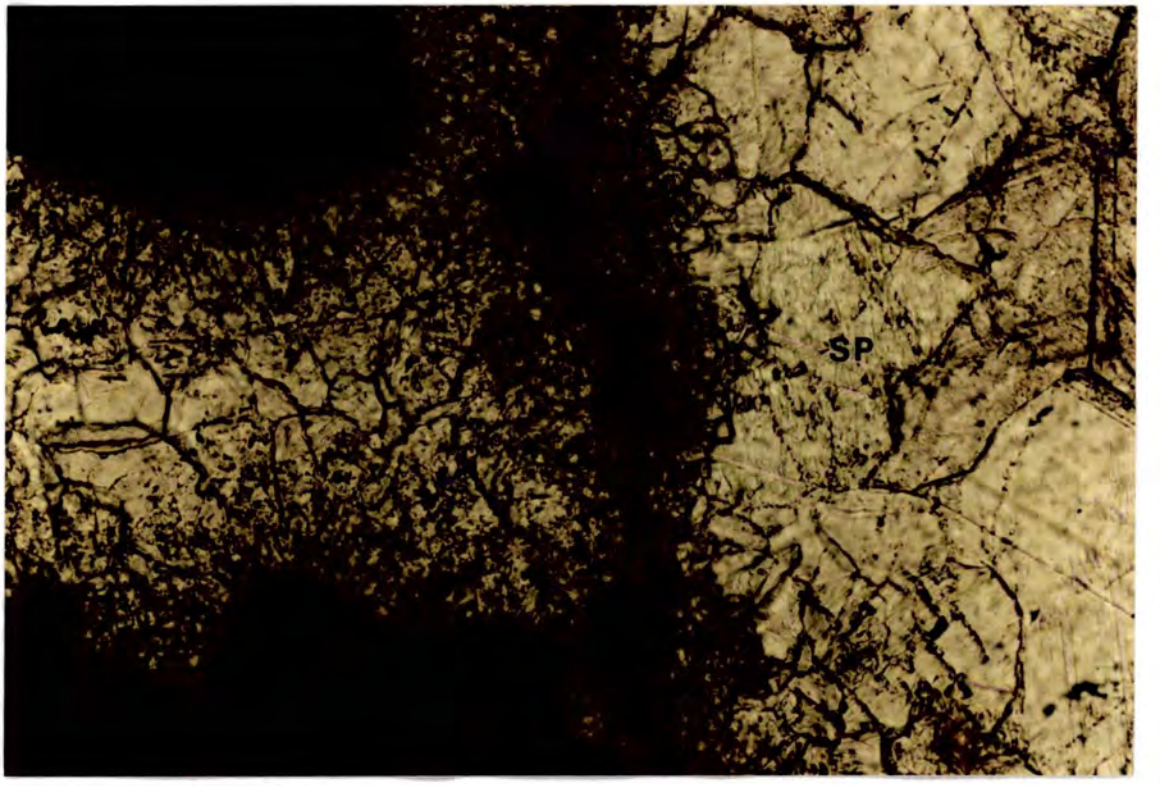

Fig.3.7c

3.8.2 Bladed isopachous cements.

This is typically seen within the shelf-margin facies of the Urgonian (see Fig.3.8). It consists of small (roughly 20 microns long; their width is slightly less, ie a small length:width ratio) stubby blade-like crystals that form an even coat around grains. They only occur on substrates lining primary inter- and intra- granular porosity. As with the isopachous acicular cements these cements are also relatively rich in inclusions and are non-luminescent.

Fig. 3.8 Bladed isopachous cements. Field of view= 0.17mm. 560/90, Aravis. Note; the bladed cement has become detached from the surface of the grain due to mechanical fracture, see section 3.10.2 for further discussion.

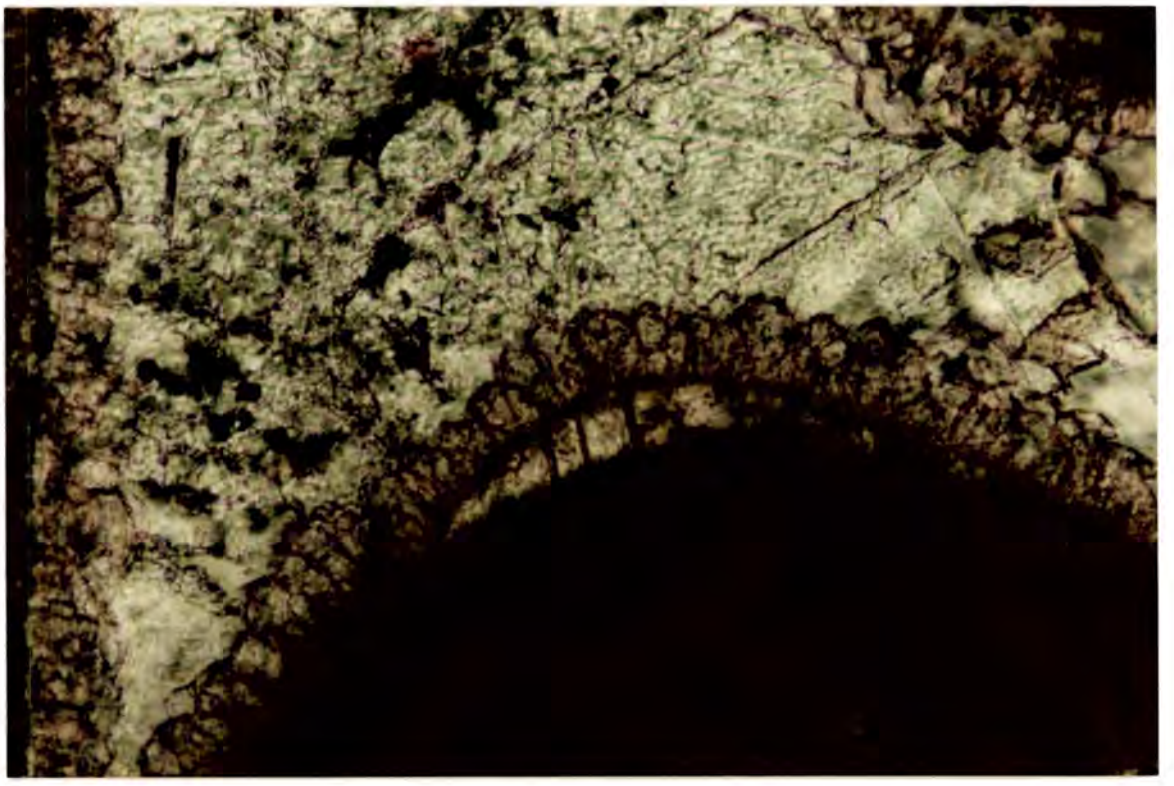

3.8.3 Radial fibrous.

Volumetrically this is the least important marine cement in the Urgonian and was only seen in a two localities (one of which is described in more detail in section 3.8.4). The cements are very coarse in comparison to the two types already described above. Individual crystals are commonly up to several millimetres long and nearly a millimetre wide and possess unit extinction and straight twin planes. Again they are inclusion-rich and non-luminescent.

3.8.4 Marine cements at Villaret Rouge, an example of radial-fibrous cements associated with a trangressive surface within the upper Urgonian of the Bauges.

The upper part of the Urgonian is exposed in a road section near the village of Villaret Rouge (location number 17 on Fig. 3.1) in the western part of the Bauges. The section is parallel to the strike of the beds, and shows well the lateral variability of the Urgonian and in particular of the Orbitolina horizons. To the author's knowledge this section has never before been described.

The Urgonian here displays all the classic features of a transgressive surface (Arnaud-Vanneau et al., 1987). Standard shelf-lagoon rudist facies (F8-F9, see section 3.5) are cut by irregular dissolution pipes, which are filled by dark blue clays (see Fig. 3.9a) often with patches of iron mineralization. Wackestones just below these dissolution surfaces contain fragments of the freshwater alga *Chara* (see Fig. 3.9b). XRD analysis (see Appendix 3) of a sample of the clay karst infill from this locality indicated that the mineralisation was pyrite (see Appendix 3). Above these are rounded pebble-sized clasts of typical Urgonian grainstones cemented by coarse, non-luminescent radial-fibrous cements (see Fig. 3.9c & 3.9d). Infilling the centre of the pore spaces there is a finely crystalline non-luminescent calcite (mineralogy confirmed by XRD, see appendix 3). Individual grains are often coated reddish fine grained material, presumably limonite. This gives a red colour to the to the rock in places (see Fig. 3.9c, area i). A rich and diverse macrofauna occurs within the horizon including irregular echinoids and large gastropods, suggesting open marine conditions. Overlying these (or possibly filling a channel feature) are Orbitolina grainstones (see Fig. 3.9e), with abundant detrital quartz.

Overall these sediments suggest that 'normal' platform sedimentation was suspended by exposure of the platform top. Possibly as a result of a relative sea-level fall, permitting meteoric diagenesis of the upper surface of the platform. This produced the dissolution pipes that are filled by the pyritic clays. A fresh water environment was established briefly, indicated by the *Chara* algae. A rise in relative sea-level caused the exposure surface to be transgressed, during which erosion and re-working occurred. The pebble-sized clasts were cemented at this stage by the pore-filling radial fibrous cements. An opportunistic fauna moved into the area from deeper environments, aided by the increase in siliciclastic material.

3.8.6 Factors controlling the occurrence of marine cements.

During transgressive events, sea-level rises pumping seawater through the sediments and there is often a greater input of siliciclastic material (hence lowering carbonate production). If the climate at the time is also of an arid nature causing hypersalinities to develop over the platform and causing more rapid CO_2 degassing, then marine cementation may be very common in some areas of the platform. In the Urgonian the F3 to F7 shelf-margin facies (see section 3.5) typically contain isopachous bladed marine cements; these facies represent the platform slope and margin and in these areas

active circulation of seawater is likely. This is the 'active' marine phreatic environment of Longman (1980). The Barremian-Aptian climate is believed to have been arid to semi-arid in nature (Deconinck, 1984; Deconinck et al., 1985; Ruffel & Batten, 1990).

Fig. 3.9a Blue-gray clays (c) infilling irregular dissolution pipes, within the Urgonian at Villaret Rouge. Several 'pebbles' of Urgonian grainstones can be seen toward the top of the photograph. Pen is approximately 140 cm long. **Fig. 3.9b** (see foldout on opposite page) Chara limestone, from Villaret Rouge. Field of view= 7mm **Fig. 3.9c** Slabbed hand sample of Urgonian from Villaret Rouge. Several clasts of Urgonian (U) grainstone can be seen, along with coarse radial-fibrous cements surrounding them (arrowed). The fine grained calcitic infill to the final pore space is labelled i. One pence for scale. **Fig .3.9d** Photomicrograph of radial-fibrous cements from Villaret Rouge. Field of view= 7mm. G= Urgonian grainstone pebble. **Fig. 3.9e** Orbitolina grainstone from Villaret Rouge. Several orbitolina are arrowed. Finger for scale. See foldout on opposite page for Figs 3.9b to 3.9e.

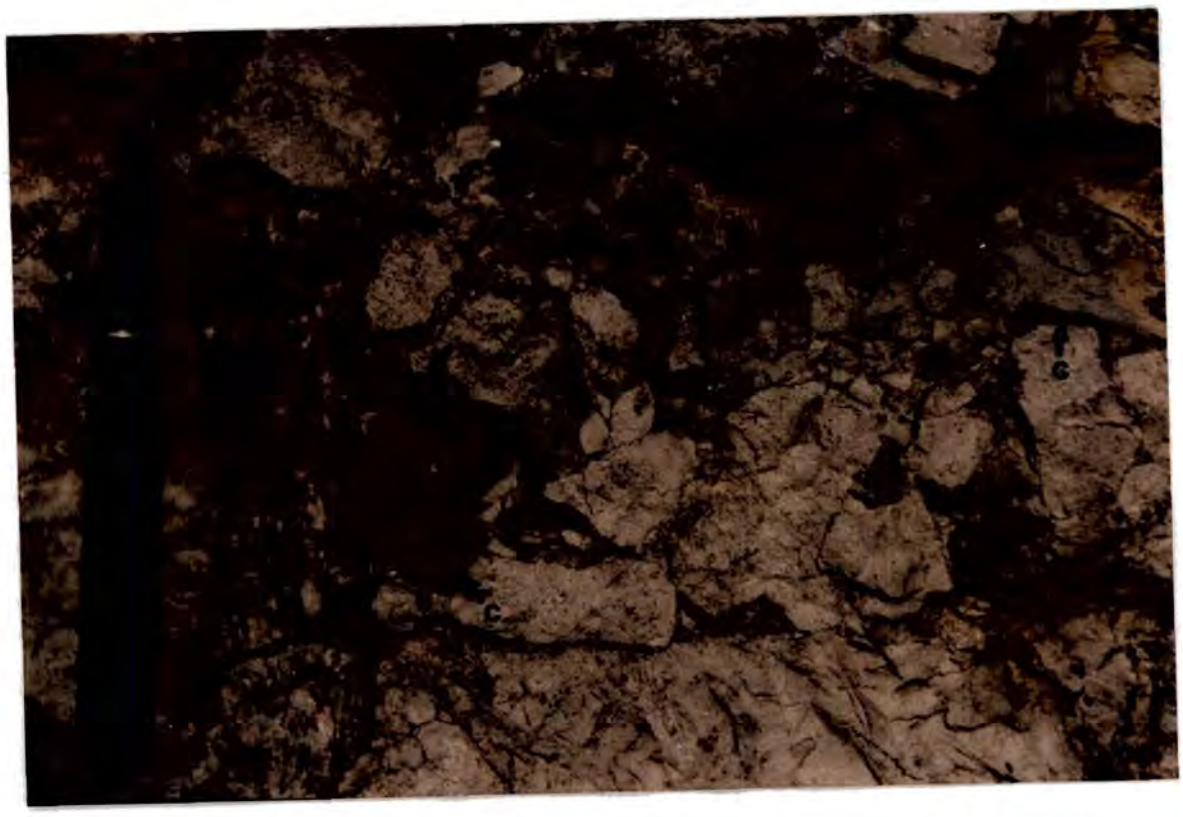

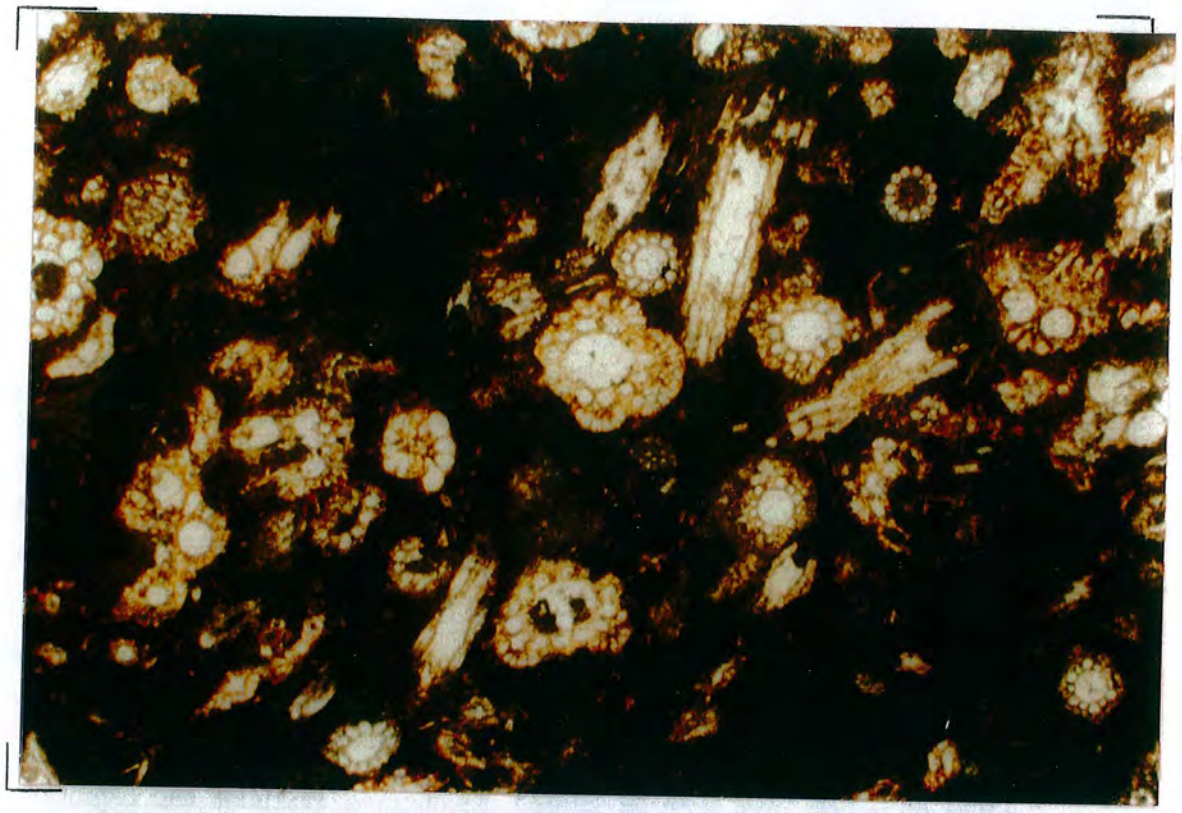

B

C

D

E

3.8.7 Marine cements synthesis and conclusions.

Like many other ancient carbonates marine cements are not common within the Urgonian except within particular facies. Marine cementation rarely accounts for the total occlusion of pore spaces, typically only providing a fairly narrow lining to the pore space.

3.9 Petrography of Rudist bivalves in the Urgonian.

This section describes and discusses the nature and diagenesis of the bi-mineralic shells of rudist bivalves.

3.9.1 Introduction to rudists and previous research associated with them.

Rudists were sessile epifaunal suspension-feeding bivalves, which were commonly inequivalve, highly asymmetric and relatively large. They were abundant in warm Cretaceous shallow-marine seas of Tethys and were capable of constructing carbonate buildups (Wilson, 1975; Masse & Philip, 1981). They have thick shells, originally composed of an outer low-Mg calcite layer and an inner aragonite layer (Kennedy & Taylor, 1968; Al-Aasm & Veizer, 1986a). The evolution of these bivalves is detailed by Skelton (1985) and their classification is discussed by Skelton & Gili (1988). Several different families of rudists have been recognised. Requienids, caprinids and caprotinids are present within the Urgonian (Arnaud-Vanneau et al., 1972; Masse & Philip, 1981; Arnaud-Vanneau et al., 1987). Figure 3.10 shows the stratigraphic distribution of rudist genera through the upper Jurassic and Cretaceous.

Several papers and theses have been written concerning rudist diagenesis and in particular the neomorphism (or calcitization) of their shells. Al-Aasm & Veizer (1986a & 1986b) studied the diagenetic stabilization of the aragonite and low Mg-calcite within the shells of several different rudist families and used both trace elements (Al-Aasm & Veizer, 1986a) and stable isotopes (Al-Aasm & Veizer, 1986b) to monitor diagenetic changes within the shells during what they envisaged as solely meteoric diagenesis. Ross (1989) also studied the skeletal diagenesis of rudists and in particular their use as an indicator of diagenetic environment. He suggested that isotopic signatures of the neomorphosed part of the shell reflected different environments of aragonite neomorphism. Enos (1986) and Minero (1988, 1991) have discussed in more general terms the diagenesis of rudist limestones from the mid-Cretaceous El Abra Formation of Mexico. Enos (1988) described the evolution of pore space within the Tamabra limestone, which is the basinward equivalent of the El Abra. The Tamabra limestone is an important oil reservoir rock in the Poza Rica trend, Mexico; within this limestone porosity is largely due to the selective dissolution of Caprinid rudists. Jacka & Brand (1977) detailed the porosity and diagenetic evolution of the lower Cretaceous Edwards rudist reef of Texas and in particular they discussed the differences in diagenesis between what they suggest are palaeo- vadose and

phreatic zones. M'Rabet et al. (1986) discussed the early lithification of micrites and environmental conditions of early diagenesis within two Senonian rudist build-ups in Tunisia. Within the mid-Cretaceous Stuart City trend of Texas partial to complete dissolution of rudist shells is important for porosity enhancement (Prezbindowski, 1985).

Fig. 3.10 The stratigraphic and taxonomic distribution of rudists, by genera, for the upper Jurassic and Cretaceous, showing that requienids, caprotinids and caprinids are likely to be present within the Urgonian, as Arnaud-Vanneau et al. (1972) and Masse & Philip (1981) suggest. Diagram re-drawn from Skelton & Gili (1988).

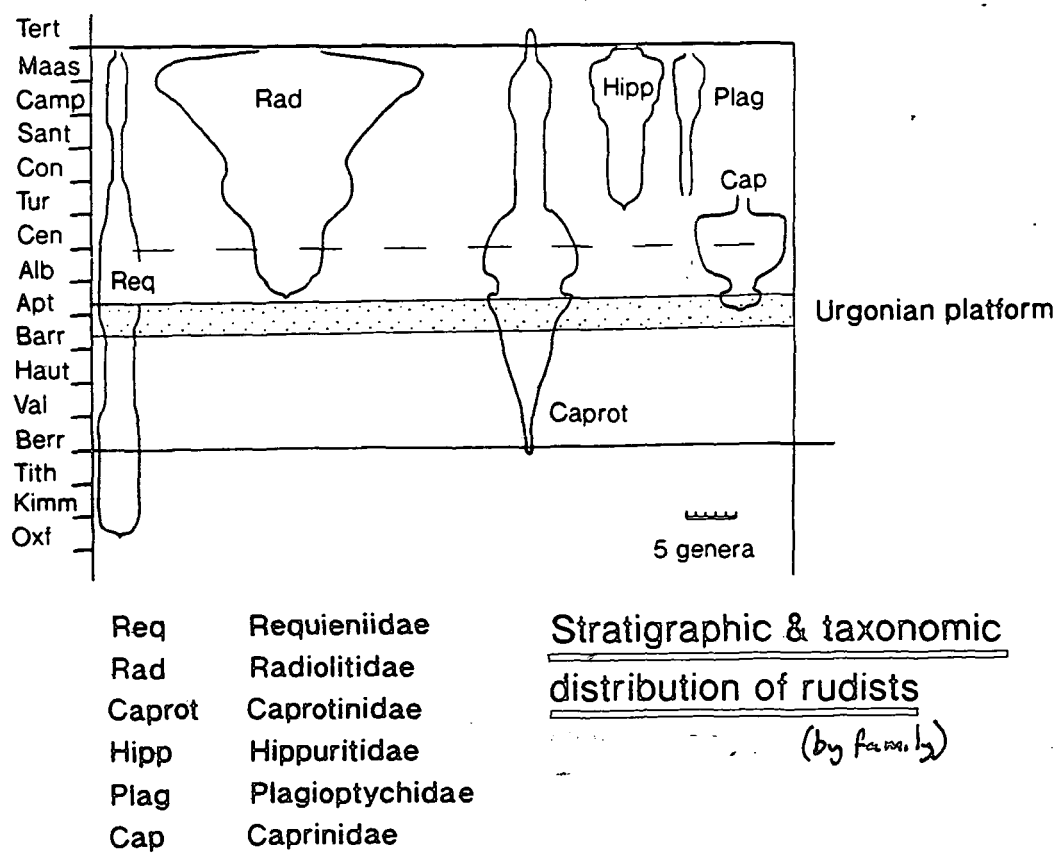

The original mineralogy and nature of rudist shells was first described by Kennedy & Taylor (1968) in well preserved examples of *Hippurites boehmi* and *Praeradiolites aguilloni* (both Santonian in age). According to Kennedy & Taylor's (1968) figure 1(a and b) an aragonitic layer with crossed-lamellar or complex crossed-lamellar structure occurs within the inner part of the shell (including internal pillars and tabulae) of the *Hippurites*. The maximum width of this layer is 1mm, whereas the outer part of the shell is composed of low Mg-calcite (LMC) blocks of fine calcite prisms, up to 12 mm thick. Within the *Praeradiolites* sample aragonite areas are up to 10mm across (Kennedy & Taylor, 1968, their figure 2); however, there is a less even distribution of aragonite within this sample. From examples of rudists with good preservation of the original shell mineralogy (i.e.

where primary shell aragonite is preserved) a prismatic arrangement of calcite needles of 3-4 microns width and 40-50 microns length is indicated for the original structure of the outer low Mg-calcite layer (Kennedy & Taylor, 1968, Bathurst, 1975, page 18). For the three families of rudists seen in the Urgonian, Al-Aasm & Veizer (1986a) (their table 1) suggested that the state of preservation of the aragonitic components is at best fair, with the outer calcite layer enjoying better states of preservation. They also noted that the original mineralogy of the outer layer of the shell in requienids, caprotinids and caprinids was a prismatic, low magnesium calcite, with aragonitic inner layers indicated by the presence of possible remnants of lamellar structure.

enjoying better states of preservation. The upper Cretaceous rudist families, hippuritidae, radiolitidae and caprinidae all seem to have a much greater potential for preserving the aragonitic inner parts of the shell. However, it should be noted that this could be partially due to the fact that for some families, Al-Aasm & Veizer only had a small number of samples to study.

3.9.2 The state of preservation of Urgonian rudists: shell dissolution.

Urgonian rudist shells, regardless of their family, show two different states of preservation of the shell: 1) shells where the former aragonitic layer has been totally dissolved leaving just the outer LMC layer preserved; and 2) shells where the whole shell is no longer preserved and the space is occluded by drusy calcite spar. The general mode of Urgonian rudist shell preservation is for the inner aragonitic part of the shell to have been removed by dissolution leaving only the outer low Mg-calcite layer. In a few instances (less than 10% of the sections studied) total shell dissolution occurred. Instances of shell dissolution are shown in Figs 3.11a and 3.11b (see also Figs 3.17c, 3.21, 3.22a and 3.22b). As mentioned in section 3.9.1 aragonite was an important part of rudist shells. However, Urgonian rudists were inspected for any signs of calcitization of aragonite, and internal ghosting features possibly indicating calcitization of the aragonite components such as those described by Ross (1989, his figure 6.6) were not seen (this is discussed further in section 3.11.3).

Fig. 3.11a (opposite page) Partial dissolution of a shell of a rudist shell, causing the collapse of internal sediment which had filled the body chamber. Remnant shell areas (S) are (presumably) the outer low Mg-calcite part of the shell. Sample 236/89, lower Bourne gorge, Vercors Massif. Field of view= 13mm **Fig. 3.11b** An example of the less common phenomenon of total shell dissolution. The former shell area is labelled fs. Note: that the Serpulid worm tubes encrusting one the side of the shell do not occur within the former shell area. The walls of the worm tubes have also been dissolved out. Sample 442/90, Mt. Trelod, Bauges. Field of view = 7mm. In both instances the secondary porosity produced is occluded by cement generations described in section 3.11.

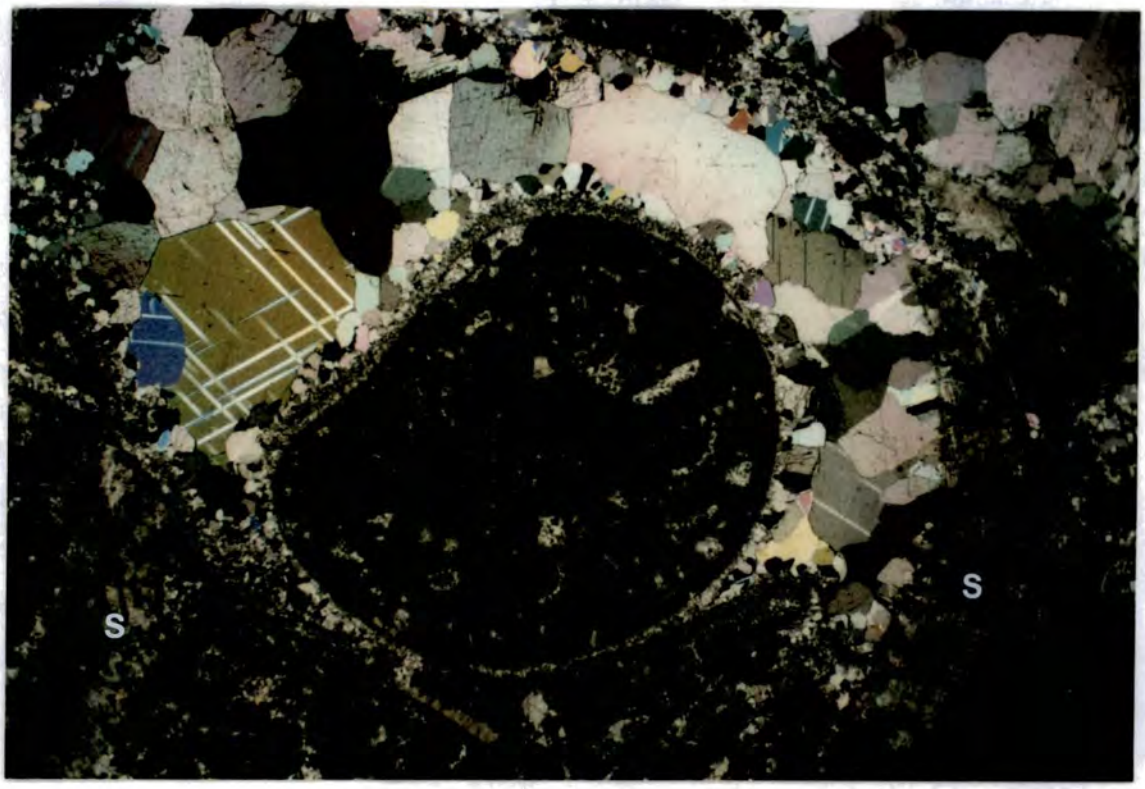

Fig. 3.11a

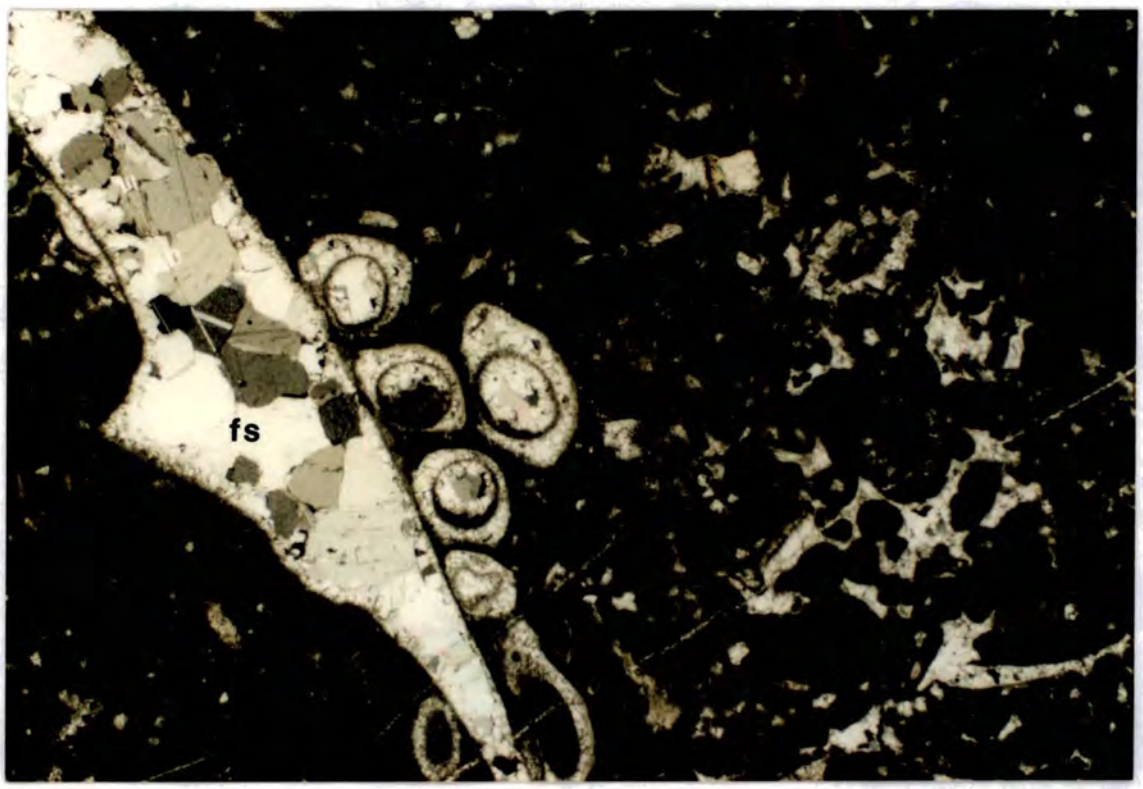

Fig. 3.11b

Mineralogical selective dissolution is apparently very common in Cretaceous rudist limestones, with similar instances being detailed by Jacka & Brand (1977), Scholle (1978, pages 85 and 193), Enos (1986, 1988), Prezbindowski (1985), M'Rabet et al. (1986), Al-Aasm & Veizer (1986a, and b) and Ross (1989). The Cretaceous was a period of aragonite-depleted seas according to Sandberg (1983; 1985) during which precipitation of calcite would be preferred. With seas undersaturated with respect to aragonite, the dissolution of aragonitic allochems could take place in marine waters, even on the sea floor (as described from certain Ordovician and Jurassic hardgrounds, Palmer et al., 1988). The cyclic changes in the dominant mineralogy of calcium carbonate (shown in Fig. 3.12) precipitated from seawater described by Sandberg (1983; 1985) have been suggested to be due to greater concentrations of atmospheric PCO_2 during these times (Wilkinson et al., 1985), The Cretaceous has been referred to as a 'greenhouse' period (Fischer, 1983), an ice-free period characterised by higher sea-levels and higher concentrations of atmospheric PCO_2. Palaeo-climatological modelling of the Cretaceous climate suggests that polar ice volume was minimal during this period (Barron et al., 1981; Barron, 1989).

Fig. 3.12 Cyclic changes in the dominant mineralogy of marine abiogenic precipitates compared to global climatic cycles, first-order eustatic sea-level and dolomite abundance. From Tucker (in press).

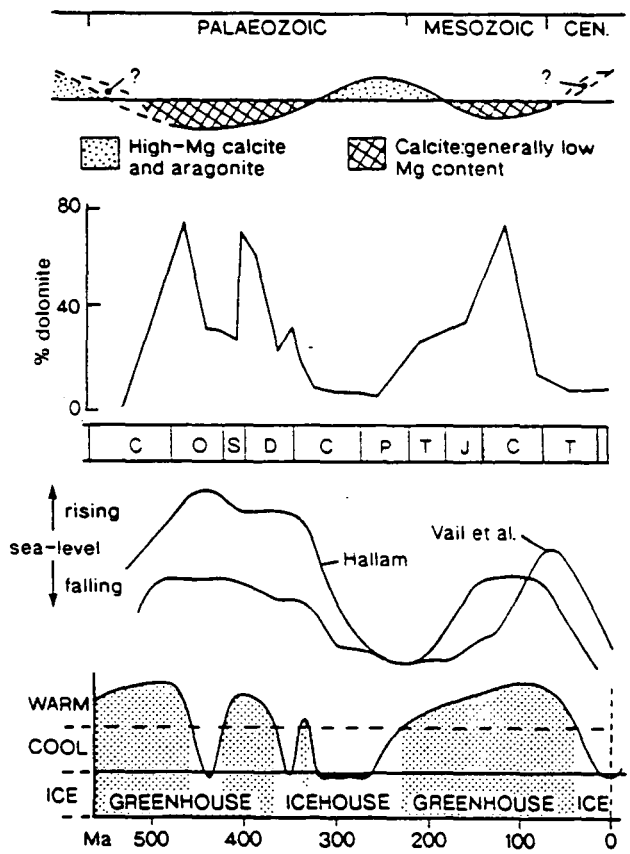

Quaternary carbonates from the first few metres below the seafloor of the Red Sea show dissolution of aragonitic pteropod shells. Horizons with aragonite dissolution coincide with times of well ventilated bottom conditions, experienced during interglacial periods. The state of preservation of shells is controlled by the degree of organic matter degradation in the sediments. With suboxic to oxic conditions and a moderate supply of organic matter, oxygen consumption and CO_2 production is increased. This lowers the pH, causing dissolution of the shells. Under anoxic, oxygen-depleted glacial intervals CO_2 is not produced, so pH increases and aragonite is well preserved (Almogi-Labin et al., 1986).

However, within the areas of partial and total shell dissolution observed within the Urgonian there was never any indication of the dissolution occurring in the marine realm. Features such as marine cements or encrustation by marine organisms (such as serpulids) are absent from these secondary pore spaces (see Figs. 3.7c and 3.11b and section 3.8). These features alone are not conclusive proof of marine dissolution as they also could be produced by fluctuating sea-level producing early (effectively syn-depositional) emergence (meteoric dissolution) followed by a return to a marine setting. This can be seen in some of the mid-Cretaceous rudist buildups of Mexico and Texas described by Enos (1986), Minero (1988) and Prezbindowski (1985). However, in such instances exposure surfaces should be expected and the secondary porosity produced should have a distribution that is related to these surfaces. The occurrence of marine cement-filled molds should decrease downwards from an exposure surface. Within the Urgonian marine cements are never seen within areas of shell dissolution (see Fig. 3.7c); it is more likely that the dissolution occurred in a meteoric setting. This is indicated by the relationship of these secondary pores to subsequent diagenetic features such as the collapse of micritic envelopes and the nature and order of cement precipitation (as discussed below). With the lack of any marine features within these pore spaces is perhaps an indication that marine pore fluids did not re-enter the sediment.

It has been argued by Giles & Marshall (1986) that the majority of secondary porosity generated in the shallow subsurface by meteoric fluids. Although Mazzullo & Harris (1992) have suggested that 'deep' (greater than 200m) burial or mesogenetic dissolution is equally important in the creation of secondary porosity in carbonates, they essentially applied the mechanism of secondary porosity production that Surdam & Crossey (1985) and Surdam et al. (1989) had proposed for sandstones. Evidence presented in the later sections (3.9.3, 3.10.1, 3.10.2 and 3.11.3) indicates that the meteoric environment is the more likely environment of rudist shell dissolution in the Urgonian. None of the petrographic associations suggested by Mazzullo & Harris (1992) to be indicative of mesogenetic porosity where seen within the Urgonian.

Rudists had relatively high inter- and intra- granular porosity, from their internal body chambers (where not filled by internal sediments) and from the open network microstructures present within the shells of some families (caprinids and radiolitids

particularly) (Al-Aasm & Veizer, 1986a). The role of initial skeletal porosity in controlling early diagenetic alteration, has been demonstrated by Martin et al. (1986) for two taxa of Pleistocene corals from Florida. This factor, along with the metastable mineralogy of the inner aragonite part of the shell, could have promoted meteoric dissolution of shell material.

3.9.3 Other instances of early dissolution within the Urgonian limestones (also see section 3.10).

Fragments of coral within the F7 facies may display the effects of dissolution on parts or all of the coral mass. Examples of this are shown in Fig. 3.13. As with the dissolution of rudist shells, in corals this process was probably aided by the very high primary intra-granular porosity. These areas can be distinguished from syn-depositional features such as borings by their lack of any internal sediment and marine cements. Often isopachous acicular cements are seen lining the walls of primary intra-granular porosity, but are not seen within the area of dissolution.

Fig. 3.13 Photomicrograph of dissolution within the framework of a corralline organism. 163/90, Les Rimets, Vercors. Field of view= 13mm. Some possibly broken (or detached) pieces of the coralline organism are healed by the later spar (see section 3.11.3(c).

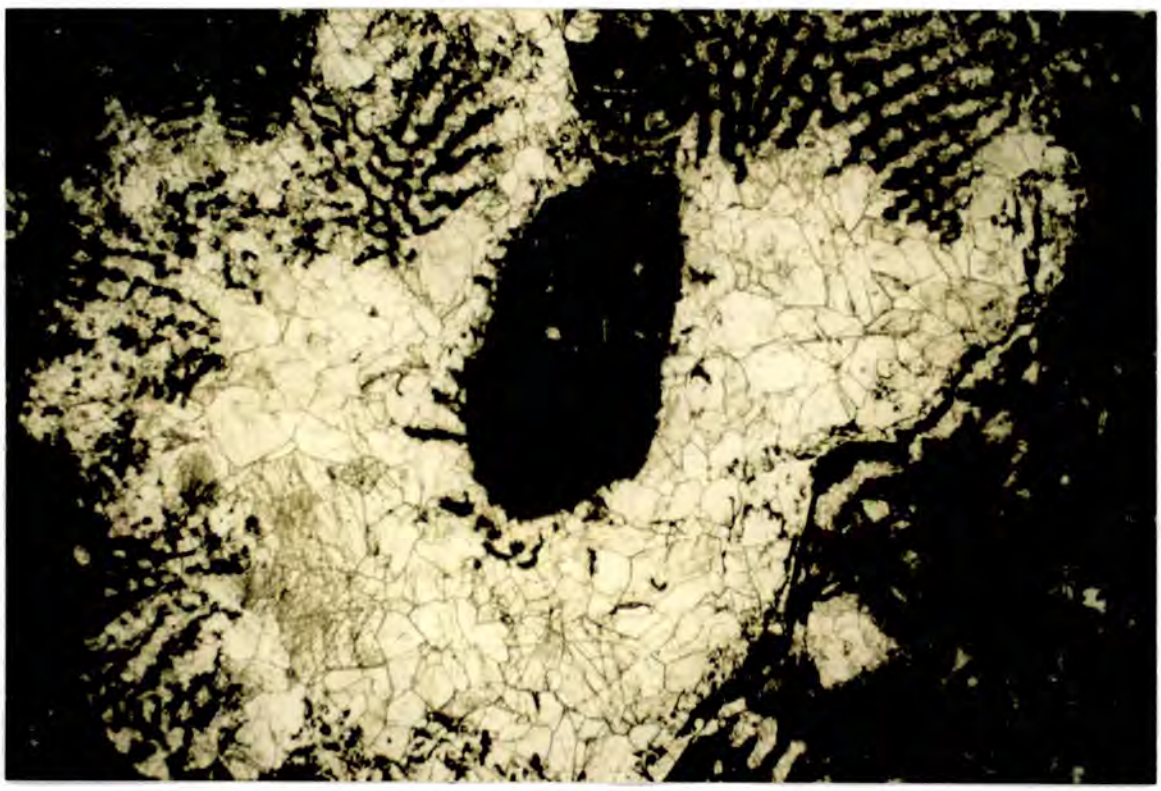

Although true barrier reefs never developed along the Urgonian shelf (Arnaud-Vanneau et al., 1987), isolated coral reefs did occur along the shelf margin. It is possible that these could have been emergent periodically allowing the local development of a meteoric lens. However, there is no evidence for locally developed karsts associated with the coral buildups. These are most likely to develop during humid climatic periods. The Barremian-Aptian, however, is believed to have been a period of semi-arid to arid climatic conditions (Deconinck, 1984; Deconinck et al., 1985; Ruffel & Batten, 1990) and this does not favour the development of such lenses. The other possibility is that the dissolution occurred in a burial setting. The petrography of the cements that infill these pore spaces and the geochemistry of the cements can give important clues to this. Both are discussed later in sections 3.11, 4.5 and 4.6 and support a meteoric setting for the dissolution.

Minor dissolution was also seen to be present within the cortices of a few ooid grains, producing very small (and presumably isolated) areas of intra-ooid porosity, aligned roughly along the concentric rings of the ooids (see section 3.10.2). Very similar dissolution rings have been observed in Holocene aragonite ooids which have been subjected to meteoric diagenesis (Budd & Land, 1990).

Several brief periods of subaerial exposure punctuate the development of the platform and a more prolonged period of subaerial exposure terminated the deposition of true Urgonian facies (Arnaud-Vanneau et al., 1987; Jacquin et al., 1991; Hunt, 1992). During these periods with the arid to semi-arid climate, mineralogical controlled dissolution would occur in the phreatic zone (see James & Choquette, 1984). Under such conditions meteoric cementation is typically minor (Hird & Tucker, 1988;Wright, 1988), which explains the lack of meteoric vadose cements. As with the instances of rudist shell dissolution, marine cements were not seen within these secondary pore spaces.

3.9.4 Petrography of the preserved part of rudist shells.

As noted above dissolution of rudist shells within the Urgonian is principally fabric selective, with the outer LMC part of the shell the only remaining part of the original shell. The calcitic mineralogy of this part of the shell was confirmed by XRD analysis of the shell wall (see Appendix 3). This part of the shell is totally occupied by a mosaic of prismatic calcite crystals arranged perpendicular to the margins of the shell wall. The calcite crystals are typically 250 to 500 microns wide and up to 2500 microns in length. Extinction within this mosaic often sweeps from one end of the shell fragment to the other (see Figs 3.14a and 3.14b). The intercrystalline boundaries between the crystals are gently curved to wavy. Enfacial junctions never occur between these crystals. These prismatic crystals are cut by an arrangement of solid inclusions (most likely remnant organic material). These inclusions transect without deviation the intercrystalline boundaries of the calcite and have a pattern reminiscent of unaltered calcite shell layers within bivalvia (Bathurst, 1975; Scoffin, 1987). Typically these inclusions have a foliated pattern and probably represent growth lines. All these features are shown in see Figs 3.14a and 3.14b.

Fig. 3.14 Typical rudist shell structure (opposite page), **(a) & (b)**, (a=XPL & b=PPL) showing the typical structure of the preserved low Mg-calcite part of the shell. The prismatic nature of the calcite can be seen, as well as the foliated pattern of inclusions. Note: the thin fracture aligned perpendicular to the shell wall. Sample 21/90, Gorge du Frou, Chartreuse Massif. Field of view= 3.25mm.

In places, the prismatic crystals of the shells are cut by thin (less than 200 microns) fractures, which are somewhat irregular in outline and are parallel to sub-parallel to the trend of the prismatic crystals. The crystals on opposite sides of the fracture go into extinction together and some of the cements infilling the fracture may also be in optical continuity with calcite crystals of the shell. These later cements fill the fractures and have petrographic and luminescent qualities which distinguish them from the areas of shell material (see Figs 3.15a, 3.15b and section 3.11.3, Figs 3.22a and 3.22b).

The prismatic crystals of the shell are consistently non-luminescent; succeeding cement generations show a different CL response, typically a non-luminescent-bright orange-dull orange/ non-luminescent zonation (see Fig. 3.23a and section 3.11.3).

3.9.5 Interpretation of the petrography of rudist shells.

The preserved rudist shells in the Urgonian are similar to previous descriptions of unaltered LMC (see section 3.9.1) rudist shell material, but are much coarser than previous descriptions. Thus it is suggested that the outer low Mg-calcite part of the shell has recrystallised to a coarser, prismatic calcite by a process of aggrading neomorphism. This fabric is produced by the growth of the prismatic diagenetic low magnesium calcite (dLMC) crystals being controlled by the shape of the original low magnesium calcite (LMC) crystals, so that the boundaries of the neomorphic calcite crystals are all preferentially aligned and are perpendicular to the walls of the shell. As mentioned in section 3.9.1 the outer part of the rudist shells had a prismatic structure, it appears then that the original structure has controlled the growth of the neomorphic prismatic calcite, but the crystals of calcite are now much coarser than in examples of preserved shell mineralogy (Kennedy & Taylor, 1968, Bathurst, 1975, page 18). This texture is the result of coalescence of the original minute subcrystals of the shell. Principally from geochemical data Al-Aasm & Veizer (1986a & 1986b) also suggested that LMC of rudist shells stabilised to dLMC during diagenesis. Geochemical arguments in favour of the alteration of LMC to dLMC within Urgonian rudist shells is presented in sections 4.2 and 4.3.

These features are similar to those described by Bathurst (1975, pages 486 to 489) for the calcitization of aragonite molluscan shell walls (see also Bathurst's figure 312, page 433, which shows a molluscan grain replaced by neomorphic spar), although of different origin. Preferential alignment of neomorphic crystals can also be seen where originally aragonitic botryoidal cements have been neomorphosed and the acicular habit of the

Fig. 3.14a

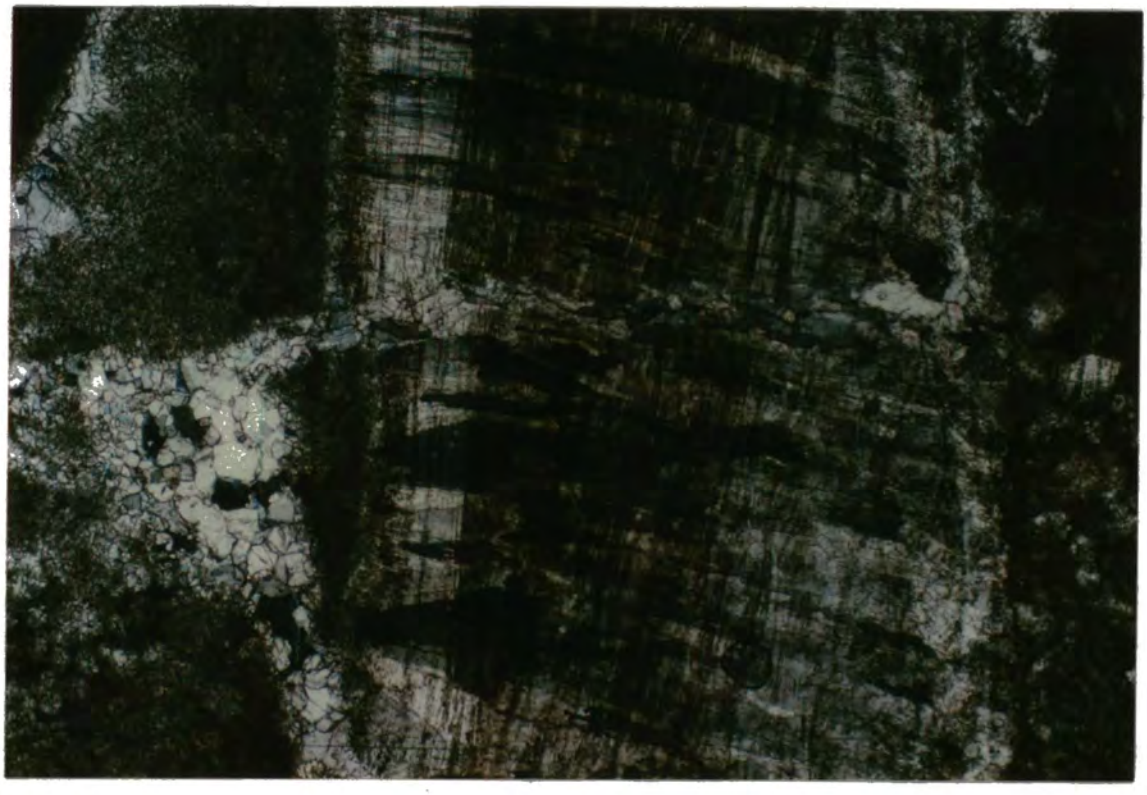

Fig. 3.14b

aragonite crystals has been followed by the calcitization (e.g. Tucker & Hollingworth, 1986). As is often the case with neomorphism, there is a fair degree of fabric retention (Wilkinson, 1983). The retention of the solid inclusions marking the position of former growth lines is also part of the original fabric of the shell.

Fig.3.15 Features dating the aggrading neomorphism of the low Mg-calcite part of the shell, **(a)** PPL photomicrograph showing where prismatic spar crystals go into extinction across a fracture. Some of the cements crystals in the fracture go into extinction with the crystals in the shell. **(b)** (opposite page) Line drawing interpretation of the above. Sample 116/91, Combe de la Orme Bauges.

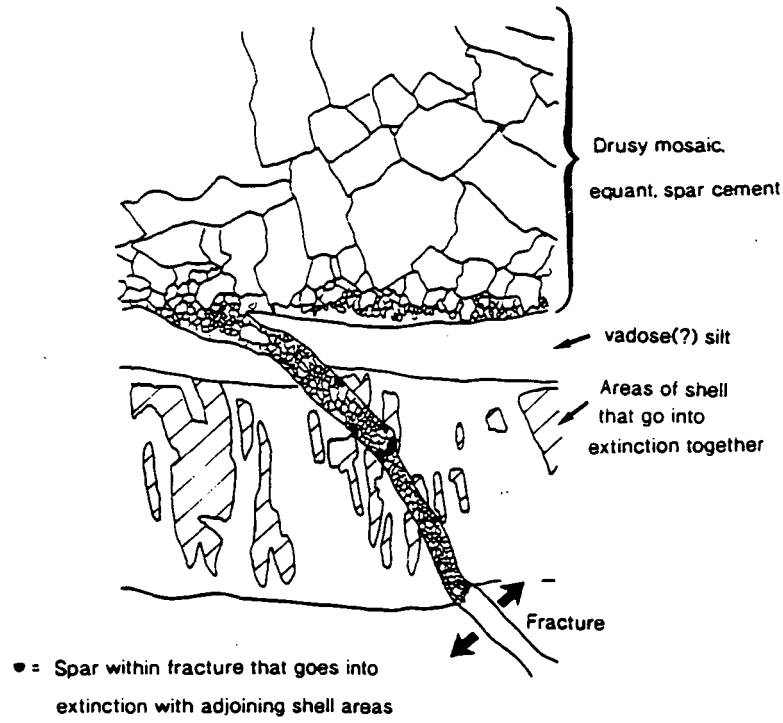

Fig. 3.15b

The criteria used to distinguish cements as actual cement generations and not as the neomorphosed aragonitic inner part of the shell, are given in section 3.11.3 Geochemically both these areas are distinct (see section 4.6). The relative timing of the recrystallization of the shells is possibly indicated by the relationship of the crystals of the shells to the thin fractures which cut the shells (see Figs 3.15a and 3.15b). These fractures follow the preferential alignment of the crystals and crystals often go into extinction across the fractures. Perhaps indicating that these fractures formed after the crystallization of the prismatic crystals, but before the precipitation of the cements which infill the fractures. The fractures are never filled by sediments and/or marine cements, which discounts them from forming near-surface or near the sea floor. The fractures are quite localised and probably formed as a result of loss of support through the dissolution of shell material, with the matrix only partly lithified at the time. These features would then indicate that the neomorphism was a relatively early event.

3.9.6 Discussion of neomorphism - environments and timing of neomorphic processes.

Neomorphism refers to processes of replacement and recrystallization where there may have been a change in mineralogy (Folk, 1965). Neomorphic processes take place in the presence of water through wet, thin-film dissolution-reprecipitation (Bathurst, 1975) with dissolution of the less stable carbonate mineral (aragonite, high Mg-calcite or very small crystals) on one side and precipitation of a more stable phase (such as low Mg-calcite or bigger crystals) on the other. This can take place within a variety of different carbonate

sediments including fine-grained carbonate muds, cements and bioclasts. The retention of relic or ghosted structures argues for an in-situ transformation without a void stage. The fabrics produced are in marked contrast to those produced by wholesale dissolution of the shell and subsequent filling of the void by cements (compare Figs 3.14a and 3.11b). Replacement textures have been divided into gross fabric obliteration and gross fabric retention by Wilkinson (1983).

Prior to the neomorphism or dissolution of shell material, syn-depositional diagenetic formation of micritic envelopes by the action of microbes, borings by endoliths and internal sedimentation in the body chambers took place. These have already been described in sections 3.5 and 3.6.

Neomorphism of shells can occur in a variety of diagenetic environments (meteoric, marine and burial). Elucidation of the environment of neomorphism often requires the use of field, regional, petrographic and geochemical data. Caution is required because several neomorphic fabrics can be generated in different environments (Wilson et al., 1983; Halley, 1987; Ross, 1989). Using a combination of some or all of these neomorphism has been recognised in burial, meteoric and marine settings (Bathurst, 1983; Sandberg & Hudson, 1983; Tucker, 1985; Ross, 1989).

Under CL, grains which have been altered often show some evidence of this alteration. For example, neomorphic spar may contain relics of an earlier cement fabric (e.g. Bathurst, 1983). In section 3.9.5 it was suggested that the preserved part of the rudist shells in the Urgonian had been altered by an aggrading neomorphism; these areas however, are non-luminescent (see Figs 3.23a and 3.23c (they are also non-ferroan). This implies that either 1) the alteration occurred in the presence of oxic pore-fluids or 2) reducing fluids lacking sufficient ratio of Fe^{2+} and Mn^{2+} within the system. From the arguments presented in 3.9.4 and the geochemistry of the shells (presented in section 4.2) either option is possible to explain the non-luminescence of the shells.

In the Urgonian there is good evidence, presented above and in the following chapter on geochemistry, that the aggrading neomorphism of the calcitic part of the shells occurred in a shallow near-surface environment.

3.9.7 Conclusions concerning Urgonian rudists.

1) The metastable original mineralogy of rudists produced a fabric-selective secondary porosity within rudistid facies of the Urgonian.

2) Typically only the outer LMC part of the rudist shell is preserved.

3) Petrographic relationships for this part of the shell suggest that it has experienced an aggrading neomorphism to preferentially aligned coarse crystals of diagenetic LMC. The neomorphic crystals are preferentially aligned with the original prismatic calcite of the outer part of the shell, but are much coarser than the original calcite is believed to have been.

4) This alteration occurred whilst the platform was in a shallow subsurface setting and prior to precipitation of drusy spar cements.

3.10 Early grain to grain dissolution and mechanical compaction.

3.10.1 Early grain to grain dissolution.

A common texture within some sections of the Urgonian is a grain fitted-fabric, the result of dissolution at grain contacts. Often it is seen in grainstones most clearly but it also occurs within micritised packstones where it usually is less easily discernable. In both it produces an overcompaction (shown in Fig. 3.16a). Often the contact between the two grains is of a concavo-convex nature with a slightly wavy appearance. The contact, however, is not sutured. Longitudinal contacts are also seen. Compactive fracture does not affect these grains, although they may be seen affecting other (more brittle) grains within the sediment. The presence of an early marine isopachous cement on the grains in question often does not seem to have impeded the grain to grain suturing (see Fig.3.16b). Scholle & Halley (1985) show a similar feature affecting upper Mississippian ooid grainstones from Tennessee. The surrounding pore spaces are occluded by cement crystals unaffected by the dissolution. These cements are of syntaxial and equant nature (see section 3.11).

This fabric suggests that there has been some dissolution at the contacts of the grains. This could be due to the effects of chemical compaction and plastic deformation in a burial environment (usually taken to be deeper than 200 to 300 metres). However,the presence of cements close to areas of fitted fabric suggests that the dissolution occurred prior to the cementation. Meyers (1980) suggested that this cement-dissolution relationship is the only time that cements can be unambiguously dated as post-dating chemical compaction. It is likely that these contacts formed relatively early on in the diagenetic history. Another possibility is that the dissolution is due to the passage through the succession of undersaturated meteoric vadose waters which have promoted the dissolution at the grain contacts. This process is referred to as 'vadose compaction' (Hird & Tucker, 1988; Tucker & Wright, 1990). This process may be aided by the initial onset of mechanical compaction with the de-watering of the sediments and re-organization of the grain packing to a tighter arrangement bringing about a greater number of grain to grain contacts. It some cases it appears that the presence of a slightly more resistant grain surface has promoted this dissolution.

3.10.2 Mechanical fracturing.

Within the Urgonian, grains and cements have experienced brittle deformation by mechanical fracturing. A variety of different fractures are shown in Figs 3.17a, 3.17b and 3.17c. Buckled and fractured marine isopachous cements are relatively common within the Urgonian (see Figs 3.8, 3.19a and 3.19b).

Fig. 3.16a Photomicrograph of an overcompacted grainstone. 66/91, Pic d'Oiellette, Chartreuse. Field of view= 3.25mm. Some of the cores of the grains have been dissolved out. **Fig. 3.16b** (opposite page) Photomicrograph of grain to grain suturing between two oolitic coated grains. 554/90, Pic de Jallouvre, Bornes. Field of view= 1.5mm

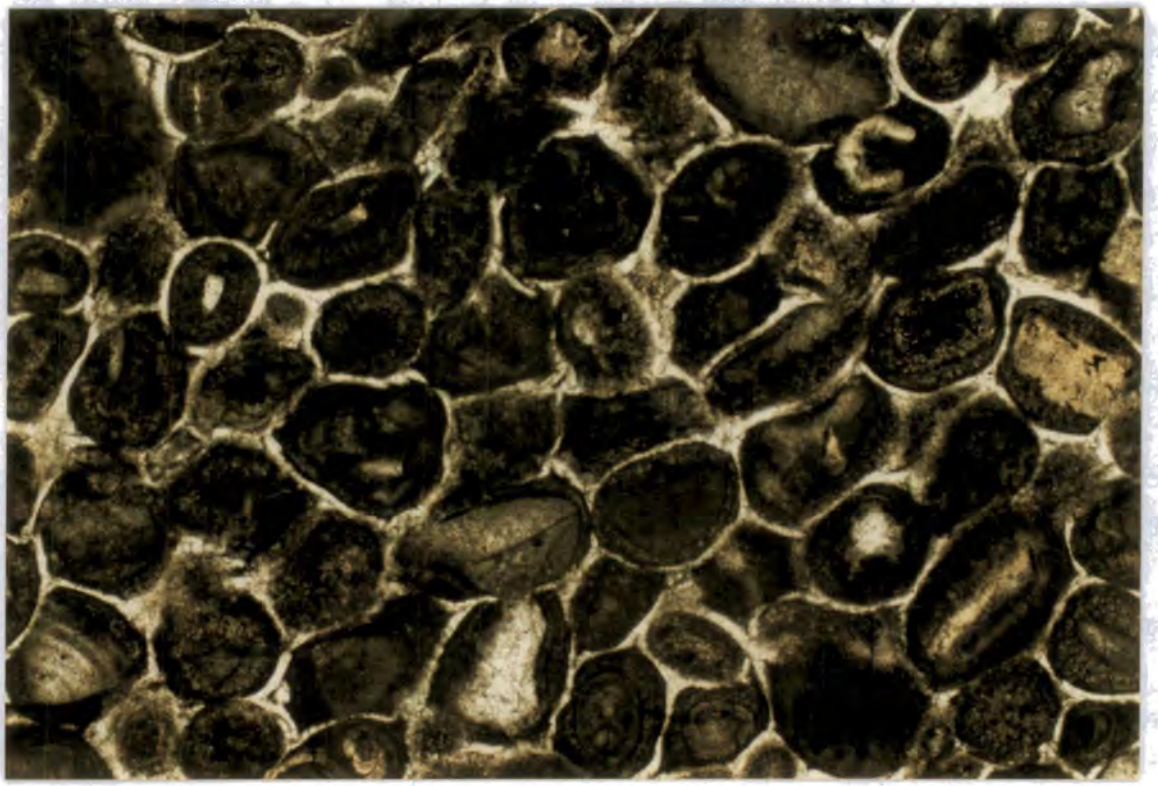

In a few oolitic grainstones, so-called 'elephantine' ('trunk to tail' or chain) structure can be seen. This unusual structure consists of zig-zag chains of crescent shaped ooid and peloidal remnants (see Fig. 3.17a). In the Urgonian examples the inner part of the ooid/peloid is never totally dissolved out. Similar structures have been described by Moore (1985), Harwood (1988) and Henton (1990). Henton (1990) proposed that these structures formed with the preferential dissolution of the ooid/peloid inner cortex/core (dissolution of the inner rings of ooids is described at the end of section 3.9.2), with the outer part of the ooid mechanically spalling off and fracturing against point contacts with adjacent grains, resulting in a flattening and interlocking of the ooid remnants. This structure indicates that there was dissolution prior to mechanical fracture and again supports the notion that this dissolution and the dissolution of the parts or all of the shells of rudists occurred relatively early on in the diagenetic history of the platform whilst it was still in a meteoric environment (see section 3.9.2).

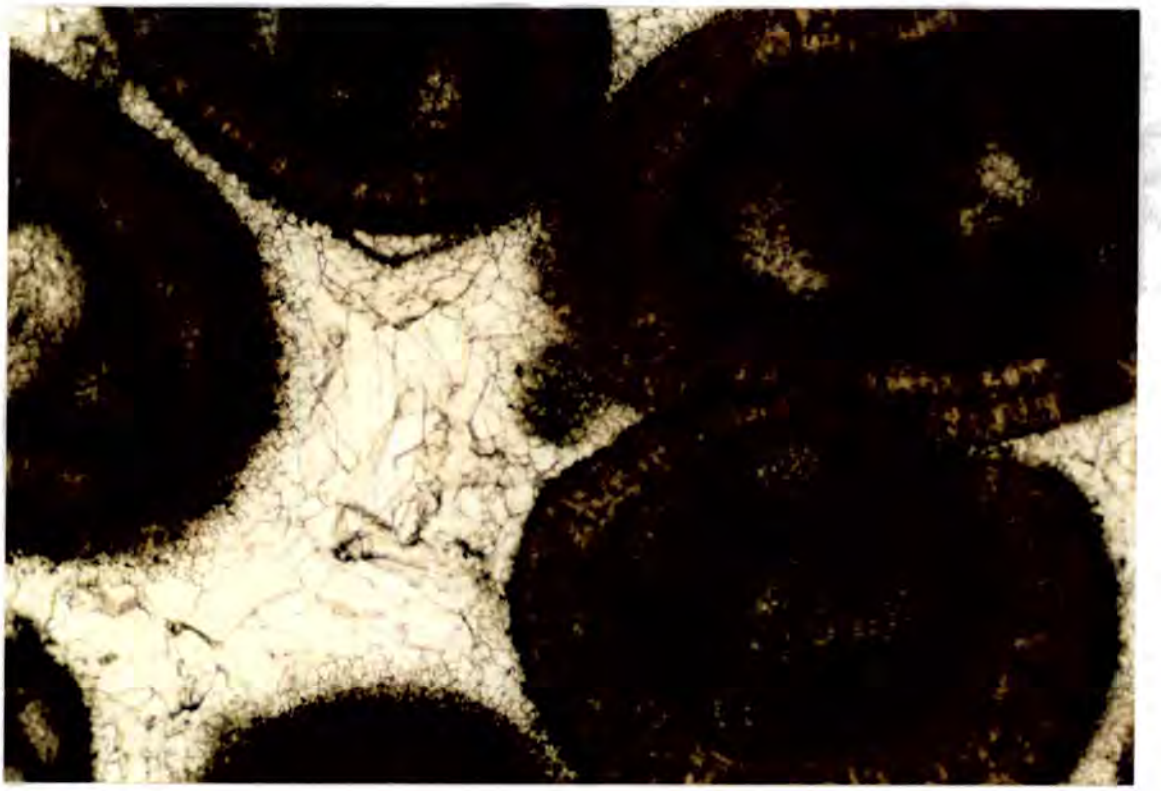

Fig. 3.16b

Fractured and collapsed micritic envelopes (see Fig. 3.17b) are a relatively common feature of the shelf-lagoon facies where partial to total shell dissolution has occurred (see section 3.9.5). Broken envelopes are most clearly seen where the envelope formerly lined the inner wall of the former body chamber wall (micritic envelopes are just as common on the outer shell wall, see section 3.7 and Fig. 3.6, but are less likely to be fractured unless total shell dissolution has occurred). With the removal of the inner part of the shell wall the relatively fragile envelopes would become susceptible to fracture. If, as suggested in section 3.9.5, the dissolution of the rudist shells was an early event, then potentially this fracture and collapse of the micritic envelopes could occur as soon as there is the slightest overburden, aided by dewatering and the mechanical re-orientation of adjacent grains. This is in line with the conclusions of Meyers (1980) from petrographic studies and Shinn & Robbin (1983) from the laboratory compaction of cores from modern marine environments. Internal sediment within the rudist body chamber has also been fractured (see Fig. 3.17c). Presumably the more rigid preserved rudist shells required a greater

amount of stress (from burial) to fracture, as in Fig. 3.14a, 3.14b and 3.15a, and so occurred in a slightly deeper burial setting.

Fig. 3.17 Photomicrographs of various features of mechanical fracturing within the Urgonian. **(a)** Elephantine structure. 365/90, Dents d' Arclusaz, Bauges. Field of view= 1.5mm **(b)** Collapsed and fractured micritic envelopes (arrowed) and a fractured rudist shell (s). 172/89, Moucherotte, Vercors. Field of view= 13mm. **(c)** Fractured internal sediments within the former body cavity of a rudist. 14/89, Dents de Crolles, Chartreuse. Field of view= 4mm. Opposite page for 3.17b and 3.17c.

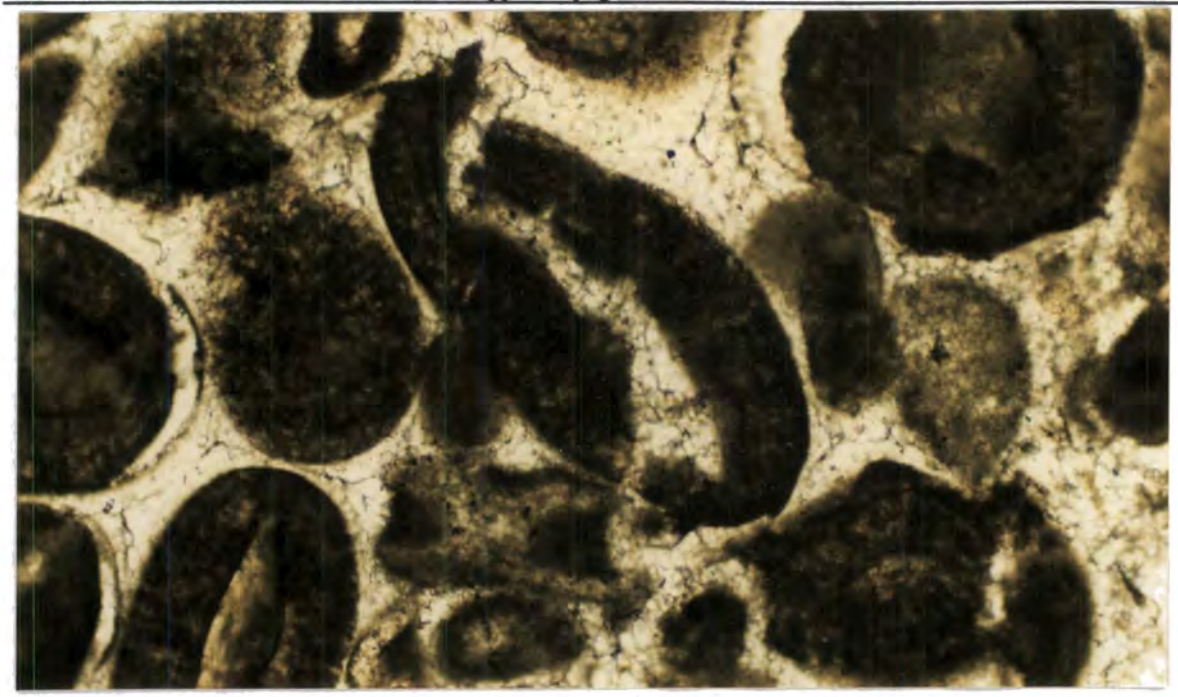

Fig. 3.17a

Fig. 3.17b

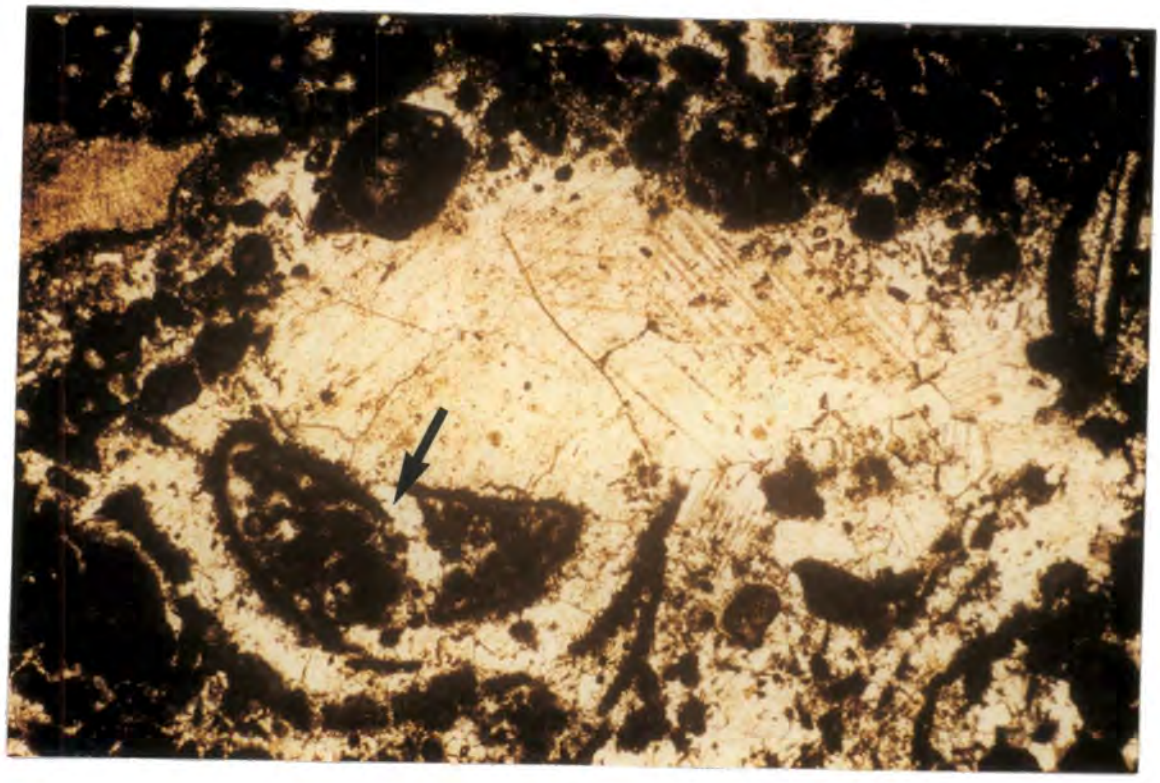

Fig. 3.17c

3.11 Later cement generations within the Urgonian.

Several other cement types can be seen within the Urgonian. Each cement type is described and interpreted as regards its possible environment of formation.

3.11.1 Methods of 'dating' cement generations.

The relative order of precipitation of cement generations can be deduced from their relationship to other diagenetic features. Essentially this comes down to deciding whether cements pre- or post- date features ascribed to forming from burial compaction (either mechanical or chemical), such as stylolites, microstylolites, compactive fractures, and hydrocarbons and their alteration products (Scholle & Halley, 1985; Choquette & James, 1987). Fig. 3.18 shows several features which can be used to date cements.

3.11.2 Syntaxial overgrowth cements.

3.11.2 (a) Description.

These enclose echinoderm grains and are typified by single, large (usually several mm in width and length) calcite crystals in optical continuity with the grain. Their often relatively large size reflects the size of the grain upon which they have nucleated, which has point contacts with the surrounding grains (see Figs 3.19a, 3.19b and 3.20b). The inner portion of the cement (nearest to the grain) is usually quite cloudy in appearance due to the

presence of inclusions. The youngest parts of these cement crystals (i.e. furthest away from the grain surface) are generally clear and may heal mechanical fractures or occlude compaction reduced porosity (see Fig. 3.19b). Typically they are non-ferroan, although in a few samples ferroan calcite was seen.

Fig. 3.18 Cross-cutting relationships that can be used to place diagenetic features in a relative time ordering and assign them to being burial in origin.

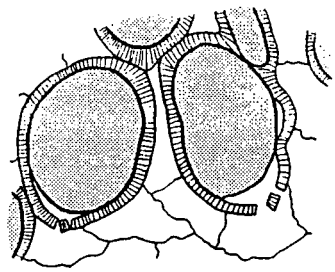

① SPAR HEALS BROKEN RIM OF EARLY CEMENT

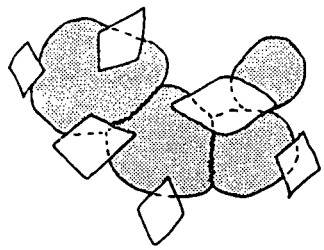

② DOLOMITE POST-DATES MECHANICAL COMPACTION AND/OR PRESSURE DISSOLUTION

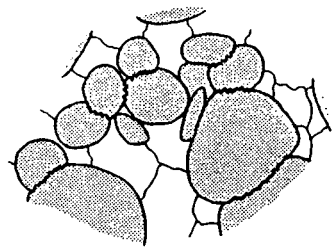

③ SPAR POSTDATES MICROSTYLOLITE FORMATION

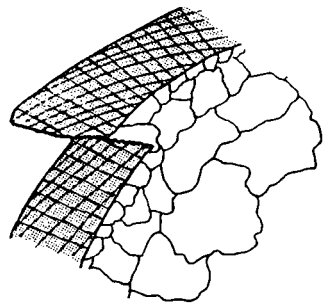

④ SPAR HEALS BROKEN BIOCLASTS AND/OR MICRITIC ENVELOPES

Often these cements show a zoning in CL of one or more bright orange bands, with a first non-luminescent generation of variable width, followed by one or more thin (40-60 micron width) bright orange bands, which are enclosed in non-luminescent to dull orange areas (see Fig. 3.20a & Fig. 3.20b). In other instances the cement is totally non-luminescent.

Fig. 3.19a Syntaxial cement covering a echinoderm grain which only has a point contact with the adjacent grain (XPL). **Fig. 3.19b** The same view in PPL, the outer part of syntaxial cement can be seen to 'heal' fractured marine cements (black arrows). Some of the non-echinoderm grains have sutured contacts (white arrow). 288/90 Croix du Nivolet, Bauges. Field of view= 3.25mm. See opposite page.

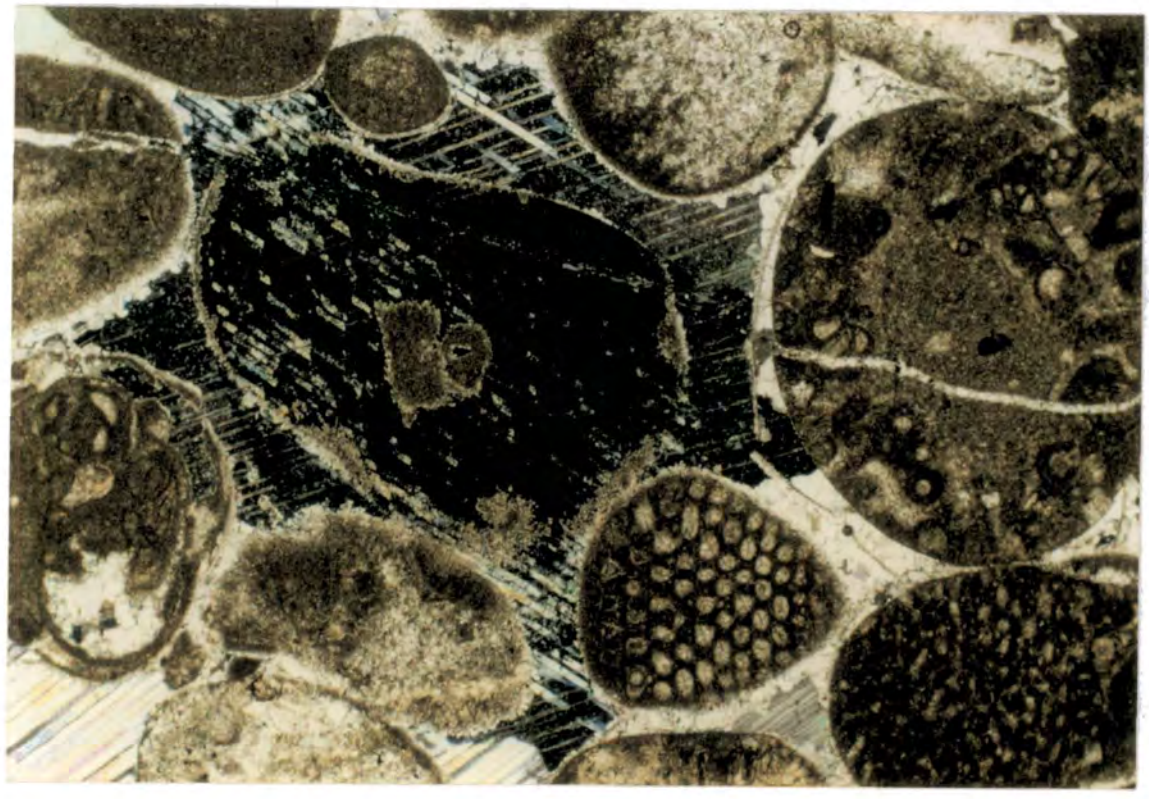

Fig. 3.19a

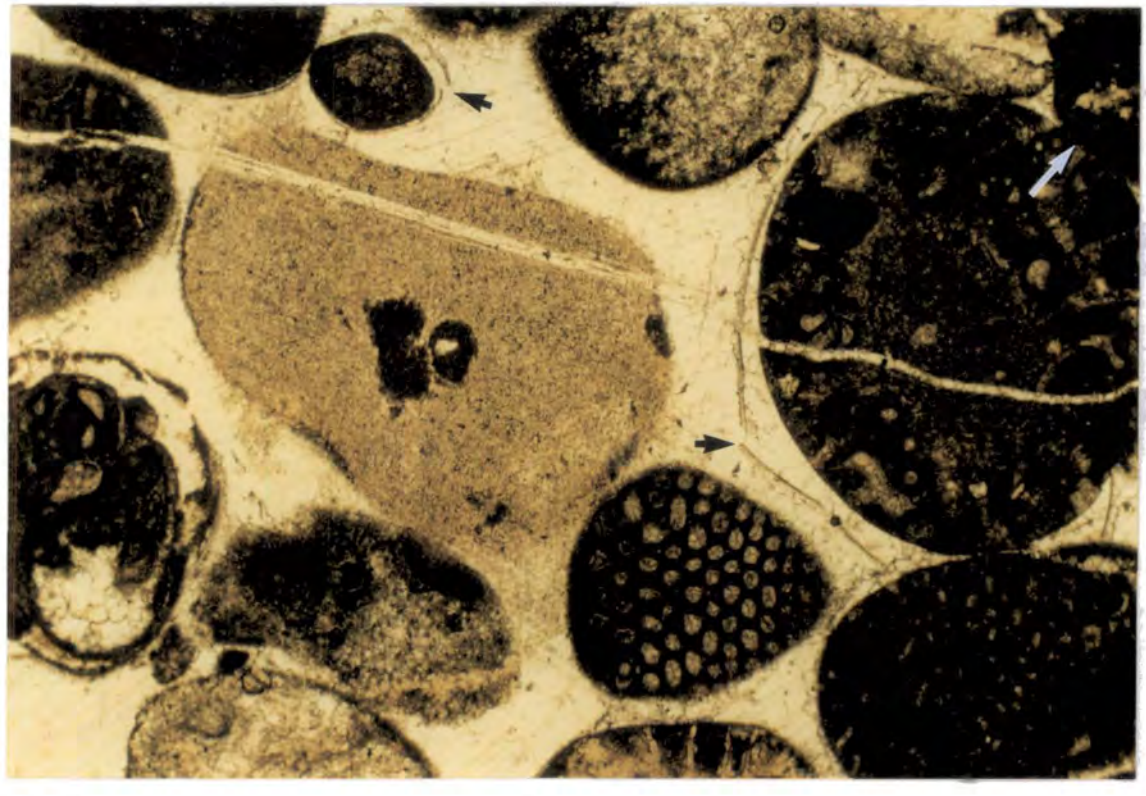

Fig. 3.19b

Fig. 3.20a CL shot of a zoned syntaxial cement. **Fig. 3.20b** PPL shot of the same field of view as Fig. 3.20a. 1/91, Grande Goulets, Vercors. Field of view= 4mm.

Fig. 3.20a

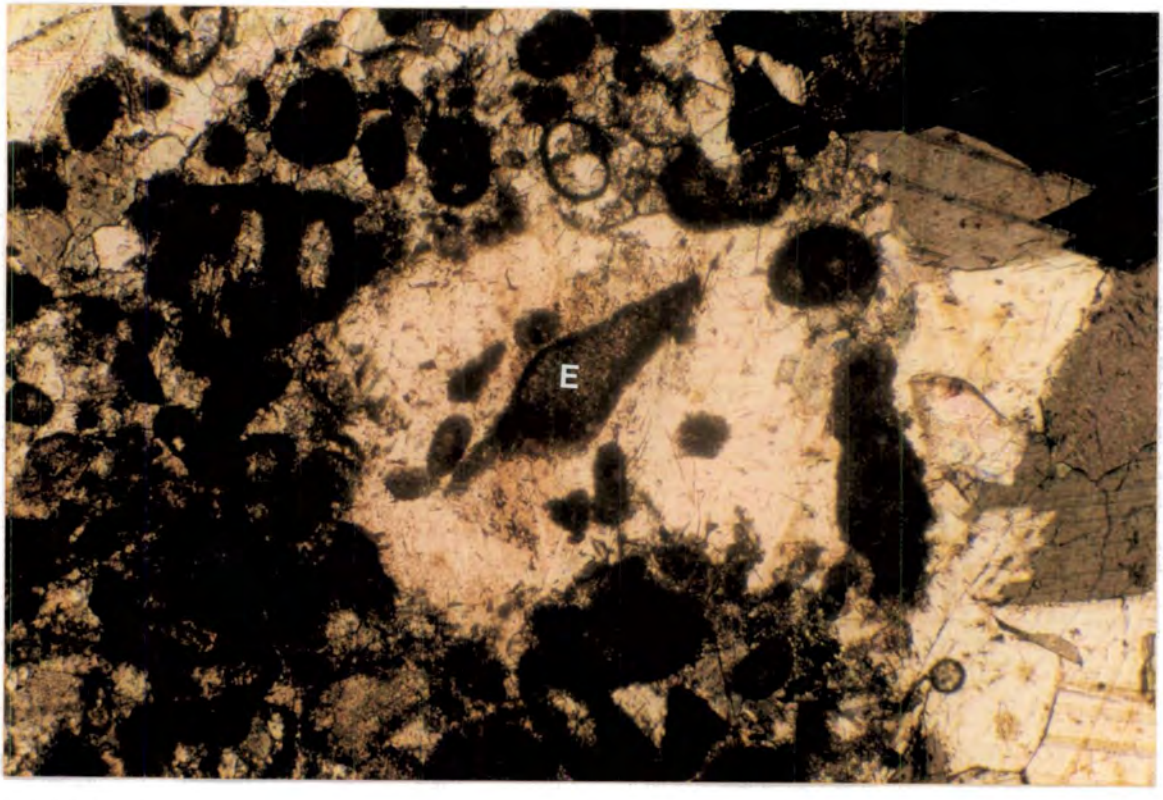

Fig. 3.20b

3.11.2 (b) Interpretation.

These features would seem to suggest that at least the earliest part of these syntaxial overgrowths began to precipitate relatively soon after deposition, even whilst the rock was still in the marine phreatic environment. This initial growth stage would have then provided a nucleation site for the precipitation of the rest of the overgrowth in either a meteoric phreatic or burial environment. The rapid growth of such cements may be aided by the fact that the echinoderm grain is made up of a single large crystal. Overgrowth cements similar to these have often been ascribed to be meteoric cements. Meyers & Lohmann (1978) offered that similar cements in Mississippian limestones of New Mexico were marine and marine-meteoric mixing-zone in origin. This idea was partly based on the presence of microdolomite rims within the earliest part of the syntaxial overgrowth. Repeated bright orange crystal growth zonations seen under CL would seem to support a meteoric origin at least for at least part of these cements, since the first CL zone is non-luminescent, which suggests oxidising porefluids and the following bright orange zone indicates that the porefluids had become reducing. These reducing conditions could have been brought about by the stagnation of porefluids. Repeated non-luminescent calcite zones could then indicate brief periods of influx of fresh meteoric waters, so that the pore fluids became oxidising, precipitating a non-luminescent cement zone (Grover & Read, 1983; Dorobek, 1987; Mussman et al., 1988; Niemann & Read, 1988). These sort of conditions are typical of shallow burial phreatic environments where freshwater recharge to the aquifer could occur sporadically. A single bright orange zone probably represents stagnation of porewaters, as the rock becomes buried (Grover & Read, 1983; Choquette & James, 1987). In instances where the cement is non-luminescent and non-ferroan it suggests that there was no source of either Fe^{2+} or Mn^{2+} or both within the system.

These cements are interpreted to have formed at least partly in a marine/meteoric setting but also partly in a burial environment as the youngest part of the cement post-dates fractures (see Fig. 3.19b)

3.11.3 Drusy mosaic, equant spar cements.

3.11.3 (a) Description.

This is a coarse, normally non-ferroan (although some may contain ferroan zones) cement which occurs in three main pore types: (1) primary and secondary porosity associated with rudist body chambers and shell dissolution; (2) areas of dissolution within coralline organisms and (3) fenestral porosity and keystone vugs. Individual crystals can be up to several millimetres across. These various pore types occur in different facies of the Urgonian, from shelf-margin coral grainstones and boundstones to supratidal wackestones but predominantly in the true Urgonian facies shelf-lagoon limestones. As equant spars are believed to form in a range of diagenetic environments (Wilson et al., 1983; James & Choquette, 1984; Choquette & James, 1987), this cement is described individually from

each pore space association (since these pore spaces occur within different facies across the platform).

Drusy mosaic simply refers to the cement fabric of crystal size increasing towards the centre of the pore. Equant shape implies that the crystals of the same generation are a similar shape and size.

3.11.3 (b) Petrography of equant spar associated with rudists.

Dissolution of rudistid bivalve shells was a common feature of the Urgonian (see section 3.9.2). Primary and secondary porosity associated with rudists is occluded by an equant, drusy mosaic calcite cement (see Figs 3.11a, 3.11b, 3.17b, 3.17c, 3.21, 3.22a and 3.22b). They can be clearly seen to post-date the mechanical fracture of unsupported micritic envelopes (see Fig. 3.19d) and the fracture of rudist shells (see Fig. 3.14a, 3.14ba and 3.15b). The earliest generation of this cement also fills the fractures which cut through rudist shells and is described in section 3.9.4 (see Figs 3.17a and 3.17b).

Fig. 3.21 Drusy calcite cements (S) infilling primary and secondary bio-moldic porosity associated with rudists (R). The shells have been partially to totally removed by meteoric dissolution (see section 3.9.2). Looking down onto a bedding surface, mid-Urgonian, Pointé Perceé, Aravis, Finger for scale.

3.11.3 (c) Cement versus neomorphic origin for the equant spar in pore spaces associated with rudists.

Sparry calcite associated with rudists occurs within areas of inferred aragonite rudist shell dissolution and the distinction between cement and neomorphic spar is critical.

If neomorphic spar after aragonite were present in these areas it would suggest a different diagenetic process (especially regarding porosity evolution and compaction - see Bathurst, 1983) and a different fluid flow history and this would require a modification of the interpretation of the geochemical analysis of these areas given in sections 4.5 and 4.6.
Criteria for the recognition of cements within rudist associated pore spaces in the Urgonian are listed below:-
1) spar occurs within both inter- and intra- granular pore spaces and in particular within non-rudist associated inter-granular pore spaces,
2) two or more generations of spar exist (often this is only discernable under CL),
3) micritised peloids and foraminifera are not altered to microspar, neither are micritic envelopes,
4) no relic structures of shells occur within the spar when viewed under transmitted light or CL and the area is relatively free of inclusions,
5) contact between spar and particles is sharp, although this may be slightly obscured by the fact that some of the crystals have nucleated on the crystals of the shell epitaxially (or syntaxially),
6) the initial substrate of spar crystals coincides with former free surfaces of particles or mold walls,
7) spar occupies the upper parts of unfilled geopetal structures,
8) spar has a pore filling form, i.e. similar to pore-filling cements recognised from modern day environments and description of cements in other limestones in the literature,
9) size of crystals increases away from the initial substrate, i.e. it displays a drusy fabric,
10) neomorphic fabrics are absent,
11) intercrystalline boundaries are made up of plane interfaces,
12) enfacial junctions are common,
These criteria were not (and should not be) applied individually, since taken in isolation some of them are not indicative of cements (especially 11 and 12), see Dickson, 1983). In some instances this cement does not have an equant shape; this is because the crystals have syntaxially nucleated upon the dLMC crystals of the adjacent rudist shell wall.
All these features are illustrated in Figs. 3.11a, 3.11b, 3.15a, 3.17b, 3.17c, 3.22a, 3.22b and 3.23b.

3.11.3 (d) CL petrography of the rudist associated drusy spar.

The CL response of the majority of these cements is shown in Figs 3.23a, 3.23b and 3.23c. The oldest part of the cement is typically non-luminescent followed by a bright orange band defining a scalenohedral shape (see Fig. 3.23a), which may be impersistent. This may be succeeded by subsequent less bright bands of very dull orange which parallel the outline of the first or non-luminescent calcite. In a few other instances the first non-

luminescent zone passes into a uniform dull orange band followed by vague zones defined by very slightly variable shades of dull orange without any bright orange band.

Fig. 3.22a Drusy calcite cement (C) infilling secondary porosity associated with a rudist. Part of the shell is still preserved (S). Crystal silt (?vadose) has settled on the bottom of the pore space prior to cementation. 86/91, Gorge du Frou, Chartreuse. Field of view= 13mm. **Fig. 3.22b** (opposite page). Drusy calcite spar infilling secondary intra- granular porosity (the former position of the inner shell wall is shown by the micrite envelope (arrowed)) and inter-granular porosity associated with internal sediments within the body cavity of the chamber. 226/90, Moucherotte, Vercors. Field of view= 3.25mm. R=Rudist IS=Internal sediment

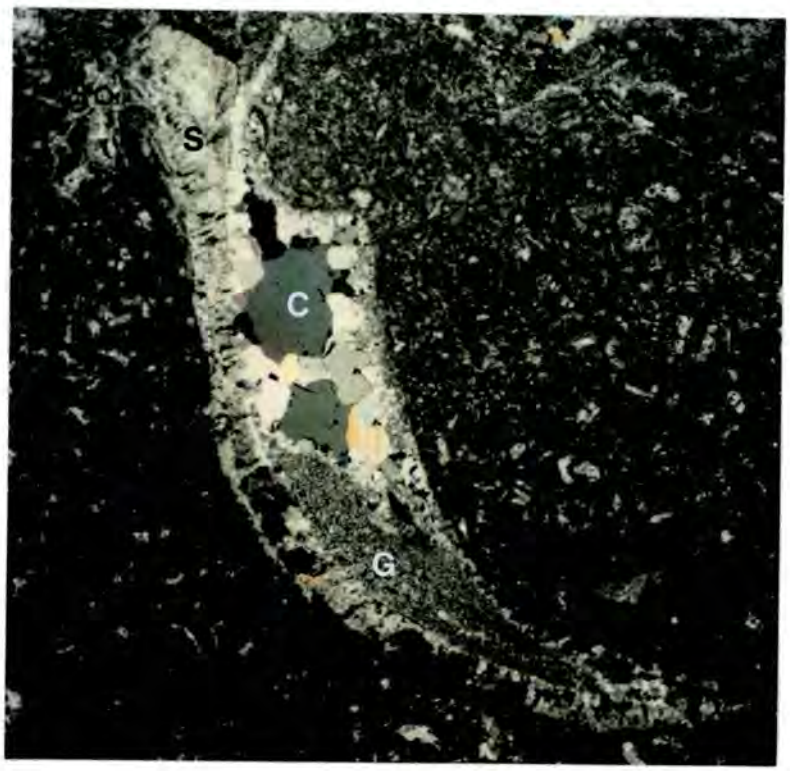

This non-luminescent - bright orange - dull orange/non-luminescent zonation appears to be quite common in limestones (Frank et al., 1982; Grover & Read, 1983; Choquette & James, 1987: Tucker & Wright, 1990) and is usually ascribed to cements precipitated in a burial setting, with the pore-fluids becoming increasingly reducing in nature. The initial non-luminescent zone coincides with pore-wall lining phreatic cements (may be marine and/or early burial in origin), precipitated from oxidising fluids (positive Eh); in which Mn^{2+} and Fe^{2+} would not be available for incorporation into any precipitates. The succeeding bright orange band(s) suggests the permanent onset of reducing conditions, so conditions are suitable for Mn^{2+} and Fe^{2+} ions to occur within the porefluid (if available).

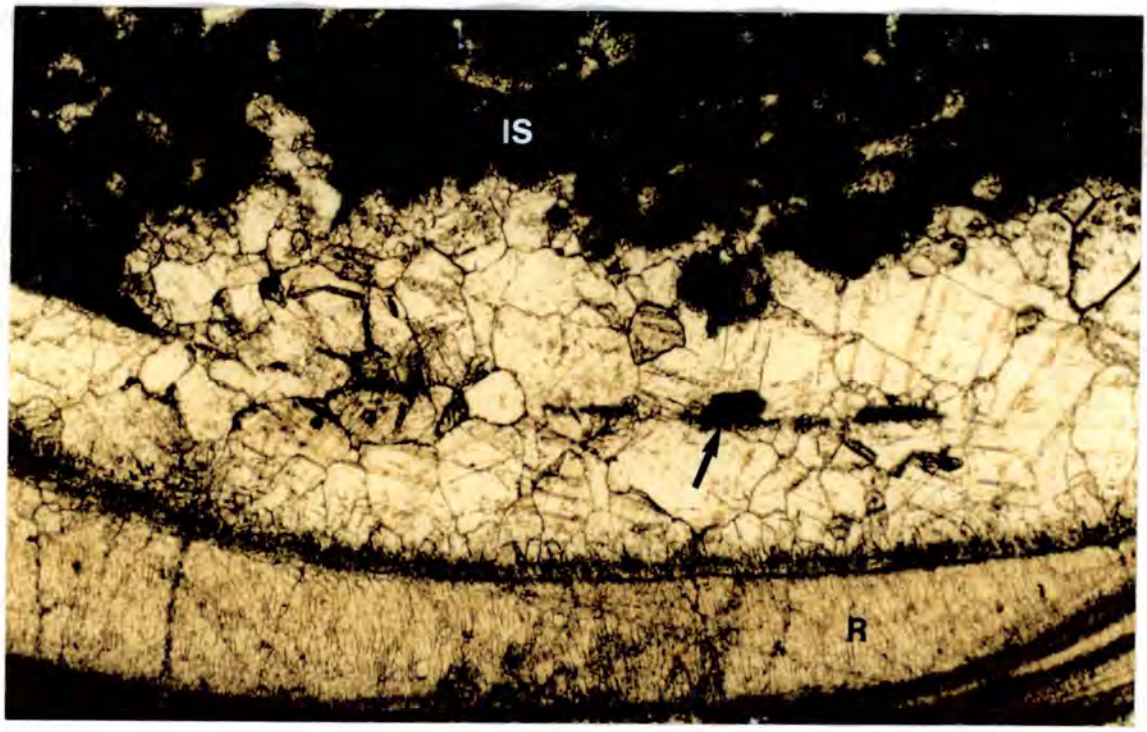

Fig. 3.22b

The final dull or non-luminescent area suggests precipitation of an increasingly more iron-rich cement. However, staining with Alizarin Red-S and potassium ferricyanide showed the bulk of these cements to be non-ferroan, so possibly this final zone simply represents precipitation from fluids with an insufficient ratio of Mn^{2+} to Fe^{2+} to precipitate luminescent cements (Hemming et al., 1987).

3.11.3 (e) Petrography of equant spar occluding areas of dissolution in corals.

Petrographically this is very similar to the spar within areas of rudist shell dissolution. However, often these cements are ferroan or possess a ferroan zone in the outer extremity of the spar crystal. These cements can be seen to heal broken pieces of micritised coralline framework (see Fig. 3.13).

Under CL they have a very vague and indistinct zonation of scalenohedral shapes defined by slight variations in the general dull orange colour of the cements. The response is similar to the final area of cement filling porosity associated with rudists. This does not imply that both are synchronous in the timing of their formation, but merely that they precipitated from fluids of similar trace element composition.

Fig. 3.23a CL shot of equant cements associated with rudists. **Fig. 3.23b** PPL shot of the same field of view as Fig. 3.23a. The calcite crystals of the cement have grown epitaxially upon the shell. 456/90, La Clusaz, Aravis. Field fo view= 4mm. **Fig. 3.23c** (opposite page). Line drawing interpretation of Fig. 3.23a.

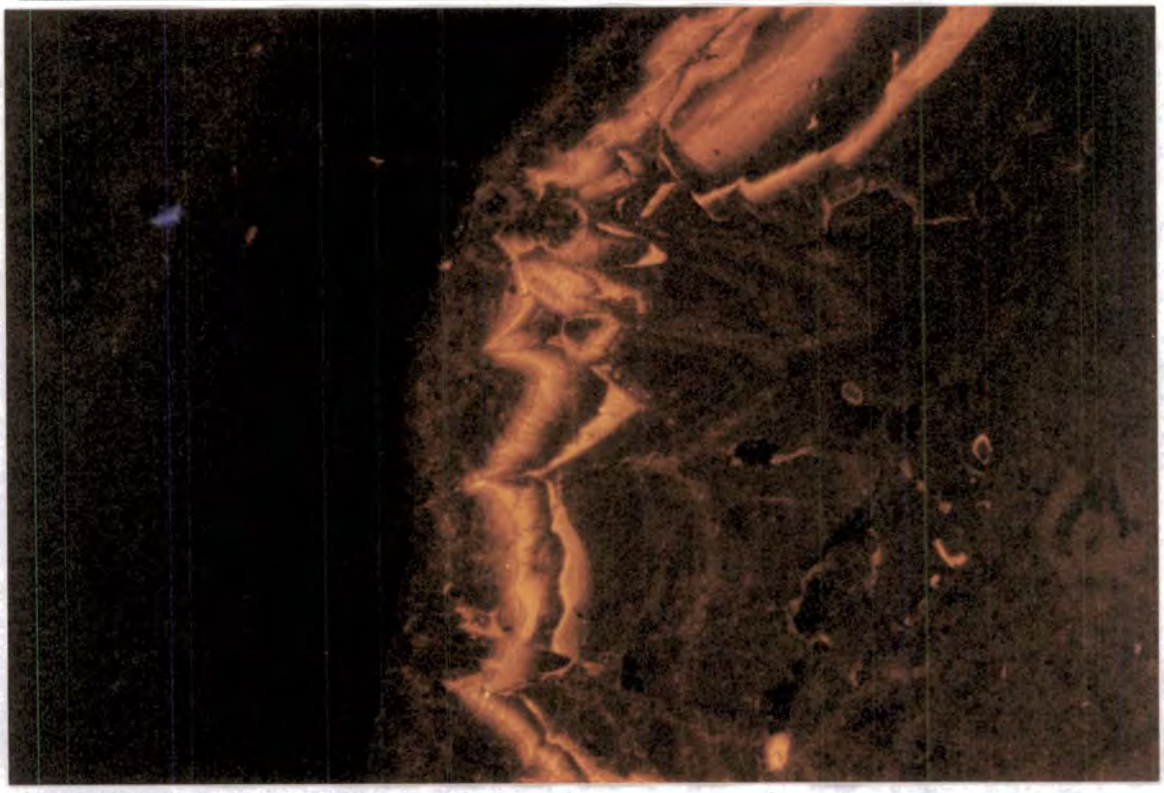

Fig. 3.23a

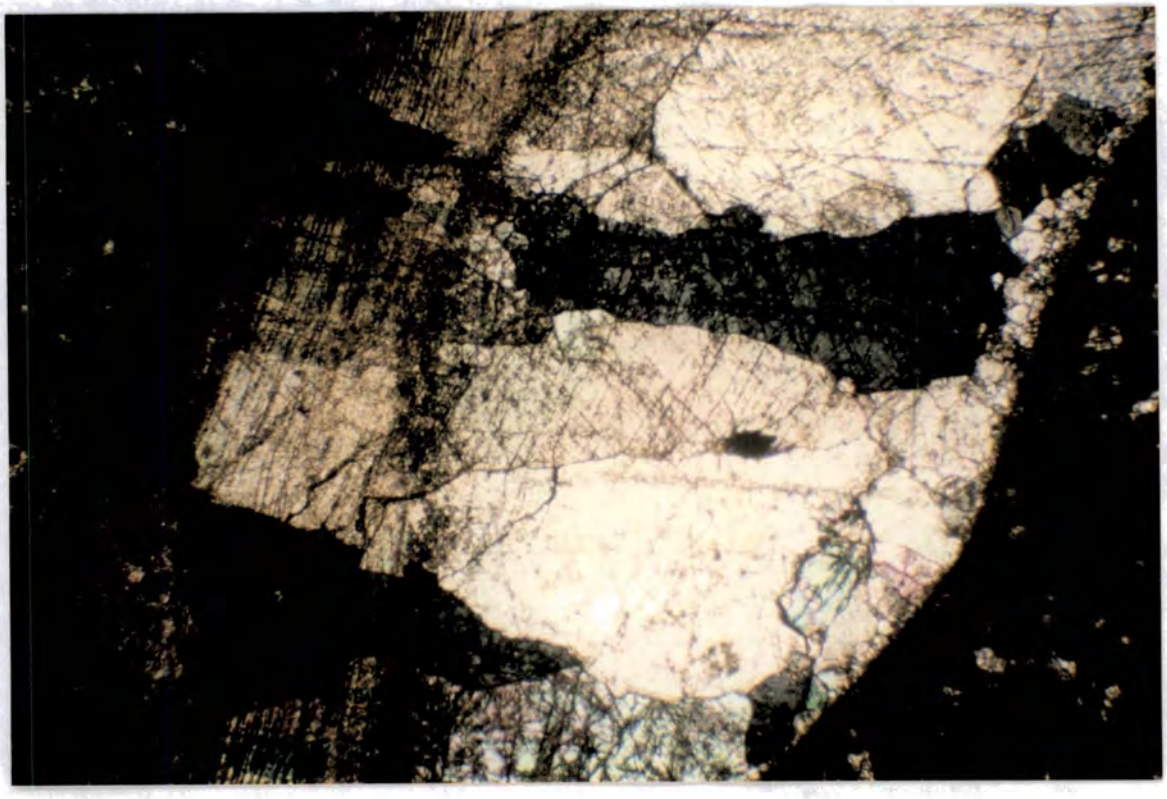

Fig. 3.23b

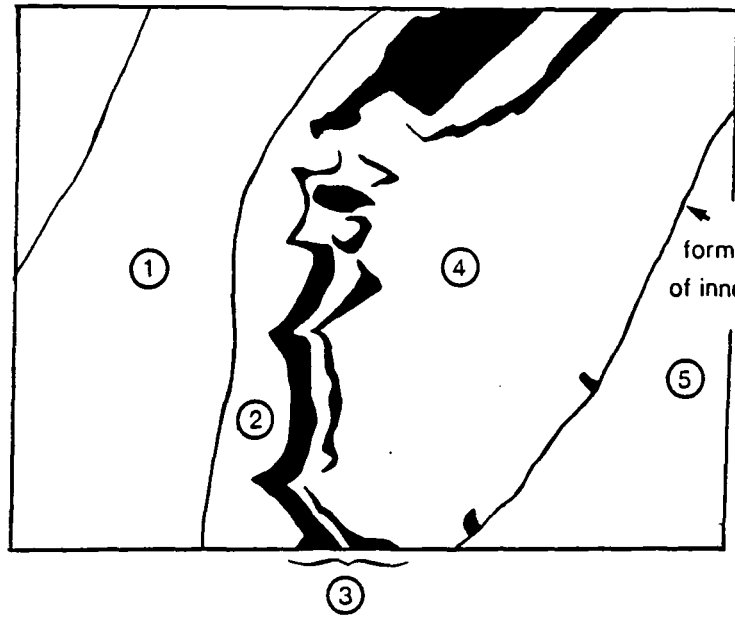

1= non-luminescent shell material

2= initial cement, uniform dull orange (may also be non-luminescent)

3= zoned BO/NL/BO cement

4= vague zones in DO passing out into non-luminescent area

5= former body cavity filled by sediment

Fig. 3.23c

3.11.3 (f) Petrography of equant spar occluding fenestral porosity and keystone vugs.

Coarse equant spar commonly occludes at least the central part of these pore spaces, which in many cases has an earlier marine cement as the first cement generation (see Figs 3.7a and 3.24a). However, within some keystone vugs they were the only cement generation. Again this spar has the same morphology to the two occurrences of spar described above.

These cements are difficult to place in a relative order using the methods described in section 3.11.1 and Fig. 3.18. This is because there is a paucity of any burial diagenetic features (such as fractured grains) near to these cements, although they are bounded by stylolites in several instances. However, as discussed in section 3.11.4 these pervasive compaction features may be of less use to date cement generations.

Under CL, the response of these cements was variable, from uniform dull orange to non-luminescent - bright orange- dull orange zonation similar to that seen in the cements associated with rudist porosity.This does not imply that both are synchronous but merely they precipitated from fluids of similar composition. Again, this does not imply that both formed diachronously, but merely they precipitated from fluids of similar trace element composition.

Fig. 3.24a Equant cement occluding fenestral porosity. 584/90, Termine road section (upper road), Bornes. Field of view= 13mm. From the upper section of the platform of Villaret Rouge road section (see section 3.8.5), Bauges. **Fig. 3.24b** (opposite page). Stylolite (arrowed) cross-cutting drusy calcite cement infilling porosity associated with a rudist (R). 309/90, Col d'Encrenaz, Bornes. Field of view= 13mm.

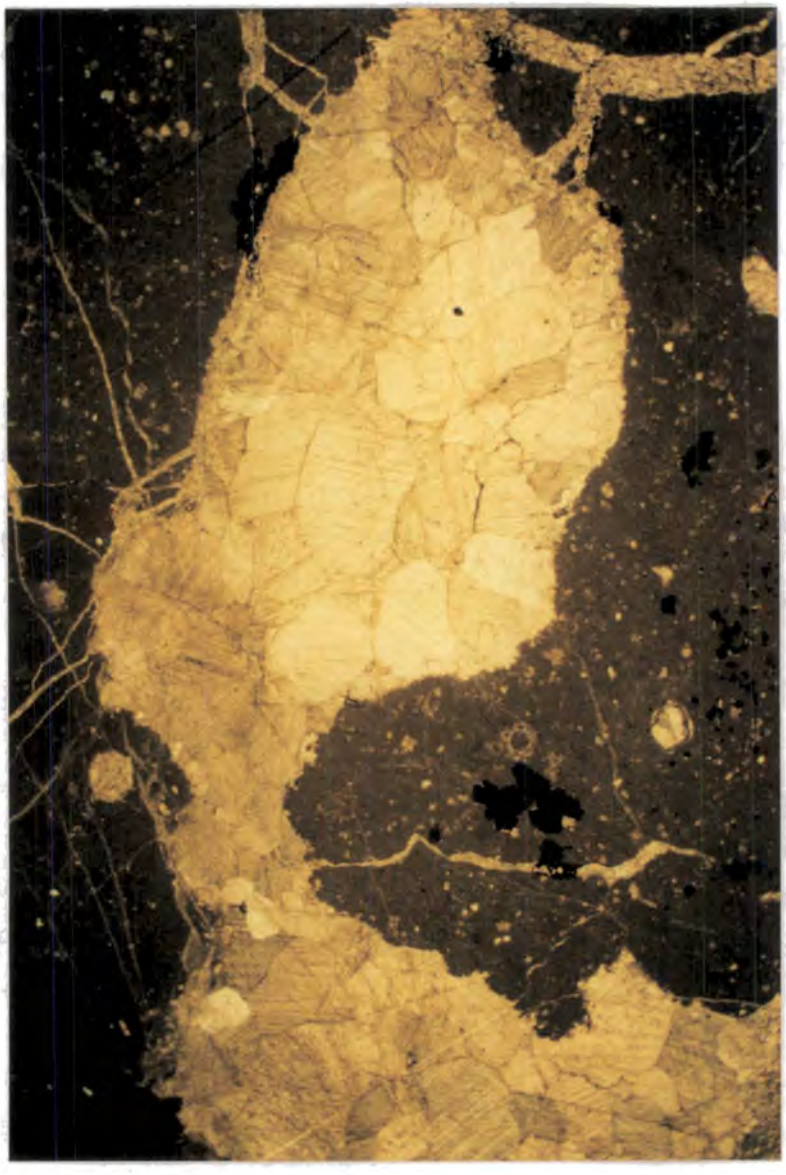

Fig. 3.24a

3.11.3 (g) Interpretation of equant, drusy mosaic cements.

From the above descriptions it is suggested that the three occurrences of drusy mosaic, formed in a similar setting. They have the same petrographic relationships to burial diagenetic features (with the exception of equant spar associated with fenestrae and keystones, see 3.11.3 (c) above) within the Urgonian, similar CL response and the same morphology (their geochemistry is also similar; this is discussed in sections 4.4 and 4.5).

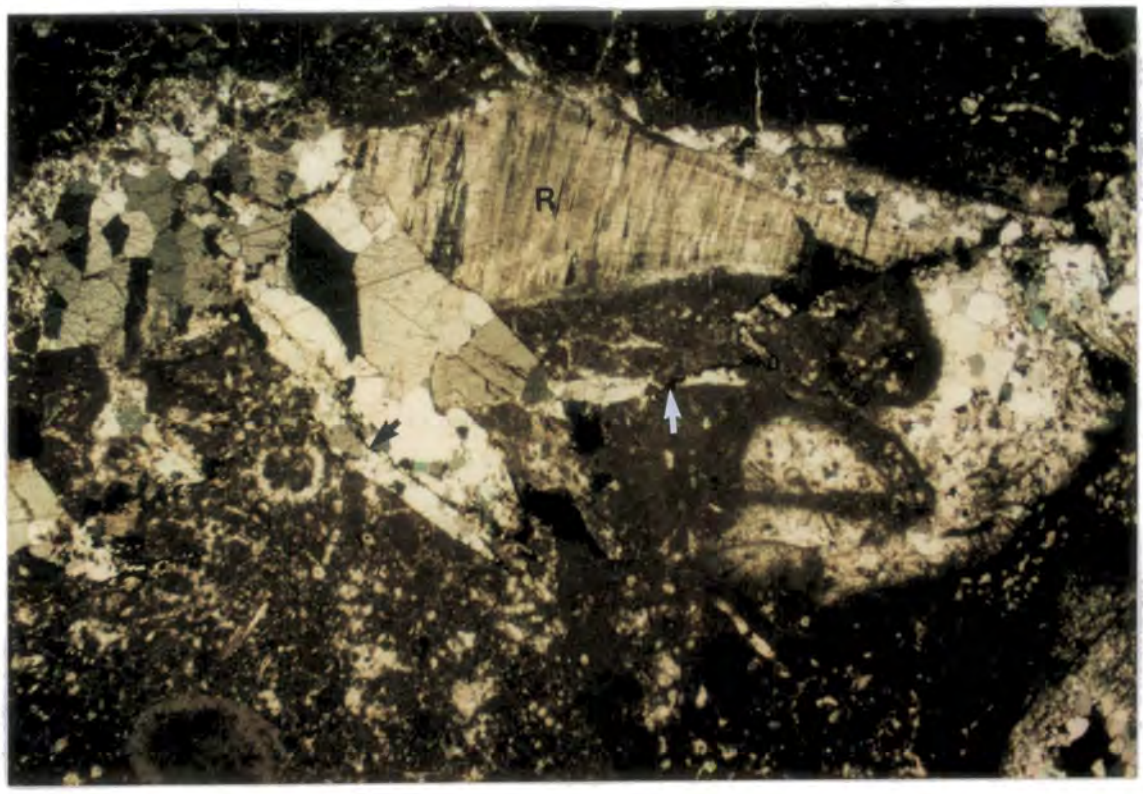

Fig. 3.24b

These cements are interpreted from their petrography to have formed post-mechanical fracture but pre- any significant chemical compaction (see section 3.11.4). Ascertaining the environment that these cements formed in from their petrography alone is problematical since their morphology is not distinctive of one diagenetic environment. However, from the relationship of the cements to burial diagenetic features it is likely that they formed whilst the Urgonian was at a burial depth of 10 to near 300 metres. The origin of the porefluids responsible for the precipitation of these cements is discussed further in the following chapter (see sections 4.4 and 4.5).

3.11.4 Relationship of the syntaxial and equant calcite spar cements to more pervasive features of chemical compaction.

These cements, although quite clearly post-date mechanical fracture and localised (grain to grain) dissolution features, are themselves quite clearly post-dated by a later more pervasive pressure dissolution, which is typically manifested by stylolites (sutured seams), cutting (apparently) indiscriminately across through the rock fabric (see Fig. 3.24b). These are typical of clean (mud free) limestones with structurally resistant elements (Wanless, 1979; Bathurst, 1987).

Chemical compaction by stylolitization is usually inferred to occur "***within the first few hundred metres of burial***" (Choquette & James, 1987), although Bathurst (1980) quoted

a figure of 300m for the onset of chemical compaction. Depth is not the only control on pressure dissolution: temperature, grain size, pore water composition, mineralogy, clay minerals, early dolomitization and the presence of liquid hydrocarbons can all influence pressure dissolution (Feazel & Schatzinger, 1985; Choquette & James, 1987). Stylolitization of the Urgonian is also not likely to be simply a response to burial depth since the area has been involved with deformation associated with the Alpine orogeny (see section 2.6). Tectonic stresses associated with this period of folding and thrusting in some instances have led to the formation of uniformly spaced dissolution cleavage similar to that described by Mitra et al.(1984), Marshak & Engelder (1985), Hancock (1985) and Price & Cosgrove (1990). This style of deformation is believed to be dependent on the presence of clays, between grain and crystal boundaries (Marshak & Engelder, 1985; Price & Cosgrove, 1990). Spaced cleavage is more common in more muddier limestones (such as the Tithonian) than in the Urgonian limestones in the Subalpine Chains. However, this does not mean that tectonic-induced pressure dissolution did not occur within the Urgonian. In reality it is likely to have been quite widespread, particularly where the Urgonian has been folded so that it has a vertical orientation (e.g. the forelimbs of hanging wall anticlines). With maximum principal stress ($\sigma 1$) orientated horizontally (perpendicular to the bedding and any previously burial-induced stylolites) thus facilitating further pressure dissolution along previously formed stylolites and the formation of new ones (the evidence for this is discussed further in section 5.3). Thus in areas such as the Subalpine Chains using stylolites as a means to date other diagenetic features requires extra caution as they are not solely the product of burial induced stresses.

3.11.5 Conclusions concerning the calcite cementation of the Urgonian.

1) Coarse equant, drusy calcite cements occlude a variety of primary and secondary pore spaces within the Urgonian.

2) Regardless of the location of the pore space occluded, the cement has similar petrographic relationship to burial diagenetic features, CL response and cement morphology and so can be said to be of the same generation, despite the fact that it occurs in rocks of very different facies across the platform.

3) Petrographically these cements are what are usually referred to as burial cements, although it is likely that their formation was at a relatively shallow burial depth. However, even though these are burial cements it does not necessarily mean they were precipitated from burial fluids (this point is discussed further in sections 4.4 and 4.5). The fluids may also have been of meteoric or marine origin.

3.12 Replacive and cement dolomites within the Urgonian.

Dolomite occurs in two stratigraphically distinct levels within the Urgonian. The volumetrically most important dolomite type within the Urgonian is a replacive, often sucrosic dolomite seen within the basal section of the platform. The other is found close to the uppermost surface of the Urgonian and is associated with transgressive surfaces and karst horizons. The latter of the two is discussed first.

3.12.1 Dolomitization associated with transgressive and micro-karst surfaces within the upper part of the Urgonian.

3.12.1 (a) Field description.

This dolomite has a very restricted occurrence; it is present infilling irregular millimetre to centimetre scale dissolution features upon the upper surface of the Urgonian (see Fig. 3.25a) at certain localities. These dissolution features are both fabric selective (usually of rudist shells) and fabric non-selective (forming irregular vertical and horizontal pipes). It has a red to yellowy-orange colour and a sandy texture. Within the matrix green and darker coloured grains (glauconite and phosphate) are discernible. Clearly visible within the dolomitic areas also are clasts of the wall rock. Often, where rudist shells are not totally dissolved out, the shells are partially silicified (see Fig. 3.26). Regionally this surface is related to a lower Aptian sea-level fall and subaerial exposure of the platform.

3.12.1 (b) Petrography.

Typically this is a cloudy (solid inclusion rich), polymodal, microcrystalline dolomite (sizes range from 100 to 500 microns for individual rhombs; see Fig. 3.25b). The rhombs are euhedral and form idiotopic mosaics. Individual rhombs may have opaque coatings, interpreted to be ferruginous in nature. Where the dolomite does not completely fill the cavity it has an astropetal fabric, i.e. it is preferentially located on the floor of the cavity (see Fig. 3.26). In one such instance baroque (or saddle) dolomite has preferentially nucleated upon the dolomite on the floor of the pore space. Baroque dolomite precipitated in a cavity containing both oil and water may show a similar texture due to the bottom half of the pore being filled with water (Tucker & Wright, 1990). The rest of the pore has been occluded by a coarse, blocky calcite spar, which encloses fractured pieces of the baroque dolomite.

The microcrystalline dolomite (and the one instance of baroque dolomite) a uniform dull red/orange luminescence. The dolomite within these dissolution features can be seen to pre-date the earliest zoned (non-luminescent, bright orange) cements which occlude both primary inter- and intra- granular pore spaces and also secondary (fabric selective) pore spaces where they are not filled by the microcrystalline dolomite (see Figs 3.27a and 3.27b).

3.12.1 (c) Interpretation and diagenetic model of formation.

A karst was produced by a relative sea-level fall in the lower Aptian (immediately following the upper Orbitolina bed, Arnaud-Vanneau & Arnaud, 1990; Jacquin et al.,

Fig. 3.25a Slabbed hand sample of top Urgonian from Dent d'Arclusaz, Bauges, (see log #7, Appendix 1) displaying the effects of sub-aerial exposure and micro-karst formation. Rudist shells have been selectively dissolved out (RS), along with non-fabric selective dissolution (KS). The orange speckled infill to these dissolution cavities is a fine grained dolomitic matrix encasing grains of quartz, glauconite and phosphate. NERC studentship for scale. **Fig. 3.25b** Photomicrograph of karst related dolomite. DWH434/98, from the top of the Urgonian of the Chartreuse, sample courtesy of Dave Hunt. r= rudist shell, p= phosphatic grain; greenish grains are glauconite. Field of view= 2mm.

Fig. 3.25a

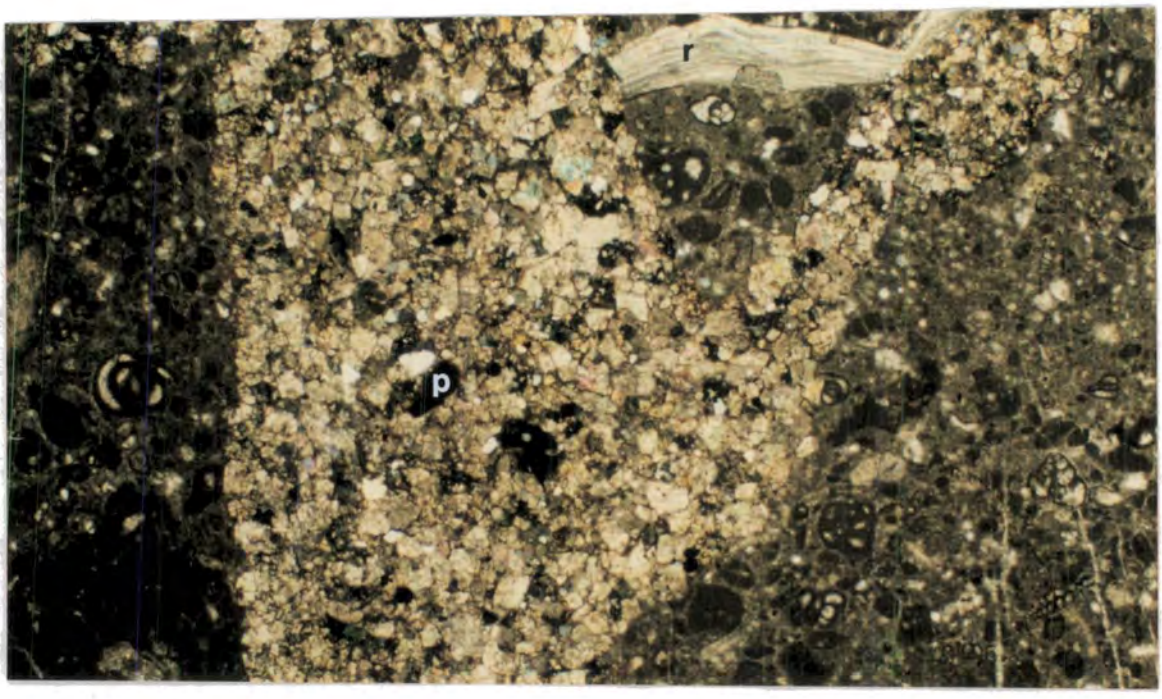

Fig. 3.25b

Fig. 3.26 Photomicrograph of microcrystalline dolomite in the bottom of karst-related dissolution cavity. 177/91, Dents d'Arclusaz, Bauges. Field of view= 13mm. C= ferroan calcite spar, d= microcrystalline dolomite, S= saddle dolomite; r= silicification of a rudist shell. Large black arrow gives way up.

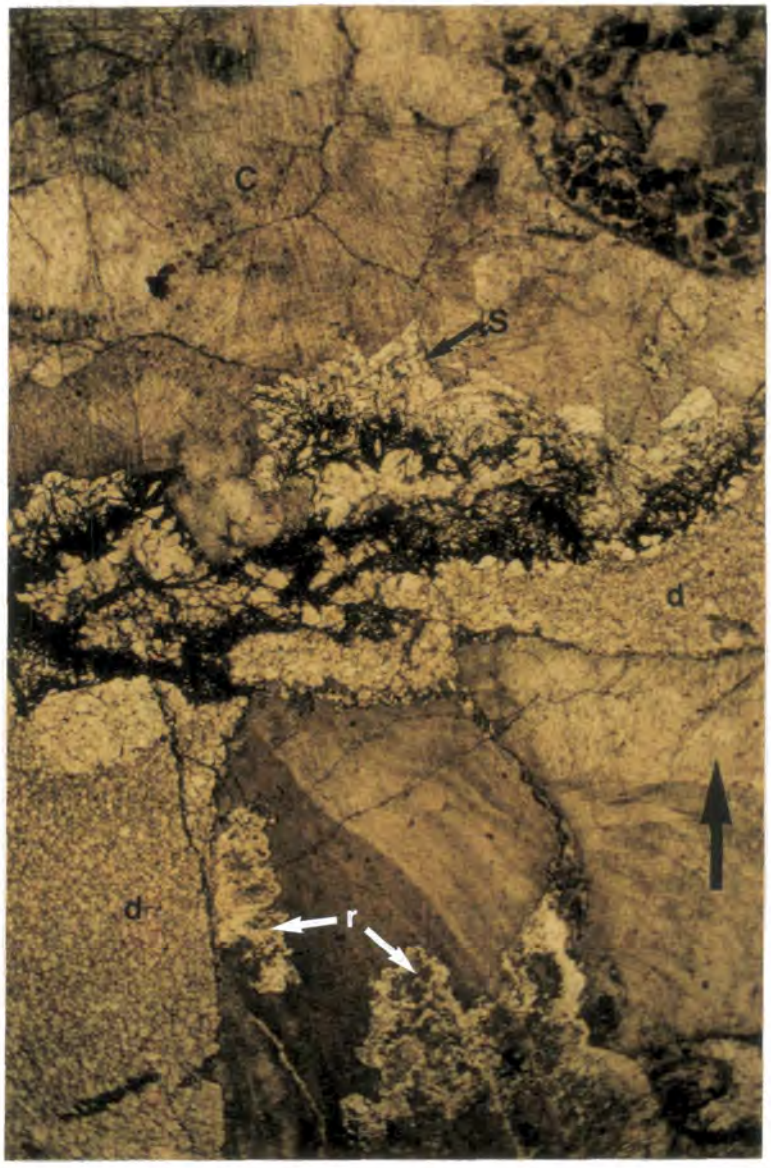

1991). The depth to which this karstification extends is minimal (two metres maximum). The Cretaceous climate is believed to have been generally semi-arid to arid in nature (Deconinck, 1984; Deconinck et al., 1985; Ruffel & Batten, 1990). Under such conditions meteoric diagenetic features such as karstification would be minimal and the surface produced can be referred to as a micro-karstic surface (James & Choquette, 1984; Choquette & James, 1988; Wright, 1988). Karst infill sediments and breccias were presumably composed of fine grained calcitic material derived from the host rock. This material was deposited inside the dissolution cavities enclosing clasts of the wall rock and had preferentially settled upon the base of the cavities first. With the following transgression siliciclastic detritus (quartz, glauconite and phosphatised grains) and

carbonate material from the erosion of the Urgonian, was deposited above the micro-karst surface and some was washed down into the dissolution features. With the renewed marine phreatic conditions and seawater being actively pumped through the upper surface of the sediment during the transgression, the calcitic karst infill was preferentially dolomitized. This would be aided by the presence of numerous nucleation sites and the fine grained nature of the inferred precursor sediments (Sibley & Gregg, 1987). A model for the formation of these dolomites is shown in Fig. 3.28.

Fig. 3.27a CL shot of the microcrystalline dolomite (d), saddle dolomite (s) and later calcite cement (c). **Fig. 3.27b** (opposite page). PPL shot of the same field of view as in Fig. 3.27a 177/91, Dents d'Arclusaz, Bauges. Field of view= 2mm.

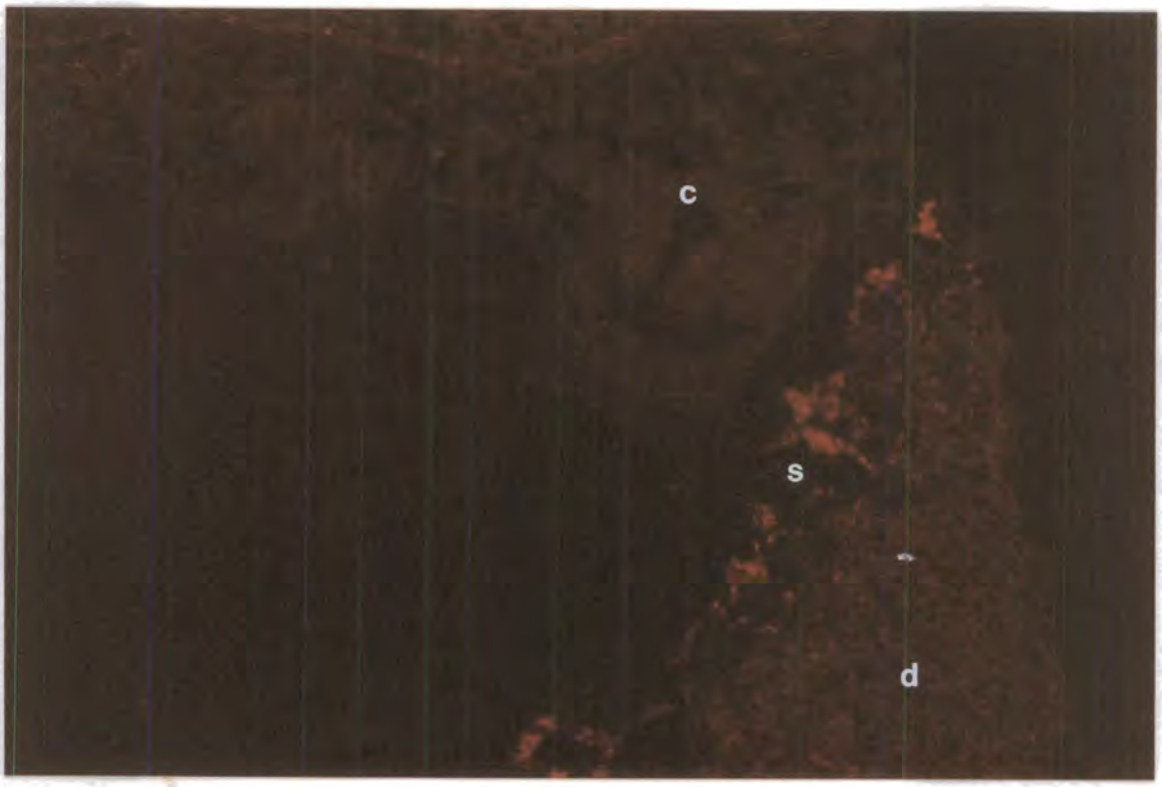

Fig. 3.27a

This style of dolomitization was not seen in association with any other exposure surfaces within the Urgonian. This could be due to overprinting and recrystallization with later dolomitization (see section 3.12.2) or possibly a reflection of the length of exposure associated with the formation of the micro-karstic upon the upper surface of the platform leading to greater production of calcitic infill. or more prolonged pumping of seawater through the top of the platform.

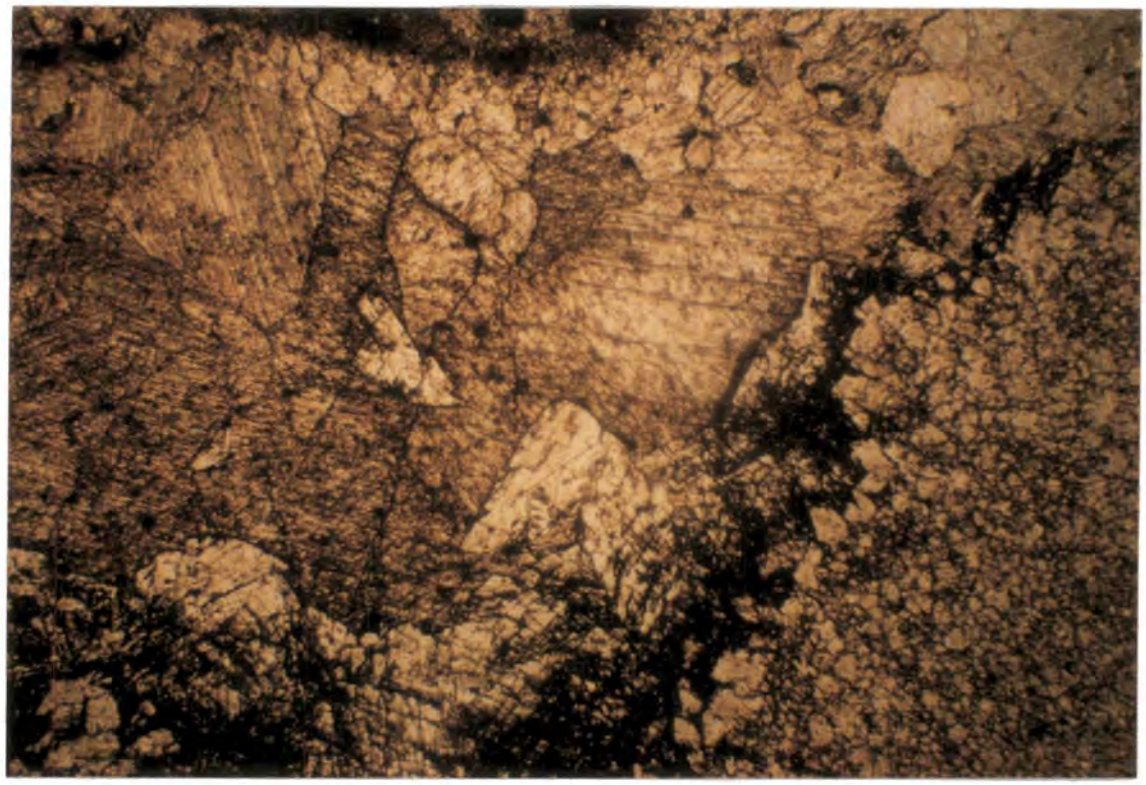

Fig 3.27b

3.12.2 Dolomitization associated with the basal section of the platform.

Volumetrically this is the most important dolomite within the platform. Petrographically it is split into two types.

3.12.2 (a) Field description.

The dolomitization of the Urgonian shows a strong facies control. It is typically restricted in extent to the shelf-margin facies (F5 to F7; typically high energy grainstones with either rounded bioclasts, ooids and/or corals, see section 3.5 and Figs 3.3 & 3.4a), which are seen within the basal section of the platform as a transgressive sequence (see Hunt, 1992). The facies association of the dolomitization was first recognised by Lory (1846), when he noted that in the Urgonian of the Grenoble region corals were commonly associated with dolomitization. This dolomitization is very variable in its thickness. For example at Gorge de Frou (see log #3 in Appendix 1, #12 on Fig. 3.1) there is only a thin (2m) single dolomitized horizon, whereas at Grande Goulets (see log #1 in Appendix 1, #3 on Fig. 3.1) the dolomitized section is 125m. Usually the dolomitized section at the base of the Urgonian has a thickness of between 10 and 40 metres (see Appendix 1). In many sections there are several dolomitized horizons within the basal part of the Urgonian.

Dolomitization fronts are normally gently discordant to sub-parallel with bedding as (shown in Fig. 3.29a) and transitional in nature with totally dolomitized limestone passing down to undolomitized limestone within the space of 30-40 mm.

Fig. 3.28 A model for the formation of the infill of the micro-karst seen at the top of the platform.

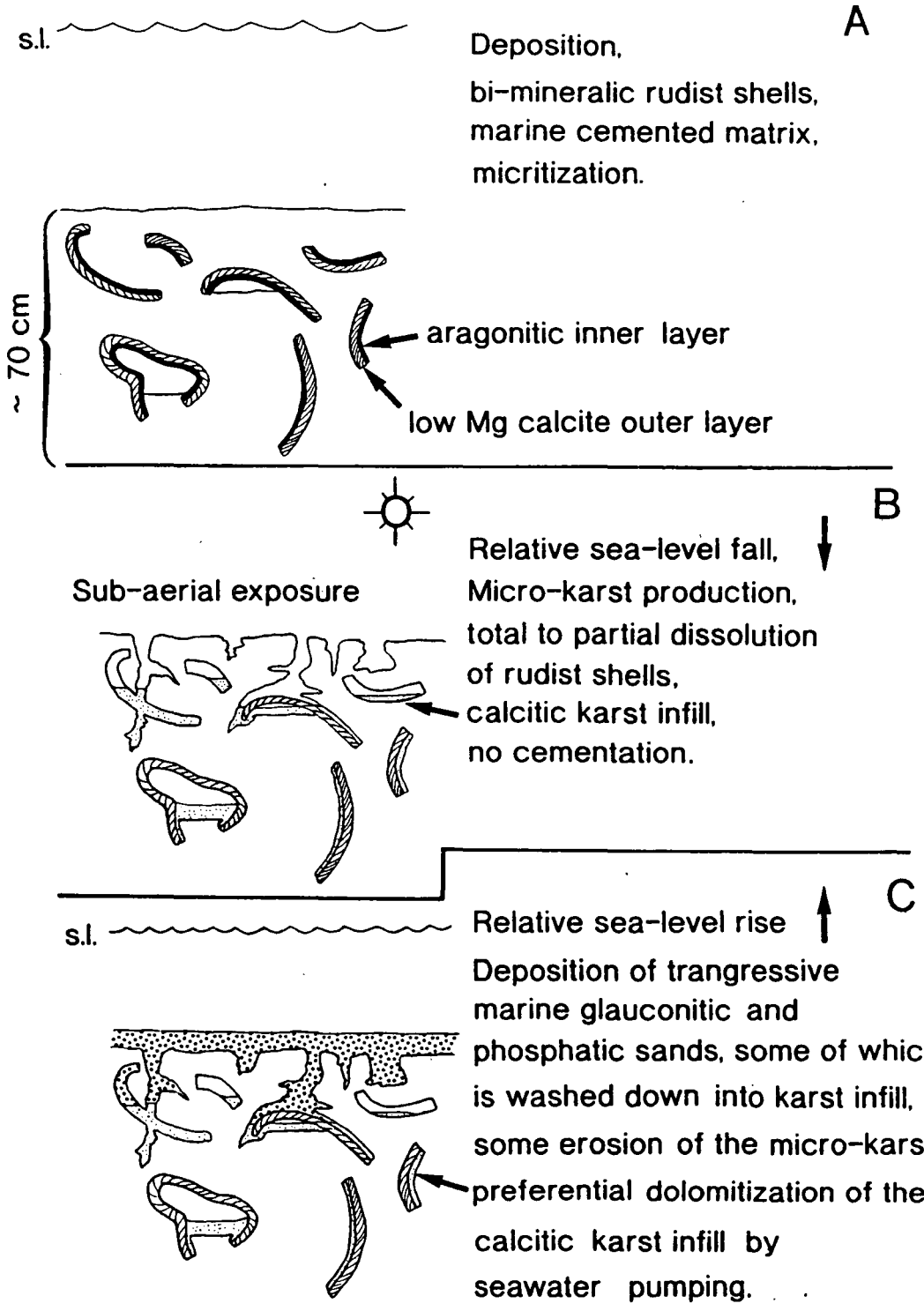

Fig. 3.29a Field shot of the dolomitization front, upper Borne Valley, Bornes massif (see log #12, Appendix 1, #23 on Fig. 3.1). Hammer= 350mm. **Fig, 3.29b** Unreplaced bioclastic grains within the basal dolomitized section of the Urgonian, La Tournette, #21 on Fig. 3.1). **Fig. 3.29c** (underneath foldout). Dolomite lining fractures through rudist shells (small black arrows). Combe de Tardevant (#28 on Fig. 3.1). Several 'clasts' of unreplaced Urgonian (labelled C) bounded by a random network of dolomite can be seen. One pence for scale.

A

B

C

In the field this dolomite is white to tan coloured and has a sucrosic appearance. This texture is identified with dolomites that have either a different mineral phase or empty pore spaces between the rhombs or mosaics of rhombs (Sibley & Gregg, 1987).

Often corals and rudists may be seen as unreplaced allochems or entire 'clasts' of unreplaced limestone (as shown in Fig. 3.29b) are seen floating within a matrix of dolomite rhombs. Occasionally, in partially dolomitized limestones dolomite rhombs can be seen to line fractures through shells (see Fig. 3.29c). The fractures are localised features. Another often common feature of the dolomitization of the Urgonian are 'clasts' (usually sub-spherical areas, several millimetres in diameter) of unreplaced host rock within a totally dolomitized matrix or surrounded by a seemingly random network of dolomitized vein-like features (see Fig. 3.29c).

In many instances dolomitization is intimately linked with the top of coarsening upward cycles. This is particularly well seen within the section in the lower part of the Gorge de la Bourne (Vercors, #4 on Fig. 3.1). Dolomitization is also frequently identified with the former areas of burrows (see Figs 3.29a and 3.30a). Within the lower Urgonian section in the lower part of the Gorge de la Bourne (Vercors, #4 on Fig. 3.1) the bioturbation also coincides with the tops of metre scale coarsening-upward cycles (see Fig. 3.30b). Both bedding surface parallel, Y-branching (? Thallassinoides) and single vertical burrows may be seen (see Figs 3.29a and 3.30a). Trough and planar cross bedding structures (typical of the higher energy shelf margin facies, F5 to F7) are also preserved in many of the totally dolomitized horizons.

The pervasive nature (although variable in thickness) and the marked stratigraphic control upon the dolomitization of the Urgonian platform suggest that dolomitization was at least in part controlled by initial porosity/permeability characteristics (initially a reflection of depositional processes) and/or the original mineralogy.

3.12.2 (b) Petrography.

Partially dolomitized limestones commonly contain unimodal, planar-e, idiotopic mosaic dolomites (Sibley & Gregg, 1987). Usually they are limpid (clear) in nature with a reddish opaque rhombohedral shaped band near the core of the dolomite rhomb. They pre-date later non-ferroan equant calcite spar. They may occur with fine grained calcitic silt, which has settled on the bottom of the pore space (i.e it has an astropetal fabric, see Fig.

Fig. 3.30a (opposite page). Preservation of (?)Thallassinoides burrows (T) within a dolomitized section of the Urgonian within the lower Urgonian section in the lower part of the Gorge de la Bourne (Vercors, #4 on Fig. 3.1). The burrowed surface marks the top of a metre scale coarsening-upward cycle and is located on Fig. 3.30b. D= dolomite; L= limestone; a slight colour change between the two is visible and the contact is transitional and undulatory. Lense cap for scale. **Fig. 3.30b** (opposite page). Detailed log of the basal Urgonian of the lower Bourne gorge (see also log #2, Appendix 1). The starred horizon is the surface shown in Fig. 3.30a.


A
T
D
L

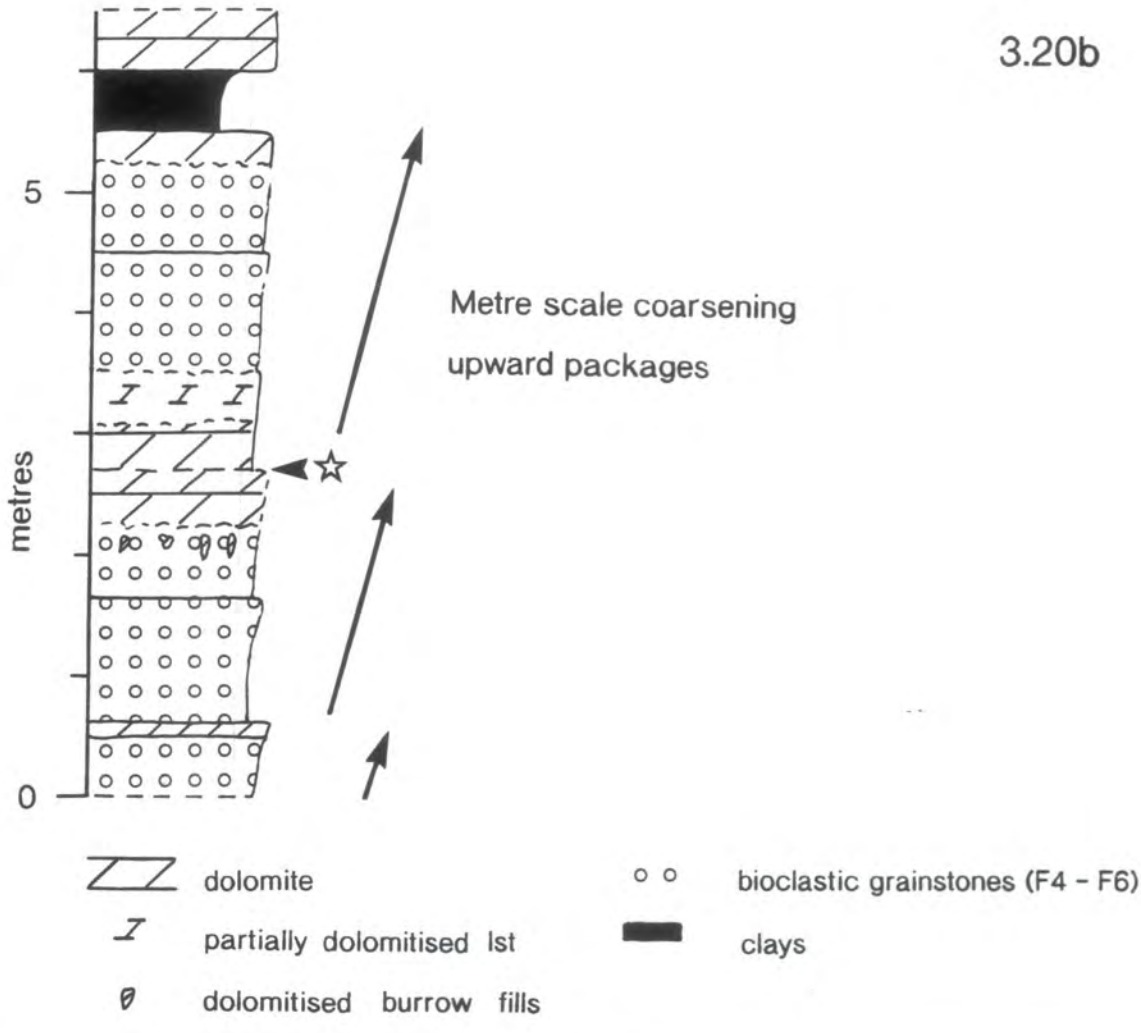
3.20b
5
metres
0
Metre scale coarsening
upward packages
dolomite
partially dolomitised lst
dolomitised burrow fills
bioclastic grainstones (F4 - F6)
clays

Fig.3.31 Photomicrograph of 130/90, Gorge du Nant (#6 on Fig. 3.1, see also log #3, Appendix 1). Field of view= 7mm. S= calcitic silt; D= dolomite rhombs. Large black arrow gives way-up.

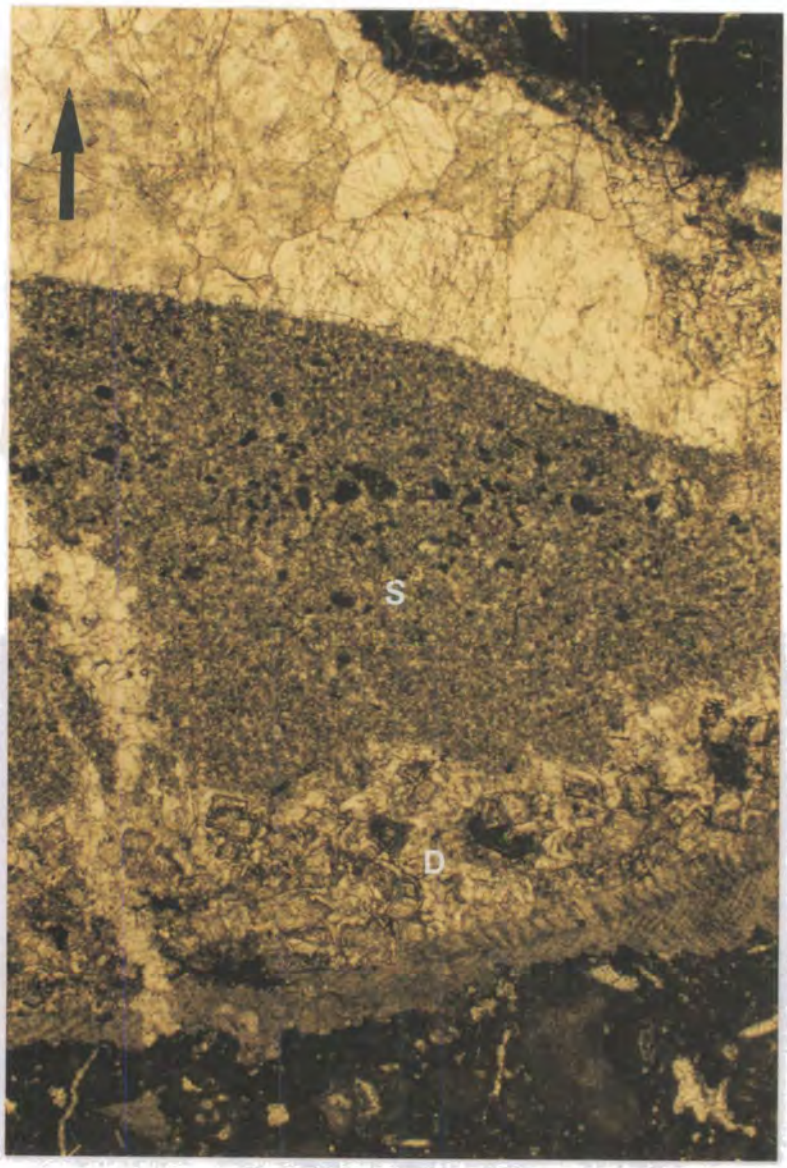

3.31, e.g. 130-90 Gorge du Nant). The dolomite usually is seen as a void filling phase (void filling is used instead of cement, as the edges of the rhombs may actually replace parts of adjacent grains and early cements). Often the edges of the rhombs that lined former pore space have been etched (see Fig. 3.32). Where replacement occurs within partially dolomitized limestones it is consistently within areas of finer grain sized material first (micritised grains, areas of micritic sediment/cement).

Fig. 3.32 Etched rims (arrowed) of pre- non-ferroan calcite spar dolomite. 641/90, Salles, Platé massif. Field of view= 1.5mm. See opposite page.

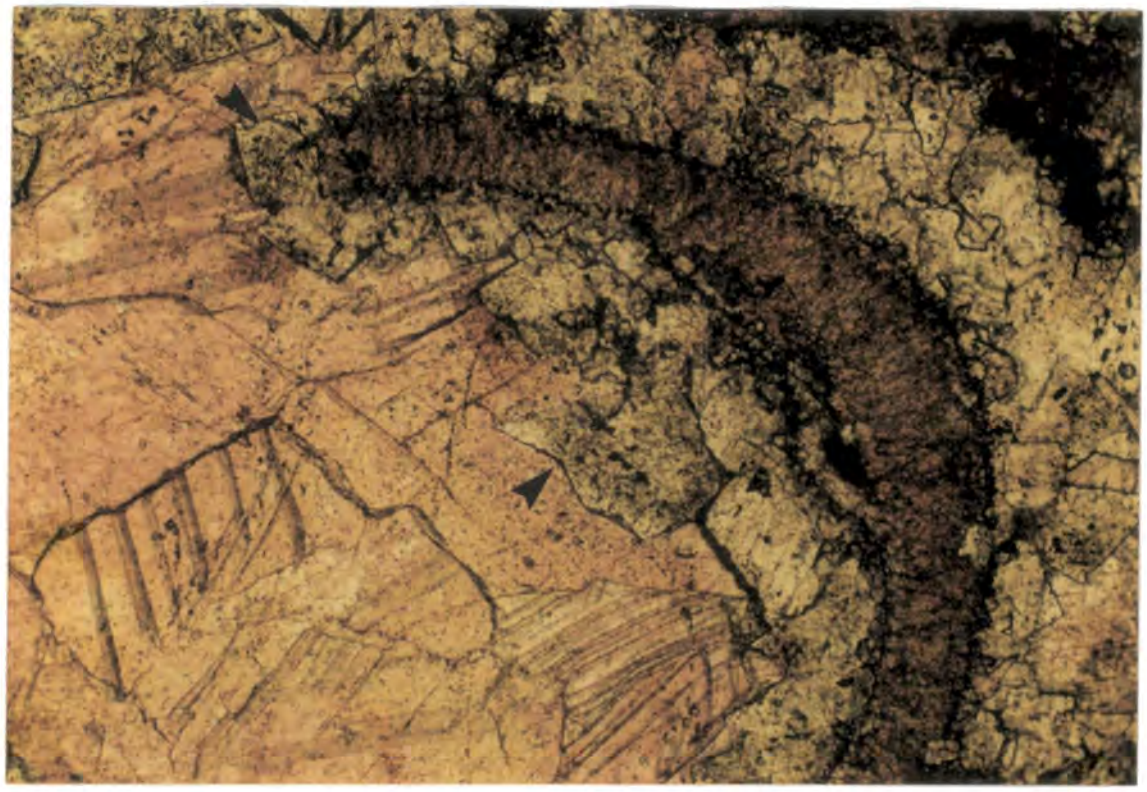

Under CL these dolomites have a dull orange core, the boundary of which coincides with the inner reddish coloured core to the dolomite rhomb seen under ppl. The outer edge is often bounded by a single bright orange band (see Figs 3.33a and 3.33b). The following limpid rim to this core is non-luminescent. If there is a second limpid rim, this typically has a dull orange luminescence.

On the thin-section scale planar-e, idiotopic mosaics of partially dolomitized limestones pass into dusty cored-limpid rimmed, planar-s, polymodal, hypidiotopic (rarely xenotopic) mosaic dolomite. Individual rhombs can be up to 0.8mm in size (see Figs 3.34a, 3.34c & 3.35).

The rhombs may show a slight undulose extinction, a feature which is usually quoted as distinctive of baroque (or saddle) dolomite (Radke & Mathis, 1980). However, the term is not used to describe these dolomites since they do not have the curved, scimitar-like crystal faces of baroque dolomite, nor marked undulose extinction or the xenotopic texture characteristic of baroque dolomite. The term baroque or saddle dolomite is perhaps best avoided in this case since it has often been used in a generic sense to imply high temperature (60° to 150°C), late diagenetic dolomitization.

Fig. 3.33a CL shot of partially dolomitized limestone, a single bright orange band can be seen. **Fig. 3.33b** PPL shot of the same field of view in Fig. 3.33a. Note: some of the rhombs can be seen to overprint sutured grain contacts (white arrow). 203/89, lower Bourne gorge, Vercors. Field of view= 2mm.

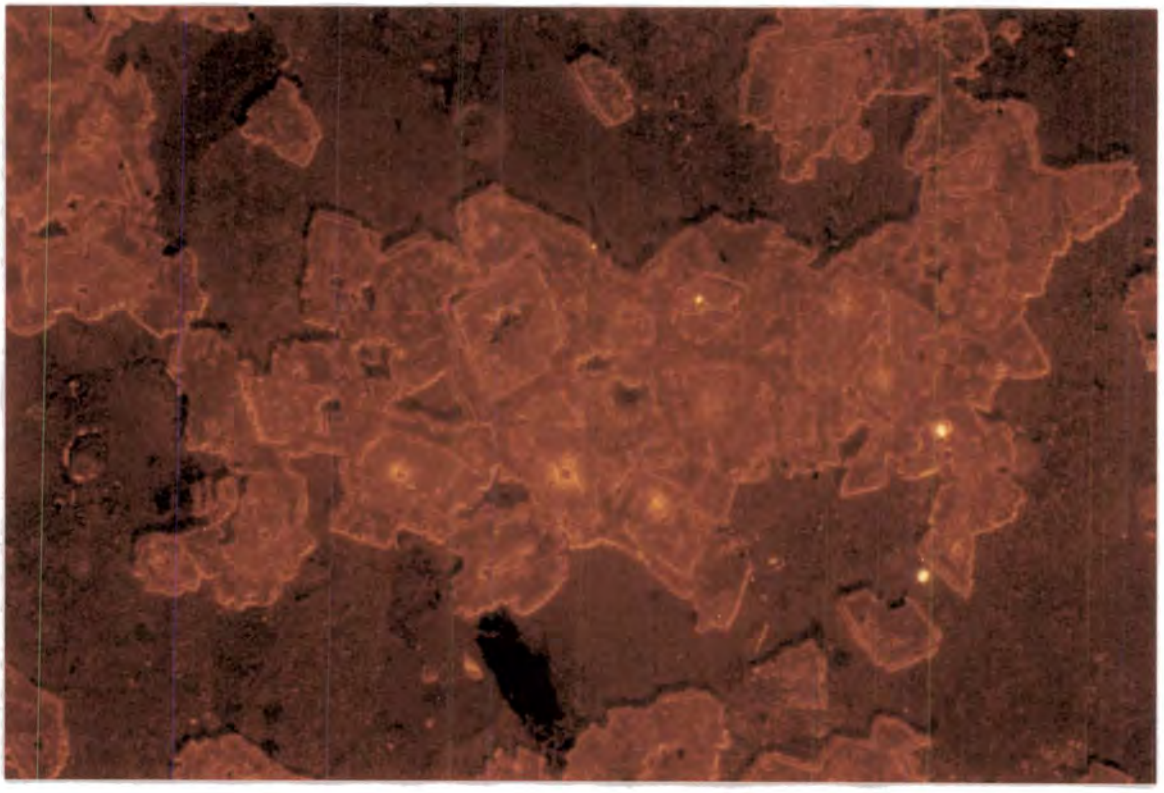

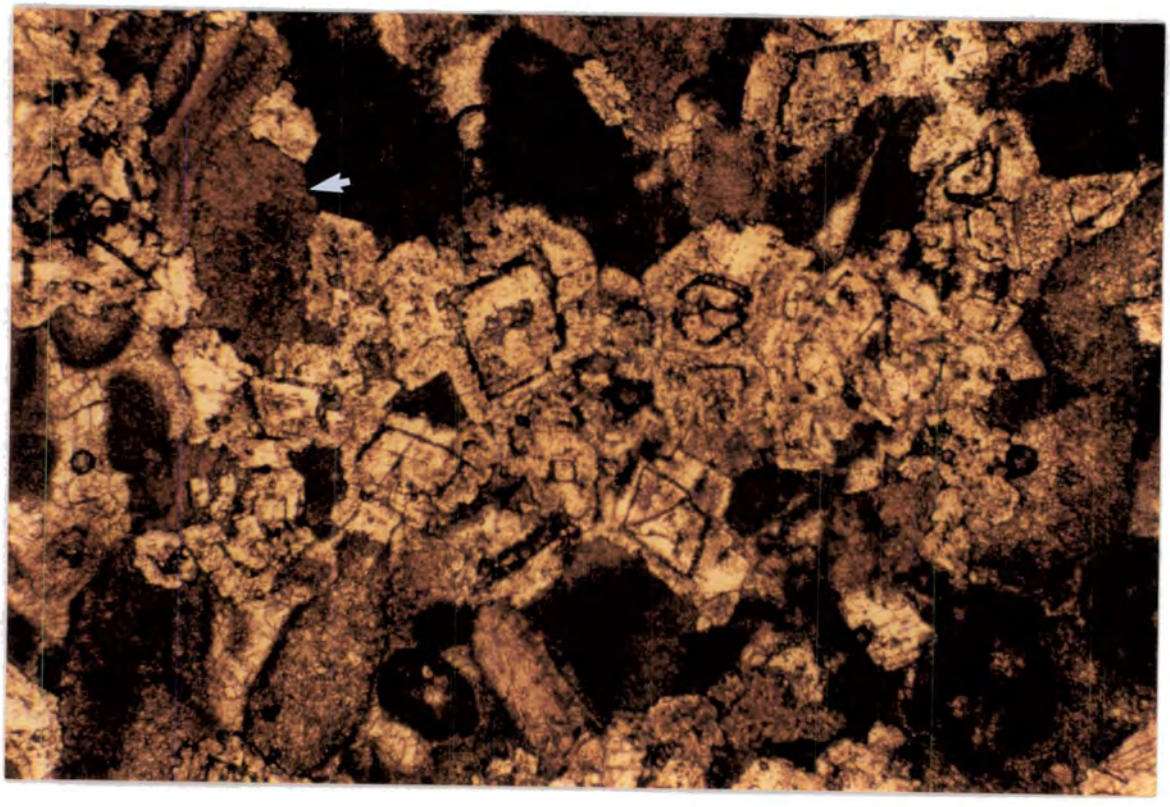

Fig. 3.34a (underneath foldout). Photomicrographs of polymodal, hypidiotopic mosaic dolomite. E= single dolomite crystal replacing an echinoderm(?) grain. 562/90, Combe de Tardevant, Aravis. Field of view= 7mm. **Fig. 3.34b** CL polymodal, hypidiotopic mosaic dolomite. A single thin bright orange band can be seen at the outer edge of some of the dolomite rhombs. The non-luminescent area to the bottom left is an area of dolomitic porosity occluded by calcite. **Fig. 3.34c** PPL shot of the same field of view as Fig. 3.34b. 255/89 Grande Goulets, Vercors.

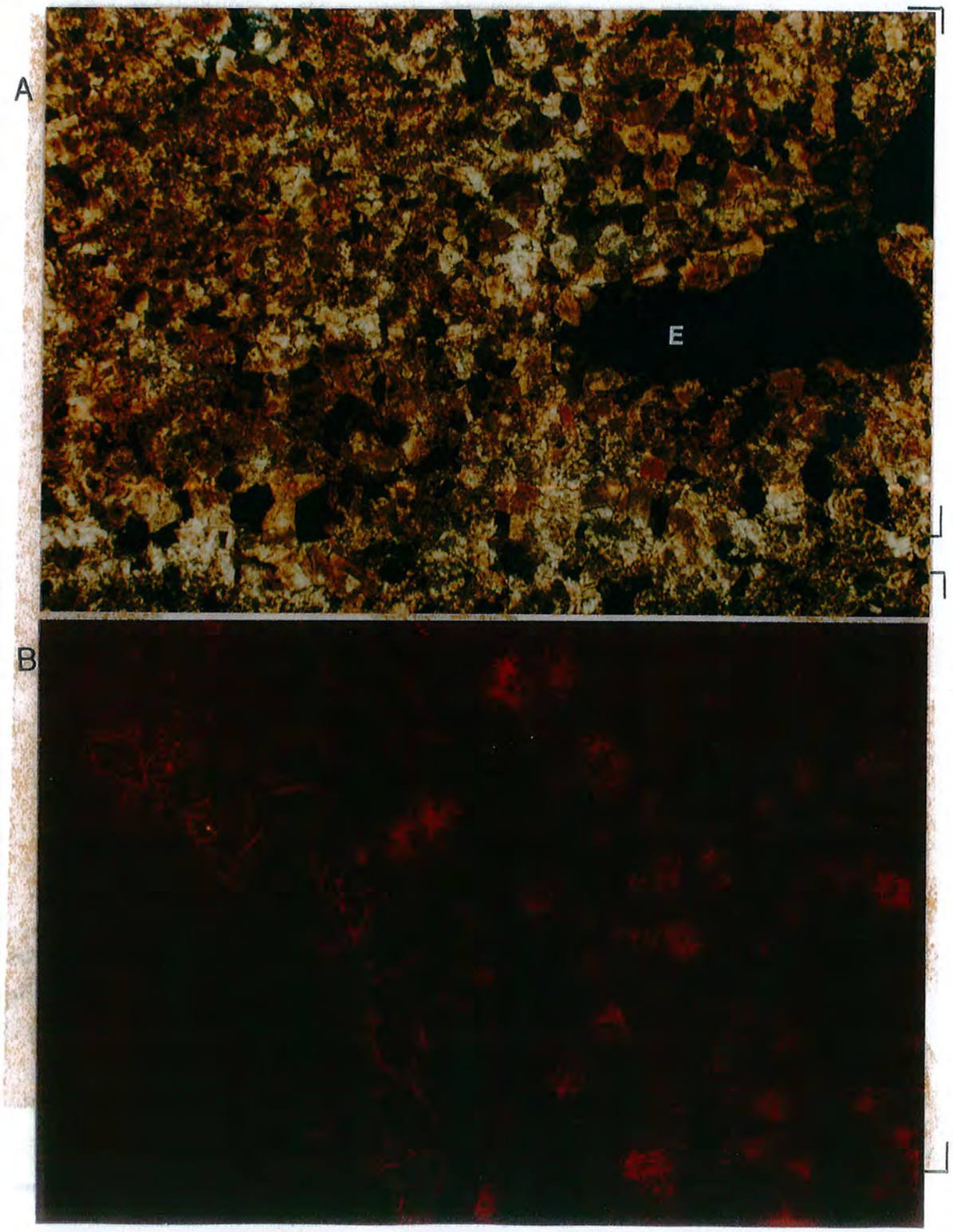

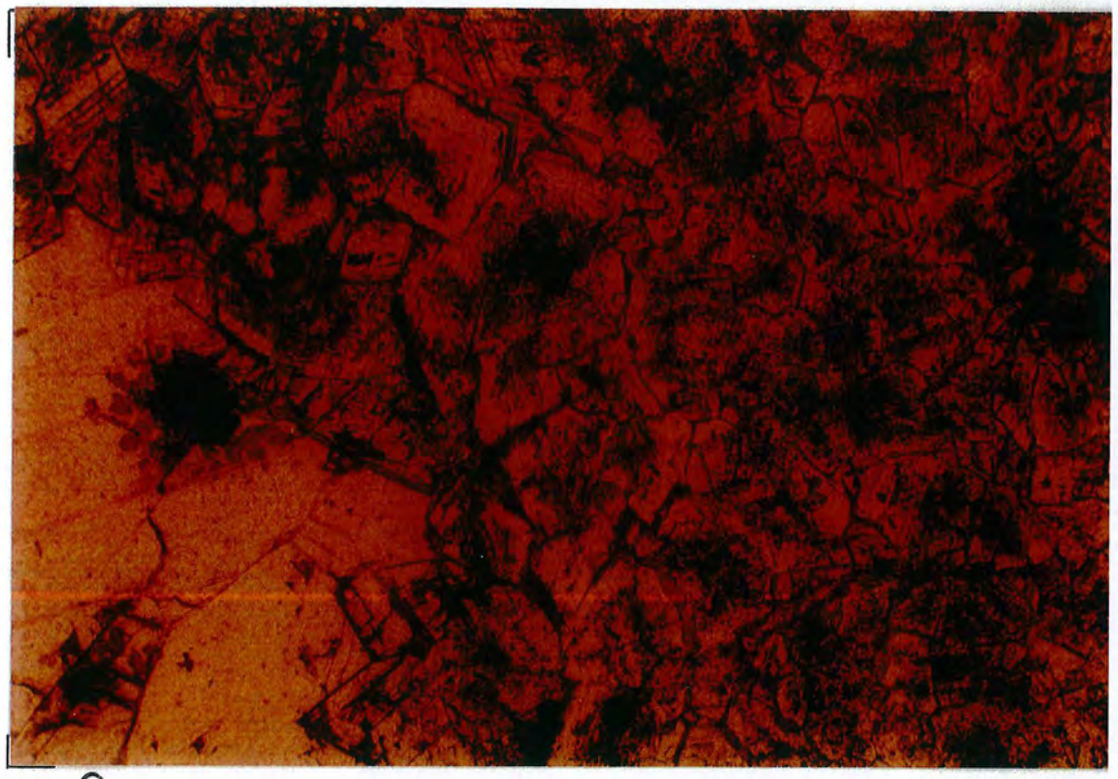

In many samples that were transitional between partially to totally dolomitized, rhombs were seen to occur preferentially along roughly linear features (see Fig.3.29c and also Fig. 3.35). This is probably a reflection of the location of nucleation sites during the dolomitization. Areas formerly dominated by micrite or micritised grains, because of their fine grained nature may have had numerous nucleation sites. However, the generally poor quality of mimetic replacement (see Fig. 3.36) within Urgonian dolomites suggests that generally nucleation sites were quite separated, allowing non-pseudomorphic replacement of the host rock (Sibley, 1982).

Fig. 3.35 Hypidiotopic dolomite mosaic following a roughly linear feature through a partially dolomitized grainstone. Note; the rhombs adjacent to the unreplaced limestone are euhedral, whilst those within the centre of the dolomitized areas are anhedral. 448/90, Combe de Paccaulay, Aravis. Field of view= 7mm.

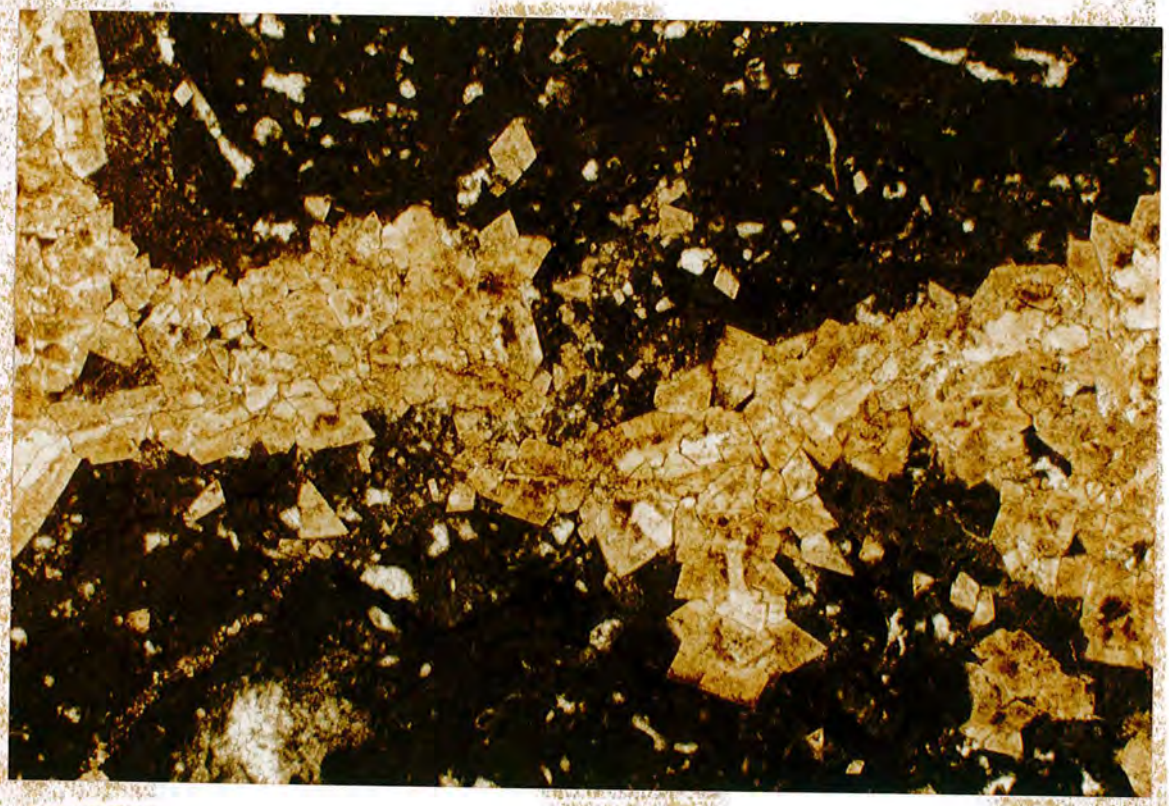

Under CL they are typically unzoned dull orange or non-luminescent with perhaps a bright orange band at the extreme outer edge of the limpid rim of the rhomb (see Figs. 3.34b and 3.34c). In the hypidiotopic mosaics parts of the limpid rims of the rhombs are actually cements not replacements, as they are precipitated in open pore space.

Within many dolomitized sections of the Urgonian, the only original grains to be preserved unreplaced are bioclastic grains, usually either rudist or coralline. Mimetic replacement of original grains and texture, a common feature of many other dolomitized

carbonate platforms (e.g. figure 8.8 of Tucker & Wright, 1990) is usually poor within the Urgonian (see Fig. 3.6). With the exception of former single crystal grains (echinoderm fragments) which are replaced by a single large dolomite crystal (see Fig. 3.34a), sometimes solid inclusions may roughly define the former position of the echinoderm. This style of replacement is probably due to the relative ease with which the dolomite could nucleate upon a single calcite crystal grain such as an echinoderm (Sibley & Gregg, 1987). The presence of dusty cores within the rhombs (probably mineral relics of the precursor sediment and/or solid inclusions) suggest that during the early stages of dolomitization, the calcium carbonate of the original grains was not totally dissolved out.

Fig. 3.36 Poor mimetic replacement of a grainstone by hypidiotopic mosaic dolomite. 368/90, Dents d'Arclusaz, Bauges. Field of view= 3.25mm.

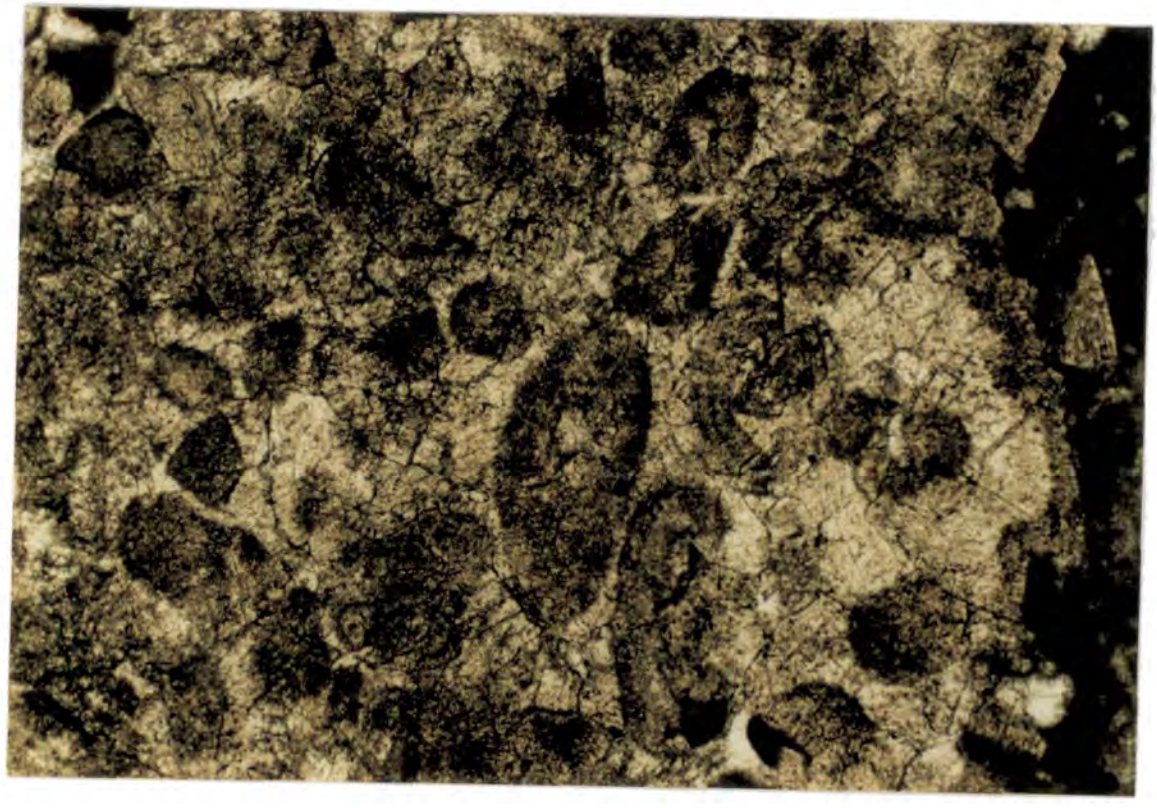

In the partially dolomitized limestones the rhombs could often be seen to overprint sutured grain contacts (see Figs 3.33b and 3.37a), also dolomite rhombs can be seen to line mechanical fractures (such as fractures through rudists, where the dolomitization passes up into shelf-margin facies, see Fig. 3.29c). The fabric destructive nature of the grain replacement means that the relationship of features such as the fracture of marine cements could not be seen. In a few samples, euhedral rhombs were seen to line sutured and non-

sutured dissolution seams (see Fig. 3.37b and 3.37c) within partially dolomitized limestones. This could be due to a solution-cannibalism of previously formed dolomite (Land, 1985). Although several authors have implied an intimate link between dolomitization and stylolitization (Wanless, 1979), these relationships suggest burial dolomitization. However, the dolomite is cut by stylolites (see Fig. 3.38), suggesting the dolomite formed in a shallow burial environment (again the same caution with using petrographic relationship to stylolites applies that was mentioned for the equant calcite cements in section 3.11.4).

Fig. 3.37a Dolomite rhomb overprinting a sutured grain to grain boundary (labelled S) between two micritised grains. The former positions of the grain boundaries are partially ghosted (labelled F) within the dolomite rhomb. These relationships suggest that the dolomite formed after suturing of the grains. 38/91, lower Bourne gorge,Vercors. Field of view= 1.5mm. **Fig. 3.37b** CL shot of a partially dolomitized limestone with rhombs lining pressure dissolution seams. 626/90, Platé massif. **Fig. 3.37c** PPL shot of the same field of view as Fig. 3.37b. Field of view= 2mm. See opposite page for 3.37b and 3.37c.

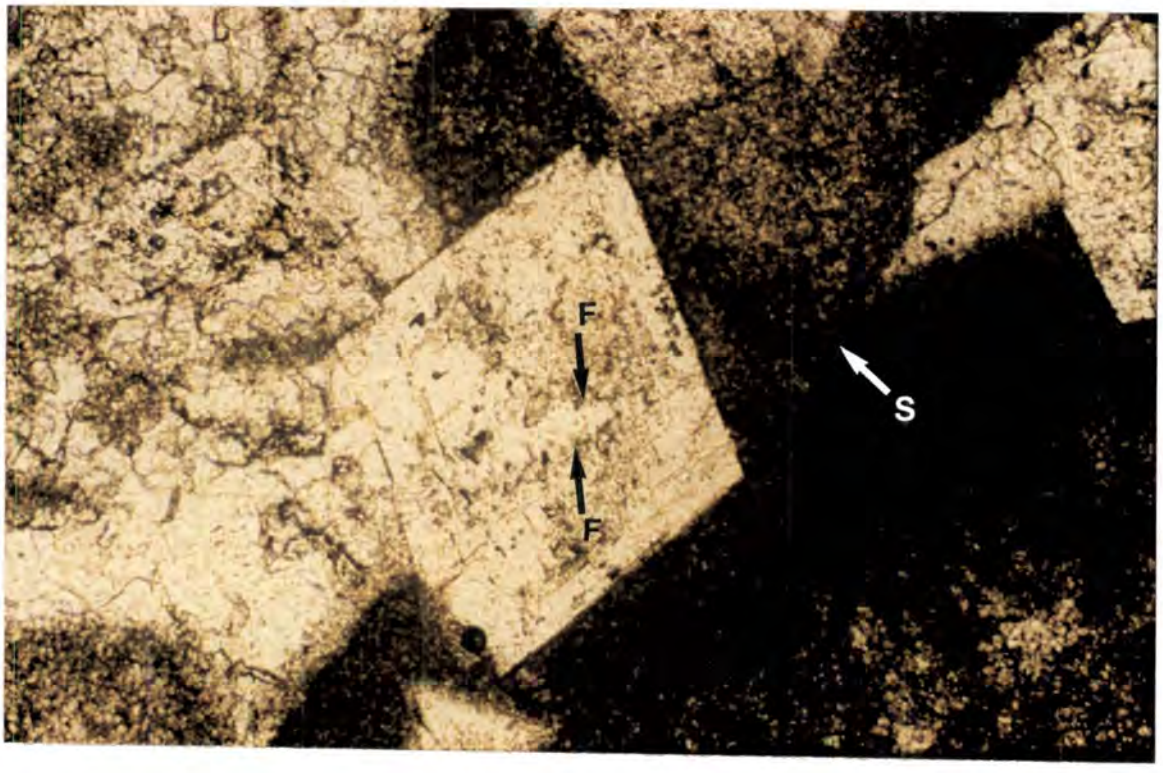

3.12.3 Baroque dolomites infilling fractures and veins.

These are not particularly abundant within the Urgonian and were only seen in samples from the eastern Bauges and Aravis. Where they do occur, the crystals have scimitar-like curved crystal faces and marked undulose extinction. Within the Urgonian

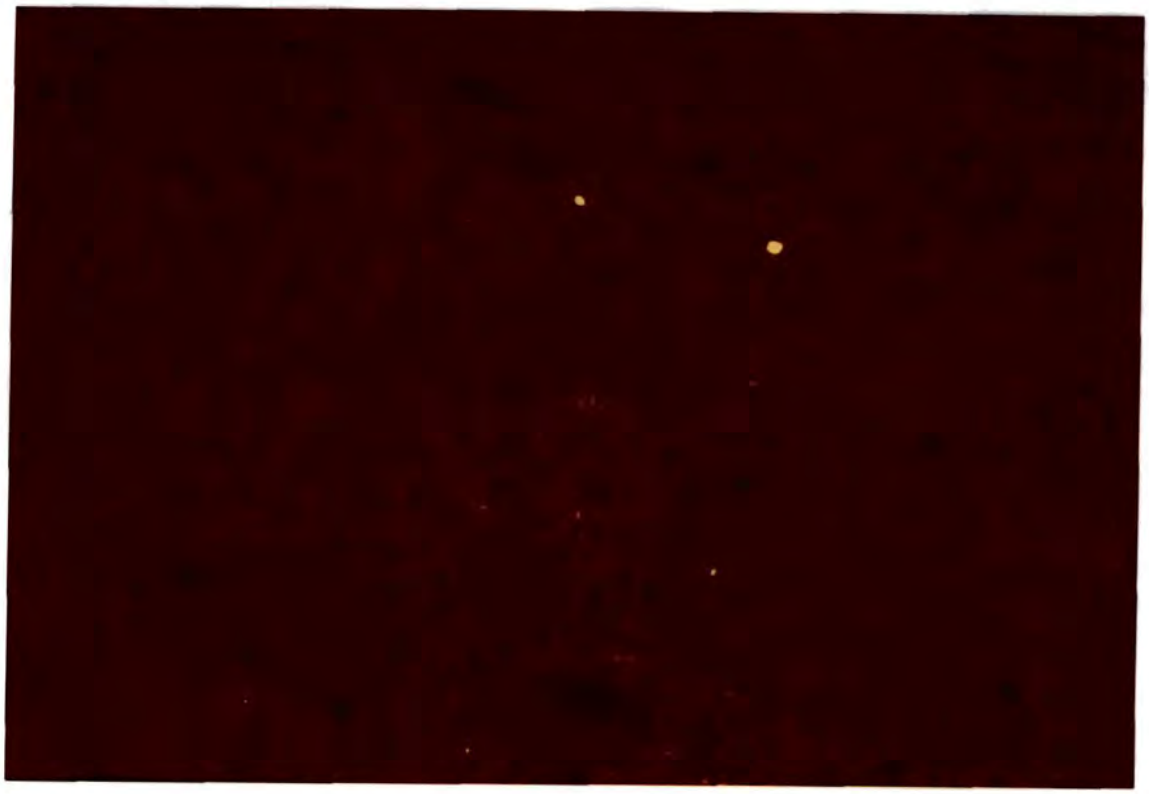

Fig. 3.37b

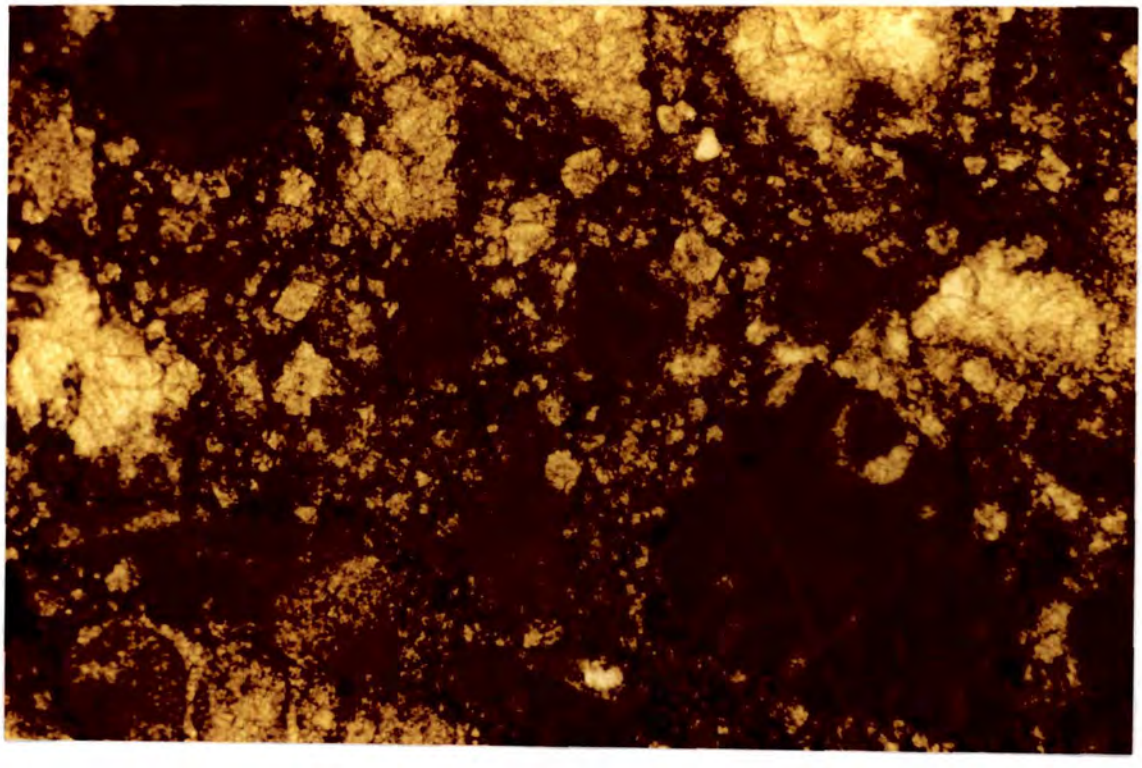

Fig. 3.37c

they line fractures and veins and have a uniform, orangey-pink luminescence (see Fig. 3.39a & 3.39b). They may be slightly etched (edges dissolved) by non-luminescent, equant calcite cements which postdate the dolomite. Dissolution of baroque dolomite is one of the criteria that Mazzullo & Harris (1992) propose for the recognition of mesogenetic (burial) dissolution.

Fig. 3.38 Post dolomite pressure dissolution seam. 205/89, lower Bourne gorge, Vercors. Field of view= 1.5mm.

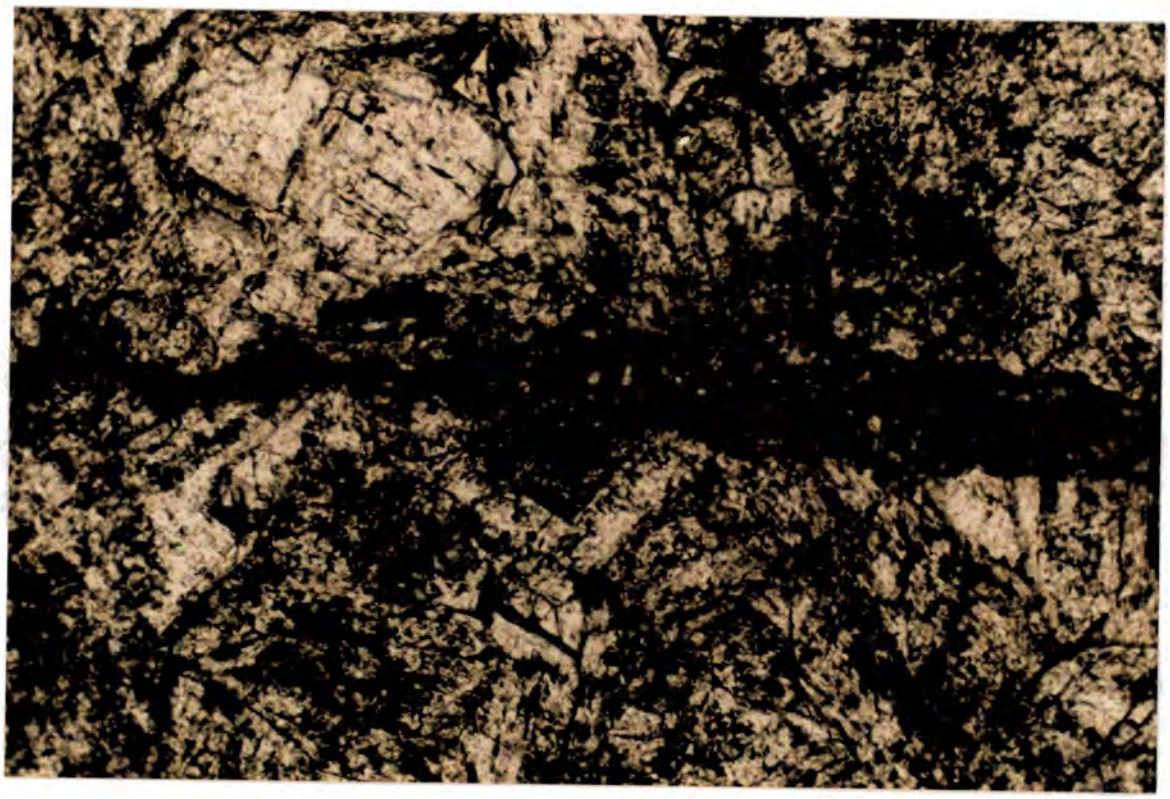

Baroque dolomite within the Urgonian is not related to any sulphide mineralisation and the fractures and veins that it lines may have formed during syn-tectonic fluid movement (see Chapter 5). The restriction of their occurrence to the eastern Bauges and Aravis may be a reflection of the greater depth of burial of the northeast part of the chain (including these two areas) during the Tertiary.

Fig. 3.39a CL shot of baroque dolomite. Note: dissolution of the dolomite (arrowed) and breakage of the terminations of one of the rhombs (f). **Fig. 3.39b** XPL shot of baroque dolomite shown in Fig. 3.39a. 485/90, Pointe de la Sambuy, Bauges. Field of view= 2mm. See opposite page. S= spar

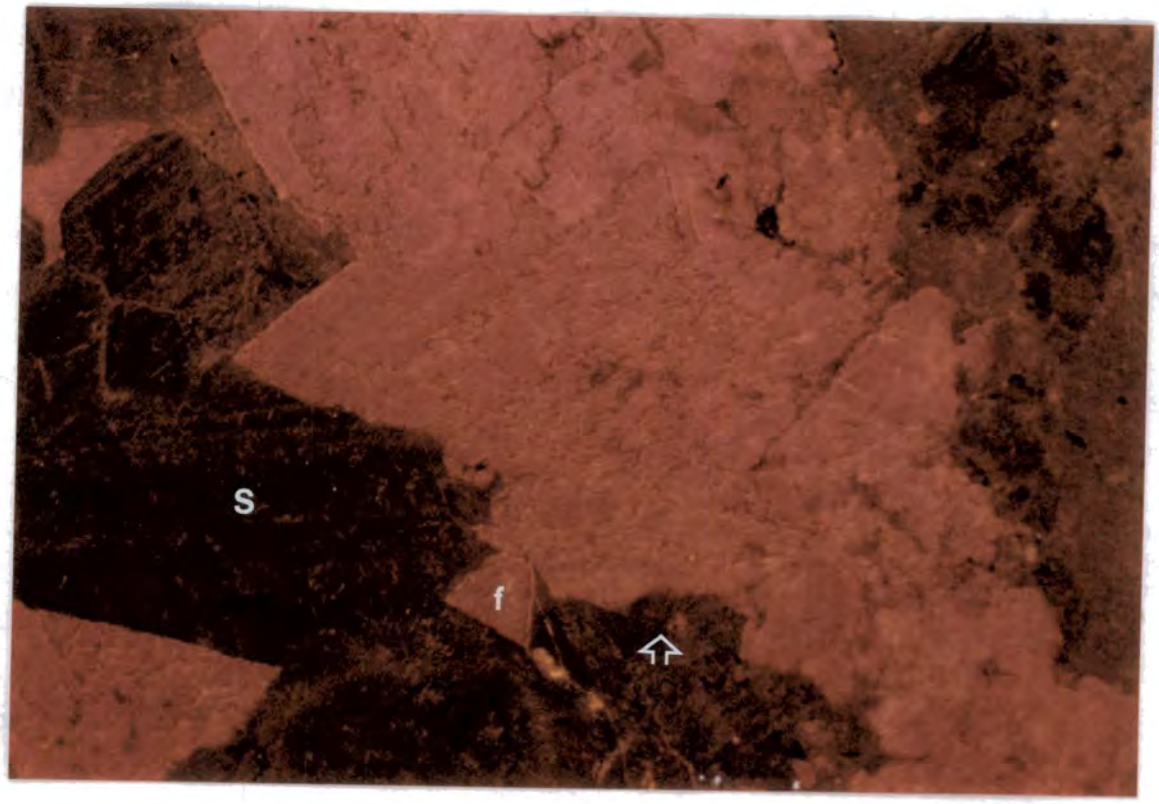

Fig. 3.39a

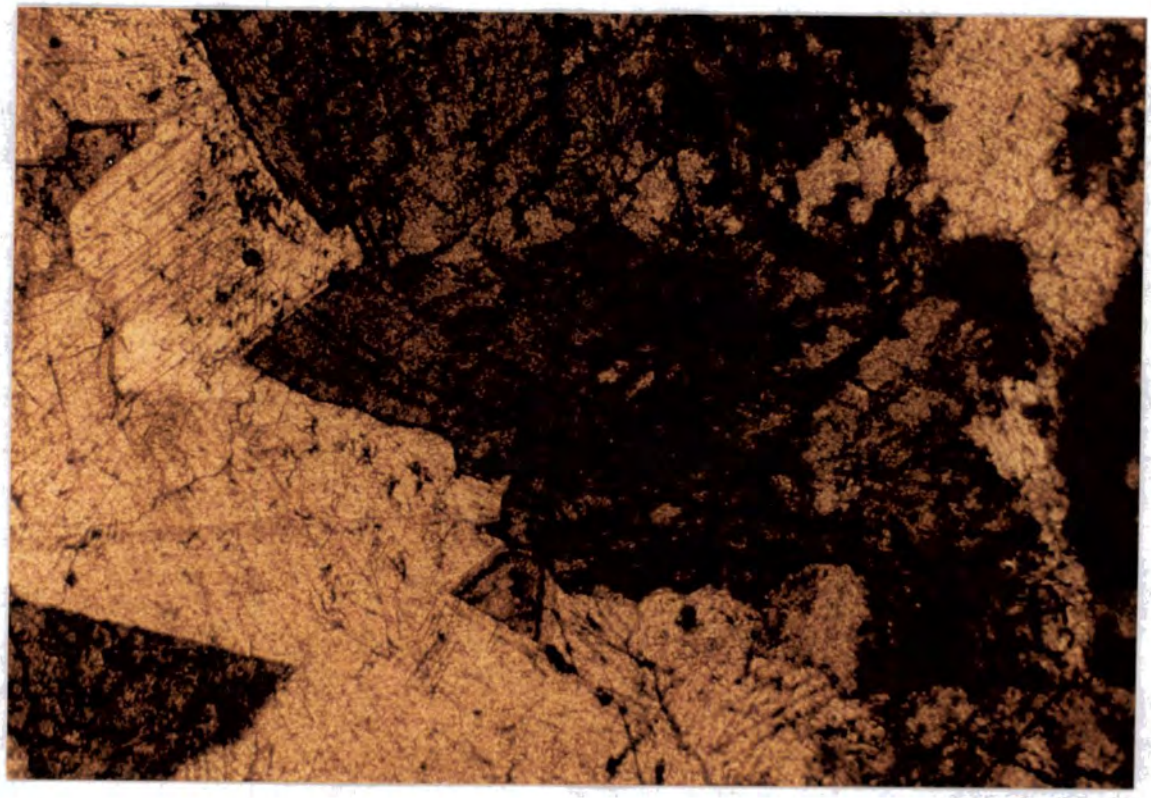

Fig. 3.39b

3.12.4 Post-dolomite spar.

3.12.4 (a) Field description.

As mentioned in section 3.12.2 (a) the basal dolomites commonly have a sucrosic texture, the intercrystalline pore spaces are infilled by coarse calcite spar.

3.12.4 (b) Petrography.

This is distinct from the calcite spar which postdates the dolomite described in section 3.12.2 (b) (see Figs 3.31 and 3.32). This spar occurs where the Urgonian has been totally dolomitized and infills intercrystalline porosity. It consists of coarse (up to 1mm), blocky, non-luminescent to dull orange, non-ferroan calcite (see Fig 3.40a). The pore spaces occluded by these cements may have shapes roughly reminiscent of bioclastic grains (such as echinoderms, see Fig. 3.40a and rudist shells).The final rims of the dolomite have partially grown into these spaces (see Fig. 3.34a) and the crystal has a euhedral form where it has grown into the pore space. This suggests that these grains were dissolved after the matrix had already been dolomitized, producing relatively large intercrystalline and moldic porosity. A similar porosity evolution has been described by Choquette et al. (1992). Later, this pore space was occluded by the coarse calcite. Placing such calcite cements in a relative time order is difficult, except to say (the obvious) that it is post-dolomitization

Where these intercrystalline pore spaces are not occluded by calcite, the Urgonian has quite good porosity (see Fig. 3.40b). Roberts (1991) obtained a permeability of up to 220 millidarcies for samples of dolomitized Urgonian from the Gorges du Bourne (Vercors Massif). Since 45% of all dolomite reservoirs in the U.S.A. have permeabilities in the range of 0 to 10 millidarcies (Schmoker et al., 1985), this permeability could make the dolomitized Urgonian a suitable reservoir rock. However, this could be a surface feature due to the dissolution of intercrystalline calcite, with buried sections of the Urgonian dolomite still cemented.

3.12.5 Environment and possible model of the dolomitization of the Urgonian.

A number of dolomitization models have been published; several variants are shown in Fig. 3.41. These are reviewed in Morrow (1982b), Land (1985), Machel & Mountjoy (1986), Hardie (1987) and Tucker & Wright (1990) and in symposium volumes (Zenger et al., 1980; Shukla & Baker, 1988) Although now there seems to be a growing consensus that dolomite can form by a variety of different mechanisms (Tucker & Wright,

---

Fig. 3.40a Former intercrystalline porosity (p), with a shape reminiscent of a (?)echinoderm grain. The pore space is occluded by blocky, non-ferroan calcite. 325/90, Col de la Fête, Platé (#30 on Fig. 3.1). Field of view= 7mm. **Fig. 3.40b** A totally dolomitized limestone, composed of a mosaic of hypidiotopic dolomite rhombs. A vuggy porosity has been produced, shown here by the blue resin. 134/91 La Tournette (#21 on Fig. 3.1, see log #8, Appendix 1). Field fo view= 1.5mm. See opposite page.

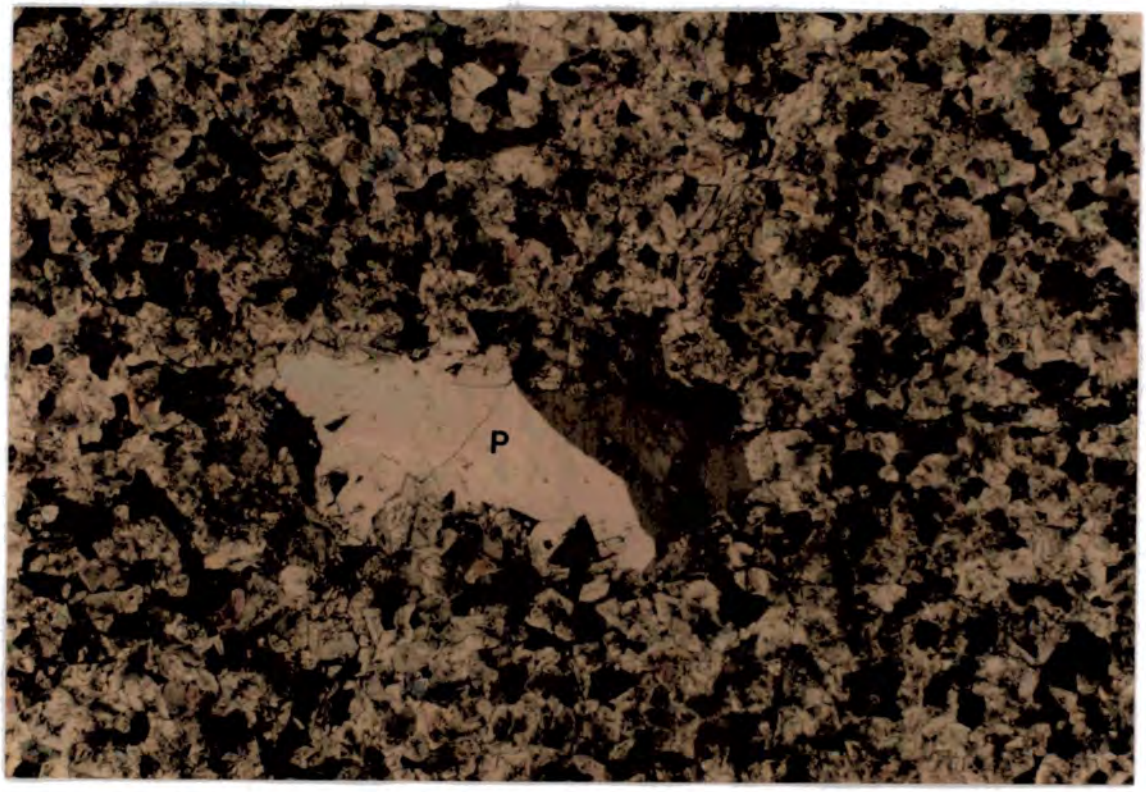

Fig. 3.40a

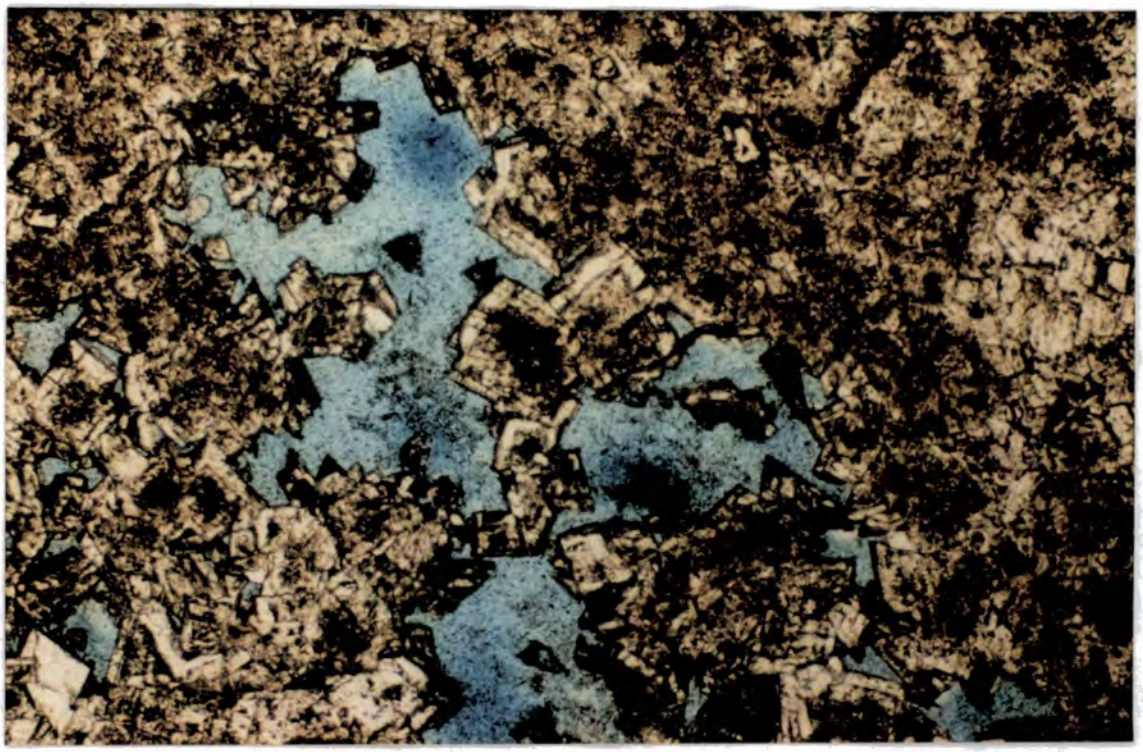

Fig. 3.40b

1990), the so-called seawater dolomitization models are currently gaining in popularity (Saller, 1984; Land, 1985; Vahrenkamp et al., 1991). Hardie (1987) in his conclusions suggested that it may not actually be possible to give an unequivocal solution to how a dolomitized limestone formed.

Fig. 3.41 Models of dolomitization. Modified from Land (1985) and Tucker & Wright (1990). wt= water table, which is elevated in the sabkha and mixing-zone models. Cross hatched area= dolomitized areas.

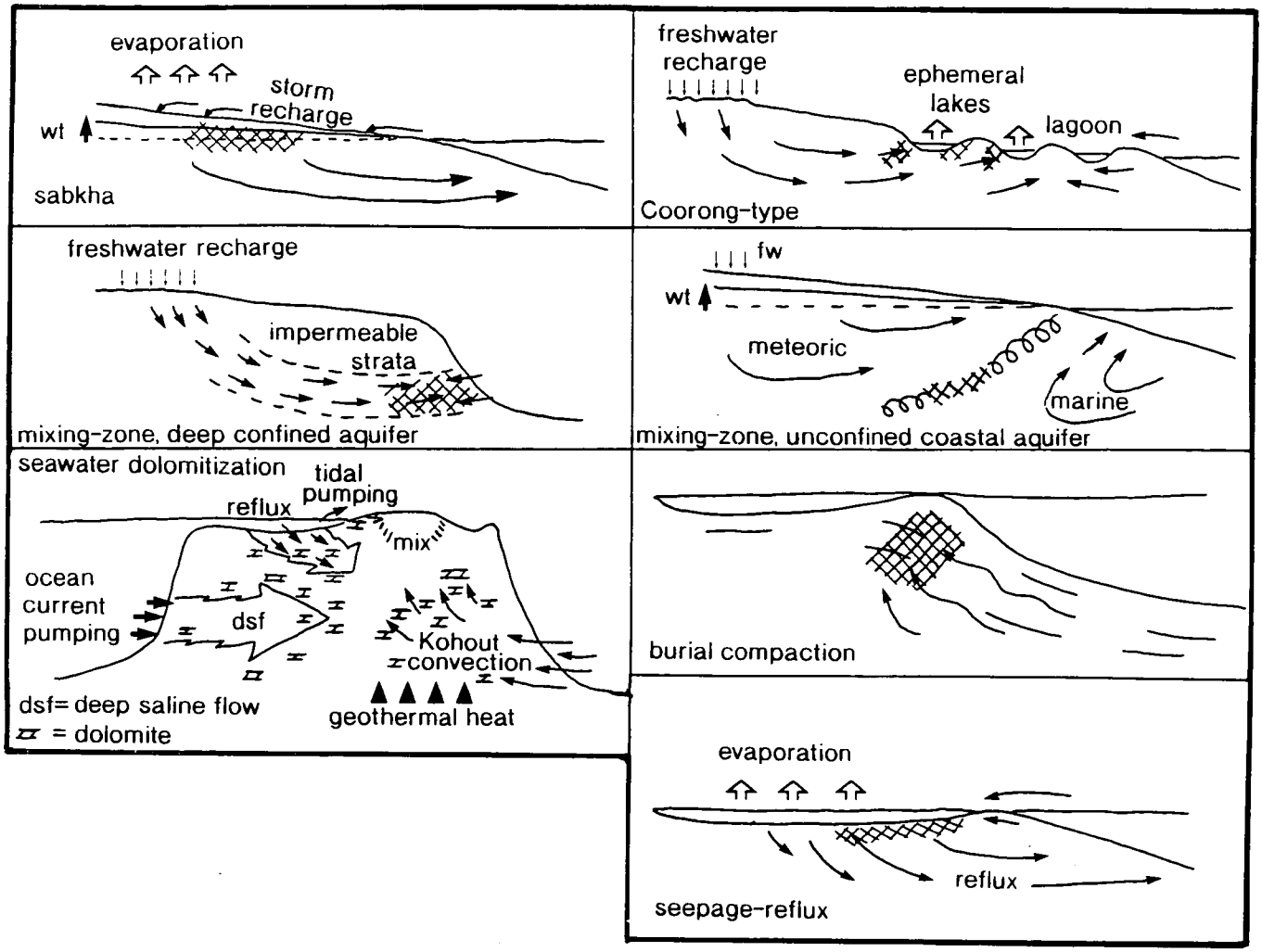

The principal requirements for large scale dolomitization are 1) a source of Mg2+, 2) an efficient hydrologic pumping mechanism and 3) reaction conditions favourable to the formation of dolomite or dolomitization of former calcium carbonate (Morrow, 1982b).

The dolomitization of the basal part of the Urgonian platform was a regionally extensive event and probably occurred whilst the platform was in a shallow burial setting (up to a kilometre). Several possible mechanisms of shallow burial dolomitization have

been presented in the literature. They are 1) seepage-reflux dolomitisation, 2) mixing-zone, 3) seawater circulation models (Kohout convection, refluxation of platform top waters and ocean tide pumping) and 4) connate seawater released with the early mechanical compaction of basinal shales.

Seepage-reflux and sabkha dolomitization seems to be highly unlikely in this case since there are no evaporites associated with the Urgonian. These models also do not adequately explain the geometry of the Urgonian dolomites (i.e. preferential association with the basal section of the platform). A reflux model would predict dolomitization to progress downward from the upper surface of the platform (see Wilson et al., 1990, their figure 13) or the petrographic relationships (which suggest a shallow burial setting).

Mixing-zone dolomitization, popularised in the seventies, is now thought to be an unlikely mechanism for extensive dolomitization (Land, 1985; Hardie, 1987; Machel & Mountjoy, 1990), because of the undersaturation with respect to dolomite of many modern day mixing-zones (e.g. Bermuda, Plummer et al., 1976) and the slow kinetics of dolomite growth and nucleation (James & Choquette, 1984). Modern day mixing-zones also do not contain much (if any) replacement dolomite, even if there is supersaturation with respect to dolomite (e.g. Bahamas, Smart et al., 1988). Plus there is a lack of dissolution of the calcite substrate (an integral part of the model) in examples interpreted to be mixing-zone in origin (Hardie, 1987). In particular one of the main criticisms is the kinetics of the reaction, in that if geologically more realistic disordered dolomite is used instead of ordered dolomite in thermodynamic calculations then the range of seawater and freshwater mixes that meet the requirements for mixing-zone dolomitization becomes very narrow (Hardie, 1987).

Dolomitization from seawater is a fairly recent addition to the list of dolomitization models. Several pumping mechanisms have been proposed, Kohout convection, refluxation of platform top waters and ocean current pumping (Saller, 1984; Simms, 1984; Land, 1985). The ocean current pumping model has some attraction since there is independent sedimentological evidence for oceanic currents encroaching on to the edge of the Dauphinois/Helvetic shelf during the upper Aptian (Delamette, 1986; 1988). Circulation of seawater could also be produced by the hydrologic action of coastal freshwater-seawater mixing (Machel & Mountjoy, 1990), or in response to the development of horizontal density gradients between cold marine waters adjacent to a platform containing geothermally heated groundwaters (referred to as Kohout convection) (Simms, 1984; Land, 1985). Seawater could also be pumped through the platform (particularly its top) in response to a salinity contrast between normal marine porewaters and slightly hyper-saline platform top waters (due to restricted circulation or moderate evaporation). As regards the applicability of the seawater models to the Urgonian, these models are certainly possible and could explain the formation of the euhedral, pre-sparite dolomite cements seen in some of the partially dolomitized limestones. However, seawater dolomite does not have a distinctive fabric and recrystallization is always possible (Land, 1985; Hardie, 1987), re-

setting the geochemistry. Thus identification of this type of dolomite has to come from the geometry and the geochemistry (i.e. if the dolomite has marine isotopic values, then the geochemistry would support a seawater origin).

Mechanical dewatering (i.e. expulsion of connate seawater from pore spaces) of shales and micrites occurs within the first 2 km of their burial (Sclater & Christie, 1980; Baldwin & Butler, 1985; Jones & Addis, 1985). Vertical migration of the expelled connate fluids into overlying porous platform limestones could cause the dolomitization of the basal section of the platform (most compactional fluids migrate vertically, Magara, 1987). This does not require Mg^{2+} to be sourced from clay transformations or scavenging Mg^{2+} from calcites, *etc*, neither does it require the lateral influx of 'special' waters. The problem with this model is that at a porosity of around 50%, dewatering of fine-grained sediments becomes increasingly more difficult due to low permeability. However, the dolomitization process may have commenced whilst deposition of the upper parts the Urgonian was still in progress.

Considering the field relationships and petrography of these dolomites a shallow burial origin due to the compactional release of connate pore fluids from the underlying mudstone succession is considered the most likely mechanism. The variable thickness of the replacement dolomitization may be due to the focusing of dolomitizing fluids initially into more porous and permeable beds. It is possible that the sediments of the vadose zone below the SbBA3 exposure surface (a sequence boundary in the basal section of the platform; see Hunt, 1992, see Fig. 3.4b) only underwent minor cementation and stabilization because of the sluggish movement of porefluids through vadose zones under the semi-arid/arid climate and so provided suitable porous and permeable beds (James & Choquette, 1984). Earlier formed dolomite cements (? from the circulation of seawater during later trangression of the platform and other seawater circulation mechanisms) may have formed the 'seeds' upon which this dolomite nucleated (cf. Zenger & Dunham, 1988). Once dolomitization has begun, and as long as the transport mechanism is maintained, the dolomitization is self perpetuating. Precipitation of dolomite from seawater leaves the solution undersaturated with respect to calcite, promoting further calcite dissolution and enhancing porosity for further dolomitization.

As mentioned earlier recrystallization of earlier formed (epigenetic) dolomite has been inferred by many authors (often because their geochemical signatures do not fit their model for the formation of the dolomite). Such a mechanism may have been operative within the dolomites of the basal Urgonian with increased fluid flow (possibly at elevated temperatures) during Tertiary compression. An example of actual dolomitization via syn-tectonic expulsion of fluids is given by Vahrenkamp & Taylor (1991). However, since dolomitization within the Urgonian is not spatially linked to tectonic features and it clearly pre-dates the formation of Alpine tectonic features (Roberts, 1991, reached the same conclusion) actual dolomitization via circulation of syn-tectonic fluids can be discounted.

However, recrystallization of earlier formed dolomite (even a early formed burial dolomite) cannot be discounted (this is discussed again in section 4.8.3).

3.12.6 Conclusions concerning the dolomitization of the Urgonian.

1) Dolomitization of the platform is regionally extensive, but highly variable in thickness.

2) It is a replacive dolomitization and has typically replaced grainstones of the shelf-margin facies association.

3) The dolomites have a coarse, sucrosic texture and consist of hypidiotopic mosaics of dusty cored/limpid rimmed planar-s rhombs.

4) Petrographically it post-dates early compactional features, such as mechanical fractures and grain contact suturing and could have been contemporaneous with early stylolitization, but it pre-dates the last phase of stylolitization (the arguments developed in section 3.11.4 for equant calcite/stylolite relationships apply to dolomitization as well).

5) A shallow burial dolomitization model is proposed to be the most suitable. The source and mechanism of Mg^{2+} movement is the dewatering of basinal sediments below the platform.

6) Dolomitization is also specifically linked to karstic dissolution features upon the upper surface of the platform. It is suggested that this dolomitization is related to the subsequent transgression and drowning of the platform in the upper Aptian.

7) Baroque dolomite also occurs within the Urgonian but is volumetrically insignificant.

3.13 Dedolomitization of the Urgonian dolomites.

Replacement of dolomite by calcite is commonly referred to as dedolomitization and is often thought of as a near-surface process (see Theriault & Hutcheon, 1987, for discussion), although it has been described from the burial realm (Budai et al., 1987).

3.13.1 Field description.

Dedolomites occur within some of the dolomitized horizons in the basal section of the Urgonian. Typically they have a fine grained, granular to crystalline texture (i.e. quite variable), but they do not possess the sucrosic texture distinctive of the dolomite. They are also variable in their colour, from grey to rusty red. Often they are very porous.

Stratigraphically dedolomites are often associated with correlatable exposure horizons, produced during brief periods of emergence. For example dedolomites at Gorge du Nant (log #6 in Appendix 1) occur at the karst between the Bs2 and Bs3 sequences of Arnaud-Vanneau et al. (1987) (SbBA3 sequence boundary of Hunt, 1992, see Fig. 3.4b).

3.13.2 Petrography of Urgonian dedolomites.

Several dedolomite textures are seen within the Urgonian and are similar to some of the dedolomites described by Henton (1990) from the Lower Muschelkalk of northeast Spain.

Fig. 3.42a Micritised dolomite rhombs can be seen on the right (area labelled A) and coarse calcite infilling vuggy porosity. 143/90 Gorge du Nant (#6 on Fig. 3.1, see log #3, Appendix 1). **Fig. 3.42**b Spectacularly zoned calcite infilling intercrystalline porosity around calcitized dolomite rhombs. 143/90 Gorge du Nant (#6 on Fig. 3.1, see log #3, Appendix 1). The dedolomitized rhombs have a bright orange core. On the basis of this distinctive luminescence these areas can be distinguished from the post-dolomite spar. Field of view= 4mm.

Typically dolomite is replaced by fine grained calcite, in some cases this mimicked the rhombohedral shape of the dolomite rhombs. In others the embayed and etched limpid dolomite rim of dolomite was preserved with the core replaced by micritic calcite; usually these dolomite remains were surrounded by micritic calcite (see Fig. 3.42a). Calcite mineralogy was confirmed by XRD analysis (see Appendix 3).

Under CL the rhombs are usually non-luminescent or uniform dull orange coloured with non-luminescent rims (similar to the original dolomite). Intervening areas of micritic calcite and areas of calcite filling vuggy porosity are spectacularly zoned (see Fig. 3.42b).

3.13.3. Interpretation.

Dedolomitization is usually ascribed to a near surface process. Several times during the basin evolution of the Subalpine Chains uplift occurred causing subaerial exposure (i.e. the late Cretaceous and early Paleogene and the end Miocene, see section 2.3.5, Chapter 8 and Moss, 1992). During these periods the replacive dolomite at the base of the Urgonian may have acted as a carrier bed for meteoric fluids (assuming the intercrystalline porosity was maintained to some extent). The passage of these fluids was responsible for the dedolomitization of parts of the basal Urgonian dolomites. The geochemistry of these dedolomites supports this suggestion (see section 4.12).

3.14 General conclusions to Chapter 3.

The Urgonian limestone is a Barremian-Aptian carbonate shelf deposit, typified by rudist bivalve and peloid/foraminifera limestones. These shelf-lagoonal limestones constitute the bulk of the Urgonian. Rudist limestones similar to those of the Urgonian in other parts of the world are important hydrocarbon reservoirs (e.g. the Poza Rica trend, Mexico, Enos, 1988).

A paragenetic sequence for the platform is presented and shows the relative ordering of diagenetic features within the platform and their magnitude. This sequence can be related to subsequent events within the basin, such as sea-level falls and uplift.

The Urgonian was partially lithified in a marine setting by a variety of marine cements.

A period of mineralogical selective dissolution of the aragonitic inner part of the rudist shells occurred early in post-depositional history of the platform. This dissolution occurred during meteoric exposure and produced abundant secondary porosity in the appropriate facies. At the same time low Mg-calcite parts of the rudists were stabilised by aggrading neomorphism. The petrography of the shells suggests that this occurred in a shallow subsurface setting.

Chemical dissolution at grain contacts and within the cortices of ooids occurred relatively early, along with the mechanical fracture of unsupported ooid rims, micritic envelopes, marine cements and rudist shells.

Final lithification of the platform occurred with the precipitation of poikilotopic and equant, drusy spar cements, notably occluding primary and secondary porosity associated with rudists. These are interpreted to be burial cements, although probably not deep burial. Syntaxial overgrowths are also common and maybe began to form in a marine setting.

The transgressive, basal part of the platform is preferentially replaced by a shallow burial dolomite, probably formed by the compactional release of entrapped connate seawater from the more muddier sections below the platform.

Uplift of the Dauphinois region in the late Cretaceous/Paleogene and the late Miocene to present allowed meteoric fluids to dedolomitize parts of the basal dolomite.

Chapter 4 Geochemistry of Urgonian rudists and diagenetic phases within the platform.

4.1 Introduction.

In the preceding chapter the Urgonian carbonate platform was introduced in terms of its age, depositional setting and facies types.

The original marine components and later diagenetic features of the platform were described and interpreted from their petrographic and field relations. This chapter discusses the geochemical signatures of these features, then discusses these results in the light of the data presented and interpretations made in Chapter 3.

4.2 Isotope geochemistry of rudist shells.

4.2.1 Introduction to the isotopic analysis of shells and their use in diagenetic studies.

Rudist shells within the Urgonian were studied primarily to provide a "diagenetic baseline" or starting line, from which studies of later diagenetic phases could be put into context. In studies of limestone diagenesis, defining the starting composition of the carbonate assemblage prior to diagenesis is important. This is because, for the majority of carbonates (and certainly in the case of the Urgonian), precipitation and deposition occur within marine waters and there is much evidence to suggest that the composition of marine waters has changed in a subtle fashion during geological time (see Fig. 4.1) (Wilson et al., 1983; James & Choquette, 1983; 1984; Given & Lohmann, 1985; Popp et al., 1986; Longstaffe, 1987; Lohmann, 1988). An estimate of the isotopic composition of marine water can be derived empirically from an analysis of primary marine components, such as brachiopods (e.g. Popp et al., 1986) or marine cements (e.g. Prezbindowski, 1985; Given & Lohmann, 1985). Brachiopods are often favoured as the best means of determining palaeo-ocean chemistry because their shells are initially low Mg-calcite (the most stable form of calcium carbonate) and so should suffer little alteration by later diagenesis. Samples for this type of study should be selected carefully, especially with regards to their stratigraphic position with respect to exposure surfaces. Even the "best preserved" fabric retentive, non-luminescent brachiopods can give isotopic values other than marine if they have been near an exposure surface where isotopic exchange with non-marine fluids may have taken place (Rush & Chafetz, 1990). Numerous previous authors have made estimates of the isotopic composition of Cretaceous seawater (Wilson et al., 1983; Czerniakowski & Lohmann, & Wilso 1984; Moldovanyi & Lohmann, 1984; Woo, 1984; Al-Aasm & Veizer, 1986b; Enos, 1988). Only three of these used rudists to estimate the isotopic composition of Cretaceous seawater (Moldovanyi & Lohmann, 1984; Al-Aasm & Veizer, 1986b; Enos 1988), and their data suggest that Cretaceous marine calcite has a composition in the region of δO^{18} -2 to -3

(PDB) and δC^{13} 1.5 to 3 (PDB). Al-Aasm & Veizer (1986b) argued that due to the similarity of the isotopic composition of rudist shells with preserved original mineralogy and microstructures to Holocene marine bivalves then Cretaceous and Holocene seawater had a comparable isotopic composition as well as a similar mode of incorporation of isotopes into their shell structure.

With rudists, because the shell is bi-mineralic and calcitization of the aragonite part of the shell may occur, it should be clearly stated which part of the shell was analysed. If for any part of the shell neomorphism had occurred in the presence of fluids other than marine waters, it will not give an accurate estimate of seawater composition.

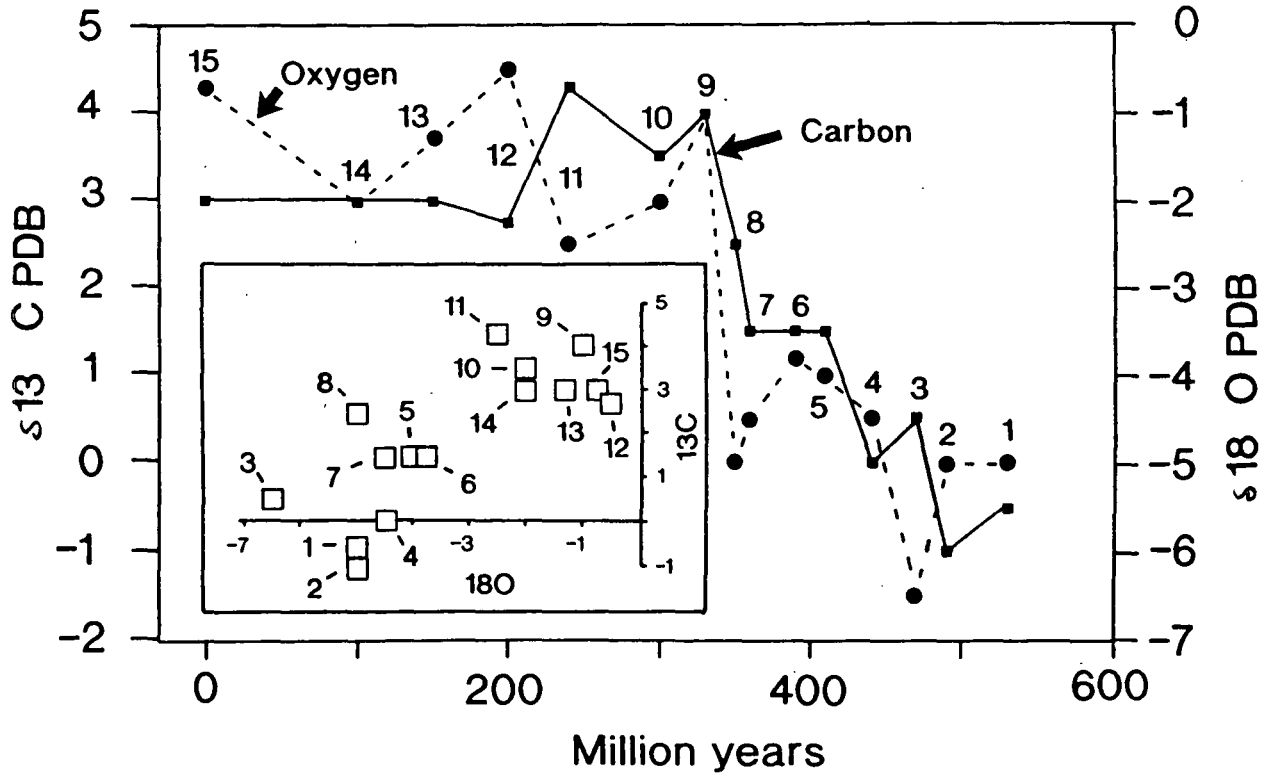

Fig. 4.1 Secular variation of carbon and oxygen isotopic composition of calcitic marine cements during the Phanerozoic. Numbered time intervals are: 15 = Holocene; 14 = Cretaceous (Aptian-Albian); 13 = Jurassic (Kimmeridgian); 12 = Triassic (Norian); 11 = Permian (Kazanian); 10 = Pennsylvanian (Moscovian); 9 = Mississippian; 8 = late Devonian (Frasnian); 7 = middle Devonian (Givetian); 6 = Late Silurian; 5 = middle Silurian; 4 = late Ordovician; 3 = mid-Ordovician; 2 = early Ordovician; 1 = early Cambrian. From Lohmann (1988). Data from low latitude reefal sequences from specific time intervals, the effects of diagenesis have been accounted for and removed so the values give primary marine calcite estimates.

In thin sections of all samples studied and from XRD analysis, it was apparent that only the outer low Mg-calcite layer was preserved (in section 3.9.5 it was suggested that this had been altered by aggrading neomorphism). If the division of bi-minerallic rudist

shells is as simple as an outer low Mg calcite and an inner aragonite (and/or low Mg calcite), then in theory (if it is unaltered) the outer part should give the original Cretaceous isotopic composition.

4.2.2 The isotopic composition of rudist shells.

Fig. 4.2 shows the isotopic compositon of rudists from the Urgonian (see Appendix 2 for full listing of results), along with values for the isotopic composition of seawater for the Cretaceous from the literature. As can be seen from Fig. 4.2 only a few of the rudists studied from the Urgonian have isotopic signatures similar to the previously quoted values for the Cretaceous. The majority of samples are depleted both in $\delta^{18}O$ and in $\delta^{13}C$. The shell samples studied have a mean isotopic of -4.1 +/- 1.16 $\delta^{18}O$ (PDB) and 1.44 +/- 1.16 $\delta^{13}C$ (PDB).

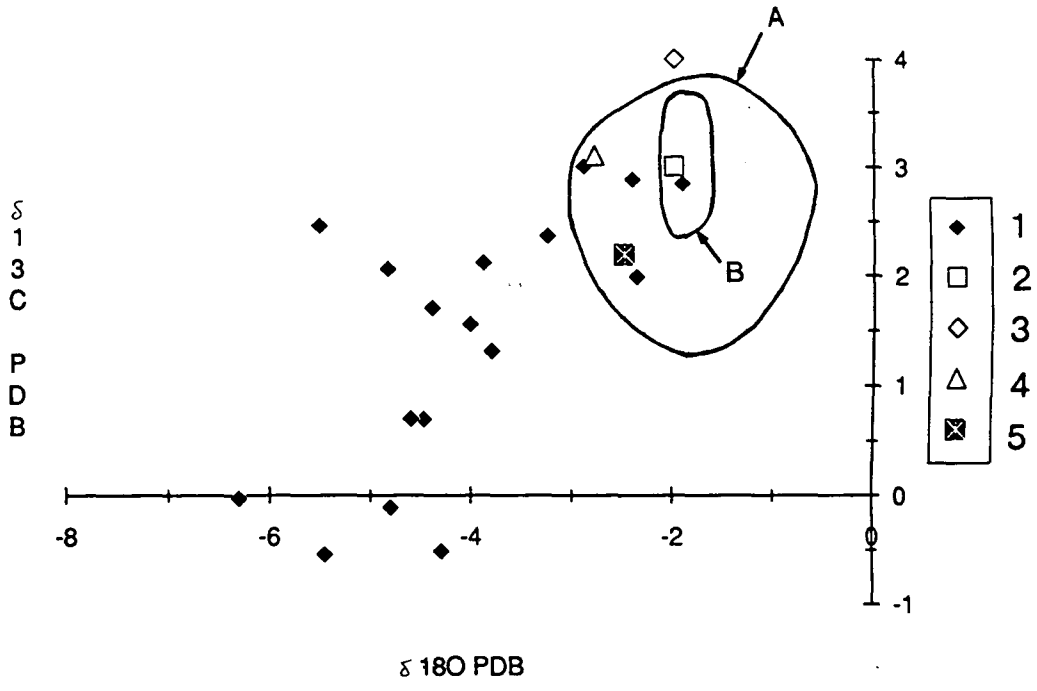

Fig. 4.2 Oxygen and carbon isotope cross-plot for Ugonian rudist shells, plotted against values from the literature for *'unaltered'* Cretaceous marine calcite. It can be seen that only a few of the rudist shells sampled have an isotopic composition similar to values usually quoted in the literature for Cretaceous marine calcite. 1= Urgonian rudists (this study); 2= Lohmann (1988) Aptian-Albian (see Fig. 4.1); 3= Moldovanyi & Lohmann (1988) lower Cretaceous rudists; 4= Enos (1988) Albian-Cenomanian 'original shell walls' of rudists; 5= Czerniakowski et al. (1984) Conacian-Santonian low magnesium calcite oysters, Field A= Woo (1986) mid-Cretaceous 'unaltered marine components'; B=Al-Aasm & Veizer (1986) preserved aragonite, Cretaceous rudists (upper Cretaceous mainly),

4.2.3 Interpretation of rudist shell isotopic compostion.

Samples with isotopic composition similar to published values for Cretaceous seawater can be considered either, 1) to be unaltered, or 2) to have been altered in the presence of marine waters and/or waters of the same chemistry (i.e. a closed system where fluids acquire a host rock signature via numerous dissolution-precipitation reactions). In section 3.9.5 it was suggested that the shells had been altered, so the second option is perhaps more likely. Petrographically samples with these isotopic compositions were identical to samples with more depleted isotope compositions.

For the samples where $\delta^{18}O$ is depleted by up to 2 per mil and $\delta^{13}C$ is unchanged to slightly depleted from values quoted for Cretaceous seawater (this applies to the majority of the samples), alteration (neomorphism) of the shell material in the presence of fluids depleted in $\delta^{18}O$ relative to co-eval seawater is suggested. $\delta^{13}C$ would be an value inherited from wall rock-fluid interaction, $\delta^{13}C$ signatures of fluids are easily 'swamped' by host rock-derived carbon because of the abundance of CO_3^{2-} in limestones.

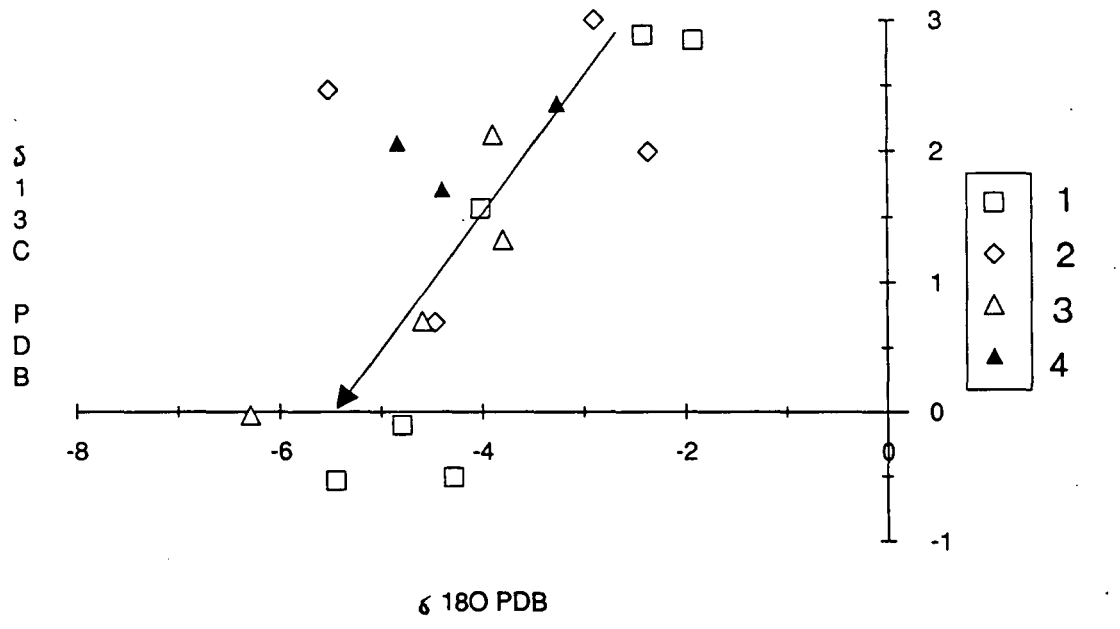

Fig. 4.3 Isotope cross-plot showing a co-variant mixing trend interpretation for the isotopic composition of rudist shells. Location of samples: 1= Chartreuse; 2- Vercors; 3= Bauges; 4= Aravis.

Those samples which are also depleted in ^{18}O (by up to 2 per mil), but are more significantly depleted in ^{13}C, suggest that the fluid was depleted in ^{18}O relative to co-eval

seawater, but had experienced a lesser degree of wall rock-fluid interaction (a more open system), with light $\delta^{13}C$ values coming from CO_2 introduced into the fluid from soil gas or from organic maturation.

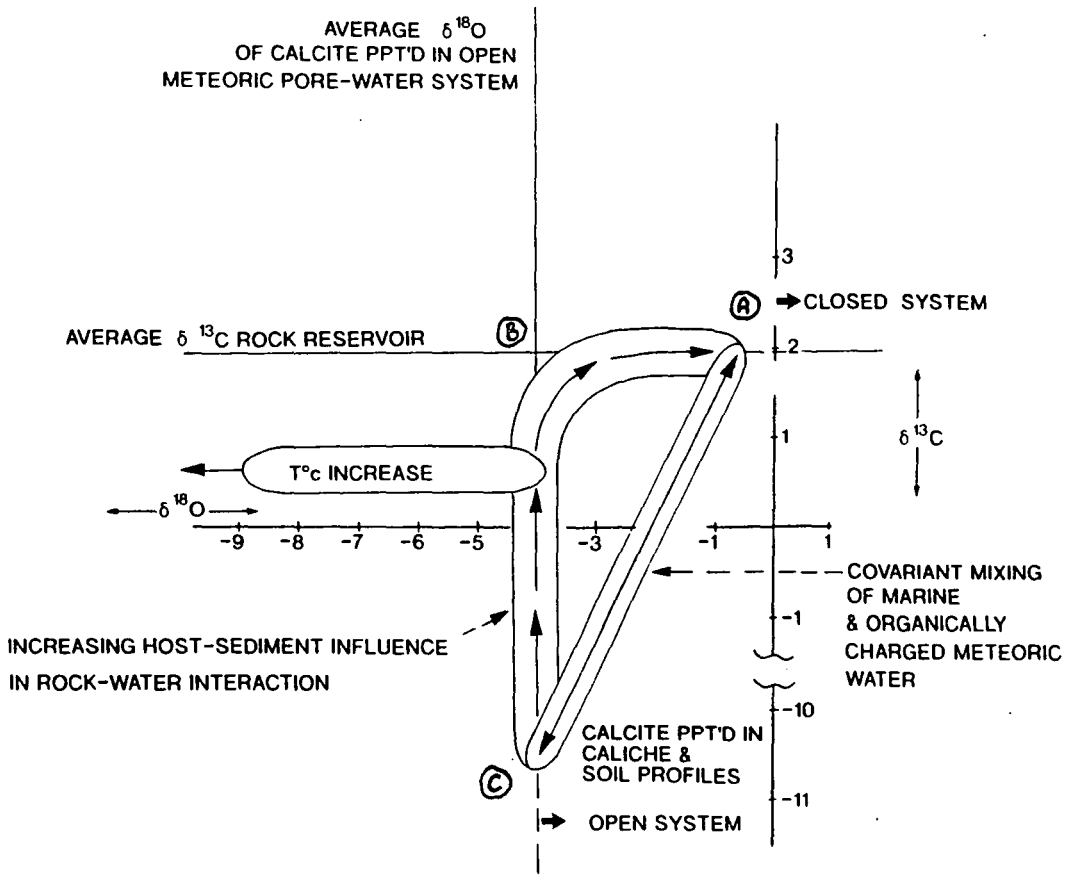

Fig.4.4 Likely oxygen and carbon isotope compositions and trends in carbonates undergoing meteoric diagenesis. Point A represents marine sediments (seawater) and ^{12}C enriched pore waters; point B represents a point where lighter meteoric oxygen has entered the system but no soil profile exists to provide light carbon and point C is typical for vadose zones where light carbon is provided from an overlying soil profile. Diagenetic calcites precipitated within a marine - meteoric mixing zone have a tendency to plot along the co-variant trend between A and B. Adapted from Allan & Matthews (1977); 1982, Hudson (1977), Wilson et al. (1983) and Lohmann (1988).

The overall trend shown by the rudist shell samples is interpreted to be a co-variant trend (as described in Wilson et al., 1983; James & Choquette, 1984; and Lohmann, 1988) produced by the mixing of marine and organically-charged meteoric water, typical of the mixed marine-meteoric phreatic or burial phreatic diagenetic environments. This trend is shown in Fig. 4.3. This sort of trend in isotope cross plots is produced by variation in the degree of rock-water interaction and indicates that there has been a variable degree of

mixing of the fluids responsible for the neomorphism of the fibrous calcite within the rudist shells studied. Figure 4.4 shows how such trends in isotopic composition can be interpreted.

In a similar way to the approach of Given & Lohmann (1985) who used marine cements, the samples with the heaviest $\delta^{18}O$ and $\delta^{13}C$ values can be used to indicate the isotopic composition of marine water and the lightest could indicate the isotopic composition of light (isotopically), meteoric water or a heavy (isotopically) formational fluid at elevated temperature (a burial neomorphism scenario).

In section 3.9 the petrography of the rudist shells within the Urgonian was presented and interpreted. It was concluded that typically only the outer part of the shell is preserved and this was stabilised from its original LMC mineralogy to dLMC in a shallow subsurface setting (during the Mesozoic the Urgonian only experienced shallow burial; see Chapter 8). If these conclusions concerning the depth at which the alteration took place are correct then the burial neomorphism by heated formational fluids looks less likely, unless hot fluids were transported into the shallow surface and retained their temperature. Thus it is more likely that meteoric fluids were involved in the neomorphism of the LMC part of rudist shells.

The meteoric fluids involved would have to be in equilibrium with calcite with a $\delta^{18}O$ value of around -4 to -6 PDB (mean value for the rudist shells is -4.1 PDB). There is independent evidence to suggest that this value is correct. The $\delta^{18}O$ of meteoric water becomes more negative with decreasing ambient temperature and increasing latitude. Compiled isotopic data on meteoric cements showed that the $\delta^{18}O$ values of meteoric calcite matched the same latitudinal changes predicted for modern environments (Hays & Grossman, 1991).

Fig. 4.5a The relationship between mean annual air temperature and the $\delta^{18}O$ of rainwater (SMOW), from Dansgaard (1964). This relationship provides a first approximation of the isotopic difference between meteoric and coeval marine waters. Assuming $\delta^{18}O$ marine = 0 per mil SMOW and a mean annual surface temperature, then an estimate of the $\delta^{18}O$ meteoric water can be made. **Fig. 4.5b** .Predicted mean annual air temperatures for the Cretaceous, modified from Barron (1986). From (a) it is apparent that mean annual surface temperatures for the palaeo-latitude of the Urgonian were in the region of 25-29°C, assuming the Cretaceous climate was hotter than the present day climate (as suggested by Barron et al., 1981; Barron, 1989). If the present day temperature range for the same latitudinal position is used the mean annual air temperature for the Urgonain would be around 22°C. Within the higher temperature range a $\delta^{18}O$ rainwater (SMOW) of around -1 per mil could be expected (according to Fig. 4.5a), whereas with the lower range a value of -2 could be expected. On Fig. 4.5a the two thin black lines (a and b) are the surface temperature range of the Urgonian assuming a hotter Cretaceous climate and the thick black line (c) assumes a present day climate to estimate of the surface temperature of the Urgonian in its Barremian-Aptian latitudinal position. Figs 4.5a and 4.5b are on the opposite page.

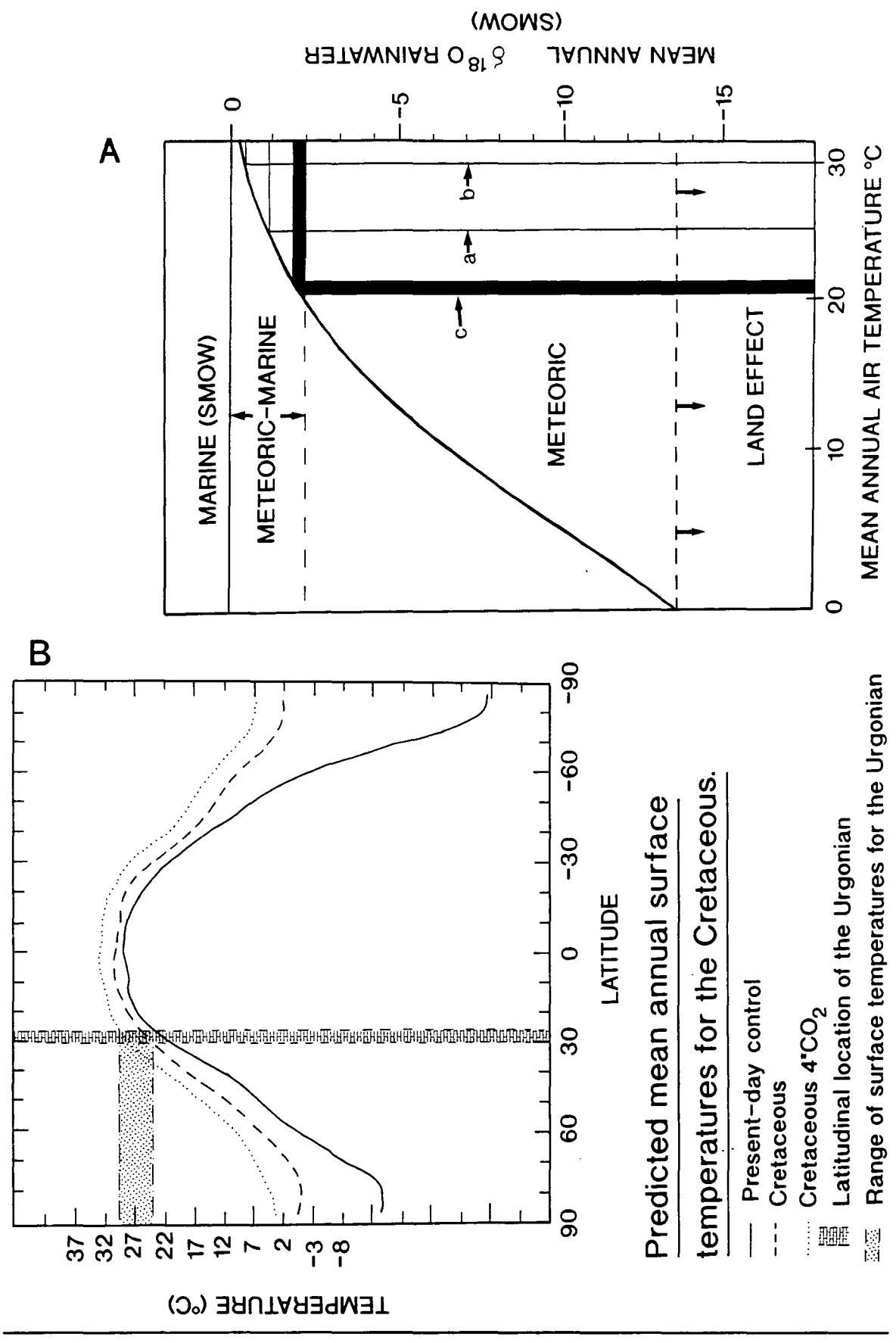
A
MEAN ANNUAL δ18O RAINWATER (SMOW)
0
-5
-10
-15
MARINE (SMOW)
METEORIC-MARINE
METEORIC
LAND EFFECT
a
b
c
0
10
20
30
MEAN ANNUAL AIR TEMPERATURE °C
B
TEMPERATURE (°C)
37
32
27
22
17
12
7
2
-3
-8
90
60
30
0
-30
-60
-90
LATITUDE
Predicted mean annual surface temperatures for the Cretaceous.
Present-day control
Cretaceous
Cretaceous 4*CO2
Latitudinal location of the Urgonian
Range of surface temperatures for the Urgonian

Fig. 4.6 Oxygen isotopic fractionation between calcite and water at sedimentary temperatues. From Anderson & Arthur (1983). If it is assumed that the calcite precipitated at temperatures of 25 to 30°C (likely surface or very shallow burial temperaures), then given that the mean value $\delta^{18}O$ PDB value for a rudist shell is -4.1, the likely $\delta^{18}O$ of water in equilibrium with it would be -2 to -1.

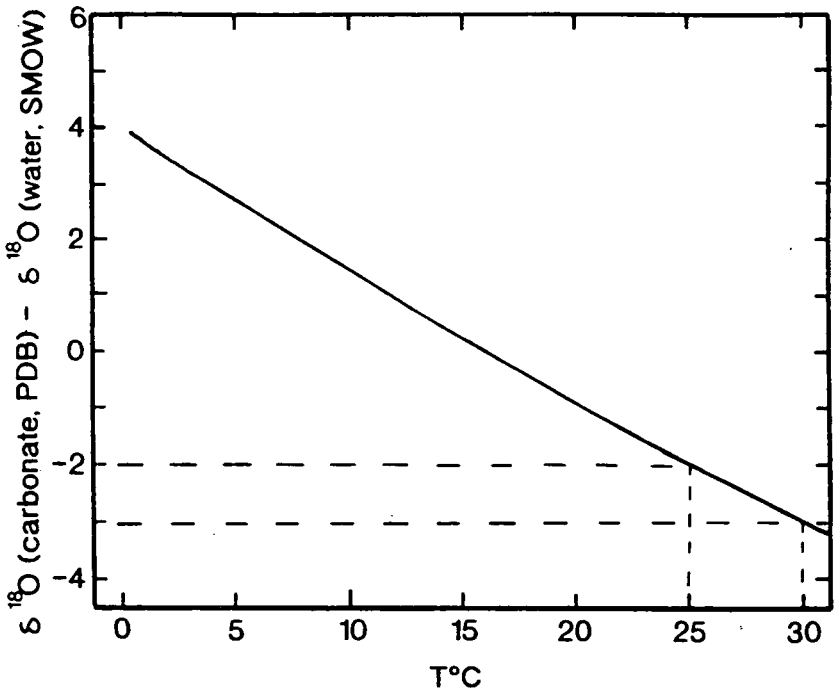

Several independant lines of evidence can be used to predict the composition of meteoric water. Dansgaard (1964) documented the relationship between mean annual air temperature (which can be roughly correlated with latitude) and the annually averaged $\delta^{18}O$ of coastal rainwater (see Fig. 4.5b). Using this relationship and an estimate of the mean annual surface temperature for the latitudinal location of the Urgonian in the Aptian (see Fig. 4.5a) suggests a rain water composition of around -1 to -2 $\delta^{18}O$ SMOW. Water with this isotopic composition should be in equilibrium with calcites with a composition of -4 to -5 $\delta^{18}O$ PDB in the temperature range of 25° to 30°C (Anderson & Arthur, 1983) (see Fig.4.6), which fits the likely temperatures for the Urgonian whilst at the surface (Fig. 4.5b).

From the diagram of Yurtsever (1975) the composition of meteoric water in the equivalent present day latitude as that for the Urgonian in the Cretaceous, is -2 to -4 $\delta^{18}O$ SMOW. It should be noted that more depleted meteoric fluids could be produced by additional fractionation due to "land effects" (the presence of mountain belts nearby, *etc.*) and if the area borders an enclosed body of seawater. However, by reference to available palaeogeographic data (see section 2.4, Mintz, 1981 and Dercourt et al., 1985, Barron, 1986; 1987) the latter two do not seem to be applicable to the Urgonian.

4.2.4 Conclusions to the isotopic study of rudist shells.

1) Mean isotopic content of the shells studied -4.1 +/- 1.16 $\delta^{18}O$ and 1.44 +/- 1.16 $\delta^{13}C$

2) Isotopic content of most of the rudists studied suggests that they have been altered.

3) The fluids present during alteration were most likely meteoric or meteoric-mixed marine in origin.

4.3. Trace element content of rudist shells.

4.3.1 Introduction to trace element studies.

ICP-AES analysis was carried out on rudist shells to determine their trace element composition. For the rudists (and for all constituents of the Urgonian studied), samples were drilled from the same areas used in the isotope study, although in some cases there was insufficient material for both isotope and trace element analysis (see Appendix 2 for full listing of results and analytical technique).

In a similar manner to the way stable isotopes from co-eval seawater are incorporated into organic and inorganic carbonates, these same precipitates will incorporate trace elements. The concentration of that trace element within an inorganic carbonate can be predicted by use of an appropriate distribution coefficient, if a straight guest/host substitution is assumed. The partitioning of a trace element at low activities (or concentrations) between liquid and solid phases is given by:

$$(m_t/m_c)\text{solid} = D.\ (m_t/m_c)\text{liquid} \qquad (4.1)$$

(where m= moles, t= trace element, c= major element, D= distribution coefficient). When D<1 the trace element is preferentially concentrated into the fluid; when D>1 the trace element is preferentially partitioned into the solid. If D=1 no partitioning occurs and the m_t/m_c ratio in the fluid and the solid are the same. The concentrations of Mg^{2+}, Sr^{2+}, Fe^{2+} and Mn^{2+} in equilibrium-precipitated inorganic calcite can be predicted using equation 4.1, if water compositions are known (see Fig. 4.7).

The above equation assumes that the mother solution is an infinite reservoir (an open system) and therefore the composition of any precipitate will be uniform. The value of D for a trace element depends on many variables (chemical composition of the fluid, crystal growth rate, nature of the reaction, temperature and pressure, Eh and pH conditions) and will not predict incorporation of elements into non-lattice sites. Several workers have expressed doubts concerning the application of commonly used distribution coefficients in diagenetic studies (Land, 1985; Moore, 1985; 1989). As regards the trace element content of rudist shells there is also the fact that biomineralization will occur from body fluids and not ambient fluids (the so-called 'vital-effect') (see Veizer, 1983, Morse and Mackenzie, 1990 and Tucker & Wright, 1990 for further discussion).

Fig. 4.7. The abundances of trace elements in calcite precipitated from waters of known composition using the partition coefficients shown. Cation concentrations in seawater are well known; for meteoric water, river water is used as an approximation and for formation waters oil field brine was used as an approximation. From Tucker & Wright (1990).

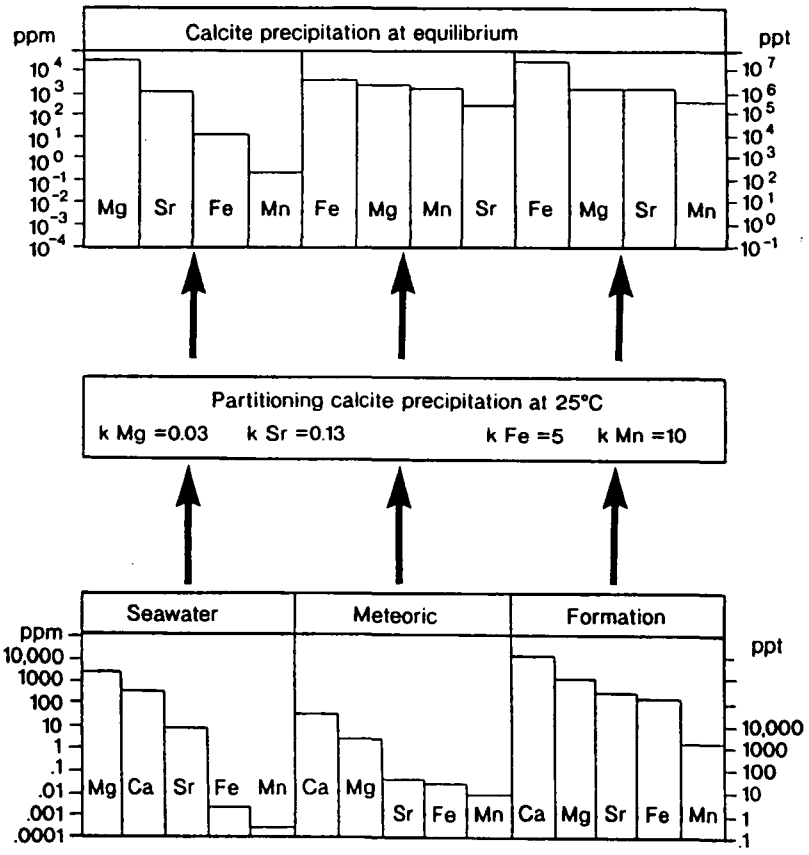

4.3.2 Trace element content of rudists.

Within the prismatic calcite (dLMC, see section 3.9) of the rudist shells sampled during this study the range of trace element compositions were as follows: Sr^{2+} 200 - 1140 ppm, Fe^{2+} 60 - 3430 ppm and Mn^{2+} 7 - 300 ppm (see Figs 4.8 and 4.9), with values widely scattered between these limits as shown by the mean and standard deviation for these three ions. For example Sr^{2+} composition of the rudist shells has a mean value of 674 +/- 305 ppm (n= 17), mean Fe^{2+} content = 375 +/- 692 and mean Mn^{2+} content = 52 +/- 55. Figs 4.8 and 4.9 show the Sr^{2+}, Mn^{2+} and Fe^{2+} composition of the shells. Fig. 4.10 shows the variation of Sr with $\delta^{18}O$ values for the same shells.

Fig. 4.8 (opposite page). Plot of Sr^{2+} versus Mn^{2+} concentrations in Urgonian rudists. Location of samples; 1= Chartreuse; 2= Vercors; 3= Bauges; 4= Aravis.

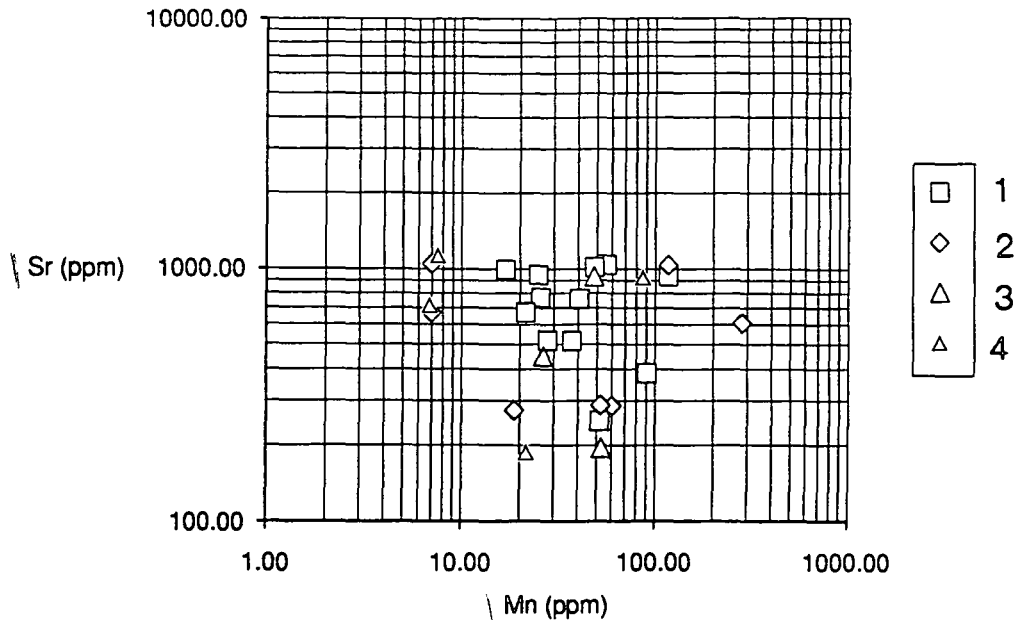

Fig. 4.9 Plot of Mn^{2+} versus Fe^{2+} concentrations in Urgonian rudists. The covariance between the two is taken to indicate that the same factors controlled the concentration of these two cations in rudist. Location of samples; 1= Chartreuse; 2= Vercors; 3= Bauges; 4= Aravis.

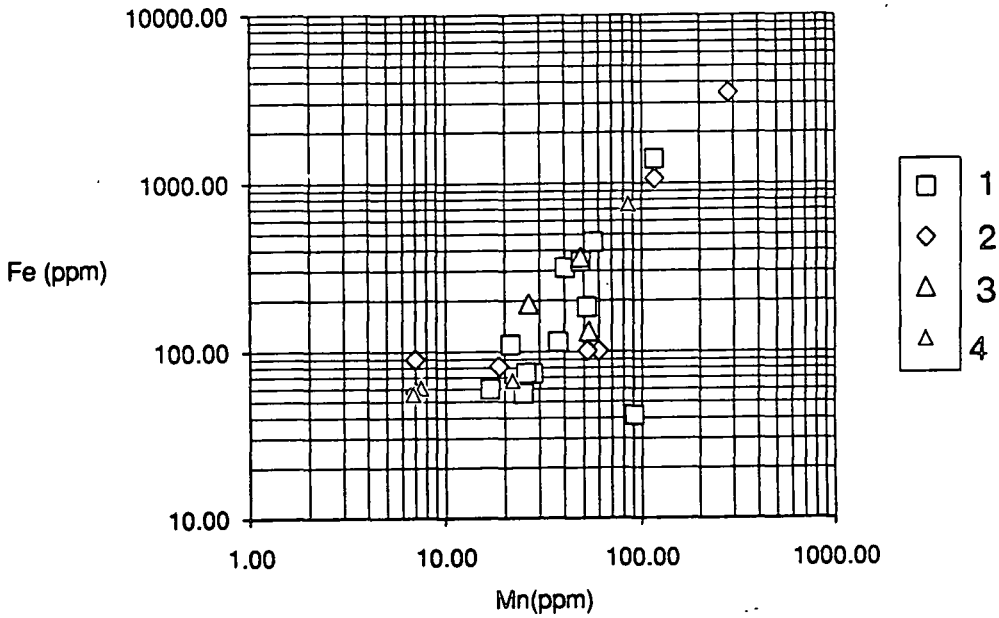

4.3.3 Interpretation of trace element contents in rudists.

For the majority of the rudist shells the Sr^{2+} content is much less than would be expected in a marine aragonite or high Mg-calcite precipitate (from Fig. 4.7). Samples of well preserved aragonite from the inner shell layers of rudists studied by Al-Aasm & Veizer (1986a) have a mean value of Sr^{2+} of 1400 ppm, whereas those without preserved

aragonite have a Sr^{2+} mean value of 430 ppm. Low Sr^{2+} values in calcite have been suggested to show precipitation or recrystallization in contact with meteoric water (Kinsman, 1969; Brand & Veizer, 1980; Veizer, 1983). When the Sr^{2+} content within the shells is compared to $\delta^{18}O$ value for the same sample there is a slight correlation. With the exception of three of the samples, there is a trend toward lower Sr^{2+} content with more depleted ^{18}O. The samples with the lowest Sr^{2+} and most depleted ^{18}O suggest alteration of the shells in 'open' diagenetic conditions. For the three samples that do not fit this trend it is suggested that local controls (number of dissolution events, lithological differences, contrasting pore residence times of fluids, *etc*) were more important, such as increased dissolution increasing the amount of Sr in the fluid.

Fig. 4.10 Plot of Sr^{2+} concentration versus $\delta^{18}O$ composition of the same shell samples. A slight correlation can be seen, more depleted ^{18}O values coincide with lower concentrations of Sr^{2+}. Location of samples; 1= Chartreuse; 2= Vercors; 3= Bauges; 4= Aravis.

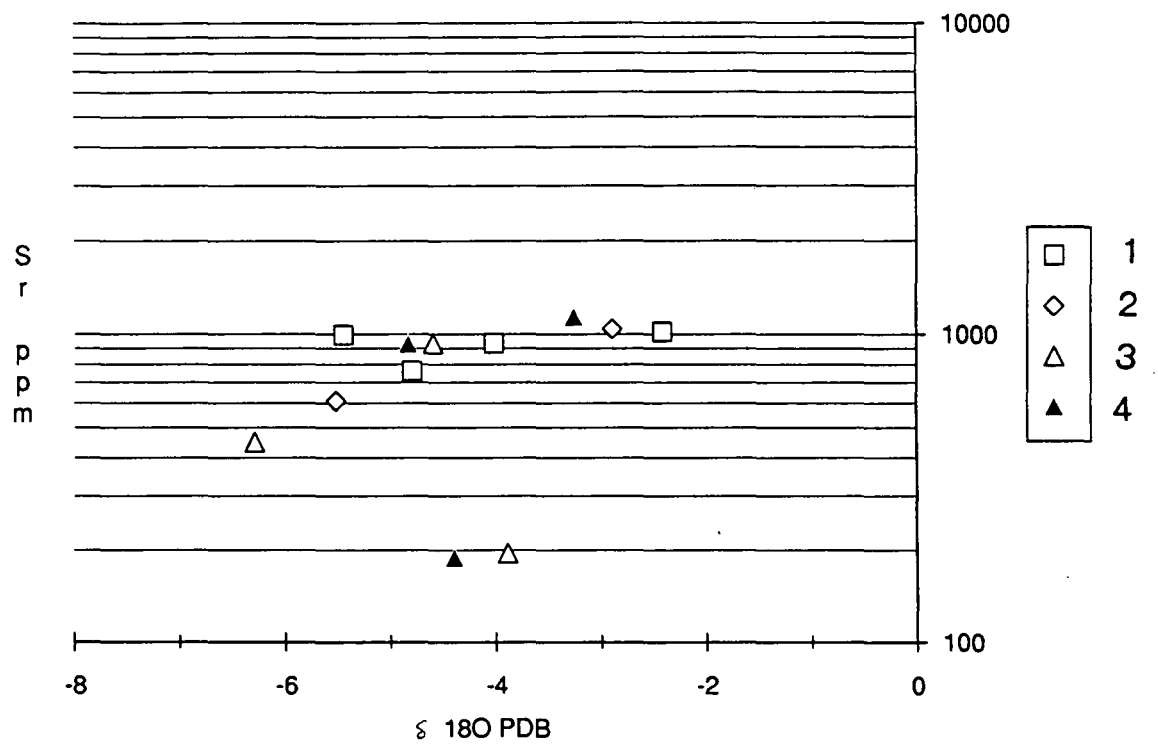

The trace element content of the rudists shows a wide variation in the content of Fe^{2+} and Mn^{2+} (see Fig. 4.9). The concentration of Fe^{2+} and Mn^{2+} in fluids and diagenetic phases is not controlled solely by partitioning between fluids and rock reservoirs, i.e. the degree of rock - water reaction, as they are not sourced from the dissolution of other carbonate phases, rather their concentration within a fluid requires reducing conditions and a local source within the sediment (Lohmann, 1988). Most Urgonian rudists have Mn^{2+}

concentrations of 100 ppm or less. This indicates that porefluids were oxidising and/or there was no source of Mn^{2+} in the system (this explains their non-luminescence). Both Fe^{2+} and Mn^{2+} concentrations within rudists would seem to be controlled by the same factors (availability and Eh - pH conditions of the fluids and similar partition coefficients); this can be seen by their co-variance between the concentrations of Mn^{2+} and Fe^{2+} (see Fig. 4.9). Al-Aasm & Veizer (1986a) found very little difference in the mean values of Fe and Mn between rudists with preserved aragonite and those without preserved aragonite (see their Table 5).

A few of the rudist samples have high Fe^{2+} content (up to 3400 ppm in one shell from the Vercors); however, the mean value is much lower (370 ppm, with a standard deviation of 690 ppm). The high iron content of some of the shells could be due to the presence of early framboidal pyrite precipitated along the shell margins, due to bacterial reduction of dissolved sulphate producing H_2S to react with Fe^{2+}. The shelf-lagoon facies would have been an area of low energy with minimal circulation and presumably initially high contents of organic matter (although this now oxygenated) which could favour the formation of some early authigenic iron minerals. Small, cubic, opaque minerals which are presumbably iron pyrite (or similar) were occasionally seen in thin section.

4.3.4 Conclusions concerning the trace element content of rudist shells.

Overall, for the Urgonian the above trace element data suggest that the fluids at the time of neomorphism were oxidising and part of an open system. The results of the isotope study suggest that the rudist shells had been altered in the presence of mixed marine-meteoric fluids indicating an open system, and this would seem to support the trace element data. Both trace element and isotopic data support the notion that the preserved LMC part of the rudist shell studied has been altered to dLMC (by neomorphism) and the degree of alteration is variable. The alteration occurred in an open pore water system with low degree of rock to water interaction.

4.4 Isotope geochemistry of burial cements.

4.4.1 Introduction to the isotopic analysis of calcite cements.

As with the shells of rudists the spar cements seen within the Urgonian were analysed for their isotopic and trace element composition. The analytical technique is given in Appendix 2, along with a full listing of samples, location and results. In section 3.11.3 (d) the CL response of these cements was described, for geochemical samples (both isotope and trace element) care was taken to sample from the centre of the pore space where the cement has a uniform luminescence (either dull orange or non-luminescent). However they are still likely to represent average values for the final stages of precipitation.

The isotope geochemistry of fluids responsible for burial cementation is largely determined by the origin of the fluid. Depleted waters can be produced either by light (meteoric) fluids (possibly slightly heated) or heavy (formation) fluids at high temperature (Prezbindowski, 1985:Woronick & Land, 1985). For the $\delta^{13}C$ isotope the possibility of light CO_2 from organic maturation or perhaps from a soil environment, is important. However, with ^{13}C the degree of rock/water interaction is also important, because the carbon reservoir within carbonate systems is so large that the original carbon signature of the fluid may be overprinted by CO_3^{2-} derived from the host-rock to show an average wallrock type value. The isotopic composition of the cement precipitated will therefore reflect the above, but will also be affected by the temperature of precipitation as regards its $\delta^{18}O$ composition, due to increasing fractionation between $^{18}O/^{16}O$ with increasing temperature (there is only minor isotopic fractionation of $^{13}C/^{12}C$ with increasing temperature, Anderson & Arthur, 1983).

4.4.2 The isotopic composition of the equant, burial cements in the Urgonian.

Figs 4.11a and 4.11b shows the isotopic composition of the equant, drusy mosaic burial cements within the Urgonian from throughout the Subalpine Chains. It can be seen that these cements plot in two different fields (spar A and spar B on Fig. 4.11b, although. there is no difference in the timing of precipitation of these two fields). Both have the same depletion in $\delta^{18}O$ (between -5.7 to -11) and are depleted relative to Cretaceous marine values and most of the rudist shell samples (see Fig. 4.2). The difference between the two fields lies in the $\delta^{13}C$ value. Spar A shows a similar to slightly depleted, composition for $\delta^{13}C$ (+3 to -1) when compared to $\delta^{13}C$ values for unaltered marine calcite (compare Figs 4.2 and 4.11). Spar B is more strongly depleted with regards $\delta^{13}C$ (-3 to -5) when compared to $\delta^{13}C$ values for unaltered marine calcite (compare Figs 4.2 and 4.11) and only occurs within the rudist associated porosity.

4.4.3 Interpretation of the isotopic composition of the equant, burial cements.

The composition of spar A field is taken to indicate internal buffering with regard to the supply of $\delta^{13}C$ and the temperature effect on $\delta^{18}O$. The $\delta^{18}O$ composition of spar B would seem to also reflect the temperature effect. For spar 2, two possibilities exist for the light $\delta^{13}C$ values. They could be due to light CO_2 coming from either organic maturation in deeper units, or from meteoric vadose zone soil gas. However, since these cements from their petrography are interpreted to have formed in a shallow burial setting (see section 3.11.3), the latter source of light ^{12}C seems unlikely, as it is difficult to envisage how such a light signature would be preserved in fluids passing through possibly several hundreds of metres of carbonate, unless there is a distinct lack of fluid/wall rock reaction. Thus it is more likely that the depletion in ^{13}C seen in spar 2 is due to the incorporation of light CO_2 from organic maturation.

Fig. 4.11a Isotope plot for equant burial spars within the Urgonian plotted for the type of pre space the cement occludes. 1= rudist associated porosity; 2= fenestral porosity; 3= coralline associated porosity. **Fig. 4.11b** Isotope plot for equant burial spars within the Urgonian plotted for the geographic location of the sample. Location of samples; 1= Chartreuse; 2= Vercors; 3= Bauges; 4= Bornes; 5= Aravis.

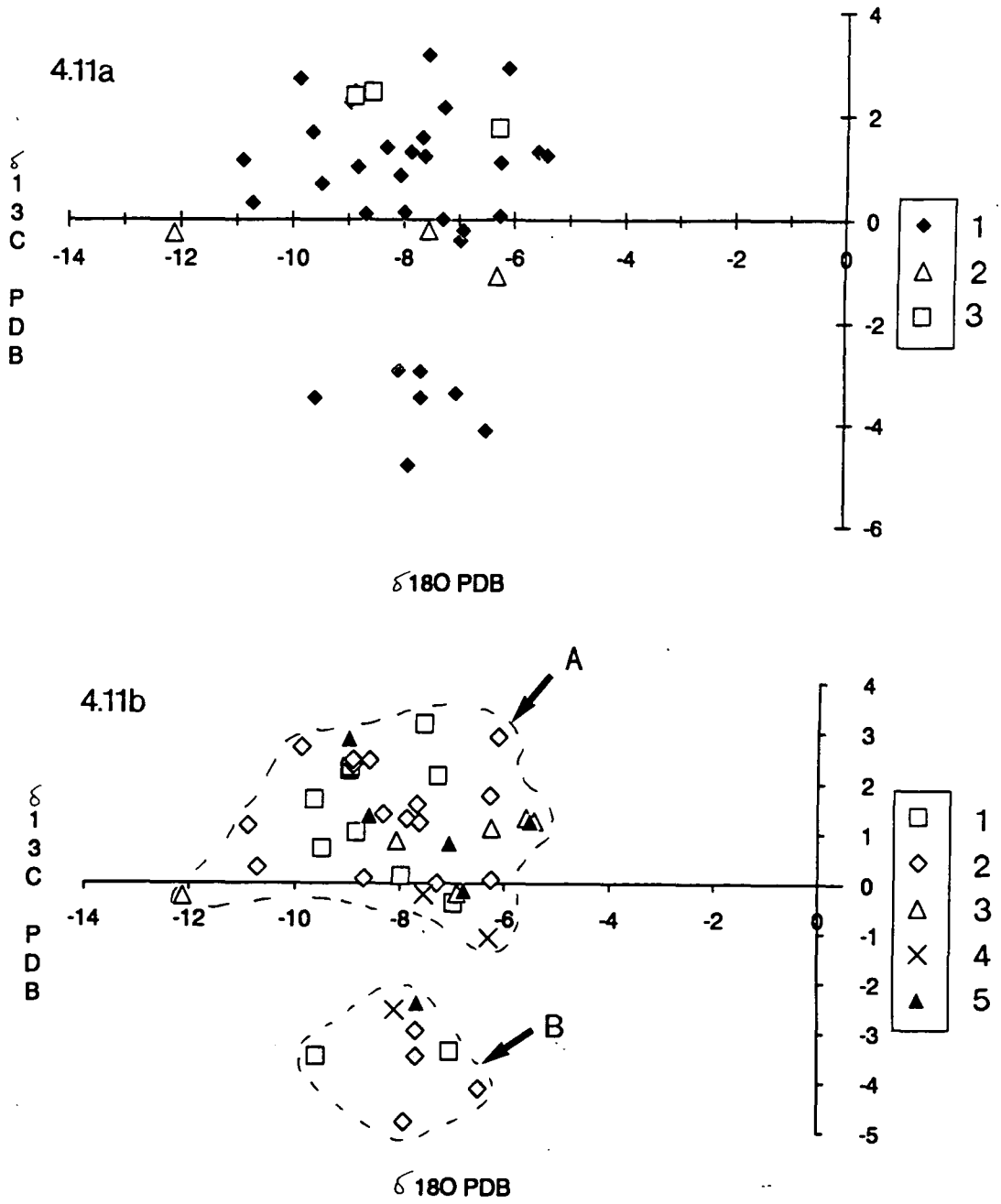

In section 3.11.3 equant calcite cements were described petrographically from three different pore type associations. There is a difference in the isotopic composition of the equant calcite in those different situations, in that depleted ^{13}C values only occur within the equant burial cements occluding porosity associated with rudists. This may be an indication of a slight 'channelization' of fluids responsible for the precipitation of these cements.

There is no difference in the isotopic composition related to geographic location (see Fig. 4.11b).

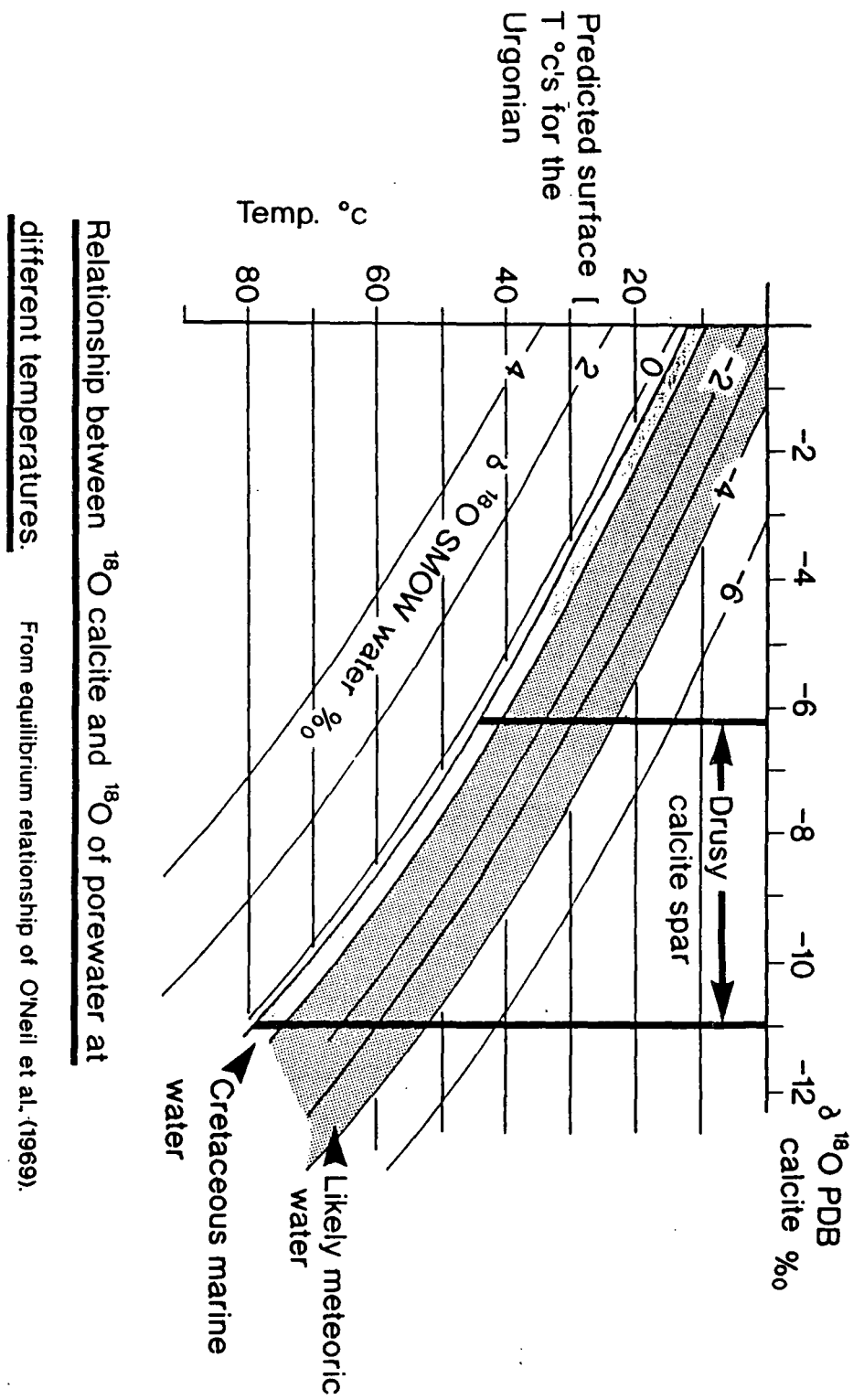

Relationship between ^{18}O calcite and ^{18}O of porewater at different temperatures. From equilibrium relationship of O'Neil et al. (1969).

Fig. 4.12a

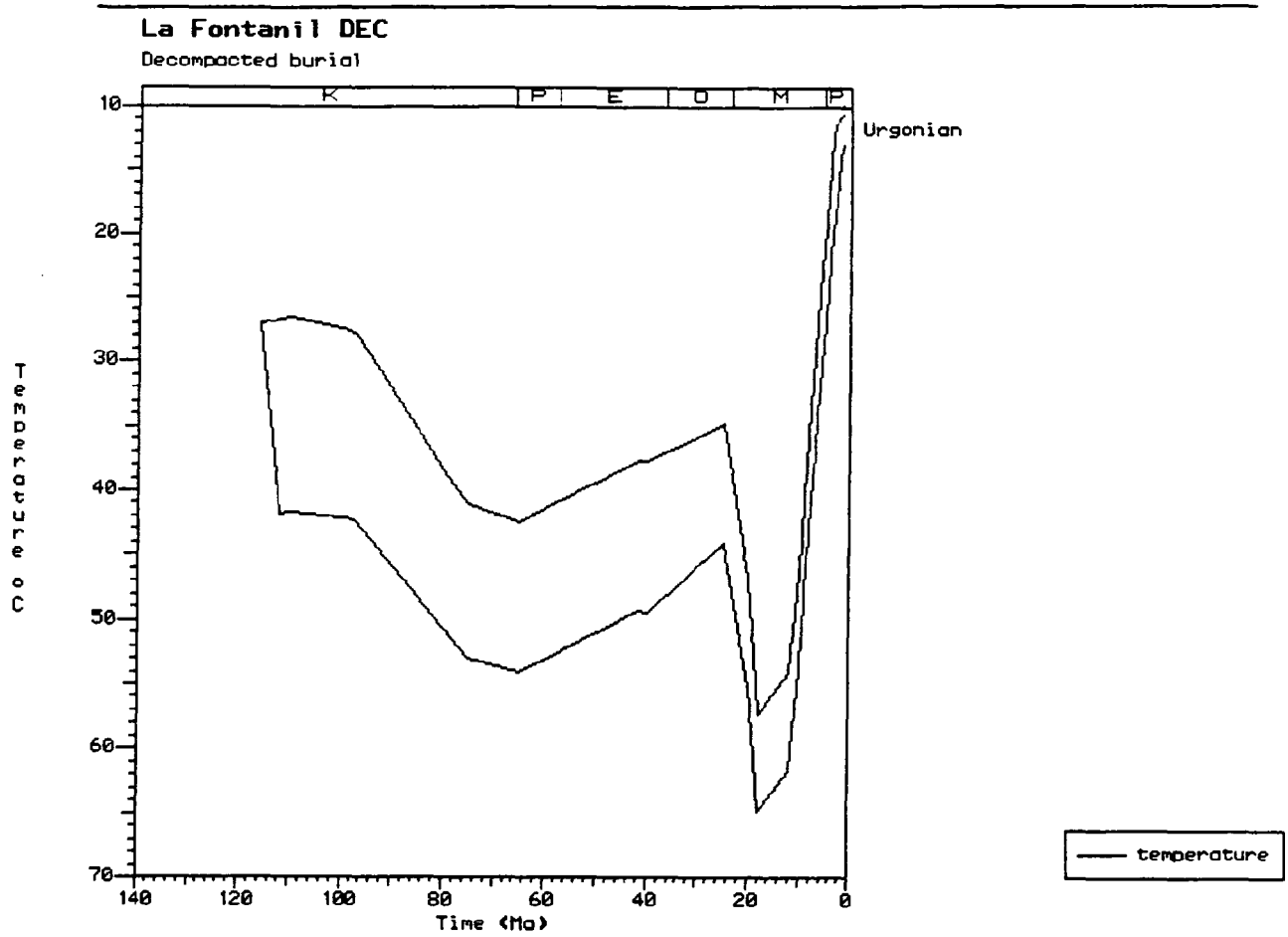

Fig. 4.12b

Fig. 4.12a (previous page). The relationship between $\delta^{18}O$ of calcite (PDB), the $\delta^{18}O$ of porewater (SMOW) and temperature (°C). Constructed from the equilibrium relationship of O'Neil et al. (1969). Values for the estimated compostion of co-eval seawater and meteoric water are marked on, along with the isotopic compostions of the equant burial cements. **Fig. 4.12b** Plot of the burial temperatures for the top and bottom of the Urgonian at La Fontanil (southern Chartreuse, see Fig. 8.7 for location). Calculated using a geotherm of 30°C/km for the Cretaceous, this figure suggests that the Urgonian experienced burial temperatures of between 45°C and 55°C during the Cretaceous. However the likely error bar on this estimate (due to factors such as under- or over- estimation of missing upper Cretaceous sediments) is likely to be around 10°C, giving a burial temperature range of 35°C to 65°C.

Fig. 4.12a shows the relationship between $\delta^{18}O$ of calcite and porewater (using the equilibrium relationship of O'Neil et al., 1969). This shows the temperature range over which the cements could have been precipitated. The $\delta^{18}O$ SMOW of marine water has varied through time in response to variations in the volume of glacial ice and other factors (Tucker & Wright, 1990). This is reflected in the secular variations seen in the oxygen isotopic composition of marine calcite shown in Fig. 4.1. Climatic modelling (Barron et al., 1981; Barron, 1989) suggests that during the Cretaceous glacial ice volume was minimal. Calculations of the effect of incorporating oxygen from glacial water suggest that relative

to modern oceans, Cretaceous sea-water had a $\delta^{18}O$ SMOW signature between -0.92 per mil and -0.52 per mil (Woo, 1986; Ross, 1989). On Fig. 4.12a it is marked on as -0.5 to -1 per mil. In section 4.2.3 it was suggested that Cretaceous meteoric water (for the latitudinal position of the Urgonian in the Barremian/Aptian) had a composition of around -1 to -2 $\delta^{18}O$ SMOW; this range is used again (on Fig. 4.12 meteoric water is shown to have a composition between -1 and -4 to account for any errors in this estimate). If these estimates of the $\delta^{18}O$ SMOW of sea-water and meteoric water are used it suggests that these cements may have precipitated from either of these fluids from temperatures just above those predicted as surface temperatures (27-30°C, see Fig. 4.5a) for the Barremian-Aptian to temperatures as high as 80°C. If the cements precipitated from seawater the temperature would have to be 5 to 7°C higher (dependant on what composition of meteoric water is used; see Fig. 4.12a). This latter possibility is discounted on the basis of the trace element content of the cements (see sections 4.6 below), from the paragenetic history of the platform (see Fig. 3.5 and section 3.6) and from petrography (see section 3.11.3). It is well established that the platform was sub-aerially exposed during several brief periods and in the lower Aptian leading to the karstification of the upper part of the platform (see sections 3.5.1 and 3.6 and Hunt, 1992). Any marine porefluids are likely to have been 'flushed' out of the platform at this stage and replaced by meteoric fluids. Only in basinal settings, usually not affected by exposure from eustatic and/or tectonic-induced sea-level controls, are porefluids likely to have remained marine in origin as the sediments passed into the shallow burial phreatic environment (Choquette & James, 1987, their table 5).

In Chapter 8 and Moss (1992) the results of burial and thermal history modelling of specific locations within the Subalpine Chains are described. Fig. 4.12b shows the calculated burial temperatures for the top and base of the Urgonian for one such location. These suggest that prior to the Tertiary the Urgonian had only been buried to maximum depths from 800m to 1.5km and based on an average geothermal gradient of 30°C/km, burial temperatures would have been in the range of 35°C to 65°C (see Fig. 4.12b). These temperatures agree with the temperatures for precipitation indicated in Fig. 4.12a and are in agreement with burial temperatures suggested for the Urgonian during the mid- to upper-Cretaceous from the thermal and burial history modelling shown in Fig. 4.12b and Chapter 8. Given the likely burial conditions of the Urgonian when this cement was precipitated, the involvement of high temperature formation fluids can be ruled out. Unless a mechanism such as fault valving is invoked (e.g. Burley et al., 1989), however in such an instance cements are likely to be spatially related to the conduit faults. This is not seen in the Urgonian. Some updip migration of fluids must of occurred to cause the light ^{13}C PDB values of the some of the cements (assuming the light ^{12}C is from organic maturation).

4.4.4 Conclusions to isotopic composition of equant, burial cements.

1) The isotopic composition of these cements can be interpreted in several ways; the most likely is that the fluids responsible for the precipitation of these cements were of meteoric origin at elevated temperatures.
2) $\delta^{13}C$ composition of the cements divides the samples into two compositional fields, those with $\delta^{13}C$ derived from host rock interaction and those with $\delta^{13}C$ derived from the input of light CO_2 from organic maturation occurring deeper in the section.

4.5 Trace element composition of equant, burial cements.

Drusy mosaic, equant spar cements were analysed for their trace element content. The same problems of using trace elements described in section 4.3.1 for rudists apply here too. Calcite cements were sampled for their trace element composition in a similar manner to the way rudist shells were studied. The analytical technique and a full listing of sample locations and results is given in Appendix 2.

4.5.1 Trace element composition of equant, burial cements.

Figs 4.13 & 4.14 show the Sr^{2+}, Mn^{2+} and Fe^{2+} contents of the drusy mosaic, equant cements. Sr^{2+} ranges from 400 to 20 ppm, mean 334 +/- 418 ppm, Mn^{2+} ranges from 400 to 10 ppm, mean 92 +/- 67 ppm and Fe^{2+} ranges from 2250 to 50 ppm, mean 213 +/- 209 ppm. Fig. 4.15 shows the Sr^{2+} composition versus $\delta^{18}O$ for the same spar samples.

Fig. 4.13 Plot of Sr^{2+} versus Mn^{2+} concntrations in equant cements in the Urgonian. Location of samples: 1= Chartreuse; 2= Vercors; 3= Bauges; 4= Aravis; 5= Bornes.

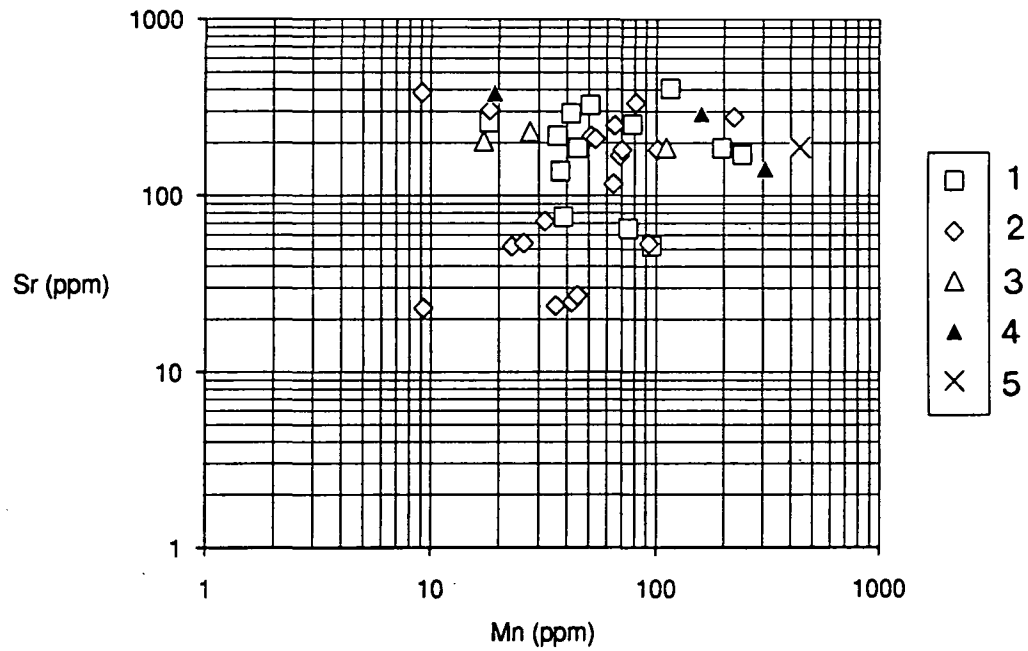

Fig. 4.14 Plot of Mn^{2+} versus Fe^{2+} concentrations in equant cements in the Urgonian. Location of samples: 1= Chartreuse; 2= Vercors; 3= Bauges; 4= Aravis; 5= Bornes.

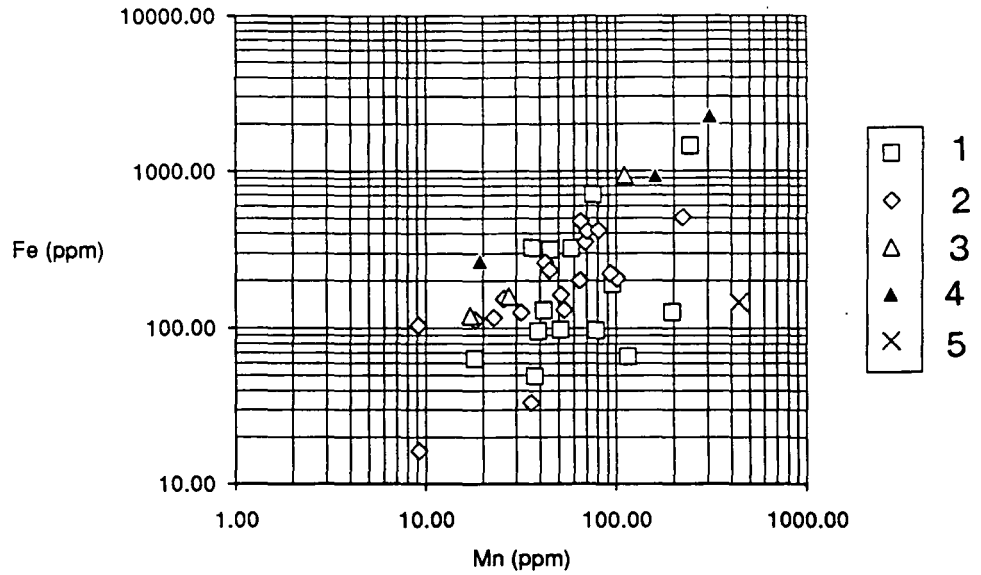

Fig. 4.15 Plot of Sr^{2+} concentration versus $\delta^{18}O$ composition of equant cements in the Urgonian. Location of samples: 1= Chartreuse; 2= Vercors; 3= Bauges; 4= Aravis; 5= Bornes.

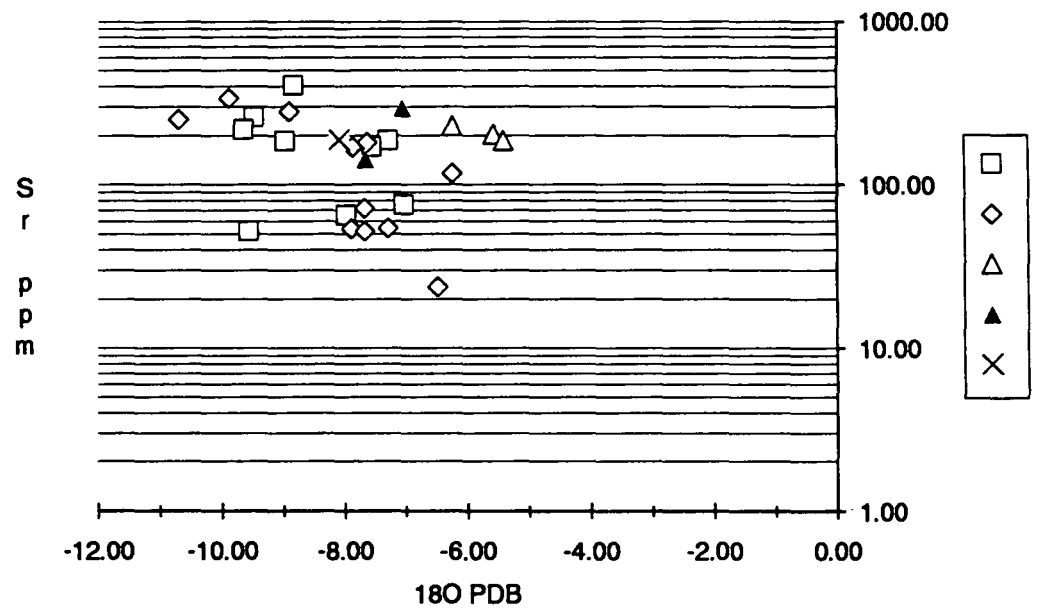

4.5.2 Interpretation of trace element composition of the equant, burial cements.

The trace element geochemistry of the equant spar cements suggests that the fluids responsible for the precipitation of the cements were meteoric in origin. This is indicated by the low Sr content of the calcite (see Fig. 4.13), which is typical of meteoric fluids

(Kinsman, 1969; Brand & Veizer, 1980; Veizer, 1983) and the low Fe^{2+} content (see Fig. 4.14). The latter seems to rule out the possibility that formational or burial fluids were responsible for the precipitaion of the cements, since these fluids usually are typically associated with high iron contents (see Fig. 4.7). However, it is also possible that the fluids simply contained little Fe^{2+} (perhaps because they had not passed through possible 'donor' beds; Emery, 1987). The Sr^{2+} values for the cements on the whole are lower by 200-300 ppm than those reported for rudists (in section 4.4.2, compare Figs 4.13 and Fig. 4.8). The Fe^{2+} and Mn^{2+} concentrations are very similar to those seen in the rudist shells and show the same roughly co-variant distribution (high values of Fe mostly coincide with high values of Mn^{2+}) (compare Figs 4.9 and 4.14). This is probably due to the similarity in distributtion coefficients and the fact that they are controlled by the same factors (see section 4.3.3). Emery (1987) shows similar trends in Fe^{2+} and Mn^{2+} for burial calcites in the Lincolnshire limestone. No particular trend can be picked out in Fig. 4.15, which shows the Sr composition versus $\delta^{18}O$ for the same spar samples. This indicates that differences in the Sr composition of the fluids were produced by local factors (degree of dissolution in the vicinity of cement precipitation, contrasting porewater residence times, *etc*), whilst the $\delta^{18}O$ of the cements was controlled by the temperature of precipitation. As with the trace element concentrations in the rudists, the large standard deviations show that the population of trace element values is widely scattered.

Overall, this suggests that the fluids which precipitated the equant cements had less of a marine influence (if any at all), but Fe^{2+} and Mn^{2+} were controlled by the same factors and a similar source as for Fe^{2+} and Mn^{2} in the rudist shells.

4.5.3 Conclusions concerning the geochemistry of equant spar cements in the Urgonian.

The equant cements in section 3.11.3 are interpreted to have precipitated in a shallow burial setting. Trace element and stable isotope data for these cements suggest that they were precipitated from meteoric fluids at slightly elevated temperatures. Supporting evidence comes from the shallow burial setting of these cements and from burial history and thermal modelling of the Subalpine Chains detailed in Chapter 8 and Moss (1992).

4.6 Synthesis of the geochemistry of rudist shells and drusy, equant spar cements in the Urgonian.

The geochemistry of both the rudist shells and these cements supports the interpretations made in sections 3.9.5 and 3.11.3 (f), regarding their environment of formation. The depletion seen in the ^{18}O isotopic composition of the equant spar cements compared to the rudist shells (see Fig. 4.16a and section 4.13) suggests that the cements were precipitated at slightly elevated temperatures (see Fig. 4.16b), supporting the shallow burial origin of these cements (see section 3.11.3 (f)). The generally lower Sr content of the

cements compared to the rudist shells (see Fig. 4.16b) indicates that the rudists have retained some of their original marine Sr^{2+} content, whereas the low Sr content of the cements supports their origin from meteoric fluids. The similarity of the Fe^{2+} and Mn^{2} concentrations within the cements and rudist shells suggests similar porefluid geochemistries at the time of shell stabilization and cement precipitation and/or similar controls on the Fe^{2+} and Mn^{2} content of diagenetic fluids involved in cement precipitation and shell stabilization. Material for the precipitation of these cements may of been derived from the dissolution of shell material and other grains (see sections 3.9.2 and 3.9.3) slightly higher up in the section.

Fig. 4.16a Comparison of the stable isotope composition of rudist shells and equant burial cements. The depletion in the $\delta^{18}O$ value and in ^{13}C (in some cases) of the equant cements reflects the increased temperature of precipitation and the incorporation of light CO_2 from organic maturation in some cases. 1= cements; 2= rudist shells. **Fig. 4.16b** Comparison of the $\delta^{18}O$ composition versus Sr concentration for rudist shells and equant cements. 1= cements; 2= rudist shells.

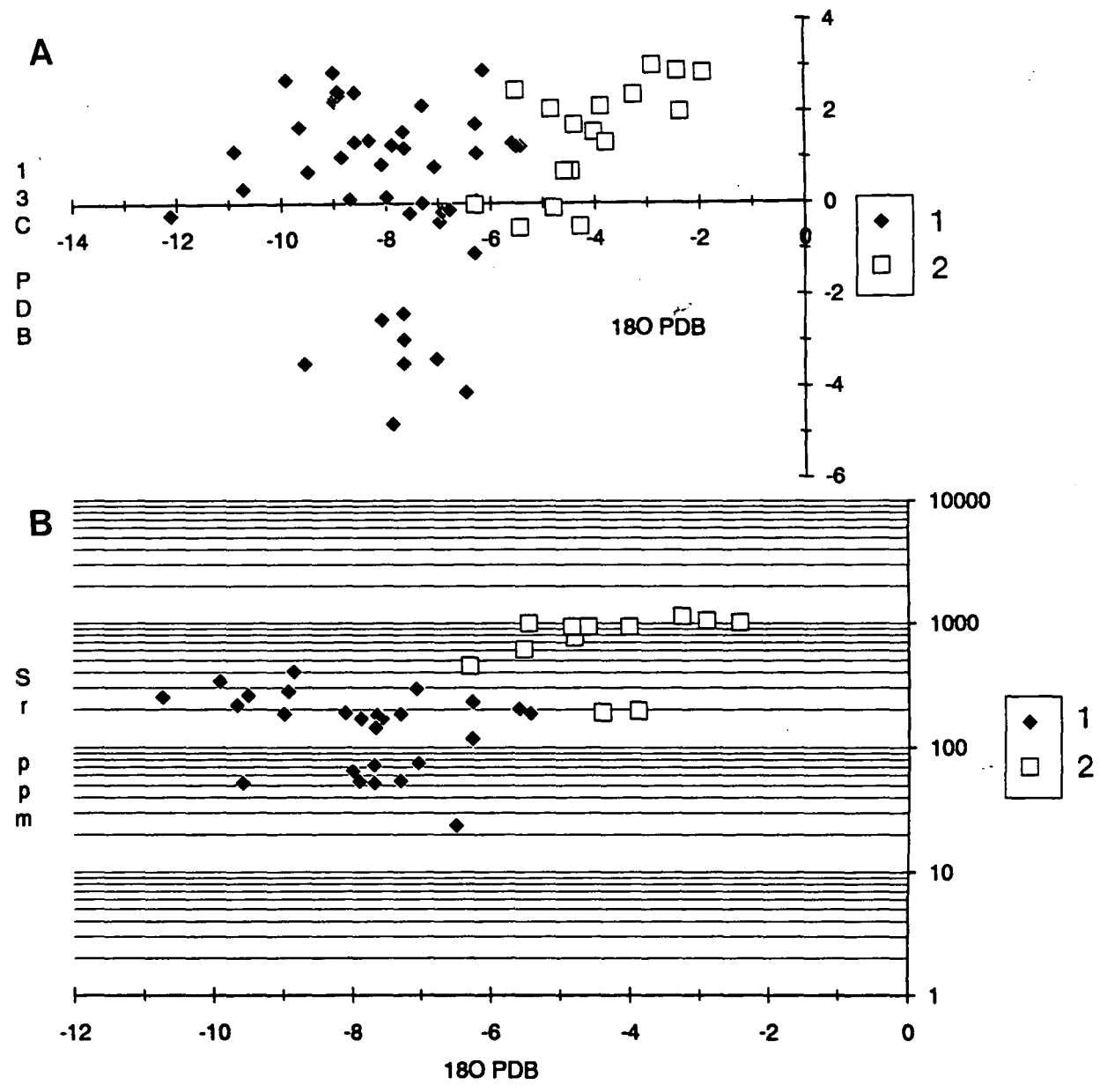

4.7 Isotopic compostion of basal replacive dolomites.

4.7.1 Introduction.

The volumetrically most important dolomite within the Urgonian is the replacive planar-s to planar-e dolomite that occurs preferentially at the base of the platform replacing the shelf-margin facies (F5 to F7). This was described and interpreted in section 3.12.5 to be a shallow burial dolomite formed by the early compactive release of connate sea-water from underlying basinal sediments. These dolomites were analysed for their stable isotopic composition at the same time as the rudist shells and equant spar cements. A full description of the analytical technique and listing of results is given in Appendix 2.

Much has been written about the geochemistry of dolomites (eg. Land, 1980; 1983; 1985; Morrow, 1982a; Hardie, 1987; Tucker & Wright, 1990) and many problems still exist. Central to these is the uncertainty concerning the nature of isotopic fractionation between dolomite and diagenetic fluids, and dolomite and calcite. However, in a similar manner to isotopes from calcite spar (see section 4.5.1), the oxygen isotope composition of dolomite is most likely to be determined by the isotopic composition of the fluid and the temperature of precipitation, whilst the carbon isotopic signature of the dolomite is strongly influenced by that of the precursor limestone and the amount of organic matter diagenesis (assuming that the geochemistry of the dolomite has not been re-set via recrystallization of the dolomite; Land, 1985; Hardie, 1987).

4.7.2 Isotopic composition of dolomites within the Urgonian.

The basal burial dolomites (see section 3.12.5) plot between -3 to -7 $\delta^{18}O$ PDB (mean = -4.88 +/- 0.92) and -1 to +3 $\delta^{13}C$ PDB (mean = 1.41 +/- 1.1); this is shown in Fig. 4.17a. Fig. 4.17b shows the isotopic composition of the burial dolomites along with the isotopic composition of two samples of microcrystalline dolomite associated with the microkarst upon the upper surface of the platform (see section 3.12.1) and three samples of baroque dolomite (see section 3.12.3). The former plots between -5.9 to -5.4 $\delta^{18}O$ PDB and 1.8 to 3.1 $\delta^{13}C$ PDB, whilst the latter has a mean $\delta^{18}O$ PDB of -5.68 +/- 0.29 O and a mean $\delta^{13}C$ PDB of 1.74 +/-0.93. It can be seen that isotopically the basal replacive dolomites are similar to the karst-related and baroque dolomite types within the Urgonian.

4.7.3 Interpretation of isotopic composition of basal replacive dolomites and other dolomite types within the Urgonian.

The isotopic composition of all three types of dolomite within the Urgonian (see Fig. 4.17b) are very similar to those previously described for dolomites of burial/mudrock dewatering origin, with negative $\delta^{18}O$ PDB (usually somewhere between -4 to -10) and positive to zero values for $\delta^{13}C$ PDB (Mattes & Mountjoy, 1980; Zenger, 1983; Gregg, 1985; Gawthorpe, 1987 and numerous other papers). However, there is the possibilty of recrystallization of earlier formed dolomite with an associated re-setting of the geochemical

Fig. 4.17a Isotopic composition of the basal dolomites, plotted for each different massif. Sample location: 1= Chartreuse; 2= Vercors; 3= Bauges; 4= Bornes; 5= Aravis. **Fig. 4.17b** Stable isotopic composition of the various dolomite types seen within the Urgonian. 1= shallow burial dolomites; 2= baroque dolomite; 3= karst-related dolomite.

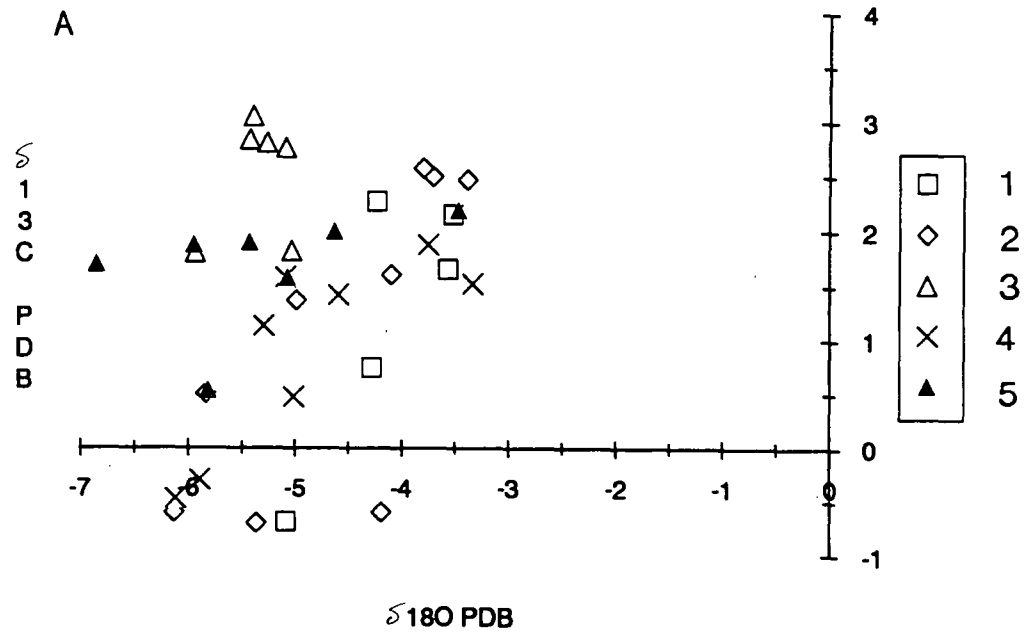

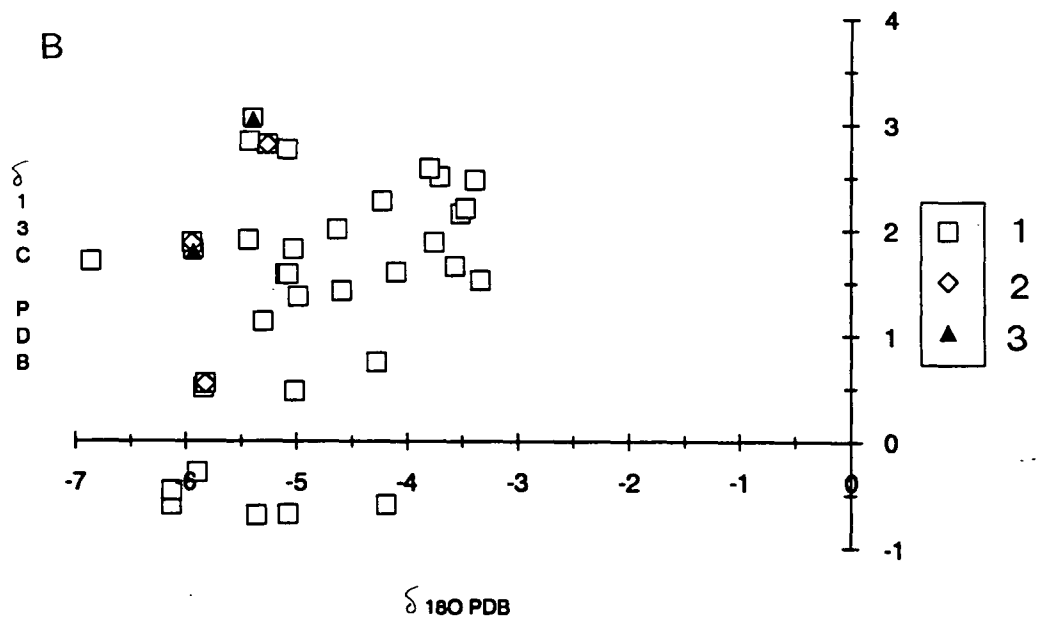

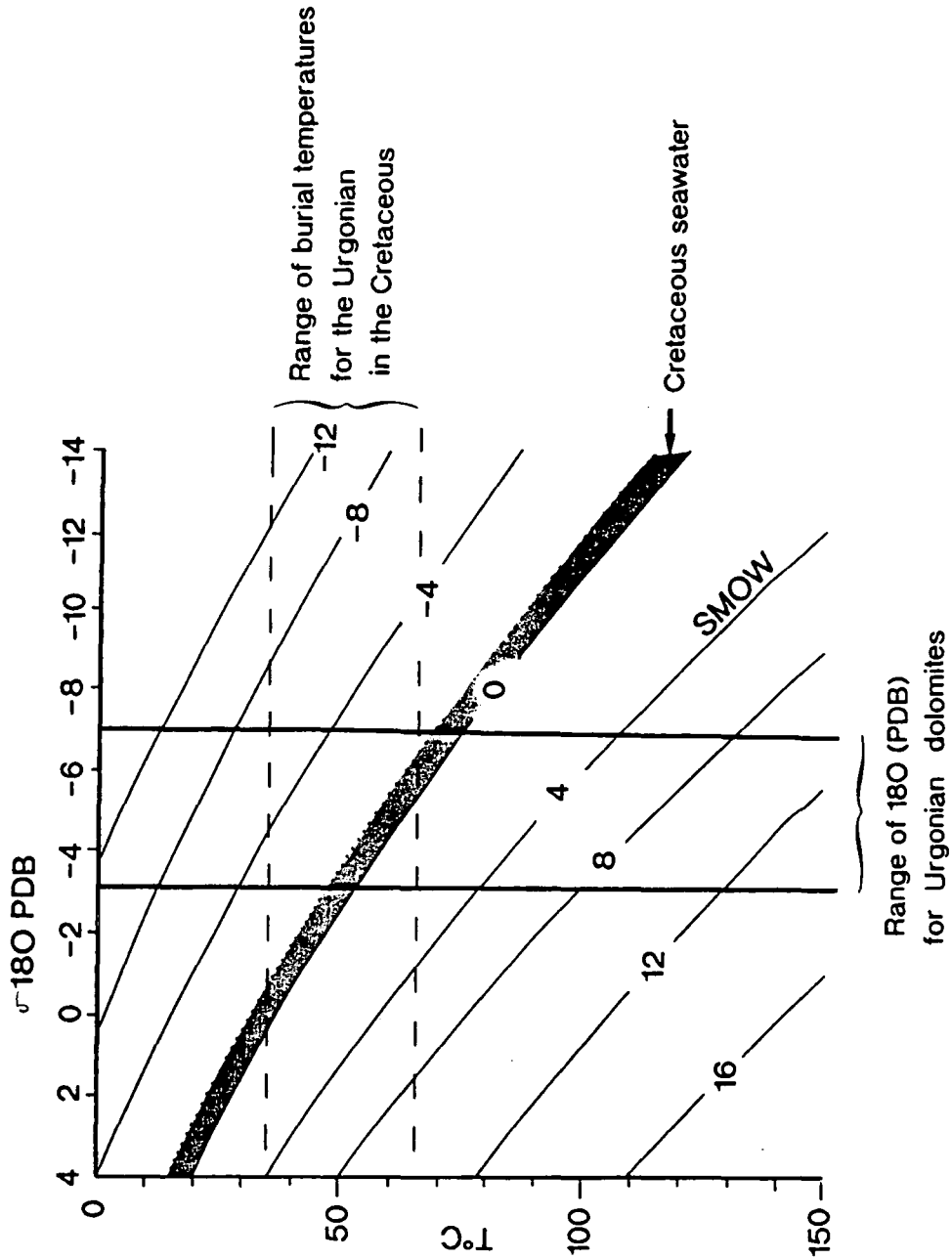

Fig. 4.18 The relationship between $\delta^{18}O$ (dolomite) versus temperature (°C) for various $\delta^{18}O$ (SMOW) (assuming the equilibrium fractionation relationship shown in Land, 1983 and Woronick & Land, 1985). The likely Cretaceous burial temperatures for the Urgonian (see Fig. 4.12b) along with the $\delta^{18}O$ composition of the basal dolomites (n.b. the upper temperature range is more applicable since these dolomites occur at the base of the platform).

signatures of the dolomite so that the isotope sigantures do not justify assigning these dolomites to a burial origin without further discussion. As with all geochemistry (perhaps especially where dolomite is concerned) the results should only be used to support a particular model of dolomite formation if the field relationships and petrography are in agreement with the model. Similarity of the isotopic composition of the planar-s, mosaic replacive dolomites and inferred early dolomites (see section 3.12.1) and baroque dolomites (see section 3.12.3) indicates either that they were precipitated from the same fluids or recrystallization of some of the dolomite occurred causing the geochemical signature of the dolomites to be re-set.

The $\delta^{13}C$ value for the majority of the dolomites sampled is a typical marine limestone signature (compare carbon values shown in Figs 4.17a and 4.17b with Fig. 4.2) and so can be interpreted as inherited from the original sediment it replaces (or in the case of the baroque dolomite cements, the $CaCO_3$ that provides a substrate for precipitation). In the case of the few samples (all from the basal replacive dolomite) with slightly negative $\delta^{13}C$ values, the incorporation of CO_2 from organic maturation, similar to the spar B field for the equant spar cements (see section 4.5.2), is the most likely explanation.

If basal replacive dolomites were precipitated from Cretaceous seawater released as connate fluids during the early compaction of underlying basinal muddier sections (as suggested in section 3.12.5), and assuming the $\delta^{18}O$ SMOW value of Cretaceous seawater (given in section 4.5.3) to be -0.52 to -0.92 $\delta^{18}O$ SMOW, then the dolomitization occurred from fluids with a temperature of 50 to 80°C (using the equilibrium fractionation relationship shown in Land, 1983 and Woronick & Land, 1985) (see Fig. 4.18). Using an average geothermal gradient (30°C/km) estimated burial temperatures for the base of the Urgonian as it experienced during burial in the upper Aptian to the late Cretaceous are in the region of 45 to 65°C (see Fig. 4.12b and Chapter 8 and Moss, 1992). Thus heated seawater or isotopically depleted heated seawater derived by the early compactional release of connate marine porewaters (see section 3.12.5) could explain the isotopic composition of the dolomites. However, the temperatures quoted above are the maximum burial temperatures reached by the Urgonian during Cretaceous burial. If the dolomitization occurred before these temperatures were attained then it suggests that the dolomitizing fluids were slightly hotter than the host sediment or fluid was more depleted than Cretaceous seawater (this is assuming that the thermal modelling of Chapter 8 and Moss, 1992, is correct and the geochemistry of the basal dolomites has not been re-set).

4.8 Trace element content of basal replacive dolomites.

In veiw of the number of factors involved, including uncertainty about the appropriate distribution coefficients, it is difficult to interpret quantitatively the trace-element contents of dolomites (Land, 1980; Mattes & Mountjoy, 1980; Hardie, 1987).

4.8.1 Trace element contents of the basal replacive dolomites.

The Sr^{2+}, Mn^{2+} and Fe^{2+} concentrations of the basal replacive dolomites and baroque dolomites are shown in Figs 4.19 and 4.20. In the basal dolomites Sr^{2+} is generally low (mean=127 +/- 27 ppm) and is fairly consistent (see Fig. 4.19), likewise Mn^{2+} is also low (mean= 97 +/- 120 ppm). Fe^{2+} content is very variable (mean=930 +/- 1246 ppm) as shown in Fig. 4.20. Two samples of baroque dolomite analysed have very similar trace element compositions and are plotted along with the basal dolomites in Figs 4.19 and 4.20. Unfortunately due to time constraints no samples of karst-related dolomite were analysed for trace element content.

Fig. 4.19 Sr^{2+} versus Mn^{2+} plot for dolomites. Sample location: 1= Chartreuse; 2= Vercors; 3= Bauges; 4= Aravis; 5= Bornes.

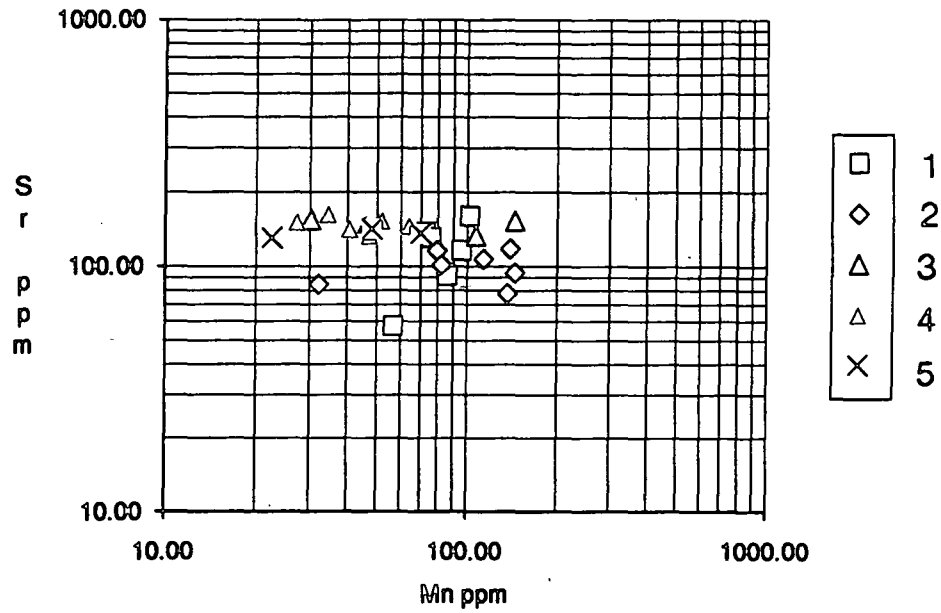

4.8.2 Interpretation of trace element contents of basal replacive dolomites.

The low Sr^{2+} content, if interpreted with the model presented in section 3.12.5 could indicate the dolomitization of stabilized marine carbonates which had already lost their Sr^{2+}. An alternative is that the low Sr^{2+} content could be produced by recrystallization of the dolomite. However, low Sr^{2+} content has also been used to suggest mixing-zone dolomitization (see Tucker & Wright, 1990, for further discussion).

The low Mn^{2+} and Fe^{2+} (in some samples) could be used to imply dolomitization from seawater, since both Mn^{2+} and Fe^{2+} are only present in very low quantities in seawater. Both Mn^{2+} and Fe^{2+} are usually abundant in burial dolomites. The variation in iron and manganese may have arisen from different local fluid compositions and/or differing trace element contents in the precursor sediments. Given the size of the field area, such wide variation in the trace element geochemistry is perhaps not surprising, with local factors (local chemical gradients, rate of through-flow of diagenetic fluids, etc.) overriding regional causes.

Fig. 4.20 Fe^{2+} versus Mn^{2+} plot for dolomites. Sample location: 1= Chartreuse; 2= Vercors; 3= Bauges; 4= Aravis; 5= Bornes. There is very little variation in Mn^{2+} compared to that shown by Fe^{2+}

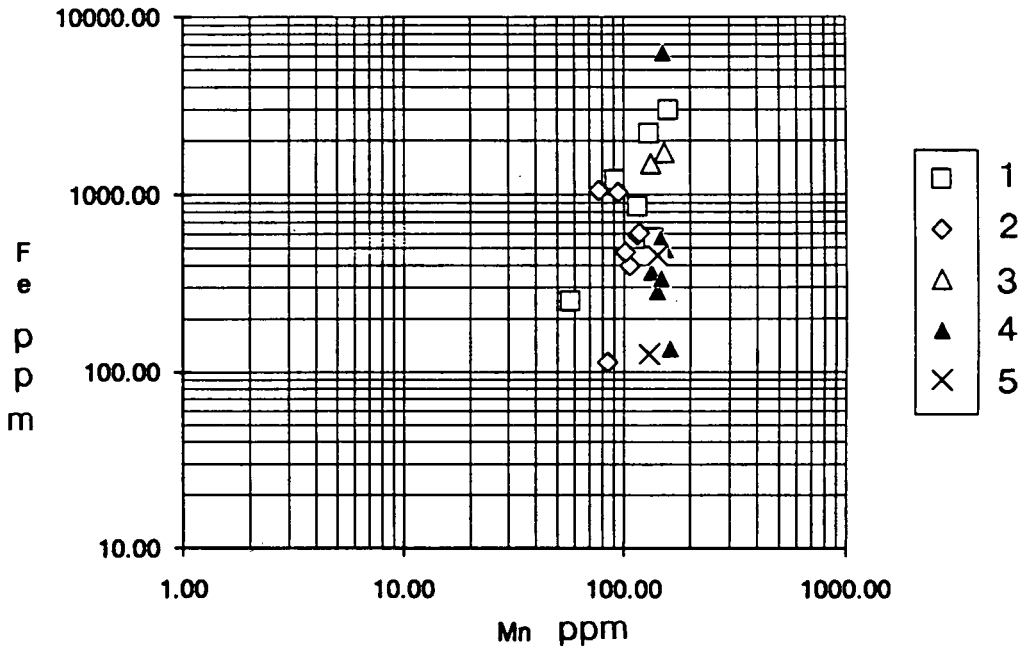

4.8.3 Conclusions to the geochemistry of basal replacive dolomites.

Stable isotope signatures do support the shallow-burial model proposed in section 3.12.5 (if the assumptions made concerning the $\delta^{18}O$ of the fluids responsible for the dolomitization are correct). Interpretations based on the trace element content can only be qualitatively interpreted (Land, 1980; Mattes & Mountjoy, 1980; Hardie, 1987) and in this case do not either really support or argue against the model of dolomitization presented in section 3.12.5, since a number of interpretations are possible. The overlap in isotopic composition between inferred burial dolomites and baroque vein dolomite with dolomite believed to have formed relatively early in the diagenesis of the platform possibly indicates that recrystallization occurred.

4.9 Geochemistry of post-dolomite spar within the Urgonian.

4.9.1 Isotopic and trace element content of post-dolomite calcite spar.

Since only relatively few samples were analysed, the isotopic and trace element contents will be described together.

The isotopic content of these calcite spars (see section 3.12.4) has a mean $\delta^{18}O$ of -8.65 +/- 3.06 and a mean $\delta^{13}C$ of -0.65 +/- 1.66. The isotopic composition of these calcite cements is shown in Fig. 4.21. As with the dolomites these coarse calcite spars have variable trace element concentrations. Sr^{2+} and Mn^{2+} are generally quite low (Sr^{2+} mean = 250 +/- 182 ppm, Mn^{2+} mean = 117 +/- 113 ppm), whilst Fe^{2+} content can be quite high (mean = 1012 +/- 940 ppm). See Figs. 4.22a and 4.22b.

Fig. 4.21 Isotope cross-plot post-dolomite spar plotted against basal dolomites. 1= basal replacive dolomites; 2= post-dolomite spar.

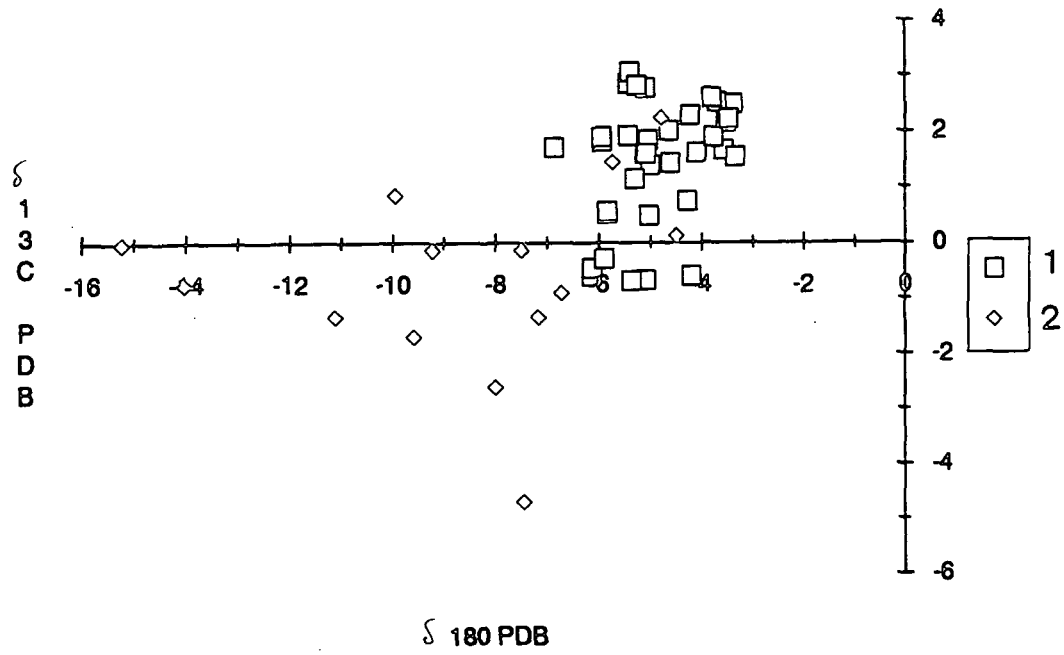

Fig. 4.22a Sr^{2+} versus Fe^{2+} plot for post-dolomite spar and dedolomitized dolomites. 1= dedolomites; 2= post-dolomite spar. **Fig. 4.22b** Fe^{2+} versus Mn^{2+} plot for post-dolomite spar. 1= dedolomites; 2= post-dolomite spar.

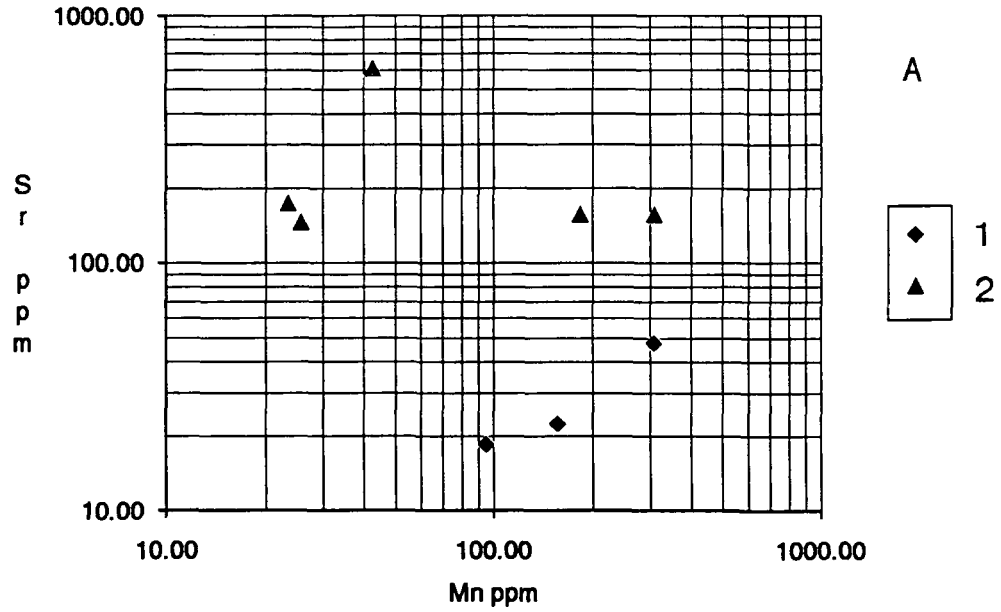

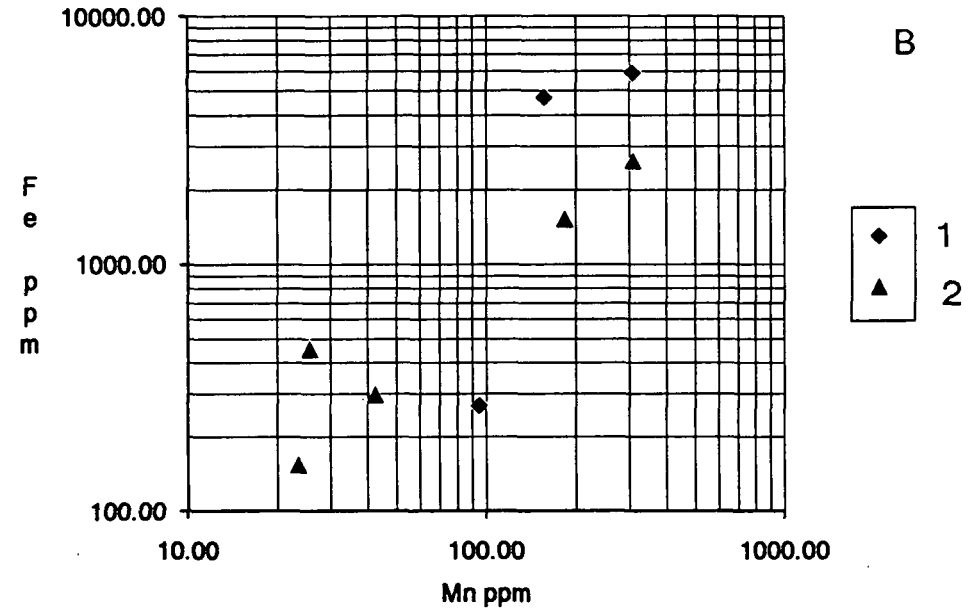

4.9.2 Interpretation of the isotopic and trace element geochemistry of post-dolomite calcite spar.

The overlap in the stable isotopes with the isotopic composition of the spar A and B fields of the equant cements (see section 4.5) suggests precipitation from fluids of similar composition (compare Figs 4.11 and 4.21). Most of the post-dolomite spars have very negative $\delta^{18}O$, this suggests precipitation at higher temperatures. The general similarity of

Sr^{2+} and Mn^{2+} contents of these post-dolomite spars with the equant spar cements (compare Figs 4.13, 4.14 and 4.22a and 4.22b) suggests precipitation from the comparable fluids, although the higher concentration of Fe^{2+} would argue for a different source, possibly a burial fluid.

4.10 Geochemistry of the dedolomites.

4.10.1 Stable isotope and trace element composition of the dedolomites.

Since only relatively few samples were analysed, the isotopic and trace element content will be described together.

The dedolomites (see section 3.13) generally have a more negative $\delta^{18}O$ value (mean = -7.12 +/- 1.4) and $\delta^{13}C$ value (mean = -4.10 +/- 2.26) than the dolomite precursor. This is shown in Fig. 4.23. The dedolomites are relatively enriched in Fe^{2+} (up to 5800 ppm; mean = 3600 +/- 2400 ppm), but have low values of Sr^{2+} and Mn^{2+} (mean values of 190 +/- 90 ppm and 30 +/- 13 ppm respectively) (Figs 4.22a and 4.22b).

Fig. 4.23 Isotopic composition for dedolomites plotted along with the isotopic composition of the basal dolomite. 1= basal dolomite; 2= dedolomite. Note: no distinction is made between whole rock dedolomite samples and areas of calcite cement infilling vuggy porosity associated with the dedolomitization (see Fig. 3.42a).

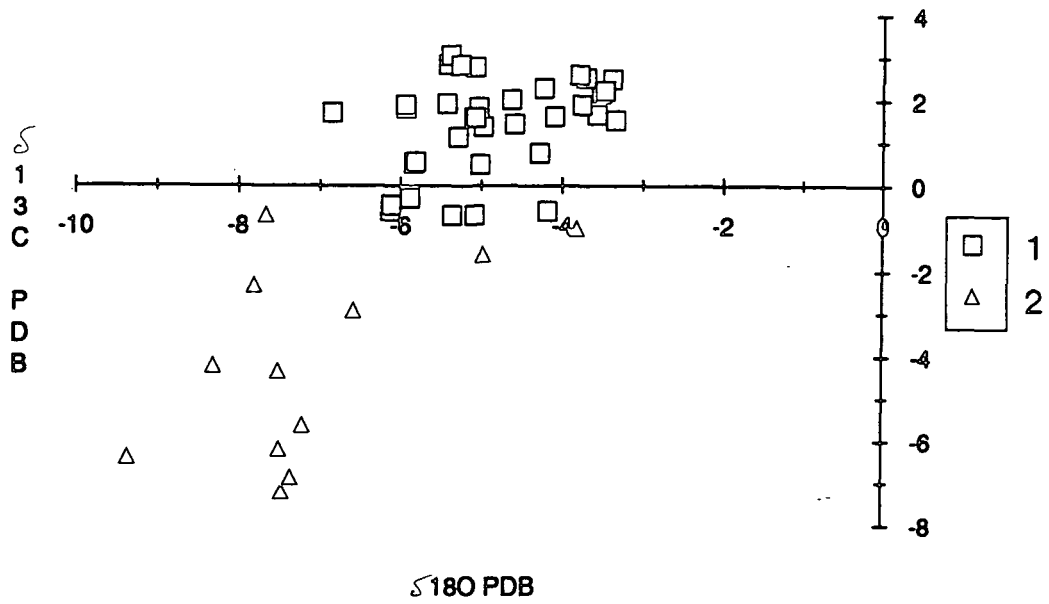

4.10.2 Interpretation of the stable isotope and trace element composition of the dedolomites.

The geochemistry supports the notion that the dedolomites are the product of meteoric processes leading to the calcitization of the dolomite. The low Sr^{2+} and Mn^{2+} values of the dedolomites suggest a meteoric setting The negative $\delta^{13}C$ values are indicative of the influence of vadose-zone derived CO_2. The $\delta^{18}O$ value would reflect the composition of meteoric water in either the late Cretaceous/early Paleogene or post-Miocene (the two times when the dedolomitization could have occurred), altered due to the effects of any significant topography and the proximity (or not) of open oceanic water bodies.

4.11 Conclusions and synthesis of the field, petrographic and geochemical data on the diagenesis of the Urgonian. A diagenetic model for the Urgonian platform.

Incorporating all the general conclusions presented in this chapter and in Chapter 3 the following model of diagenesis and lithification of the Urgonian platform is presented (see Fig.4.25). The following stages are not isolated steps but rather overlapping and represent a continuum of processes i.e. parts of the platform will be entering the shallow burial stage D, whilst upper parts of the platform may still be exposed.

Stage A: corresponds to deposition of the platform. Diagenetic features formed during this stage include marine cements, micritization and grain repacking. Several brief periods of exposure interrupt normal platform sedimentation; however, meteoric diagenesis during these periods was minor due to the prevalent semi-arid climate. The lack of marine cements within fabric selective dissolution porosity shows most dissolution took place during Stage B or that marine porefluids did not re-enter the sediment.

Stage B: corresponds to the exposure of the platform in the lower Aptian, following a more pronounced relative sea level fall. The prevalent semi-arid climate prevented deep, penetrative karstification and resulted in a shallow micro-karst forming upon the exposed upper surface of the platform. Fabric selective dissolution of aragonitic shell material and the stabilization of low magnesium calcite, occurred in the presence of mixed-meteoric fluids. Dissolution will of provided material for cementation downdip.

Figs 4.25 (opposite page) Model of the pre-Tertiary diagenesis of the Urgonian platform. No horizontal scale is implied. Nor is any specific location, although west is on the left hand side of the diagram. The Urgonian is shown by the brickwork pattern. Compactionally released connate fluids moving into the base of the platform are responsible for the dolomitization of the basal section of parts of the platform,

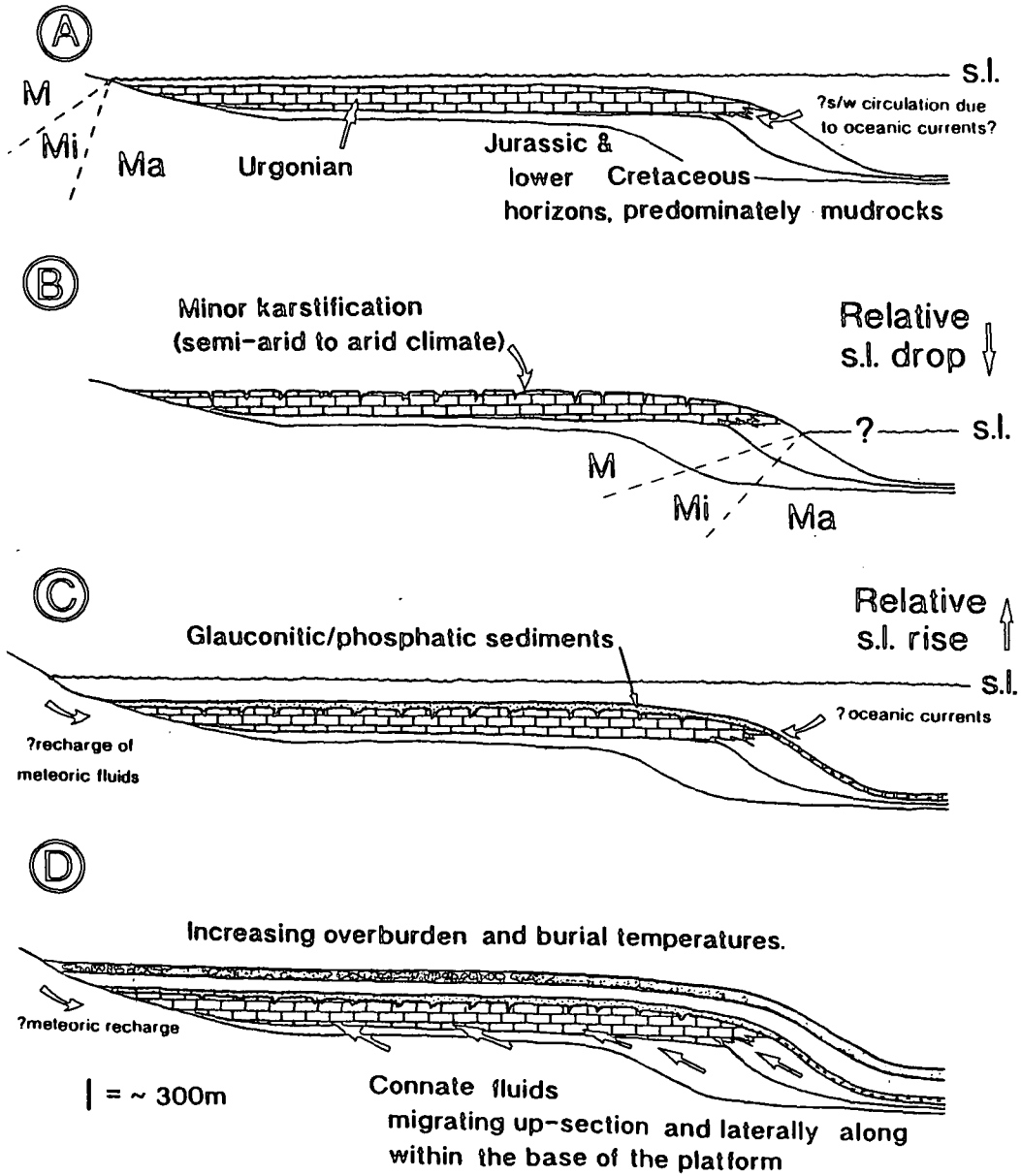

Platform formation

Marine phreatic diagenesis

- Micritization
- Marine cementation
- Grain re-packing
- ?Seawater dolomitization?

Platform exposure

Meteoric diagenesis

- Aragonite dissolution
- Calcite recrystallization

Drowning of the platform

- Grain breakage
- Grain sutering

Meteoric phreatic diagenesis

Shallow burial

Burial diagenesis

- Drusy spar cements
- Replacive burial dolomitization
- Pressure dissolution

M = meteoric porewaters Mi = mixing zone waters Ma = marine porewaters

Stage C: corresponds to drowning of the platform in the upper Aptian. This transgression removed the microkarstic surface in some localities; in others the karstic surface was re-worked by hardground formation in the Albian. During the transgression calcitic silt was dolomitised by the action of seawater moving through the upper part of the former carbonate platform. During this period there is the possibility that 'cold' oceanic waters were pumped into the shelf margin grainstones of the basal section of the platform, leading to the formation of some dolomite. Fluid circulation could have been driven by one or more of three possible mechanisms: 1) oceanic currents encroaching onto the drowned platform; 2) Kohout convection; or 3) meteoric-mixing zone driven convection. Early mechanical fracturing of grains continued as the platform was gradually buried.

Stage D: corresponds to shallow burial during the Albian to the end of the Cretaceous. Shallow burial resulted in the release of connate seawater by mechanical compaction of the basinal muds below the platform, causing widespread replacement dolomitization of the platform margin grainstones. Focusing of the flow of the fluids responsible for dolomitization produced the variable thickness of the dolomite. Precipitation of burial cements from moderately heated meteoric fluids (?possibly from meteoric recharge), occluding post-mechanical fracture porosity. Material for precipitation could be provided from fabric selective dissolution, within the platform by meteoric fluids and the downdip movement of this fluid. Intra-crystalline porosity with the burial dolomites is occluded.The platform is now fully lithified.

Stage E: corresponds to the post Cretaceous to the present day. Basin inversion in the early Palaeogene locally led to renewed exposure of the platform. Dedolomitization occurred in some sections. In the Eocene onwards compressional tectonics caused the folding and faulting of the platform (and of the whole succession), and syn-tectonic fluid movement occurred through the platform via fractures (see Chapter 5). Post-Miocene times saw the gradual uplift of the platform. Again dedolomitization of some of the burial dolomites took place.

Chapter 5 Syn-tectonic veining within the Subalpine Chains.

5.1 Introduction.

This chapter deals with the outcrop pattern, petrography and geochemistry of veins from the Subalpine Chains. The vast majority of these veins have a direct field association with Alpine tectonic structures and from both their field relationships and their petrography they can be described as syn-tectonic. Both field and petrographic relationships show that while these veins and other microstructural features were forming there was also net volume loss via numerous pressure dissolution seams. Both veins and pressure dissolution seams often possess a systematic relationship to the axes of major folds (i.e. hanging wall anticlines) and the trend of thrust faults.

Within this framework the stable isotope and trace element composition of the veins was analysed. The geochemistry at first sight appears to be random, although on closer inspection there are several trends; these are described and discussed in the text.

5.2 Geometry of brittle microstructures in fold/thrust belts.

The structure of the Subalpine Chains is typified by fold/thrust structures (see section 2.7). Microtectonic features will show a geometrical relationship to the fold and/or thrust structures developed (Price & Cosgrove, 1990). The variety of structures include bedding parallel and perpendicular sutured pressure dissolution seams (stylolites), extension, shear and hybrid joints (veins, if filled), small scale faults (mesofaults, can be either extensional, contractional or conjugate) and shear zones. Hancock (1985) and Price & Cosgrove (1990) have shown how microstructures formed during folding may be related geometrically to major structures (see Fig. 5.1a). The exact orientations of structures will change from locality to locality according to variations in the plunge of folds and orientation of the fold axial plane. To avoid confusion caused by the use of absolute orientations, it is beneficial to use a notation to describe the fractures that is not dependent on absolute orientation. One such system is to refer the geometry of the microstructures to an orthogonal fabric cross, the axes of which are labelled *a*, *b* and *c*. These do not have any kinematic or dynamic implications (Hancock, 1985). The orthogonal fabric cross along with the common arrangement of microstructures seen in the Urgonian in the Subalpine Chains is shown in Fig. 5.1b; similar arrangements of brittle microstructures are shown in Droxler & Schaer (1979) and Hancock (1985). Because of the higher level of exposure and its regionally uniform sedimentology, this study was principally carried out on the Urgonian limestone, although examples from other parts of the stratigraphy were studied as well. With basinal, muddier sediments stratigraphically above and below, the Urgonian would have acted as a brittle layer interbedded with more ductile layers.

Fig. 5.1a (opposite page) Trends of minor fractures in a folded competent unit (Price & Cosgrove, 1990). R and T are shear and extensional fractures respectively. **Fig. 5.1b** Common brittle deformation structures seen within the Urgonian.

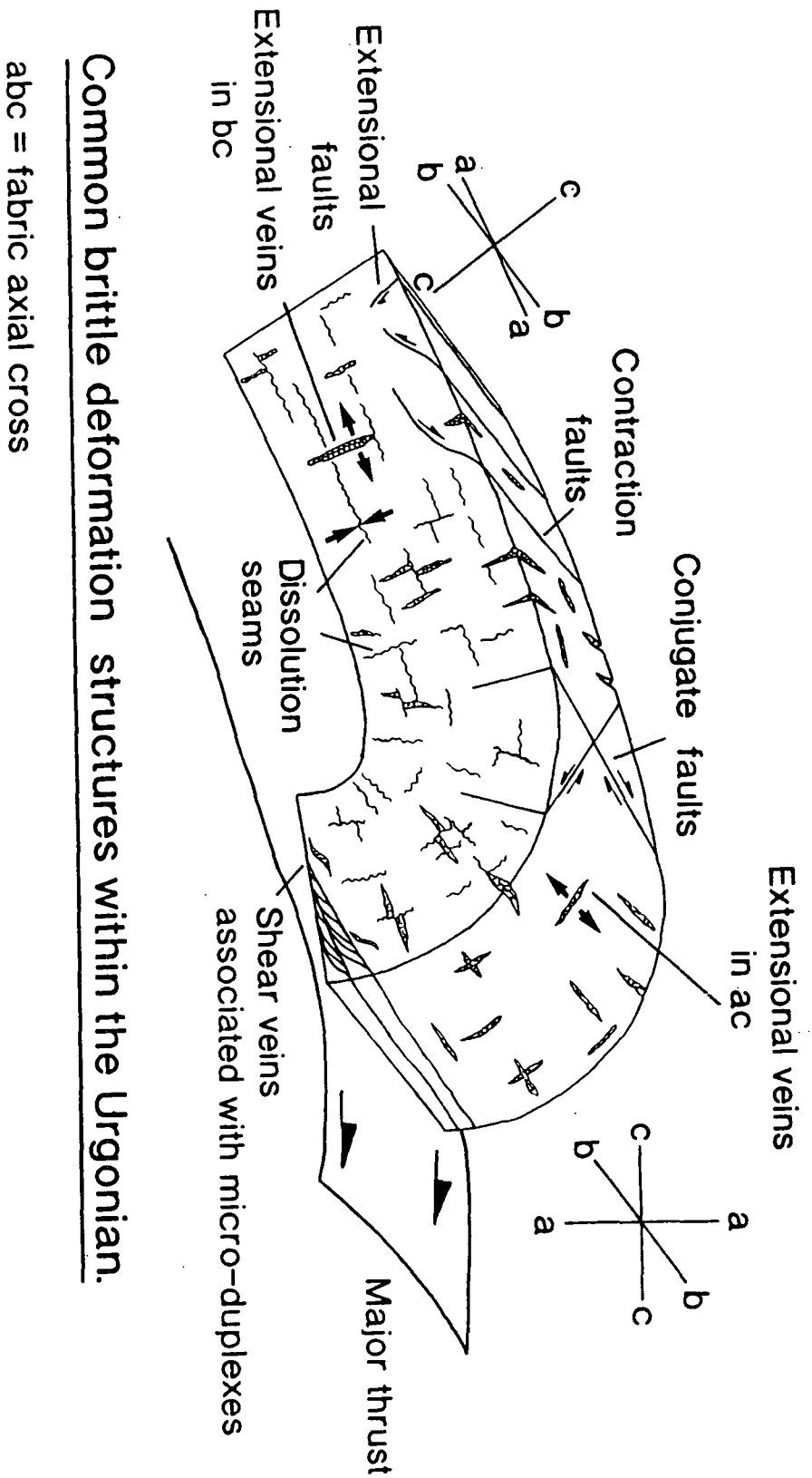

Fig. 5.1b

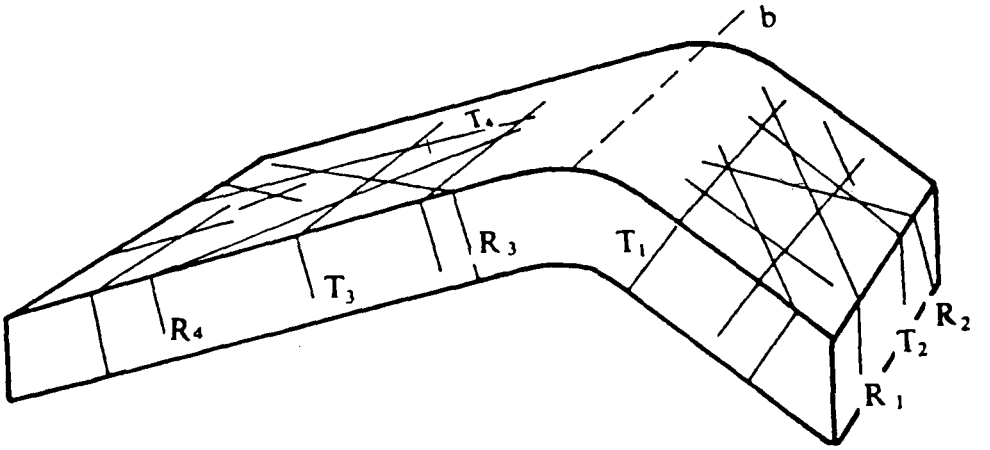

Fig. 5.1a

The geometrical relationship of the microstructures to major structural features as shown in Fig. 5.1b strongly argues for their formation being syn-tectonic. Fracturing could have occurred at several times, during initial pre-thrust folding, with earthquake activity (possibly occurring deeper in the section, e.g. see Roberts; in press), during thrust faulting and refolding and rotation (as rock units are moved over ramps for example) and with uplift. Fractures occurring well away from thrust zones may form early on in the deformational history, as suggested by Roberts (1990a and in press) for veins in the hanging wall to the Rencurel thrust in the central Vercors. It is more than likely that some of these microstructures have different orientations due to the differing stress conditions at different times during the deformation; i.e. structures with orientations that are geometrically related to the present position and orientation of folds will have most likely formed during the final phase of folding. However, as shown by Price & Cosgrove (1990) and Butler (1992a) folding and eventual thrusting often reflect a complex strain rate history, beginning with minor structures such as small intraformational thrusts and ending with the final thrust faulting. In addition, slight changes in the thrusting direction could well alter the orientation of subsequent microstructures (as suggested by Ramsay, 1981 for curved vein fibres in the root zone of the Morcles nappe and by Huggenberger & Wildi, 1991 for veins in the Bornes massif).

5.3 Field description of veins.

The veins studied usually showed a geometrical relationship to the major structures; typically they were either aligned in *bc* or in *ac* (see Fig. 5.1b), that is either parallel to the hinge of a fold or perpendicular to it, so they record extension or shear-extension in these orientations. As such they are either perpendicular to or parallel to the maximum principal stress ($\sigma 1$). Since the folds are intimately related to the thrusts, usually being cut by a thrust

Fig. 5.2.a Thrust parallel veins (indicated by the small black arrows) from just above a thrust fault plane (T) in the Urgonian, near St. Christophe-sur-Guiers, Chartreuse. Lense cap for scale (C). Numerous non-sutured pressure dissolution seams can be seen running parallel to the main thrust. **Fig. 5.2b** Vein containing 'clasts' (some of which are arrowed) of wall rock. Upper Jurassic, to the northwest of La Place, Bauges. Fingers for scale.

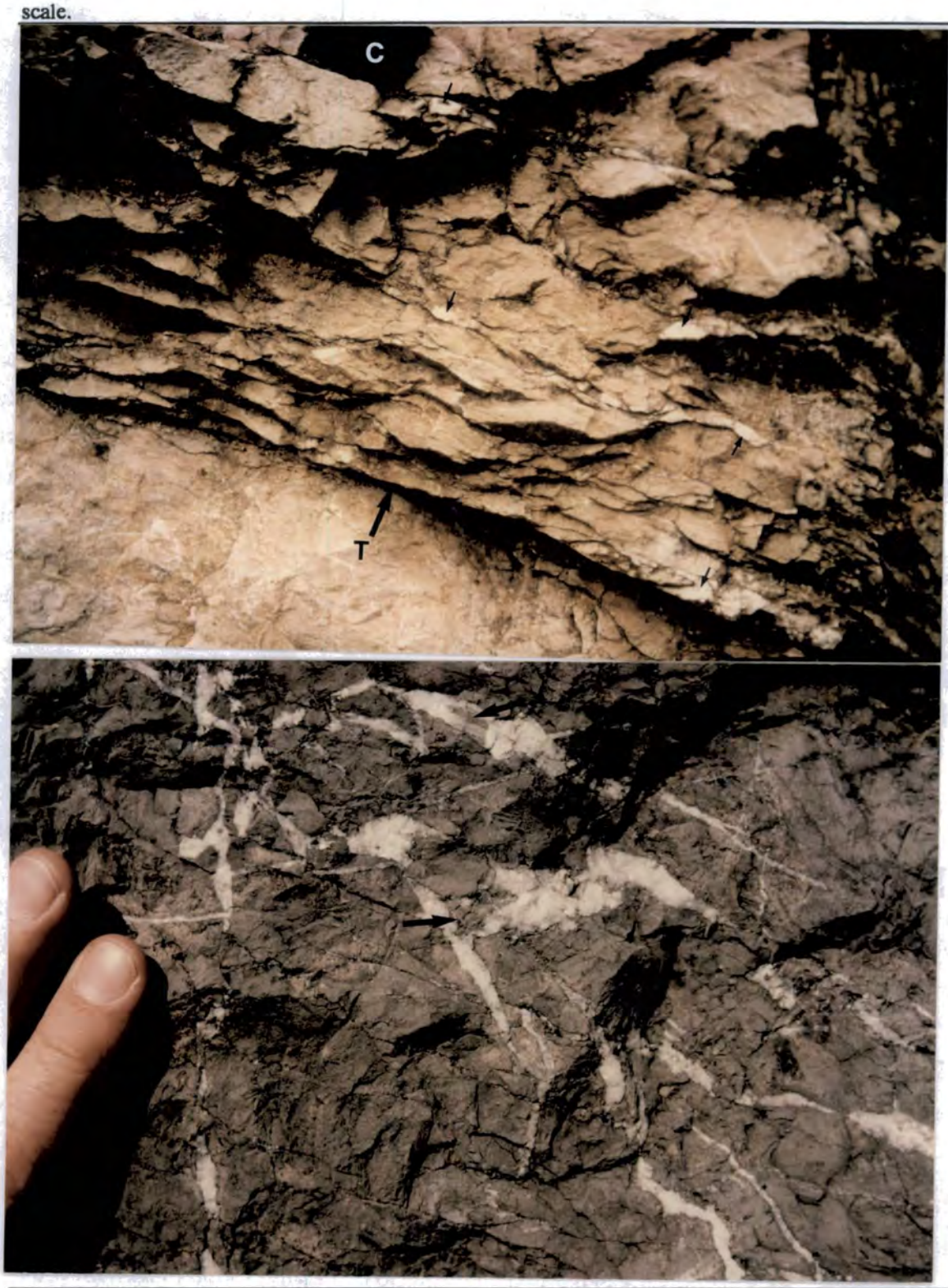

through their steeper forelimb, the veins are also geometrically related to the thrust structures. Vein density also shows a direct relationship to structure, particularly faults, and in many instances can be seen to increase in number toward a thrust fault. Pressure dissolution seams also showed the same relationship. Several other authors have also noted the increase of veins and stylolite density toward faults planes (Sibson, 1981; Butler et al., 1987; Coli & Sani, 1990). Within thrust fault zones and in the vicinity of thrusts (up to 10 metres or so from the fault) veins parallel or sub-parallel to the fault plane were sometimes seen (see Fig. 5.2a). Coli & Sani (1990) reported veins with similar orientations from the hanging wall of the Cervarola thrust in the Apennines.

The veins are usually fairly straight-walled, although with closer inspection the contact between wall rock and vein may actually be sutured. Often they contain 'clasts' of the wall rock within the vein (see Fig. 5.2b).

The spacing of the veins is very varied (several mm to metres); this is controlled by the mechanical properties of the rock. Fractures are formed by non-hydraulic processes; fractures will form at a separation governed by the lithology and bed thickness (Price & Cosgrove, 1990). However, if the fractures have formed hydraulically through fluid pressure exceeding the tensile strength of the rock and the minimum principal stress ($\sigma 3$), the veins will then have a spacing dependant on the permeability of the unfractured rock (Price & Cosgrove, 1990).

Often in the crests of small anticlines veins that were orientated parallel to the fold axis (extension in *bc*, see Fig. 5.1b) would taper downwards from the top of the bedding surface (see Fig. 5.3a). This suggests that the fractures opened in response to extension of the bed as it was folded (see Price & Cosgrove, 1990, see Fig. 5.3b). Similar extensional fractures are reported by Droxler & Schaer (1979) from folds in the Pierre Jaune-de-Neuchâtel (Hauterivian, oolitic grainstones) of the Jura.

In the field veins are seen to be cross-cut and to cut through pervasive, sutured, dissolution features (stylolites) (see Fig. 5.3c). Often there appears to be an apparent displacement of the vein or dissolution seam. In the majority of cases this was due to the orientation of the vein and stylolite relative to the observer. Although shear and hybrid shear-extensional fractures would produce similar features, it was usually impossible to show conclusively displacement on the fractures. Both bedding parallel and bedding perpendicular orientations of stylolites are seen. Often these are referred to as 'diagenetic' (i.e. formed due to lithostatic stress with burial) and 'tectonic' (i.e. formed due to tectonic stresses) stylolites respectively (for example, Droxler & Schaer, 1979). However, if the beds have been folded this distinction is likely to be invalidated since it is likely that the beds will become orientated perpendicular to the maximum principal stress ($\sigma 1$, which will be orientated horizontal and directed from orogenic hinterland to foreland, see Price & Cosgrove, 1990). Once the beds have been folded re-newed pressure dissolution (perhaps re-activating old 'diagenetic' stylolites) may occur parallel to the beds even though the

pressure dissolution is a response to tectonic stresses. This is shown in cartoon form in Fig. 5.4.

Fig. 5.3a Fold axis parallel, bed perpendicular vein (X) produced by extension in *bc* in Berriasian wackestones. The vein (X) can be seen to taper to a point (1/90, from the Entremont road section, see Fig. 5.10G for location. Continuous vein (labelled Y) was produced by extension in *ac* and cross-cuts vein X. Slab cut oblique to both veins. Isotopic composition of the veins is shown in Fig. 5.18a). **Fig. 5.3b** The formation of extension fractures parallel to a fold axis in a small fold (from Price & Cosgrove, 1990). **Fig. 5.3c** Extensional veins in *bc* in the base of the Urgonian at the Gorge du Frou (see Fig. 5.10F for location). Veins can be seen to both cut through stylolites (white arrow) and be cut through by stylolites (black arrow). Y= younging direction. **Fig. 5.3d** Cross-cutting relationships of several vein generations following similar and perpendicular orientations. Looking down onto a bedding surface within the Nummulitique of Grande Platières. Compass-clino for scale. See opposite page for Figs 5.3c and 5.3d.

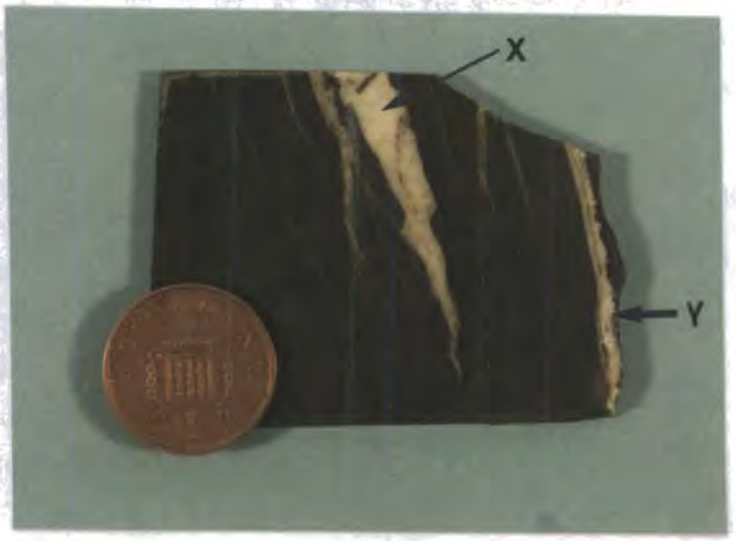

A

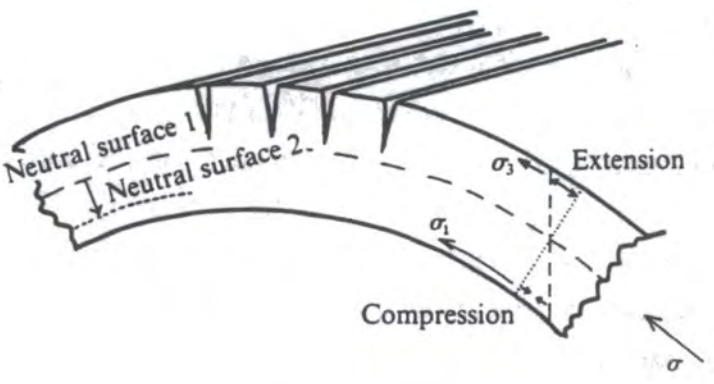

B

C

D

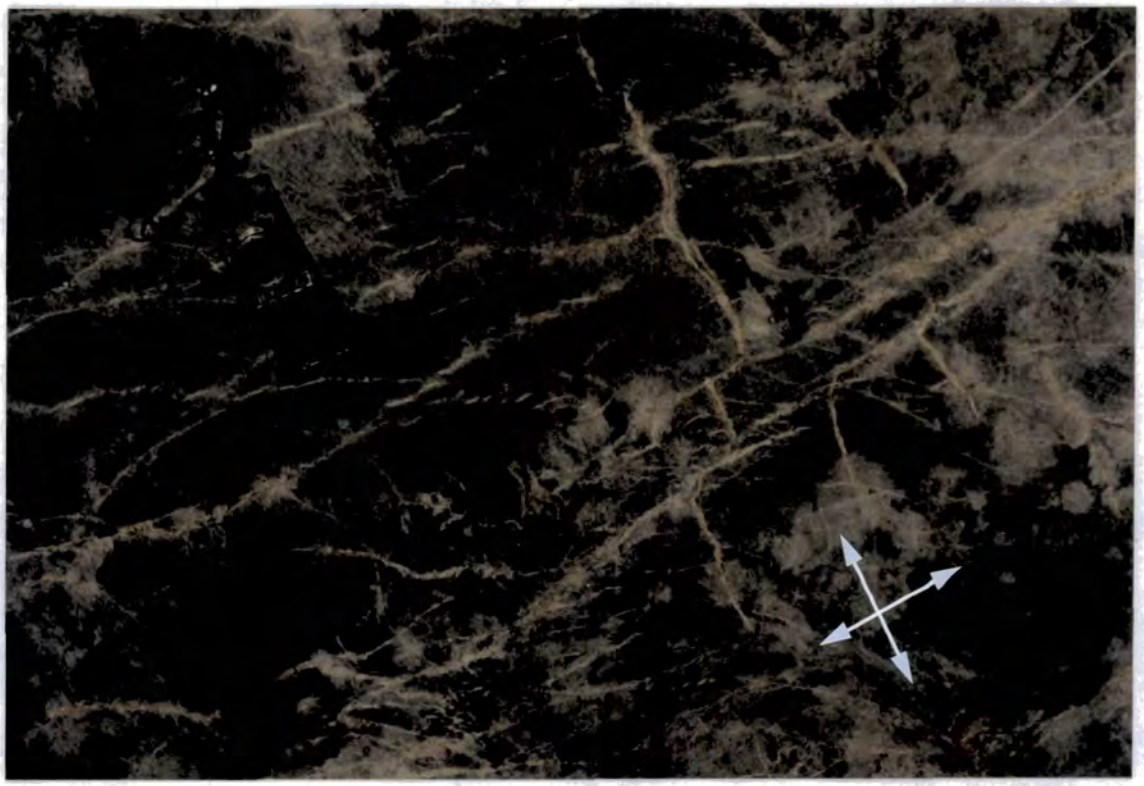

Fig. 5.4 Cartoon sketch of the relative timing of 'diagenetic' and 'tectonic' stylolites.

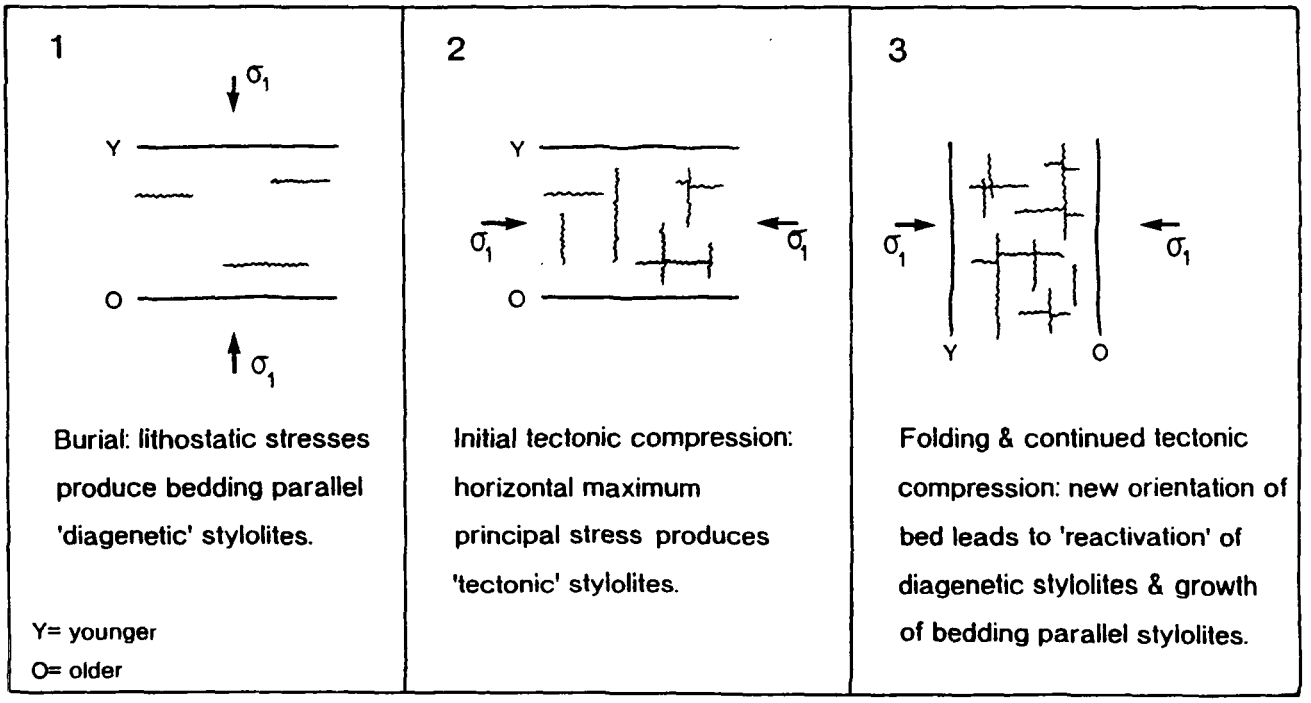

Veins are also cut by often numerous subsequent veins following orientations which are similar to or perpendicular to (see Fig. 5.3d) their own orientation. This suggests that repeated fracturing occurred along similar orientations (i.e. *ac* or *bc*).

5.4 Petrography of veins.

The veins are filled by a coarse, often drusy, calcite cement. Vein fills are ferroan to non-ferroan in nature and most are non-luminescent, although a few zoned examples do occur (see Fig. 5.5a). Under CL vein fills are typically either uniform dull-orange or non-luminescent, although occasionally veins fills have a zonation (see Figs 5.5b and 5.5c).

Often within the vein fill are clasts of detached wall rock (see Fig. 5.2b). Within these slivers and in the wall rock, the fracturing and subsequent vein fill can be seen to postdate other diagenetic features such as equant cements (described in Chapter 3). In some instances the wall rock and earlier vein(s) have been brecciated over a distance of several centimetres (see Fig. 5.5d). Brecciation of the wall rock and of pre-existing veins suggests that hydraulic fracturing occurred when there is an abrupt drop in fluid pressure following fracturing (i.e. the permeability produced with fracturing allows fluid pressure to drop, Sibson, 1981; 1990).

Fig. 5.5a Zoning within a calcite vein fill as revealed by staining. Field of view= 17mm. 210/89, Urgonian, lower Bourne gorge, Vercors. **Fig. 5.5b** CL shot of zoned calcite within a vein fill. 553/90, Urgonian, Pic de Jallouvre, Bornes. Field of view= 4mm. **Fig. 5.5c** PPL shot of the same field of view as Fig. 5.4b. **Fig. 5.5d** Clasts of brecciated wall rock within a vein. 342/90, Nummulite limestone, Tête du Sallaz, Aravis. Field of view= 3.25mm. Figs 5.5c and 5.5d are undeneath the foldout.

A

B

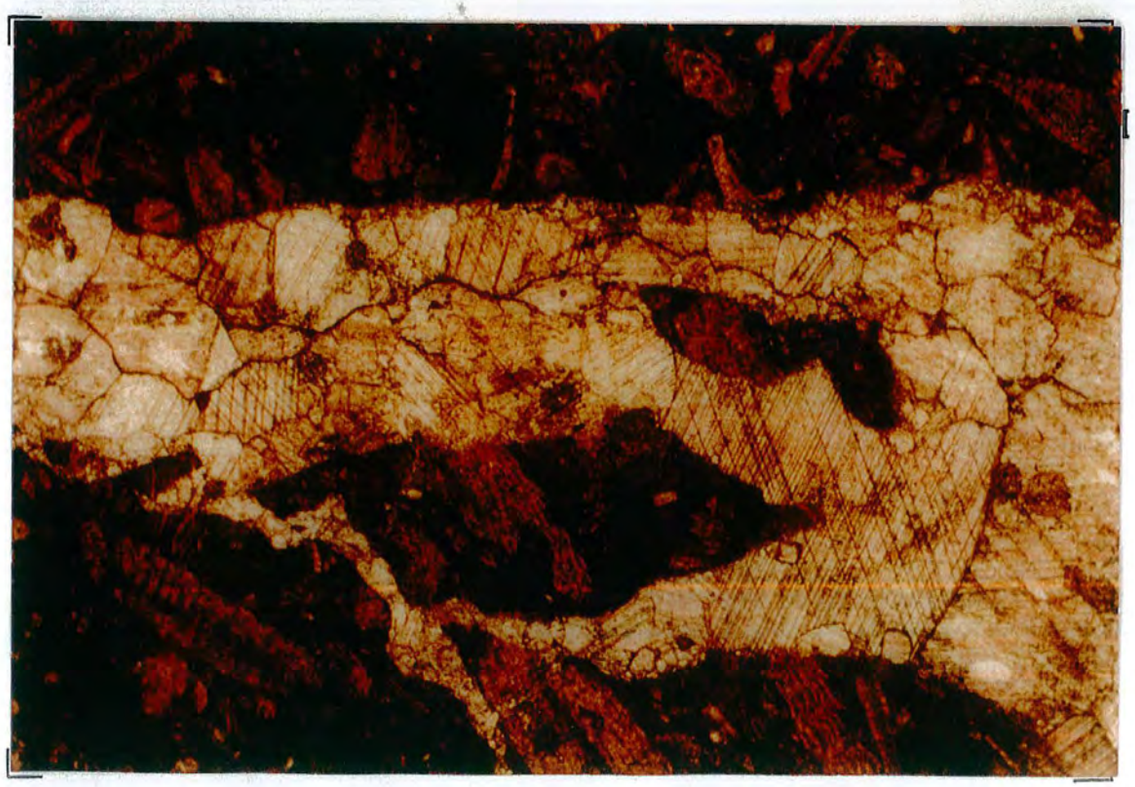

Veins are often cut through their central section or along one of their walls by a subsequent vein with a similar orientation. This arises from the initial veining producing an anisotropy in the rocks, along which subsequent failure occurs, if the right conditions are met again. Within some veins comminuted clasts of wall rock and/or vein fill material are present. This suggests that slight movements have caused mechanical fracturing and grain size reduction of the wall rocks and/or pre-existing vein material to produce a fault gouge-like material (see Fig. 5.6). Late shear fractures associated with the rupture of fault tip propagation have been shown by Roberts (1990) to have nucleated upon earlier formed extensional fractures in the hanging wall of the Ferrière thrust (upper part of the Bourne Gorge, Vercors, see Figs 2.17a and 3.1).

Fig. 5.6 Comminuted clasts of wall rock and earlier vein fill (labelled as C). W= wall of the vein(s). 81/90, Valanginian grainstone, Epernay (location H on Fig. 5.9). Field of view= 17mm.

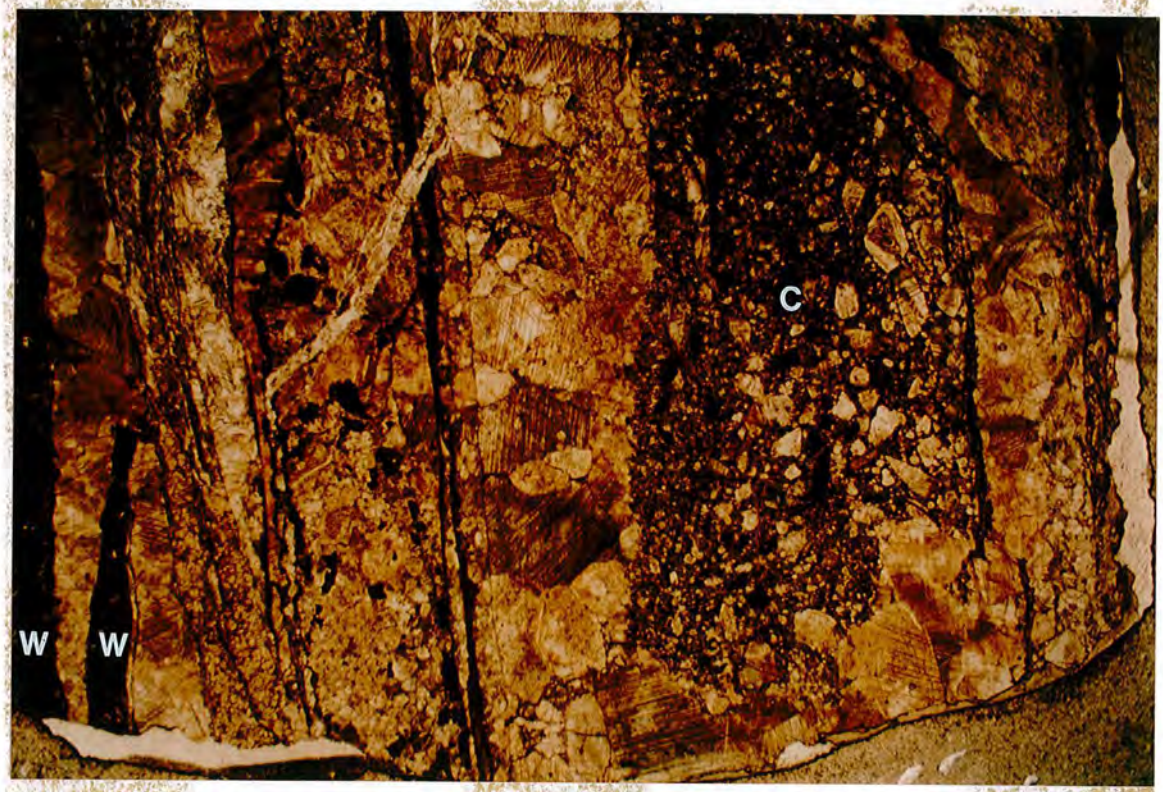

Inclusion trails are common within the calcite crystals of the vein fill (see Fig. 5.7a). These are distinct from the line of twin or cleavage planes within the calcite. These trails are not unique to individual crystals and often parallel the margin of the vein wall. A similar feature is also seen where thin slivers of wall rock have been repeatedly fractured off and healed by the subsequent vein fill (see Figs 5.5d and 5.7b, also Ramsay, 1981; Ramsay & Huber, 1987). This is called 'crack-seal' texture (Ramsay, 1980; Ramsay & Huber, 1987). This is common in rocks which have experienced temperatures and pressures

Fig. 5.7a Inclusion trails in a calcite crystal of a vein fill. The thin white arrows indicate the orientation of the trails. 337/90, Urgonian, La Colonne, Platé. Field of view= 0.7mm **Fig. 5.7b** Several healed slivers of detached wall rock. Note also the stylolite lining one of the vein walls and the stylolite cutting through part of the vein (both arrowed). 360/90, from the same locality as Fig. 5.2b. Field of view= 17mm.

A

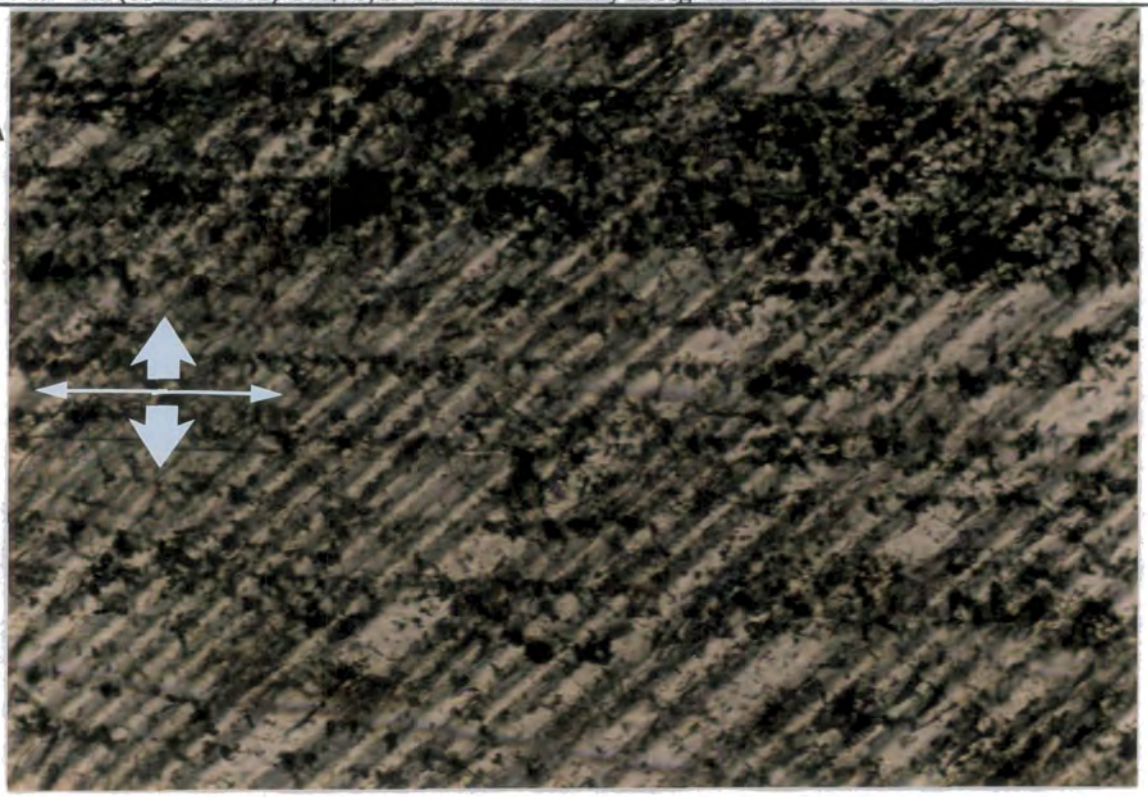

B

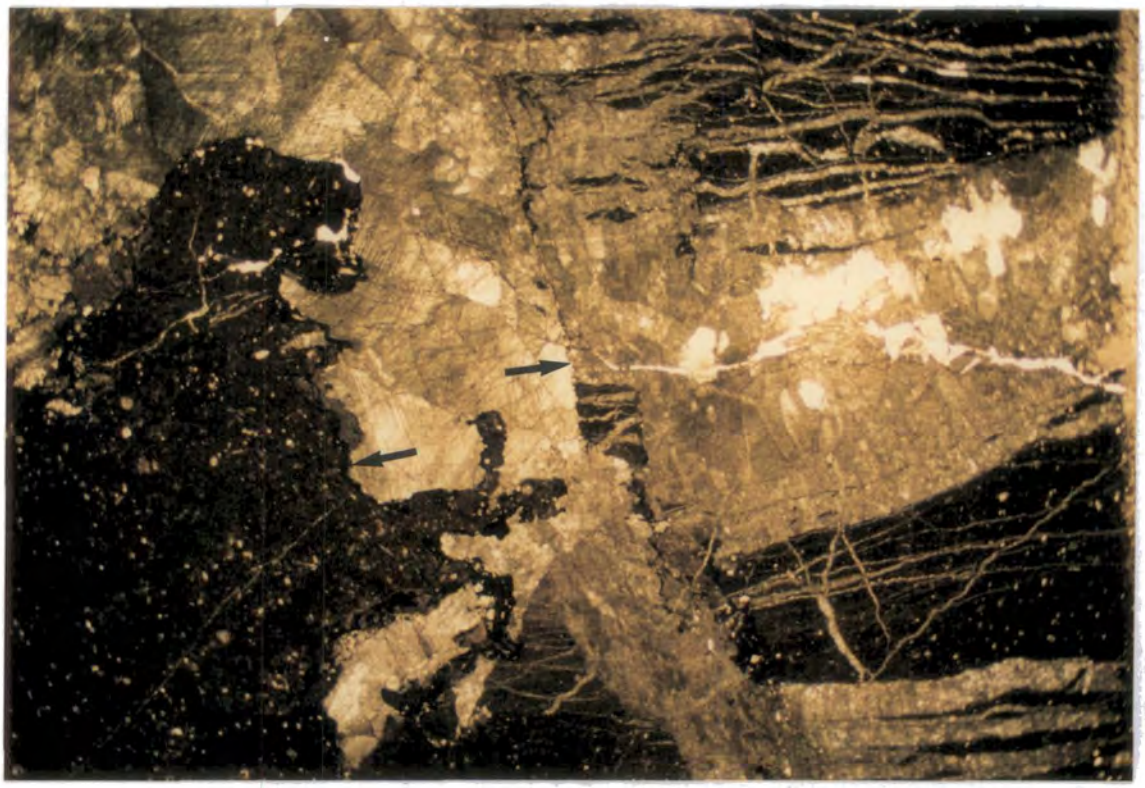

below that of upper greenschist facies (i.e. have experienced brittle deformation), which certainly applies to the Subalpine Chains (see Chapters 6, 7 and 8). The texture suggests that the opening process was episodic and the sudden release of stored energy progressively tore away parts of the wall rock which was then healed by material crystallizing from the fluid which filled the crack. The repeated fracturing indicated by crack-seal veins suggests a process induced by hydraulic fracturing under cyclic changes in pore pressure. Such repeated build-ups of pore pressure are likely only to be found during tectonism. Studies of the geometries of ubiquitous veins in the western Helvetic nappes suggest that periodic energy releases and crack formation was one of the most common expressions of rock extension in the Helvetic nappes (Durney, 1972; Ramsay, 1981). A similar feature occurs within calcite vein fills in fractures in the Silurian-Devonian of the central Appalachians (Dorobek, 1989).

Twinning of calcite crystals is quite common (see Fig. 5.8); the density of the twin planes is variable. Deformed and curved twins were also seen in vein fills (see Fig. 5.8). Such features may be a reflection of the effects of higher temperature and pressure on these rocks and suggest that deformation was still occurring after the formation of the veins.

Fig. 5.8 High density of twin planes which are also deformed (labelled D) within vein fill calcite crystals. Note also that the vein has a stylolitic contact with the wall-rock (black arrow) 208/89, Urgonian upper Bourne Gorge, Vercors. Field of view= 3.25mm.

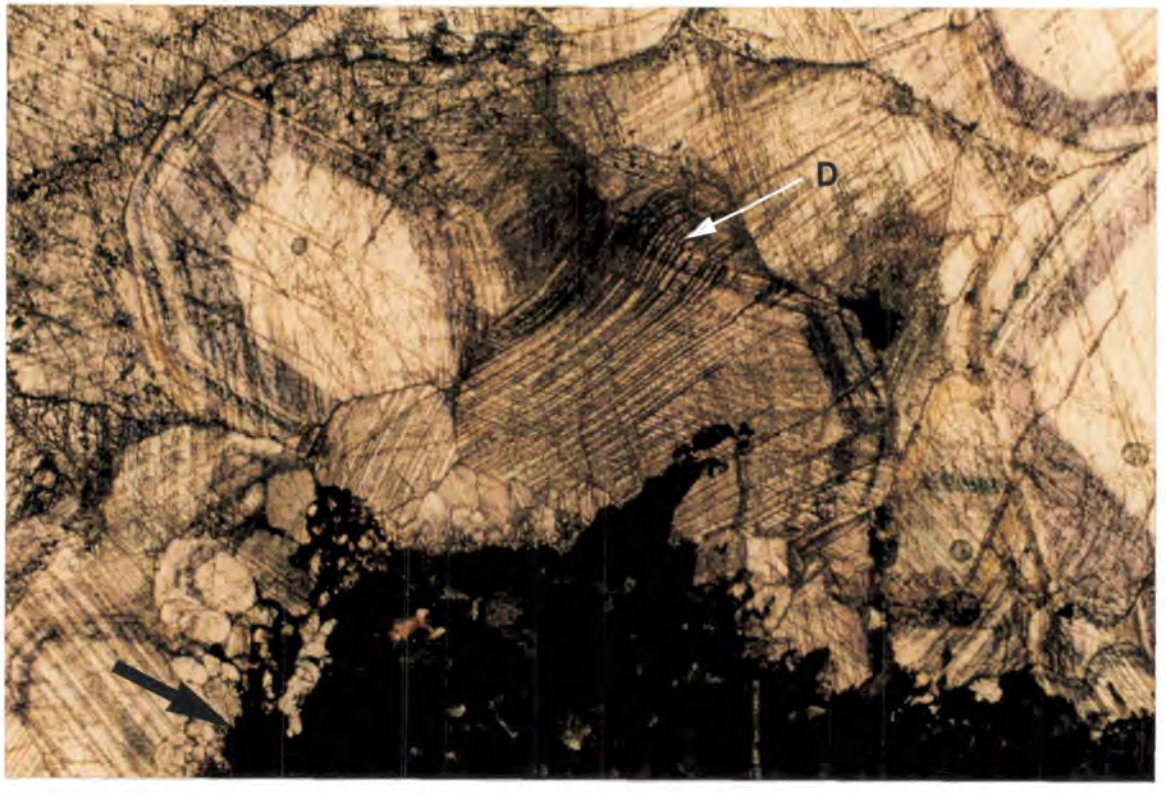

As seen in the field the veins both cross-cut and are cut themselves by pressure dissolution seams (usually sutured stylolites) (see Figs 5.3c, 5.7b, 5.8, 5.9a and 5.9b). Within a single sample they may cut through pressure dissolution features such as stylolites but at the same time be cut through or lined by stylolites themselves (see Fig. 5.9a). Often one or both of the vein walls is stylolitic in nature (see Figs 5.7b, 5.8 and 5.9b). This is brought about by the competence contrast of the vein fill and the wall rock and inhomogeneity introduced into the rock causing a stress build-up and pressure dissolution. The association of the vein fills and pressure dissolution phenomena may be linked in that the closure of pore spaces brought about by pressure dissolution could be important in the build up of high pore pressure required for repeated crack-seal fracturing (Ramsay & Huber, 1987). Presssure dissolution within the system could also have supplied material for precipitation within the veins (Durney, 1972). Dietrich et al. (1983) have noted the increasing importance of pressure dissolution in supplying material for precipitation in successively younger veins from the Doldenhorn nappe in central Switzerland. The complexity of pressure dissolution and fracturing induced by fold/thrust related deformation has been described by Droxler & Schaer (1979) for the Hauterivian of the Jura; Budai (1985) for Mississippian aged carbonates of Wyoming and Utah; by Rispoli (1981) for the Jurassic of the Languedoc and Coli & Sani (1990) for Tertiary turbidites of the Apennines.

The veins are always completely filled. This perhaps negates the possibility that the veins formed with very late uplift of the chain, when only partially filled or unfilled fractures might be expected. Since the veins are completely filled it follows that a large volume of fluid must have passed through the fractures and the fluid was in connection with a source of ions for the precipitation of the vein fills. One obvious possible source of material for precipitation is from pressure dissolution. Possible fluid sources involved in the deformation of the Subalpine Chains are discussed later (see section 5.7).

5.5 Interpretation of the field relationships and petrography of the veins.

Both the field relationships and the petrography of the veins indicate a syn-tectonic origin for the veins. However, this is still quite a wide time band since veins could have formed with initial folding and intraformational thrusting, during earthquakes produced by the orogeny (perhaps occurring at some distance from the site of fracturing), by thrusting and re-folding. Other times when the veins could have formed are with the release of fluids from overpressured areas during burial and with uplift. However, it is difficult to reconcile the evidence for cyclicity of fracturing seen within the veins, the relationship of the veins to larger structural features and their relationship to pressure dissolution if either of these two are invoked.

Fig. 5.9a A stylolite (arrowed) that has cut through a vein, only to be cut through itself by subsequent veining 117/90, basal Urgonian, Pas de Foullet, Vercors. Field of view= 2mm. **Fig. 5.9b** Oldest vein (labelled 1) which is lined and cut through its centre by stylolites (black arrows), younger, ferroan, vein generation (labelled i) cuts through the stylolites. 121/91, Urgonian, Pont de l'Abime (see Fig. 5.11A, n.b. this sample has not been analysed geochemically). Note the difference in twin densities in the calcite crystals of the two vein generations. Field of view= 17mm.

A

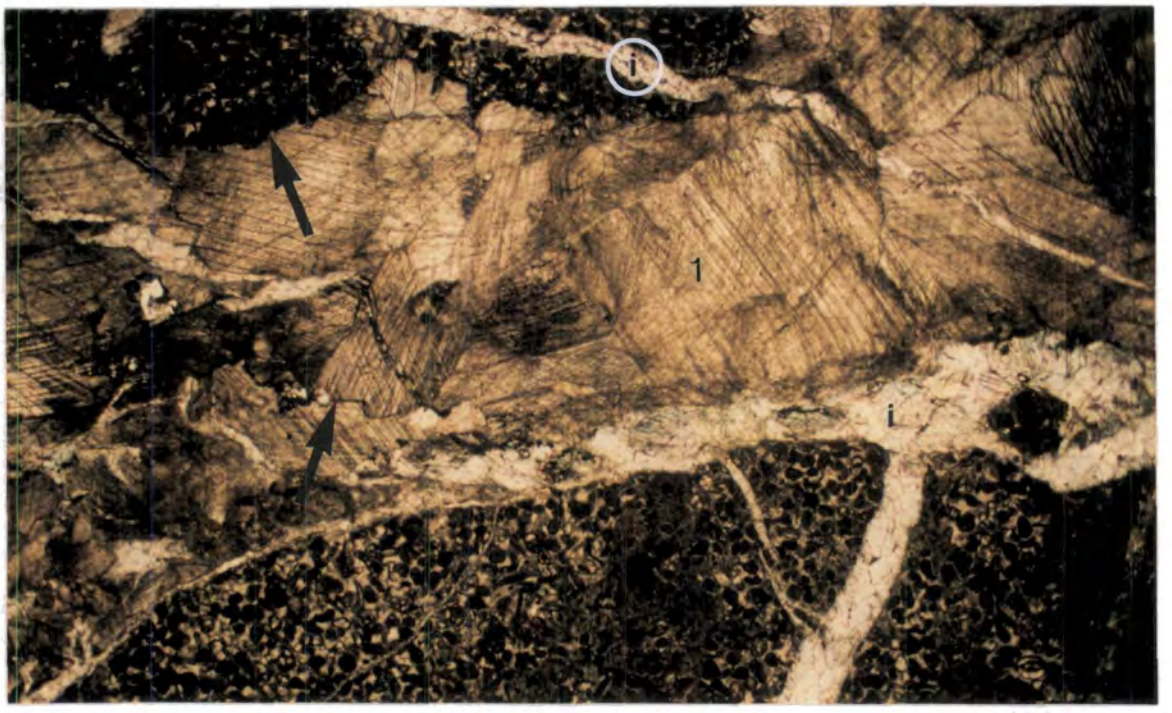

B

5.6 Geochemistry of vein fills.

Calcite cement vein fills were analysed for their stable isotope and trace element composition in a similar manner to the diagenetic phases within the Urgonian. A full listing of the results and analytical technique are given in Appendix 2.

As was described in section 5.4 veins may be cut by subsequent vein generations (see Figs 5.3d, 5.6 and 5.7b) or may be zoned (see Figs 5.5a and 5.5b). Great care was taken to ensure that only a single vein generation was sampled and where possible from an area of uniform CL response and/or stain (for example, the central, youngest part of the vein with a uniform cathodoluminescence response); however, in the few examples like shown in Fig. 5.5b this was not possible). Where possible two generations of a vein were sampled or two areas of the vein were sampled (i.e. an older part next to the vein walls and a younger area in the central section of the vein); the results of this study are described in section 5.6.3 and shown in Figs 5.18a, 5.18b and 5.18c.

Stable isotope and trace element studies in carbonate diagenesis have been introduced and discussed in general terms already in sections 4.3.1 and 4.4.1; the points raised in those sections apply equally well to the geochemistry of calcite vein fills. Particularly for trace element concentrations within the veins, the importance of local conditions (such as the degree of dissolution in the local vicinity, porewater residence times, temperature, pressure and crystal growth rate) is likely to be such that only qualitative interpretations are possible.

5.6.1 (a) Veins related to structures of the Chartreuse massif.

Fig. 5.10 shows the locations of veins from the Chartreuse with respect to major structures and the isotopic composition of those veins.

5.6.1 (b) Veins related to structures of the Bauges massif.

Fig. 5.11 shows the positions of sites from which the orientations of veins with respect to major structures were recorded and the isotopic composition of those veins.

Figs 5.10 and 5.11 show that there is very little pattern to the isotopic composition of the veins when related to the structural features of the Chartreuse and Bauges. Very little in the way of consistent trends or correlations between structure and stratigraphy can be picked out from these data. One feature which does come from close inspection of Figs 5.10 and 5.11 is that veins with negative ^{13}C PDB values are restricted to the basal Urgonian section (F1 on Fig. 5.10 and E1 on Fig. 5.11) or they are next to small thrusts within the Urgonian (G1 on Fig. 5.10 and A1 on Fig. 5.11). This could suggest that fluids that filled these veins had originated in or passed through areas deeper in the section where organic maturation was occurring (see Chapter 7).

Fig. 5.10 Location of sample sites in the Chartreuse and simplified structural geology of the area (see Fig. 2.18a for more detail) and isotopic composition of vein fills (O = $\delta^{18}O$ PDB; C= $\delta^{13}C$ PDB). VT= Voreppe thrust; CSP= principal Subalpine thrust (the *'chevauchement subalpin principal'*). Black arrow indicates main thrusting direction (from Butler, in press a). LdP= St. Laurent du Pont; PC= St. Pierre-en-Chartreuse.
A = Canaple, small 'horse' structure with a slice of Urgonian limestones bounded by Valanginian grainstones (in the hanging wall to the Urgonian) and Senonian wackestones (in the footwall to the Urgonian), 1= (?)bedding parallel extension vein in the Valanginian; 2= extensional vein above a small intra-formational thrust in the Urgonian; 3 = extensional vein in *bc* in the core of a footwall syncline in the Senonian.
B =Col de la Cachete, Urgonian in the hanging wall to the CSP thrust, 4= extensional (in *ac*) veins in the Urgonian at Col de la Chachete. **C** = west of Pont St. Pierre, hanging wall anticline of Tithonian limestones with Urgonian in the footwall, a highly tectonised, (?vertical) sliver of Valanginian occurs between the two in a small horse structure; 1= Extensional veins in *bc*, perpendicular to bedding in the Tithonian; 2= ? bedding parallel extensional veins in Valanginian grainstone; 3= extensional veins in the Urgonian in the footwall.
D = Fourvoire, several small thrust slices in the hanging wall of VT (see Fig. 2.18a), 1= two vein generations from Valanginian grainstones related to several small thrusts, 2= extensional vein above a small intra-formational thrust within Urgonian grainstones in the immediate hanging wall to VT. **E** = St. Christophe-sur-Guiers, extensional veins in *bc* on the forelimb of a hanging wall anticline in the Urgonian (=3).
F = Gorge du Frou, basal Urgonian section, 1= extensional veins in *bc*.
G = west of St. Pierre-de-Entremont, Berriasian thrust onto several small thrust bound slices of Urgonian. 1= two cross-cutting vein generations, older *bc* orientated vein is cut by younger *ac* orientated vein (arrow points from older to younger) in the Berriasian; 2= cross-cutting extensional vein generations related to small intra-formational thrusts within the Urgonian; 3 = extensional veins in *ac* in the Urgonian.
H = Epernay, Tithonian, Berriasian and Valanginian in the hanging wall with a thrust bound imbricate of Urgonian in the footwall; 1= extensional veins in ac in the Tithonian (arrow points from older to younger); 2= extensional veins associated with small intra-formational thrusts within the Valanginian; 3= veins within highly tectonised Urgonian of the footwall imbricate.

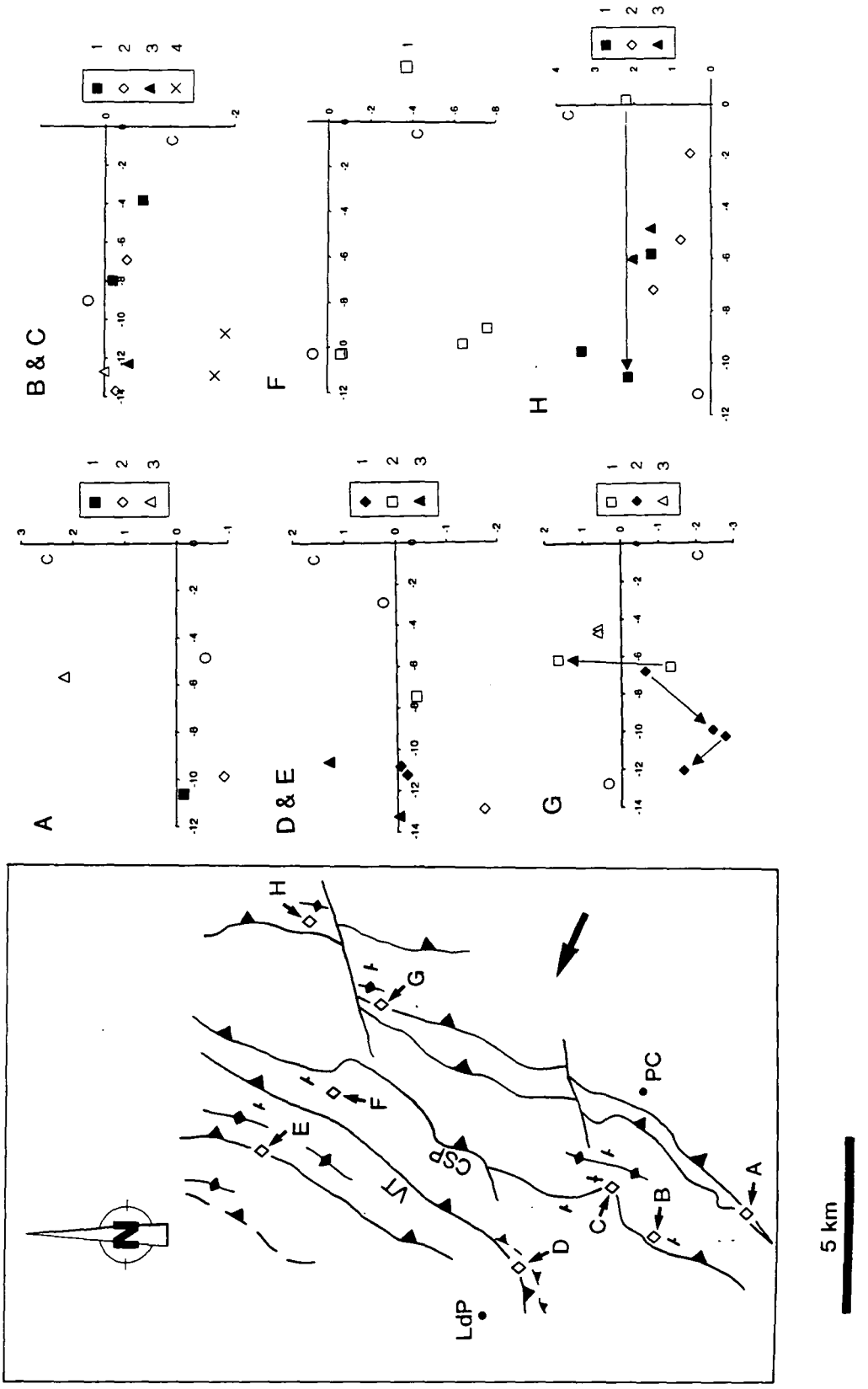

Fig. 5.10

Fig. 5.11 Location of vein sample sites in the Bauges, simplified structural geology of the Bauges (see Fig. 2.19 for more detail) and isotope geochemistry of the vein fills. Black arrow indicates main thrusting direction (from Butler, in press a). RT= Revard thrust; SA= Semnoz anticline; FA= Arcaclod fault. ClE= Challes-les-Eaux; LC= Le Chatelard. (O = $\delta^{18}O$ PDB; C= $\delta^{13}C$ PDB).

A and A' = Imbricated Urgonian in the immediate footwall to RT, Valangian in the hanging wall. 1= extensional veins related to minor intra-formational thrusts (arrows point from older to younger) within the Urgonian at Pont de l'Abime; 2= extensional vein in *bc* in Valanginian grainstones in the HW to RT; **A'** (=3)= extensional vein in *ac* in Urgonian grainstones in the rear limb of SA. **B**= extensional veins in *ac* in upper Urgonian limestones.

C and D Folded Urgonian, upper Cretaceous and Tertiary from the Mount Trelod syncline (C) and western limb of the Dents d'Arclusaz syncline (D). 1= three extensional vein generations from the upper Urgonian of Dents d'Arclusaz; 2= upper Urgonian and Senonian veins (both extension in *ac*) from the western limb of the Trelod syncline; 3= extensional veins in *bc* in the Senonian and Tertiary in the core of the syncline.

E = Croix-du-Nivolet, 1= extensional veins in *ac* in the basal Urgonian; 2= extensional vein in Valanginian grainstones in the hanging wall of a small thrust.

F and G = Urgonian thrust over Valanginian near Pointe de Galloppaz and several small thrusts within the upper Jurassic of the Curienne region; 1= extensional vein in *ac* in Urgonian in the hanging wall; 2= veins associated with small intra-formational thrusts in Valanginian limestones in the footwall; 3= veins in Tithonian limestones in the hanging wall of a small thrust.

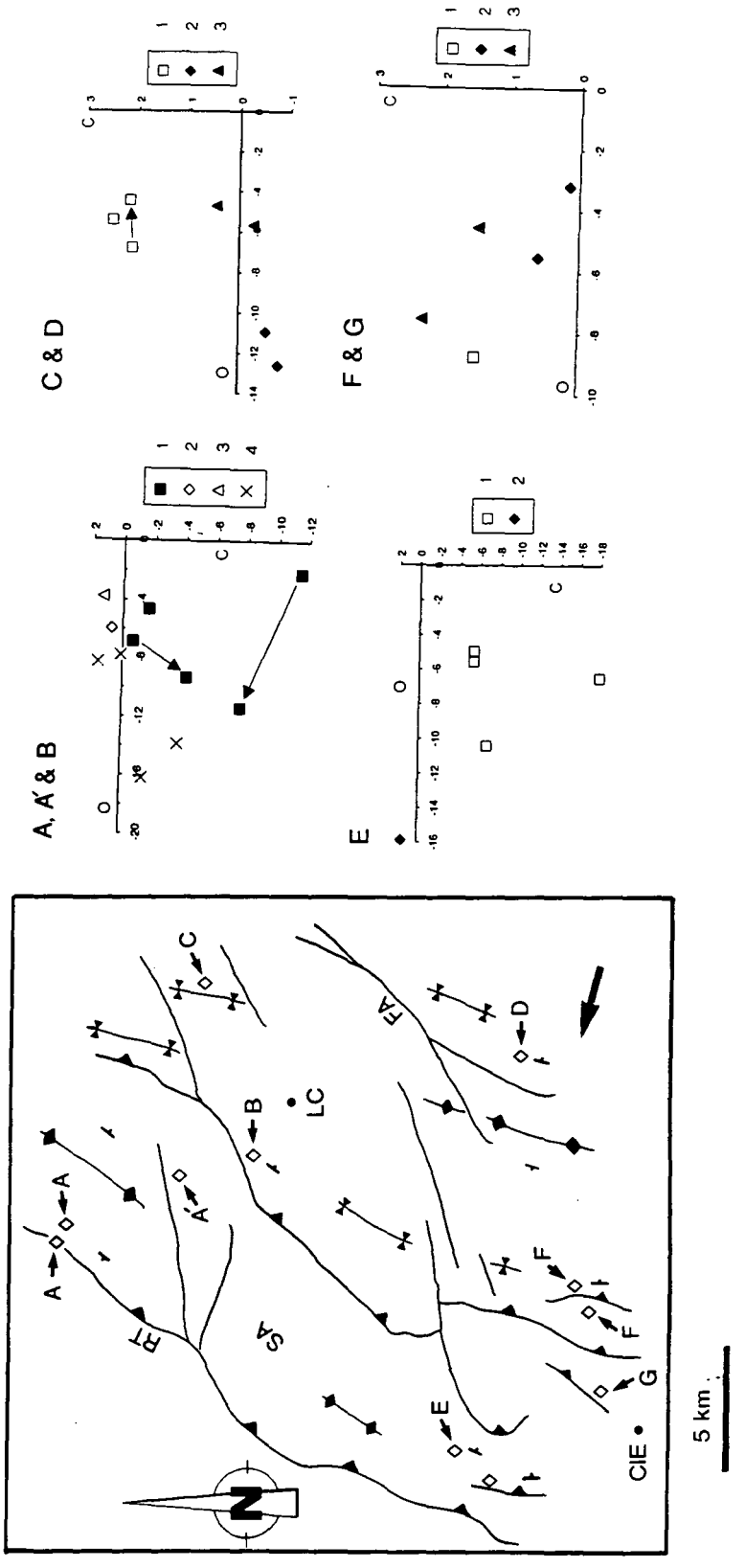

Fig. 5.11

5.6.2 (a) Geochemistry of veins in the vicinity of and within thrust zones within the Urgonian and stratigraphically within the Urgonian.

Figs 5.12a, 5.12b and 5.12c show the isotopic geochemistry of veins within the Urgonian, plotted into the following groups: veins from in the vicinity (roughly 5 to 10 metres or less) of thrust faults; veins from the basal part of the platform; and veins from the upper and middle part of the platform (the latter two often showed a geometrical relationship to larger structural features as shown in Fig. 5.1b). This tri-partite division was used to see if there was any difference in the geochemistry of fluids responsible for filling fractures at different levels within the Urgonian and within thrust zones within the Urgonian. Fig. 5.13 shows the isotopic composition of all three types of Urgonian vein along with the compositional fields for the Urgonian equant burial spars (see section 4.4.2 and Figs 4.11a and 4.11b).

Fig. 5.12a Isotope geochemistry of veins in the vicinity of and within thrust zones within the Urgonian. 1= Chartreuse; 2= Vercors; 3= Bauges; 4= Bornes; 5= Aravis; 6= Platé and Haut-Giffre. **Fig. 5.12b** Isotope plot for veins in the basal section of the Urgonian. 1= Chartreuse; 2= Vercors; 3= Bauges; 4= Bornes; 5= Aravis; 6= Platé and Haut-Giffre. **Fig. 5.12c** Isotope plot for veins from the upper and middle sections of the Urgonian. 1= Chartreuse; 2= Vercors; 3= Bauges; 4= Aravis.

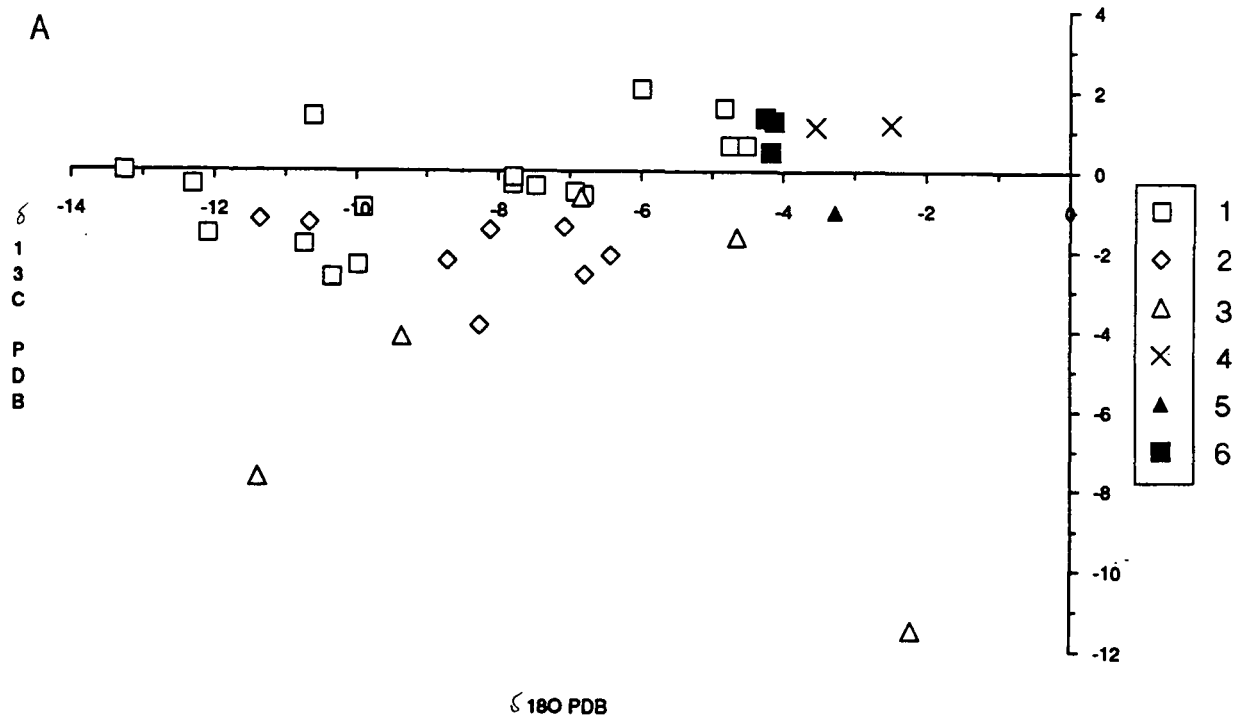

Fig. 5.12a

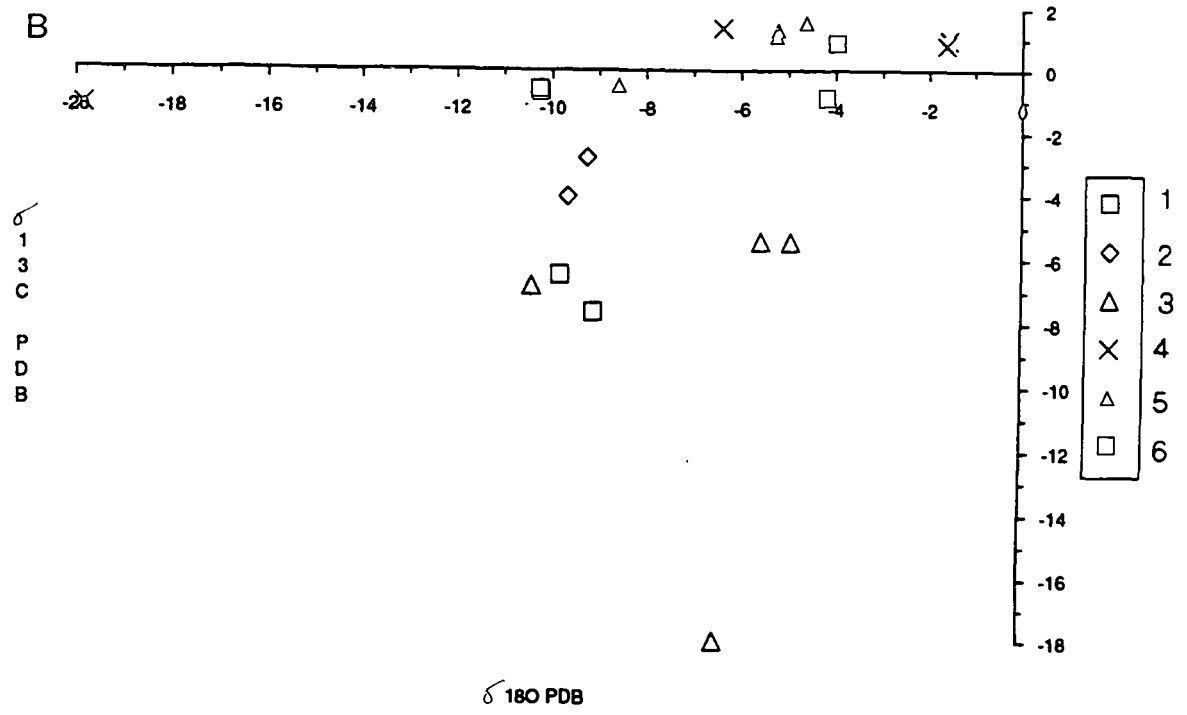

Fig. 5.12b

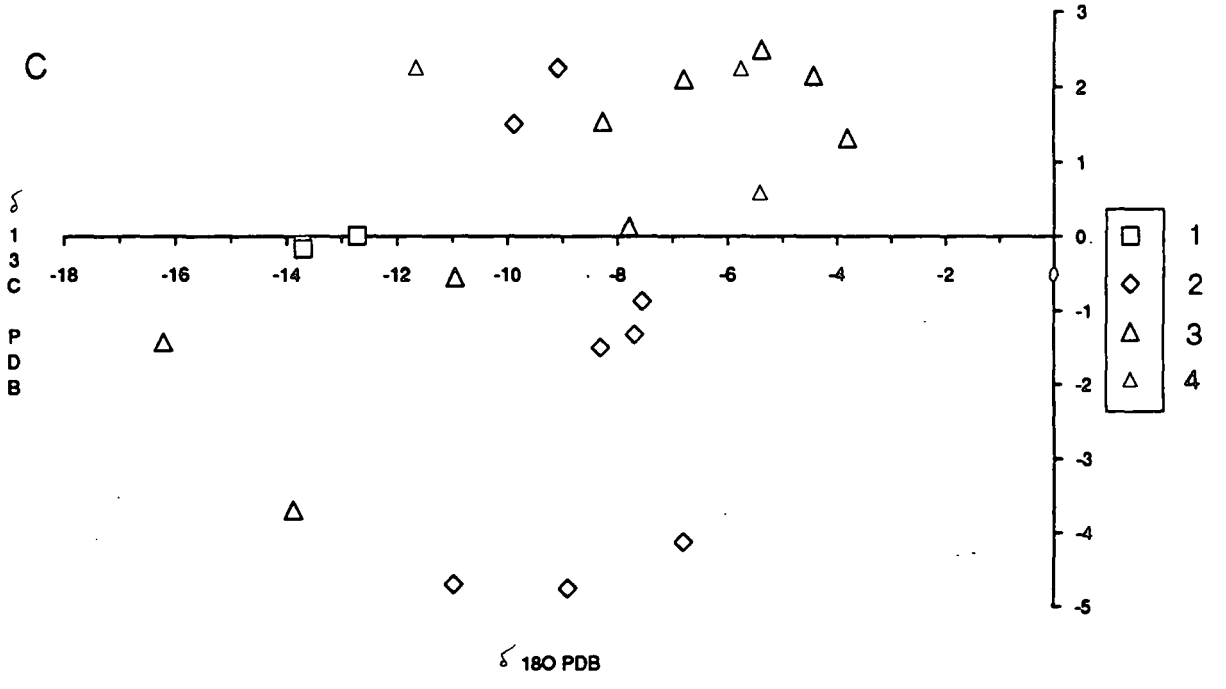

Fig. 5.12c

With two exceptions veins from in the vicinity of thrust zones plot in a roughly linear field from -2 to -13 ^{18}O PDB and 2 to -2 ^{13}C PDB (see Fig. 5.12a). The two exceptions are both from Pont l'Abime (380v1/90 and 380v2/90, located at A on Fig. 5.11, see also Fig. 5.18c) and indicate the incorporation of light CO_2 from organic maturation into fluids moving through the footwall to the Revard thrust. However, the majority of veins within Urgonian thrust zones plot within the roughly linear field described above. Two important features of this plot are firstly that the light ^{13}C values (around -3 $\delta^{13}C$ PDB) have correspondingly light ^{18}O values (around -10 $\delta^{18}O$ PDB). This could mean that hotter syn-tectonic fluids moving through the Urgonian had also been influenced by light CO_2 from organic maturation. Secondly, there is a marked regional bias in this linear trend, such that veins from the north east part of the chain (Haut-Giffre, Platé, Aravis and Bornes) plot at the less depleted end, whilst veins from the south-western part of the chain plot toward the more depleted end of this trend. This could indicate that isotopically heavier (formational) fluids were more common as syn-tectonic fluids in the north-east and perhaps these fluids were involved in a greater degree of wallrock-fluid interaction.

Veins from the basal section of the Urgonian show a similar trend (see Fig. 5.12b) to that described above for veins from thrust zones, in that veins from the north east part of the belt have (with one notable exception) less negative $\delta^{18}O$ PDB and $\delta^{13}C$ PDB values than veins from the south west of the chain. Again, this could indicate that isotopically heavier fluids were more common as syn-tectonic fluids in the north-east and these fluids were involved to a greater degree in wallrock-fluid interaction. Veins from the basal Urgonian from the south western massifs are quite depleted in ^{13}C and this suggests that fluids had migrated up section from deeper horizons undergoing organic maturation (see Chapter 7 for description of regional maturation levels within the Subalpine Chains). The one exception to this is a vein from the base of the Urgonian of the Bornes, with an exceptionally negative $\delta^{18}O$ PDB value (-19.84). Whatever the fluid source, this vein fill was precipitated from a particularly hot fluid.

Veins from the upper and middle sections of the Urgonian plot in a more wider field (see Fig. 5.12c) and are less easy to interpret. No consistent trends can be seen within this group, for example veins from the upper and middle sections of the Urgonian of the Bauges (number 3 on Fig. 5.13) can be seen to plot just about anywhere.

Fig. 5.13 (oppposite page). Isotope plot for all veins studied from the Urgonian. 1= thrust zone related veins; 2= basal Urgonian veins and 3= veins from the upper and middle sections of the Urgonian. Fields A and B are the two compositional fields within which the equant burial cements plot (see section 4.4.2).

Fig. 5.13 is a compilation plot of all the veins analysed from the Urgonian and shows that there is much of overlap in the isotopic composition of veins within the

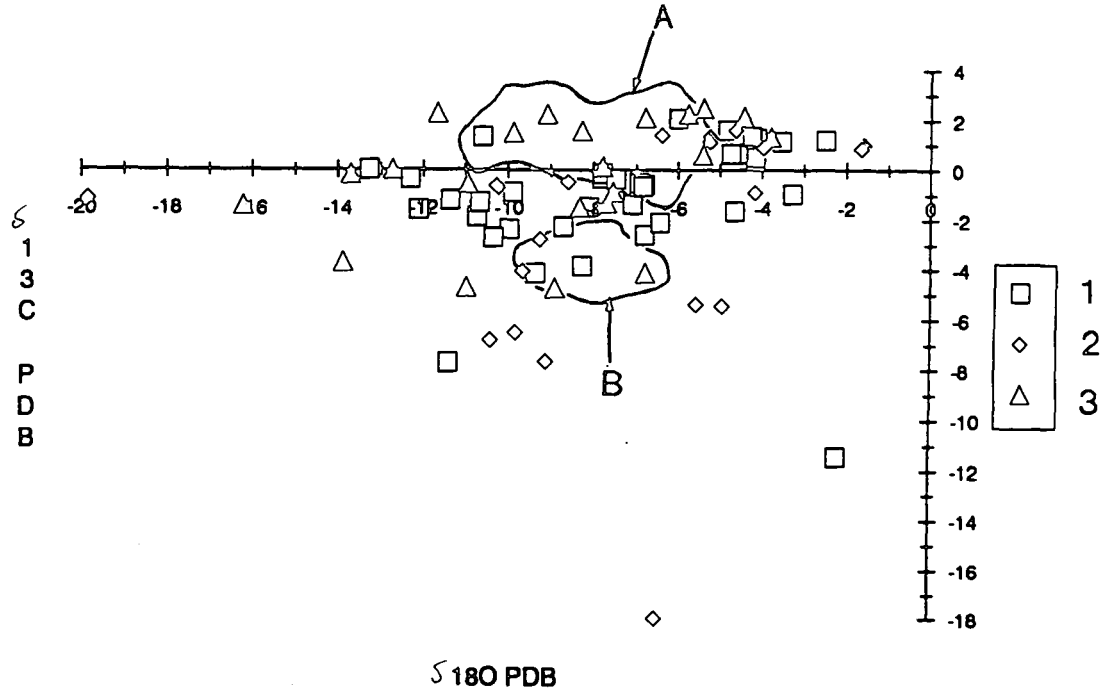

Fig. 5.13

Urgonian, despite the fact that they occur within different settings within the Urgonian. Veins from the basal Urgonian do show a slight trend in being more depleted $\delta^{13}C$ than veins from other settings. Veins from the upper and middle parts of the Urgonian generally seem to have a $\delta^{13}C$ signature similar to a likely host rock composition (2 to 3 $\delta^{13}C$ PDB), perhaps due to the effects of incorporating more wallrock-derived CO_2. The two compositional fields in which equant burial cements from the Urgonian plot are also shown in Fig. 5.13. Even though some of the veins overlap with the isotopic composition of the cements, it shows that the veins must have been precipitated from a wider range of fluid compositions, and probably at a wider range of temperatures too.

The trace element content of the veins is shown in Figs 5.14a and 5.14b and a plot of Sr^{2+} content versus $\delta^{18}O$ value for Urgonian veins is shown in Fig. 5.14c. Fig. 5.14b shows a slight correlation between the concentration of Fe^{2+} and Mn^{2+} within these veins and is comparable to similar trends seen in rudist shells and equant burial cements within the Urgonian (see Figs 4.9 and 4.14 respectively).

Generally the veins have a similar trace element composition to the equant burial cements within the Urgonian. Comparison of Figs 5.14a, 5.14b and 5.14c with Figs 4.13, 4.14 and 4.15 shows the overlap in the trace element composition of the veins and the equant burial spar within the Urgonian. Veins within the Urgonian have a mean Sr^{2+} content of 285 +/- 270, a mean Mn^{2+} content of 90 +/- 70 and a mean Fe^{2+} content of 500 +/- 480. These values are compared to those for the equant burial spars in the Urgonian and rudist

Fig. 5.14a Sr^{2+} versus Mn^{2+} plot for veins within the Urgonian. Key as in Fig. 5.13. **Fig. 5.14b** Fe^{2+} versus Mn^{2+} plot for Urgonian veins. Key as in Fig. 5.13. **Fig. 5.14c** Plot of Sr^{2+} versus $\delta^{18}O$ PDB for veins from the Urgonian. Key as in Fig. 5.13. **Fig. 5.14d** Table of the means and standard deviations for Sr^{2+}, Mn^{2+} and Fe^{2+} concentrations within rudist shells, equant burial cements (both from the Urgonian), veins from the Urgonian and veins from other parts of the stratigraphy. See opposite page fot Figs 5.14c and 5.14d.

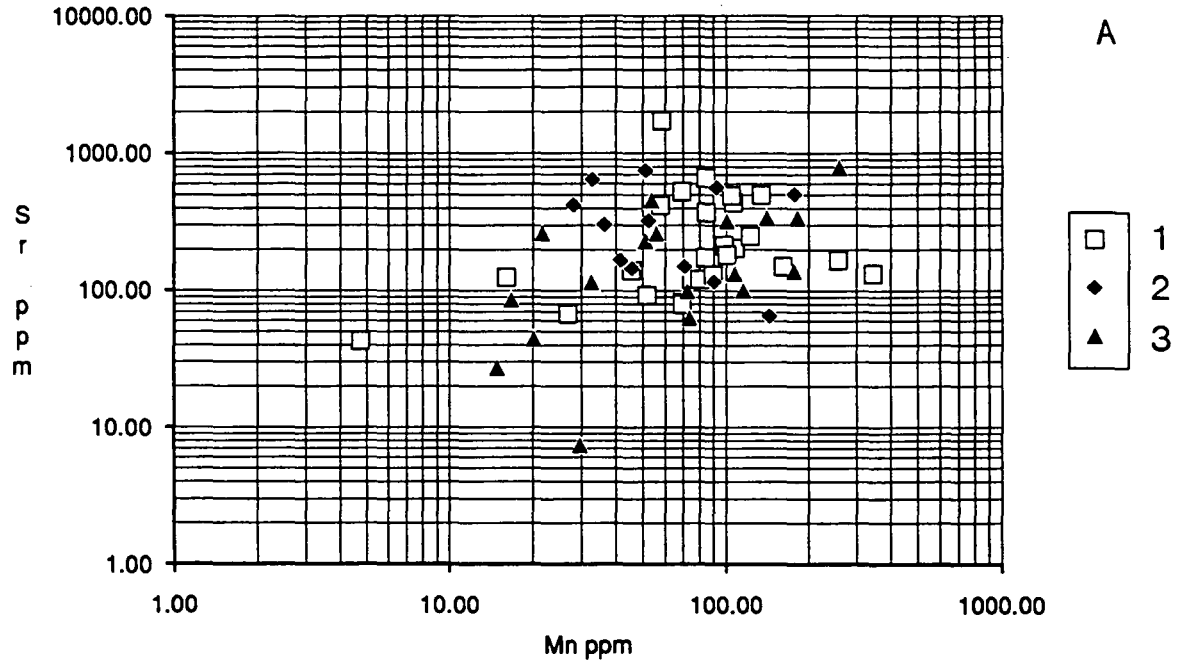

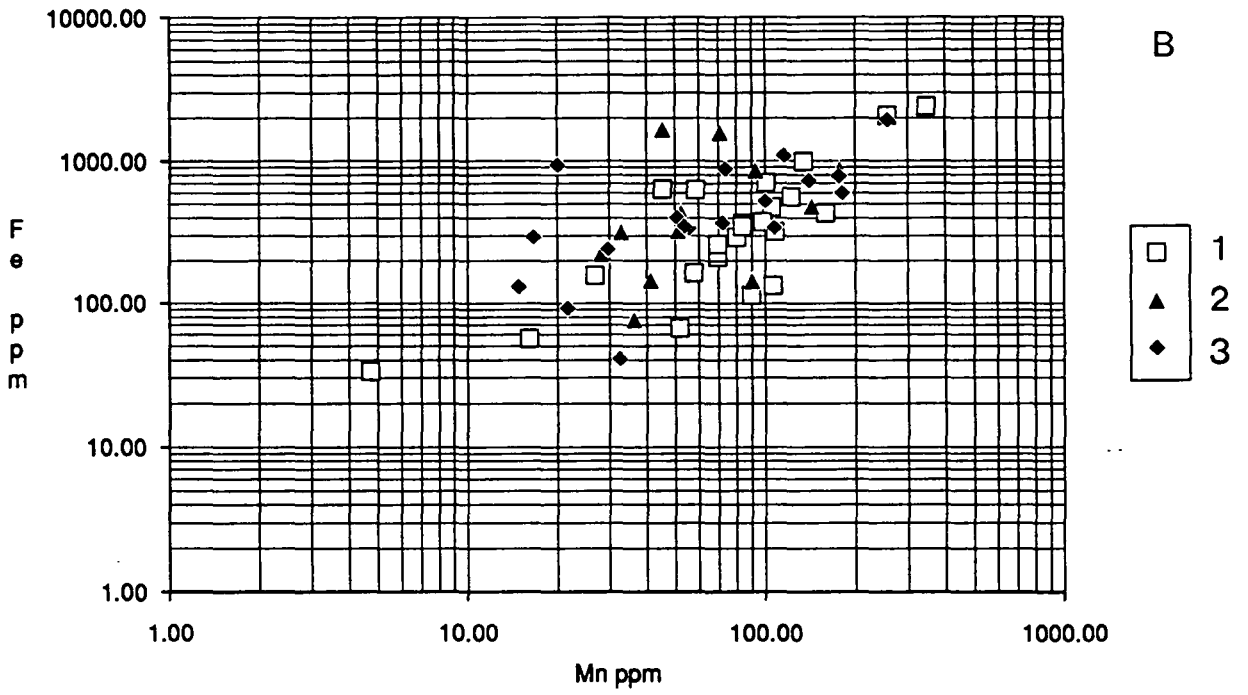

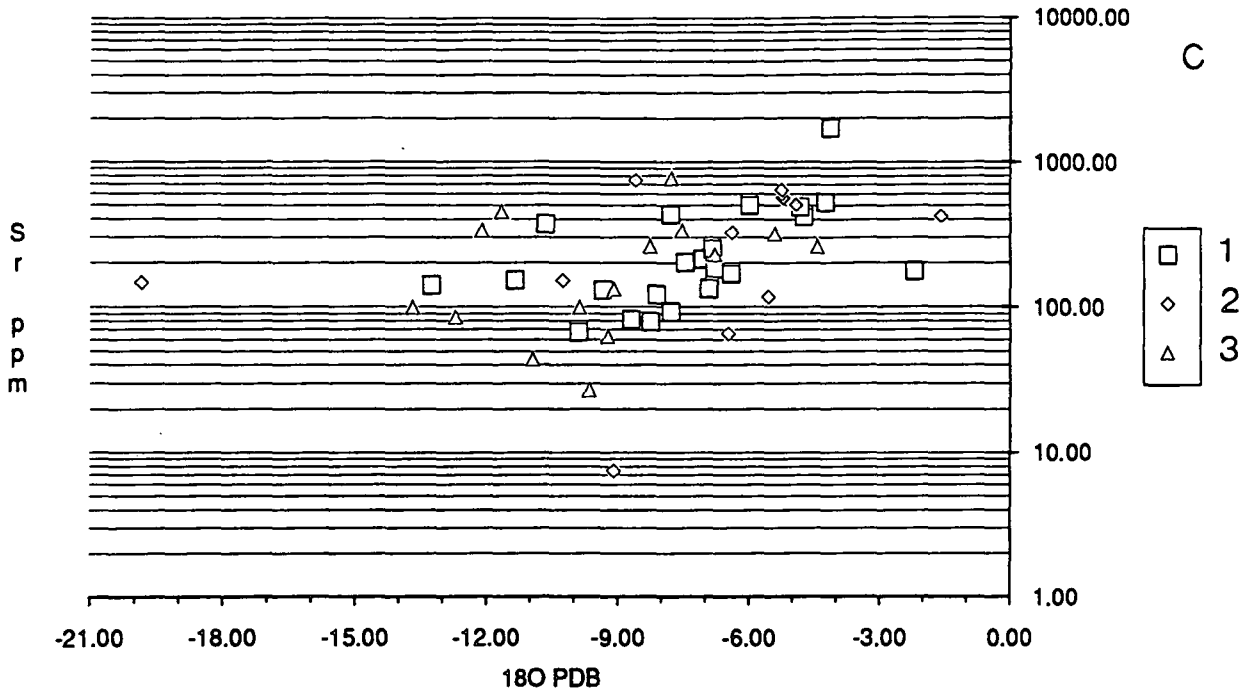

Fig. 5.14c

	Urgonian veins				Non-Urgonian veins		
	Fe	Mn	Sr		Fe	Mn	Sr
Mean	499.2	91.9	285.1	Mean	1050.3	207.5	690.9
Std.Dev.	484.7	69.7	270.7	Std.Dev.	929.9	228.8	673.6
Max.	2381.7	346.6	1693.5	Max.	3290.5	1235.9	3360.6
Min.	33.1	4.7	7.4	Min.	81.0	27.8	94.5
	Burial cements				Rudist shells		
	Fe	Mn	Sr		Fe	Mn	Sr
Mean	213	92	334	Mean	375	52	674
Std.Dev.	209	67	418	Std.Dev.	692	55	305
Max.	2250	200	400	Max.	3430	300	1140
Min.	50	10	20	Min.	60	7	200

Fig. 5.14d

shells (see sections 4.5.1 and 4.3.2 respectively), as well as values obtained for veins within other parts of the stratigraphy in Fig. 5.14d. The large standard deviations seen in Fig. 5.14d indicates that the populations are widely dispersed for trace element concentrations both within the veins and the cements and shells. The broad similarity of the trace element concentrations between the veins from within the Urgonian and the cements and rudist shells may possibly indicate that pressure dissolution within the Urgonian was

quite important for supplying material for precipitation within some of the fractures. The fact that veins from other parts of the stratigraphy have slightly different trace element concentrations (see sections 5.6.2 (b) and Figs 5.16a, 5.16b and 5.16c) supports this interpretation somewhat and suggests that the fluids responsible for the precipitation of these vein fills had not been influenced by pressure dissolution within the Urgonian or perhaps had not passed through the Urgonian. Fig. 5.14c, which shows the Sr content versus the $\delta^{18}O$ PDB value for the same veins shows a slight correlation, in that higher Sr^{2+} content generally occurs with less depleted values of $\delta^{18}O$ PDB.

Over such a broad sample set a wide scattering of isotopic compositions and trace element concentrations is perhaps inevitable. The interpretations given above are made on a limited number of data points in some instances (and perhaps too many in others!), such as veins in the north east part of the chain (due to the inaccessibility of some of the outcrops in the north east). More data points may well fill in the gaps and confirm the interpretations made in the section above; however they could just as easily disprove them!

5.6.2 (b) Geochemistry of veins within other parts of the stratigraphy.

Figs 5.15a and 5.15b show the isotopic composition of veins in other parts of the stratigraphy. the wall/host range in age from Tithonian to Eocene. Figs 5.16a, 5.16b and 5.15c show the trace element composition of these veins and a plot of Sr^{2+} content and $\delta^{18}O$ value for these veins. Fig. 5.14d shows the mean concentrations and standard deviations for Sr^{2+}, Mn^{2+} and Fe^{2+} concentrations within these veins.

When plotted according to their location (see Fig. 5.15a) the only consistent trend is that veins from the Haut-Giffre and Platé plot along a roughly linear vertical trend around -5 $\delta^{18}O$ PDB with more variable $\delta^{13}C$ PDB, whilst veins from the other areas are more diverse in their isotopic composition. When plotted according to their age no real pattern or trend can be seen.

The trace element concentrations of the non-Urgonian veins (see Figs 5.16a, 5.16b, 5.16c and 5.14d), have broadly similar trends to those from the Urgonian (see Figs 5.14a, 5.14b and 5.14c). There is quite a good correlation between Fe^{2+} and Mn^{2+} within these veins (see Fig. 5.16b); similar trends for Fe^{2+} and Mn^{2+} concentrations were also seen for rudist shells and equant burial cements within the Urgonian (see Figs 4.9 and 4.14 respectively) and also with veins in the Urgonian (see Fig. 5.14b).

Fig. 5.15a Isotopic composition of veins within other parts of the stratigraphy, plotted for location. 1= Chartreuse; 2= Vercors; 3= Bauges; 4= Bornes; 5= Aravis; 6= Platé and Haut-Giffre. **Fig. 5.15b** Isotopic composition of veins within other parts of the stratigraphy plotted for age. 1= upper Jurassic; 2= Berriasian; 3= Valanginian; 4= upper Cretaceous; 5= Tertiary. See opposite page.

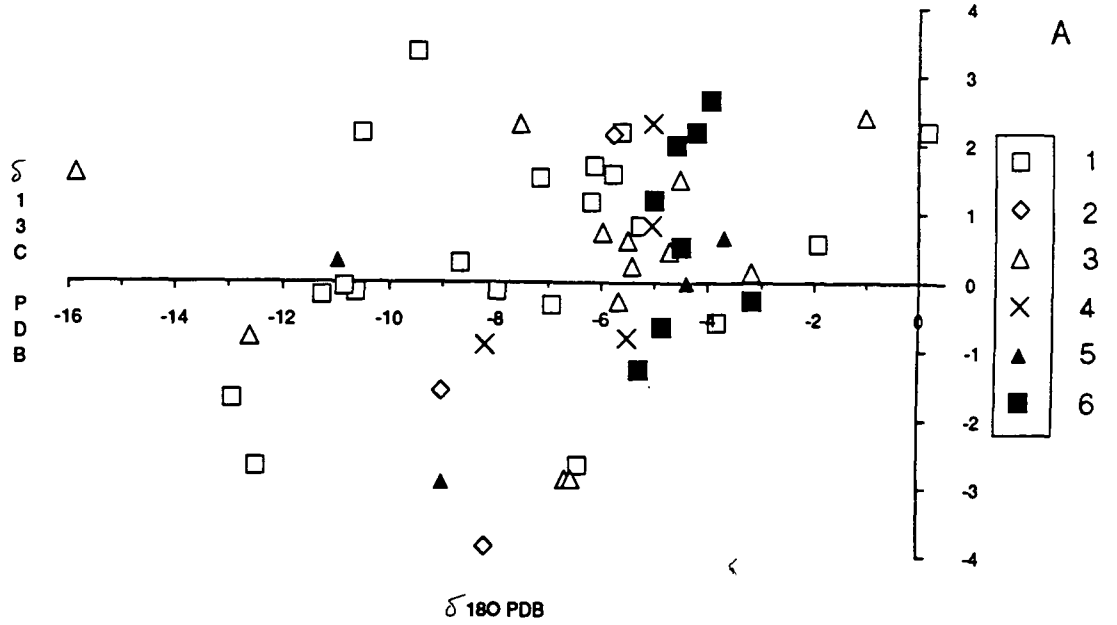

Fig. 5.15a

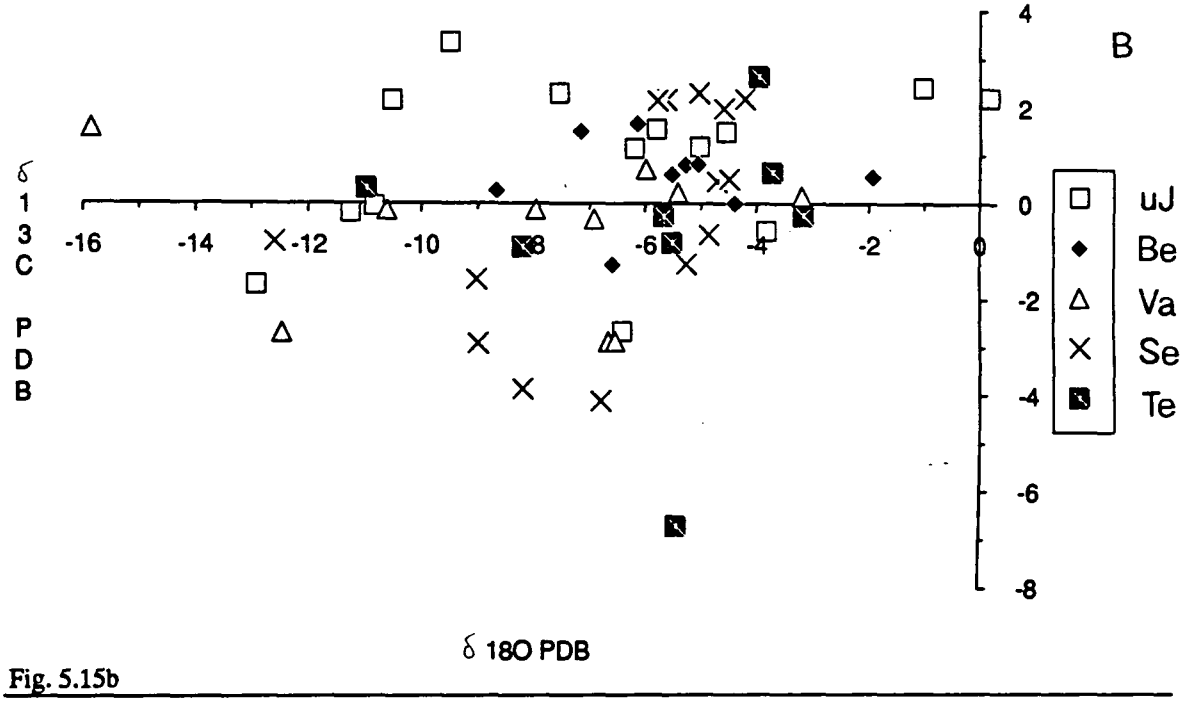

Fig. 5.15b

Fig. 5.16a Sr^{2+} versus Mn^{2+} plot for veins within other parts of the stratigraphy, plotted for location. 1= Chartreuse; 2 = Vercors; 3= Bauges; 4= Bornes; 5= Aravis; 6=Platé and Haut-Giffre. **Fig. 5.16b** Fe^{2+} versus Mn^{2+} plot for non-Urgonian veins. Key as in Fig. 5.16a. **Fig. 5.16c** plot of Sr^{2+} content versus $\delta^{18}O$ PDB for the same veins. Key as in Fig. 5.16a. See opposite page for Fig. 5.16c.

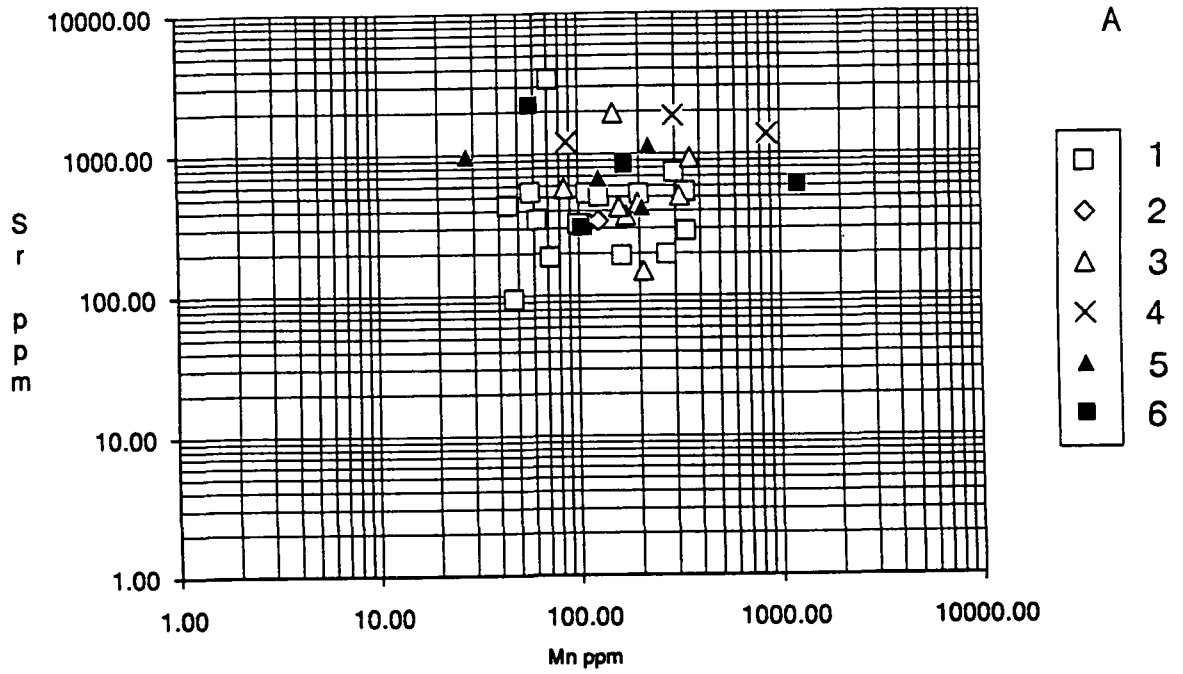

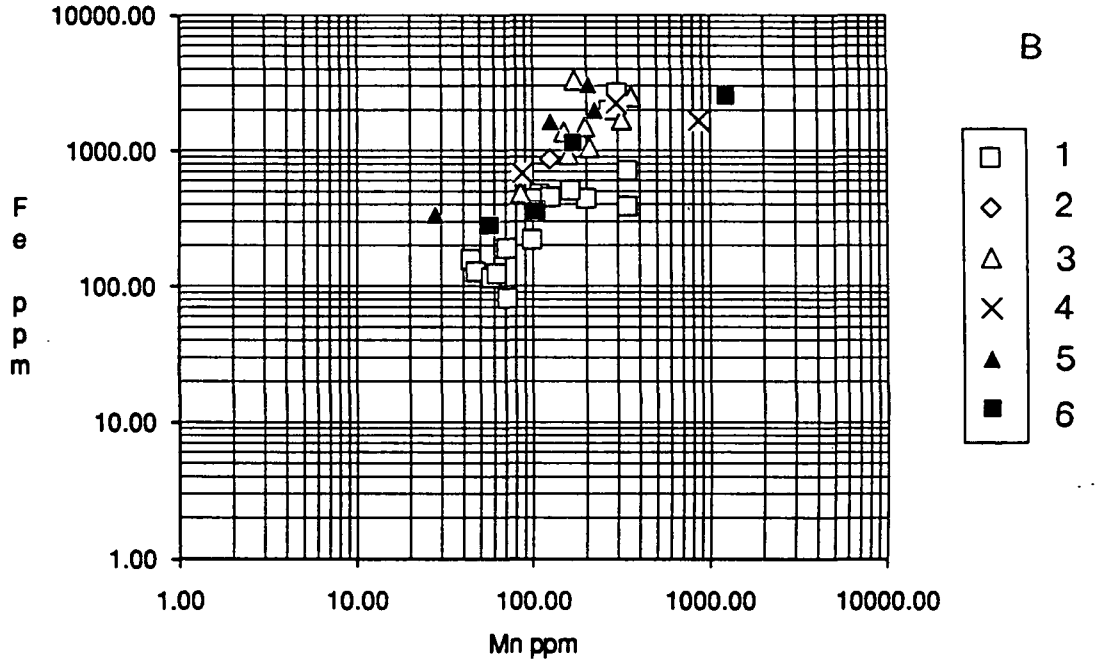

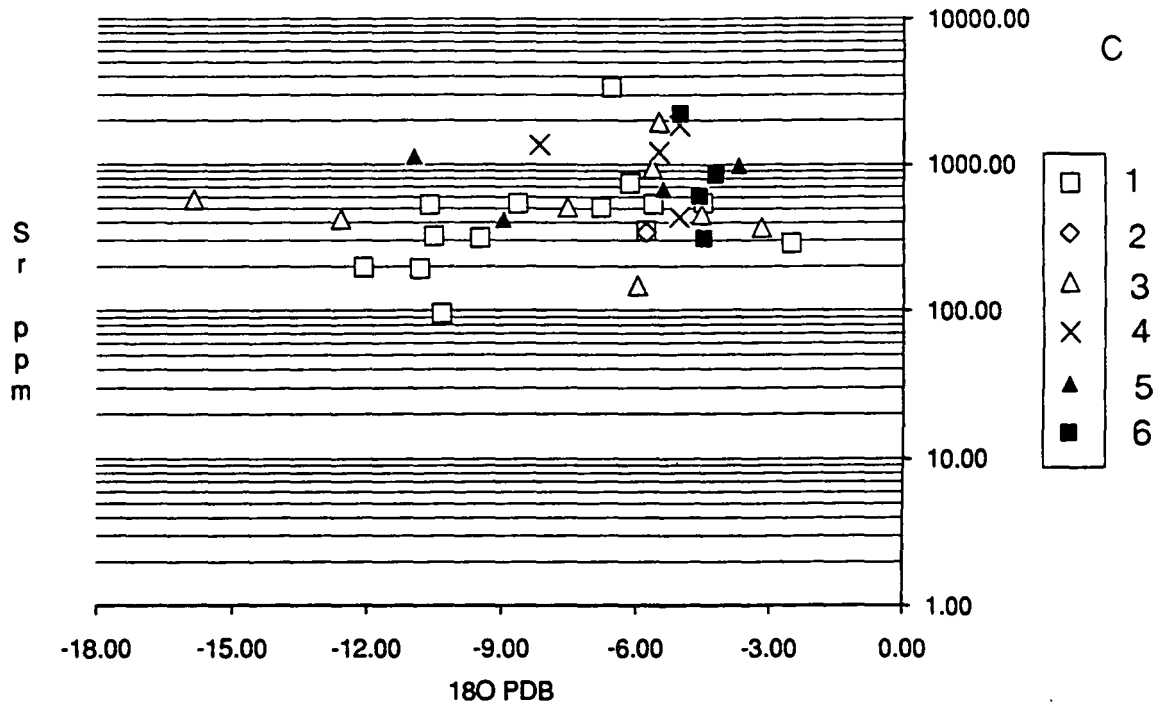

Fig. 5.16c

5.6.2 (c) Comparison of the geochemistry of veins from within the Urgonian with those from other parts of the stratigraphy.

The isotope and trace element geochemistry of both the veins within the Urgonian and from other parts of the stratigraphy are shown in Figs 5.17a, 5.17b, 5.17c and 5.17d.

In very general terms some trends can be picked out from Fig. 5.17a. Firstly veins from other horizons have more positive $\delta^{13}C$ values than a lot of the veins from the Urgonian (veins from the Urgonian have a mean $\delta^{13}C$ value of -1.29 +/- 3.30, non-Urgonian veins have a mean $\delta^{13}C$ value of 0.04 +/- 1.95). This could suggest that the Urgonian was an aquifer for fluids that had been derived from or had passed through areas where organic maturation was occurring. The clustering of isotopic compositions for veins from other parts of the stratigraphy around -5 $\delta^{18}O$ and 2 $\delta^{13}C$ suggests that perhaps fluids responsible for the precipitation of these vein fills had interacted isotopically with the wallrock (assuming an average bulk rock limestone to have a composition of -4 to -2 $\delta^{18}O$ and 3 to 2 $\delta^{13}C$ PDB).

Fig. 5.17a Isotope plot of all veins. 1= veins within the Urgonian; 2= veins within non-Urgonian strata. **Fig. 5.17b** Sr^{2+} versus Mn^{2+} for all veins. Key as for 5.17a. **Fig. 5.17c** Fe^{2+} and Mn^{2+} plot for all veins. Key as for 5.17a. **Fig. 5.17d** Sr^{2+} versus $\delta^{18}O$ PDB plot for all veins. Key as for 5.17a. See opposite page for Fig.s 5.17c and 5.17d.

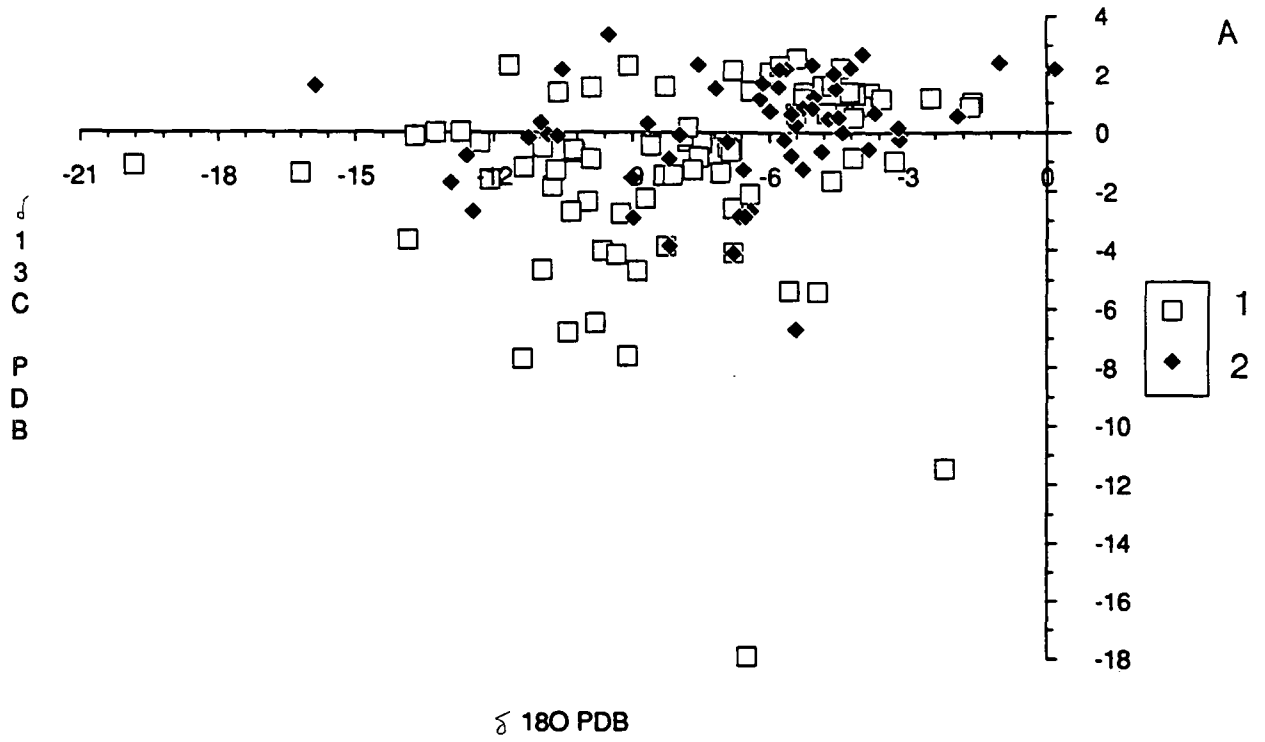

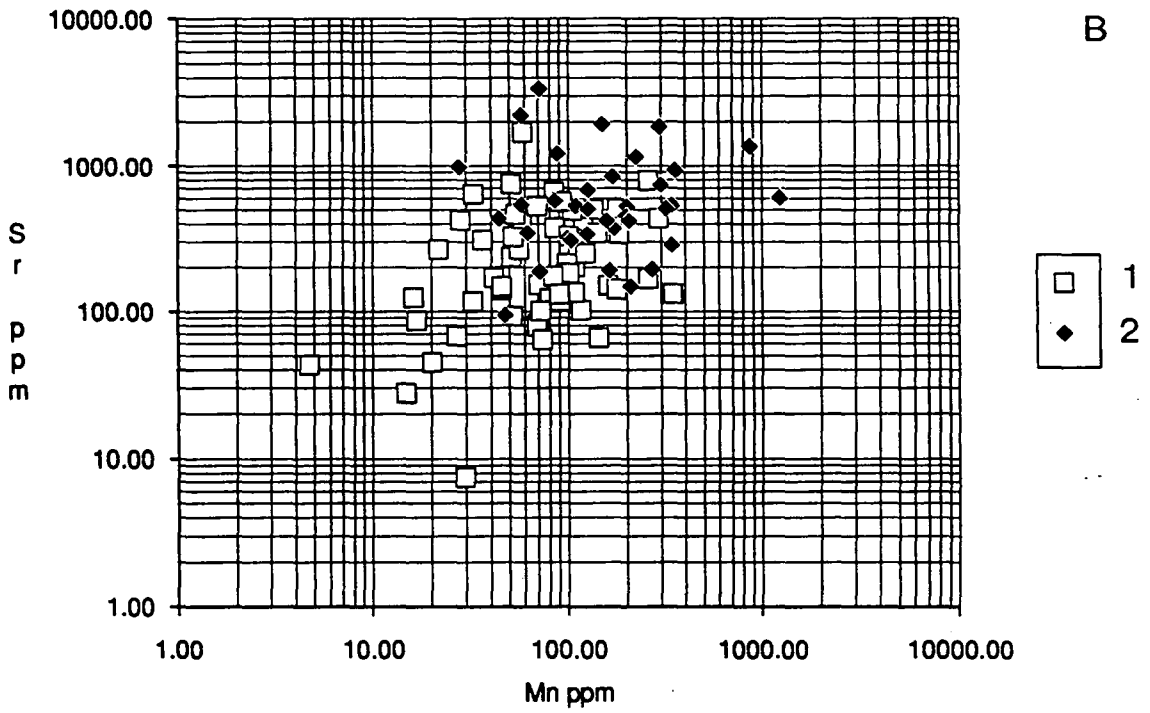

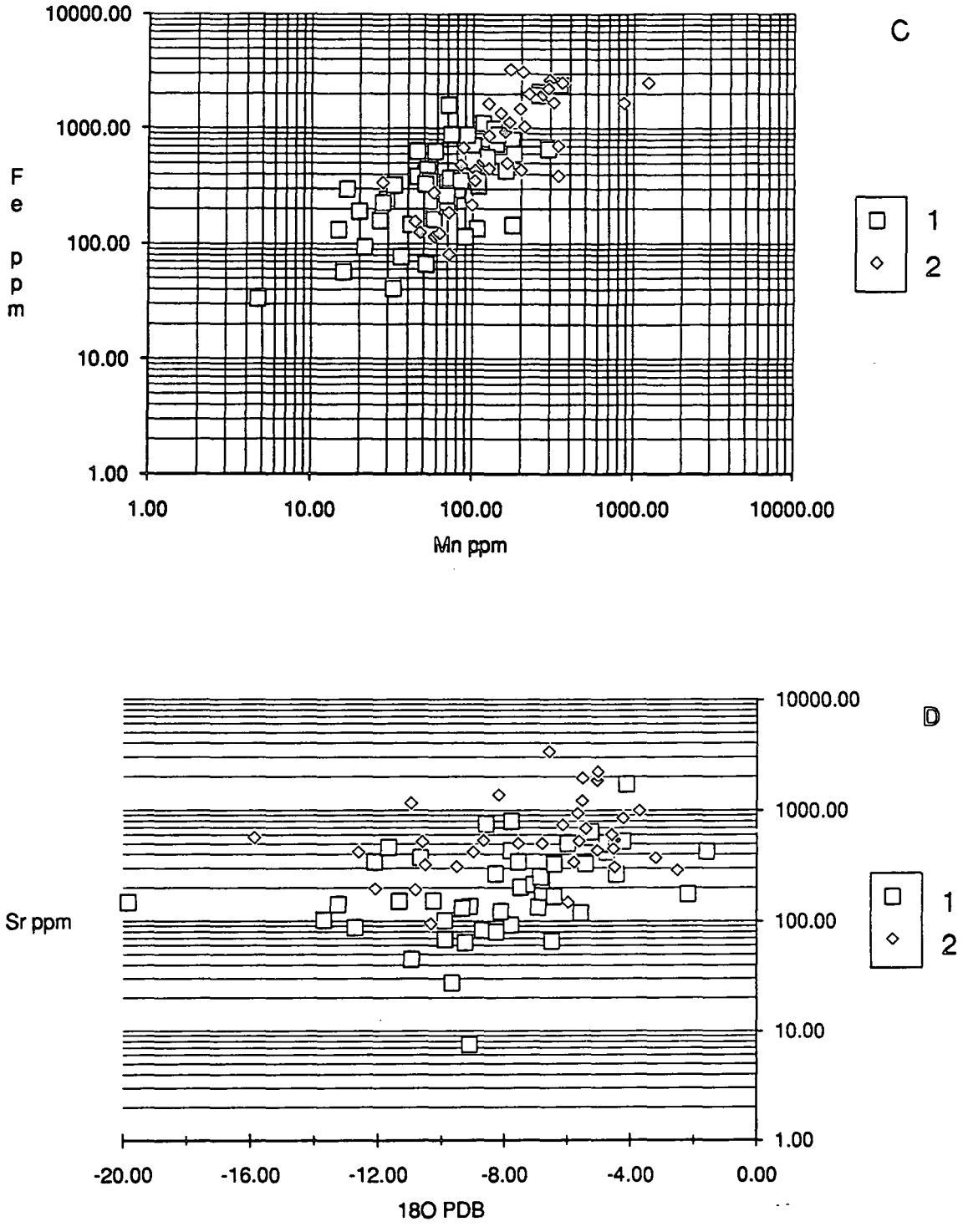

Both veins within the Urgonian and within other parts of the stratigraphy have generally very similar ranges of trace elements (see Figs 5.17b, 5.17c and 5.17d). However as can be seen from the mean values shown Fig. 5.14d (and Figs 5.17b, 5.17c and 5.17d)

the non-Urgonian veins tend to have slightly higher concentrations of Fe^{2+}, Mn^{2+} and Sr^{2+} than veins from the Urgonian. As was suggested earlier this could reflect the influence of pressure dissolution within the Urgonian affecting the trace element composition of fluids passing through the Urgonian and precipitates from these fluids within fractures in the Urgonian.

5.6.3 Isotopic composition of cross-cutting veins and the 'oldest' and 'youngest' areas of the same veins.

Numerous localities displayed two or more generations of veining; where possible the order of formation was deduced from cross-cutting relationships and, if the thickness of the veins permitted, two generations were sampled and analysed isotopically. Due to the greater amount of material required for trace element analysis often one of the two vein generations could not be sampled. Figs 5.18a, 5.18b and 5.18c show the isotopic compositions for cross-cutting veins from the Chartreuse, Vercors and Bauges, Bornes and Aravis respectively.

Fig. 5.18a Isotopic composition of cross-cutting veins from the Chartreuse. Arrows point from older to younger. 1v/90= two vein generations in the Berriasian, older non-ferroan, *bc* vein cut by ferroan vein orientated perpendicular to it (*ac*) (G1 on Fig. 5.10); 3v/90= two non-ferroan veins in the Urgonian (G2 on Fig. 5.10); 4v/90= two *ac* veins, both non-ferroan in the Urgonian (G3 on Fig. 5.10); 18v/90= two ferroan *bc* veins in the Urgonian (not possible to establish age relationship) (F on Fig. 5.10); 156v/89= two *ac* veins in the Tithonian (H1 on Fig. 5.10), older vein is ferroan; 124v/89= two veins in the Valanginian related to intra-formational thrusts (D2 on Fig. 5.10) older vein is ferroan. **Fig. 5.18b** Isotopic composition of cross-cutting veins from the Vercors. 192v-90= non-ferroan, *bc* vein from the upper part of the Urgonian, Pas de Montbrand, central Vercors; older part of the vein to central, youngest part of the vein; 208v/89=bedding parallel, ferroan, zoned vein from Pont de Goule Noire, Bourne Gorge, Vercors. Older outer part of the vein to younger, inner part of the vein. **Fig. 5.18c** Isotopic composition of cross-cutting veins from the Bauges, Bornes and Aravis. 255v/90= two extensional veins within the Valanginian, older non-ferroan cut by younger ferroan vein; 278v/90= non-ferroan *ac* veins in the Urgonian (E1 on Fig. 5.11) (not possible to establish age relationship) 374v/90= both non-ferroan veins from the upper Urgonian of Dents d'Arclusaz (D1 on Fig. 5.11); 380v/90 & 381v/90= extensional veins related to intraformational thrusts in the Urgonian, Pont de l'Abime (A1 on Fig. 5.11), 380v/90 ferroan older vein cut by younger non-ferroan vein, 381v/90 older, zoned ferroan outer part of the vein and inner, younger unzoned part of the same vein; 553v/90= non-ferroan vein from the basal section of the Urgonian (Pic de Jallouvre, Bornes), older, outer part of the vein and inner, younger part of the vein; 493/90= two vein generations from the upper Urgonian of the Aravis (Combe du Grande Cret). See foldout for Fig. 5.18c.

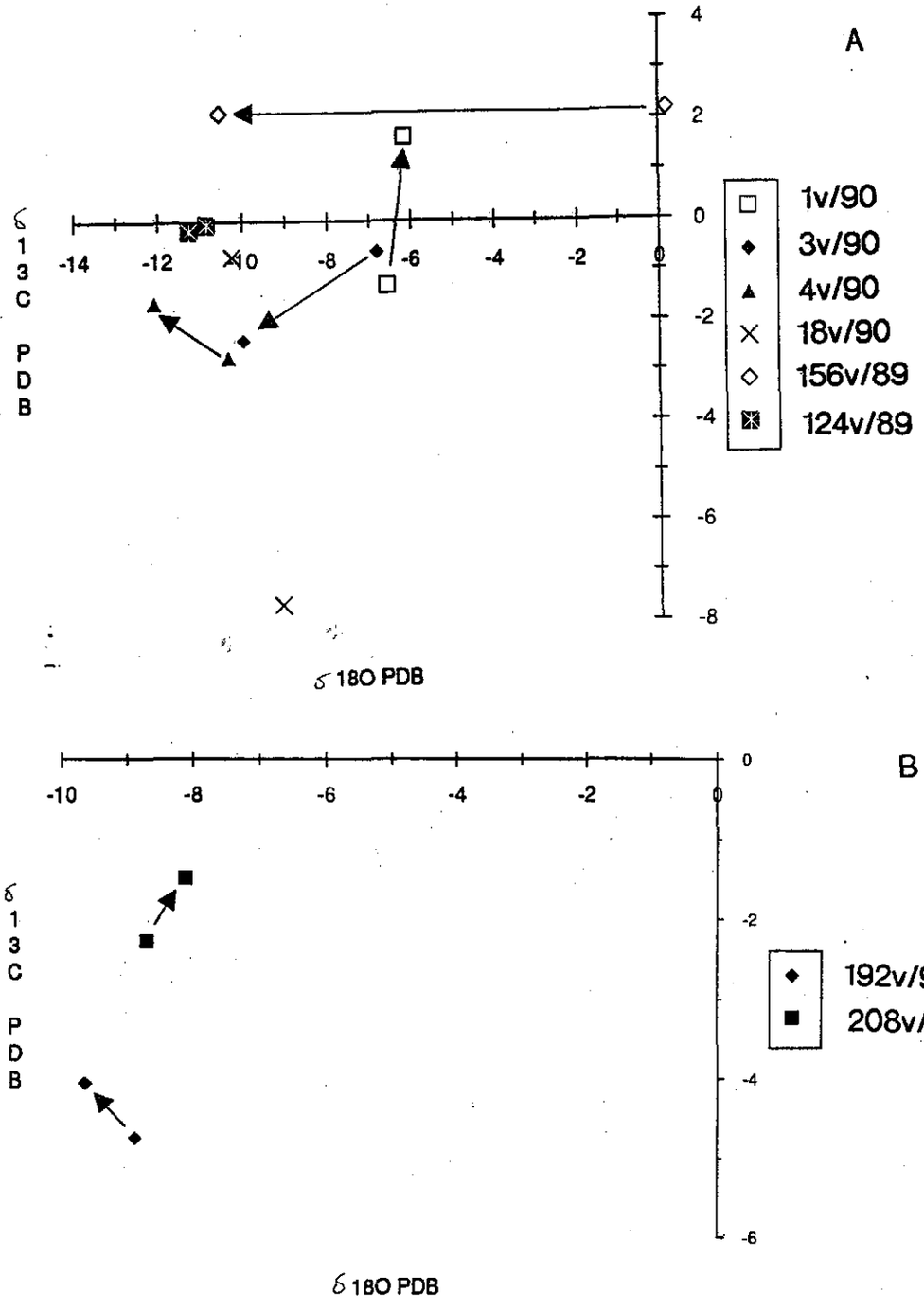
A
δ 13C PDB
δ 18O PDB
1v/90
3v/90
4v/90
18v/90
156v/89
124v/89
B
δ 13C PDB
δ 18O PDB
192v/90
208v/89

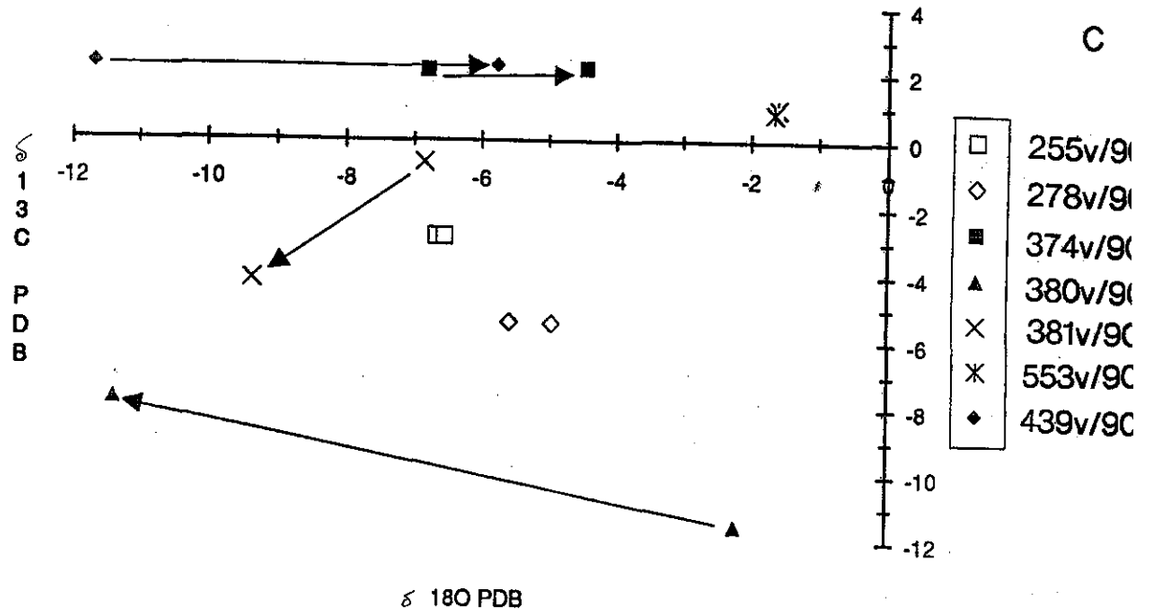
C
δ 13C PDB
δ 18O PDB
255v/9
278v/9
374v/9
380v/9
381v/9
553v/9
439v/9

Figs 5.18a, 5.18b and 5.18c show is that there is no consistent trend in the isotope geochemistry from older to younger veins. This could be a reflection that not enough cross-cutting veins were analysed. Veins that show a depletion in ^{18}O from older to younger could show the effects of increased temperature of the fluids responsible for precipitating the vein fill. Veins and successive vein generations which show the opposite trend (less depleted from older to younger) could be due to the younger generation precipitated from isotopically heavier fluids (such as formational fluids). Budai (1985) suggested that similar temporal changes in isotopic composition (combined with changes in mineralogy and luminescence) indicated rapid allochthonous migrations of fluids during deformation.

For samples 156v/89, 374v/90 and 439v/90 (shown on Figs 5.18a and 5.18c) there is virtually no change in their $\delta^{13}C$ values from older to younger. This suggests that the carbon reservoir within the fluids was strongly controlled by the input of CO_2 derived by pressure dissolution. This is unlike the evolution of isotopic compositions of earlier to later formed veins reported from the Doldenhorn nappe of Switzerland by Dietrich et al. (1983) and from the Rencurel thrust (central Vercors, see Fig. 3.1, number 5) by Roberts (1991 and in press). In both cases the earlier formed veins were more depleted in ^{13}C relative to the host rock signature, whilst later veins have $\delta^{13}C$ PDB signatures similar to the host rock. Both authors suggested that this was due to a switch from a chemically open to closed environment with pressure dissolution becoming increasingly important. A similar trend is seen for sample 1v/90 (see Fig. 5.18a). A different picture is presented by Rye & Bradbury (1988), who suggest from their isotope data from veins within a thrust ramp of the Pineta thrust complex that exchange between host rock and syn-tectonic fluids diminished as fluid flow became more 'channelized' with time. The two patterns of isotopic evolution for vein fills shown by Dietrich et al. (1983) and Roberts (1991 and in press) are perhaps intuitively the most predictable scenario, i.e. with increasing deformation (and stylolitisation) the composition of veins fills will shift toward that of the host rock (particularly as regards $\delta^{13}C$ PDB signatures). Departures from this trend are possibly due to one or more factors such as lack of connectivity between fluid flow conduits and sites of pressure dissolution, rates of reaction, the amount of fluid passing through (a large mass of water equilibrating with a small mass of rock will show little change in isotopic composition, Hanor, 1987), temperature and the original composition of the fluid and host rock.

5.7 Discussion.

A whole range of possible fluid sources has been suggested to be involved in fold/thrust belts. These include meteoric water derived from uplifted parts of the thrust belt acting as recharge points (Garven & Freeze, 1984; Bethke & Marshak, 1990; Sverjensky & Garven, 1992), formation fluids from within the thrust stack as it de-waters (with increased

burial with tectonic loading (see Fig. 8.5), as suggested by Dietrich et al., 1983, for the Doldenhorn nappe, Bradbury & Woodwell, 1987; for the Canadian Cordillera and Yardley, et al., 1989 for the Central Pyrenees), from ascending metamorphic fluids from deeper within the thrust stack (as suggested by Bradbury & Woodwell, 1987 and Rye & Bradbury, 1988 for the Southern Pyrenees) and possibly from the circulation of sea water which has infiltrated fractures and faults (if the syn-orogenic surface was covered by sea-water at the time). For the Subalpine Chains the least likely fluid source is the metamorphic option. Although these fluids are likely to have been produced in the orogenic hinterland to the east, by such fluids at the time they may have had migrated (several tens of kilometres at least) to reach the Subalpine Chains it is likely that it would be unrecognisable due to mixing with fluids of other sources (Drever, 1982). The distances involved in the migration of fluids if one or more of the fluid sources listed above are invoked are likely to be less than 5 kilometres (similar distances are quoted by Bradbury & Woodwell, 1987 and Yardley et al., 1989).

The geochemistry shows that the composition of the fluids and the temperature of the fluids varied considerably temporally and spatially. Budai (1985) also shows spatial and temporal variations in the isotopic composition and the mineralogy of veins. A variety of fluid sources can be invoked (discussed above) to account for the isotopic composition of the vein fills, both slightly heated 'light' meteoric water or hot 'heavy' formational fluids could account for the isotopic composition of the vein fills. The trace element data does not really clarify this, except that fluids that flowed through the Urgonian have a broadly similar trace element content to the host rock values (ie. rudist shells and burial spars).

The variety of different fluids could be a reflection of several factors such as the degree to which faults are acting as conduits for fluids to move along, to what depths faults can source fluids, which horizons had better permeability characteristics during the deformation (e.g. the basal dolomitised section of the Urgonian if it still possessed its inter-crystalline porosity, could be a good aquifer) and which areas were uplifted and acted as recharge points at the time. The fact that none of the veins from other horizons showed the depleted ^{13}C values that some of the veins in the base of the Urgonian show, may suggest that the Urgonian was a regional aquifer for fluids released from units undergoing organic maturation deeper in the section. These fluids could have possibly utilised Paleogene normal faults and/or Alpine thrust faults to get to the Urgonian and flowed laterally within the Urgonian until suitable fractures were produced for precipitation.

It has been suggested that the hot fluids responsible for the precipitation of various cements within the Tartan oil field of the North Sea migrated up-section along normal faults (Burley et al., 1989). With regional thermo-baric fluid flow responsible for building high enough fluid pressures next to faults to allow faulting to occur. This mechanism is directly analogous to the seismic valving mechanism suggested by Sibson (1981; 1990). The other mechanism for fluid flow along faults by Sibson (1981) is the seismic 'pump'

model, where post-seismic flow occurs through the collapse of pre-failure dilatant fractures. Although Sibson (1990) suggested that the favoured crustal levels for fault valve activity is where P-T conditions are in the range of 300-400°C, σv (vertical stress) <0.4 GPa (low to mid-greenschist environment). He also noted that the high fluid pressures required for fault-valve behaviour are most likely to develop in compressional regimes through de-watering of thrust stacks, so may occur at shallower depths in instances such as the Subalpine Chains. Both normal and reverse faults in the Subalpine Chains were probably similarly important for providing fluids from which the vein fills were precipitated and may at times have acted both fluid 'pumps' or 'valves' for fluid migration (Roberts, 1990, suggested that seismic pumping has been important within the hanging wall of the Ferrière thrust).

Had it been possible to employ a finer resolution of sampling, enabling more than just two parts of a vein or two vein generations to be sampled, then perhaps a more detailed picture of the fluctuations of the geochemistry could be presented. Roberts (1991 and in press) has already presented the results of an isotopic study of veins within a single thrust zone.

5.8 Chapter conclusions.

1) Both field relationships and petrography point to a syn-tectonic origin for the veins. Petrography also shows that a lot of the fracturing was induced by hydraulic fracturing under cyclic changes in pore pressure, producing 'crack-seal' textures within the veins.

2) Varied geochemistry not surprisingly indicates a variety of possible fluid sources

3) The predominant isovariant trend in the $\delta^{18}O$ isotopes of all the veins sampled (see Fig. 5.17a) indicates the importance of temperature of the porefluids and the likely wide range of temperatures of syn-tectonic porefluids.

4) More depleted ^{13}C values of vein fills within the Urgonian suggest that the Urgonian was an aquifer for fluids which had been derived from or had passed through areas of undergoing organic maturation.

5) The overlap in the trace element geochemistry of veins and shell material and cements within the Urgonian suggests that fluids filling fractures within the Urgonian were influenced by pressure dissolution of the Urgonian.

6) The temporal and spatial changes in fluid geochemistry suggest that fairly rapid migrations of fluids of different sources (and probably temperatures) occurred during deformation within the Subalpine Chains.

Chapter 6 Clay mineral transformations within lower Cretaceous (Hauterivian) mudstones.

6.1 Introduction.

This chapter details the results of an X-ray diffraction analysis of the clay fraction from one particular mudstone unit from within the study area. Lower Cretaceous (Hauterivian) aged mudrocks were analysed for changes in clay mineral composition in particular, and changes in the ordering of the illite/smectite (I/S) mixed-layer species. The results of this study are used to infer regional differences in the burial and thermal history of the Subalpine Chains.

Within the northern part of the study area (Haut-Giffre, Platé and Aravis massifs) illite/chlorite assemblages dominate the Hauterivian and the illite/smectite mixed-layer clay mineral has an ISII ordering. In the southern part of the area (Vercors, Chartreuse and Bauges massifs) by way of contrast smectite and mixed-layer I/S assemblages dominate clay fractions from the Hauterivian and the I/S has a random ordering. These results indicate that the northern part of the area has experienced a greater depth of burial than the southern area. The implications of this study are discussed at greater length in Chapter 8.

6.2 Background to clay mineral changes in sedimentary rocks.

Early work by Burst (1969), Weaver (1960), Perry & Hower (1970), and later by Hower et al. (1976), showed that increasing burial depth caused the transformation of expandable smectite clay mineral species to non-expandable illite and chlorite. Mixed-layer illite-smectite (I/S) forms an intermediate series, with the percentage of non-expandable illite layers increasing with the loss of expandable smectite layers as the horizon becomes more deeply buried. The compositional differences between smectite, which is similar to pyrophyllite, and illite, which is more akin to muscovite, is shown in the "magic triangle" shown in Fig. 6.1. This transformation was documented within the clay fraction, which is usually taken to be the less than 2 micron size fraction. The interstratification of illite and smectite layers becomes more ordered (or less random) and hence more predictable (Reynolds & Hower, 1970). The progress of the reaction from an assemblage dominated by smectite to randomly interstratified I/S to well ordered ISII interstratification to illite can be followed by X-ray diffraction (XRD) profiles (Reynolds & Hower, 1970; Hower et al., 1976; Wilson, 1987). The ideal nature of the transformation of smectite into ordered I/S is by the formation of thin illite particles (the so-called "fundamental" clay particles) stacking on top of each other giving rise to interparticle expansion and the XRD characteristics of I/S. This is shown diagrammatically in Fig. 6.2. The main compositional changes that

Fig. 6.1. The illite-smectite compositional field and generalised chemical relationships. The contours of expandability are at 90%, 45% and 10% and are based on approximately 100 analyses. Re-drawn from Sroden & Eberl (1984).

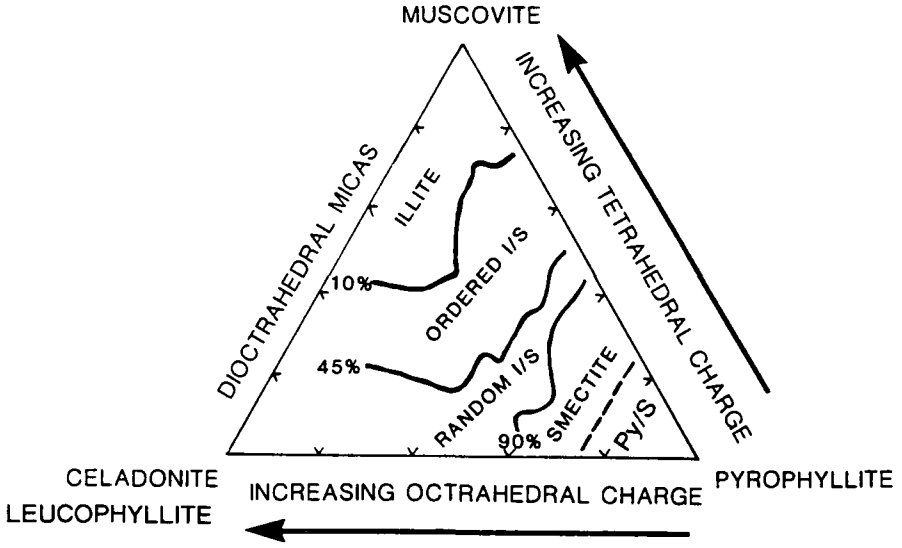

CHEMICAL RELATIONSHIPS BETWEEN ILLITE AND RELATED MINERALS.

From Sroden and Eberl (1984).

Celadonite Leucophyllite	$(AlFeMg)_2Si_4O_{10}(OH)_2K$
Pyrophyllite	$Al_2Si_4O_{10}(OH)_2$
Muscovite	$Al_2(Si_3Al)O_{10}(OH)_2K$

occur with increasing illite layers are a gain of interlayer potassium, increasing substitution of aluminium for silicon in the tetrahedral layer, loss of octahedral magnesium and iron and probable reduction of octahedral iron from ferric to ferrous (see Hower, 1981; Sroden & Eberl, 1984 for discussion). Assuming the original smectite 2:1 layers remain intact and that the mineralogical change only involves ionic substitution, the overall reaction in Tertiary of the Gulf Coast is:

smectite + Al^{3+} + K^+ = illite + chlorite + quartz (Hower et al., 1976)

This implies a layer-for-layer conversion of smectite to illite. It has been suggested by Pearson & Small (1988) that a similar reaction has occurred in shales of Permo-Triassic to Quaternary age in the Viking Graben and Moray Firth areas of the North Sea, where the input of K^+ and Al^{3+} was again considered to be from the breakdown of detrital potassium feldspar. Boles & Frank (1979) suggested a slightly different reaction with the aluminium required for the reaction being concentrated in the illite/smectite by decomposition of the

Fig. 6.2. The idealised transformation of smectite into ordered I/S by the formation of thin illite particles. Taken from Sroden & Eberl (1984).

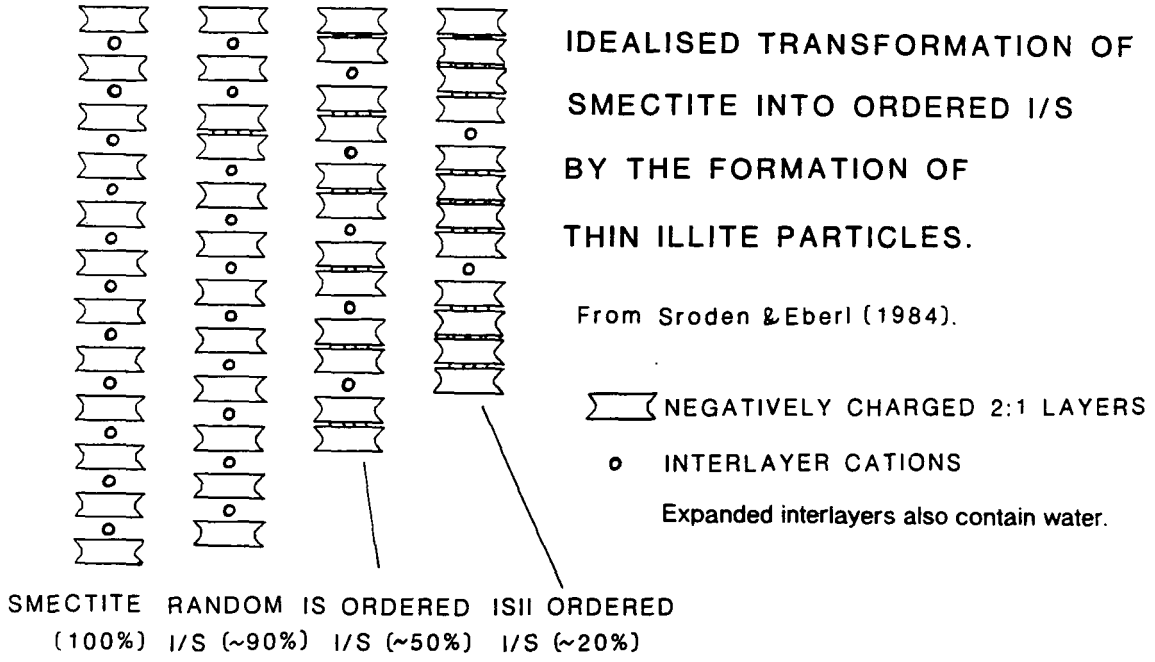

2:1 layer (i.e. some of the smectite is consumed during the conversion process), along with loss of silica and formation of a smaller number of illite layers than initial smectite layers. This reaction results in the concentration of the potassium already present, and so requires less potassium to be supplied by K-feldspar decomposition or other sources. The reaction is as follows:

K^+ + smectite = illite + chlorite + quartz + H^+ (Boles & Frank, 1979)

The mechanism of authigenic illite growth still has many controversial aspects, particularly with regard to how the original components of the smectite are accommodated within the structure of illite (see Freed & Peacor, 1992, for discussion). For further consideration of the chemistry of smectite, mixed-layer I/S and illite and the nature of the transformation from smectite to illite observed in sedimentary basins is given in reviews by Hower (1981), Sroden & Eberl, (1984), Weaver et al., 1984, Nadeau & Bain (1986) and Weaver (1989).

The loss of smectite and increase of illite with depth is not a reversible reaction, and so is not affected by later uplift. The transformation has been correlated with increasing temperature and differences in diagenetic grade (Heroux et al., 1979; Hoffman & Hower, 1986 and can be used to make a rough estimate of palaeotemperatures, and so to trace the thermal and burial histories of sedimentary basins (Hower et al., 1976; Monnier, 1979;

Smart & Clayton, 1985; Guthrie et al., 1986; Hoffman & Hower, 1986; Jennings and Thompson, 1986; Pollastro & Barker, 1986; Hagen & Surdam, 1989; Hillier & Clayton, 1989). When the percentage of illite in I/S (often referred to as expandability) is plotted against temperature for several basins, it can be seen that changes in the I/S composition occur at different temperatures in different basins (see Fig. 6.3), so that the transformation

Fig. 6.3. The percentage decrease in illite present in mixed-layer I/S versus temperature from various sedimentary basins. It can be seen from this figure that the expandability (the percentage of smectite within the mixed-layer I/S) is not solely a function of temperature. The other controls upon the reaction are discussed within the text (section 6.2). Figure re-drawn from Hoffman & Hower (1986; Sroden & Eberl (1984).

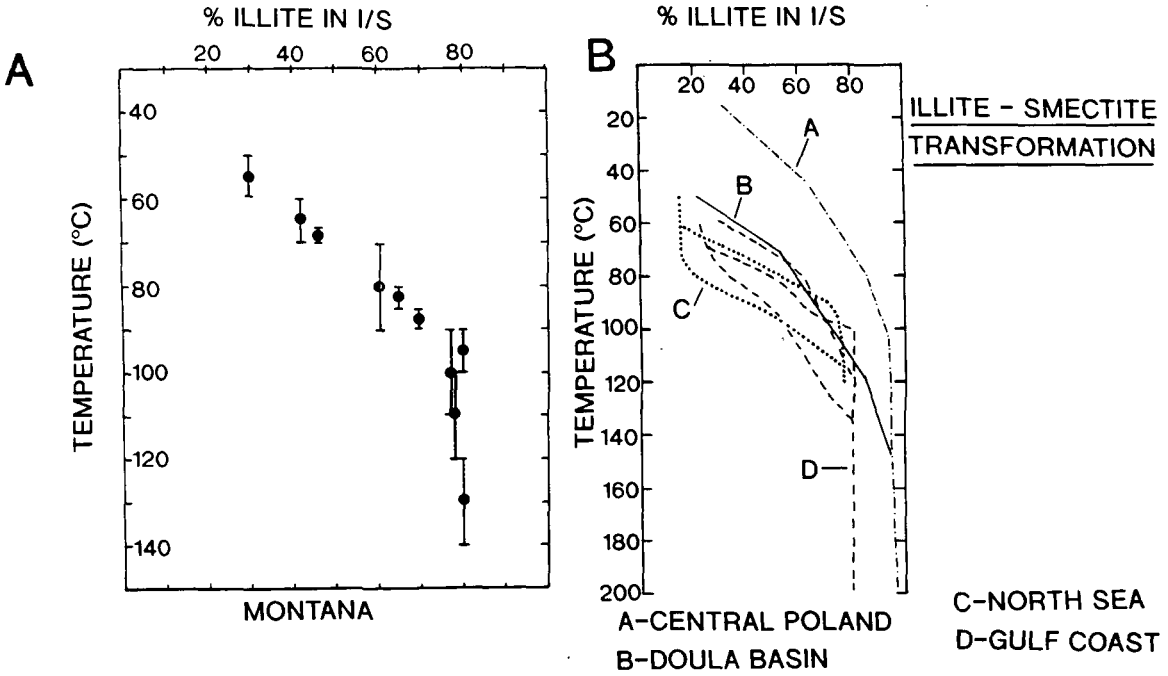

of smectite to illite via mixed-layer steps is not solely a function of temperature. This means the smectite to illite transformation is much less accurate than other currently available palaeogeothermometers, such as fluid inclusions, fission tracks and vitrinite reflectance, since the reaction is controlled by a number of factors other than just simply temperature (Hower, 1981; Sroden & Eberl, 1984). In fact, the precise nature of the reaction is still not fully understood (Sroden & Eberl, 1984; Nadeau & Bain, 1986; Elliot et al., 1991). In the Gulf Coast the smectite to illite transition occurs over a narrow range of temperatures in a given well but occurs over a wide range when several wells are considered (Freed & Peacor, 1989a). For the completion of the reaction, the temperatures ranged from 80 to 140°C, whilst temperatures for the onset of the reaction ranged from 60 to 90°C (see Freed & Peacor, 1989a; their fig. 3). Heling (1974) reported temperatures as

low as 72°C for the disappearance of smectite in the Tertiary of the Rhine Graben, whilst Dunoyer De Segonzac (1970) recorded temperatures as high as 140°C for the same reaction in the Cretaceous of Cameroon. Similarly, Smart & Clayton (1985) from the Carboniferous of the northern Pennines and Hillier & Clayton (1989) from the Devonian of the Orcadian basin have both described the relationship between vitrinite reflectance (see Chapter 7) and changes in the compositon of the I/S fraction. In both instances they found a good inverse relationship between increasing vitrinite reflectance and decreasing percentage of smectite within the I/S, but in each case the specific relationship was different for different localities in the area studied (e.g. between the Alston and Askrigg blocks). From changes in the I/S composition from seven wells in the Viking Graben and Moray Firth, Pearson & Small (1988) concluded that the change from random to ordered I/S occurs at a similar temperature (87°-100°C) and a similar level of vitrinite reflectance. Despite these limitations, the illite-smectite reaction can still be used as a tool in basin analysis and thermal modelling if it is used in a more qualitative manner and compared to other thermal indicators whenever possible (Guthrie et al., 1986; McCulloh & Naeser, 1989). Differences in the reaction rate and temperature of the growth of diagenetic illite and changes in vitrinite reflectance may make the former technique more applicable to regional studies because it is less likely to be affected by short-lived thermal perturbations such as small intrusions (Smart & Clayton, 1985). Thus in no instance should the transition of smectite to illite be used as an absolute geothermometer.

The transformation of smectite to illite is believed to be controlled by a number of factors including temperature, pressure, pore-fluid composition, variation in the rock/water ratio, bulk shale chemistry, original smectite composition and possible chemical heterogeneity of original smectite, porosity-permeability properties of the host rock, sources of potassium and reaction time (Hower, 1981). From the above list of factors the transition can be seen to be highly dependent on local geological factors. As well as these intrinsic factors there are also several external factors which may influence the appearance of certain minerals within a buried sequence, as pointed out by Jennings & Thompson (1986). They are the depositional environment, provenance of the sediments, tectonic setting and climate, which all exert an influence on the detrital mineralogy of the rocks before they are buried.

Pytte & Reynolds (1989) suggested that the reaction is kinetically controlled because of the strong correlation of I/S composition with temperature and time, with temperature the dominant control. This view is shared by Elliot et al. (1991), who concluded that temperature from burial is the most important control on 'illitization', although factors such as solution chemistry and variations in shale chemistry are important on a local scale. The sixth-order kinetic expression proposed by Elliot et al. (1991) would cause the reaction rate of the illitization process to slow down drastically for a given temperature as the composition approaches that of pure illite. In documented examples,

after reaching compositions of around 80% illite, the reaction does appear to slow down dramatically or even to stop (see Fig. 6.3). In Gulf Coast wells this phenomenon has been ascribed to the cessation of potassium availability (Perry & Hower, 1970; Weaver & Beck, 1971; Hower et al. 1976; Boles & Frank, 1979). The source of potassium is usually attributed to the breakdown of feldspars or the influx of potassium-charged fluids from an external source (Weaver & Beck, 1971). However, the supply of potassium from the breakdown of feldspars might not be such an important factor, since Freed & Peacor (1989b, 1992) suggested that the transformation was not limited by abundance of potassium feldspar. Potassium feldspar was found at all depths in a well through the Tertiary of Texas, indicating that the smectite-illite transition was not equivalent to complete loss of potassium feldspar and so perhaps the transition is not as dependent on the breakdown of feldspar as previously thought. Velde et al. (1986) came to a similar conclusion from the study of upper Cretaceous mudstones of the Niger delta area, where they suggested that increasing illite content within the I/S was due to the temperature of diagenesis and not the supply of potassium.

The uses of the transformation of smectite to illite via I/S is reviewed in Hower (1981) and Weaver (1989) and several recent case histories are given in a special edition of the Journal of Clay Minerals (edited by Morgan, 1989).

Illite crystallinity (Weaver, 1960; Kübler, 1964) is an empirical method of relating the change in shape of the 10 Å diffraction peak of illitic minerals to metamorphic grade, for which there are several ways to measure the crystallinity (Blenkinsop, 1988; Eberl and Velde, 1989: Weaver, 1989, p.449;). An increase in illite crystallinity reflects an increase in diagenetic/metamorphic grade. This technique is most useful for the recognition of low grade metamorphism and variation in grade in pelitic rocks at sub-greenschist facies level and has been applied particularly to anchizone (very low grade metamorphic) slates. For example, Weaver et al. (1984) used illite crystallinity to define different grades of, and changes in, the metamorphism for Palaeozoic slates of the southern Appalachians. As such, for reasons that will become clear later in this chapter and Chapters 7 and 8, this technique is more applicable to regions that have experienced late diagenesis to anchizone and epizone regional metamorphism (areas where burial temperatures of 250°C to 400°C have been reached and the effects of lateral deformation are clearly seen in such features as slaty cleavage) (Weaver, 1989). As discussed below some authors have used the illite crystallinity method in the Western Alps.

6.3 Previous clay mineral work in the western Alps.

There have been several previous studies of changes in clay mineralogy within sediments from the Western Alps, some of which are pioneer works in the field of clay

mineral diagenesis and low grade metamorphism. Frey (1970; 1974), Kübler (1979), Monnier (1979), Frey et al. (1980), Kisch, 1980: Aprahamian (1988) and Mosar (1988) have all used clay mineral changes and in particular the 'crystallinity indices' of illites. These studies are all from the Swiss Alps (the Bernesse and Glarus Alps) and from the Swiss Molasse basin, to the north and north-east of the study area. In a review paper Kübler et al. (1974) described the existence of low-grade metamorphic minerals (lawsonite, pumpellyite and prehnite) and illite crystallinity within Oligocene sediments in the Helvetic region of Switzerland and the border region with France (Haut-Giffre). The presence of these minerals in the volcaniclastic turbidites of the Taveyannaz sandstones was used to indicate anchizone metamorphism. However, illite crystallinity measurements from the Globigerina shales and the Diablerets beds (stratigraphically below) and shale beds intercalated with the sandstones, suggest that the anchizone has not been reached in this area (Frey et al., 1974: Kübler et al., 1974; Aprahamian, 1988). This is probably due to a lag in reaction time between the formation of such low grade metamorphic minerals and increases in illite crystallinity and also the relative importance of controlling factors such as porosity, porewater composition, CO_2 and H_2O activities, temperature and pressure controlling the formation of metamorphic minerals compared to the factors which control illite crystallinity. Sawatzki (1975), as part of an unpublished Ph.D thesis, studied the burial metamorphism of the Taveyannaz and Val d'Illiez sandstones within the Thônes syncline (which divides the Bornes and Aravis massifs). From the presence of certain clay minerals (such as corrensite) he suggested that these flysch units had experienced burial temperatures in the region of 100°C to 200°C. This temperature range is lower than the usually quoted value for the lower limit of anchizone metamorphism, which is usually thought to start at around 250°C (Stalder, 1979; Weaver, 1989), although Burkhard (1988) postulated that it may start at 200°C and Sroden & Eberl (1984) offered a value of 280°C as the boundary between diagenesis and anchimetamorphism.

The papers by Frey et al. (1974) and Aprahamian (1988) each present a map of the metamorphism within the Western Alps, based on illite crystallinity and mineral assemblages. Both maps show that anchizonal metamorphism has not affected the area studied, with the exception of the Haut-Giffre and Platé massifs. These maps are shown in Fig. 6.4. Aprahamian & Pairis (1981) detailed a reverse gradient in the very low grade metamorphism of the Arve valley section on the edge of the Platé massif (see Fig.6.5), and suggested that the cause of an inverted metamorphic grade of illite crystallinity was due to frictional heating along the thrust plane of the pre-Alpine thrust sheets. This area of inverted metamorphic gradient is shown as an "outlier" of anchizone metamorphism in Aprahamian's (1988) map.

Fig. 6.4. Low grade metamorphic zones in the Western Alps, based upon illite crystllinity and the presence/absence of zone minerals. Based on data from Frey et al. (1974) and Aprahamian (1988). This figure clearly shows the discrepancy in the positioning of the anchizone boundary between using zone minerals (as used by Frey et al., 1974) and illite crystallinity (as used principally by Aprahamian, 1988). Both Frey et al. (1974) and Aprahamian (1988) have the region of the Haut-Giffre massif in the anchizone. The section shown in Fig. 6.5 (Pointe du Derochoir) is shown in this figure as the small outlier of anchizone metamorphism (as defined by Aprahamian, 1988) just to the north of the Arve river.

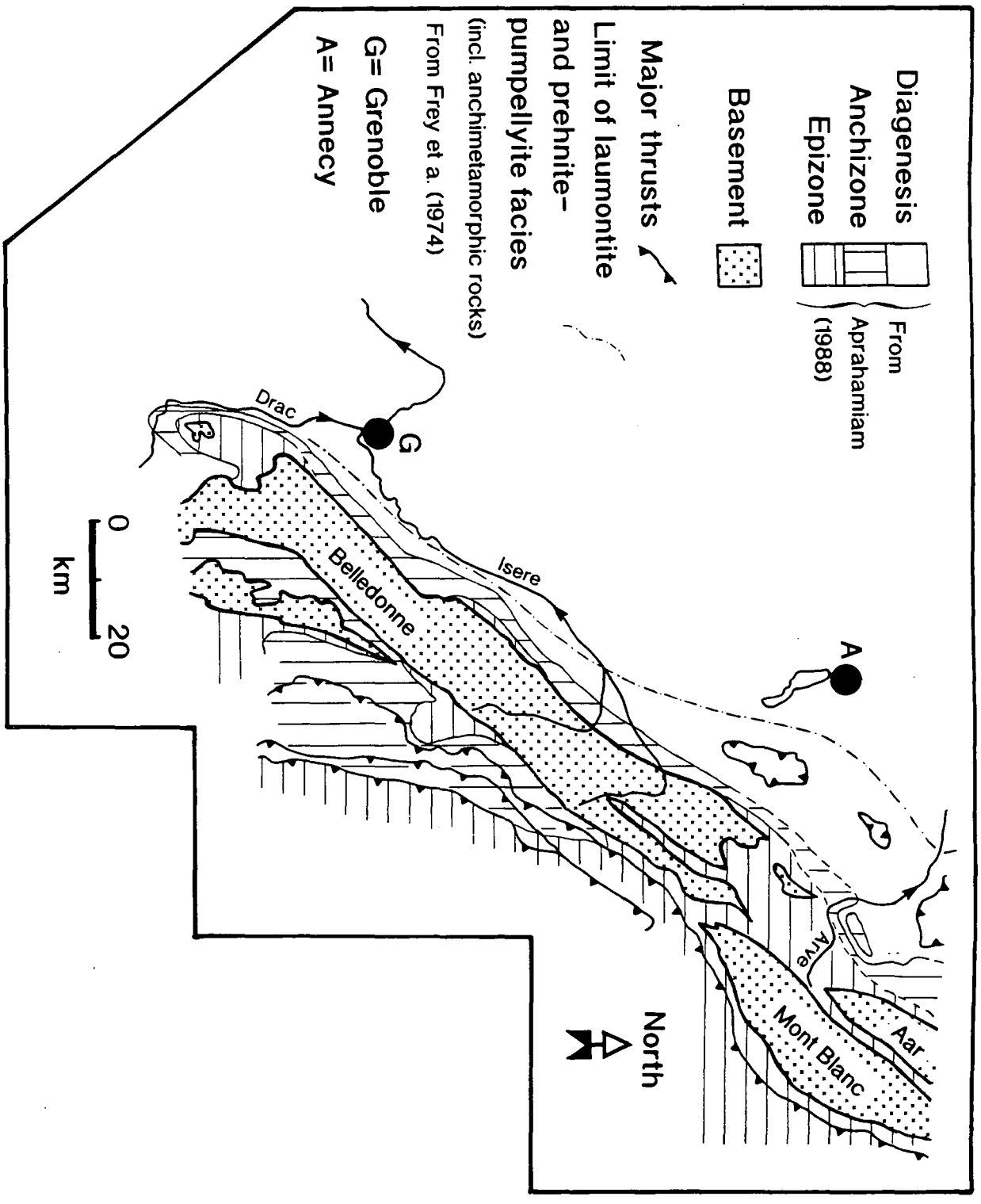

Fig. 6.5. Illite crystallinity plotted against altitude and the section for Pointe du Derochoir, located on the southern end of the Platé massif. The Hauterivian, Neocomian and upper Jurassic all have sub-anchizone crystallinities, whilst stratigraphically older Jurassic units and Urgonian, Gault and Tertiary units in relative proximity to the thrust plane of the Pre-alpine klippen have anchizone crystallinities. This apparent inverted metamorphic gradient was suggested by Aprahamian & Pairis (1981) to have formed as a result of the frictional heating along the base of the Pre-alpine nappes. This is discussed further in the text. Diagram from Aprahamian & Pairis (1981).

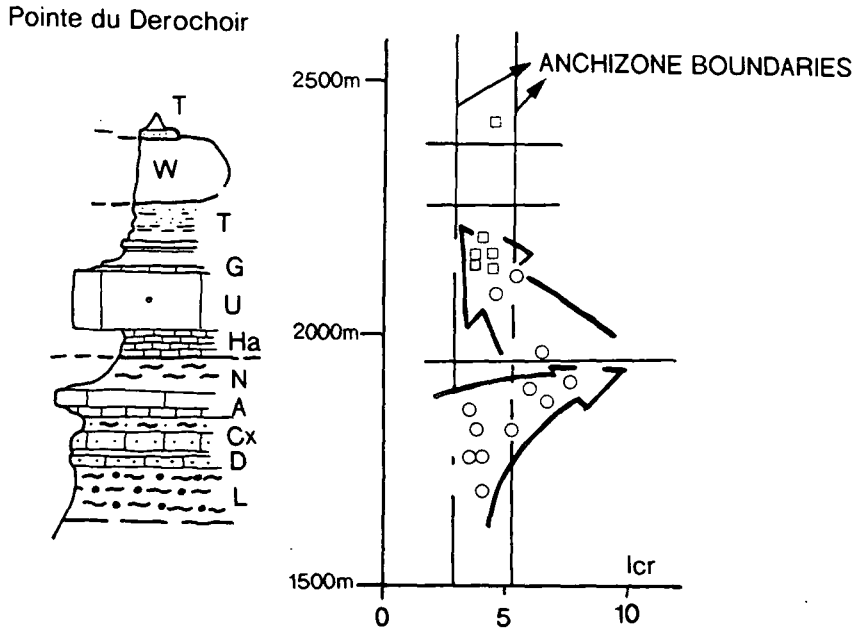

Levels of low-grade metamorphism have been demonstrated to change with structural position within a traverse across the Morcles nappe in central Switzerland (Goy-

Eggenberger & Kübler, 1990). Chaplet (1989), Deconinck (1984) and Deconinck & Debrabant (1985) determined the clay mineralogy of the upper Cretaceous and related the increase of illite and chlorite in samples from east of the Dent d'Arclusaz fault (eastern Bauges) to greater depth of burial of the upper Cretaceous. A decrease from west to east in the percentage of smectite within the I/S of the Oligocene and lower Miocene sediments of the Annecy molasse basin (Plateau des Bornes) has been documented by Schegg (1992a). Both Deconinck & Charollais (1986) and Mosar (1988) have studied the clay mineral diagenesis of the Pre-alpine klippen in France (Sulens klippen, see Figs 2.19 and 2.20a)) and Switzerland (Chablais and Romandes, see Fig. 2.21) respectively. Both show an west to east increase in the degree of diagensis/low grade metamorphism within their respective study areas.

Previous work carried out (using both clay mineral changes, illite crystallinity and vitrinite reflectance) in the Western Alps has predominantly concentrated on differences in the thermal history across strike of the regional structure instead of along strike, which is the major objective of this paper. To this purpose one unit was chosen to be studied regionally for any changes in the clay mineral composition. This was a lower Cretaceous mudstone, Hauterivian in age. For convenience, since no formation name has been designated, this will be referred to as the Hauterivian.

6.4 Regional differences in the clay mineralogy of the Hauterivian of the Subalpine Chains.

6.4.1. Analytical techniques.

All analysed samples were taken from fresh field exposures and were washed in distilled water before preparation. Preparation of samples for XRD analysis is described in Appendix 3. For all samples a whole rock sample was run prior to a run of the clay fraction in order to ascertain the percentage of clay minerals within the sample, as well as the bulk mineralogy of the sample. A few samples were analysed by X-ray fluoresecnce to determine the bulk chemistry of the Hauterivian. Preparation techniques and results are listed in Appendix 3.

6.4.2. Variation of detrital clay mineralogy in various sedimentary settings and the detrital clay composition of the Hauterivian.

The lower Cretaceous Hauterivian argillaceous lime mudstones of the Subalpine Chains were deposited in a basinal setting during a period of relative high sea-level. The Hauterivian sediments of the Subalpine Chains were deposited on a hemipelagic ramp bounding the shallower Jura-Bas Dauphine platform to the west and north-west (see Fig. 2 7a). The argillaceous lime mudstones of the Hauterivian typically contain sponge spicules,

Fig. 6.6a. Field shot of a typical exposure of the Hauterivian in the Subalpine massifs. Location: Guiers Mort Gorge, central Chartreuse. **Fig. 6.6b.** Decimetric bedded pack-/wacke- stone, from approximately1.5 metres below the top of the Hauterivian with *Toxaster* shells clearly visible. Location: Pas du Rocheplane, eastern Chartreuse.

A

B

silt-sized quartz and glauconite. These lime mudstones are interbedded with nodular wackestones ('calcaires à miches') (see Fig. 6.6a) and more calcareous centrimetric packstones with peloids and small foraminifera. Within the nodular limestones, irregular

echinoids are common at certain horizons, especially the genus *Toxaster* (Charollais et al., 1981; Arnaud-Vanneau et al., 1987; Arnaud-Vanneau & Arnaud, 1991) (see Fig. 6.6b).

Fig. 6.7. The partition of clay minerals and quartz on a idealised carbonate platform. Re-drawn from Arnaud-Vanneau et al. (1987). It can be seen that smectite is preferentially concentrated in basin and slope/ramp settings, whilst micas (synonomous with illite) and chlorite are concentrated in shallow water areas.

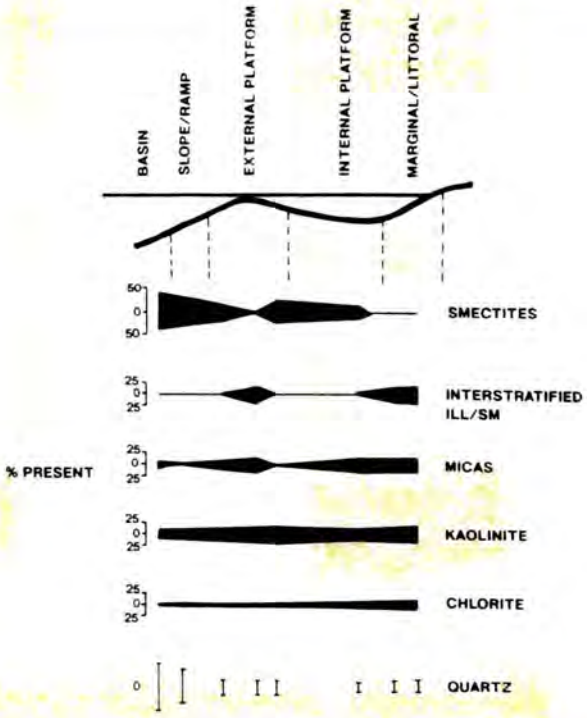

During the Hauterivian, the future area of the Subalpine chains was located to the south of the 30° North latitude line (Mintz, 1981; Dercourt et al., 1985; Barron, 1986; 1989). The area was tectonically stable and the climate in western Europe at the time is believed to have been humid (Deconinck, 1984; Deconinck et al., 1985; Ruffel & Batten, 1990). Shorelines during this period were located farther to the west and north (approaching the Paris basin, see Tyson & Funnel, 1987; their fig. 3), although some authors believe the sea did not extend so far and have placed the shoreline in the Jura. In the Chambotte section (located next to Lac du Bourget, north-west of Chambery), the Hauterivian is represented by two formations, the "Marnes Bleues d'Hauterive" (blue marls) and the overlying "Pierre Jaune de Neuchâtel" (bioclastic grainstone and packstones). Both are marine deposits (see Vieban, 1983; Zweidler, 1985; Arnaud-Vanneau et al. 1987, for further discussion). Under such conditions active peneplanation and pedogenesis would occur on land areas, producing smectite and kaolinite-rich soils and supplying a large amount of smectite to marine areas (Chamley & Deconinck, 1985). As a

result of the differential settling of different-sized clay floccules illite and kaolinite will be preferentially trapped on shallower platform areas (i.e. the Jura-Bas Dauphine and Provençe regions during the Hauterivian). Sedimentation in basinal areas of the Dauphinois region would be dominated by smectite (Darsac, 1983; Deconinck, 1984; Deconinck et al., 1985; Joseph et al., 1985). This effect is shown in Fig. 6.7.

Whole rock analysis of the Hauterivian mudstones (listed in full in Appendix 3) shows them to be lime mudstones with variable proportions of quartz and only minor amounts of clay (see Fig. 6.8). The quartz content in some instances is the dominant fraction

Fig. 6.8. The mean percentage of different constituents within the Hauterivian derived by whole rock X-ray diffraction analysis.

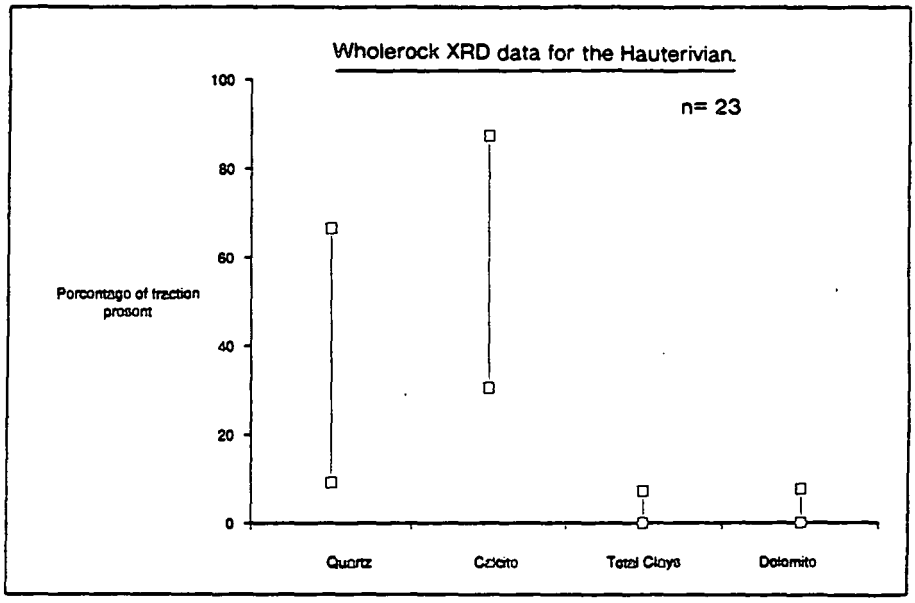

(up to 66%), although the calcite fraction is more commonly the major constituent. The percentage of total clay in the rocks studied is minor, with an average of 2.5 % (n=27). It should be pointed out here that the Hauterivian does not contain any detrital feldspar (or the amounts are below the detection limit of the XRD in Durham), which is the often quoted source of K^+ and Al_2O_3 required for the illitization reaction. X-ray fluorescence analysis was carried out on 12 whole rock samples of the Hauterivian from the Vercors, Chartreuse and Aravis to determine the variability (if any) of major elements and specifically the content of K^+ and Al_2O_3 within these mudstones. Fig. 6.9 shows the average weight percent of K_2O and Al_2O_3 within the Hauterivian compared to seven other mudrocks from around the world from which the illite to smectite transition has been described. It can be seen from this diagram that in the other mudrocks the average amount of K_2O and Al_2O_3 present is always over 3% and 13% respectively, whilst the Hauterivian

samples have an average of 0.66% and 3.8% respectively. Given the small percentage of clays within the Hauterivian and lack of any feldspar being detected on the XRD analysis

Fig. 6.9. The mean abundance of K_2O and Al_2O_3 for the Hauterivian compared to values for other shale units quoted in the literature: 1= Mesozoic, Disturbed belt, Montana; 2= Mesozoic, Sweetgrass Arch, Montana (both Hoffman & Hower, 1986); 3=Tertiary, Gulf Coast (Hower et al. 1976); 4= Tertiary, Gulf Coast (Perry & Hower, 1970); 5= Plio-Pleistocene, Colorado River (Jennings & Thompson, 1986); 6= Devonian, Moray Firth; 7= Devonian, Caithness, (both Hillier & Clayton, 1989) and 8= Hauterivian of the French Subalpine Chains (this study).

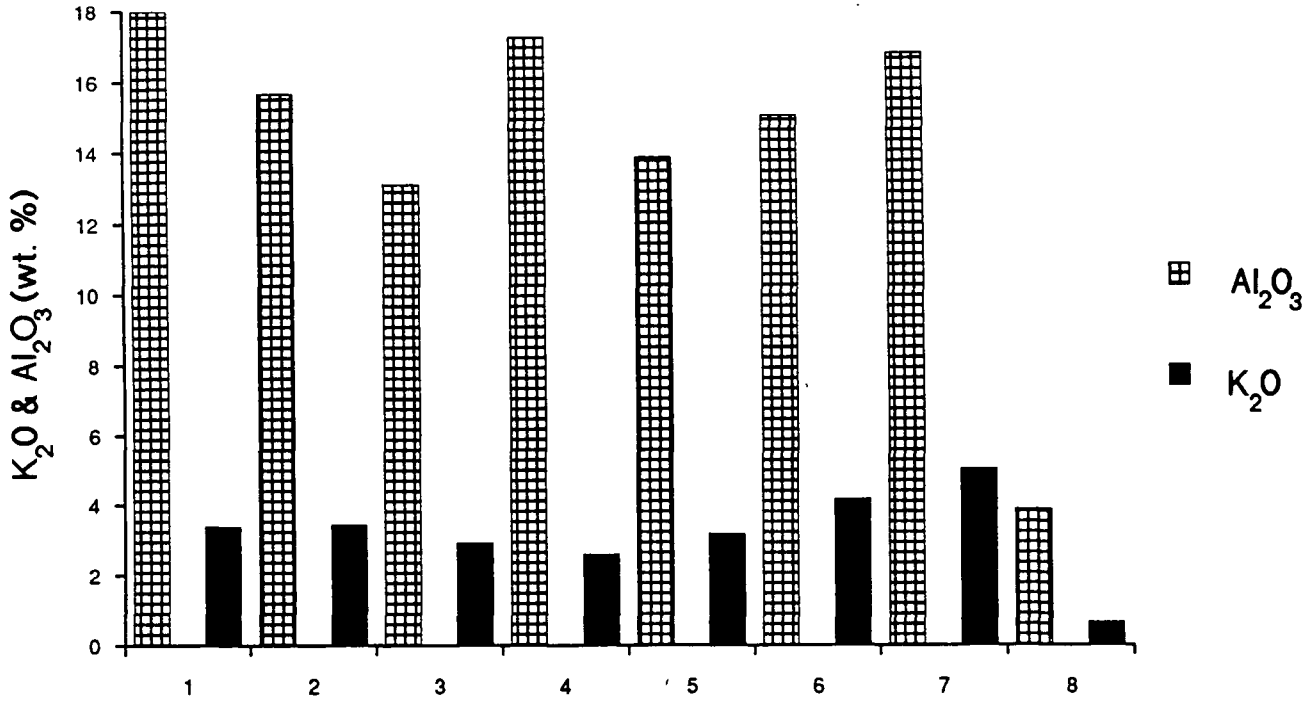

of bulk rock samples, these values are perhaps not surprising. However, this poses a major question as to the source of K^+ and Al^{3+} for the conversion of detrital smectite to illite. It may be nesessary to invoke an external source of K and Al from deep circulating fluids. This question will be addressed later in this chapter.

6.4.3. Composition, abundance and distribution of clay minerals within the clay fraction of the Hauterivian.

In the following section the nature of the clay assemblages will be described and then interpreted, firstly in the south-west part (Vercors, Chartreuse, southern Bauges massifs) of the study area and secondly in the north-east (northern Bauges, Bornes, Aravis,

Platé and Haut-Giffre massifs) part of the study area, (see Figs 2.1 and 2.17 to 2.21 for the location of these areas).

6.4.3 (a) The south-west part of the study area.

Figure 6.10 shows the nature of the Hauterivian clay mineral assemblages (<2 micron size fraction) in the south-west part of the study area. In both the Vercors and the Chartreuse massifs the assemblage is dominated by smectite, with the proportion of smectite ranging from 61% to 96% (average = 75%, n=16; not all the points are shown on Fig.6.10). The rest of the fraction is composed of illite (24% to 6%) and illite-smectite mixed-layer species (3.5% to 21%). One sample differs dramatically from this in being dominated by illite-smectite (78%) and minor illite (8%) and smectite (13%). This sample (#187/89) comes from l'Embossu on the extreme eastern edge of the Vercors massif, which is part of the Moucherotte thrust sheet (see Fig.2.17a). In the western part of the Bauges massif the Hauterivian clay fraction has a very similar clay fraction to that of the Chartreuse and the Vercors, but with slightly less smectite. In no sample from this area was chlorite present in the <2 micron size fraction (see Fig. 6.10). Fig. 6.11 shows a cross section through the Vercors massif with the clay mineral assemblages for the Hauterivian drawn on. From this diagram a progressive decrease in the smectite content can be seen from west to east, with the most easterly sample (#187/89) being dominated by mixed-layer I/S.

6.4.3 (b) The north-east of the study area (including Bauges massif).

Figure 6.12 shows the nature of Hauterivian clay mineral assemblages in the north-east part of the study area. In the Aravis, Platé, Haut-Giffre massifs, eastern parts of the Bornes and Bauges massifs, the <2 micron size fraction of the Hauterivian is dominated by illite (up to 75%; average 66%; n=7) and to some extent by chlorite (up to 21%; average 16%; n=7). Smectite and illite-smectite are also present within these samples but to a much lesser extent than in the south-west part of the Subalpine Chains (see 6.3.3a). In the western part of the Bauges massif the Hauterivian clay fraction has a very similar clay fraction to that of the Chartreuse and the Vercors, but with slightly less smectite (see 6.3.3a and Figs 6.10 & 6.11). In these two instances (both recorded in Deconinck, 1984) from the Bauges, smectite dominates, with lesser amounts of illite and mixed-layer illite-smectite and no chlorite. In the eastern part of the Bauges (i.e. to the east of the Arcalod fault) the Hauterivian is dominated by illite and contains roughly equal amounts of smectite, mixed-layer I/S and chlorite. A similar relationship for clay mineral assemblages of the upper Cretaceous (Sublithographic limestones) for the Bauges and southern part of the Aravis and Bornes massifs has been described by Deconinck & Debrabant (1985). Their fig. 10 is shown in Fig. 6.13. This figure shows that the upper Cretaceous from the west of the Arcalod fault is dominated by smectite with lesser amounts of illite, I/S and chlorite (only

Fig. 6.10. The distribution and nature of clay mineral assemblages in the south-west part of the chain (Vercors and Chartreuse massifs). See Figs 2.17a and 2.17b for the geology of the Vercors.

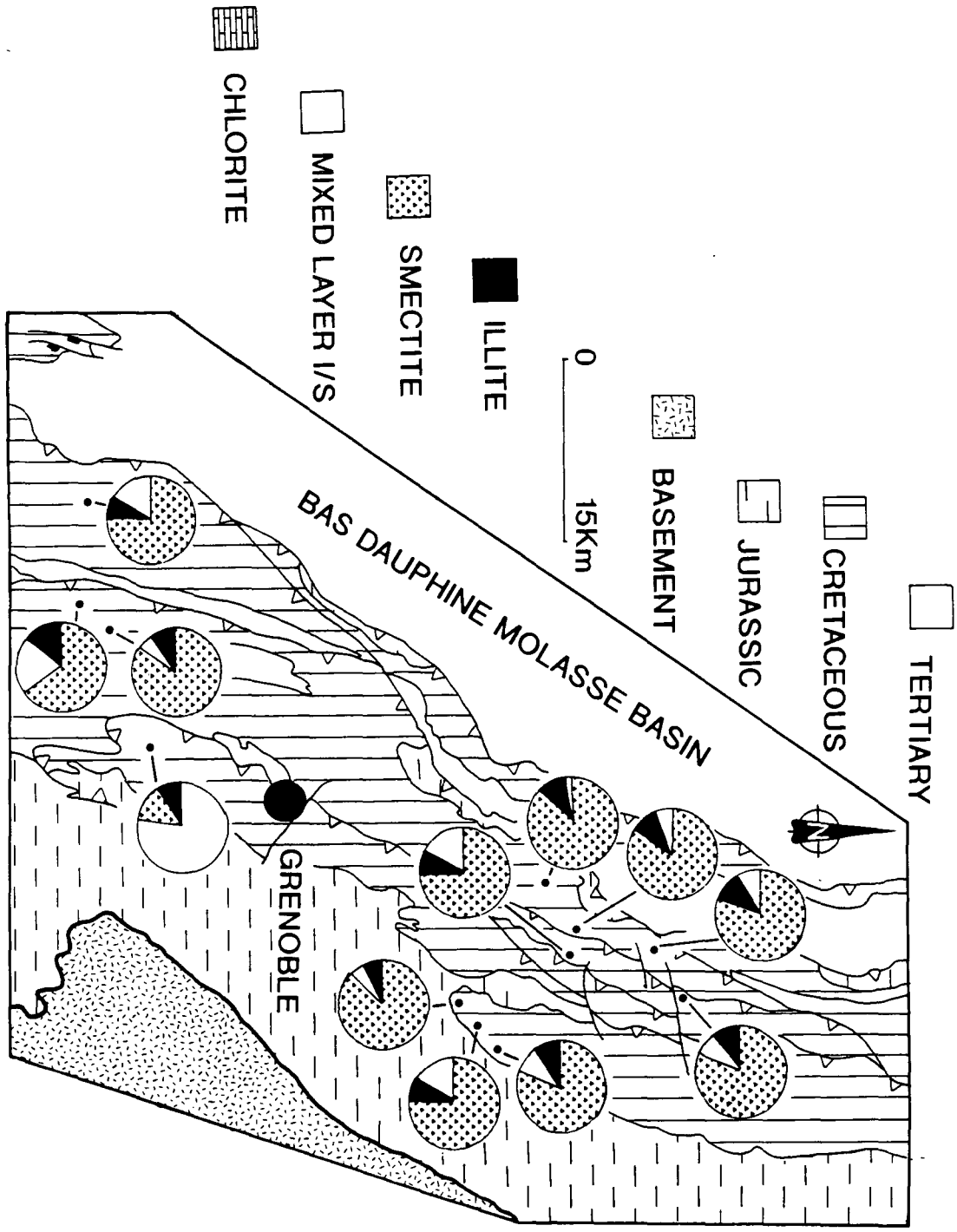

Fig. 6.11. East-west cross section through the Vercors massif, with the clay mineral assemblage for the Hauterivian drawn on. Section re-drawn from Butler et al. (1987). See Figs 2.17a and 2.17b for the geology of the Vercors.

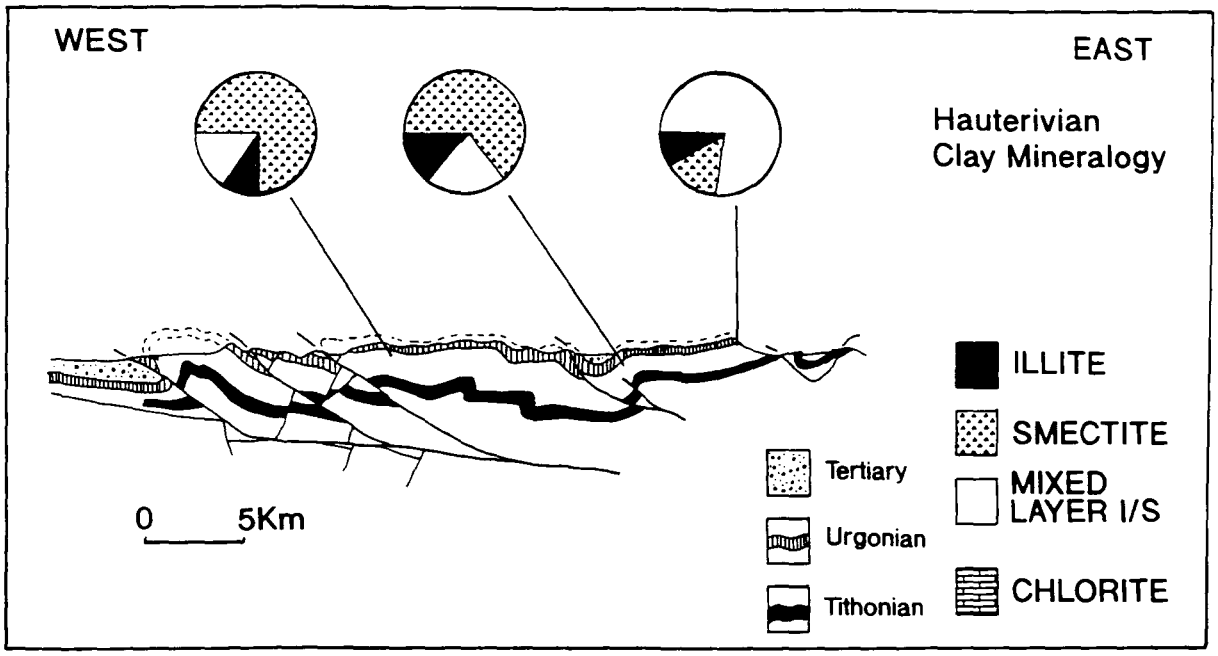

in two samples), whilst to the east of the Arcalod fault illite dominates the clay mineral assemblage with lesser amounts of I/S and chlorite but no smectite. In the western part of the Bornes massif (near Haut-Rumilly, see Fig.6.12) roughly equal amounts of illite and mixed-layer illite-smectite are present with lesser amounts of chlorite and smectite. Fig. 6.14 shows a cross section across the Bornes and Aravis massifs with the clay mineral assemblages of the Hauterivian drawn on. A west to east increase in the percentage of illite and decrease in the percentage of smectite can be clearly seen, along with an increase in the percentage of chlorite.

6.4.3 (c)Variation in the composition of the illite-smectite mixed-layer species within the clay fraction of the Hauterivian.

Fig. 6.15 shows a comparison of three XRD runs of the <2 micron size fraction of the Hauterivian from three different localities. In the Chartreuse, Vercors and western Bauges (west of the Arcalod fault), the mixed-layer I/S has a random ordering, indicative of less than 65% illite within the I/S. Further to the north and east in the Bornes and eastern Bauges (east of the Arcalod fault) the mixed-layer I/S in the <2 micron size fraction of the Hauterivian has an IIS 'allevardite' or short-range ordering (Wilson, 1987), typical of 65% to 80% illite within the I/S, whilst, in the Aravis, Platé and Haut-Giffre massifs the mixed-

Fig. 6.12. The distribution and nature of clay mineral assemblages in the Hauterivian in the north-east part of the chain (Bauges, Bornes, Aravis, Platé and Haut-Giffre massifs). See Figs 2.20a and 2.21ab for geology of the Bornes/Aravis, Platé and haut-Giffre.

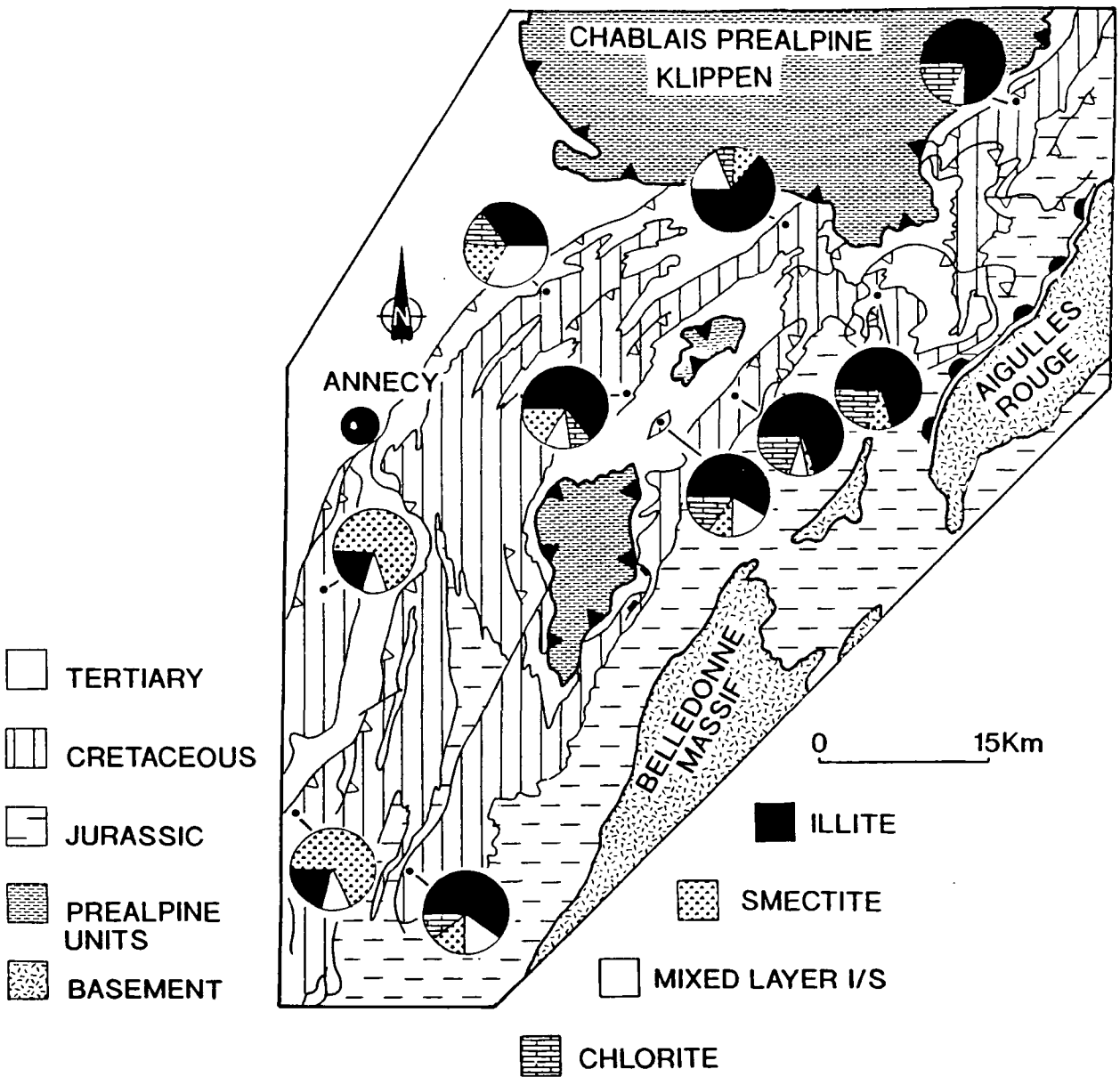

Fig. 6.13. Clay mineral assemblages of the upper Creatceous in the Bauges and southern Bornes and Aravis massifs. The clay mineral assemblages with a high smectite content (i.e. those to the west of the Arcalod fault) are detrital in origin, whereas those with a high illite and chlorite content, to the east of the Arcalod fault, are diagenetic in origin. One sample from west of the Arcalod fault also had a minor kaolinite content, not shown in the diagram. From Deconinck & Debrabant (1985).

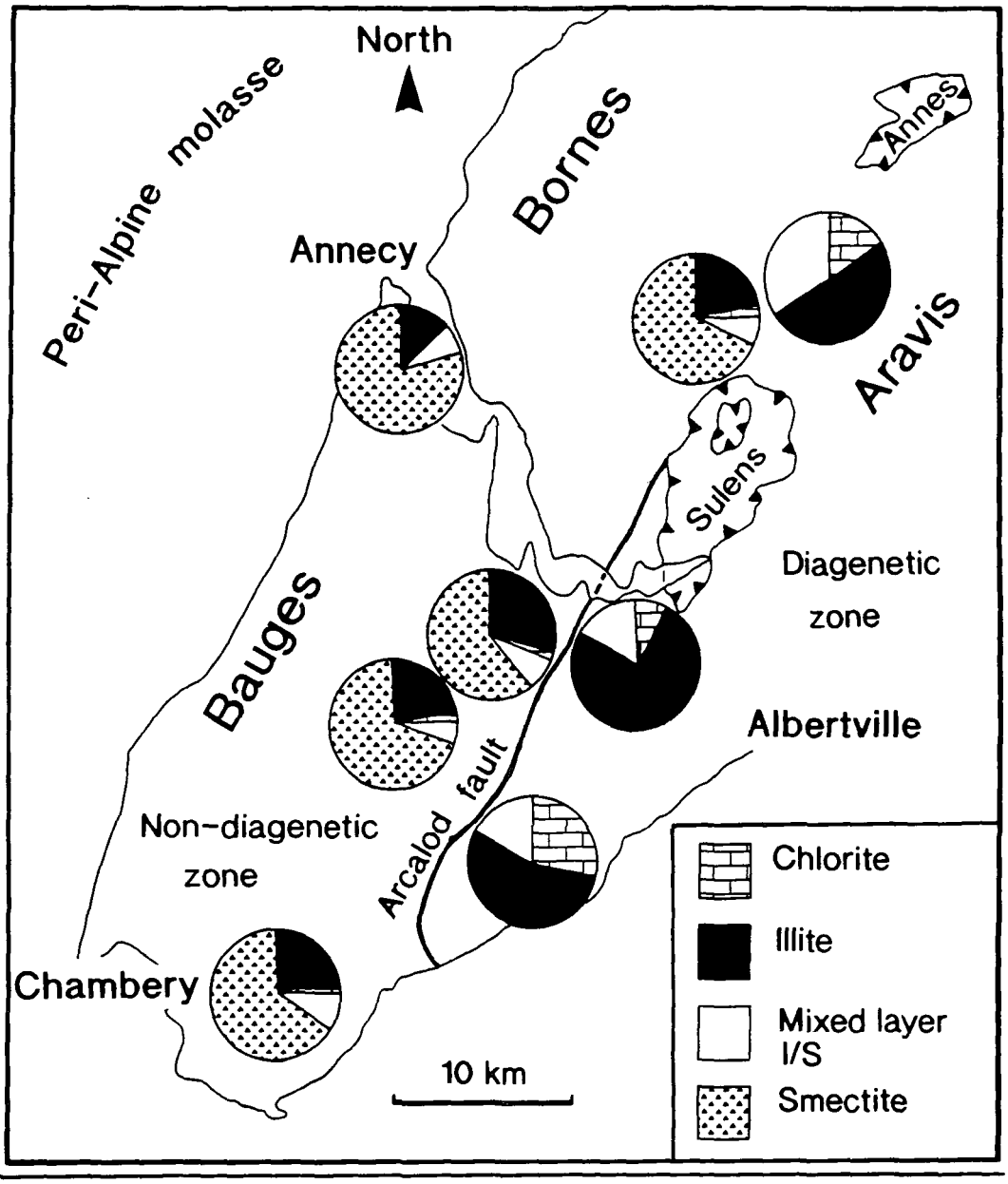

layer species within the <2 micron size fraction of the Hauterivian has an IIIS 'kalkberg' or long-range ordering with over 80% illite within the I/S.

Several authors have ascribed the changes in ordering (or illite percentage present in the I/S) to specific temperatures, usually derived from corrected bottom-hole temperatures from bore holes. An example from several basins is shown in Fig. 6.3. These should always be used with caution not only because of the improbability that the reaction within two

separate basins is similar but also because of the errors inherent in the calculation of bottom-hole temperatures.

Fig. 6.14. East-west cross section through the Bornes and Aravis massifs. Section re-drawn from Butler et al. (1987). See Figs 2.20a and 2.20b for geology of the Bornes/Aravis,

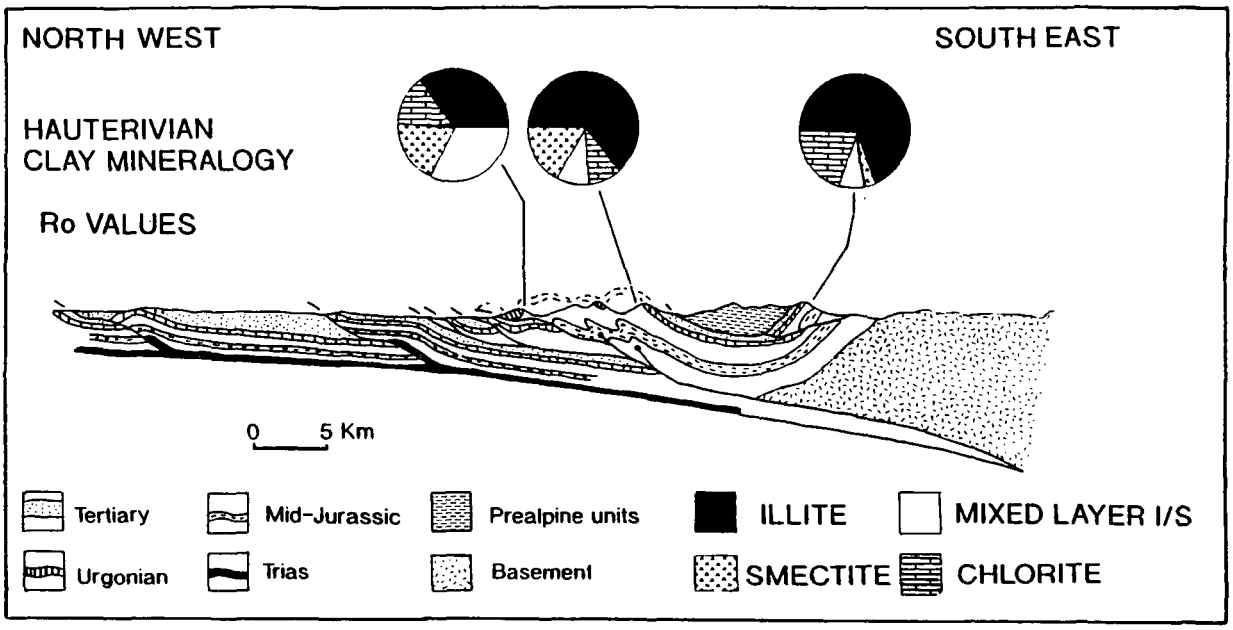

6.5 Implications for the burial history of the Subalpine Chains.

6.5.1 Interpretation of the clay mineral assemblages in the Hauterivian in the south-west part of the area.

The clay fraction of the Hauterivian and the composition of the mixed-layer I/S in the Vercors and Chartreuse (see Figs 6.10, 6.11, 6.12, 6.14 and 6.15) suggest that these two regions have not been subjected to deep burial (that is, burial to 3-5 km or more). The dominance of smectite, both of the overall clay fraction and as the dominant fraction in the mixed-layer I/S, suggests that this area has only been buried to shallow burial depths (which are discussed further in Chapter 8). The similarity of the Hauterivian clay fraction in the western part of the Bauges massif argues for a similar depth of burial, possibly slightly deeper (and therefore presumably hotter) to account for the decrease in smectite. The composition of the mixed-layer I/S, with less than 65% illite within the I/S, suggests that the Hauterivian in these areas has experienced temperatures less than 100°C, if the relationship between temperature and percentage illite in I/S obtained from other basins is

Fig. 6.15. X-ray diffractograms of the <2 micron clay size fraction showing the compositional changes seen in the Hauterivian from different areas of the Subalpine Chains. In the Vercors, Chartreuse and western Bauges the I/S has a random ordering. In the Bornes and eastern Bauges the I/S has an ISII 'allevardite' short range ordering, whilst in the Aravis, Platé and Haut-Giffre massifs the I/S in the Hauterivian has an ISIII 'kalkberg' long range ordering. I/S random= <65% illite; I/S Allevardite= 65-80% illite; I/S Kalkberg= >80% illite (Wilson, 1987)

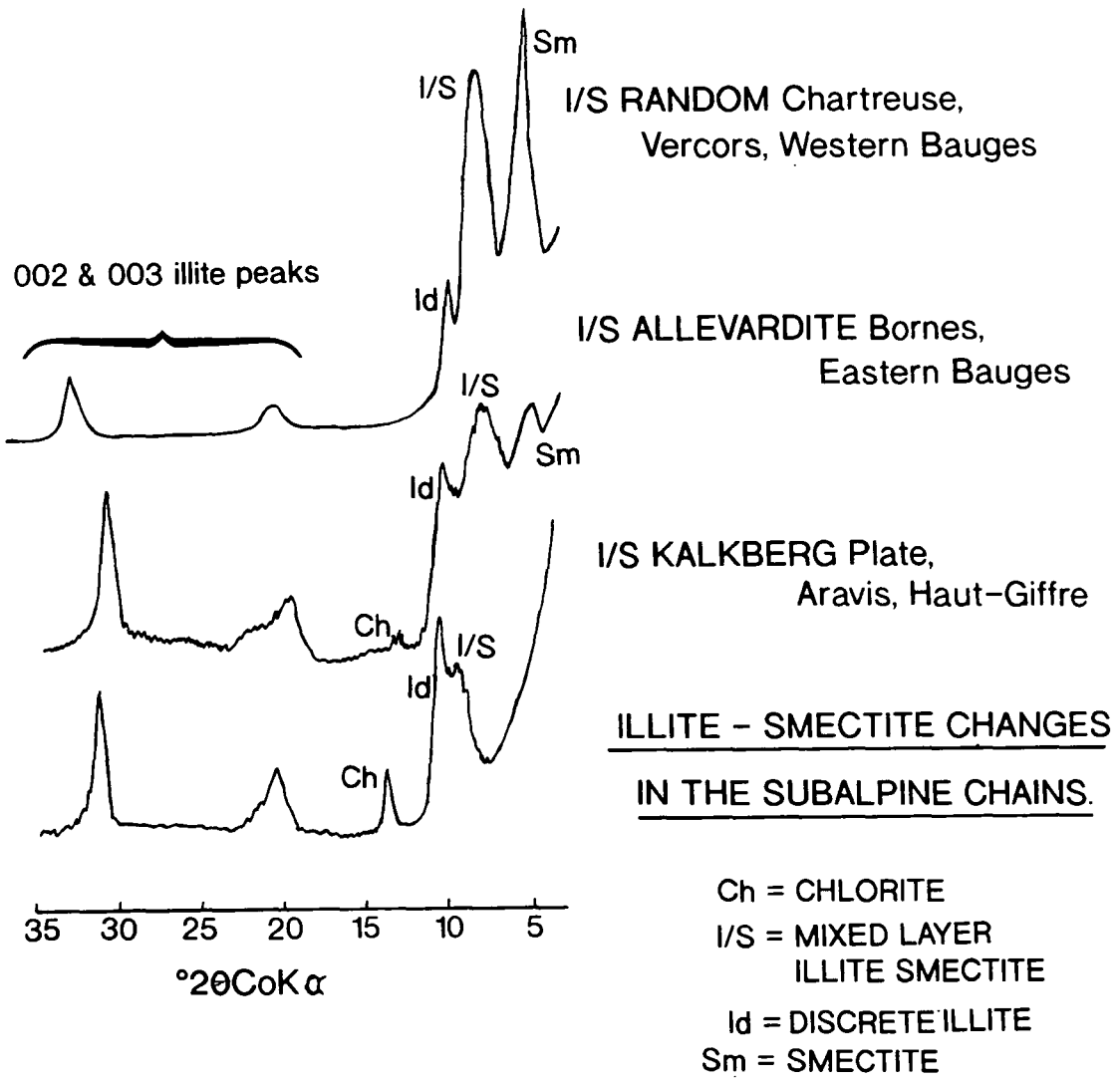

Orientated, ethyl glycol saturated slides of the less than 2 micron clay size fraction.

used (see Fig. 6.3). However, these at best can only be a very approximate estimate of temperature, since it is very unlikely that the controls upon the reaction in the Subalpine Chains are very different from the controls on the reaction in the basins shown in Fig. 6.3 (see section 6.2). Estimates of the burial temperatures to which these rocks have been exposed are discussed again in Chapter 7 and again in more detail in Chapter 8.

6.5.2 Interpretation of the clay mineral assemblages in the Hauterivian in the north-east part of the area.

The dominance of illite and the appearance of chlorite in the clay mineral assemblages of the Aravis, Platé and Haut-Giffre (see Figs 6.12, 6.14 and 6.15) massifs indicate that these areas have been more deeply buried than the areas described above (section 6.4.1.) and have experienced greater burial temperatures. Comparison with other sedimentary basins and the temperature range of the illite-smectite transformation (Fig.6.3) suggest that the kalkberg ordering seen in the I/S in the Hauterivian in these areas is due to temperatures over 100°C. In the Bornes and the eastern part of the Bauges the allevardite ordering and the lesser amount of illite suggest that the Hauterivian in these areas has been buried to shallower depths than the Aravis, Platé and Haut-Giffre. The possible temperature range estimated from the percent of illite in I/S (Fig.6.3) for these rocks is 80°C to 130°C. According to McDowell & Elders (1980) in the Holocene of the Salton Sea geothermal field, chlorite appears at temperatures of 190°C, whilst in the Cambrian Conasauga shale of the Appalachians chlorite appears at 240°C (Weaver et al., 1984). This is an illustration of the fact that such clay mineral growths are governed by a multiplicity of factors. In the Salton Sea example, the role of hot fluids, particularly as an ion transport mechanism, would seem to be main reason why the same mineral changes seen in the Conasauga shale, occur at consistently lower temperatures (50-70°C). It also indicates that time may not be so important, since the Salton Sea shales and sandstones are only Holocene in age. Estimates of the burial temperatures to which these rocks have been exposed are discussed again in Chapter 7 and in more detail in Chapter 8.

6.5.3 An alternative explanation.

An alternative to a burial temperataure control is that the clay mineral assemblages of the Hauterivian have not been affected at all by diagenetic changes but that the differences described above (see Figs 6.10, 6.11, 6.12, 6.14 and 6.15) are due to original differences in the detrital clay mineralogy. However, if this were true the clay mineral assemblages on the western side of the Subalpine Chains (the more landward side during the Hauterivian) should contain more illite and chlorite (and possibly kaolinite) than those to the east (see palaeogeographic description of the area in sections 2.3.1 and 2.4.1). A detrital origin for the regional differences in the clay mineral assemblage also does not explain the changes in the composition in the mixed-layer I/S species within the clay

fraction (shown in Fig. 6.15). Data presented in the following chapter on vitrinite reflectance and in the thermal modelling section of Chapter 8 agree with the regional differences in burial depth revealed by the clay mineral changes and indicate that certainly the north-east part of the chain has reached burial temperatures at which the smectite to illite transformation is known to occur in other basins (Sroden & Eberl, 1984). However, given the size of the area studied, it is possible that there were some differences in the original clay assemblage composition of the Hauterivian. These, however; have now been masked by subsequent Alpine-induced deeper burial.

6.6 The role of potassium and aluminium in the diagenesis of smectite and the growth of illite: some problems posed by the chemical composition of the Hauterivian and regional changes in the clay mineral assemblages of the Hauterivian.

K^+ and Al^{3+} are required for the transformation of smectite to illite as mentioned in section 6.2. However, as mentioned in section 6.3.2 the Hauterivian does not contain any detectable detrital feldspar and the weight percentages of K^+ and Al^{3+} are much lower than in mudrocks from other basins from which the illite-smectite transformation has been described. Since the reaction has been demonstrated to have occurred in the Hauterivian of the Subalpine Chains (described in above sections and also in sediments of other ages in Deconinck, 1984 and Deconinck & Debrabant, 1985), several major questions arise: is the breakdown of detrital feldspar as important to the reaction as has been previously described? (both Velde et al., 1986 and Freed & Peacor, 1989b; 1992; have also suggested this). Is it not possible for the K^+ and Al^{3+} to be solely sourced from the original detrital smectite? Or to what degree is the import of K+ from deeper sources nescessary (as suggested in Weaver & Beck, 1971 and Hanor et al., 1988). In such an environment with little K^+ and Al^{3+}, to what degree is the time required for the reaction increased?

6.7 Comparison with other studies in the Western Alps.

Previous studies of clay mineralogy changes in the Western Alps have tended to concentrate on illite crystallinity measurements, particularly in the central part of Swiss Helvetics (Frey, 1970; Kübler et al., 1974; Kisch, 1980; Burkhard, 1988; Goy-Eggenberger & Kübler, 1990). The clay mineralogy of the south-west part of the area has not been described before in terms of possible diagenetic changes. Some of the previous studies have extended into the Haut-Giffre, Platé and Aravis massifs. Several studies mentioned in section 6.2 suggest that the Tertiary strata of the aforementioned areas have reached the anchizone, which would seem to contradict the evidence presented here for the level of diagenesis in the Hauterivian, which at least in the Aravis and Platé massifs has not reached

the anchizone. This conclusion is supported by Aprahamian & Pairis (1981). In their figure 2 (see Fig. 6.6) they show the Hauterivian to have an illite crystallinity below (i.e. not to have reached) the anchizone boundary. This suggests that there is marked lithological control on the reaction rate of the smectite-illite transformation and the growth of certain minerals between the andesitic volcaniclastics of the Tertiary and the underlying Mesozoic. As already mentioned in section 6.3, Kübler (1974) and Frey et al. (1974) pointed out the discrepancy between the degree of diagenesis/low grade metamorphism indicated by the presence of certain zone minerals in the Taveyannaz sandstones and the degree of diagenesis indicated by the illite crystallinity from horizons stratigraphically below. The presence of laumonite and corrensite in the Tertiary volcaniclastics of the Thônes syncline suggests temperatures of 100-200°C for the Tertiary according to Sawatzki (1975), ans would agree with the deeper Hauterivian having experienced temperatures over 100°C in the north east of the area. However, since the formation of these zone minerals is probably controlled by different factors from clay mineral changes (see section 6.3) then Sawatzki's data can only be used with caution.

The maps of low grade metamorphic zones in the Western Alps (see Fig. 6.4) suggest that anchizone metamorphism is restricted to the Haut-Giffre and the area farther to the north and east in Switzerland. Kübler et al. (1979), on the basis of 200 vitrinite reflectances, presence of certain minerals and changes in illite crystallinity from the Jura, the Molasse basin (both western Switzerland) and Bornes, Aravis and Platé massifs, also suggested that these areas have not reached the anchizone. They are considered to be in their zones 3 and 4 and correspond to vitrinite reflectances of 0.6 to 2.6%, whereas they suggested that the Haut-Giffre had reached the anchizone. Schegg (1992a) used illite crystallinity to show that the Oligocene and lower Miocene of the Annecy molasse basin had not experienced anchizone conditions. However, the illite content of these sediments does increase toward the east (and the Subalpine Chains) and matches the trends shown for the Hauterivian for the same area (see Fig. 6.14).

The data presented by Deconinck (1984) and Deconinck & Debrabant (1985) for the upper Cretaceous and Hauterivian of the northern Bauges and the southern Aravis agree with the data presented in this chapter. The thermal history of the Subalpine Chains is discussed in greater detail in Chapter 8.

6.8 Conclusions.

The transformation of smectite to illite and chlorite via mixed I/S steps and changes in the composition of the I/S have been investigated using one mudstone unit from the study area, the lower Cretaceous Hauterivian. The results of this study suggest that the south-west area of the Subalpine Chains has only experienced limited burial and has

therefore not been exposed to high burial temperatures. In contrast, in the north-east part of the study area the dominance of illite and chlorite in the clay mineral assemblages and the illitic composition of the mixed-layer I/S indicate that these rocks have experienced relatively deep burial and temperatures, although anchizonal metamorphism is only restricted to the extreme north-east of the study area (the Haut-Giffre massif).

Chapter 7 Levels of organic maturity within the Subalpine Chains.

7.1 Introduction.

Levels of organic maturity of Mesozoic and Tertiary strata have been established using vitrinite reflectance (Ro) and spore fluorescence. In the southwestern part of the chain, values of Ro for the Mesozoic units from the Vercors and Chartreuse massifs are generally low, with all Cretaceous units having values of less than 0.5% Ro. Older Jurassic horizons have higher values, up to 1.25% for the mid-Jurassic (Oxfordian). When compared to values from the same horizons and from younger Tertiary units (published data and new values) from the north-eastern part of the chain, it is clear that this part of the belt has encountered higher temperatures, produced by greater depth of burial. In the Haut-Giffre and Aravis massifs Mesozoic units have Ro values as high as 2.7% and, in terms of hydrocarbon generation, can be considered overmature.

The causes of greater depth of burial of the north-eastern part of the belt are discussed briefly at the end of this chapter and more fully at the end of Chapter 8.

7.2 Background to studies of organic maturation and the use of such studies in basin analysis.

Vitrinite reflectance (hereafter referred to as Ro) and spore fluorescence are techniques which have been in use for several years as a means of estimating palaeotemperatures and geothermal gradients (Barker & Pawlewicz, 1986; Tissot et al., 1987). Both are optical techniques for assessing the thermal maturity of sedimentary organic material. The reflectance of vitrinite macerals is probably the most widely used method of quantifying organic diagenesis. It provides a scale against which other diagenetic indicators can be compared and can be directly related to hydrocarbon maturation. For example 0.5% Ro and 1.3% Ro are the usually quoted values for the start and end of oil generation respectively (Hood et al., 1975; Teichmüller, 1987). The term "vitrinite reflectance" refers to the amount of light of a certain wavelength reflected from a polished surface of vitrinite. The measurement is compared to a standard of known reflectance. The sample is viewed and reflection measurements made, under oil immersion, employing an oil with a known refractive index (R.I.). (The wavelength of the light and the refractive index of the oil are given in Appendix 4, along with a full description of the analytical technique). With increasing levels of diagenesis of organic matter, Ro increases from a minimum of around 0.15-0.2% to greater than 5.5% at a level equivalent to the lower greenschist metamorphic facies. Vitrinite, a type 3 kerogen[1], and common coal maceral, is derived from cellulose, lignin and tannins (see Stach et al., 1982 for further

[1] Footnote: kerogen is the part of organic matter which is insoluble in the usual organic solvents; the definition is in practice extended to all solid fossil organic matter (Robert, 1988).

discussion). It is most often an abundant constituent of the organic fraction of sedimentary rocks (the organic fraction is usually under 1% of the rock), particularly those of a continental origin. The Ro method offers several advantages as a measure of organic diagenesis:

1) it is a broadly accepted and standardized method;
2) vitrinite, like most organic material, is sensitive to minor changes in the level of burial temperature and matures in a regular manner;
3) vitrinite is a common constituent of the organic fraction of many sedimentary rocks;
4) the method is applicable throughout the entire range of diagenesis up to lower greenschist metamorphic facies, although it becomes more sensitive at higher maturities;
5) since it is a microscopic method, measurements are always made on the same physical components (dependant on the skill of the operator).

As with all analytical techniques, the method has a few limitations:

1) reworked vitrinite may be present leading to spurious results;
2) vitrinite may be difficult to discriminate from other macerals (such as inertinite);
3) oxidised vitrinite has a different reflectance from that which is unoxidised.
4) since the vitrinite measured is at the discretion of the observer, the measurements are subjective;
5) at low maturities readings of Ro are prone to scatter;
6) the level of Ro readings within a sample can be reduced if the rock is impregated with liquid hydrocarbons (Price & Barker, 1985),
7) different laboratories may attain different levels of Ro for the same sample.

The blue light fluorescent colour (shortened to simply 'fluorescent' or 'fluorescence' in this thesis) of liptinite (and exinite, types 1 and 2 kerogen, see Stach et al., 1982 and Robert, 1988 for further discussion of the coal maceral groups) can similarly be used to show maturity. This method is based on the premise that the liptinitic component of organic matter, derived from algae, spores, pollen, resin and cutin, autofluoresces when irradiated by fluorescent (UV) and low wavelength visible light. The intensity and fluorescent colours of liptinite vary both with type of liptinite and the level of diagenesis. The colours will vary between spores, cuticle, resin and algae. For example, a rock with light orange fluorescing spores will have yellow/orange fluorescing algae at the same level of maturity. The changes in fluorescence of spores when viewed under fluorescent light are similar to those seen under low wavelength white light. The colours can also be determined visually or by use of an arbitary numerical scale and standardized by comparison to reference samples. One such scale in wide use is the 'thermal alteration index' (TAI) scale (Barnes et al., 1984). Marshall (1991) has recently described a technique using the CEI (Commission Internationale de l'Eclairage) colour system which allows a quantification of the colour changes in spores when under white light. This approach is flawed, however,

because the maturity of the rocks has to be known beforehand to know exactly where the rocks studied should lie on the graphs he produced (see his fig. 9, which shows that samples with the same Ro can plot in a variety of positions upon the cusp-shaped curve produced). Under fluorescent light with increasing levels of diagenesis the fluorescent intensity decreases and there is a shift in colour from lower to higher wavelengths (Teichmüller & Durand, 1983). Compared to Ro changes, fluorescence of liptinite materials is somewhat irregular, with rapid shifts in the fluorescence occurring at between 0.35 to 0.5% and 0.8 to 0.9% Ro (Teichmüller & Durand, 1983). Above levels of diagenesis equivalent to a Ro of about 1.0% the intensity of fluorescence is so low that it cannot be measured. The observation of colour changes in organic matter under fluorescent light is less precise, since it depends upon the judgement of the observer. The changes in the fluorescent colours of spores are as follows:

Fluorescent colour	**Maturity**	**Equivalent Ro value (approx.)**
Green	immature	<0.2 %
Yellow	immature	0.2% to 0.35
Orange/Yellow	sub-mature/mature	0.35% to 0.5%
Orange/Red	mature	0.5% to 0.9%
Brown/Black	mature/overmature	over 0.9%

It should be noted that the colours given above are not fixed but depend on the excitation wavelength used and the value of the barrier filter used. The colours given above are the most appropiate for the conditions used (see Appendix 4) (J.M. Jones, pers. comm., 1992). Similar scales are given in Murchison et al. (1985) and Marshall (1990).

Figure 7.1 shows the relationship between changes in vitrinite reflectance and spore fluorescence in relation to the zones of hydrocarbon generation and destruction, whilst Fig. 7.2 (taken from Robert, 1988) pictorially shows the fluorescent rank-related alteration of the algae Tasmanites and the relationship of the colour changes to Ro and the generation of oil (note that in Fig. 7.2 P. Robert has used different conditions (i.e. wavelength of light anf barrier filters) from those used in this thesis). The use of Ro and spore fluorescence in basin analysis and thermal modelling is reviewed in Bustin et al. (1985), Teichmüller (1987), Robert (1988) and Barker (1989).

Ro values are principally governed by the geothermal gradient and the length of exposure time to maximum burial temperatures experienced by the rocks in question. The nature of the geothermal gradient encompasses other variables such as thermal conductivity of each horizon, heat flow within the area and the burial depth which governs the position on the geotherm of each horizon. Differences in the hydrocarbon content of the total organic fraction and variations in the kinetic properties of the macerals involved are also important and should be considered. Various models for the increases in Ro with temperature and/or time have been published and can be used to obtain a value for the

Fig. 7.1. Correlation between the stages of hydrocarbon generation and destruction, and values of vitrinite reflectance (Ro %) and spore fluorescence under fluorescent light. After Tissot & Welte, (1984); Murchison et al. (1985); Teichmüller (1987) and Marshall (1990).

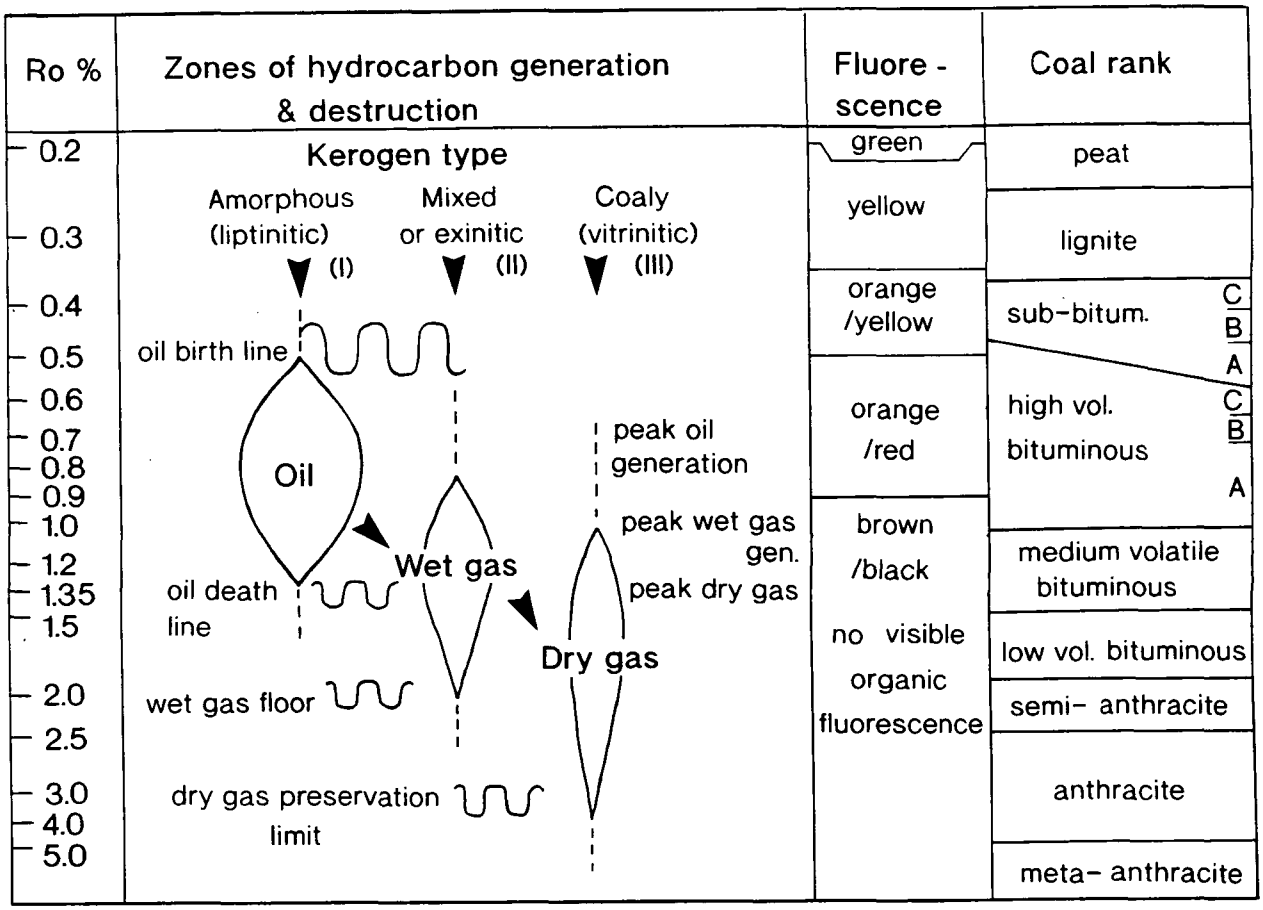

temperature to which a series of rocks has been exposed. Published models vary greatly in their level of sophistication, partly because of the uncertainties concerning the importance of time in the maturation of vitrinite macerals and activation energies of different macerals. Consequently a number of different nomograms of Ro versus temperature and time have been presented and some have taken kinetic considerations into account too. Price (1983) and Barker & Pawlewicz (1986) suggested that full thermal maturation oforganic matter is controlled principally by maximum temperature, with time showing little or no influence. Following their ideas the Ro method is therefore essentially an absolute palaeogeothermometer. It was thought that full maturation is achieved after only an exposure time to maximum burial temperatures of about 10000 years. In a recent review Barker (1989) stated that there is evidence that only 10^6 to 10^7 years are required for kerogen to stabilise during thermal maturation via burial diagenesis. For geothermal

Fig. 7.2. Changes in the fluorescent colour of the alga *Tasmanites* and relationship of these changes to vitrinite reflectance and oil generation (Genèse de l'huile). Diagram from Robert (1988). N.B. The excitation wavelength and the barrier filter used in this study are different from those used by the current author, hence the discrepancy between the colours seen in this plate and the fluorescent colours reported for spores in this thesis.

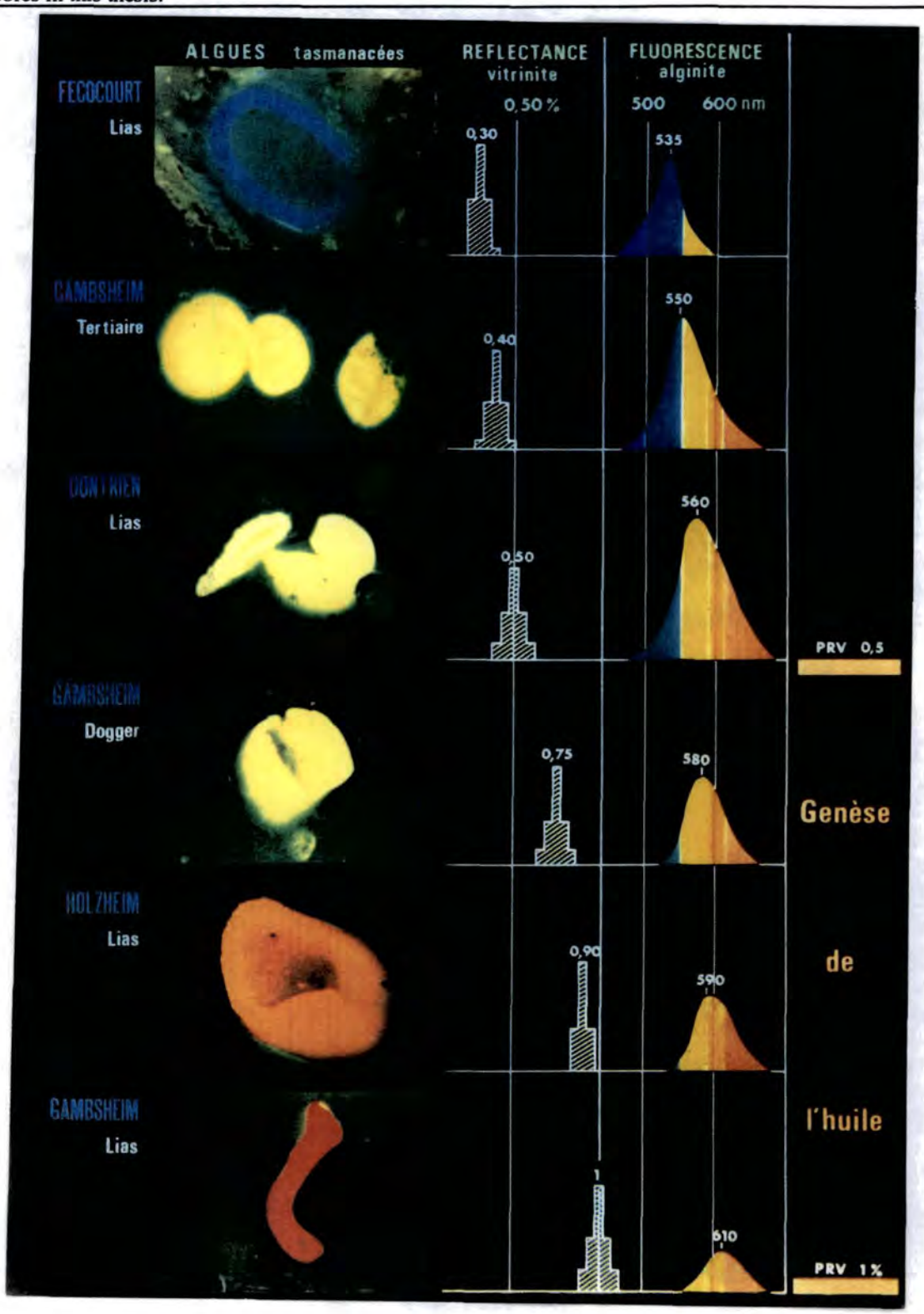

systems and contact metamorphism organic matter stabilizes over a shorter time span of 10^4 and 10^{-1} to 10^0 years respectively. Barker concluded that models of organic maturation which consider both temperature and time or just temperature alone will predict palaeotemperatures with the same precision. Burnham & Sweeney (1989) and Sweeney & Burnham (1990) have published the most recent model of vitrinite maturation; their equation integrates chemical kinetic equations for activation energies of vitrinite over time and temperature. Their nomogram of Ro versus exposure time and maximum temperature for their equation is shown in Fig. 7.3, along with those for several other equations for Ro (Hood et al., 1975; Bostick et al., 1978; Middleton, 1982). The Sweeney & Burnham equation is preferred and used in this chapter to estimate temperatures, because it incorporates a distribution of activation energies with several parallel reactions to account for the diversity of composition and distribution of chemical bond types seen in kerogens, as well as temperature and time. This models the maturation of vitrinite macerals more accurately, since a single activation energy does not do so.

Fig.7.3. Nomograms of vitrinite reflectance versus exposure time and temperature after Hood et al. (1975), Middleton (1982) and Bostick et al. (1978) and calculated using the EASY%Ro model developed by Sweeney and Burnham (1990).

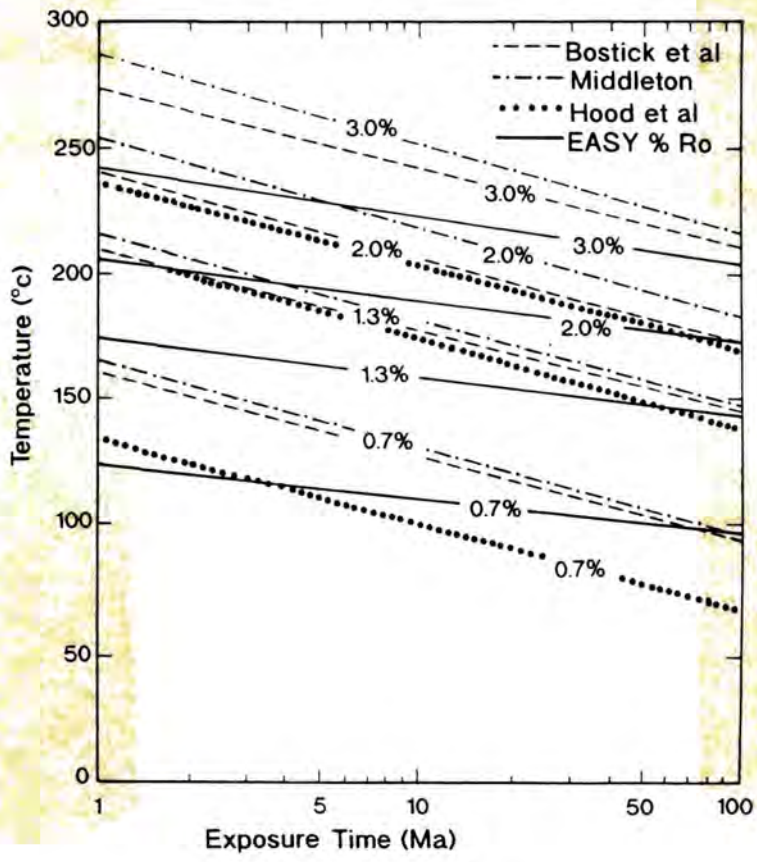

7.3 Previous work on organic maturity in the Western Alps.

Several previous papers have been published concerning the organic maturity of various horizons in the Tertiary and Mesozoic of the external Western Alps. Levels of Ro in western Switzerland and Haute-Savoie region of France (Annecy molasse basin, Bornes and Aravis) have been presented by Kübler et al. (1979) for the Tertiary and Mesozoic and by Schegg (1992a; 1992b). Similar studies of Ro have been carried out by Kisch (1980) and Burkhard & Kalkreuth (1989) for Tertiary units farther round the arc in the Swiss Helvetics (see Fig. 2.1). Gorin et al. (1989) and Gorin & Monteil (1990) looked at the thermal maturity of lower Tertiary and upper Cretacous from the Jura, Bornes, Aravis and Bauges using the Rock-Eval T_{max} and Thermal Alteration Index (TAI) techniques. What is common to Kübler et al. (1979), Schegg (1991, 1992), Gorin et al. (1989) and Gorin & Monteil (1990) is the increase in maturity from west to east, that is, towards the orogenic hinterland. This is usually described as being due to the effects of tectonic induced overburden, although Schegg (1992a; 1992b) has suggested that increased regional discharge of warm fluids may have played a second order role in the thermal history of the Plateau and Subalpine molasse of western Switzerland. The possible role of migrating warm fluids in the thermal history of the Subalpine chains is discussed in Chapter 8.

7.4 Abundance and occurrence of organic material in the Mesozoic and Tertiary of the Subalpine Chains.

Readings of Ro and spore fluorescence were made from samples prepared from fresh outcrop samples from argillaceous lime mudstones, shales and sandstones from Mesozoic and Tertiary units. Readings of Ro would ideally be made on more than 20 vitrinite particles; however, the average number of readings was generally less than this. This could be expected since the samples mainly come from muddy carbonate rocks which were deposited in oxygen-rich environments, in which organic material is readily oxidised. Vitrinite macerals, derived from land plants, are typically more common in continental\marginal clastic marine facies rocks than fully marine rocks, the former being closer to sources of terrestrial organic matter supply. Most carbonate rocks contain non-generative organic material, mainly highly oxidised Type 4 kerogens (inertinite). This is the organic facies D of Jones (1985). Source rock potential in the Subalpine Chains is further discussed in section 7.6.

7.5 Levels and regional variation of organic maturity within the Subalpine Chains.

The results of the Ro study are detailed in Appendix 4 and are shown in Figs 7.4, 7.5, 7.6, 7.7 and 7.8 for the south-west and north-east parts of the study area respectively

Fig. 7.4. Mean Ro (%) values for the south-west part of the study area (Vercors, Chartreuse and southern Bauges massifs). Stratigraphic ages of the samples studied are indicated by the abbreviations: Mio= Miocene; Ha= Hauterivian; Va= Valanginian; Be= Berriasian; Ki= Kimmeridgian; Ti=Tthonian; Oxfordian. From Moss (1992). Fig. 6.10 shows the nature and distribution of clay mineral assemblages in the Hauterivian for the same area and provides a useful comparison. See Figs 2.17a and 2.17b for the regional geology of the Vercors.

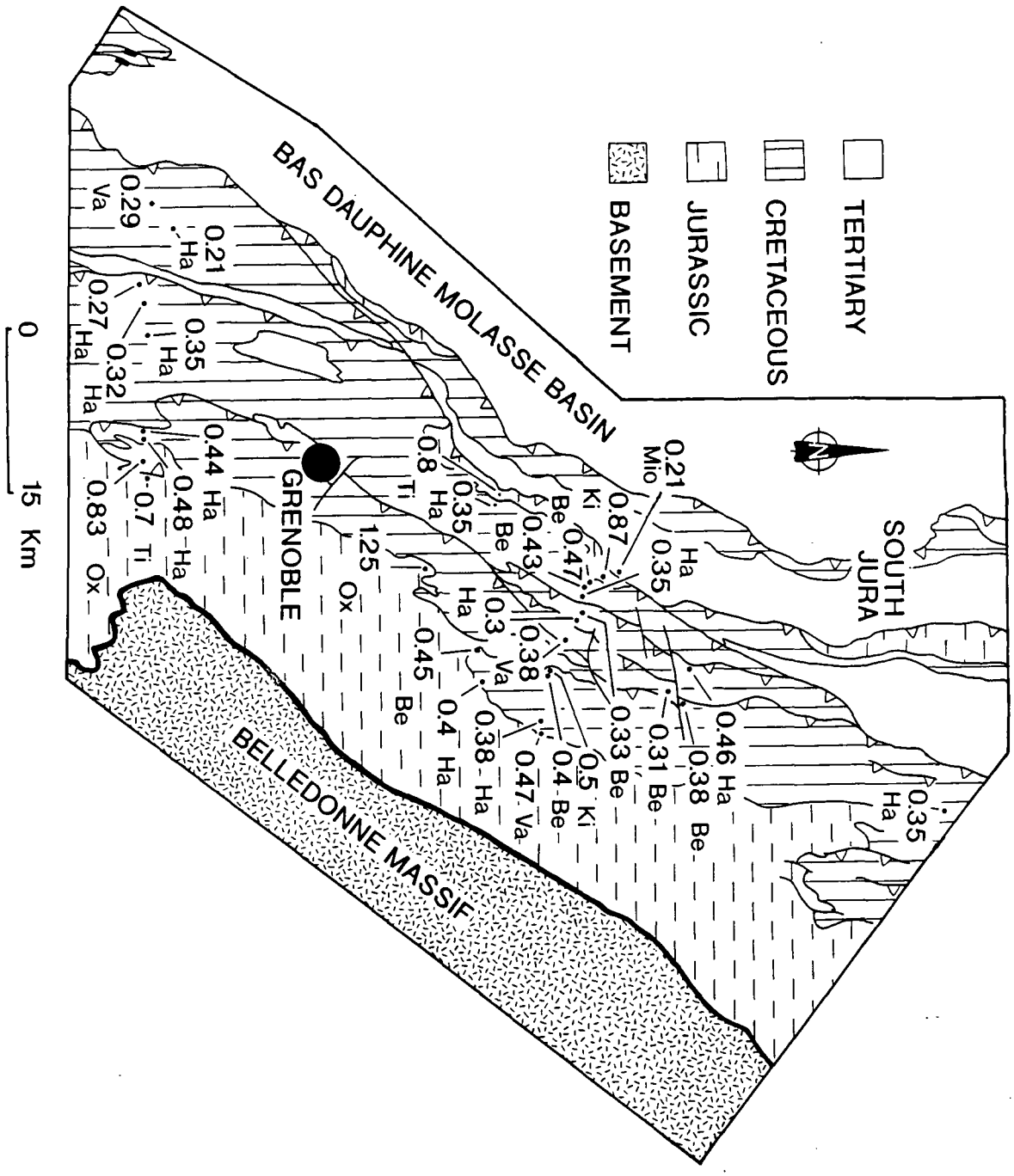

7.5.1 South-west part of the Subalpine Chains.

In the Chartreuse and Vercors massifs (see Fig. 2.1 for location), Lower Cretaceous units such as the Berriasian, Valanginian and Hauterivian have low values of Ro, generally in the region of 0.35 to 0.45% (see Fig. 7.4). Seen under fluorescent light, spores from these horizons are green/yellow to yellow, sometimes with a slightly orange fluorescence, which is consistent with the vitrinite values recorded for these horizons. Upper Jurassic to mid-Jurassic units from these same areas of the Subalpine Chains have higher values of Ro, as would be expected since they come from 500m to 900m lower down in the stratigraphy, with values of Ro ranging from 0.5% for the uppermost Jurassic (Kimmeridgian) to 1.25% for the mid-Jurassic (Oxfordian); see Table A4.1 (in Appendix 4 and Fig. 7.4). Spores from the Jurassic show a range of fluorescence, from yellow/orange to orange to brown to dark/non fluorescent. Again the fluorescence matches the values obtained for Ro for each respective sample (see Figs 7.1 and 7.2). Only one Ro value was recorded from the upper Tertiary (Miocene) molasse deposits in this part of the chain, from the western edge of the Chartreuse massif, of 0.21% Ro. Spores within this sample had a bright green fluorescence. Fig. 7.5 shows an east to west cross-section through the Vercors massif. The Hauterivian on the eastern edge of the Vercors has a slightly higher value of Ro than the same unit on the western edge of the massif although it should be borne in mind that below values of 0.5 % readings of Ro can be prone to scatter (Barker, 1989).

Fig. 7.5. Cross section through the Vercors massif, in the southwest part of the Subalpine Chains. Mean Ro (%) values for different horizons along the line of the section are shown. A west to east increase in the level of Ro can be seen. However, values of Ro below 0.5% can be prone to scatter (Barker, 1989). The section is based on Butler et al. (1987) and the diagram is from Moss (1992). Fig. 6.11 is the same section line but with the clay mineral assemblages of the Hauterivian marked along the line of section and is a useful comparison. Stratigraphic ages are given by the abbreviations shown in Figs 7.4 and 7.6. See Figs 2.17a and 2.17b for the regional geology of the Verors.

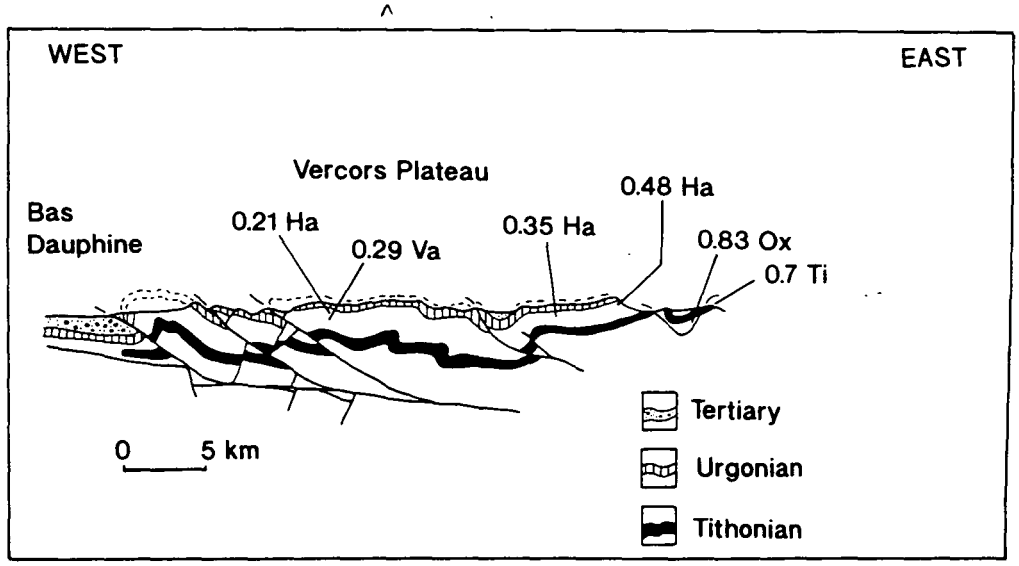

7.5.2 North-east part of the Subalpine Chains.

Further to the north-east, along strike of the Subalpine Chains, in the Haut-Giffre, Platé and Aravis massifs (see Fig. 2.1 for location) the Lower Cretaceous units of the Hauterivian and Berriasian have much higher Ro values than the areas to the south-west discussed above. Ro values for the Hauterivian range from 1.7% in the Aravis to 2.0% in the Platé. In the Haut-Giffre massif a value of 2.1% was recorded for the Berriasian, whilst the mid-Jurassic (Oxfordian) reaches an Ro value of 2.8%; see Table A4.1 (in Appendix 4) and Fig. 7.6. Under fluorescent light, these samples appeared dark and non-fluorescent, typical of rocks which have Ro values greater than 1.4 to 1.5% Similarly, Tertiary units of the Aravis, Platé and Haut-Giffre massifs have relatively high values of Ro. Upper Eocene coaly beds of the Diablerets beds have an Ro of 1.49% in the vicinity of Lac des Chambres (Haut-Giffre), whilst slightly younger upper Eocene shales from below Pointe d'Anterne (Platé) have an Ro of 1.23%. Farther to the south-west still, Oligocene-aged shales from Mt. Charvin (Aravis) have an Ro of 0.75% (see Fig. 7.6). Towards the west (i.e. the Bornes massif) there is a marked decrease in the level of Ro. For example, Ro values for the Hauterivian from the Platé and Aravis to the Bornes, with a value of Ro 1.1 for the Hauterivian in the western Bornes (Glierés plateau) (see Figs 7.6 & 7.8). Again this trend can be seen in the Tertiary strata of these massifs. With the Eocene/Oligocene of the Bornes massif having Ro values which range from 0.42% to 0.8% from north-west to south-east across the Bornes massif; that is they range from being similar to, to being higher than the Ro values for the Cretaceous of the Chartreuse and Vercors massifs to the south-west (compare Figs 7.4 and 7.5 with 7.6, 7.7 and 7.8). Some of the Ro values shown in Figs 7.6 and 7.7 are from Kübler et al. (1979); a full listing of the Ro values is given in Table A4.1 in Appendix 4.

7.5.3 Interpretation of levels of organic maturity in the south-west part of the Subalpine Chains.

The Ro values recorded from the Chartreuse and Vercors suggest that the Lower Cretaceous strata have experienced maximum temperatures considerably less than 100°C (see Fig. 7.3), if the nomogram of Sweeney & Burnham (1990) is used. Roberts (unpubl. Ph.D. thesis 1990) obtained similar maximum burial temperatures (40°C to 80°C) for the Hauterivian of the Vercors. This suggests that neither the depth of burial nor the residence time at maximum depth of burial were sufficient to cause any significant heating (in terms of organic maturity). Periods of burial related to foredeep formation and deformation are likely to be short in comparison to other basinal areas, such as mid-continental basins, with only very short periods, of up to 10 Ma, for residence time at maximum burial depth (see discussion on burial and thermal history in the region in Chapter 8).

Fig. 7.6. Mean Ro (%) values for the north-east of the study area (northern Bauges, Bornes, Aravis, Platé and Haut-Giffre massifs). Stratigraphic ages of the samples studied are indicated by the abbreviations: Ol= Oligocene; Eo= Eocene; Ha= Hauterivian; Be= Berriasian; Ox= Oxfordian. From Moss (1992). This diagram can be compared to Fig. 6.12, which shows the nature and distribution of clay mineral assemblages in the Hauterivian in the same area. Diagram from Moss (1992). Some of the Ro values on this diagram are from Kübler et al. (1979); these are listed in Table A4.1 in Appendix 4. See Figs 2.20a and 2.20b for geology of the Bornes/Aravis,

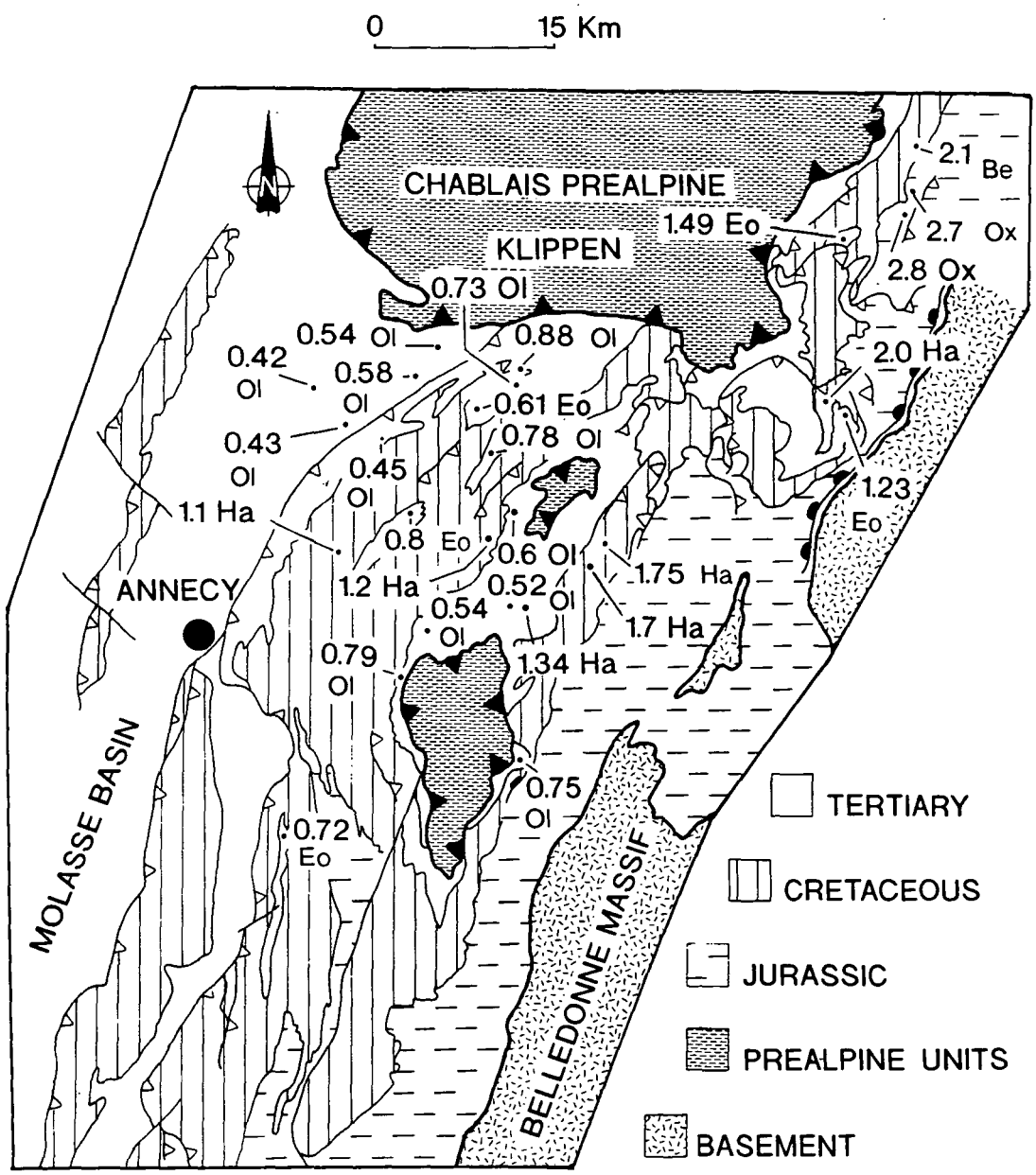

Ro values from upper Jurassic (Tithonian) to mid-Jurassic (Oxfordian) units suggest temperatures of between 100°C to 160°C using the nomogram of Sweeney & Burnham (1990) (see Fig. 7.3) and assuming a heating duration of up to 10 Ma (see Chapter 8 on the burial history of the Subalpine Chains for discussion). In terms of oil generation these rocks can still be considered mature.

Overall, the data for the level of organic maturity of Mesozoic and Tertiary units in the Chartreuse and Vercors massifs suggest that this part of the Subalpine Chains has only been subjected to shallow burial, short residence times, abnormally low geothermal gradients, or all three. Foreland areas are typified by low geotherms (Allen & Allen, 1990) and it is also likely that maximum burial depths were slight for this part of the Subalpine Chains. Thus it is possible that a combination of these factors produced the low levels of thermal maturity in this region. Both geothermal gradients and maximum depths of burial are discussed in the section on burial history.

Fig. 7.7. Northwest to southeast cross section through the Bornes and Aravis massifs, in the north-east part of the Subalpine Chains, showing the values of Ro along the line of section. A general increase in the level of vitrinite reflectance can be seen towards the eastern end of the section in both the Hauterivian and Oligocene. The diagram is from Moss (1992) and the section is based upon Butler et al. (1987). This diagram makes a useful comparison with Fig. 6.14, which shows the same section but with the changes in the clay mineral assemblage of the Hauterivian. Both suggest a general easterly increase in the level of diagenesis. Stratigraphic ages are given by the abbreviations shown in Figs 7.4 and 7.6. See Figs 2.20a and 2.20b for geology of the Bornes/Aravis.

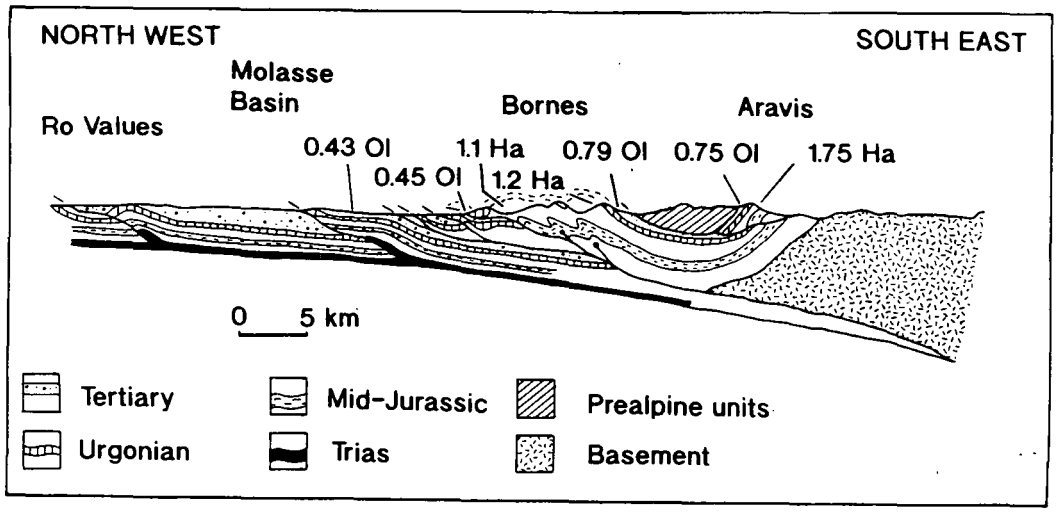

7.5.4 Interpretation of levels of organic maturity in the north-east part of the Subalpine Chains.

Using the nomogram shown in Fig. 7.3 the Ro values from the north-eastern part of the belt suggest that the Cretaceous to mid-Jurassic rocks there have experienced temperatures of around 150°C to 230°C, assuming the length of exposure time to these maximum temperatures was up to 10 Ma. The former temperature is for the Hauterivian of the western Bornes massif (see Figs 7.6 & 7.7) and the latter temperature is for the Oxfordian of the Haut-Giffre massif (see Figs 7.6 & 7.8). These temperatures suggest that the Cretaceous and Jurassic rocks of the north-eastern part of the belt have been buried more deeply than their equivalent horizons to the south-west or that they have experienced a radically different thermal history (see Chapter 8 for discussion).

Fig. 7.8. West to east section throughout the Haut-Giffre massif, in the extreme north-east of the study area, showing the mean Ro (%) values along the line of section. Section after Butler et al. (1987). The Urgonian is of Barremian-Aptian age, so the unmarked area between the Malm and Urgonian is the lower Cretaceous. The unmarked area between the Malm and the Bajocian is the Callovian and Bathonian, whilst the Aalenian and the Lias is represented by the unmarked area below the Bajocian. The unmarked area above the Urgonian is the mid- to upper Cretaceous and the Tertiary. Stratigraphic ages(next to Ro values) are given by the abbreviations shown in Figs 7.4 and 7.6. See Fig. 2.21a for the geology of the Haut-Giffre.

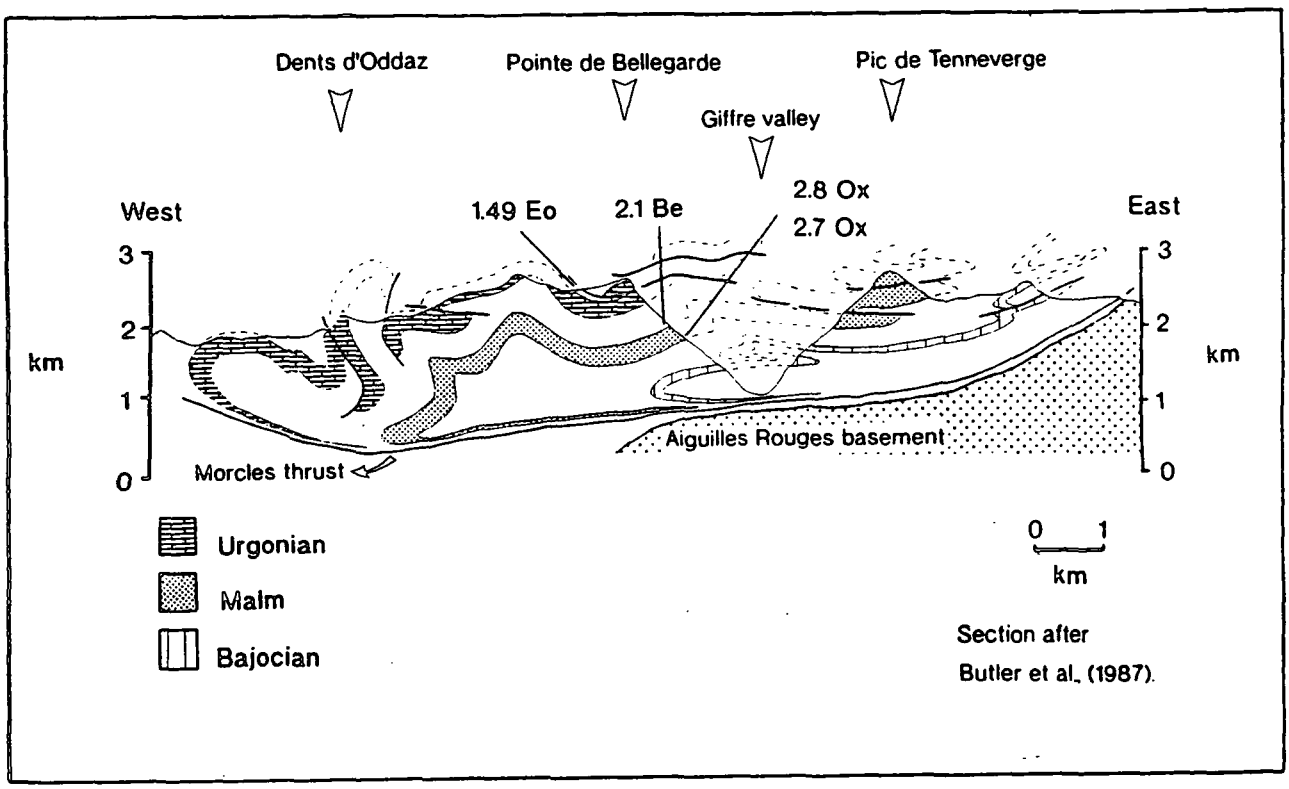

The Ro values for Eocene and Oligocene units in the Bornes (up to 0.8; see Figs 7.6 & 7.7) suggest that maximum burial temperatures of up to 135°C were reached (see Fig. 7.3) for these horizons. Higher Ro values for the sediments of the same age farther to the east suggest slightly higher temperatures of 180°C (assuming a heating time of up to 10

Ma). This shows that the Tertiary of the north-eastern part of the Subalpine Chains has experienced greater burial temperatures than the older Cretaceous and Upper Jurassic of the south-western part of the belt, and reached levels of organic maturity similar to (and in one instance higher than) those of the mid-Jurassic (Oxfordian) of the south-western part of the belt (compare Figs 7.4 and 7.5 with 7.6, 7.7 and 7.8).

7.6 Implications for burial and thermal history and comparison to previous estimates of organic maturity of the Subalpine Chains.

Figs 7.9a and 7.10a show the present day surface distribution of Tertiary and Cretaceous rocks which are still within the oil generation window (the area between the oil birth and death lines in Fig. 7.1). Both Fig. 7.9a and 7.10a are drawn using the data shown in Figs 7.4 and 7.6.

From Fig. 7.9a it can be seen that no Tertiary rocks from the Vercors, Chartreuse and Bauges massifs have entered the oil generation window. The oil birth line for the Tertiary lies roughly within the central part of the Bornes massif and trends north-south, whilst the oil death line lies to the east of the Aravis massif and up to the eastern edge of the Platé massif. Fig. 7.9b is taken from Schegg (1992a) and shows the isoreflectance lines for the Tertiary of the Annecy molasse basin (Plateau des Bornes) and western Bornes massif and can be seen to broadly match Fig. 7.9a.

Fig. 7.10a shows the distribution of Cretaceous rocks (which are now at the surface) which have entered the oil generation window. By comparison to Fig. 7.9a the oil birth line for the Cretaceous is located farther to the west (towards Annecy city and the central Bauges massif, see Fig. 7.10a). The oil death line is similarly shifted to the west and runs roughly north-south through the Thônes syncline area (between the Bornes and the Aravis massifs). As with the Tertiary the Cretaceous rocks now exposed at the surface in the Vercors, Chartreuse and south-western Bauges have not reached the oil generation window. Fig. 7.10a should be compared to Fig. 7.10b, which is taken from Gorin & Monteil (1990), who used Rock-Eval T_{max}, Thermal Alteration Index (TAI) and the fluorescent colour of dinoflagellates to calculate thermal maturity and the equivalent Ro values for the upper Maastrichtian Wang Formation of the Chartreuse, Bauges, Bornes and Aravis massifs. The isomaturity lines shown in Fig. 7.10b match closely the oil birth and death lines for the Cretaceous in Fig. 7.10a. However, it should be noted that the fluorescent colour of dinoflagellates is a shade or two down on those seen from spores. For example, a yellow fluorescing dinoflagellate could be found in rocks in which the spores have a yellow/orange or light orange fluorescence.

In all the areas were the Jurassic was sampled it had reached the oil generation window(the western, frontal edge of the Chartreuse for example) or had passed through it

Fig. 7.9a. Tentative present day surface distribution of Tertiary rocks (based on the data presented in Figs 7.4, 7.5, 7.6, 7.7 and 7.8) which have entered the oil generation window (roughly equivalent to an Ro of between 0.5 to 1.3%, see Fig. 7.1). In the Vercors, Chartreuse and southern Bauges the Cretaceous is immature. Whilst in the Aravis, Platé and Haut-Giffre massifs it is mature to overmature and mature in the Bornes massif.

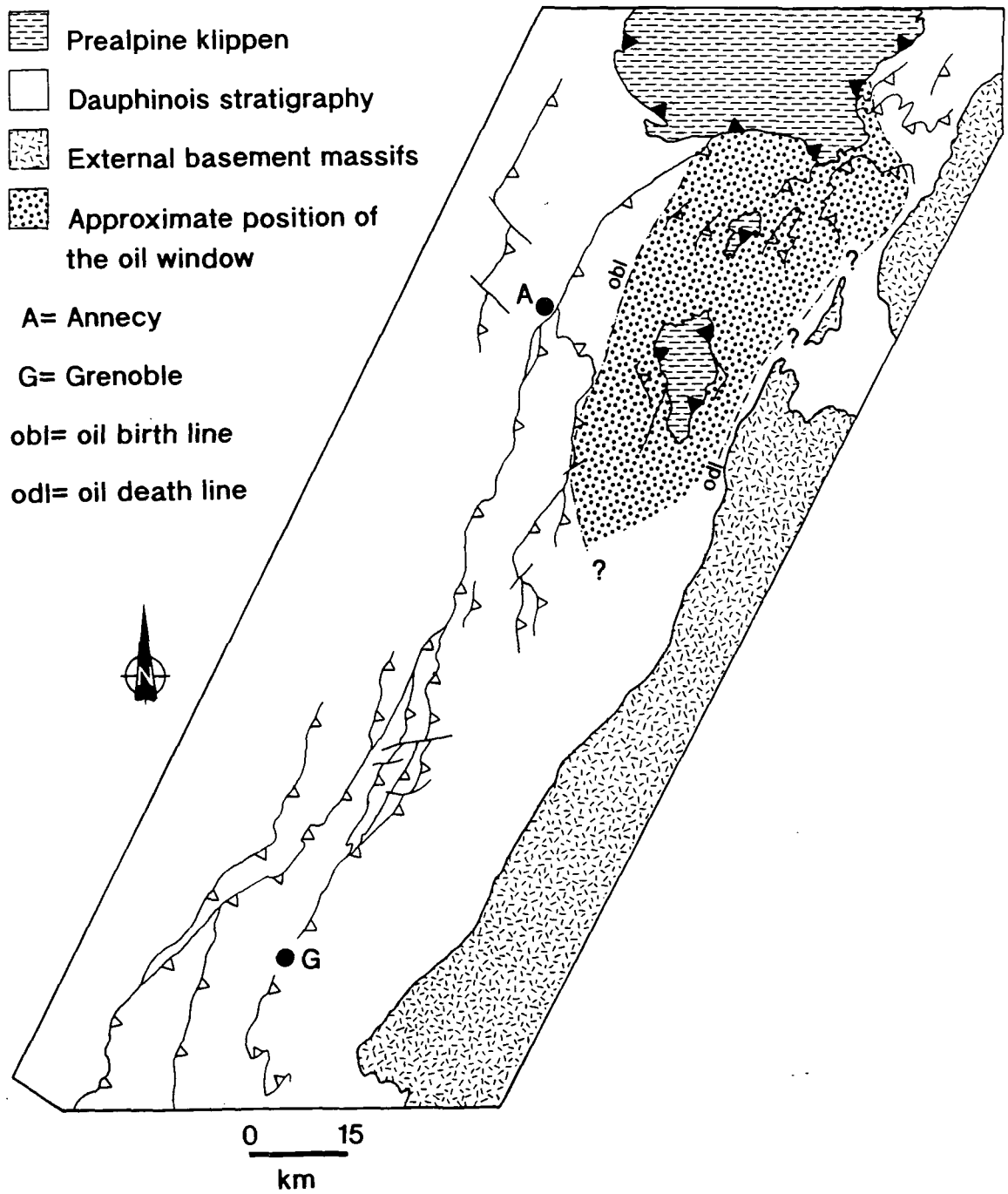

Fig. 7.9b Calculated isoreflectance for the Oligocene and lower Miocene of the Annecy molasse basin and western edge of the Bornes massif (from Schegg, 1992a). This figure generally compares well with Fig. 7.9a. The NW-SE trending, stippled region (labelled TA) has slightly higher maturity due to the circulation of hot fluids. It should be noted that Kübler et al. (1979) (their table 4) suggest that the Oligocene in that region has a lower maturity (see Fig. 7.6) than that suggested by Schegg (1992a).

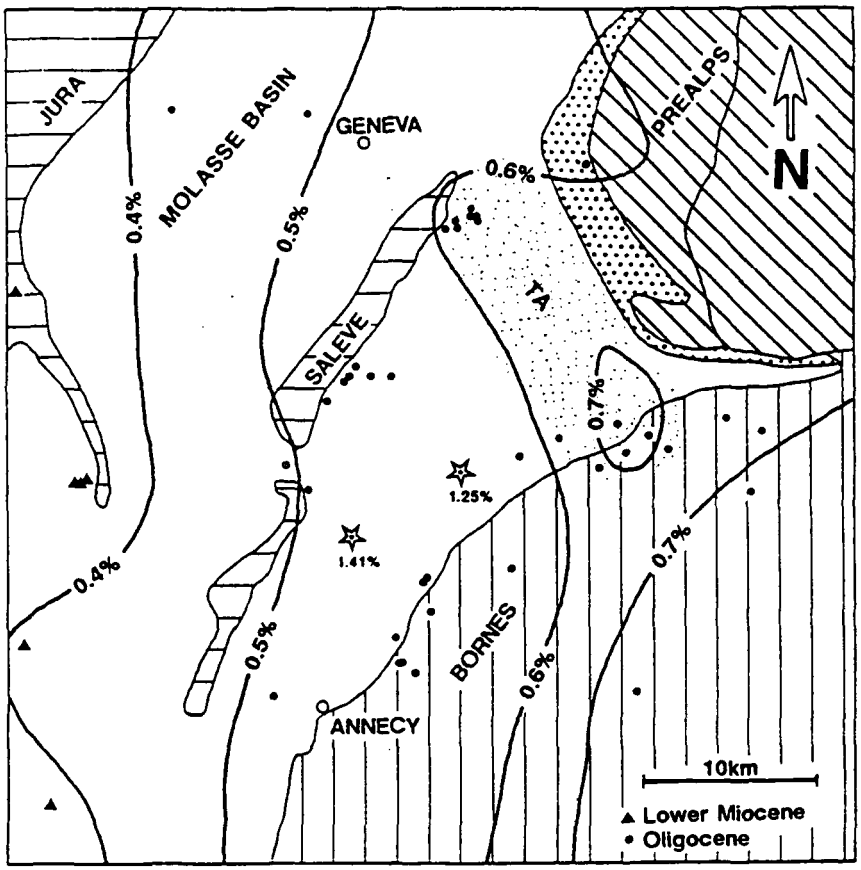

(in the Haut-Giffre massif for example). However, in the southern Jura region (to the north-west of Aix-les-Bains) upper Jurassic Kimeridigian lagoonal limestones are thermally immature (<0.5% Ro) (Gorin et al., 1989) and Purbeckian facies rocks of upper Jurassic/lower Cretaceous age at Salève (to the north-west of Annecy) have an Ro of between 0.25 and 0.40% (Kübler et al., 1979); see Fig. 7.10a.

The data presented in this chapter (and in Moss, 1992) in general terms agrees with those presented elsewhere (Kübler et al., 1979; Gorin et al., 1989; Gorin & Monteil, 1990; Schegg, 1992a). These previous works have concentrated on the Bornes/Aravis and the Annecy molasse basin regions, so the thermal data presented in this chapter and in Moss (1992) is significant since the first recording of maturity levels in the south west (Grenoble) region of the Subalpine Chains.

Fig. 7.10a. Tentative present day surface distribution of Cretaceous rocks which are in the oil window. Both this figure and Fig. 7.9a compare well with Fig. 6.4, which shows the approximate position of the lower boundary of anchizone metamorphism. These two maps (7.9a and 7.10a) of the approximate position of the oil generation window for the Tertiary and Cretaceous are in agreement with Kübler et al. (1979), their figure 2.

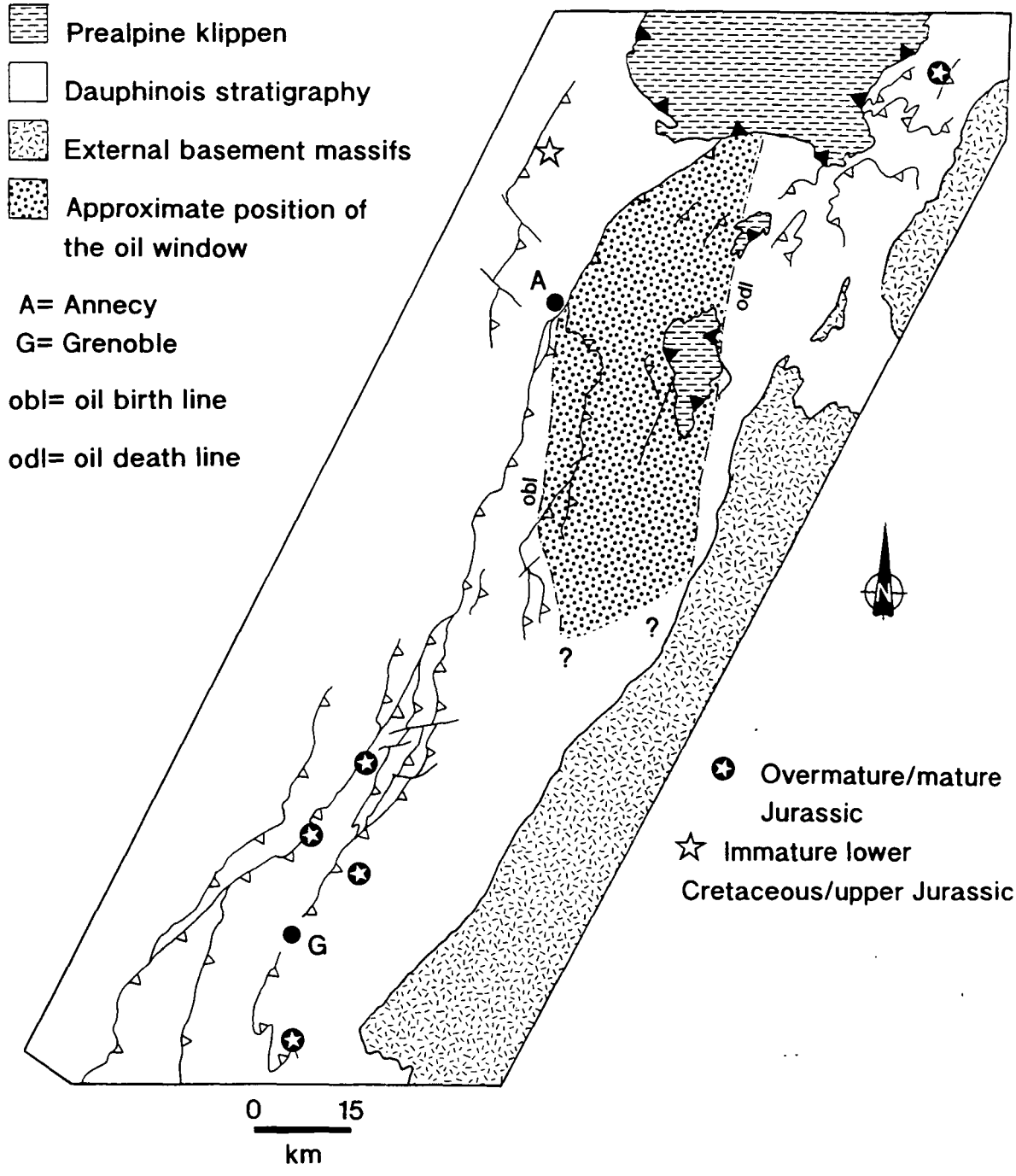

Fig. 7.10b. Maturity data for the upper Cretaceous Wang Formation in the Aravis, Bornes, Bauges and Chartreuse massifs (from Gorin & Monteil, 1990). This figure should be compared to Fig. 7.10a. N.B. as noted in the text (in section 7.5) the fluorescence of dinoflagellate cysts is a shade or two below that shown by spores.

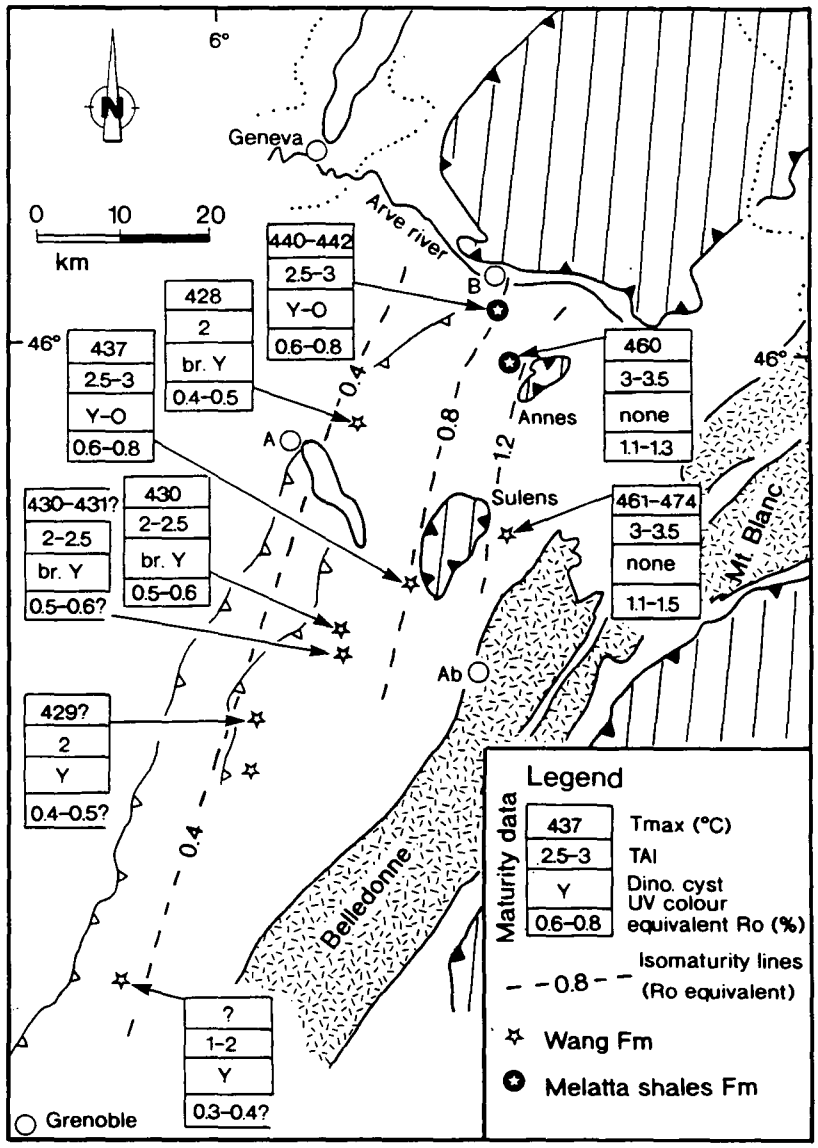

A= Annecy Ab= Albertville B= Bonneville

Prealpine units

External zone basement

Y= yellow UV fluorescence br. Y= bright yellow UV fluorescence

Y-O= yellow-orange UV fluorescence

Some of the views expressed in this chapter are different to those of a recently published account of modelling hydrocarbon maturation in the northeast part of the chain. This study carried out by Butler (1992b) is primarily based on the out-dated Time-

Temperature Index (TTI) method of assessing maturity. This method and Butler's conclusion's are discussed in Chapter 8.

Using indicators of organic maturity in the Subalpine Chains shows that the maximum burial depths and time at those depths, and therefore the highest temperatures experienced, were in the north-east of the belt. The greatest variation in maximum burial temperatures is along strike of the fold/thrust belt, although temperatures do vary across the belt (see Figs 7.4, 7.5, 7.6, 7.7 and 7.8), with higher temperatures experienced on the eastern side, closest to the orogenic hinterland. The values recorded for the south-west parts of the chain are explicable by sedimentary burial alone and are apparently little disturbed by tectonic burial (see Chapter 8). Similar variations in temperature across strike of fold/thrust belts have been documented by Hoffman & Hower (1986), Guthrie et al., 1986; Kalkreuth & McMechan (1988), and Underwood et al. (1988).

7.7 Hydrocarbon source rock potential in the French Subalpine Chains.

A source rock is a volume of rock that has been or is generating and expelling hydrocarbons or has the capability to do so in sufficient quantities to form commercial oil and gas accumulations (Brooks et al., 1987). The contained sedimentary organic matter must meet minimum criteria of organic richness, kerogen type and organic maturity, except for a potential source rock which has not yet reached the required levels of organic maturation to allow hydrocarbon generation. The organic fraction (or kerogen component) of most sedimentary rocks is generally small; with the total organic carbon (TOC) expressed as a weight percent, it is usually much less than 1%. Obvious exceptions to this are coals and oil-shales. In the petroleum industry a TOC of about 0.5 % is usually used to mark the lower limit of source rock potential (Tissot & Welte, 1984). Although for carbonate source rocks a minimum figure of 0.3 weight percent has been suggested (Jones, 1985). Listed below are the ratings of source rock potential based on TOC:

TOC (weight percent)	**Rating**
<0.5	very poor
0.5-1.0	poor
1.0-2.0	fair
2.0-4.0	good
4.0-12.0	very good
>12.0	excellent (oil shale)

The lower rating (0.5%) may be optimistic, since the type of organic matter present is also important. It should always be borne in mind that these ratings describe the amount of organic matter within the rock and not the hydrocarbon source potential (Cornford, 1984).

For example, a rock may have a TOC of 2.0% but if the kerogen type is predominantly type 4 then the rock has no hydrocarbon source potential.

The TOC of marine sediments is believed to be controlled by an interplay of six intimately related parameters (Tyson, 1987):

1) sediment texture (especially grain size).
2) water depth.
3) primary productivity.
4) rate of allochthonous (terrestrial and marine) organic matter supply.
5) rate of sediment accumulation.
6) bottom water oxygenation.

Tyson (1987) proposed that the main factor for the formation of petroleum source rocks in a marine setting is the bottom water oxygenation, which correlates with the location of the Eh interface and the intensity of macrobenthic activity. As pointed out by Tyson (1987), high TOC's and high contents of marine organic matter are *"predominantly correlated with dark-coloured, fine grained mudrocks having the sedimentological, palaeoecological and geochemical characteristics associated with deposition under oxygen-deficient or oxygen-free bottom waters."*

In Europe, a stratigraphic survey of Mesozoic organic rich shales by Hallam (1987) and papers on specific horizons (Arthur et al., 1987 and Schlanger et al., 1987 (upper Cretaceous of Europe); de Graciansky et al., 1987 (Cretaceous of the north Atlantic); Farrimond et al., 1989; (the Toarcian of Europe)) show five periods within the European/north Atlantic Tethyan realm during which the formation of organic-rich sediments is particularly concentrated. They are the mid-Jurassic (Toarcian), two periods during the upper Jurassic (Callovian and Kimmeridgian to Tithonian), the mid-Cretaceous (Aptian-Albian) and the upper Cretaceous (Cenomanian-Turonian). Some of these time periods may also have seen the accumulation of organic rich sediments in the Dauphinois/Helvetic basin, since the basin was part of western Tethys which was connected to the northern Atlantic during the Jurassic and Cretaceous (Dercourt et al., 1984; Lemoine et al., 1986; Barron, 1989). For example the Aptian-Albian 'Marnes bleues' Formation of the Vocontian basin (to the south of the Vercors; see Fig. 2.7a) has several organic rich intervals (up to 3% TOC; kerogen types 1 and 2), believed to have formed by a stratified water column leading to the development of anoxic bottom water conditions during transgressive pulses (Bréhéret, 1988). The same events are recognisable in other Alpine and Tethyan regions.

The important properties for the characterization of a potential source rock are the TOC, type of organic matter, thickness of the unit, areal extent and lateral variation, the presence of interbedded sands or silts for drainage and regional maturity boundaries.

In the following part of this section, potential source rocks within the Subalpine Chains are described first. Then the actual hydrocarbon occurrences and the results of hydrocarbon exploration wells are described. It should be borne in mind that, as previously stated, a rock which has a high TOC does not automatically have a high hydrocarbon source rock potential.

Within the Subalpine Chains several horizons have been shown to possess high enough TOC values and suitable kerogen type to make them at least a potential source rocks. These are listed in Fig. 7.11 and shown in Fig. 7.12 for the Cretaceous and Tertiary. From these two it can be seen that the Tertiary Diablerets Beds and the Melatta Shales are

Fig. 7.11. Table showing the stratigraphy, location (usually where the samples were sampled), TOC, kerogen content and maturity (at the sample locality) of possible source rocks in the Subalpine Chains. Data from BRGM (1988); Lateltin (1988); Gorin et al. (1989) and Gorin & Monteil (1990). The Oxfordian of the Bornes (in the Brizon #1 well) is mentioned by Charollais & Jamet (1991), to be rich in organic material. No data exists for the TOC and kerogen type within the Toarcian and Carboniferous of the Subalpine Chains; however, from regional evidence they could represent possible source rocks. N.K. = not known.

Horizon	Age	Locality	TOC	Kerogen type	Maturity
Val d'Illiez ssts	Oligocene	Bornes, N. Morcles (Swiss)	0.60 -0.85	III	mature to overmature
Gres Taveyannaz ssts	Oligocene	Aravis	0.47	N.K.	mature to overmature
Melatta shales	Oligocene	Bornes, N. Morcles (Swiss)	0.83 -1.80	II/III	sub-mature to mature
Foraminifera shales	Eo-Oligocene	Aravis, Bornes	0.32 -0.69	II/III	mature to overmature
Diablerets beds	upper Eocene	Bornes	upto 7.42	II/III	mature to overmature
Wang Fm	Maastrichtian	Bauges, Chartreuse, Bornes	0.0 -0.9	mainly III	immature to mature
"	Hauterivian to	Bornes	<0.25	N.K.	mature
"	Berriasian	Bornes	<0.25	N.K.	mature
"	Kimmeridgian	Jura	<0.25 -2.09	II	immature
"	Kimmeridgian	Aravis	0.0	N.K.	overmature
"	Oxfordian	Aravis	<0.25	N.K.	overmature
"	Bathonian	Aravis	<0.25	N.K.	overmature
"	Toarcian	regionally	N.K.	N.K.	overmature
"	Carboniferous	regionally	N.K.	N.K.	overmature

the most promising potential source rocks within the Subalpine Chains (see *'notice explicative'* BRGM 1988; Gorin et al. 1989; Gorin & Monteil, 1990). The upper Eocene Diablerets Formation has a TOC of up to 7.42% (see Table 7.11 and Fig.7.12) and shales

of the lower to middle Oligocene Melatta Shales Formation with a TOC of up to 1.32% (see Fig. 7.11 and Fig. 7.12), have mixed type II/III kerogens and both are sub-mature to overmature (depending on location). The latter formation, in the east of the Bornes massif where it is mature, is probably responsible for local oil impregnation of the Val d'Illiez sandstones (Gorin et al., 1989). Butler (1991) suggested that the Berriasian may be a source

Fig. 7.12. TOC and hydrogen index versus stratigraphic age for the Tertiary and Mesozoic of the Bornes massif from Gorin (1987; reproduced in BRGM, 1988). This diagram and the table in Fig. 7.11 both emphasize that the Oligocene Melatta shales and the Eocene Diablerets beds are the only realistic source rocks within the region.

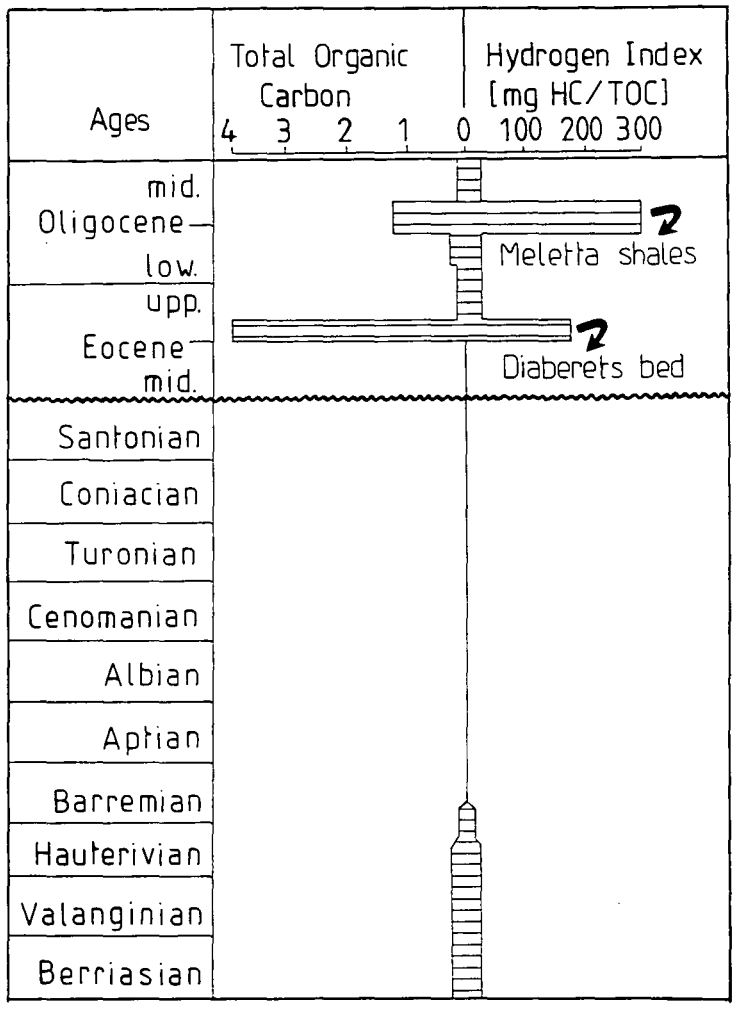

rock in the Bornes/Aravis region, however, from the organic geochemistry of Gorin et al. (1989) this is highly unlikely (see Fig. 7.11). TOC data presented in Appendix 4 shows that a sample of the Berriasian from Pas l'Ours (near Refuge de la Vogealle, Haut-Giffre) has a

TOC of 2.17%, however the hydrogen index of this sample indicates the kerogens ... are type IV (inertinite) so of no value as a hydrocarbon source rock. Kimmeridgian lagoonal marly limestones of the Bellegarde anticline (north-west of Aix-les-Bains) in the southern Jura have TOC's ranging from <0.25 to 2.09% and are oil prone, but they are still immature (Gorin et al., 1989). Regional maturity patterns for the Tertiary and the Cretaceous are shown in Figs 7.9a and 7.10.

Deeper hydrocarbon source rocks could possibly be the Toarcian shales and Carboniferous coals. Toarcian shales are known from other areas of the Tethyan realm to contain organic-rich sediments produced by a single oceanic anoxic event (Farrimond et al., 1989). This horizon could possibly be a source of oil. The Oxfordian of the Bornes though not exposed at the surface is described from the Brizon #1 well (see Fig.7.13 for location) as "rich in organic matter" (Charollais & Jamet, 1991) Similarly the upper Oxfordian basinal shales and muddy limestones in the GPF-Balazuc well (located in the Ardèche region, on the western margin of the Mesozoic Subalpine basin) is reported to have TOC values up to 1.1% (Dromart et al., 1992). However, in the Aravis it has a TOC of <0.25 (Gorin et al., 1989), so is probably less likely to be a source rock. Carboniferous (upper Westphalian and lower Stephanian) coal has been mined from remnant basins in and around the Belledonne and Pelvoux external basement massifs (part of the so-called "Zone Houillère Externe", BRGM, 1979a, 1979b). It is also present in the other external basement massifs (Aiguilles Rouges and Aar massifs, Trümpy, 1980; BRGM, 1985) and could be a possible source of gas. Carboniferous coal basins could also exist below the Jura, the Molasse basin and the Subalpine Chains. In the western foot of the Jura, at Lons-le Saunier, a subsuface coal deposit was explored in the 1950's (Trümpy, 1980). Permo-Carboniferous deposits within a small fault bounded basin have been imaged seismically and penetrated by the FAY 1 well (see Fig. 7.13 for location) within the Annecy molasse basin area (Charollais & Jamet, 1990; Huggenberger & Wildi, 1991). Whether any coal deposits exist within this small basin is not stated. For both of these latter two sources a secondary migration would mostly have to be involved if the hydrocarbons were to reach a suitable reservoir rock.

Several actual occurrences of hydrocarbons in the north-east of the Subalpine Chains have been detailed in the literature. Michal & Caillon (1957) very briefly mentioned oil shows within the Aquitanian molasse sediments, in the conglomerate/breccia at the base of the Tertiary succession, in the paleokarstic and fissured top of the mid-Cretaceous Urgonian limestones and the upper Jurassic of exploration wells drilled in the area immediately west of Annecy (see Fig. 7.13, wells numbered Sv101, Sv104, etc). In most cases the quantities of hydrocarbons were small and production testing of the wells was impossible because of the very low permeability of the "reservoir" rocks and/or the amounts of oil were so small (possibly because they are only the remnant traces of a former

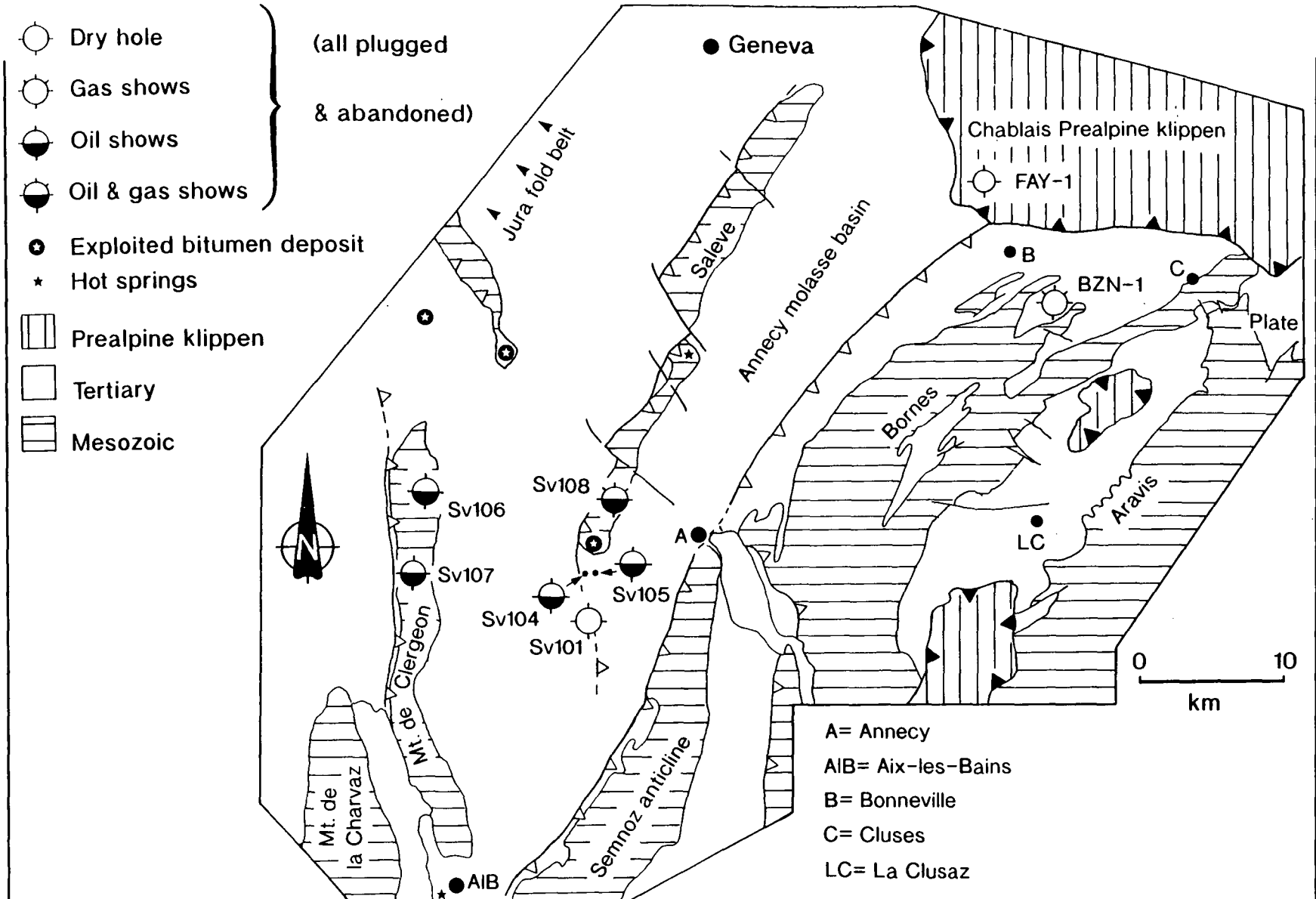
Dry hole
Gas shows
Oil shows
Oil & gas shows
(all plugged & abandoned)
Exploited bitumen deposit
Hot springs
Prealpine klippen
Tertiary
Mesozoic
Geneva
Jura fold belt
Salève
Annecy molasse basin
Chablais Prealpine klippen
FAY-1
B
C
BZN-1
Plate
Bornes
Aravis
LC
A
Sv108
Sv106
Sv107
Sv105
Sv104
Sv101
Mt. de Clergeon
Mt. de la Charvaz
Semnoz anticline
AIB
N
0
10
km
A= Annecy
AIB= Aix-les-Bains
B= Bonneville
C= Cluses
LC= La Clusaz

Fig. 7.13. (previous page). The location of exploration wells drilled in the Bornes massif and Bas-Dauphine molasse basin in the Annecy region. Compiled from data in Michel & Caillon (1957), Charollais & Jamet, (1990) and Butler (1992b).

migration pathway?). In some instances the hydrocarbons were oxidised, and this could indicate that biodegradation has occurred due to the invasion of the host rock by surface-derived meteoric water carrying dissolved oxygen and micro-organisms (Tissot & Welte, 1984). Previously worked asphalt[2] mines are also known to occur in the Annecy area (Butler, 1991). Similar asphalt occurrences have also been documented from the more external region of the Swiss Jura by Trümpy (1980a) and Zweidler (1985). At Val de Travers (to the north-west of Lac Neuchâtel, in the Swiss Jura) a large asphalt deposit is mined, where the bitumen is resident within the lower Cretaceous "Pierre jaune de Neuchâtel" and Urgonian formations beneath a southward dipping thrust (Trümpy, 1980a). At Val de Travers migration occurred before Jura folding, with sedimentological (stratigraphic) traps. Jura folding led to re-migration and biodegradation of the deposits (Zweidler, 1985). The Brizon # 1 well (BZN-1) drilled in 1987 to the south-west of Bonneville in the Bornes Massif, had gas shows (Charollais & Jamet 1990; see Fig.7.13), although the Faucigny # 1 well (FAY 1), drilled roughly 10km to the north-east, on the edge of the Chablais Pre-alpine Klippen in 1970 was a dry hole (op. cit.). Trümpy (1980a, page 101) details the results of hydrocarbon prospecting in the Swiss alpine region, where, initially sandstones of the Oligocene and Miocene Marine and Freshwater Molasse of the Molasse Basin were the main targets. These only furnished very modest results. However, a large number of very small oil and gas fields do exist in the Munich region of the Molasse Basin (Bachmann & Müller, 1991), where a variety of reservoir rocks (fractured Mesozoic carbonates, Mesozoic sandy horizons such as the Keuper and the molasse sandstones) and source rocks (Carboniferous shales and coals, Cretaceous shales, Oligocene shales and thin coals) exist. The lack of success in exploration within the French sector of the external French Alps, where similar conditions exist, is likely to be a reflection of several factors, such as the lack of suitable traps available at the time of migration of any hydrocarbons produced.

7.8 Discussion of the results and the thermal history of the Subalpine Chains.

[2] **Footnote:** asphalts are a viscous form of bitumen which is a general term for partly hydrocarbonated compounds (liquid or solid). Bitumen is first and foremost a *secondary* product of the thermal transformation of organic matter and it may be migrated or generated in-situ by the degradation of kerogen (Robert, 1988). Asphalt is classified as bitumen with an Ro <0.7 and a melting point below 104°C (see table VIII in Robert, 1988).

The results of this study of vitrinite reflectance show that the variation in maximum burial temperature is more marked along strike of the Subalpine Chains than across strike. Although an across strike variation in the maximum temperatures experienced does exist (see Figs 7.4, 7.5, 7.6, 7.7 and 7.8), this variation is not as marked, especially in the Chartreuse and Vercors massifs where there is little difference in the recorded Ro value from east to west. Ro values in these two areas for the Cretaceous and Tertiary are low, less than 0.5%. At such low values, Ro readings are generally prone to scatter and are generally less accurate than readings made from rocks which have reached higher levels of maturity (Barker, 1989). However, the values recorded for the Ro in these areas are consistent with the fluorescence of spores from the same samples (see Appendix 4).

7.9 Conclusions.

Organic maturity indicators demonstrate both across and along strike variations in the maximum depth of burial and burial temperatures within the French Subalpine Chains, with the greatest variation being along strike of this foreland fold/thrust belt. In terms of organic maturity the Cretaceous of the south-west part of the chain can be considered immature, whilst in the north-east the Cretaceous can be considered to be mature to overmature.

Two trends in the increase in organic maturity are recognised; firstly, across structural strike of the fold/thrust belt (roughly from west to east) and secondly, along strike of the fold/thrust belt (from south-west to north-east). This latter trend shows the greatest change in organic maturity and suggests that the north-east of the fold/thrust belt has experienced greater burial temperatures. These results are discussed further and modelled in the following chapter.

Chapter 8 Burial History and Thermal History Modelling of the Subalpine Chains.

8.1 Introduction.

This chapter details the procedures and results of PC-based modelling of both the burial and thermal histories of selected locations within the Subalpine Chains. The key factors which need to be considered when speculating on the thermal evolution of a basin are discussed in the context of foreland fold/thrust belts.

A simple thermal model is described along with the results of modelling the thermal history of specific locations within the Subalpine Chains The assumptions and choice of values for these factors for the Subalpine Chains are discussed. The validity of this model is checked by comparison to measured values of the organic maturity of the Subalpine Chains (from Chapter 7). The likely causes of the increased burial temperatures of the northeast part of the chain are discussed.

8.2 Introduction to basin modelling of sedimentary sequences.

Basin modelling has become an integral part of research in basin studies both in acedemia and in industry. Several different types of model exist. Burial history models are plots of stratigraphic age versus thickness (decompacted or not) and have become a common tool in basin analysis (van Hinte, 1978; Falvey & Deighton, 1982; Guidish et al., 1985; Angevine et al., 1990; Waples et al., 1992a, 1992b). Geohistory models take the process a step further and incorporate changes in sea-level and palaeobathymetry. Geohistory plots include the contribution from all factors that are believed to affect subsidence; these also can be taken a step further to show purely the affects of tectonic-produced subsidence by the application of isostatic equations, to produce backstripped or tectonic subsidence curves (Guidish et al., 1985; Angevine et al., 1990, Loup, 1992a; 1992b).

Many problems are involved with the modelling of sedimentary successions. They include: 1) dating of successions, for example in areas lacking good zone fossils or with limited biostratigraphic or radiometric evidence (similar problems are discussed by Rudkiewicz, 1988; Wildi et al., 1989; Loup, 1992 and in press); 2) converting ages indicated by fossils into numbers; 3) the choice of timescale used; 4) the unknown effects of unconformities (how much of the succession is missing and what lithologies?); and 5) the empirical nature of correcting sedimentary thicknesses for the effects of compaction (decompaction). With geohistory modelling and backstripping there are the problems of estimating palaeobathymetry and deciding which sea level curve to chose. Added to this for backstripping is the choice of which isostatic equation to employ (Pratt or Airey). There is always the problem that not all basins form by isostatically-driven subsidence (flexural and

thermal subsidence are also important mechanisms in basin formation), so equations which take these into account rather than isostasy must be employed (Angevine et al., 1990).

The modelling in this thesis was carried out to estimate the amount of extra burial that the northeast part of the chain has undergone. As indicated by the study of clay mineralogy of the Hauterivian (Chapter 6) and the study of vitrinite reflectance and spore colouration (Chapter 7). To this purpose a simplistic thermal model of the Subalpine Chains and used to produce thermal models of specific locations within the Subalpine Chains.

8.3 Thermal modelling of sedimentary successions.

8.3.1.Controls on subsurface temperature.

Several intrinsic and extrinsic factors govern subsurface temperatures (Garven & Freeze, 1984; Deming & Chapman, 1985; Allen & Allen, 1990) and are listed below:-

i) thermal conductivity, this in turn depends on the matrix conductivity (framework mineralogy and percentage of fine grained material), the porosity of the rocks, the temperature of the rocks and the nature (density and vicosity) and volume of the pore filling fluid. The fundamental importance of thermal conductivity to conductive heat transport and heat flux (q) is shown by Fourier's law:

$$q = -K(dT/dy) \qquad (8.1)$$

where K is the coefficient of thermal conductivity, T is the temperature at a given point and y is the coordinate in the direction of temperature variation (n.b. this applies only to one dimensional cases; an equation for two dimensional cases is presented in Hagen & Surdam, 1989).

ii) hydraulic conductivity, heat transport by convection will become stronger as fluid-flow rates increase; conversely with lower rates of fluid flow, thermal conductivity dominates the thermal regime.

iii) thermal diffusivity.

iv) climate and surface temperatures.

v) topography within the basin; this essentially determines the water table configuration.

vi) basin geometry; factors such as the size and structure of a basin.

vii) internal heat sources; these are minimal for carbonates, but potentially high for volcanogenic sediments.

viii) sedimentation and erosion.

ix) heat flow; this combined with the thermal conductivity governs the geothermal gradient (g). The relationship is:

$$g = q/K \qquad (8.2)$$

where q is the heat flow and K the coefficient of thermal conductivity. In areas devoid of active tectonics and/or volcanicity heat flow appears to be inversely related to the age of the rocks and crustal thickness (see Figs 8.1a and 8.1b).

Fig. 8.1a Summary of the typical heat flows associated with the various types of sedimentary basins (Allen & Allen, 1990). Fig. 8.1b The relationship between crustal thickness and heat flow density (Teichmüller & Teichmüller, 1986; Teichmüller, 1987).

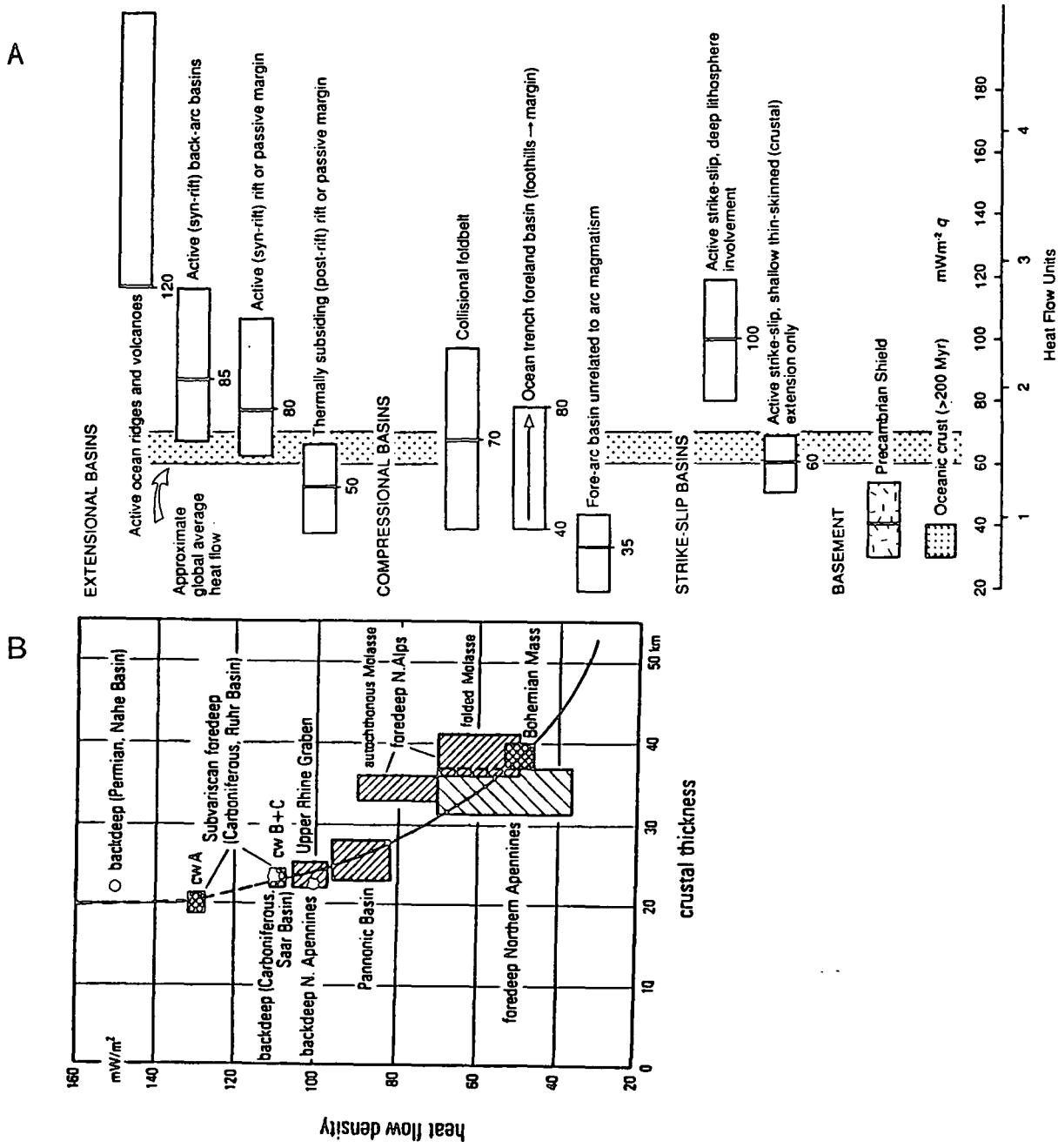

8.3.2. Thermal characteristics and subsidence of foreland fold/thrust belts.

8.3.2 (a) Thermal characteristics of foreland fold/thrust belts.

Foreland basins are typically cooler than other sedimentary basins and have been referred to as hypothermal (Robert, 1988; Allen & Allen , 1990), since they have not had the time to re-equilibrate thermally, thickening of the lithosphere and commonly large amounts of "cold", low conductivity, sediments have been deposited within them at high sedimentation rates (Kominz & Bond, 1986). As a result geotherms are likely to be reduced to around 20°C to 24°C/km. Fig. 8.1a suggests that heat flow will have increased from around 50 mWm^{-2} to around 70 mWm^{-2} with the change from a thermal subsiding passive margin to a collisional foldbelt. However, with the increased crustal thickness the geothermal gradient will be lowered (see equation 8.2) (Teichmüller & Teichmüller, 1986; Teichmüller, 1987). Low present-day geothermal gradients were recorded by Deming & Chapman (1985) in the Utah-Wyoming thrust belt using bottom-hole temperatures, and give gradients between 23°C/km and 24°C/km. Deming & Chapman (1985) estimated a heat flow of 60 (+/- 8) mWm^{-2} for the Utah-Wyoming thrust belt.

Further thermal perturbations in foreland areas are produced with the emplacement of tectonic loads, and the migration of fluids associated with forelands (both during and after formation) also play an important role in the thermal evolution of foreland fold/thrust belts. Numerous papers have been written on the subject of thermal evolution of fold/thrust belts based on both deductive studies of thermal data from fold/thrust belts and theoretical modelling (e.g. Brewer, 1981; Angevine & Turcotte, 1983; Bustin, 1983; Edman & Surdam, 1984; Furlong & Edman, 1984; 1989; Edman & Furlong, 1987; Warner & Royse, 1987; Underwood et al., 1988; Deming & Chapman, 1985; Yonkee et al., 1989; Lewis & Hower, 1990). The models of thermal evolution presented by the above authors typically include one or more of the following mechanisms of increased heat production: (1) normal burial heating via both tectonic and stratigraphic burial, (2) thermal inversion (or disequilibrium) by emplacement of a thrust sheet with a hotter base producing the 'sawtooth' geotherm profile seen in many models; and (3) frictional heating next to thrust planes. Frictional heating in thrust belts has been considered to have been important only locally (Bustin, 1983; Underwood et al., 1988). Although Brewer (1981) does argue for its importance in producing a zonation in metamorphic minerals next to large scale thrusts involving crystalline basement. In thin-skinned thrust belts such as the Subalpine Chains the effects are likely to be negligible. The major factor against frictional heating being important on anything larger than a local scale is the likely removal of heat generated along the fault plane by advective means. The development of 'sawtooth' geotherm profiles (thermal inversion or disequilibrium) is potentially important in regions of thick (> 10km) overthrusts which usually involve crystalline basement, but in thinned-skinned fold/thrust belts (such as the study area for this thesis) the affect is geologically ephemeral, so thermal

equilibrium is maintained. Any temperature inversion produced is likely to dissipate over a geologically short period, to produce a monotonically increasing geotherm from the surface downward. What is important within thinned-skinned fold/thrust belts is the depth to which the footwall is buried, how much the hangingwall is cooled, the fault motion and the rates and timing of post-thrusting erosion and uplift. Some aspects of how geotherms are affected by thrust faulting and subsequent erosion are shown in Figs 8.2. Many models of the thermal evolution of thinned-skinned fold/thrust belts suggest that the hanging wall is exposed at the syn-orogenic surface (Angevine & Turcotte, 1983; Furlong & Edman, 1984) and this aids greatly in the cooling of the upper plate. However, in many cases this is not likely to be the case since higher thrust sheets and/or syn-orogenic sediments are likely to provide a mantle over the area, at least until isostatic uplift and erosion force the exposure of the hanging wall.

Likewise both theoretical models (Oliver, 1986; Ge & Garven, 1989; Deming et al., 1990) and studies of geological evidence (such as heat flow patterns, Hitchon, 1984; Majorowicz et al., 1984; Bethke & Marshak, 1990; Bethke et al., 1991; Sverjensky & Garven, 1992) have shown the relationship of fluid migration to temperatures and heat flow in foreland areas. In forelands, areas of increased heat flow and geothermal gradients and the location of mineral and hydrocarbon deposits (see Fig. 8.3) can be explained by the basin scale circulation of groundwater driven away from the newly formed mountain belt under the force of gravity to the shallow edges of the foreland platform. It has been suggested that flow rates of between 1 and 10m yr^{-1} can be achieved and sustained for several millions of years (Bethke & Marshak, 1990; Sverjensky & Garven, 1992). Fig. 8.4 shows how gravity-driven circulation of groundwaters can explain high heat flows and temperature gradients on the margins of foreland basins such as the heat flow distributions described by Hitchon (1984) and Majorwicz et al. (1984) from Alberta. Higher temperature gradients and geotherms are restricted to the front of the fold /thrust belt where these fluids discharge, whilst the topographically higher fold/thrust belt is cooled with the influx of meteoric water (rainfall). Subsidence driven compaction fluid flow and fault related fluid flow (seismic pumping and fault valving, as described by Sibson, 1981; 1990) during the formation of the fold/thrust belt may both contribute to this but are likely to be of relatively minor importance. Both are relatively short-lived, also subsidence driven compaction fluid flow produces very small fluid flow rates and is dependent on the permeability architecture in the basin (Bethke and Marshak, 1990; Deming et al. 1990), whilst the effects of seismic pumping and valving will only be localised to the area (100m to 200m perhaps, suggested in Hooper, 1991) of the fault which is providing the conduit for migration. In Chapter 5 the field relationships, petrography and isotope geochemistry of syn-tectonic veins within the Subalpine Chains were described. From isotopic compositions reported in Chapter 5 it can

be seen that some hot fluids have migrated through the thrust belt during deformation. However, it is likely that these events were relatively short-lived and restricted in extent.

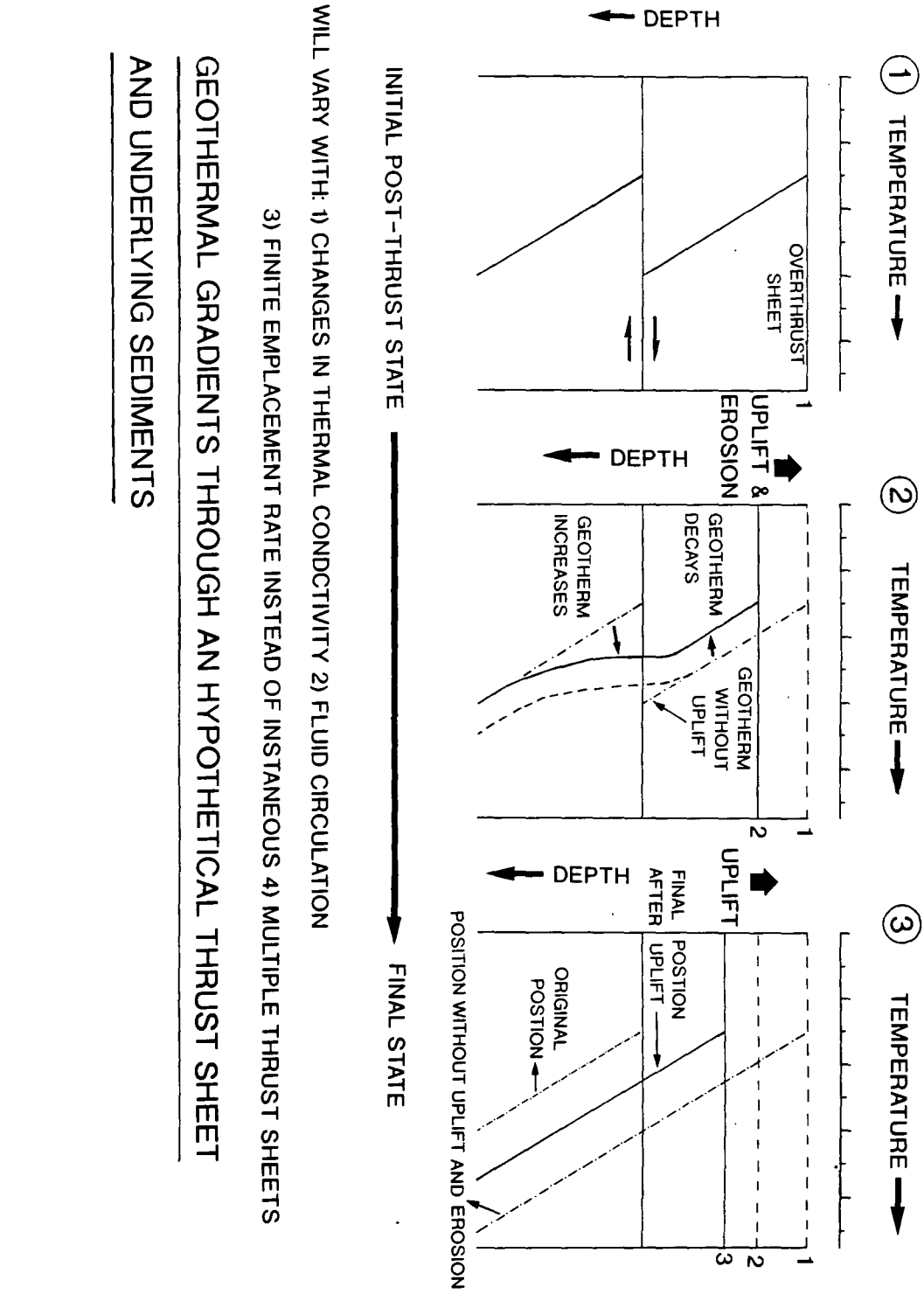

Fig. 8.2 (previous page). Changes in the profile of a geothermal gradient across a hypothetical thrust sheet. Stage 1 is the immediate post-thrust state, a 'saw-tooth' profile is produced due to differences in the temperature of the hanging wall and footwall. Stage 2 sees uplift and erosion, so the geotherm in the upper sheet (in the hanging wall) decay whilst the geotherm in the lower sheet will increase due to deeper burial. State 3 sees attainment of thermal equilibrium and a monotonically increasing geotherm. Note that the final position of the geotherm after uplift and erosion is lower on the temperature scale than the position without uplift and erosion.

From the above discussion, it can be suggested that normal burial heating via both stratigraphic and tectonic burial is the most likely cause of thermal perturbation within foreland fold/thrust belts. This is shown diagrammatically in Fig. 8.5.

Fig. 8.3 Location of hydrocarbon deposits in relation to fold/thrust belts in the U.S.A and inferred migration pathways. Re-drawn from Bethke & Marshak, 1990).

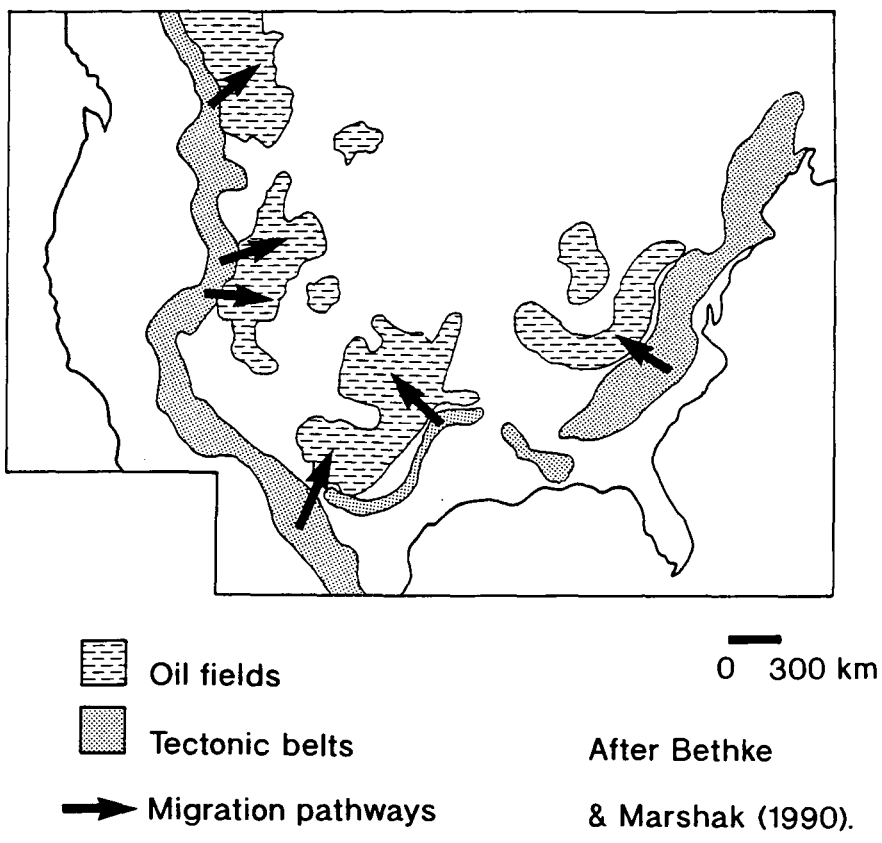

Fig. 8.4 Topographically driven groundwater flow in a hypothetical foreland area. Re-drawn from Garven & Freeze (1984) and Sverjensky & Garven (1992). Note: it is likely that such a fluid flow system would be added too from other fluid sources, such as de-watering of the thrust stack.

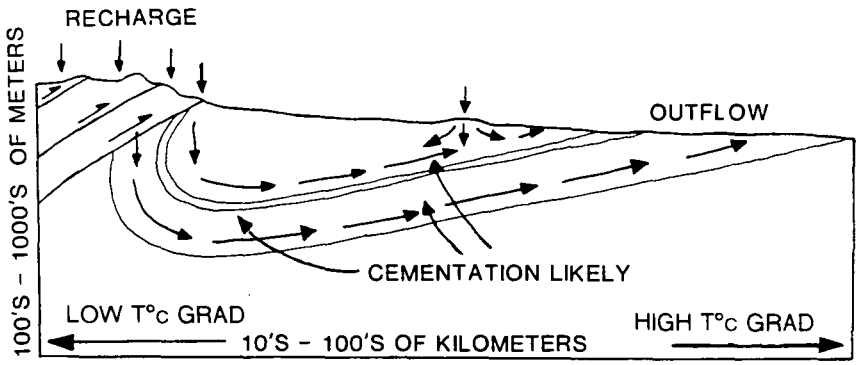

SCHEMATIC CROSS-SECTION OF A FORELAND BASIN, SHOWING HYDROLOGIC FLOW DIRECTIONS AND TEMPERATURE GRADIENTS. BASED ON THE ALBERTA BASIN,

8.3.2 (b) Subsidence characteristics of foreland basins.

Subsidence of foreland basins occurs through flexure of the lithosphere due to the emplacement of thrust sheets, deposition of sediments and the effects of subsurface loads (Beaumont, 1981; Karner & Watts, 1983; Angevine et al., 1990). Tectonic subsidence of these basins reflects the rate of thrusting in the adjacent orogen and the sedimentation rate in the basin. A representative collection of tectonic subsidence curves from forelands and from other types of basin is shown in Fig. 8.6. Subsidence history curves from forelands are typified by 1) the sudden onset of rapid and often considerable subsidence coinciding with foredeep formation, 2) a segmented profile, reflecting discontinuous loading and 3) high rates of flexural uplift ('re-bound') with the removal of the original load. These characteristics can also be seen in more simplified burial history curves for the Subalpine Chains and the Swiss Molasse basin (e.g. Lemcke,1974; Moss, 1992; see Fig. 8.7). Prior to the onset of foredeep subsidence the tectonic subsidence curves for foreland areas shown in Fig. 8.6 show typical passive margin style subsidence. This same pattern is also seen in the burial history plots of Lemcke (1974) and Moss (1992) and in geohistory plots presented by Funk (1985),Rudkiewicz (1988) and Wildi et al. (1989) and tectonic subsidence plots (Loup, 1992a; 1992b). The plots shown in Lemcke (1974) and Moss (1992) also clearly

show the post-orogenic uplift of the western Molasse basin and the Subalpine Chains (see also Fig. 8.7).

Fig. 8.5 Increased burial of a former passive margin stratigraphy due to the emplacement of tectonic loads and the deposition of syn-orogenic sediments.

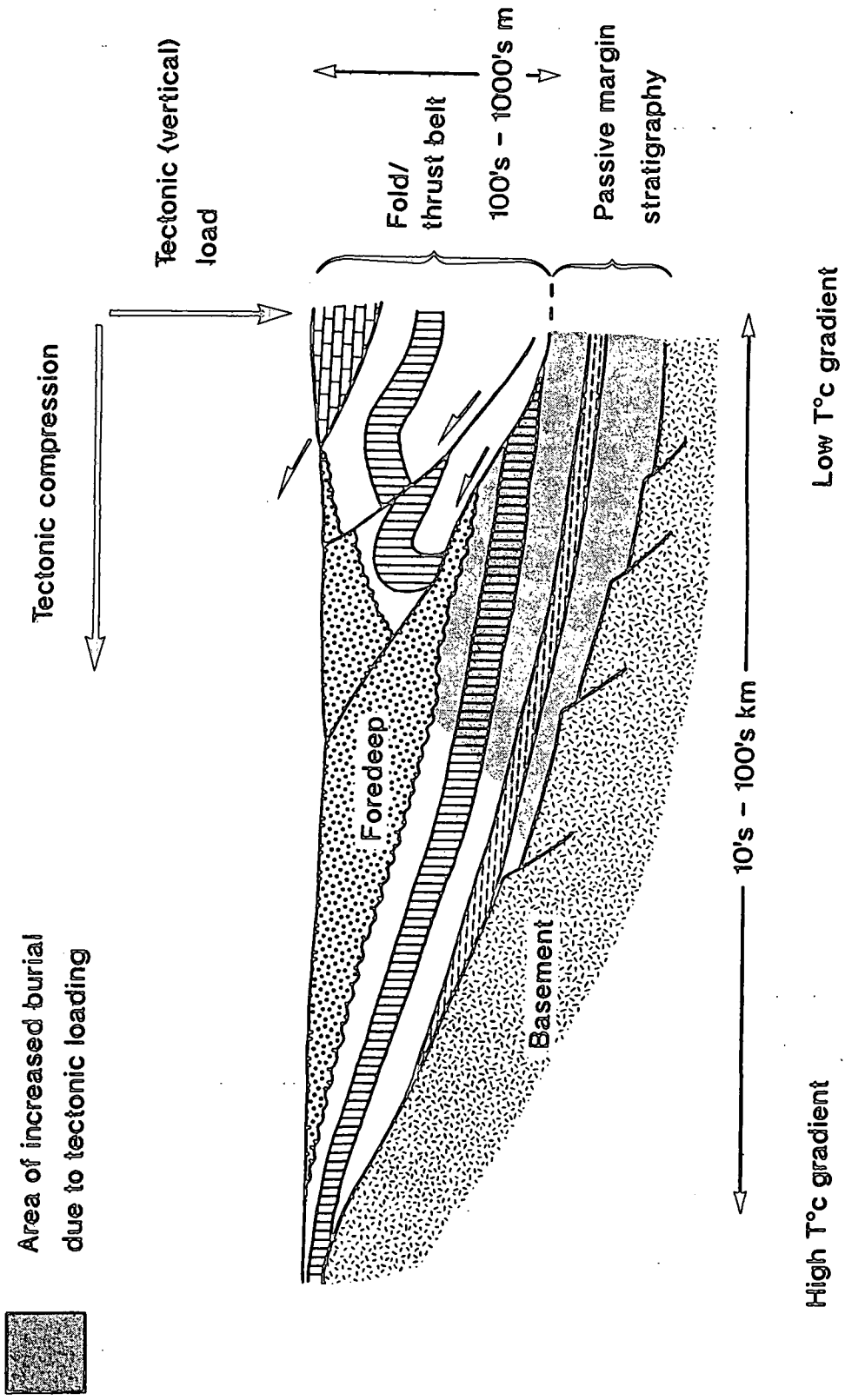

Fig. 8.6 Representative subsidence history curves from a variety of different tectonic settings including forelands (from Angevine et al., 1990).

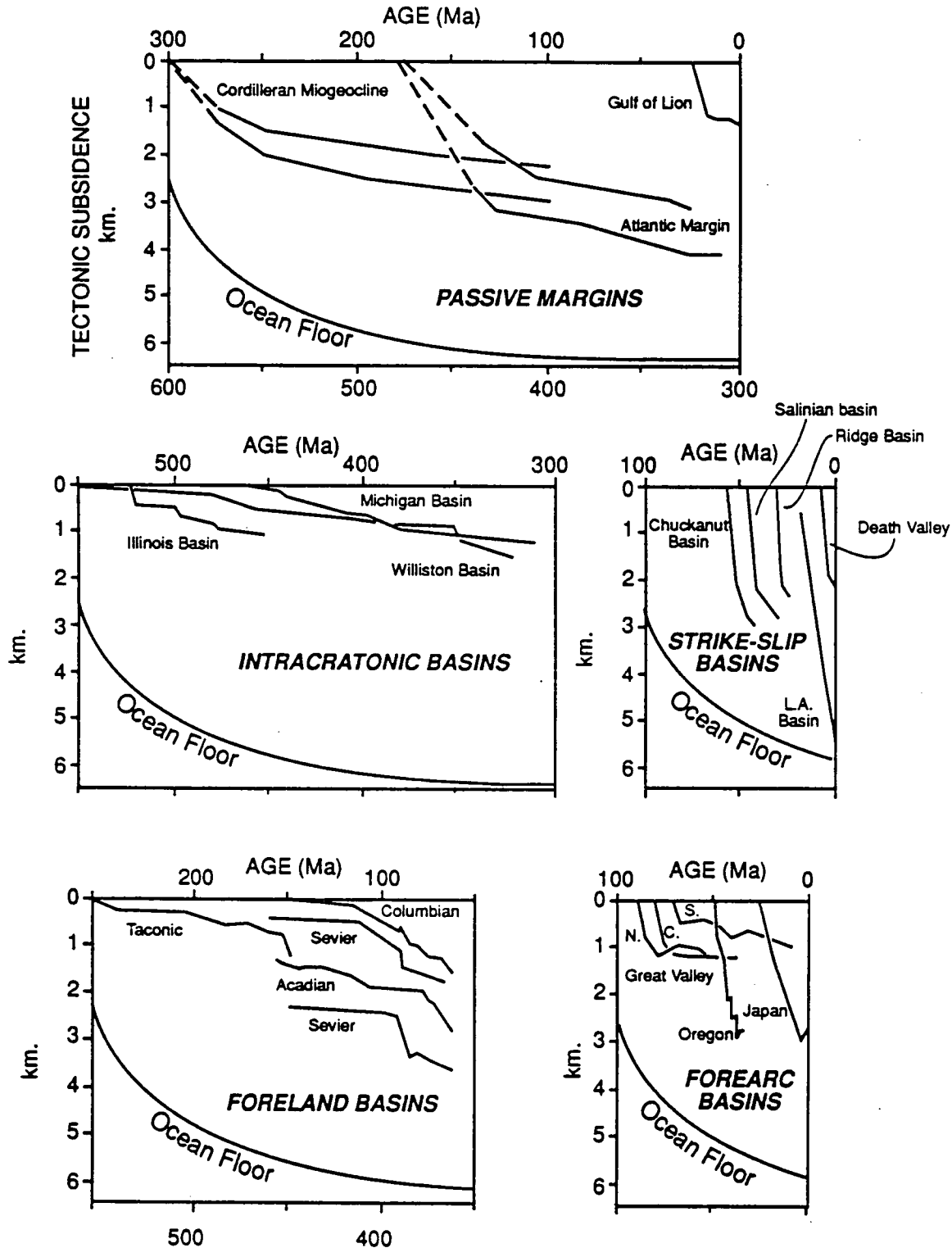

8.4 The thermal model and results of the thermal and burial history modelling.

One dimensional burial history models are used in this thesis to provide a framework for modelling the thermal history of specific locations within the Subalpine Chains (a similar approach has been used by Kalkreuth & McMechan, 1988; Burkhard & Kalkreuth, 1989; Waples 1990; Waples et al., 1992a; 1992b). The modelling was carried out using the Basinmod Modular Basin Modelling software. It should be noted that this software package was designed primarily to model borehole data from hydrocarbon provinces in sedimentary basins such as the North Sea and not faulted and uplifted areas such as the Subalpine Chains. The results of the modelling are presented and shown in Fig. 8.7 and have also been described in Moss (1992). In the following, firstly the results are briefly described, then the assumptions and selection of values used in this modelling are described and discussed.

A simple thermal model was used in the production of the models shown in Fig. 8.7. The assumptions and choices of values behind this model are described in section 8.5. The following conditions were used in the thermal model:

heat flow	$70mWm^{-2}$
geotherms	131 Ma to 32Ma = 30°C/km
geotherms	32 Ma to 0 Ma = 20°C/km

8.4 1 Description of the results.

The plots shown in Fig. 8.7 bring out several features of the burial history of the Subalpine Chains. In the south-west, after a period of uplift and erosion in the Paleogene, the rate of burial increased with the onset of molasse-style deposition (plots for the St. Lattier borehole, Villard-de-Lans and Pic d'Oeillette). However, this depositional event was not long enough to cause significant thermal maturation of the Mesozoic units of the Subalpine Chains, except for stratigraphically deeper units such as the mid-Jurassic (Oxfordian). In the St. Lattier borehole on the western front of the Vercors massif Miocene molasse sediments are only 590m thick (BRGM, 1975). To the east of this locality, actually within the Vercors massif, the Miocene deposits were probably much thicker, in the region of 1200m (now preserved in synclinal cores, such as the one at Villard-de-Lans and Lans-en-Vercors). This is deduced from the Ro values and the clay mineralogy of the Hauterivian (see sections 7.4 and 6.4), which show that the Mesozoic rocks have experienced a slightly higher degree of thermal alteration than the same horizons farther to the west (see Figs 6.11 and 7.5). Farther to the north-east, hydrocarbon exploration boreholes to the west and south-west of Annecy, at Chapery, Poisy and Chavanod (these boreholes are located on Fig. 7.13, Sv 101 *etc,*) show the Miocene to be up to 1950m thick

Fig. 8.7 Burial history models for several locations in the Subalpine Chains with isotherms predicted by the thermal model shown. For simplicity only two horizons are shown; they are the base of the Hauterivian (the lower of the two) and the upper (stippled) horizon is the base of the inferred Tertiary load (foredeep sediments and/or tectonic loads).

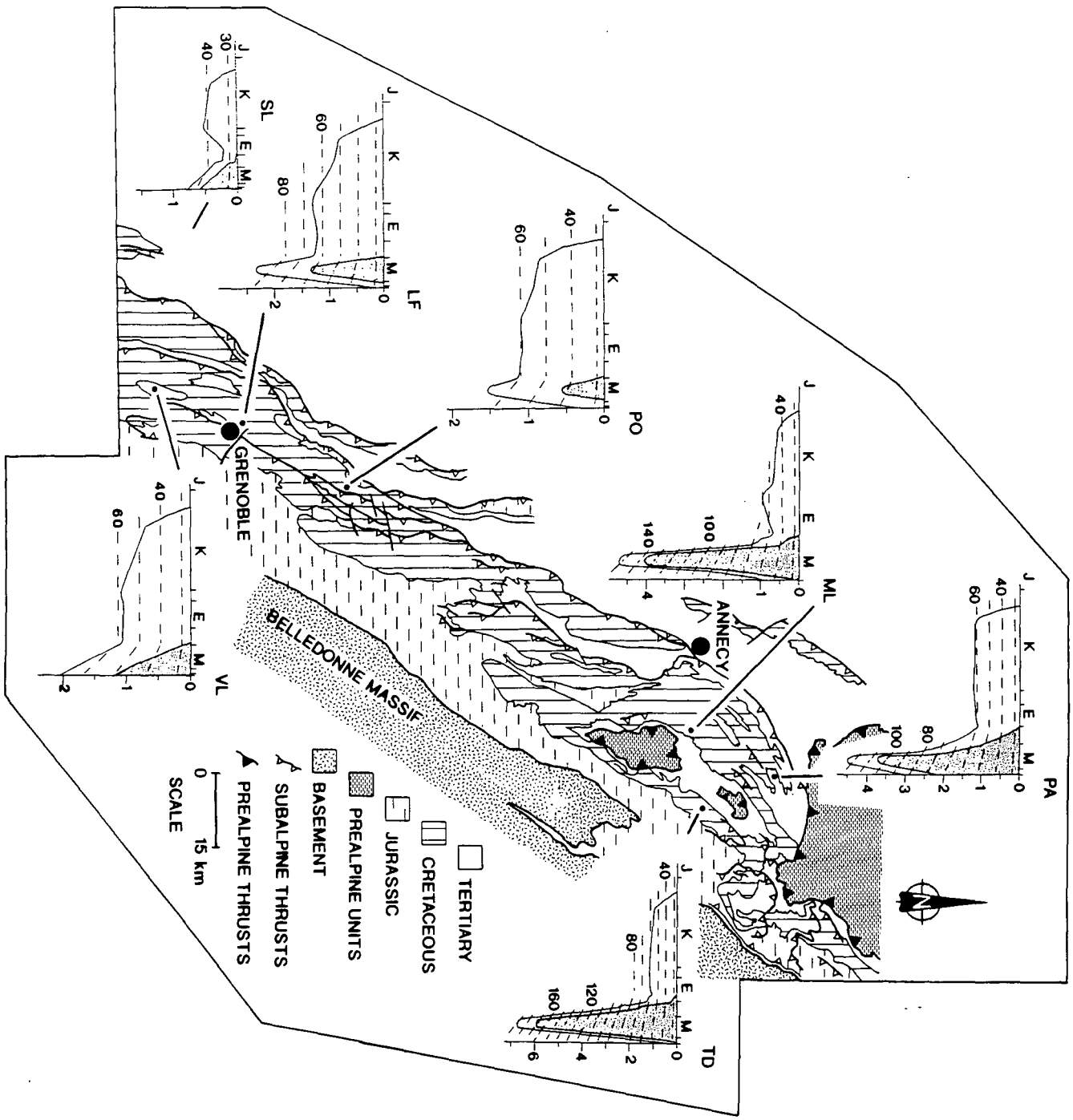

(Michel & Caillon, 1957). This increase in the thickness of the molasse may reflect the fact that the Pre-alpine thrust sheets, emplaced in the upper Oligocene on to the Subalpine Chains to the east/north-east of these localities, provided a far greater quantity of detritus to the molasse basin in front (i.e. to the west) of the north-east part of the Subalpine Chains (the Bornes, Aravis, Platé and Haut-Giffre massifs) and the presence of a depositional trench at this time.

The greater effects of foredeep formation on the thermal history of the north east part of the chain compared to the south west of the chain can be seen in Figs 8.8a,and 8.8b. Fig. 8.8a shows the temperature rate (i.e. the increase/decrease in temperature versus time) for the top Hauterivian calculated for Villard-de-Lans and Tardevant (see Fig. 8.7 for location) using the thermal model. Both show a similar Mesozoic temperature rate with a notable increase during the deposition of the Urgonian corresponding to a higher rate of sedimentation (the 'Barremian crisis' of Arnaud, 1988; see also section 2.3.4). However they differ dramatically in the Tertiary, with only a slight perturbation in the temperature rate in the plot for Villard-de-Lans. The temperature for the top Hauterivian at Tardevant increases dramatically with burial below foredeep sediments and tectonic loads, then decreases with uplift of the area. Fig. 8.8b show the calculated maturity (in Ro) versus time curves for four of the localities modelled and shown in Fig. 8.7. Two are from the southwestern part of the chain (Pic d'Oillette and La Fontanil, in the Chartreuse). The maturity of the Mesozoic units in these two localities shows no perturbation during foredeep formation. The values of predicted Ro compare well with the calculated values of Ro for the Mesozoic of the Chartreuse (see Fig. 7.4). The other two curves shown are from locations in the north-eastern part of the chain (Tardevant, Aravis and Mont Lachat, Bornes), in both there is a marked increase in the maturity of Mesozoic and Tertiary during foredeep formation. In particular in the Tardevant profile there is a very rapid increase in maturity with time during the Oligocene and Miocene. By comparison to Fig. 7.6, it can be seen that the calculated final Ro values for the two localities are broadly similar to the recorded values for the same areas (differences in the calculated maturity (Ro) and recorded values of Ro are discussed in section 8.6).

Several different models (with differing thicknesses of Tertiary burial) were tried, the results described above (in Fig. 8.7) produced the 'best fit' with the measured Ro data (described in Chapter 7). This is discussed in section 8.6. However, before this is discussed the assumptions and choices of values in those assumptions are described in more detail.

Fig. 8.8a Temperature rate for the top Hauterivian at Villard-de-Lans. and temperature rate for the top Hauterivian at Tardevant. See Fig. 8.7 for locations.

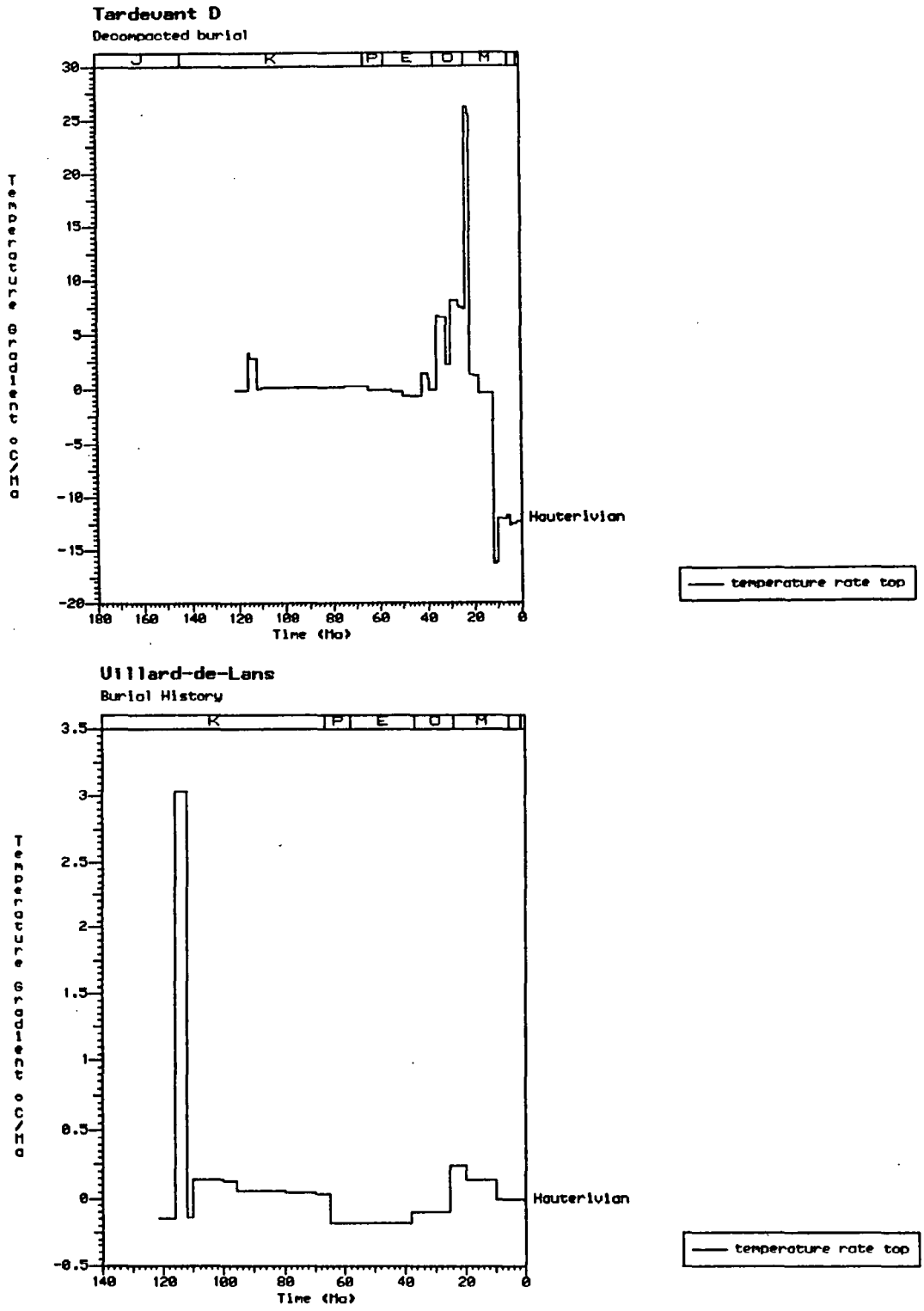

Fig. 8.8b Maturity (Ro) versus time curves for four locations that were modelled. The locations are shown in Figure 8.7. The profiles are, unless otherwise stated, maturity bottom. Haut.= Hauterivian; Tav. ssts= Taveyannaz sandstones; Kimm.= Kimmeridgian. Any differences between the calculated final Ro values of the horizons and the recorded values shown in Figs 7.4 and 7.6 could be due to a number of factors which are discussed in section 8.6 and the fact that the recorded values may be from slightly different positions in the stratigraphy than the calculated profiles shown.

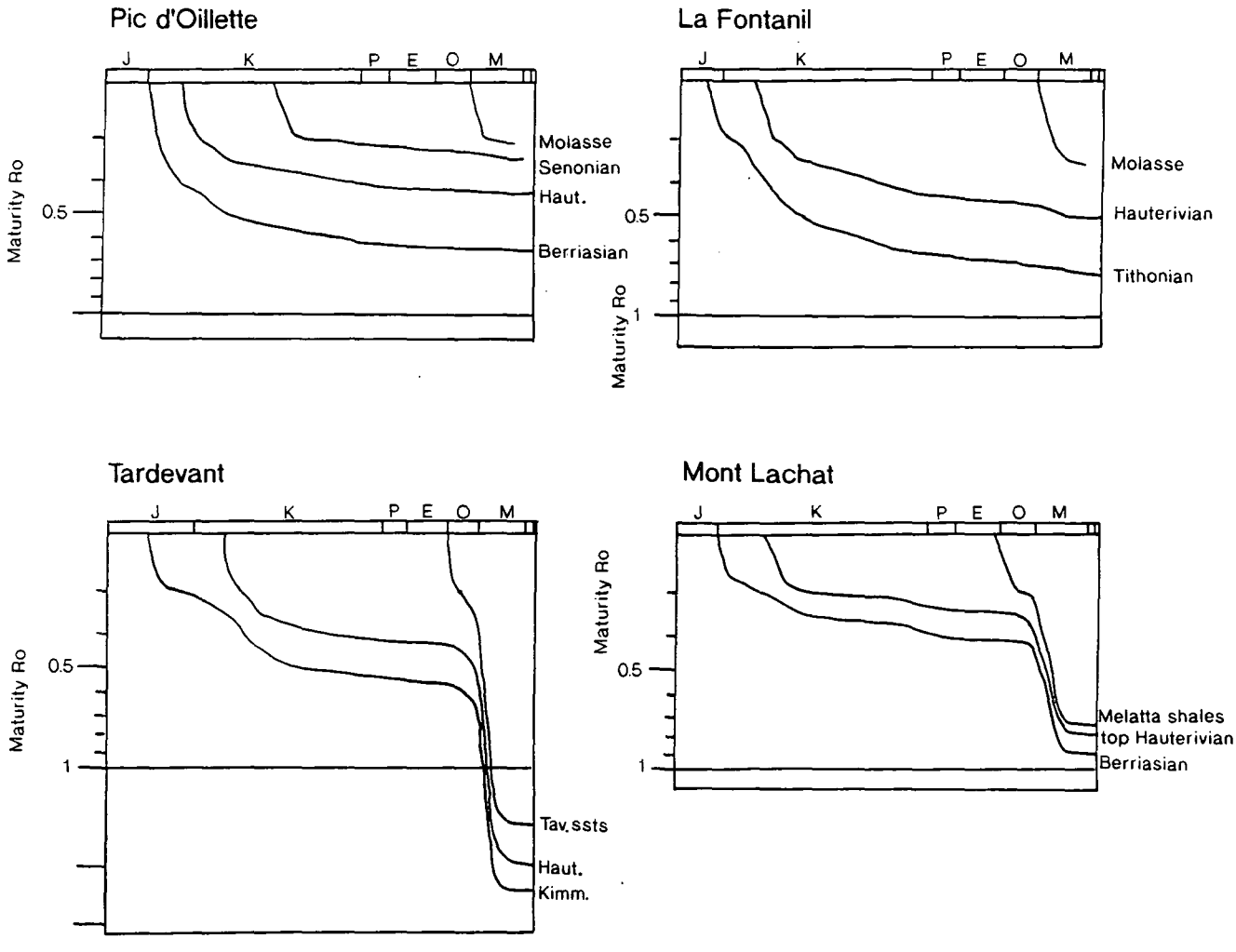

8.5 Principal assumptions used in the modelling and the selection of values used in the modelling.

8.5.1 The principal assumptions used in the modelling.

The following are the principal assumptions that were made during this modelling:

i) no radiogenic heat sources within the basin,

ii) no convective heat transport is considered in the 1-D model; heat transfer is by conductive means,

iii) equilibrium thermal conditions, i.e. heat flow at the base is equal to that at the surface,

iv) similar geotherms are considered to have affected the area,

v) uplift occurred soon after thrusting,
vi) uplift occurred at a constant rate,
vii) surface temperatures are modelled as remaining constant.
These assumptions i) to iii) are similar to assumptions made by Waples et al. (1992a) in their modelling of a single well from Hokkaido, Japan. Assumptions iv) to vi) were used to model the Subalpine Chains in the absence of any hard data to the contrary. Assumption vii) was used because the models are not true subsidence curves but assume that deposition occurred at zero metres elevation, so an average surface temperature was used.

8.5.2 Uplift and residence times.

Very little hard data are available on the timing and rate of uplift of the Subalpine Chains after the end of the collisional events responsible for uplifting sediments originally deposited below wave base (several hundred metres in the case of some of the Tertiary flysch and Mesozioc units) and near wave base (in the case of some of the molasse units) to heights of more than two thousand metres above sea level. The timing and rate of uplift are important because they will have affected the residence time of any given unit at a certain temperature (see section 8.3.2 (a)). All modelling was done using the assumption that uplift occurred instantaneously after the final episode of burial and thrusting. Following this assumption, episodes of thrusting can be roughly approximated by using shortening rates within the Alpine arc (Butler, 1989a; 1992b) and the dating of the youngest sediments in footwall localities (Mugnier et al., 1990) to estimate the dates of deformation (see also section 2.6.4). For the north-east part of the chain deformation began during the Oligocene (Burkhard, 1990), whilst more external areas, such as the south-west part of the chain, experienced deformation much later in the Tertiary (mid- to end- Miocene, Burkhard, 1990; Mugnier et al., 1990). Deformation ended in the Late Miocene (see discussion in Burkhard, 1990). Timing of the uplift and exhumation of the external crystalline massifs based on fission track and K/Ar isotope data (see Mugnier et al., 1990, for references and discussion) can also be used to constrain the timing and rate of uplift of the Subalpine Chains. Burkhard & Kalkreuth (1989) used the timing and rate of uplift of the crystalline Aar massif to estimate a rate of uplift of between 0·5 - 1mm yr^{-1}, starting at 12 Ma to 6 Ma respectively for the Kander Valley region of the Swiss Helvetics. Subsidence history curves for the Swiss Molasse Basin presented by Lemcke (1974) show an average net rise of 0·3-0·4 mm yr^{-1} starting in the late Miocene.

There are some published data on the recent rate of rock uplift (as opposed to surface uplift, see England & Molnar, 1990, for discussion) within the Subalpine Chains. From re-levelling studies Fourniquet (1977) put the rate of present uplift of the St. Pierre de Albigny area of the Bauges at 1mm yr^{-1} (1km Ma^{-1}). This seems unrealistically fast. Vernet (1980), also from re-levelling studies, gave more realistic values for the rate of uplift of the Cluse d' Iseran (around Grenoble) and the Arve valley (in the north-east of the

chain) of 0.3mm yr^{-1} (0.3km Ma^{-1}) and 0.4mm yr^{-1} (0.4km Ma^{-1}) respectively. Kaelin et al. (1991) used compaction trends derived from studying sonic and density logs to estimate missing stratigraphic thicknesses in the Swiss Molasse Basin and so calculate the rate and starting date of uplift, which they put at 0.5mm yr^{-1}, starting at 12 Ma. The starting time of uplift for the Subalpine Chains is similar to the values suggested by Mugnier & Menard (1986), estimated by dating of the uplift and cooling of the external basement massifs, and by Butler (1989a; 1992b), estimated from shortening rates across the Western Alps, and by Mugnier et al. (1990). Using the values quoted by Vernet (1980) uplift and erosion beginning at around 12-10 Ma could account for the present relief and level of erosion of the Subalpine Chains. This was the value used in the modelling, assuming the rate of uplift was constant throughout this period.

From the above discussion it is possible that periods of residence time at maximum burial depth are likely to be short, in the region of 5-6 Ma, some authors, notably Lemcke (1974, his figure 5) and Schegg (1992a, his figure 5), show much shorter periods (roughly 1 Ma) at maximum burial depths. However, given the length of time between the onset of foredeep sedimentation and uplift, the slowness of Alpine convergence and the inertia of heating and cooling rocks, broader burial history curves are more realistic. Burkhard & Kalkreuth (1989) discussed this point at greater length.

8.5.3 Stratigraphic input to the modelling.

The basic stratigraphic data (thicknesses and ages) used in the modelling are shown in Figs 2.8 and 2.11. These data are based on information from numerous French works summarised in Debelmas & Kerckhove (1980), Debrand-Passard et al. (1984) and several unpublished Ph.D. theses (Rivano-Garcia, 1978; Nicolet, 1979; Delamette, 1986; Chaplet, 1989; Deconinck, 1984; Lateltin, 1988; Detraz, 1989; Villars, 1992). Dating of sediments (always a possible source of error in burial history curve construction) at the localties modelled was carried out principally using facies correlation to sections where a biostratigraphy has been established. Owing to the known facies diachronism in the Helvetics, Wildi et al., (1989) speculate that errors of up to 3 Ma could be introduced into any burial history models by using facies correlation.

8.5.4 Decompaction of the Subalpine Chains.

The Basinmod program was used to decompact the curves assuming that the original thickness of the sediments was reduced by a predictable amount according to the lithology and the depth of burial. Fig. 8.9 shows a comparison between a burial history plot uncorrected for compaction and the decompacted curves for the same plot. The basic lithological data for all the plots are shown in Appendix 5. Using these data the program computes the initial porosity for that particular lithological mix; the computed initial

porosities of the units are shown in Appendix 5. These were checked by comparison with thin sections and reference to the porosities of similar recent sediments. Using these porosities the program calculated a compaction factor for each horizon, using the compaction equation chosen, which in this case was the Falvey & Middleton (1981) equation:

$$1/\emptyset = 1\emptyset o + kh \qquad (8.3)$$

where k= lithology dependent constant, h= depth, Ø = porosity and Øo = the initial (uncompacted) porosity at the surface. This assumes that incremental change on porosity is proportional to the change in the load and ratio of void space to grain volume.

It should be noted that this approach neglects the timing of cementation, which has the potential to lessen the effects of compaction, especially if the cementation is early (Gallagher, 1990). However, errors in the predicted burial history curve are likely to be quite small, in the region of +/-100m (Gallagher, 1990). This approach also neglects the possibility of dissolution, overpressure development, hydrocarbon expulsion and possible decompaction during periods of uplift and erosion, all of which can cause departures from the standard porosity-depth relationships employed in decompaction.

Fig. 8.9 This figure shows the effects of decompaction, the hashed lines are the uncorrected curves (really stratigraphic accumulation curves) whilst the dark lines are the compaction-corrected burial curves for La Fontanil in the southern Chartreuse (see Fig. 8.7 for location).

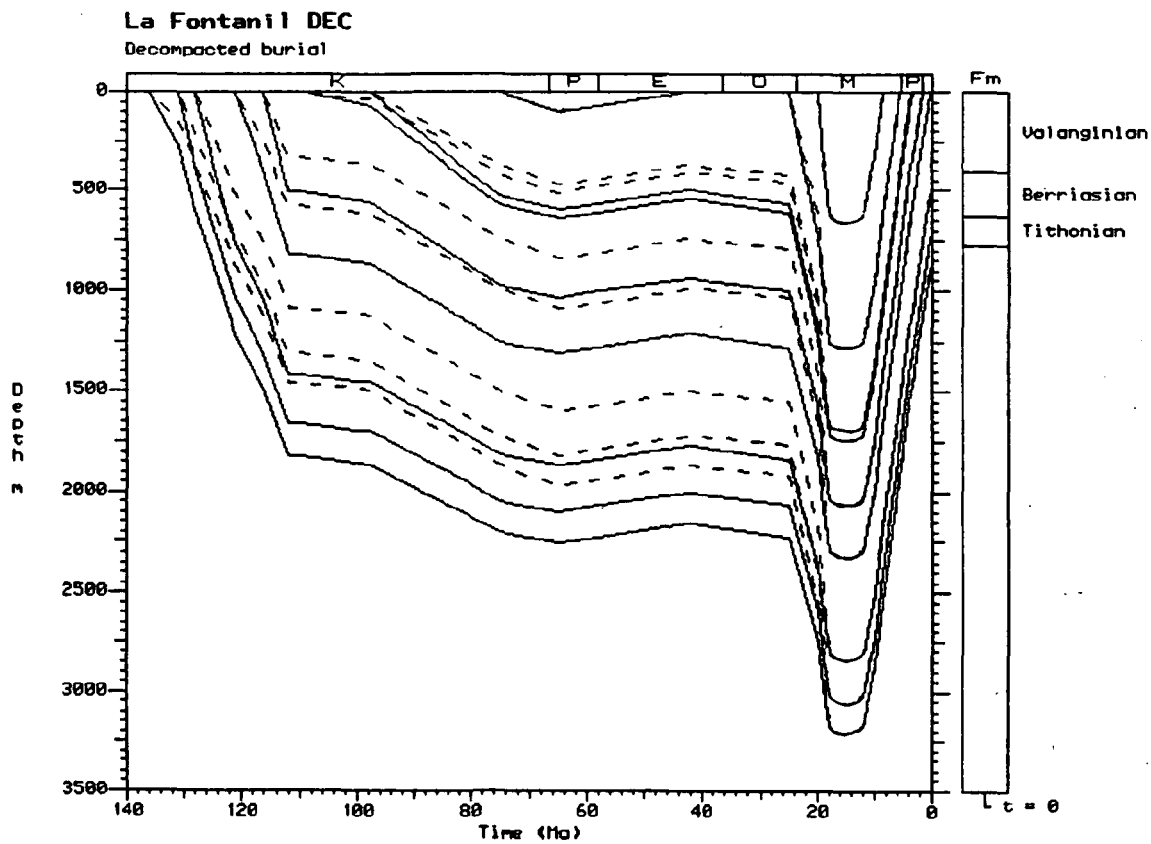

8.5.5 Modelling the thermal evolution of the Subalpine Chains and the selection of values used in the thermal modelling.

8.5.5 (a) Palaeogeothermal gradients

Burial history modelling was performed using the premise that the geothermal gradient was the same throughout the whole of the Subalpine Chains. The sedimentary units of the north-eastern massifs of the Haut-Giffre, Platé and Aravis originated slightly farther to the oceanic side of the continental margin (and are therefore more internal within the Alpine system) than the south-western massifs of the Vercors, Chartreuse and western Bauges (more external). Thus it is possible that they experienced a different thermal history prior to the Alpine orogeny as well as during the collisional event when they quite clearly experienced greater burial depths and temperatures (see Chapters 6 and 7). With no evidence to the contrary it is assumed that any thermal anomalies developed prior to the Tertiary were completely overprinted.

The low geothermal gradient of 20°C/km from 32 Ma to 0 Ma was taken from recorded geothermal gradients in the North Alpine Foreland Basin (Teichmüller & Teichmüller, 1986; Teichmüller, 1987; Rybach & Bodmer, 1980; Rybach et al., 1980). Teichmüller & Teichmüller (1986) and Teichmüller (1987) showed the geothermal gradient (based on Ro measurements from borehole samples) at the front of the northern Alps (Helvetics) of Switzerland to be 20°C/km and to increase away from the Alps to a figure of 23°C/km (see Teichmüller, 1987, figure 38). Rybach & Bodmer (1980) presented details of the present geothermal gradient from the Rhine Graben to the western Swiss Alps; the geothermal gradient on the Alpine side of the traverse (near Luzern) was recorded at <20°C/km (see Fig. 8.10). Rybach et al. (1980) also showed the results of Ro measurements in the Swiss Molasse Basin. Their data show that a low temperature geotherm has been in existence in this area since the deposition of the molasse and like today's geotherm in the area the palaeogeotherm decreases towards the Alps. Prior to foredeep formation the gradient is likely to have been higher, in the region of 25°C/km to 30°C/km, which is typical for old passive margins (Allen & Allen, 1990). The European passive margin formed in lower and middle Jurassic times (200-165 Ma, Lemoine et al., 1986) (see section 2.3) and so can be considered as old.

8.5.5 (b) Heat flow.

The heat flow of 70mWm^{-2} used in the model was taken from values for the heat flow density (HFD) for the Western Alps shown in Della Vedova et al. (1990, see their figure 2). Allen & Allen (1990, see Fig. 8.1a) gave 70mWm^{-2} as typical for collisional foldbelts. Geophysical studies of the Western Alps indicate a crustal thickness of 30-35 km for the Subalpine Chains region (Perrier, 1980; Bayer et al., 1987; see also Fig .2.14). The typical heat flow through such a crustal thickness is in the region of 80 to 60 mWm^{-2}

(Teichmüller & Teichmüller, 1986; see Fig. 8.1b), so the value chosen was assumed to be a good estimate of the likely value of heat flow in the study area.

Fig. 8.10 Geothermal gradients along the Basel-Luzern section, in western Switzerland. From Rybach & Bodmer (1980). A clear decrease in the geothermal gradient toward the Alps can be seen.

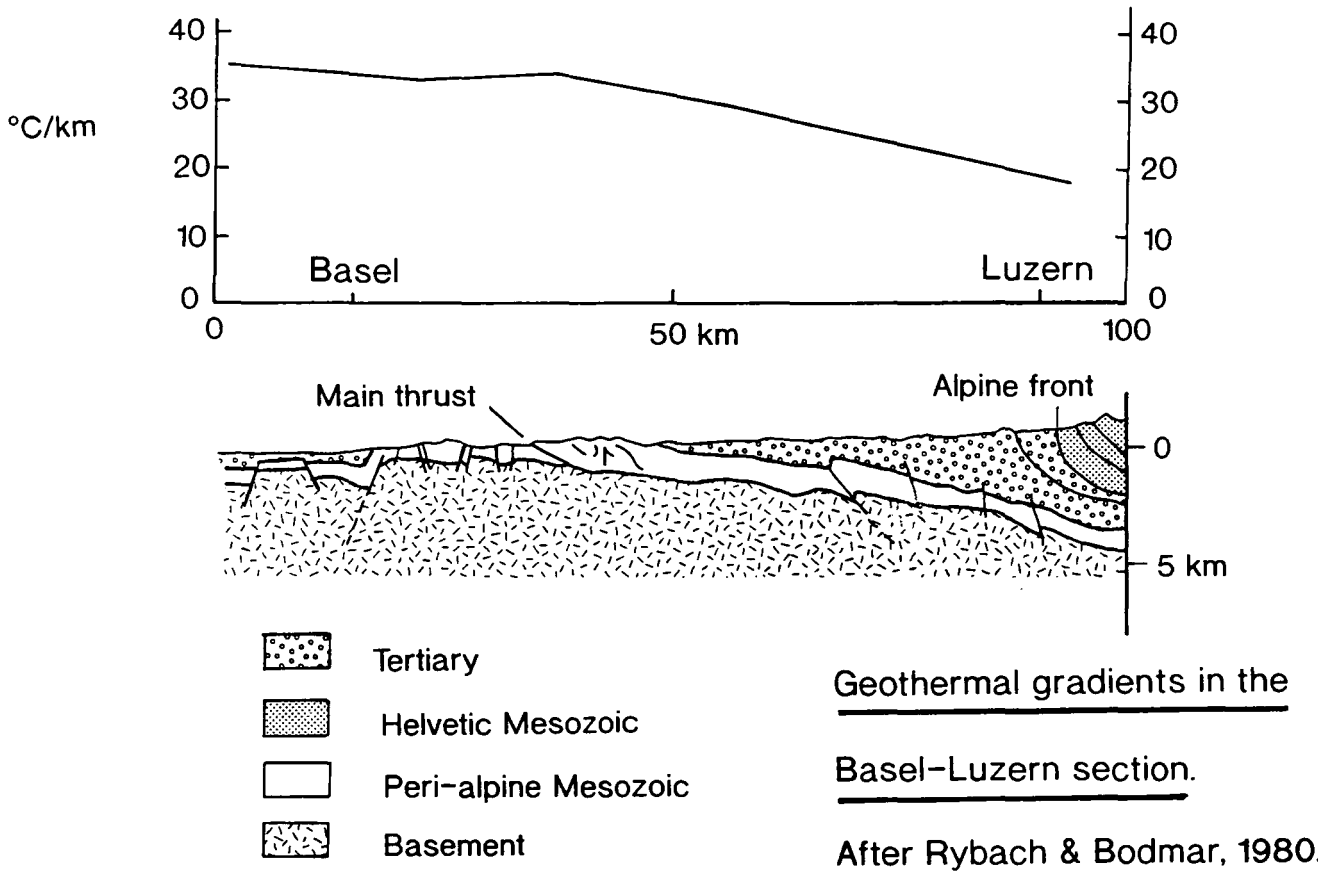

8.5.5 (c) Calculation of maturity.

Modelled thermal maturity was calculated by the Basinmod program using kinetically-based equations of maturation with time and temperature, developed by the Lawrence Livermore National Laboratories (LLNL), California (Burnham & Sweeney, 1989; Sweeney & Burnham, 1990 and section 7.2). These equations were used in favour of other methods such as the Time Temperature Index (TTI) which contains several fundamental errors (see Waples et al., 1992b, for discussion). Interestingly, Waples, who first popularised this method, now recommends the use of kinetic models such as the LLNL equations in its place, even though some authors still persist in its use (Butler, 1992b).

8.6 Comparison of the model results to real data.

Calculated thermal maturity vs depth profiles for each of the burial history models were plotted against Ro values vs depth for each respective area of the Subalpine Chains. Regression analysis was carried out on the plots of vitrinite data and compared to the vitrinite maturity profile calculated by the program using the appropriate burial history model. The match or mis-match between the data set and the thermal model was then used to check the accuracy of the burial history model. This was used to test the validity of each burial history curve. The results are shown in Fig. 8.11. A similar approach was used by Middleton & Falvey (1983) to test their thermal and burial history models of the Otway Basin on the southern Australian continental margin. Any difference between the calculated and the 'real' thermal profile could be due to a number of factors, including mistakes in the decompaction and real depth of burial, miscalculation of the amount of erosion, under- or over- estimation of the size of tectonic loads, the effects of convective heat flow (Schegg, 1992a; 1992b), error in the geothermal gradients used, error in the timing of deposition of certain units (Homewood, 1983; Wildi et al., 1989) and in the timing of emplacement of orogenic loads (Ramsay, 1981; 1989; Mugnier et al., 1990; see section 2.6.3) and miscalculation of the Ro data. It should also be noted that the Ro data were obtained from samples solely from outcrops within the vicinity of the point being modelled and not from an individual borehole, as most commonly seen in the literature. All the values plotted, however, were from individual thrust sheets and not from a mix of units from hanging wall and footwall locations. The generally good first order agreement of the Ro data with the modelled maturity suggests that the values used in the thermal modelling are generally correct.

Thus the northeast part of chain (eastern Bauges and Bornes, Aravis, Platé and Haut-Giffre) must of experienced up to 5km greater depth of burial in the Tertiary. From the geology of the area (see section 2.6) and the burial history plots for the Aravis and Haut-Giffre massifs (see Fig. 8.7), it is apparent that the major cause of enhanced burial of this part of the chain occurred during the Tertiary and the major contribution to this was the of the Pre-alpine thrust sheets. Either by being emplaced onto the Subalpine Chains or by increasing the supply of detrital sediments to the area increasing the thickness of foredeep sediments or a combination of both. This latter point is discussed in section 8.7.

The models are taken to be good first order representations of the thermal history of the Subalpine Chains and can be considered satisfactory. However, they do <u>not</u> represent correct solutions. The number of assumptions involved and the level of data make the attainment of geologically correct models unlikely for the Subalpine Chains. Waples et al. (1992b) came to a similar conclusion when they modelled the thermal history of a single well from Hokkaido, Japan. The modelling was performed to get a rough estimate on the

burial depths of the specific locations of Subalpine Chains had experienced and in particular how much deeper was the northeast part of the chain buried. The results have already been described in Fig. 8.7.

Fig.8.11 Comparison of maturity regression for measured Ro values (see Chapter 7, Figs 7.4 to 7.8 inclusive and Appendix 4) vs. calculated maturity regression from the modelling, plotted against depth for four of the burial history plots shown in Fig. 8.6. Dashed lines are the maturity regression curves for the measured Ro values; solid lines are the maturity regression curves calculated by the burial history plot for each location and the thermal model used. Recorded Ro values are shown by the black triangles. PO = Pic d'Oeilette; LF = La Fontanil; VL = Villard-de-Lans; TD = Tardevant. See Fig. 8.6 for location.

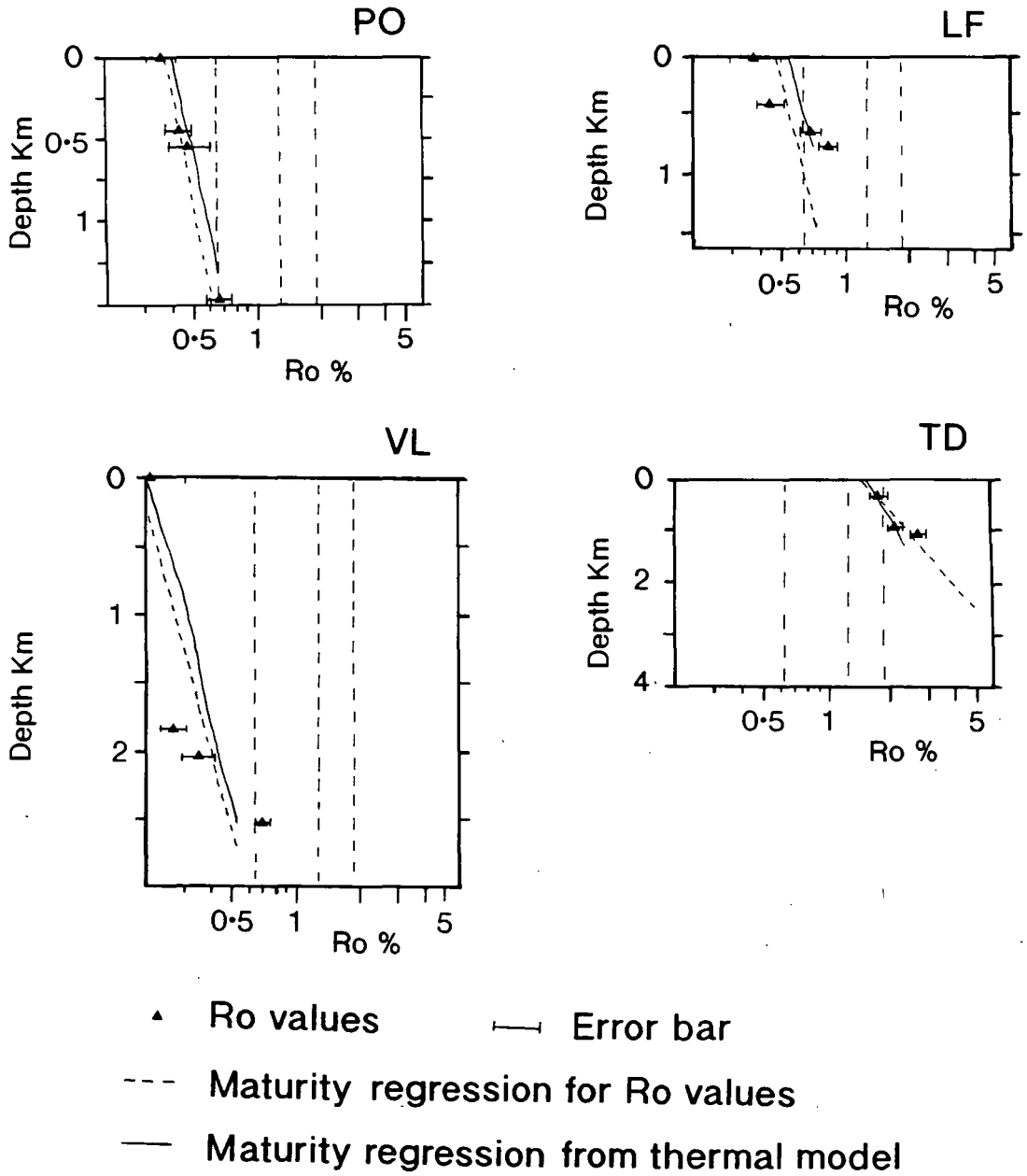

8.7 Discussion.

In section 8.3.2 several mechanisms of producing thermal perturbations in foreland fold/thrust belts was discussed. They were: (1) normal burial heating via both tectonic and stratigraphic burial; (2) migration of hot fluids; (3) thermal inversion by emplacement of a thrust sheet with a hotter base producing the 'sawtooth' geotherm profile seen in many models; and (4) frictional heating next to thrust fault planes. The major factor against frictional heating being important on anything larger than a local scale is that the high fluid content expected with the emplacement of the Pre-alpine sheets (Ramsay, 1981) and the likely significant amount of fluids involved in tectonic deformation of the Subalpine Chains, which would quickly dissipate any frictionally-produced higher temperatures. This suggestion goes against the ideas of Aprahamian & Pairis (1981), who proposed that frictional heating was the cause of an inverse low-grade metamorphic gradient in the Tertiary Taveyannaz sandstones of the Platé Massifs. As regards thermal inversion, it is likely that the units forming the Pre-alpine thrust sheets were not significantly hotter than the Subalpine units they were thrust onto, although the base of the Pre-alpine sheets was probably hotter than the top of the Subalpine units at the time of thrusting. Schegg (1992a; 1992b) has suggested that the migration of warm fluids (see section 8.3.2) has been important in the thermal history of the Tertiary sediments of the Annecy molasse (Plateau des Bornes) and Molasse basin of western Switzerland (i.e. to the front of the Subalpine Chains). This postulated fluid migration produced a second order pattern of slightly higher Ro values (second order to the first order pattern produced by the emplacement of the Pre-alpine klippen). The thermal effects of migrating groundwaters are considered here to be of minor importance for the Subalpine Chains. Even though high heat flows recorded in the Zürich region of the Swiss Molasse basin and several hot springs within the Annecy region (see Fig. 7.13) are believed to be due to the deep migration of groundwater (Dazy & Grillot, 1982; Dazy et al., 1987; Rybach et al., 1987). They are produced by the present-day water-table configuration (i.e. uplifted in the Subalpine/Helvetic region relative to the molasse region in front), so the effect upon the Subalpine Chains would be to promote the 'cooling' of the area as it was uplifted.

Thus it is suggested here that the major contribution to the greater burial temperatures experienced in the north-east of the Subalpine Chains was normal burial heating via tectonic and stratigraphic loading.

A similar attempt to model hydrocarbon generation along a single section through the Jura and Bornes/Aravis (part of the section shown in Fig. 2.20b) has been made by Butler (1992b), who used the TTI method and the peak temperature method (Quigley & Mackenzie, 1988) to calculate maturation. From his results he suggests that maturation occurred in the Subalpine Chains during foredeep subsidence, prior to thrust sheet loading.

The TTI method (used principally by Butler, 1992b) is fundamentally flawed since it assumes that the kinetic reaction involved in organic maturation doubles its reaction rate for every 10°C rise in temperature over a range of temperatures from 30 to 250°C (Quigley & Mackenzie, 1988; Burnham & Sweeney, 1989; Sweeney & Burnham, 1990; Waples et al., 1992b; see also section 7.2). The TTI method was initially designed to predict the Ro of coals, so should not (strictly speaking) be used to estimate hydrocarbon generation. Since the kinetics are very different (Waples, 1992b). The Waples (1980) TTI-Ro calibration was used by Butler (1992b) to estimate hydrocarbon generation windows instead of the more appropriate compaction-corrected TTI-Ro calibration (referred to as CTTI) offered by Dykstra (1987). Although this would not alter the absolute degree of maturity it does change the timing of oil and gas generation. The estimates for the timing of oil generation given by Butler (1992b) for the base of the Berriasian then require modification and based on his figure 11 would begin roughly 5 Ma later than he predicted. Another source of error in the modelling carried out by Butler (1992b) is the choice of geothermal gradient (pre-thrust gradient of 28°C/km, post-thrust gradient of 30°C/km). The main justification for the 30°C/km geotherm he suggested comes from the work of Sawatzki (1975) on the distribution of zone minerals in the Thônes syncline. However, the only mention of geotherms in Sawatzkis thesis is the following: *"Laumonite and corrensite are typical for a temperature of formation of 100°C to 200°C. With a normal geothermal gradient of 30°C/km and a surface temperature of 20°C the maximum overburden of the prealpine units is equivalent to an ancient burial depth of 2.7 km and 6 km and to pressures of 0.7 kbar and 6.0 kbar respectively."* Nowhere does Sawatzki (1975) suggest that his results indicate a geotherm of 30°C/km and as was pointed out in section 6.3, the growth of such zone minerals is dependent on many other factors apart from time and temperature and so are unreliable as estimates of geothermal gradients. Further to this there is evidence that the present-day geotherm and the palaeogeotherm (since the onset of molasse deposition) in the Subalpine Chains are unknown but by analogy to western Switzerland much lower, around 20°C to 23°C/km (see section 8.5.5 (a) and Fig. 8.10), and are similar to geothermal gradients recorded from other foreland areas (see section 8.3.2 (a)). Thus palaeotemperatures are overestimated in this model. This invalidates the peak temperature method discussion in Butler (1992b), since with a lower geotherm peak temperatures would be reached at a different time, unless the depth of burial was increased. Given the above discussion the results of the modelling and conclusions drawn by Butler appear to be unsound.

There are two possible causes of the along strike variation in burial temperature: (1) increasing stratigraphic burial in the north-east part of the belt due to increased thickness of foredeep sediments (the favoured method of Butler, 1992b); and (2) increased burial via emplacement of allochthonous thrust sheets and increased intensity of deformation within

some areas of the Subalpine units (i.e. Haut-Giffre, Platé and Aravis, which represent the south-western termination of the Helvetic nappes). Point (1) is less important since it appears there was little difference in the thickness of foredeep sediments in the north-east of the belt compared with the south-west part of the belt (see Fig. 2.11). Although it is impossible to ascertain the exact thickness of the foredeep succession in the north-east part, since the emplacement of the Pre-alpine thrust sheets may have cut out an unknown thickness of the upper part of the succession, it is likely that it was not much greater than 2km (Kübler et al., 1974; Lemcke, 1974; Charollais & Jamet, 1990; Schegg, 1992a). In the Annecy region of the chains there is presently 2km of molasse sediment within the molasse basin (Michel & Caillon, 1957), resting unconformably on the mid-Cretaceous "Urgonian" limestone. This thickness of molasse sediment thins to the south-west to a thickness of between 1.5km and 0.5km, suggesting that there was a less prolific source of detritus feeding the molasse basin in this direction or the existence of a depositional trench in the north-east part of the chain at this time. Point (1) is also less likely since the Kimmeridgian of the southern Jura and the upper Jurassic/lower Cretaceous of the Salève anticline (to the north of Annecy, see Fig. 7.13 and section 7.6) are immature (both have an Ro of less than 0.5). This suggests that neither area has been deeply buried, either in the Mesozoic or in the Tertiary by a thick cover of molasse.

It is considered here that the main cause of the increased burial of the north-east part of the chain was the emplacement of the Pre-alpine thrust sheets on to this part of the belt in the upper Oligocene (as suggested by Ramsay, 1989; Homewood et al., 1986; Lateltin, 1988; Burkhard, 1990; Mugnier & Menard, 1990; see Fig. 2.11), which did not occur in the south-west part of the belt. This Pre-alpine roof was then involved in the folding and thrusting of the Helvetic nappes over the basement massifs of the Aiguilles Rouges and Aar (Ramsay, 1981). This deformation will have further increased the burial of certain areas of the north-east part of the Subalpine Chains (i.e. inverted limbs of recumbent folds, as reported by Goy-Eggenberger & Kübler, 1990, and footwall locations). Of lesser importance is the fact that the north-east part of the study area is the south-west termination of the Helvetic nappe pile, which thickens farther round the Alpine arc into Switzerland to a thickness of 8km (Ramsay, 1981). There are no data to suggest the possibilty of further molasse deposition above these thrust sheets, so they have been modelled with the thrust sheet emplacement as the final burial event in these areas. The importance of the Pre-alpine thrust sheets to increasing the overburden and thermal maturity in the north-east part of the chain has already been noted by Sawatzki (1975), Kübler et al. (1979), Mosar (1988); Gorin et al. (1989) and Schegg (1992a; 1992b).

8.8 Conclusions.

1) The results of thermal modelling suggest that the Haut-Giffre, Platé, Aravis and parts of the eastern Bornes and Bauges massifs have experienced up to 5km greater depth of burial than the Chartreuse and Vercors massifs and western parts of the Bauges and Bornes massifs.

2) This greater depth of burial was produced by two factors, namely, the earlier initiation of foredeep sedimentation and marked differences in the structural style producing differences in the sizes of tectonic loads.

3) It is suggested that the earlier initiation of the foredeep and its sedimentation (mid- to late Eocene compared to mid-Miocene) in the north-east, although not of greater thickness than the foredeep sediments to the south-west, caused the earlier beginning of deeper burial in the north-east part of the chain. This was followed by the emplacement of Pre-alpine thrust sheets, the main cause of burying this part of the chain to a greater depth than the massifs to the south-west.

4) The thermal models presented are considered to be good representations of the thermal evolution of the area, but are not unique solutions and should not be viewed as correct solutions. They are one of a number of possible viable models. A good model is one which is plausible or satisfactory in most respects, a model correct in all respects is beyond attainment given the data set and the uncertainty about the choice of values for certain parameters.

Chapter 9. Thesis conclusions.

9.1 Principal conclusions to the chapters and of this thesis.

9.1.1 Conclusions regarding the diagenesis of the Urgonian carbonate platform.

The Barremian-Aptian Urgonian carbonate shelf deposit is typified by rudist bivalve and peloid/foraminifera limestones. These shelf-lagoonal limestones constitute the bulk of the Urgonian. Rudist limestones similar to those of the Urgonian in other parts of the world are important hydrocarbon reservoirs (e.g. the Poza Rica trend, Mexico, Enos, 1988). A paragenetic sequence for the platform is presented and shows the relative ordering of diagenetic features within the platform and their magnitude. This sequence can be related to subsequent events within the basin, such as sea level falls and uplift. The Urgonian was partially lithified in a marine setting by a variety of marine cements.

A period of mineralogical selective dissolution of the aragonitic part of the rudist shells occurred early in post-depositional history of the platform. This dissolution occurred during meteoric exposure related to a major sea level drop and produced abundant secondary porosity in the appropriate facies. At the same time low Mg-calcite parts of the rudists were stabilised by aggrading neomorphism. The petrography of the shells suggests that this occurred in a shallow subsurface setting. Chemical dissolution at grain contacts and within the cortices of ooids occurred relatively early, along with the mechanical fracture of unsupported ooid rims, micritic envelopes, marine cements and rudist shells.

Final lithification of the platform occurred with the precipitation of equant, drusy spar cements, notably occluding primary and secondary porosity associated with rudists. These are interpreted to be burial cements, although probably not deep burial. Syntaxial overgrowths are also common and probably began to form in a shallow subsurface setting. The transgressive, basal part of the platform is preferentially replaced by a shallow burial dolomite, probably formed by the compactional release of entrapped connate sea-water from the more muddier sections below the platform.

Uplift of the Dauphinois region in the late Cretaceous/Paleogene and the late Miocene to present allowed meteoric fluids to dedolomitize parts of the basal dolomite.

Incorporating all the general conclusions presented in this chapter and in Chapter 3 the following model of diagenesis and lithification of the Urgonian platform is presented.

Stage A: corresponds to deposition of the platform. Diagenetic features formed during this stage included marine cements, micritization, grain repacking. Several brief periods of exposure interupt normal platform sedimentation; however, meteoric diagenesis during these periods was minor due to the prevaling semi-arid climate. The lack of marine cements within fabric selective dissolution porosity shows most dissolution took place during Stage B.

Stage B: corresponds to the exposure of the platform in the lower Aptian, following a more pronounced relative sea level fall. The prevalent semi-arid climate prevented deep, penetrative karstification and resulted in a shallow micro-karst forming upon the exposed upper surface of the platform. Fabric selective dissolution of aragonitic shell material and the stabilization of low magnesium calcite, occurred in the presence of meteoric fluids.

Stage C: corresponds to drowning of the platform in the upper Aptian. This transgression removed the microkarstic surface in some localities; however in others the karstic surface was re-worked by hardground formation in the Albian. During the transgression calcitic silt was dolomitised by the action of sea water moving through the upper part of the former carbonate platform. During this period there is the possibility that 'cold' oceanic waters were pumped into the shelf margin grainstones of the basal section of the platform, leading to the formation of some dolomite. Fluid circulation could have been driven by one or more of three possible mechanisms: 1) oceanic currents encroaching onto the drowned platform; 2) Kohout convection or 3) meteoric-mixing zone driven convection. Early mechanical fracturing of grains continued as the platform was gradually buried.

Stage D: corresponds to shallow burial during the Albian to the end of the Cretaceous. Shallow burial resulted in the release of connate seawater by mechanical compaction of the basinal muds below the platform, causing widespread replacement dolomitization of the platform margin grainstones. Focusing of the fluid flow responsible for dolomitization produced the variable thickness of the dolomite. Precipitation of burial cements from moderately heated meteoric fluids, occluded post-mechanical fracture porosity. Intra-crystalline porosity with the burial dolomites was occluded by calcite The platform was now fully lithified.

Stage E: corresponds to the post Cretaceous to the present day. Basin inversion in the early Paleogene locally led to renewed exposure of the platform. Dedolomitization occurred in some sections. From the Eocene onwards compressional tectonics caused the folding and faulting of the platform (and of the whole succession), and syn-tectonic fluid movement occurred through the platform via fractures (see Chapter 5). Post-Miocene times saw the gradual uplift of the platform. Again dedolomitization of some of the burial dolomites took place.

9.1.2 Conclusions regarding syn-tectonic fluid flow through the Subalpine Chains.

Both field relationships and petrography point to a syn-tectonic origin for the veins. Petrography also shows that much of the fracturing was induced by hydraulic fracturing under cyclic changes in pore pressure, producing 'crack-seal' textures within the veins.

Varied geochemistry not surprisingly indicates a variety of possible fluid sources. The predominant isovariant trend in the ^{18}O isotopes of all the veins sampled (see Fig. 5.17a) indicates the importance of temperature of the porefluids and the likely wide range of temperatures of syn-tectonic porefluids. More depleted ^{13}C values of vein fills within the Urgonian suggest that the Urgonian was an aquifer for fluids which were derived from or had passed through areas of undergoing organic maturation. The overlap in the trace element geochemistry of veins within the Urgonian and shell material and cements within the Urgonian suggests that fluids filling fractures within the Urgonian were influenced by pressure dissolution of the Urgonian.

The temporal and spatial changes in fluid geochemistry suggest that fairly rapid in-migrations of fluids of different sources (and probably temperatures) occurred during deformation within the Subalpine Chains.

9.1.3 Conclusions regarding the regional variations in burial temperatures and the thermal history of the Subalpine Chains.

The transformation of smectite to illite and chlorite via mixed I/S steps and changes in the composition of the I/S have been investigated using one mudstone unit from the study area, the lower Cretaceous Hauterivian. The results of this study suggest that the south-west area of the Subalpine Chains only experienced limited burial and therefore has not been exposed to high burial temperatures. In contrast, in the north-east part of the study area the dominance of illite and chlorite in the clay mineral assemblages and the illitic composition of the mixed-layer I/S indicate that these rocks have experienced relatively deep burial and temperatures, although anchizonal metamorphism is only restricted to the extreme north-east of the study area (the Haut-Giffre massif).

Organic maturity indicators demonstrate both across and along strike variations in the maximum depth of burial and burial temperatures within the French Subalpine Chains, with the greatest variation being along strike of this foreland fold/thrust belt. In terms of organic maturity the Cretaceous of the south-west part of the chain can be considered immature, whilst in the north-east the Cretaceous can be considered to be mature to overmature. The regional trend seen in organic maturity matches well the data presented for clay mineral changes in the Hauterivian.

Two trends in the increase in organic maturity are recognised, firstly, across structural strike of the fold/thrust belt (roughly from west to east) and secondly, along strike of the fold/thrust belt (from south-west to north-east). The latter trend shows the greatest change in organic maturity and suggests that the north-east of the fold/thrust belt has experienced greater burial temperatures.

The results of thermal modelling suggest that the Haut-Giffre, Platé, Aravis and parts of the eastern Bornes and Bauges massifs have experienced up to 5km greater depth

of burial than the Chartreuse and Vercors massifs and western parts of the Bauges and Bornes massifs (if the simple thermal model employed is correct).

This greater depth of burial was produced by two factors, namely, the earlier initiation of foredeep sedimentation and marked differences in the structural style producing differences in the sizes of tectonic loads. It is suggested that the earlier initiation of the foredeep and its sedimentation (mid- to late Eocene compared to mid-Miocene) in the north-east, although not of greater thickness than the foredeep sediments to the south-west, caused the earlier beginning of deeper burial in the north-east part of the chain. This was followed by the emplacement of Pre-alpine thrust sheets, the main cause of burying this part of the chain to a greater depth than the massifs to the south-west. The data in chapter 5 suggest that hot fluids have migrated through the Subalpine Chains during deformation. The role of migrating hot fluids in altering the temperature of parts of the Subalpine Chains is deemed to have only been of secondary importance, after burial beneath the Pre-alpine klippen.

The thermal models presented are considered to be good representations of the thermal evolution of the area, but are not unique solutions and should not be viewed as correct solutions. They are one of a number of possible viable models. A good model is one which is plausible or satisfactory in most respects; a model correct in all respects is beyond attainment given the data set and the uncertainity about the choice of values for certain parameters.

References.

Al Aasm, I.S. & Veizer, J. 1986a. Diagenetic stabilization of aragonite and low-Mg calcite, 1. Trace elements in rudists. *Journal of Sedimentary Petrology,* 56, p. 138-152.

Al Aasm, I.S. & Veizer, J. 1986b. Diagenetic stabilization of aragonite and low-Mg calcite, 2. Stable isotopes in rudists. *Journal of Sedimentary Petrology,* 56, p.763-770.

Allan, J.R. & Matthews, R.K. 1977. Carbon and oxygen isotopes as diagenetic and stratigraphic tools: Surface and subsurface data, Barbados and West Indies. *Geology,* 5, 16-20.

Allan, J.R. & Matthews, R.K. 1982. Isotope signatures associated with early meteoric diagenesis. *Sedimentology,* 29, 797-817.

Allen, P. A. & Allen, J. R. 1990. *Basin Analysis.* Blackwell Scientific Publications, Oxford, pp. 451.

Allen, P.A., Mange-Rajetzky, M., Matter, A. & Homewood, P. 1985. Dynamic palaeogeography of the open Burdigalian seaway, Swiss Molasse Basin. *Eclogae géologicae Helveticae,* 78, 351-381.

Allen, P.A., Crampton, S.L. & Sinclair, H.D. 1991. The inception and early evolution of the North Alpine Foreland basin, Switzerland. *Basin Research,* 3, 143-163.

Almogi-Labin, A., Luz, B. & Duplessy, J-C. 1986. Quaternary paleo-oceanography, pteropod preservation and stable-isotope record of the Red Sea. *Palaeogeography, Palaeoclimatology, Palaeoecology,* 57, 195-211.

Anderson, T.F. & Arthur, M.A. 1983. Stable isotopes of oxygen and carbon and their application to sedimentologic and paleoenvironmental problems. In: *Stable Isotopes in Sedimentary Geology.* M.A. Arthur & T.F. Anderson (eds). Soc. Econ. Palaeo. Min. Short Course #10, Dallas, 1983.

Angevine, C.L. & Turcotte, D.L. 1983. Oil generation in overthrust belts. *American Association of Petroleum Geologists Bulletin,* 67, 235-241.

Angevine, C.L., Heller, P.L. & Paola, C. 1990. *Quantitative Sedimentary Basin Modelling.* American Association Petroleum Geologists, Continuing Education Course Note Series #32.

Aprahamian, J. 1988. Cartographie du métamorphisme faible à très faible dans les Alpes françaises externes par l'utilisation de la cristallinité de l'illite. *Geodinamica Acta (Paris)* 2, 1, 25-32.

Aprahamian, J. & Pairis, J. L. 1981. Very low grade metamorphism with a reverse gradient induced by an overthrust in the Haute-Savoie (France). In: *Thrust and Nappe Tectonics.* 1981. K. R. McClay & N. J. Price (eds) Geological Society London, special publication, # 9, 159-165.

Arnaud-Vanneau, A., Arnaud, H., Foury, G., & Masse, J.P. 1972. *L'Urgonien de Haute Provence et du Vercors.* Fieldguide L'association des geologues du sud-est et du groupe Français du Cretace, 9-12 Octobre, 1972.

Arnaud-Vanneau, A. 1980. Micropaléontologie, paléoécologie et sédimentologie d'une plate-forme carbonatée de la marge passive de la Téthys: l'Urgonien du Vercors septentrional et de la Chartreuse (Alpes occidentales). *Géologie Alpine*, mém 10, pp.874

Arnaud, H. 1981. De la plate-forme urgonienne au bassin vocontien: le Barrémo-Bédoulien des Alpes occidentales entre Isère et Buëch (Vercors méridional, Diois oriental et Dévoluy). *Géologie Alpine*, mém. 11, pp.804.

Arnaud-Vanneau, A., Arnaud, H., Adatte, T., Argot, M., Rumley, G. & Thieuloy, J.-P. 1987. *The Lower Cretaceous from the Jura platform to the Vocontian basin (Swiss Jura, France).* Third International Cretaceous Symposium Fieldguide Guide. pp.128.

Arnaud, H. 1988. Subsidence in certain domains of southeastern France during the Ligurian Tethys opening and spreading stages. *Bulletin Societé géologie France,* IV (8), 725-732.

Arnaud, H. & Arnaud-Vanneau, A. 1989. Séquences de dépôt et variations du niveau relatif de la mer au Barrémien à l'Aptien inférieur dans les massifs sub-alpins septentrinoux et la Jura (SE de la France). *Bulletin Societé géologie France,* V (8), 651-660.

Arnaud-Vanneau, A. & Arnaud, H. 1990. Hauterivian to Lower Aptian carbonate shelf sedimentation and sequence stratigraphy in the Jura and northern Subalpine chains (southeastern France and Swiss Jura). *In: Carbonate Platforms.* Tucker, M.E. J.L. Wilson, P.D. Crevello, J.F. Sarg & J.F. Read (eds). Int. Assoc. Sedim. spec. publ. 9, 203-233.

Arnaud-Vanneau, A. & Arnaud, H. 1991. Sedimentation et variations relatives du niveau de la mer sur les plate-formes carbonatées du Berriasien-Valanginien inférieur et du Barrémian dans les massifs subalpins septentrionaux et la jura (Sud-Est de la France). *Bulletin Societé géologie France,* VII (8), 535-545.

Ayrton, S. 1980. La géologie de la zone Martigny-Chamonix (versant suisse) et l'origine de la nappe de Morcles (un exemple de subduction continentale). *Eclogae géologicae Helveticae,* 73, 137-172.

Bachmann, G.H. & Müller, M. 1991. The Molasse basin, Germany: evolution of a classic petroliferous foreland basin. In: *Generation, accumulation and production of Europe's hydrocarbons.* A.M. Spencer. Spec. Publ. European Assoc. Petroleum Geoscientists, #1, 263-276. Oxford University Press, Oxford.

Baldwin, B. & Butler, C.O. 1985. Compaction Curves. *American Association of Petroleum Geologists Bulletin,* 69, 622-626.

Barker, C. E. 1989, Temperature and time in the thermal maturation of sedimentary organic matter. In: *Thermal History of Sedimentary Basins. Methods and Case Histories.* N. D. Naeser & T. H. McCulloh (eds), 73-98, Springer-Verlag, New York.

Barker, C. E. & Pawlewiscz, M. J. 1986. The correlation of vitrinite reflectance with maximum temperature in humic organic matter. In: *Paleogeothermics,* G. Buntebarth & L. Stegena, (eds), 79-93, Springer-Verlag, New York.

Barnaby, R.J. & Rimstidt, J.D. 1989. Redox conditions of calcite cementation interpreted from Mn and Fe contents of authigenic calcites. *Geological Society of America Bulletin,* 101,0.795-804.

Barnes, M.A., Barnes, W.C. & Bustin, R.M. 1984. Diagenesis 8. Chemistry and evolution of organic matter. *Geoscience Canada,* 11, 103-114.

Barron, E.J., Thompson, S.L. & Schneider, S.H. 1981. An ice-free Cretaceous? Results from climate model simulations. *Science,* 212, 501-508.

Barron, E.J. 1986. Modelling in paleooceanography. *Surveys in Geophysics*, 8, p.1-23.

Barron, E.J. 1987. Cretaceous plate tectonic reconstructions. *Palaeogeography, Palaeoclimatology, Palaeoecology,* **56**, 3-29.

Barron, E.J. 1989. Studies of Cretaceous climate. In: *Aeronomy and Paleoclimates.* International Union of Geodsey and Geophysics and American Geophysical Union. p. 149-157.

Bathurst, R.G.C. 1975. *Carbonate sediments and their diagenesis.* Second edition, Elsevier, New York, 658pp.

Bathurst, R.G.C. 1980. Lithification of carbonate sediments. *Science Progress,* Oxford, 66, 451-471.

Bathurst, R.G.C. 1983. Neomorphic spar versus cement in some Jurassic grainstones: significance for porosity evaluation and compaction. *Journal Geological of Society, London*, 140, 229-237.

Bathurst, R.G.C. 1986. Carbonate diagenesis and reservoir development: conservation, destruction, and creation of pores. *Quart. Journal of Colorado school of Mines,* 81, p.1-25.

Bathurst, R.G.C. 1987. Diagenetically enhanced bedding in argillaceous platform limestones: stratified cementation and selective compaction. *Sedimentology,* 34, 749-778.

Bayer, R., Cazes, M., Piaz, G. V., Damotte, B., Elter, G., Gosso, G., Hirn, A., Lanza, R., Lombardo, B., Mugnier, J-L., Nicolas, A., Polino, R., Roure, F., Sacchi, R., Scarascia, S., Tabacco, I., Tapponnier, P., Tardy, M., Taylor, M., Thouvenot, F., Torreilles, G. & Villien, A. 1987. Premiers résultats de la traversée des Alpes occidentales par sismique reflexion verticale (Programme ECORS-CROP). *Comptes Rendus Académie Sciences, Paris.* 305, Serie II, 1461-1470.

Beaumont, C. 1981. Foreland basins. *Geophysical Journal of the Royal astronomical Society,* 65, 291-329.

Bergerat, F., Mugnier, J-L., Guellec, S., Truffert, C., Cazes, M., Damotte, B. & Roure, F. Extensional tectonics and subsidence of the Bresse basin: an interpretation from

ECORS data. In: *Deep Structure of the Alps.* F. Roure, P. Heitzmann & R. Polino (eds). Memoire Société géologique de France, Paris, # 156, 145-156.

Bethke, C.M. & Marshak, S. 1990. Brine migrations across North America - the plate tectonics of groundwater. *Annual Review of Earth & Planetary Sciences,* 18, 287-315.

Bethke, C.M. Reed, J.D. & Oltz, D.F. 1991. Long-range petroleum migration in the Illinois basin. *American Association of Petroleum Geologists Bulletin,* 75, 925-945.

Blenkinsop, T.G. 1988. Defination of low-grade metamorphic zones using illite crystallinity. *Journal of Metamorphic Geology,* 6, p.623-636.

Bles, J.L., Bonijoly, C., Casraing, C. & Gros, Y. 1989. Successive post-Varsican stress fields in the French Massif Central and its borders (Western Eurpoean Plate): comparison with geodynamic data. *Tectonophysics,* 169, 79-111.

Boles, J.R. & Franks, S.G. 1979. Clay diagenesis in the Wilcox sandstones of southwest Texas; Implications of smectite diagenesis on sandstone cementation. *Journal of Sedimentary Petrology,* 49, p.55-70.

Bostick, N. H., Cashman, S. M., McColluh, T. H. & Waddel, C. T. 1978, Gradients of vitrinite reflectance and present temperature in the Los Angeles and Ventura basins, California. In: *Low Temperature Metamorphism of Kerogen and Clay Mineral: Pacific section of the Society of Economic Paleontologists & Mineralogists, special symposium,* D.F. Oltz (ed.), 65-96.

Boyer, S.E. & Elliot, D. 1982. Thrust systems. *American Association of Petroleum Geologists Bulletin,* 66, 1196-1230.

Bradbury, H.J. & Woodwell, G.R. 1987. Ancient fluid flow within foreland terrains. In: *Fluid Flow in Sedimentary Basins and Aquifers.* J.C. Goff & B.P.J. Williams (eds) Geological Society London, special publication, 34, 87-102.

Brand, U. & Veizer, J. 1980. Chemical diagenesis of a multicomponent carbonate system - 1: Trace elements. *Journal of Sedimentary Petrology,* 50, 1219-1236.

Bréhéret, J-G. 1988. Épisodes de sédimentation riche en matière organique dans les marnes bleues d'âge aptien et albien de la partie pélagique du bassin vocontien. *Bulletin Societé géologie France,* 8, p.349-356.

Brewer, J. 1981. Thermal effects of thrust faulting. *Earth & Planetary Science Letters,* 56, 233-244.

Brooks. J., Cornford, C. & Archer, R. 1987. The role of hydrocarbon source rocks in petroleum exploration. In: *Marine Petroleum Source Rocks.* J. Brooks & A.J. Fleet (eds). Geological Society London, special publication, #26, p.17-46.

Budai, J.M. 1985. Evidence for rapid migration during deformation, Madison Group, Wyoming and Utah overthrust belt. In: *Rocky Mountain Carbonate Reservoirs: A Core Workshop.* M.W. Longman, K.W. Shanley, R.F. Lindsay & D.E. Eby (eds). SEPM Core Workshop #7.

Budai, J.M., Lohmann, K.C. & Owen, R.C. 1984. Burial dedolomite in the Mississippian Madisson Limestone, Wyoming and Utah thrust belt. *Journal of Sedimentary Petrology,* 54, 276-288.

Budd, D.A. & Land, L.S. 1990. Geochemical imprint of meteoric diagenesis in Holocene ooid sands, Schooner Cays, Bahamas: Correlation of calcite cement geochemistry with extant groundwaters. *Journal of Sedimentary Petrology,* 60, #3, p.361-378.

Bureau de Recherches Géologiques et Minières (BRGM), 1975. *Carte Géologique à, 1/50000, Romans-sur-Isère.*

Bureau de Recherches Géologiques et Minières (BRGM), 1979a. *Carte Géologique à, 1/250000, Annecy.*

Bureau de Recherches Géologiques et Minières (BRGM), 1979b. *Carte Géologique à, 1/250000, Lyon.*

Bureau de Recherches Géologiques et Minières (BRGM), 1985. *Carte Géologique à, Thonon-les-Bains.*

Bureau de Recherches Géologiques et Minières (BRGM), 1988. *Carte Géologique à 1/50000, Annecy-Bonneville.*

Burkhard, M. 1988. L'Helevetique de la bordure occidentale du massif l'Aar (évolution tectonique et métamorphique). *Eclogae géologicae Helveticae,* 81/1, p.63-114.

Burkhard, M. & Kalkreuth, W. 1989. Coalification in the northern Wildhorn nappe and adjacent units, western Switzerland. Implications for tectonic burial histories. *International Journal of Coal Geology,* 11, 47-64.

Burkhard, M. 1990. Aspects of the large-scale deformation in the most external part of the Swiss Alps (Subalpine Molasse to Jura fold belt). *Eclogae géologicae Helveticae,* 83/3, p. 559-583.

Burley, S.D., Mullis, J. & Matter, A. 1989. Timing diagenesis in the Tartan Reservoir (UK North Sea): constraints from combined cathodoluminescence microscopy and fluid inclusion studies. *Marine and Petroleum Geology,* 6, 98-120.

Burnham, A.K. & Sweeney, J.J. 1989. A chemical kinetic model of vitrinite maturation and reflectance. *Geochimica et Cosmochimica Acta,* 53, 2649-2657.

Burst, J.F. 1969. Diagenesis of Gulf Coast clayey sediments and its possible relation to petroleum migration. *American Association Petroleum Geologists Bulletin,* 53, p.73-93.

Bustin, R. M. 1983. Heating during thrust faulting in the Rocky Mountains: friction or fiction? *Tectonophysics.* 95, 309-328.

Bustin, R.M., Barnes, M.A. & Barnes, W.C. 1985. Diagenesis 10. Quantification and modelling of organic diagenesis. *Geoscience Canada,* 12, p.3-21.

Butler, R.W.H. 1985. The restoration of thrust systems and displacement continuity around the Mont Blanc massif, NW external Alpine thrust belt. *Journal of Structural Geology,* 7, 569-582.

Butler, R.W.H., Welborn, A., Gillcrist, R. & Coward, M.P. 1987, *The external Western Alpine thrust belt,* Tectonic Studies Group Field excursion guide 18th July- 1st Aug. 1987.

Butler, R.W.H. 1989a. The geometry of crustal shortening in the Western Alps. In: *Tectonic evolution of the Tethyan region.* A.M.C Sengor (ed.), Kluwar Acad. Publ., 43-76.

Butler, R.W.H. 1989b. The influence of pre-existing basin structure on thrust systems evolution in the Western Alps. *In: Inversion Tectonics.* M.A. Cooper & G.D. Williams. (eds). Geological Society London, special publication, 44, 105-122.

Butler, R.W.H. 1991a. Structural evolution of the western Chartreuse fold and thrust system, NW French Subalpine Chains. In: *Thrust Tectonics.* K.R. McClay (ed), Harper Collins Acedemic, 287-298.

Butler, R.W.H. 1992b, Hydrocarbon maturation, migration and thrust sheet loading in the Western Alpine foreland thrust belt. In: *Petroleum Migration.* Geological Society London, special publication, # 59, W.A. England & A.J. Fleet (eds.), p. 227-244.

Butler, R.W.H. In press a. Thrusting patterns in the NW French Subalpine Chains. *Geological Magazine,*

Butler. R.W.H. In press b. Evolution of Alpine fold-thrust complexes: a linked kinematic approach. In: *Structural geology of fold and thrust belts.* S. Mitra & G. Fisher (eds), John Hopkins University Press, Baltimore.

Chamley, H. & Deconinck, J-F. 1985. Expression de l'évolution géodymanique des domaines nord-atlantique et subalpin au Mésozoïque supérieur, d'aprés sédimentaires argileuses. *Comptes Rendus Académie Sciences, Paris,* t.300, Série II, #20, p.1007-1012.

Chaplet, M. 1989. *Etude géologique du Massif Subalpin des Bornes (Haute-Savoie).* Ph.D. thesis, Univ. de Savoie, Chambery, Travaux du Dépt. des Sciences de la Terre #11.

Charollais, J., Hochuli, P.A., Oertli, H.J. Perch-Nielsen, K., Tourmarkine, M., Rögl, F. & Pairis, J-L. 1980. Les Marnes à Foraminifères et les Schistes à Meletta des chaînes subalpines septentrionales (Haute-Savoie, France). *Eclogae géologicae Helveticae,* 73, 9-69.

Charollais, J., Arnaud-Vanneau, A., Busnardo, R., Clavel, B., Donze, P., Fauconnier, D., Manivit, H., Oertli, H.J., Septifontaine, M., Steinhauser, N. & Strasser, A. 1981. Groupe Français du Crétacé - Reunion en Haute-Savoie. Livret-guide. *Publ. du Dépt. de Géologie et de Paléontologie de l'Université de Genève.*

Charollais, J & Jamet, M. 1990. Principaux résultats géologiques du forage Brizon 1 (BZN 1), Haute-Savoie, France. In: *Deep Structure of the Alps.* F. Roure, P. Heitzmann & R. Polino (eds). Memoire Société géologique de France, Paris, # 156, p.185-202.

Choquette, P.W. & Pray, L.C. 1970. Geologic nomenclature and classification of porosity in sedimentary carbonates. *American Association of Petroleum Geologists Bulletin,* 54, p. 207-250.

Choquette, P.W. & James, N.P. 1987. Diagenesis in limestones - 3. The deep burial environment. Geoscience Canada, 14, p.3-35.

Choquette, P.W. & James, N.P. 1988. Introduction. In: *Paleokarst.* N.P. James & P.W. Choquette (eds), Springer-Verlag, New York, 1-21.

Choquette, P.W., Cox, A. & Meyers, W.J. 1992. Characteristics, distribution and origin of porosity in shelf dolostones: Burlington-Keokuk Formation (Mississippian), U.S. mid-continent. *Journal of Sedimentary Petrology,* 62, 167-189.

Clavel, B., Busnardo, R. & Charollais, J. 1986. Chronologie de la mise en place de la plate-forme urgonienne du Jura au vercors (France) *Comptes Rendus Académie Sciences, Paris,* 302 (II), 583-586.

Clavel, B., Charollais, J. & Busnardo, R. 1987. Données biostratigraphiques nouvelles sur l'apparation des facies urgoniens du Jura au Vercors. *Eclogae Géologicae Helveticae,* 80, 59-68.

Coli, M. & Sani, F. 1990. Vein distribution in a thrust zone: a case history from the Northern Apennines, Italy. In: *Deformation mechanisms, Rheology and Tectonics.* R.J. Knipe & E.H. Rutter (eds), Geological Society London special publication, 54, 475-482.

Cornford, C. 1984. Source rocks and hydrocarbons of the North Sea. In: *Introduction to the Petroleum Geology of the North Sea.* K.W. Glennie (ed.), Blackwell, p.171-204.

Coward, M. & Dietrich, D. 1989. Alpine tectonics - an overview. In: *Alpine Tectonics.* Geological Society of London, special publication 45. M.P. Coward, D. Dietrich & R.G. Park (eds), 1-29.

Curnelle, R. & Dubois, P. 1986. Evolution mésozoïque des grands bassins sédimentaires français: bassins de Paris, d'Aquitaine et du Sud-Est. *Bulletin Societé géologie France,* II(8), 529-546.

Czerniakowski, L.A., Lohmann, K.C. & Wilson, J.L. 1984. Closed-system marine burial diagenesis: isotopic data from the Austin Chalk and its components. *Sedimentology,* 31, p.863-877.

Dansgaard, W. 1964. Stable isotopes in precipitation. *Tellus,* v. 16, p. 436-468.

Darsac, C. 1983. *La plate-forme berriaso-valanginienne du Jura méridional aux massifs subalpins (Ain, Savoie).* Thèse 3e cycle, Univ. Grenoble, 319p.

Dazy, J. & Grillot, J-C. 1982. Le thermominéralisme péri-alpin: exemple de la région savoyarde (France). *Revue de géologie dynamique et de géographique physique,* 23, #4, 319-328.

Dazy, J., Dray, M., Jusserand, C., Pasqualotto, M. & Zuppi, G.M. 1987. Characterisation isotopique des eaux thermominerales des alpes du nord Franco-Italiennes. In: *Isotope Techniques in Water Resources Development.* International Atomic Energy Agency, Vienna, 1987.

Debelmas, J. 1983. *Alpes du Dauphiné.* Guides Géologiques Régionaux de France. 198p.

Debelmas, J. & Kerckhove, Cl. 1980. Les Alpes franco-Italiennes. *Géologie Alpine,* 50, 22-90.

Debelmas, J. Escher, A. & Trümpy, R. 1983. Profiles through the Western Alps. In: *Profiles of Orogenic Belts.* N. Rast & F.M. Delaney (eds), Geodynamic Series, 10, American Geophysical Union & the Geological Society of America.

Debrand-Passard, S. Courbouleix, S. & Lienhardt, M-J. 1984. (editors). *Synthèse gèologique du Sud-Est de la France. Volume 1- Stratigraphy.* Mémoire de Bureau Recherches Géologiques et Minieres, #125.

Deconinck, J-F. 1984. *Sédimentation et diagenese des minéraux argileux du Jurassique supérieur-Cretacé dans le Jura meridional et le domaine subalpin (France-Sud-est). Comparaison avec le domaine atlantique Nord.* Ph.D. thésis, 3è, Univ. des Sciences et Techniques de Lille, France, 150pp.

Deconinck, J-F. & Debrabant, P. 1985. Diagenèse des argiles dans le domaine subalpin: rôles respectifs de la lithologie, de l'enfouissement et de la surcharge tectonique. *Revue de géol. dynamique et de géog. physique,* 26, #5, p.321-330.

Deconinck, J-F., Beaudoin, B., Chamley, H., Joseph, P. & Raoult, J-F. 1985. Contrôles tectonique, eustique et climatique de la sédimentation argileuse du domaine subalpin français au Malm-Crétacé. *Revue de géol. dynamique et de géog. physique,* 26, #5, p.311-320.

Deconinck, J.F. & Charollais, J. 1986. Mineraux argileux des formations Cretacees et Tertiarires du domaine ultra-Helvetique (unite de Nantbellet, klippe de Sulens: Haute-Savoie): Diagenese et paleoenvironment. *Géologie Alpine,* t62, 11-30.

Delamette, M. 1986. *L'évolution du domiane helvétique (entre Bauges et Morcles) de l'Aptien supérieur au Turonien: série condensées, phosphorites et circulations océaniques (Alpes occidentales franco-suisses).* Publ. Dépt. géol. et paléont. Univ. Genève, thèse #2237, 316pp.

Delamette, M. 1988. Relation between the condensed Albian deposits of the Helvetic domain and the oceanic-current influenced continental margin of the northern Tethys. *Bulletin Societé géologie France,.* IV(8), 739-745.

Della Vedova, B. Lucazeau, F. Pellis, G. & Pasquale, V. 1990. Heat flow and tectonics along the EGT southern segment. In: *Proceedings IV th EGT project workshop - data compilations and synoptic interpretation.* R. Freeman & St. Mueller (eds), March, 1990, 431-440.

Deming, D. & Chapman, D. S. 1985. Thermal histories and hydrocarbon generation: An example from the Utah-Wyoming thrust belt. *American Association of Petroleum Geologists Bulletin,* 73, #12, 1455-1471.

Deming, D., Nunn, J.A. & Evans, D.G. 1990. Thermal effects of compaction-driven groundwater flow from overthrust belts. *Journal of Geophysical Research,* 95, 6669-6683.

Dercourt, J., Zonenshain, L.P., Ricou, L-E., Kazmin, V.G., Pichon, X.L., Knipper, A.L., Grandjaquet, C., Sborshchikov, I.M. Boulin, J., Sorokhtin, O. Geyssant, J., Lepvrier, C., Biju-Duval, B., Sibuet, J-C., Savostin, L.A., Westphal, M., & Lauer, J-P. 1985. Presentation of 9 paleogeographic maps at 20 millions scale from Atlantic to Pamir between Lias and Present. *Bulletin Societé géologie France,* 8, p. 637-652.

Detraz, H. & Steinhauser, N. 1988. Le bassin delphino-helvétique savoyard et sa marge jurassienne sous contrôle tectonique entre le Kiméridgian et le Valangien. *Eclogae géologicae Helveticae,* 81, 69-108.

Detraz, H. 1989. *Evolution Paleogeograpihique de la marge Jurassienne de la tethys entre Chartreuse et Morcles (Alpes occidentales franco-suisses et Jura méridional) du Tithonique au Valanginien: tectonique synsédimentaire et eustatisme.* Publ. Dépt. géol. et paléont. Univ. Genève, thèse # 2338, pp.227.

Dewey, J.F. Pitman, W.C. Ryan, W, & Bonin, J. 1973. Plate tectonics and the evolution of the Alpine system. *Bulletin Geological Society of America,* 84, 3137-3180.

Dickson, J.A.D. 1983. Graphical modelling of crystal aggregates and its relevance to cement diagnosis. *Philosphical Transactions of the Royal Society, London,* A, 309, 465-502.

Dietrich, D., McKenzie, J.A. & Song, H. 1983. Origin of calcite in syn-tectonic veins as determined from carbon-isotope ratios. *Geology,* 11, 547-551.

Dorobek, S.L. 1987. Petrography, geochemistry and origin of burial diagenetic facies, Siluro-Devonian Helderberg Group (Carbonate Rocks), Central Appalachians. *American Association of Petroleum Geologists Bulletin,* 71, #5, 492-514.

Dorobek, S.L. 1989. Migration of orogenic fluids through the Siluro-Devonian Helderberg Group during late Paleozoic deformation: constraints on fluid sources and implications for thermal histories of sedimentary basins. *Tectonophysics,* 159, 25-45.

Doudoux, B., Mercier de Lepinay, B. & Tardy, M. 1982a. Une interprétation nouvelle de la structure des massifs subalpins savoyards (Alpes occidentales): nappes de charriage oligocènes et déformations superposées. *Comptes Rendus Académie Science Paris,* t 295, Série II, 63-68.

Doudoux, B., Rampnoux, J.P. & Tardy, M. 1984. Degre d'allochtonie et age des structures Savoyardes dans le massif des Bauges. *Géologie profonde de la France,* Doc. BRGM, 326-335.

Doudoux, B., Chaplet, M. & Tardy, M. 1987. Les series marine Paleogenes post-Lutetiennes du massif subalpin des Bornes (Alpes occidentales). *Géologie Alpine,* Mém. h.s. 13, 299-312.

Drever, J.J. 1982 *The Geochemistry of Natural Waters.* Prentice-Hall, New York, pp. 388.

Dromart, G., Courtinat, B. & Curial, A. 1992. Hydrogen-rich oranic facies in carbonate lowstand complexes: the upper Oxfordian of the western Subalpine Basin (southeastern

France). In: *Sequence Stratigraphy of European Basins: Conference abstracts volume,* CNRS-IFP, Dijon, France, May, 1992, p.342.

Droxler, A. & Schaer, J.P. 1979. Déformation cataclastique plastique lors du plissement, sous faible couverture, de strates calcaires. *Eclogae géologicae Helveticae,* 72, 551-570.

Dunoyer De Segonzac, G. 1970. The transformation of clay minerals during diagenesis and low grade metamorphism: A review. *Sedimentology,* 15, p.281-346.

Durney, D. 1972. *Deformation history of the western Helvetic Nappes.* Ph.D thesis, Imperial College, London, 327pp.

Dykstra, J. 1987. Compaction correction for burial history curves: Application to Lopatin's method for source rock maturation determination. *Geobyte,* 2, #4, 16-23.

Eberl, D.D. & Velde, B. 1989. Beyond the Kübler index. *Clay Minerals,* 24, p.571-577.

Edman, J.D. & Surdam, R.C. 1984. Influence of overthrusting on maturation of hydrocarbons in Phosphoria Formation, Wyoming-Idaho-Utah overthrust belt. *American Association of Petroleum Geologists Bulletin,* 68, 1803-1817.

Edman, J.D. & Furlong, K.P. 1987. Thrust faulting and hydrocarbon generation: reply. *American Association of Petroleum Geologists Bulletin,* 71, 890-896.

Elliot,W.C., Aronson, J.L., Matisoff, G. & Gautier, D.L. 1991. Kinetics of the smectite to illite transformation in the Denver Basin: Clay mineral, K-Ar data, and mathematical model results. *American Association of Petroleum Geologists Bulletin,* 75, p.436-462.

Emery, D. 1987 Trace-element source and mobility during limestone burial diagenesis-an example from the Middle Jurassic of Eastern England. In: *Diagenesis of Sedimentary Sequences.* J.D. Marshall (ed). Geological Society of London, special publication #36, 201-217.

England, P. & Molnar, P. 1990. Surface uplift, uplift of rocks, and exhumation of rocks. *Geology,* 18, 1173-1177.

Enos, P. 1986. Diagenesis of mid-Cretaceous rudist reefs, Valles platform, Mexico. In: *Reef Diagenesis.* J.H. Schroeder & B.H. Purser (eds), Springer-verlag, Berlin, p. 160-185.

Enos, P. 1988. Evolution of porespace in the Poza Rica trend (mid-Cretaceous) Mexico. *Sedimentology,* 35, p.287-325.

Fairchild, I.J., Hendry, G., Quest, M. & Tucker, M. 1988. Chemical analysis of sedimentary rocks. In: *Techniques in Sedimentology.* M. Tucker (ed.), Blackwells Scientific Publications, 274-354.

Falvey, D.G. & Middleton, M.F. 1981. Passive continental margins: evidence for prebreakup deep crustal metaamorphic subsidence mechanism. *Oceanologica Acta,* 103-114.

Falvey, D.A. & Deighton, I. 1982. Recent advances in burial and thermal geohistory analysis. *Australian Petroleum Explorationists Association Journal,* 22, 65-81.

Farrimond, P., Eglinton, G., Brassell. S.C. & Jenkyns, H. 1989. Toarcian anoxic event

in Europe: an organic geochemical study. *Marine and Petroleum Geology,* 6, 136-147.

Feazel, C.T. & Schatzinger, R.A. 1985. Prevention of carbonate cementation in petroleum reservoirs. In: *Carbonate Cements.* N. Schneidermann & P.M. Harris (eds), Spec. Publ. Soc. Econ. Palaeo. Miner., #36, 97-106.

Fischer, A.G. 1983. Long-term climatic oscillations recorded in stratigraphy. In *Climate in earth history.* W. Berger (ed.) p. 97-104, National Acedemy of Sciences, Washington, D.C.

Folk, R.L. 1965. Some aspects of recrystallization in ancient limestones. In: *Dolomitization and limestone diagenesis.* L.C. Pray and R.C. Murray (eds). Spec. Publ. Soc. Econ. Paleont. Mineral., 13, p.14-48.

Fourmiquet, J. 1977. Mise en évidence de mouvements actuels, verticaux, dans le Sud-Est de al France par comparision de nivellements successifs. *Comptes Rendus Sommaires Société géologique de France.* Fasc. 5, 266-268.

Frank, J.R., Carpenter, A.B. & Oglesby, T.W. 1982. Cathodoluminescence and composition of calcite cement in the Taum Sauk limestone (upper Cambrian), southeast Missouri. *Journal of Sedimentary Petrology,* 52, 631-638.

Freed, R.L. & Peacor, D.R. 1989a. Variability in temperature of the smectite/illite reaction in Gulf Coast sediments. *Clay Minerals,* 24, p.171-180.

Freed, R.L. & Peacor, D.R. 1989b. Feldspar diagenesis and the smectite to illite transformation in Texas Gulf Coast shales (abs.). *American Association of Petroleum Geologists Bulletin,* 73, p.356.

Freed, R.L. & Peacor, D.R. 1992. Diagenesis and the formation of authigenic illite-rich I/S crystals in Gulf Coast shales: TEM study of clay separates. *Journal of Sedimentary Petrology,* 62, 220-234.

Frey, M. 1970. The step from diagenesis to metamorphism in pelitic rocks during Alpine orogenesis. *Sedimentology,* 15, 261-279.

Frey, M. 1974. Alpine metamorphism of pelitic and marly rocks of the Central Alps, *Schweizerische Mineralogische und Petrographische Mitteilungen,* 54, 2/3, 489-506.

Frey, M., Teichmüller, M., Teichmüller, R., Mullis, J., Künzi, B., Breitschmid, A., Gruner, U., & Schwizer, B. 1980. Very low grade metamorphism in the external parts of the Central Alps. Illite crystallinity, coal rank, and fluid inclusion data. *Eclogae géologicae Helveticae,* 73/1, 173-203.

Funk, H. 1985. Mesozoische Subsidenzgesschichte im Helvetischen Schelf der Ostschweiz. *Eclogae géologicae Helveticae,* 78, 249-272.

Funk, H. 1988. The "Urgonian" platform in northwestern Tethys. In: *Evolution of the northern margin of Tethys, Volume 1.* M. Rakus, J. Dercourt & A.E.M. Nairn (eds). Mém. Soc. Géol. France, Paris, Nouvelle série # 154, p.131-135.

Furlong, K.P. & Edman, J.D. 1984. Graphic approach to determination of hydrocarbon maturation in overthrust terrains. *American Association of Petroleum Geologists Bulletin,* 68, 1818-1824.

Furlong, K.P. & Edman, J.D. 1989. Hydrocarbon maturation in thrust belts: thermal considerations. In: *Origin and evolution of Sedimentary basins and their Energy and Mineral Resources.* R.A. Price (ed.), 137-144.

Gallagher, K. 1990. An examination of some uncertainties associated with estimates of sedimentation rates and tectonic subsidence. *Basin Research.* 2, 97-114.

Garven & Freeze, 1984. Theoretical analysis of the role of groundwater flow in the genesis of stratabound ore deposits 2. Quantitative results. *American Journal of Science,* 284, 1125-1174.

Gawthorpe, 1987. Burial dolomitization and porosity development in a mixed carbonate-clastic sequence: an example from the Bowland Basin, northern England. *Sedimentology,* 34, 533-558.

Ge & Garven, 1989. Tectonically induced transient groundwater flow in foreland basin. In: *Origin and evolution of Sedimentary basins and their Energy and Mineral Resources.* R.A. Price (ed.), 145-157.

Gidon, M. 1981. La structure de l'extrémité mérionale du massif de la Chartreuse aux abords de Grenoble et son prolongement en Vercors. *Géologie Alpine,* 57, 93-107.

Giles, M.R. & Marshall, J.D. 1986. Constraints on the development of secondary porosity in the subsurface: re-evaluation of the processes. *Marine and Petroleum Geology,* 3, 243-255.

Gillchrist, R., Coward, M. & Mugnier, J.-L. 1987. Structural inversion and its controls: examples from the Alpine foreland and the French Alps. *Geodinamica Acta* 1(1), 5-34.

Given, R.K. & Lohmann, K.C. 1985. Derivation of the original isotopic composition of Permian marine cements. *Journal of Sedimentary Petrology,*55, p.430-439.

Gorin, G., Gülaçar, F. & Cornioley, Y. 1989. Organic geochemistry, maturity, palynofacies and palaeoenvironments of Upper Kimmeridgian and Lower Tertiary organic-rich samples in the southern Jura (Ain, France) and Subalpine massifs (Haute-Savoie, France). *Eclogae géologicae Helveticae,* 82/2, p.491-515.

Gorin, G. & Monteil, E. 1990. Preliminary note on the organic facies, thermal maturity and dinoflagellate cysts of the Upper Maastrichtian Wang Formation in the northern subalpine massifs (Western Alps, France). *Eclogae géologicae Helveticae,* 82/3, p.265-285.

Goy-Eggenberger, D. & Kübler, B. 1990. Résultats préliminaires d'un essai de zonéographie métamorphique à travers les formations calcaires de la Nappe de Morcles. *Schweizerische Mineralogische und Petrographische Mitteilungen,* 70, 83-88.

Graciansky, P.-C., Brosse, E., Deroo, G., Herbin, J.-P., Montadert, L. Müller, C., Sigal, J. & Schaaf, A. 1987. Organic-rich sediments and palaeoenvironmental

reconstructions of the Cretaceous North Atlantic. In: *Marine Petroleum Source Rocks.* J. Brooks & A.J. Fleet (eds). Geological Society London, special publication, #26, p.317-344.

Graciansky, P.-C. & Lemoine, M. 1988. Early Cretaceous extensional tectonics in the southwestern French Alps: a consequence of North Atlantic rifting during Tethyan spreading. *Bulletin Societé géologie France,* IV, 733-739.

Gregg, J.M. 1985. Regional epigenetic dolomitization in the Bonneterre Dolomite (Cambrian), southeastern Missouri. *Geology,* 13, 503-506.

Grover, G. Jr. & Read, J.F. 1983. Paleoaquifer and deep burial related cements defined by regional cathodoluminescent patterns, Middle Ordovician carbonates, Virginia. *American Association of Petroleum Geologists,* 67, 1275-1303.

Guellec, S., Mugnier, J-L., Tardy, M. & Roure, F. 1990. Neogene evolution of the western Alpine foreland in the light of ECORS data and balanced cross-section. In: *Deep Structure of the Alps.* F. Roure, P. Heitzmann & R. Polino (eds). Memoire Société géologique de France, Paris, # 156, p. 165-184.

Guildish, T.M., Kendall, C.G.St.C., Lerche, I., Toth, D.J. & Yarzab, R.F. 1985. Basin evaluation using burial history calculations: an overview. *American Association of Petroleum Geologists Bulletin,* 69, 92-105.

Guthrie, J. M., Houseknecht, D. W. & Johns, W. D. 1986. Relationships among vitrinte reflectance, illite crystallinity and organic geochemistry in Carboniferous strata, Ouchita Mountains, Oklahoma and Arkansas. *American Association Petroleum Geologists Bulletin,* 70, 26-38.

Hagem, E.S. & Surdam, R.C. 1989. Thermal evolution of Laramide-style basins: Constraints from tht Northern Bighorn Basin, Wyoming and Montana. In: *Thermal History of Sedimentary Basins: Methods and case histories.* N.D Naeser and T.H. McCulloh (eds), p.277-296, Springer-Verlag, New York.

Hallam, A. 1987. Mesozoic marine organic-rich shales. In: *Marine Petroleum Source Rocks.* J. Brooks & A.J. Fleet (eds). Geological Society London, special publication, #26, p.251-261.

Halley, R.B. 1987. Burial diagenesis of carbonate rocks. *Quarterly Journal of Colorado School of Mines,* 82, 1-15.

Hancock, P.L. 1985. Brittle microtectonics: principle and practice. *Journal of Structural Geology,* 7, 437-457.

Hanor, J.S. 1987. *Origin and Migration of Subsurface brines.* Soc. Econ. Paleo. Miner., Short Course #21, Lectures Notes.

Hanor, J.S., Kharaka, Y.K. & Land, L.S. 1988. Penrose Conference report: Geochemistry of waters in deep sedimentary basins. *Geology,* 16, 560-561.

Haq, B.U., Hardenbol, J. & Vail, P.R. 1987. Chronology of fluctuating sea levels since the Triassic. *Science* **235**, 1156-1167.

Haq, B.U., Hardenbol, J. & Vail, P.R. 1988. Mesozoic and Cenozoic chronostratigraphy and cycles of sea-level change. *In: Sea-level Changes: an Integrated Approach.* C. K. Wilgus, B. S. Hastings, C. G. St.C. Kendall, H. W. Posamentier, C. A. Ross & J. C. Van Wagoner (eds). Spec. Publ. Soc. Econ. Paleont. Mineral. 42, 71-108.

Hardie, L.A. 1987. Dolomitization: a critical review of some current views. *Journal of Sedimentary Petrology,* 57, 166-183.

Hardy, R.G. & Tucker, M.E. 1988. X-ray powder diffraction of sediments. In: *Techniques in Sedimentology,* M.E. Tucker, (ed), Blackwells, 191-228.

Harris, P.M., Kendall, C.G. st. C. & Lerche, I. 1985. Carbonate cementation - a brief review. In: *Carbonate Cements.* N. Schneidermann & P.M. Harris (eds), Soc. Econ. Paleo. Min. spec. publ. #36, 79-95.

Harwood, G. 1988. Microscopical techniques: II. Principles of sedimentary petrography. In: *Techniques in Sedimentology.* M.E. Tucker (ed.), Blackwells, p.108-173.

Hays, P.D. & Grossman, E.L. 1991. Oxygen isotopes in meteoric calcite cements as indicators of continental paleoclimate. *Geology,* 19, 441-444.

Heling, D. 1974. Diagenetic alteration of smectite in argillaceous sediments of the Rhinegraben. *Sedimentology,* 21, p.463-472.

Hemming, N.G., Meyers, W.J. & Grams, J.C. 1989. Cathodoluminescence in diagenetic calcites: the roles of Fe and Mn deduced from electron probe and spectrophotometric measurements. *Journal of Sedimentary Petrology,* 59, 404-411.

Henton, J.M. 1990. *Dolomitization and diagenesis of the lower Muschelkalk, northeast Spain.* Unpublished Ph.D thesis, University of Durham.

Heroux, Y., Chagnon, A. & Bertrand, R. 1979. Compliation and correlation of major thermal indicators. *American Association of Petroleum Geologists Bulletin,* 63, 2128-2144.

Hillier, S. & Clayton, T. 1989. Illite/smectite diagenesis in Devonian lacustrine mudrocks from northern Scotland and its relationship to organic maturity indicators. *Clay Minerals,* 24, p.181-196.

Hinte, J. E., van, 1978. Geohistory analysis - application of micropaleontology in exploration geology. *American Association of Petroleum Geologists Bulletin,* 62, 201-222.

Hird, K. & Tucker, M.E. 1988. Contrasting diagenesis of two Carboniferous oolites from South Wales: a tale of climatic influence. *Sedimentology* **35**, 587-602.

Hitchon, B. 1984. Geothermal gradients, hydrodynamics and hydrocarbon generation, Alberta, Canada. *American Association of Petroleum Geologists Bulletin,* 68, 713-743.

Hoffman, J. & Hower, J. 1986. Clay mineral assemblages as low grade metamorphic geothermometers: application to the thrust faulted disturbed belt of Montana, USA. In:

Aspects of Diagenesis, P.A. Scholle & P.R. Schluger (eds), Soc. Econ. Paleo. Min. Spec. publ., # 26, 55-79.

Homewood, P. 1983. Palaeogeography of Alpine flysch. *Paleogeography, Palaeoclimatology, Paleoecology,* 44, 169-184.

Homewood, P., Allan., P.A. & Williams, G.D. 1986. Dynamics of the Molasse Basin of western Switzerland. In: *Foreland Basins.* International Association of Sedimentologists, special publication #8 P.A. Allan & P. Homewood (eds.), 199-217, Blackwells, Scientific Publications, Oxford.

Homewood, P. & Lateltin, O. 1988. Classic swiss clastics (flysch and molasse): The Alpine connection. *Geodinamica Acta,* 2, 1-11.

Hood, A., Gutjahr, C. M. & Peacock, R. L. 1975. Organic metamorphism and the generation of petroleum. *American Association of Petroleum Geologists Bulletin,* 59, 986-996.

Hooper, E.C.D. 1991. Fluid migration along growth faults in compacting sediments. *Journal of Petroleum Geology,* 14, 161-180.

Hower, J., Eslinger, E.V., Hower, M.E. & Perry, E.A. 1976. Mechanics of burial metamorphism of argillaceous sediment: 1. Mineralogical and chemical evidence *Geological Society of America Bulletin.* 87, p.725-737.

Hower, J. 1981. Shale diagenesis. In: *Clays and resource geology.* Min. Assoc. Canada, p. 60-80.

Hudson, J.D. 1977. Isotopes and limestone lithification: *Journal Geological Society London,* 133, 637-660.

Huggenberger, P. & Wildi, W. 1991. La tectonique du massif des Bornes (Chaînes Subalpine, Haute-Savoie, France). *Eclogae geologié Helveticae,* 84, 125-149.

Hunt, D. 1992. *Application of sequence stratigraphic concepts to the Cretaceous Urgonian carbonate platform, southeast France.* Unpublished Ph.D, University of Durham, 410 pp.

Hunt, D & Tucker, M.E. 1992. The sequence stratigraphy of carbonate shelves with an example from the mid-Cretaceous of S.E. France. *In: Stratigraphy and Facies associations in a sequence stratigraphic Framework* H. Posamentier, C.P. Summerhayes, B.U. Haq & G.P. Allen (eds). Int. Assoc. Sedim. Spec. Publ. 15, in press.

Hunziker, J. C., Frey, M., Clauer, N., Dallmeyer, R. D., Friedrichsen, H., Flehmig, W., Hochstrasser, K., Roggwiler, P. & Schwander, H. 1986. The evolution of illite to muscovite: mineralogical and isotopic data from the Glarus Alps, Switzerland. *Contributions to Mineralology and Petrology,* 92, 157-180.

Hurford, A.J., Hunziker, J.C. & Stöckhert, B. 1991. Constraints of the late thermotectonic evolution of the western Alps: evidence for rapid uplift. *Tectonics,* 10, 758-769.

Jacka, A.D. & Brand, J.P. 1977. Biofacies and development and differential occlusion of porosity in a lower Cretaceous (Edwards) reef. *Journal of Sedimentary Petrology,* 47, 366-381.

Jacquin, T., Arnaud-Vanneau, A., Arnaud, H., Ravenne, C. & Vail, P.R. 1991. Systems tracts and depositional sequences in a carbonate setting: a study of continuous outcrops from platform to basin at the scale of seismic lines. *Marine and Petroleum Geology,* **8**, 122-139.

James, N.P. & Choquette, P.W. 1983. Diagenesis 6. Limestones- the sea floor diagenetic environment. *Geoscience Canada,* 10, p.162-180.

James, N.P. & Choquette, P.W. 1984. Diagenesis 9. Limestones- the meteoric diagenetic environment. *Geoscience Canada* **11**, 161-194.

Jennings, S. & Thompson, G.R. 1986. Diagenesis of Plio-Pleistocne sediments of the Colorado River delta, southern California. *Journal of Sedimentary Petrology,* 56, p.89-98.

Jones, M.A. & Addis, M.A. 1985. Burial of argillaceous sediments. *Marine and Petroleum Geology,* 2, 247-253.

Jones, R.W. 1985. Comparison of carbonate and shale source rocks. In: *Petroleum Geochemistry and Source Rock Potential of Carbonate Rocks.* J.G. Palacas (ed.). American Association of Petroleum Geologists, Studies in Geology, #18, 163-180.

Joseph, P., Beaudoin, B., Fries, G. & Deconinck, J.F. 1985. Megasequences and resediments in the subalpine basin, France (Malm - Cretaceous). *Proceedings 6th European regional meeting of sedimentology.*

Kaelin, B. Rybach, L. & Kempter, E. H. K. 1991. Deposition, uplift and erosion in the Swiss molasse basin, estimated from sonic and density logs. *Terra Abstracts,* 3, #1, 370, VIth EUG, Strasbourg, 24-28 March, 1991.

Kalkreuth, W. & McMechan, M. 1988. Burial history and thermal maturity, Rocky Mountain Front Ranges, Foothills, and Foreland, East Central British Columbia and adjacent Alberta, Canada. *American Association Petroleum Geologists Bulletin,* 72, 1395-1410.

Karner, G. D. & Watts, A. B. 1983. Gravity anomalies and flexure of the lithosphere at mountain ranges. *Journal Geophysical Research,* 88, 10449-10477.

Kennedy, W.J. & Taylor, J.D., 1968. Aragonite in rudists. *Proceedings of the Geological Society, London,* 1645, 325-331.

Kindler, P. 1988. *Géologie des wildflyschs entre Arve et Giffre (Haute-savoie, France).* Publ. Dépt. de Géologie et de Paléontologie de l'université de Genève. #6.

Kinsman, D.J.J. 1969. Interpretation of Sr^{2+} concentrations in carbonate minerals and rocks. *Journal of Sedimentary Petrology,* 39, 486-508.

Kisch, H. J. 1980. Illite crystallinity and coal rank associated with lowest-grade metamorphism of the Taveyanne greywacke in the Helvetic zone of the Swiss Alps. *Eclogae géologicae Helveticae,* 73/3, 753-777.

Kominz, M. A. & Bond, G. C. 1986. Geophysical modelling of the thermal history of foreland basins. *Nature,* 320, 252-256.

Kübler, B. 1964. Les argiles, indicateurs de métamorphisme. *Rev. Inst. France Petrole.* 19, p.1093-1112.

Kübler, B. Martini, J. & Vuagnat, M. 1974. Very low grade metemorphism in the Western Alps. *Schweizerische Mineralogische und Petrographische Mitteilungen,* 54, parts 2-3, 461-469.

Kübler, B., Pittion, J-L., Heroux, Y., Charollais, J. & Weidmann, M. 1979. Sur le pouvoir réflecteur de la vitrinite dans quelques roches du Jura, de la Molasse et des Nappes préalpines, helvétiques et penniques. *Eclogae géologicae Helveticae,* 72/2, 347-373.

Land, L.S. 1980. The isotopic and trace element geochemistry of dolomite: the state of the art. In: *Concepts and Models of Dolomitization.* D.H. Zenger, J.B. Dunham & R.L. Ethington (eds). Soc. Econ. Palaeo. Min., spec. publ. #28, p.87-110.

Land, L.S. 1983. The application of stable isotopes to studies of the origin of dolomite and to problems of diagenesis of clastic sediments. In: *Stable isotopes in Sedimentary Geology.* M.A. Arthur & T.F. Anderson (eds). Soc. econ. Paleont. Miner. Short Couse, #10, 4.1-4.22.

Land, L.S. 1985. The origin of massive dolomite. *Journal of Geology Education,* 33, 112-125.

Lateltin, O. & Müller, D. 1987. Evolution paléogéographique du bassin des Grès de Taveyannaz dans les Aravis (Haute-Savoie) à la fin du Paléogene. *Eclogae géologicae Helveticaee,* 80, 127-140.

Lateltin, O. 1988. *Les dépôts turbiditiques oligocènes d'avant-pays entre Annecy (Haute-Savoie et le Sanetsch, Suisse). Grès de Taveyannaz et du Val d'Illiez.* Ph.D. Thèse Faculté des Sciences de l'Université de Fribourg (Suisse).

Lemcke, M. 1974. Vertikalbewegungen des vormesozoisch Sockels im nördlichin Alpenvorland vom Perm bis zur Gegenwart. *Eclogae géologicae Helveticae,* 67/1, p.121-133.

Lemoine, M., Bas, T., Arnaud-Vanneau, A., Arnaud, H., Dumont, T., Gidon, M., Bourbon, M., de Graciansky, P.-C., Rudiewicz, J.-L., Megard-Galli, J. & Tricart, P. 1986. The continental margin of the Mesozoic Tethys in the Western Alps. *Marine and Petroleum Geology,* 3, 179-199.

Lemoine, M. & Trümpy, R. 1987. Pre-oceanic rifting in the Alps. *Tectonophysics* 133, 305-320.

Lewis, S.E. & Hower, J.C. 1990. Implications of thermal events on thrust emplacement sequence in the Appalachian fold and thrust belt: some new vitrinite reflectance data. *Journal of Geology,* 98, 927-942.

Lohmann, K.C. 1988. Geochemical patterns of meteoric diagenetic systems and they application to studies of paleokarst. In: *Paleokarst.* N.P. James & P.W. Choquette (eds), Springer-Verlag, New York, p.58-80.

Longman, M.W. 1980. Carbonate diagenetic textures fron nearshore diagenetic environments. *American Association of Petroleum Geologists Bulletin,* 64, 461-487.

Longstaffe, F.J. 1987. Stable isotope studies of diagenetic processes. In: *A short course in stable isotope geochemistry of low temperature fluids.* K.T. Kyser (ed.), Saskatoon, May, 1987. Min. Assoc. Canada, Vol. 13, p.187-257.

Lory, C. 1846. *Desription géologique du Dauphiné pour servir à l'explication de la carte géologique de cette province.* Savy édit., Paris. 1ère partie, 1-240, 2ère partie, 241-500, 3ère partie, 501-747.

Loup, B. 1992a. *Evolution de la partie septentrionale du domaine helvétique. en Suisse occidentale au Trias et au Lias: contrôle par subsidence themique et variations du niveau marin.* Université de Genève, publications du département de géologie et paléontologie, #12, 247pp.

Loup, B. 1992b. Mesozoic subsidence and stretching models of the lithosphere in Switzerland (Jura, Swiss Plateau and Helvetic realm). *Eclogae géologicae Helveticae,* 85/3, in press.

Machel, H. 1985. Cathodoluminescence in calcite and dolomite and its chemical interpretation. *Geoscience Canada,* 12, #4, p.139-147.

Machel, H. & Montjoy, E. 1986. Chemistry and Environments of dolomitization - A reappraisal. *Earth Science Reviews,* 23, 177-222.

Machel, H. & Mountjoy, E. 1990. Coastal mixing zone dolomite, forward modelling, and massive dolomitization of platform-margin carbonates - discussion. *Journal of Sedimentary Petrology,* 60, 1008-1012.

Magara, K. 1987 Fluid flow due to sediment loading-an application to the Arabian Gulf Region. In: *Fluid Flow in Sedimentary Basins and Aquifers.* J.C. Goff and B.P.J. Williams (eds) Geological Society of London special publication #34, 19-28.

Majorowicz, J.A., Jones, F.W., Lam, H.L. & Jessop, A.M. 1984. The variability of heat flow both regional and with depth in southern Alberta, Canada: effect of groundwater flow? *Tectonphysics,* 106, 1-29.

Mange-Rajekzky, M. & Oberhänsli, R. 1982. Detrital lawsonite and blue sodic amphibole in the Molasse of Savoy, France and their significance in assessing Alpine Evolution. *Schweizerische Mineralogische und Petrographische Mitteilungen,* 62, 415-436.

Marshak, S. & Engelder, T. 1985. Development of cleavage in limestones of a fold-thrust belt in eastern New York. *Journal of Struct. Geol.,* 7, 345-359.

Marshall, J.E.A. 1990. Determination of Thermal Maturity. In: *Palaeobiology - a synthesis.* D.E.G. Briggs & P.R. Crowther (eds), p.511-515.

Marshall, J.E.A. 1991. Quantative spore colour. *Journal Geological Society, London,* 148, 223-233.

Martin, G.D., Wilkinson, B.H. & Lohmann, K.C. 1985. The role of skeletal porosity in aragonite neomorphism- *Strombus* and *Montastrea* from the Pleistocene Key Largo limestone, Florida. *Journal of Sedimentary Petrology,* 56, 194-203.

Masse, J.-P. & Philip, J. 1981. Cretaceous coral-rudist buildups of France. *In: European Fossil Reef Models.* D.F. Toomey (ed.). Spec. Publ. Soc. Econ. Paleont. Mineral. 30, 399-426.

Mattes, B.W. & Mountjoy, E.W. 1980. Burial dolomitization of the upper Devonian Miette buildup, Jasper National Park, Alberta. In: *Concepts and Models of Dolomitization.* D.H. Zenger, J.B. Dunham & R.L. Ethington (eds). Soc. econ. Paleont. Miner., spec publ., #28, 259-297.

Mazzullo S.J. & Harris, P.M. 1992. Mesogenetic dissolution: Its role in porosity development in carbonate reservoirs. *American Association of Petroleum Geologists Bulletin,* 76, 607-620.

McDowell, S.D. & Elders, W.A. 1980. Authigenic layer silicate minerals in borehole Elmore 1, Salton Sea geothermal field. California, U.S.A. *Contributions Mineralogy & Petrology,* 74, p.293-310.

McCulloh, T.H. & Naeser, N.D. 1989. Thermal history of sedimentary basins: Introduction and overview. In: *Thermal history of sedimentary basins. Methods and case histories.* N.D. Naeser & T.H. McCulloh (eds), p.1-11, Springer-Verlag, New York.

Meyers W.J. 1980. Compaction in Mississippian skeletal limestones, southwestern New Mexico. *Journal of Sedimentary Petrology,* 50, 547-474.

Meyers, W.J. & Lohmann, K.C. 1978. Microdolomite-rich syntaxial cements: proposed meteoric-marine mixing zone phreatic cements from Mississippian limestones, New Mexico. *Journal of Sedimentary Petrology,* 48, 475-488.

Michel, P. & Caillon, G. 1957. Quelques résultats des sondages exécutés en Savoie par la Regie autonome des Petroles. *Bulletin société Géologique de France,* 7, série 6, 995-1008.

Middleton, M. F. 1982. Tectonic history from vitrinite reflectance. *Geophysical Journal Royal astronomical Society,* 68, 121-132.

Middleton, M. F. & Falvey, D. A. 1983. Maturation modelling in the Otway Basin, Australia. *American Association of Petroleum Geologists Bulletin,* 67, 271-279.

Minero, C.J. 1988. Sedimentation and diagenesis along an island sheltered platform margin, El Abra formation, Cretaceous of Mexico. In: *Paleokarst.* N.P. James & P.W. Choquette (eds), Springer-Verlag, New York, p. 385-405.

Minero, C.J. 1991. Sedimentation and diagenesis along open and island protected windward carbonate platform margins of the Cretaceous El Abra Formation, Mexico. *Sedimentary Geology*, 71, p.261-288.

Mintz, L.W. 1981. *Historical Geology.* Charles E. Merril Publ. Co., Columbus. Ohio, 611pp.

Mitra, G., Yonkee, W.A. & Gentry, D.J. 1984. Solution cleavage and its relationship to major structures an the Idaho-Utah-Wyoming thrust belt. *Geology,* 12, 354-358.

Moldovanyi, E.V. & Lohmann, K.C. 1984. Isotopic and petrographic record of phreatic diagenesis: lower Cretaceous Sligo and Cupido formations. *Journal of Sedimentary Petrology,*54, p.972-985.

Monnier, F. 1979. Thermal diagenesis in the Swiss Molasse basin: implications for oil generation. *Canadian Journal Earth Sciences,* 19, 328-342.

Moore, C.H. 1985. Upper Jurassic subsurface cements: a case history. In: *Carbonate Cements.* N. Schneidermann & P.M. Harris (eds). Spec. Publ. Soc. Econ. Palaeo. Min., # 36, p.291-308.

Moore, C.H. 1989. *Carbonate diagenesis and porosity.* Elsevier, 338pp.

Morgan, D.J. 1989. (editor). Clay minerals issue devoted to papers read at 'Clay diagenesis in hydrocarbon reservoirs and shales,' Cambridge, March, 1988. *Clay Minerals,* 24, #2.

Morrow, 1982a. Diagenesis I. Dolomite - part 1. The chemistry of dolomitization and dolomite precipitation. *Geoscience Canada,* 9, 5-13.

Morrow, 1982b. Diagenesis II. Dolomite - part 2. Dolomitization models and ancient dolostones. *Geoscience Canada,* 9, 95-107.

Mosar, J. 1988. Métamorphisme transporté dans les Préalpes. *Schweizerische Mineralogische und Petrographische Mitteilungen,* 68, 77-94.

Morse, J.W. & Mackenzie, F.T. 1990. *Geochemistry of Sedimentary Carbonates.* Developments in Sedimentology 48. Elsevier, Amsterdam. 707pp.

Moss, S. 1992. Organic maturation in the French Subalpine Chains: regional differences in burial history and the size of tectonic loads. *Journal Geological Society London,* 149, 503-515.

M'Rabet, A., Negra, M.H., Purser, B.H., Sassi, S. & Ayed, B. 1986. Micrite diagenesis in Senomanian rudist buildups in central Tunisia. In: *Reef Diagenesis.* J.H. Schroeder & B.H. Puser (eds), Springer-Verlag, Berlin, 210-223.

Mugnier, J-L. & Menard, G. 1986. The development of the Swiss molasse basin and the evolution of the external Alps: A kinematic model. *Bulletin Centres Recherches Exploration-Production, Elf Aquitaine,* 167-180.

Mugnier, J-L., Arpin, R. & Thouvenot. 1987. Coupes équilibrées à travers le massif subalpin de al Chartreuse. *Geodinamica Acta,* 1. 125-137.

Mugnier, J-L., Guellec, S., Menard, G., Roure, F., Tardy., M & Vialon, P. 1990. A crustal scale balanced cross-section through the external Alps deduced from the ECORS profile. In: *Deep Structure of the Alps.* F. Roure, P. Heitzmann & R. Polino (eds). Memoire Société géologique de France, Paris, # 156, p.203-216.

Mussman, W.J., Montanez, I.P. & Read, J.F. 1988. Ordovician Knox paleokarst unconformity, Appalachians. In: *Paleokarst.* N.P. James & P.W. Choquette (eds), Springer-Verlag, New York, 211-228.

Murchison, D.G., Cook, A.C. & Raymond, A.C. 1985. Optical properties of organic matter in relation to thermal gradients and structural deformation. *Phil. Trans. Royal Soc. London,* A, 315, p.157-186.

Nadeau, P.H. & Bain, D.C. 1986. Composition of some smectites and diagenetic illitic clay and implications for their origin. *Clays and Clay Minerals,* 34, p.455-464.

Nicolet, C. 1979. *Le Bas-Dauphine Septentrional étude stratigraphiqué et sedimentologiqué.* Ph.D. These 3è cycle, Univ. Grenoble.

Niemann, J.C. & Read, J.F. 1987. Regional cementation from unconformity-recharged aquifer and burial fluids, Mississippian Newman Limestone, Kentucky. *Journal of Sedimentary Petrology,* 58, 688-705.

Oliver, J. 1986. Fluids expelled tectonically from orogenic belts: their role in hydrocarbon migration and other geologic phenomena. *Geology,* 14, 99-102.

O'Neil, J.R., Clayton, R.N. & Meyeda, T.K. 1969. Oxygen isotope fractionation in divalent metal carbonate. *Journal of Chemical Physics,* 51, 5547-5558.

Pairis, B. & Pairis, J-L. 1975. Précisions nouvelles sur le Tertiare du Massif de Platé (Haute-Savoie). *Géologie Alpine.* t.51, 83-127.

Palmer, T.J. Hudson, J.D. & Wilson, M.A. 1988. Palaeoecological evidence for early aragonite dissolution in ancient calcite seas. *Nature,* V. 335, #27, p.809-810.

Pearson, M.J. & Small, J.S. 1988. Illite-smectite diagenesis and palaeotemperatures in northern North Sea Quaternary to Mesozoic shale sequences. *Clay Minerals,* 23, p.109-132.

Perrier, G. 1980. La structure des Alpes occidentales dédiute des données géophysiques. *Eclogae géologicae Helveticae,* 73, 407-424.

Perry, E.A. & Hower, J. 1970. Burial diagenesis in Gulf Coast pelitic sediments. *Clays and clay minerals.* 18, p.165-177.

Pierson, B. & Shinn, E. 1985. Cement distribution and carbonate mineral stabilization in Pleistocene limestones of Hogsty Reef, Bahamas. In: *Carbonate Cements.* N. Schneidermann & P.M. Harris (eds), Spec. Publ. Soc. Econ. Pal. & Min. # 36, 153-168.

Plummer, L.N., Vacher, H.L., MacKenzie, F.T., Bricker, O.P. and Land, L.S. 1976 Hydrochemistry of Bermuda: A case history of groundwater and diagenesis of biocalcarenites. *Geological Society of America Bulletin,* 87, 1301-1316.

Pollastro, R.M. & Barker, C.E. 1986. Application of clay mineral, vitrinite reflectance and fluid inclusion studies to the thermal and burial history of the Pinedale anticline, Green River Basin, Wyoming. In: *Roles of Organic Matter in Sediment Diagenesis.* D.L. Gautier (ed.) special publication Soc. Econ. Paleo. Min., # 38, p.73-83.

Popp, B.N., Anderson, T.F. & Sandberg. P.A. 1986. Brachiopods as indicators of original isotopic composition in some Palaeozoic limestones. *Geological Society of America Bulletin,* 94, p.1262-1269.

Prezbindowski, D.R. 1985. Burial cementation - is it important? A case study, Stuart City Trend. In: *Carbonate Cements.* N. Schneidermann & P.M. Harris (eds), Spec. Publ. Soc. Econ. Pal. & Min. # 36, p241-264.

Price, L. C. 1983. Geologic time as a parameter in organic metamorphism and vitrinite reflectance as an absolute paleogeothermometer. *Journal of Petroleum Geology,* 6, 5-38.

Price, L.C. & Barker, C.E. 1985. Suppression of vitrinite reflectance in amorphous rich kerogen - a major unrecognised problem. *Journal of Petroleum Geology,* 8, 59-84.

Price, N.J. & Cosgrove, J.W. 1990. *Analysis of Geological Structures.* CUP, Cambridge, 502pp.

Pytte, A.M. & Reynolds, R.C. 1989. The thermal transformation of smectite to illite. In: *Thermal History of Sedimentary Basins: Methods and Case Histories.* N.D. Naeser & T.H. McCulloh (eds), Springer-Verlag, New York, p.133-140.

Quigley, T.M. & Mackenzie, A.S. 1988. The temperature of oil and gas formation in the subsurface. *Nature,* 333, 549-552.

Radke, B.H. & Mathis, R.L. 1980. On the formation and occurrence of saddle dolomite. *Journal of Sedimentary Petrology,* 50, 1149-1168.

Ramsay, J.G. 1980. The 'crack-seal' mechanism of rock deformation. *Nature,* 284, 135-9.

Ramsay, J. G. 1981. Tectonics of the Helvetic nappes. In: *Thrust and nappe tectonics.* K.R. McClay & N.J. Price (eds), Geological Society, London, special publication, # 9, 293-309.

Ramsay, J.G., Casey, M. & Kligfield, R. 1983. Role of shear in development of the Helvetic fold-thrust belt of Switzerland. *Geology,* 11, 439-442.

Ramsay, J. G. 1989. Fold and fault geometry in the western Helvetic nappes of Switzerland and France and its implication for the evolution of the arc of the Western Alps. In: *Alpine Tectonics,* M. P. Coward, D. Dietrich & R. G. Park (eds), Geological Society, London, special publication, #45, 33-45.

Ramsay, J.G. & Huber, M.I. 1987. *The Techniques of Modern Structural Geology. Volume 2: Folds and Fractures.* Acedemic Press, London. 663pp.

Reynolds, R.C. & Hower, J. 1970. The nature of interlayering in mixed-layer illite montmorillonite. *Clays and clay minerals.* 18, p.25-55.

Rivano-Garcia, S. 1978. *Contribution a l'etude geologique du SE du massif des Bornes: La partie meridionale de la chaine des Aravis entre le Col des Aravis et la Cluse de Faverges-Ugine (Haute-Savoie, France).* Thèsè diplome de Docteur de 3e cycle à l'université. Pierre et Marie-Curie, Paris, VI.

Rispoli, R. 1981. Stress fields about strike-slip faults inferred from stylolites and tension gashes. *Tectonophysics,* 75, T29-T36.

Robert, P. 1988. *Organic Metamorphism and Geothermal History.* Elf-Aquitaine and Reidel Publ. Co.

Roberts, G.P. 1990. Structural controls on fluid migration in foreland thrust belts. In: *Petroleum and Tectonics in Mobile Belts.* J. Letouzey, (ed), Editions Technip, Paris, 193-210.

Roberts, G.P. 1991. *Deformation and diagenetic histories around foreland thrust faults.* Unpublished Ph.D thesis, University of Durham, 161pp.

Roberts, G.P. in press. Displacement localisation and palaeo-seismicity of foreland thrust zones: examples from the Rencurel thrust sheet, French Subalpine Chains. *Journal of Structural Geology,*

Ross, D.J. 1989. *Facies analysis and diagenesis of Tethyan Rudist Reef complexes.* Unpublished PhD thesis, University of Wales, 206pp.

Roure, F., Heitzmann, P. & Polino, R. 1990. (editors). *Deep Structure of the Alps.* Memoire Société géologique de France, Paris, # 156, pp.320.

Roure, F. Brun, J.-P., Coletta, & van den Driessche, J. 1992. Geometry and kinematics of extensional structures in the Alpine foreland basin of southeastern France. *Journal of Structural Geology,* 14, 503-519.

Roux, M., Bourseau, J-P., Bas, T., Dumont, T., Graciansky, P.-C., Lemoine, M. & Rudkiewicz, J.-L. 1988. Bathymetric evolution of the Tethyan margin in the Western Alps (data from stalked crinoids): a reappraisal of eustatism during the Jurassic. *Bulletin Societé géologie France,* IV(8) 633-641.

Rudkiewicz, J.-L. 1988. Quantitive subsidence and thermal structure of the European continental margin of the Tethys during early and middle Jurassic times in the western Alps (Grenoble-Briançon transect). *Bulletin Societé géologie France,* IV(8) 623-632.

Ruffel, A. H. & Batten, D. J. 1990. The Barremian-Aptian arid phase in western Europe. *Palaeogeography, Palaeoclimatology, Palaeoecology,* 80, 197-212.

Rush, P.F. & Chafetz, H.S. 1990. Fabric retentive, non-luminescent brachiopods as an indicator of original $\delta^{13}C$ and $\delta^{18}O$ composition: A test. *Journal of Sedimentary Petrology,* 60, 968-981.

Rybach, V. L. & Bodmer, P. 1980. Die goethermischen Verhältnisse der Schweizer Geotraverse im Abschnitt Basel-Luzern. *Eclogae géologicae Helveticae,* 73/2, 501-512.

Rybach, V. L., Büchi, U. P., Bodmer, P. & Krüsi, H. R. 1980. Die Tiefengrundwässer des schweizerischen Mittellandes aus geothermischer Sicht. *Eclogae géologicae Helveticae,* 73/1, 293-310.

Rybach, V.L., Eugster, W. & Griesser, J-C., 1987. Die geothermischen Verhältnisse in der Nordschweiz. *Eclogae géologicae Helveticae,* 80, 521-534.

Rye, D.M. & Bradbury, H.J. 1988. Fluid flow in the crust: an example from a Pyrenean thrust ramp. *American Journal of Science,* 288, 197-235.

Saller, A.H. 1984. Petrologic and geochemical constraints on the origin of subsurface dolomite, Enewetak Atoll: an example of dolomitization by normal seawater. *Geology,* 12, 217-220.

Sandberg, P.A. & Hudson, J.D., 1983. Aragonite relic preservation in Jurassic calcite-replaced bivalves. *Sedimentology,* 30, 879-892.

Sandberg, P.A. 1983. An oscillating trend in Phanerozoic non-skeletal mineralogy. *Nature* 305, 19-22.

Sandberg, P.A. 1985. Aragonite cements and their occurrence in ancient limestones. In: *Carbonate Cements.* N. Schneidermann & P.M. Harris, (eds), Spec. Publ. Soc. Econ. Pal. & Min. # 36, 33-57.

Sarg, J.F. 1988. Carbonate sequence stratigraphy. *In: Sea-level Changes: an Integrated Approach.* C. K. Wilgus, B. S. Hastings, C. G. St.C. Kendall, H. W. Posamentier, C. A. Ross & J. C. Van Wagoner (eds). Spec. Publ. Soc. Econ. Paleont. Mineral. 42, 155-181.

Sawatzki, G.G. 1975. *Etude Géologique et Minéralogique des flyschs a grauwackes volcaniques du synclinal de Thônes (Haute-Savoie, France).* Thèse # 1643, Université de Genève, 368pp.

Schegg, R. 1992a. Coalification, shale diagenesis and thermal modelling in the Alpine foreland basin: the Western Molasse Basin (Switzerland, France). *Organic Geochemistry,* in press.

Schegg, R. 1992b. Thermal maturity of the Swiss Molasse Basin: indications for paleogeothermal anomalies? *Eclogae Geologicae Helvtetiae,* 85/3, in press.

Schlanger, S.O. Arthur, M.A., Jenkyns, H.C. & Scholle, P.A. 1987. The Cenomanian-Turonian oceanic anoxic event, 1. Stratigraphy and distribution of organic carbon-rich beds and the marine $\delta^{13}C$ excursion. In: *Marine Petroleum Source Rocks.* J. Brooks & A.J. Fleet (eds), Geological Society London, special publication, #26, p.371-400.

Schmoker, J.W., Krystinik, K.B. & Halley, R.B. 1985. Selected characteristics of limestone and dolomite reservoirs in the United States. *American Association of Petroleum Geologists Bulletin,* 69, p.733-741.

Scholle, P.A. 1978. *A colour illustrated guide to carbonate rock constituents, textures, cements and porosities.* American Association Petroleum Geologists, Memoire 27, Tulsa, 241pp.

Scholle, P.A. & Halley, R.B. 1985. Burial cements- out of sight, out of mind. In: *Carbonate Cements.* N. Schneidermann & P.M. Harris (eds), Spec. Publ. Soc. Econ. Pal. Min. # 36, 309-334.

Scholle, P.A., Stemmerik, L. & Ulmer, D.S. 1991. Diagenetic history and hydrocarbon potential of upper Permian carbonate buildups, Wegener Halvo area, Jameson Land Basin, East Greenland. *American Association of Petroleum Geology Bulletin*, 75, 701-725.

Sclater, J.G. & Christie, P.A.F. 1980. Continental stretching: an explanation of the post-mid-Cretaceous subsidence of the central North Sea basin. *Journal of Geophysical Research,* 85, 3711-3739.

Scoffin, T.P. 1987. *An Inroduction to Carbonate Sediments and Rocks.* Blackie, 274pp.

Searl, A. 1988. The limitation of 'cement stratigraphy' as revealed in some lower Carboniferous oolites from South Wales. *Sedimentary Geology,* 57, p.171-183.

Shinn, E.A. & Robbin, D.M. 1983. Mechanical and chemical compaction in fine grained shallow-water limestones. *Journal of Sedimentary Petrology,* 53, 595-618.

Shukla, V. & Baker, P.A. 1988. (editors). *Sedimentology and Geochemistry of Dolostones.* Soc. Econ. Paleao. Miner. Spec. Publ. 43, pp.266.

Sibley, D.F. 1982. The origin of common dolomite fabrics. *Journal of Sedimentary Petrology,* 52, 1987-1100.

Sibley, D.F. & Gregg, J.M. 1987. Classification of dolomite rock texture.*Journal of Sedimentary Petrology*, 57, 967-975.

Sibson, R.H. 1981. Fluid flow accompanying faulting: field evidence and models. In: *Earthquake prediction: An international review.* D.W. Simpson & P.G. Richards (eds). American Geophysical Union, Maurice Ewing Series, 4, 593-603.

Sibson, R.H. 1990. Conditions for fault valve behaviour. In: *Deformation Mechanisms, Rheology and Tectonics.* R.J. Knipe & E.H. Rutter (eds). Geological Society London special publication, #54, 15-28.

Siddans, A.W.B. 1979. Arcuate fold and thrust patterns in the Subalpine Chains of Southeast France. *Journal of Structural Geology,* 1, 117-126.

Simms, M. 1984. Dolomitization by groundwater-flow systems in carbonate platforms. *Gulf Coast Assoc. Geol. Soc. Trans.,* 34, 411-420.

Skelton, P.W. 1985. Preadaptation and evolutionary innovation in rudist bivalves. *Special papers in Palaeontology,* 33, p.159-173.

Skelton, P.W. & Gili, E. 1988. Palaeoecological classification of rudist morphtypes. *First Int. Conf. on rudists,* Belgrade, Oct. 1988.

Smart, G. & Clayton, T. 1985. The progressive illitization of interstratified illite-smectite from Carboniferous sediments of northern England and its relationship to organic maturity indicators. *Clay Minerals,* 20, p.455-466.

Smart, P.L., Dawans, J.M. & Whitaker, F. 1988. Carbonate dissolution in a modern mixing zone. *Nature,* 335, 811-813.

Stach, E., Mackowsky, M., Taylor, G.H., Chandra, D. & Teichmüller, R. 1982. *Stach's textbook of coal petrology.* (third edition) Berlin, Gebruder Borntaeger, 535pp.

Stalder, P.J. 1979. Organic and inorganic metamorphism in the Taveyannaz Sandstones of the Swiss Alps and equivalent sandstones in France and Italy. *Journal of Sedimentary Petrology,* 49, p.463-482.

Sroden, J. & Eberl, D.D. 1984. Illite. In: *Micas,* S.W. Bailey (ed.). Reviews in Mineralogy, # 13, p. 495-544. Mineralogical Society of America, Washington, D.C.

Surdam, R.C. & Crossey, L.J. 1985. Organic-inorganic reactions during progressive burial: key to porosity and permeability enhancement and preservation. *Philosphical Transactions Royal Society London,* A 315, 135-156.

Surdam,R.C., Crossey, L.J., Hagen, E.S. & Heasler, H.P. 1989. Organic-inorganic interactions and sandstone diagenesis. *American Association of Petroleum Geologists Bulletin,* 73, 1-23.

Sverjensky, D.A. & Garven, G. 1992. Tracing great fluid migrations. *Nature,* 356, 481-482.

Sweeney, J.J. & Burnham, A.K. 1990 Evaluation of a simple model of vitrinite reflectance based on chemical kinetics. *American Association of Petroleum Geologists Bulletin,* 74, 1559-1570.

Teichmüller, M. & Durand, B. 1983. Fluorescence microscopical rank studies on liptinites and vitrinites in peats and coals, and comparision with results of rock-eval pyrolysis. *International Journal of Coal Petrology,* 2, p.197-320.

Teichmüller, R. & Teichmüller, M. 1986. Relations between coalification and palaeogeothermics in Variscan and Alpidic foredeeps of Western Europe. In: *Paleogeothermics,* Lecture notes in Earth Sciences, 5, G. Buntebarth & L. Stegena (eds.), 53-78, Springer-Verlag, New York.

Teichmüller, M. 1987. Recent advances in coalification studies and their application to geology. In: *Coal and Coal Bearing Strata: Recent advances.* A. C. Scott (ed.), Geological Society, London, special publication, #32, 127-169.

Theriault, F. & Hutcheon, I. 1987. Dolomitzation and calcitization of the Devonian Grosmont Formation, northern Alberta. *Journal of Sedimentary Petrology,* 57, 955-966.

Tissot, B.P. & Welte, D.H. 1984. *Petroleum Formation and Occurrence. A new approach to oil and gas exploration.* Springer-Verlag, pp538.

Tissot, B. P., Pelet, R. & Ungerer, Ph. 1987. Thermal history of sedimentary basins, maturation indices and kinetics of oil and gas generation. *American Association Petroleum Geologists Bulletin,* 71, 1445-1466.

Trümpy, R. 1980. *Geology of Switzerland a guide book. Part A: An outline of the geology of Switzerland.* Wepf & Co., Basel. pp104.

Tucker, M.E. 1985. Calcitised aragonite ooids and cements from the late Precambrian Biri formation of southern Norway. *Sedimentary Geology,* 43, p.67-84.

Tucker, M.E. & Hollingworth, N.T.J. 1986. The upper Permian reef complex (EZ) of north east England: diagenesis in a marine to evaporitic setting. In: *Reef diagenesis.* J.H. Schroeder & B.H. Purser, (eds), Springer-Verlag, Beriln, p.270-290..

Tucker, M.E. 1988. (editor). *Techniques in Sedimentology.* Blackwells,

Tucker, M.E. & Wright, V.P. 1990. *Carbonate Sedimentology.* Blackwell Scientific Publications, Oxford. 482pp.

Tucker, M.E. 1992. Carbonate diagenesis and sequence stratigraphy. In: *Sedimentary Reviews* (Ed. by V.P. Wright). 1, in press.

Tyson, R.V. 1987. The genesis and palynofacies characteristics of marine petroleum source rocks. In: *Marine Petroleum Source Rocks.* J. Brooks & A.J. Fleet (eds), Geological Society London special publication, #26, p.47-67.

Tyson, R.V. & Funnel, B.M. 1987. European Cretaceous shorelines, stage by stage. *Palaeogeography, Palaeoclimatology Palaeoecology,* 59, 69-91.

Underwood, M. B., Fulton, D. A. & McDonald, K. W. 1988. Thrust control on thermal maturity of the frontal Ouachita Mountains, central Arkansas, USA. *Journal of Petroleum Geology,* ll (3), 325-339.

Vahrenkamp, V.C., Swart, P.K. & Ruiz, J. 1991. Episodic dolomitization of late Cenozoic carbonates in the Bahamas: evidence from strontium isotopes. *Journal of Sedimentary Petrology,* 61, 1002-1014.

Vahrenkamp, V.C. & Taylor, S.R. 1991. Deep burial dolomitization driven by plate collision: evidence fron strontium isotopes of Jurassic Arab IV dolomites from offshore Qatar. *American Association Petroleum Geologists Bulletin,* 75, 686.

Veizer, J. 1983. Chemical diagenesis of carbonates: Theory and application of trace element technique. In: *Stable isotopes in sedimentary geology.* M.A. Arthur & T.F. Anderson (eds) SEPM short course #10, Dallas, 1983. p.3-1 to 3-100.

Velde, B., Suzuki, T. & Nicot, E. 1986. Pressure-temperature-composition of illite/smectite mixed-layer minerals: Niger delta mudstones and other examples. *Clays and Clay Minerals,* 34, 4335-441.

Vernet, J. 1980. Mise en évidence d'une orogenèse et d'une tectonique alpines actuelles par les mesures de nivellement. *Comptes Rendues sommaires géologie de France,* Fasc. 6, 246-249.

Villars, F. 1986. Structure et cinématique des déformations dans la chaîne des Aravis (Zone delphino-helvétique, Haute-Savoie, France): implications régionales. *Géologie Alpine,* 62, 107-116.

Villars, F. 1988. Progradation de la Formation de Wang dans les chaînes subalpines septentrionales (Alpes occidentales, France) au Maastrichtien supérieur: biostratigraphique et milieu de dépôt. *Eclogae géologicae Helveticae,* 81, 669-687.

Villars, F. 1992. *Evolution paléogéographique du domaine delphino-helvétique (entre Chartreuse et Morcles) au Crétacé supérieur (Turonien-Maastrichtien): Biostratigraphique, sédimentologie et dynamique sédimentaire sur une rampe carbonatée.* Publication du Département de Géologie et de Paléontologie, Univ. de Genève, pp. 173.

Villars, F., Müller, D. & Lateltin, O. 1988. Analyse de la structure du Mont Charvin (Haute-Savoie) en termes de tectonique synsédimentaire paléogène: Conséquences pour l'interprétation structurale des chaînes septentrionales. *Comptes Rendus Academie Sciences, Paris,* 307/2, 1087-1090.

Wanless, H.R. 1979. Limestone response to stress: pressure solution and dolomitization. *Journal of Sedimentary Petrology,* 49, 437-462.

Waples, D.W. 1990. Maturity modelling of sedimentary basins: Approaches, limitations and prediction of future developements. In: *Quantitative Dynamic Stratigraphy.* T.A. Cross (ed.), Prentice Hall, 181-193.

Waples, D.W., Kamata, H. & Suizu, M. 1992a. The art of maturity modelling. Part 1: Finding a satisfactory geologic model. *American Association of Petroleum Geologists Bulletin,* 76, 31-46.

Waples, D.W., Kamata, H. & Suizu, M. 1992b. The art of maturity modelling. Part 2: Alternative models and sensitivity analysis. *American Association of Petroleum Geologists Bulletin,* 76, 47-66.

Warner, M.A. & Royse, F. 1987. Thrust faulting and hydrocarbon generation: discussion. *American Association of Petroleum Geologists Bulletin,* 71, 882-889.

Weaver, C.E. 1960. Possible use of clay minerals in the search for oil. *American Association Petroleum Geologists Bulletin,* 44, p.1505-1518.

Weaver, C.E. & Beck, K.C. 1971. Clay water diagenesis during burial: how mud becomes gneiss. *Geological Society of America, Special paper,* 134. 96pp.

Weaver, C.E. & Associates. 1984. *Shale-slate metamorphism in the southern Appalachians.* Developments in Sedimentology, 10, Elsevier, Amsterdam, 239pp.

Weaver, C.E. 1989. *Clays, muds and shales.* Developments in Sedimentology, 44. Elsevier, New York, 819pp.

Welbon, A.I. 1988. *Deformation styles and localisation of thrust faults in the external French Alps.* Unpublished Ph.D, Univeristy of Leeds.

Wildi, W., Funk., H., Loup, B., Amato, E. & Huggenberger, P. 1989. Mesozoic subsidence history of the European marginal shelves of the Alpine Tethys (Helvetic realm, Swiss Plateau and Jura). *Eclogae géologicae Helveticae,* 82, 817-840.

Wilkinson, B.H. (1979). Biomineralisation, palaeooceanography and the evolution of calcareous marine organisms. *Geology* 7, 526-527.

Wilkinson, B.H. 1983. *Carbonate petrography.* American Association of Petroleum Geologists Short Course, Part III, p.1-35

Wilkinson, B.H. Smith, A.L & Carrol, A.R. 1985. Submarine hydrothermal weathering, global eustacy, and carbonate polymorphism. *Journal Sedimentary Petrology* 55, 171-183.

Wilson, E.N., Hardie, L.A. & Philips, O.M. 1990. Dolomitization front geometry, fluid flow patterns and the origin of massive dolomite: The Triassic Latemar buildup, northern Italy. *American Journal of Science,* 290, 741-796.

Wilson, J.L. 1975. *Carbonate Facies in Geologic History.* Springer-Verlag, Berlin. 471pp.

Wilson, J.L., Wilkinson, B.H., Lohmann, K.C. & Hurley, N.F. 1983. *New ideas and methods for exploration for carbonate reservoirs - a short course.* Dallas Geological Society, American Association of Petroleum Geologists Annual meeting.

Wilson, M.J. 1987. (editor). *A Handbook Of Determinative Methods in Clay Mineralogy.* Blackie, 308pp.

Woo, K.S. 1986. *Isotopical-textural-chemical studies of mid-Cretaceous limestones: implications for carbonate diagenesis and paleao-oceanography.* Unpubl. PhD thesis, University of Illinois at Urbana-Champaign.

Woronick, R.E.& Land, L.S. 1985. Late burial diagenesis, Lower Cretaceous Pearsall and Lower Glen Rose formations, South Texasa. In: *Carbonate Cements.* N. Schneidermann & P.M. Harris (eds),. Special Publication Soc. Econ. Paleao. Min., #36, 265-275.

Wright, V.P. 1988. Palaeokarsts and palaeosols as indicators of palaeoclimate and porosity evolution: a case study from the Carboniferous of South Wales. *In: Paleokarst.* N.P. James & P.W. Choquette, (eds), Springer-Verlag, Berlin. 329-341.

Yardley, B.W.D., Banks, D.A., Davies, G.R., McCraig, A.M. & Grant, N.T. 1989. Chemistry and isotopic composition of fluid from a deep thrust zone, Central Pyrenees. In: *Water-Rock Interaction.* WRI-6. D.L. Miles (ed), A.A.Balkema, Rotterdam, 789-792.

Yonkee, W.A, Parry, W.T., Bruhn, R.L. & Cashman, P.H. 1989. Thermal effects of thrust faulting: constraints from fluid-inclusion observations, Willard thrust sheet, Idaho-Utah-Wyoming thrust belt. *Geological Society of America Bulletin,* 101, 304-313.

Yurtsever, Y. 1975. Worldwide survey of stable isotopes in precipitation. Report section of isotope hydrology. *I.A.E.A.,* Nov., 1975.

Zenger, D.H., Dunham, J.B. & Ethington, R.L. 1980. (editors) *Concepts and Models of Dolomitization.* Soc. Econ. Paleao. Mineral., Spec. Publ., #28, 320pp.

Zenger, D.H. 1983. Burial dolomitization in the Lost Burro Formation (Devonian) east-central California and the significance of late diagenetic dolomitization. *Geology,* 11, 519-522.

Zenger, D.H. & Dunham, J.B. 1988. Dolomitization of Siluro-Devonian in a deep core (5,350 m), southeastern New Mexico. In: *Sedimentology and Geochemistry of Dolostones.* V Shukla & P. A Baker (eds) Soc. Econ. Paleao. Mineral., Spec. Publ., #43, 161-174.

Zweidler, D. 1985. *Genesé des Gisements d'Asphalte des Formations de la Pierre Jaune de Neuchâtel et Calcaire Urgoniens du Jura (Jura Neuchâtelois et Nord Vaudois).* Ph.D. Thèsè Faculté des Sciences, Université de Neuchâtel.

Appendix 1. Graphic logs through the Urgonian and location of samples.

In localities with good continuous exposure and access, the Urgonian was logged and sampled in detail. The following are simplified versions of these logs with the positions of samples collected on them.

1) Grand Goulets (#3 on Fig.3.1).

Located on the D518 road to the north-east of the small hamlet of les Baraques-en-Vercors. The section begins at the western end of the Grand Goulets, at the first of a series of small tunnels.

2) Gorge de la Bourne (#4 on Fig.3.1).

Located on the D531 road between la Balme-de-Rencurel and Pont-en-Royans (Vercors). The section starts at the base of the Urgonian escarpment in the lower western half of the gorge, just to the east of a spot height (522m).

3) Gorge du Nant (#6 on Fig. 3.1).

Located on the D22 road to the east of the small town of Cognin-les-Gorges (on the northwestern corner of the Vercors, on the N532 main road). The section begins at the base of the Urgonian escarpment on the eastern side of a series of road tunnels and avalanche shelters.

4) Dent de Crolles (#9 on Fig.3.1).

Dent de Crolles is located in the southeast corner of the Chartreuse. The section runs up the footpath which leads up from Col du Coq (on the D30e road). It begins at the lower most exposures of the Urgonian.

5) Pic d'Oeillette (#11 on Fig. 3.1).

Located on the D520b road to the west of St. Pierre-en-Chartreuse and Pont St. Bruno. The section begins at the base of the Urgonian escarpment to the west of the prominent rock which is Pic d'Oeillette.

6) Gorge du Frou (#12 on Fig.3.1).

Located on the D520c road to the east of Le Châtelard (central Chartreuse). The section begins at the base of the Urgonian escarpment to the west of the road tunnel and below the Pas de Frou.

7) Dents d'Arclusaz (#16 on Fig.3.1).

This section is located in the eastern Bauges massif and runs up the footpath which approaches Dents d'Arclusaz from the village of Epernay (located on the D911 road). The section begins at the lowermost exposures of the Urgonian.

8) La Tournette (#21 on Fig. 3.1).

This section is located on the western face of La Tournette (which is to the east of Lac d'Annecy, in the southwestern corner of the Bornes Massif), and begins at the base of the Urgonian cliff face to the east of the Refuge de la Tournette.

9) Pic de Jallouvre (#26 on Fig. 3.1).

Pic de Jallouvre is located on the eastern edge of the Bornes massif. The section follows the footpath from Col du Rasoir up the northwestern face of Pic de Jallouvre (located just to the west of the Col de la Columbière, on the D4 road).

10) Northwest Termine road section (upper road) (#25 on Fig.3.1).

This section is located 1 km to the north of the small village of Termine on the small unnamed road which runs parallel to the main D12 road, which is a few 100 metres below. The section begins at the southeastern end (Termine end) of the outcrop.

11) Northwest Termine road section (lower road) (#25 on Fig.3.1).

This section is located 1 km to the north of the small village of Termine on the D12 road in the Bornes massif. The section begins at the southeastern end (Termine end) of a small gorge.

12) Upper part of the Borne valley (#23 on Fig. 3.1).

Located at the eastern end of the Borne valley (eastern edge of the Bornes massif) on the D12 road, about 1.5 km to the north of St.-Jean-de-Sixt. The section begins at the western end of a small gorge.

13) La Clusaz (#22 on Fig.3.1).

This section is located to the immediate northwest of La Clusaz, in the Thônes valley (between the Bornes and Aravis). The section begins near the 1030m spot height and starts in the lower Urgonian.

The logs and key for them are shown in Data Tables A.1.

Appendix 2. Geochemical Data.

A.2.1.1 Stable Isotopic Analysis.

All stable isotopic determinations were made at the NERC Isotope Geosciences Laboratory, at Keyworth, Nottingham.

All carbon and oxygen isotopic compositions are relative to the PDB international standard in per mil (‰) using the δ notation:

$$d(x) = [R(z) - R(std)] / R(std) \times 1000$$

where $R(z) = {}^{13}C/{}^{12}C$ or ${}^{18}O/{}^{16}O$ sample

and $R(std) = {}^{13}C/{}^{12}C$ or ${}^{18}O/{}^{16}O$ standard PDB

Isotopic fractionation between two substances A and B during some physio-chemical process is expressed as a fractionation factor, αA-B

$$\alpha A\text{-}B = R(A)/R(B) = [1000 + \delta(A)]/[1000 + d(B)]$$

A.2.1.2 Sampling method.

Isotopic analysis of carbonates was performed after petrographic study and generally after cation analysis. Samples were produced using a hand held dentistry drill with varying sizes of tungsten carbide drill bit (from 0.4 to 1.2 mm) depending on the size of the area to be sampled.

A.2.1.3 Analytical method.

About 10mg of carbonate powder were left for up to 24 hours to completely react under vacuum with 4ml of anhydrous 100% phosphoric acid in a temperature bath at 25°C for calcites and at 55°C for dolomites. During the first dolomite batch the same samples were also reacted at 25°C for a duration of sixty hours, to check for any fractionation effects. The difference between the two runs was negligible, so all future dolomite batches were reacted at 25°C for sixty hours.

The evolved carbon dioxide gas was collected and analysed on a VG Isogas SIRA 10 (series 2) mass spectrometer. The samples were generally run in batches of sixteen unknowns, two duplicates from previous runs and two samples of laboratory standards (MCS 11 was used for both calcites and for dolomites).

Additional correction factors were required to correct for the temperature dependant fractionation for ${}^{18}O$ during the acid reaction (see Fairchild et al., 1988). The factors used were:

$$\text{calcite } \alpha^{25} = 1.01025$$

$$\text{dolomite } \alpha^{25} = 1.01109$$

and were applied using:

$$\delta^{18}O \text{ solid} = (\delta^{18}O \text{ gas, measured} + 1000) / \alpha - 1000$$

A.2.1.4 Estimation of error.

A random selection of twenty MCS standards that were run during three visits to Keyworth MCS with each batch of calcite or dolomite unknowns gave:

	n	$\delta^{18}O$	S.D.	$\delta^{13}C$	S.D.
MCS 11	20	-9.19	+/-0.07	-0.7	+/-0.03

Sample duplicates were run in batch and the average reproducibility (based on 10 batches of 1 sample) is:

$\delta^{18}O$ = 0.06 +/-

$\delta^{13}C$ = 0.03 +/-

A.2.2.1 Carbonate cation chemistry.

Trace element concentrations within calcites and dolomites were made on the (Inductively Coupled Plasma - Atomic Emission Spectrometry (ICP-AES) at RHBNC, Egham.

A.2.2.2 Sample preparation.

The sampling techniques are as for the stable isotopic analysis, described above in section A.

A.2.2.3 Analytical method.

An accurately determined mass of 40.0 mg (+/- 0.1mg) of oven-dried powder were reacted with 5mL of 10% HCl and placed in an oven at 60°C for two hours and then 5ml of deionised water was added to each sample. Blanks and standards (spec-pure calcium carbonate) were prepared in a similar way.

Calcium carbonate standards and laboratory standards were run every ten unknowns to check for drift.

Comparison of analyses of samples of spec-pure calcite prepared as above and those prepared in exactly the same way but with rapid reaction under room conditions in a few minutes (instead of two in the oven) were identical (within analytical error); thus evaporation during oven-warming was insignificant. Therefore the volume can be taken as 10ml.

A.2.2.3 Data correction.

The ICP-AES measures wavelength intensity and these are processed on-line to give concentrations (assuming 100mg of sample in 10ml of solution). The ICP-AES output was of the form:

sample	CaO (wt%)	MgO (wt%)	Fe_2O3(wt%)	MN (ppm)	SR(ppm)
X	CAO	MGO	FE2O3	MN	SR

and for each sample there is a mass of sample (dissolved in 10mL) in mg = MAS.

? Standards!

A SPSS-X statistics program was written to convert the above to:

CAR = % carbonate fraction (assuming all Ca and Mg are from calcite and/or stoichiometric dolomite).

DOL = % dolomite fraction (assuming that all the Mg is from stoichiometric dolomite and that there is no high Mg-calcite).

DoC = % dolomite in the carbonate fraction.

FE, MN, SR = Fe, Mn, Sr expressed as ppm of the carbonate fraction.

CAR = (CAO * [$CaCO_3$]/[CaO] + MGO*[$MgCO_3$]/[MgO]*100/MAS

= (CAO * 1.784 +MGO*2.092) * 100/MAS

DOL =(MGO * [$CaMg(CO_3)2$]/[MgO] * 100/MAS

=MGO * 4.575 * 100/MAS

DoC = DOL/CAR * 100

Fe = FE2O3 * 100/MAS * 100/CAR * [FE2O3]/[FeO] * 10000

= FE2O3 * 100/MAS * 100/CAR * 3497

Mn = MN * 100/MAS *100/CAR

Sr = SR * 100/MAS * 100/CAR

(where [$CaCO_3$] denotes the relative formula mass of calcite *etc*).

A.2.2.4 Error estimation.

Drift was found to be negligible and the reproducibility was excellent. The following values are on-line calculations for 15 determinations of the KC11 laboratory standard, which was run every 10 unknowns during one analysis session:

KC11 CaO = 6.58 +/- 0.06%

MgO = 4.10 +/- 0.05%

Fe_2O_3 = 8.83 +/- 0.09%

Mn = 1069 +/- 10ppm

Sr = 376 +/- 5ppm

The error at this stage is therefore *ca.* 1%. The estimated error in the CAR is *ca.* 3% leading to an error of *ca.* 6% in DOL. The error in Mn, Fe and Sr is estimated to be *ca.* 5%.

A.2.3. Stable isotope and trace element data sheets.

The results of the stable isotope and ICP-AES study are listed in the following data tables:

Appendix 3 X-Ray Diffraction and X-Ray Fluorescence analysis of whole rock and clay separate samples.

A.3.1. Whole rock XRD analysis.

This technique was performed on a variety of different samples. Principally it was used to ascertain the composition of Hauterivian mudstones. It was also used to discover the composition of rudist shells (aragonite or calcite), karst infill material and the presence or absence of dolomite (in unsectioned rocks).

A.3.1.1 Sample preparation.

All samples were produced using either a hand held dentistry drill on slabbed and cleaned surfaces of a sample or by crushing a cleaned sample by hand with an agate mortar and pestle.

In the case of whole rock mudstone analysis, the sample was crushed by hand using a tungsten mill and then sieved through a 150 micron mesh sieve onto a glass slide coated with double-sided sticky tape. This proved to be an effective way of producing randomly orientated slides.

A.3.2 Clay separation XRD analysis.

Clay separation slides were made by treating hand-crushed powders with Jackson's solution (a Na acetate buffer of 82g NaOAc plus 27ml of HOAc per litre) to remove carbonates. This procedure was followed after advice from Dr. D. Eberl (USGS, Boulder, Colorado, USA, pers. comms, 1989). 40 g of sample were digested in 160 ml of buffer for 30 minutes at about 50°C using a magnetic stirrer. The residue was then dialysed with distilled water, re-washed with buffer under the same conditions and then re-dialysed. The samples were left to settle out for 3.5 hours at 25°C, after which the top 5cm containing the <2 micron fraction was pipetted off (after Hardy & Tucker, 1988). This solution was then centrifuged onto four glass slides, so that reproducibility of results could be checked.

All samples were run first in their air dried state, then after being treated with ethylene glycol for over four hours, and finally after being heated up to 400°C for thirty minutes. This procedure enabled the identification of all clay mineral species within the Hauterivian (Wilson, 1987). Several samples were ran in duplicate to check if the results were reproducible, which they were.

Percentages present of respective minerals was calculated using an Albrit Polar Planimeter.

Composition of the mixed-layer illite/smectite species was estimated from the position of the I/S peak (see Fig. 6.15 and Wilson, 1987).

All samples were run on a Philips PW1130 3Kw X-Ray Diffractometer, using CoKα, running at 40 kv and 25ma.

A.3.3 Miscellaneous XRD analysis.

XRD analysis was also carried out on rudist shell samples, material infilling karst related dissolution and pore filling fine grained material from Villaret Rouge (see section 3.8.4) to ascertain the composition of these. The samples were prepared as in section A (above, for whole rock XRD analysis) and analysed as randomly orientated samples by settling the powder on to glass slides from acetone solution. The running conditions are the given above (in B).

A.3.4 Whole rock X-ray fluorescence analysis.

A selected batch of twelve samples of Hauterivian mudstone were analysed for their major element geochemistry using X-Ray Fluorescence.

A.3.4.1 Preparation.

Samples were cleaned using distilled water and any weathered surfaces removed. Initial crushing of the samples was done by jaw crusher. The samples were then crushed to a fine powder, approximately 50 microns, using a Tema Tungsten Carbide Swing Mill. The powders were mixed with a 4% solution of polyvinyl alcohol (Mowoil) and then pelleted into discs (30 mm diameter) using a Specac Hydraulic Press operating at 7 tons pressure.

A.3.4.2 Analysis.

The unknown samples together with a selection of Sedimentary International Geochemical Standards and in-house standards were analysed for major oxides SiO_2, Al_2O, Fe_2O_3 (as total Fe), MgO, CaO, Na_2O, K_2O, TiO_2.

The analysis was carried out using a Philips PW 1400 X-Ray Spectrometer system incorporating a PW1500/10 Automatic Sample Changer. Excitation was from a Rhodwin 3Kw X-Ray tube.

Calibration of the background corrected intensity data with the composition of the standards and the determination and correction for interelement influence effects were carried out by means of the Philips X41 software package called ALPHAS.

A.3.5 XRD and XRF data tables.

Results of both XRD and XRF analysis are shown in the following data tables:

Data Table A.3.1 XRD analysis of Hauterivian whole rock samples.

Data Table A.3.2 XRD analysis of Hauterivian clay samples.

Data Table A.3.3 Miscellaneous XRD results.

Data Table A.3.4 Whole rock Hauterivian XRF results.

Appendix 4 Organic maturity and Total Organic Carbon analysis and data.

A.4.1 Vitrinite reflectance and spore fluorescence.

A.4.1.1 Vitrinite reflectance.

The samples were prepared by firstly being gently crushed by hand until the material was granular in nature. Then set in epoxy resin and the blocks produced polished.

The vitrinite reflectance values given in this thesis are average values (Ro_{aver}), that is measurements were made in polarised light but the stage was not rotated. Measurements were in oil of 1.518 refractive index at a wavelength of 546nm. All measurements were made on a Zeiss Standard Universal microscope with x600 magnification.

A.4.1.2 Spore fluorescence.

The same samples used for the vitrinite reflectance measurement were used to study the spore fluoresence within the samples. All samples were inspected under a Zeiss Blue Light U.V. microscope using an HBO 100 watt mercury lamp. The exciting wavelength was 370-420nm, the dichroic mirror set at 470nm and the barrier filter at 530nm. The colours produced were estimated visually.

A.4.2 T_{max} analysis and total organic carbon - procedures and results.

A.4.2.1 Rock-Eval analysis (T_{max}).

Rock-Eval analysis (T_{max}) was carried out on hand powdered samples, using a LECO THA-200 Thermolytic Hydrocarbon Analyser at NRG, Newcastle.

Samples were run with the Kimmeridge Clay standard:

S1 - 0.51/0.43 mgg^{-1}

S2 - 37.9/36.6 mgg^{-1}

Tmax 422/421°C

All samples were run in duplicate.

A.4.2.2 Total Organic Carbon determinations.

Total Organic Carbon values were obtained by flushing through the powdered homogenized samples with 50% hydrochloric acid twice. This removed any inorganic carbon. The samples were then rinsed four times with distilled water. Copper and iron were added (to produce an increase in burning temperature of the samples), which were analysed on a LECO Carbon Analyser at NRG, Newcastle.

A rough guide to kerogen type can be obtained by the hydrogen index (S2/TOC*100). However without the oxygen index this is only speculative indication. For example type IV kerogens may be indicated by a low hydrogen index, but may in fact due to the oxidation of a different kerogen type in the depositional environment.

A.4.3 Organic maturity and TOC data tables.

Measured values of Ro, estimates of spore fluoresecence and the results of the Rock-Eval and TOC anlysis are given in the data tables:

Data Table A.4.1 Organic maturity data.

Data Table A.4.2 Rock-Eval and TOC results.

Appendix 5. Basin modelling data tables.

A.5.1 Lithological data and computed values for initial porosity, compaction factor.

The Basinmod modular modelling software package, version 2.83 (developed by Platte River Associates) was used to model the burial and thermal history of selected locations within the Subalpine Chains (see Chapter 8).

The basic lithological data used in the construction of these plots is shown in the data sheet along with the compaction factor (using the Falvey & Middleton, 1981, equation, see equation 8.3) and the calculated initial porosity for each formation.

The ages, lithological data and computed values for initial porosity, compaction factor used in the modellling are shown in the data table:

Data Table A.5.1 Basinmod data.

Data table A.1.

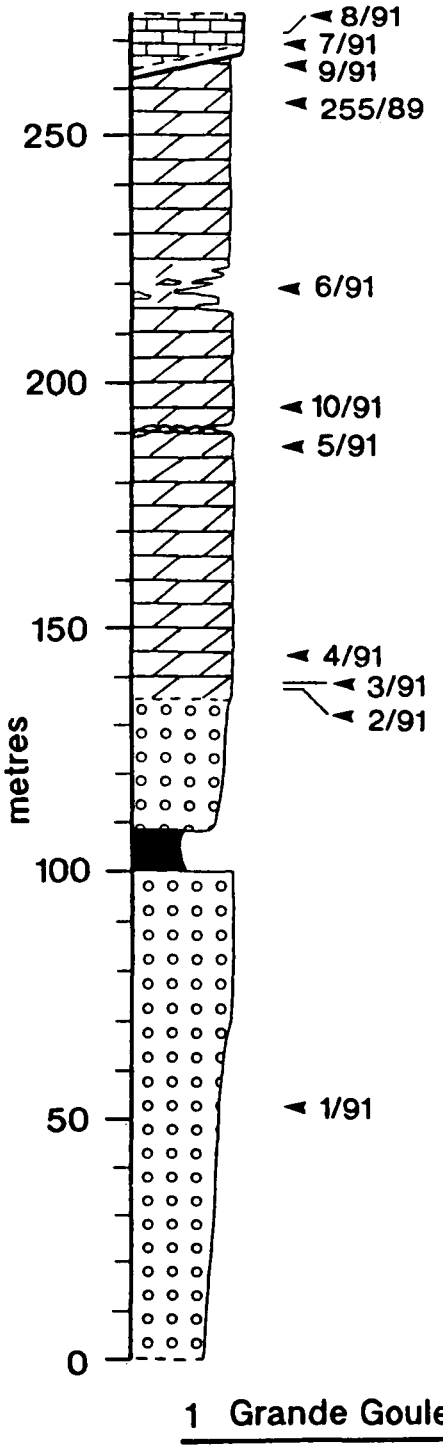

1 Grande Goulets

Key (applies to all logs)

- platform shelf facies (rudist facies)
- platform margin facies
- dolomitized limestone
- partially dolomitized limestone
- shale
- Aptian/Albian glauconitic sands
- ..... beach facies
- ~~~~ chara wackestones
- dissolution cavities
- karst horizons/exposure surfaces

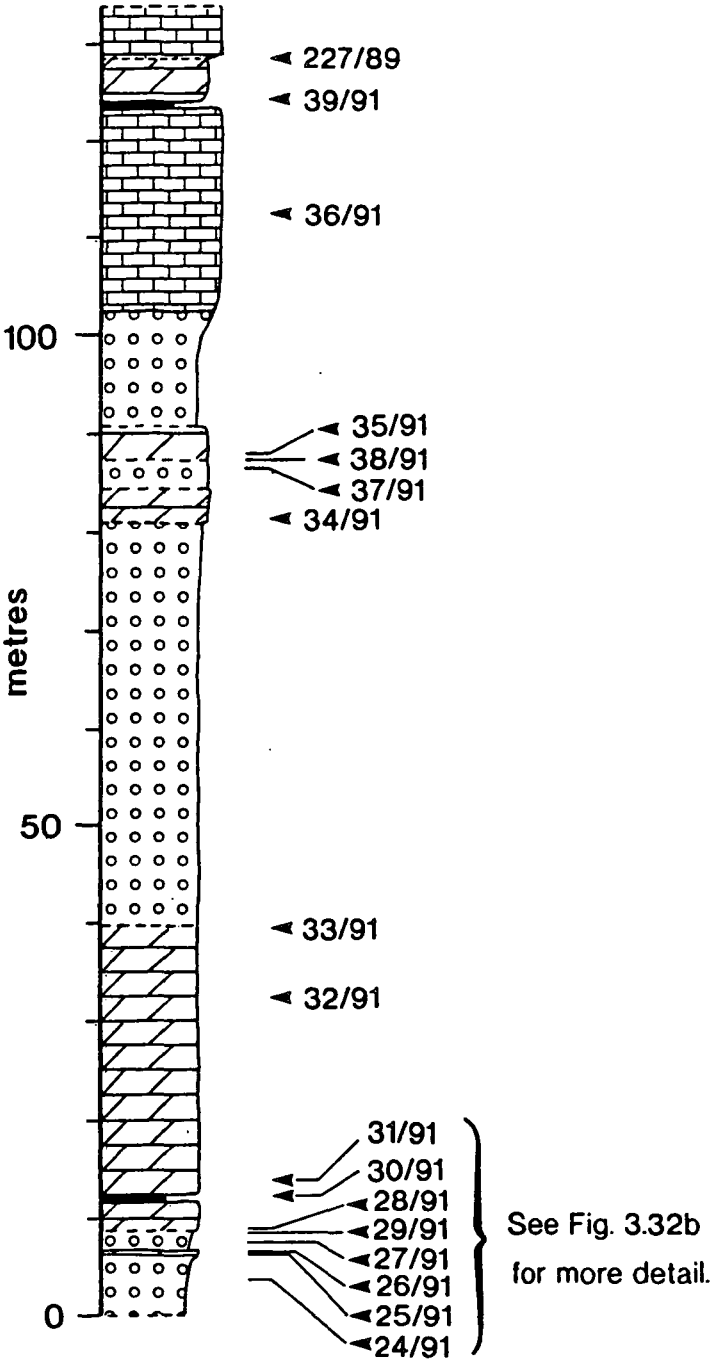

2 Gorge de la Bourne

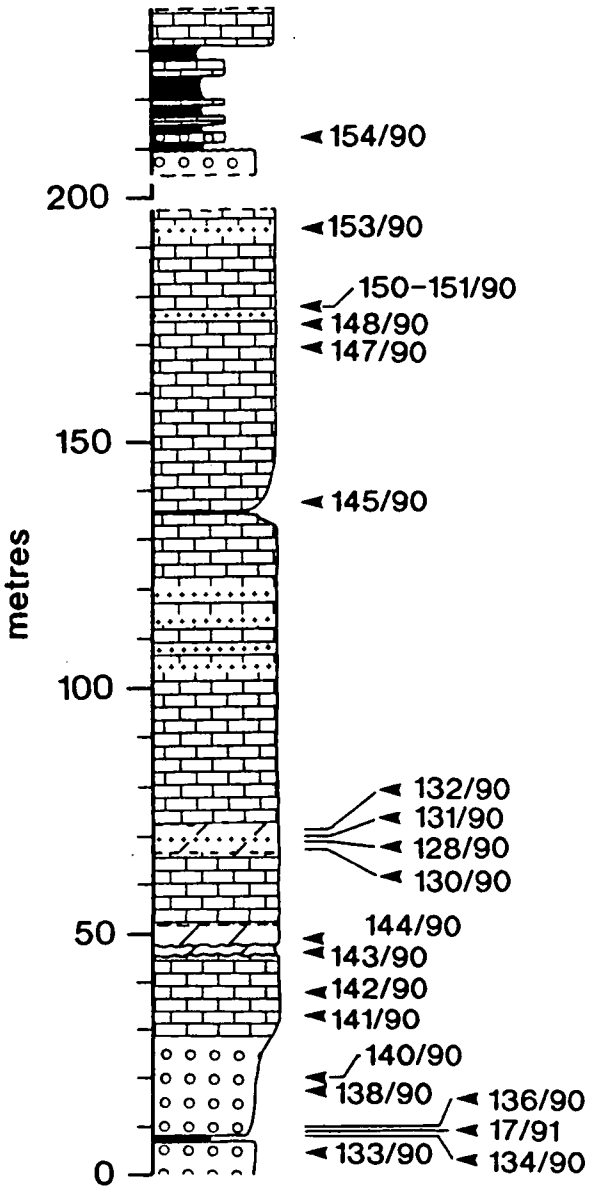

3 Gorge du Nant

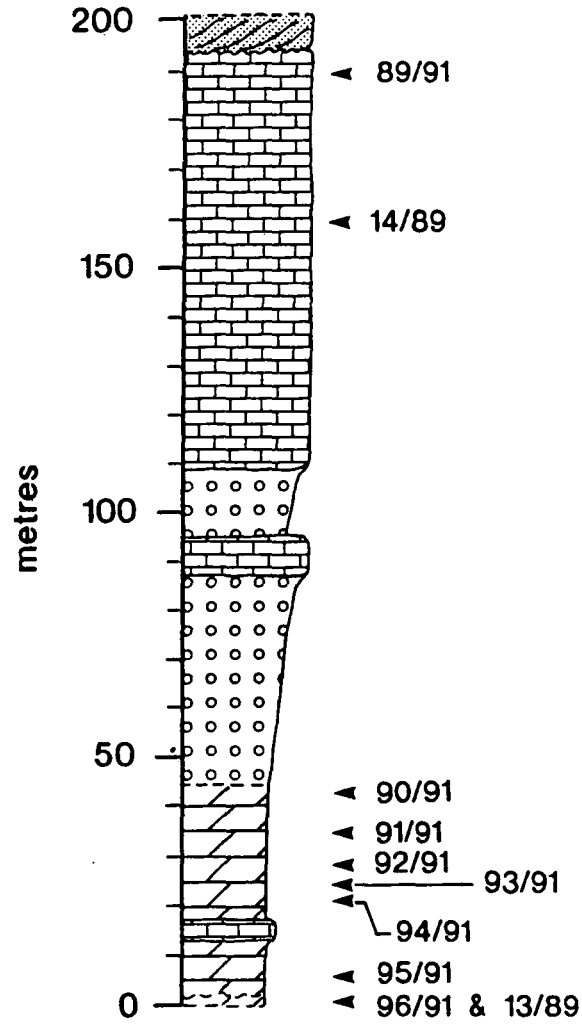

4 Dent des Crolles

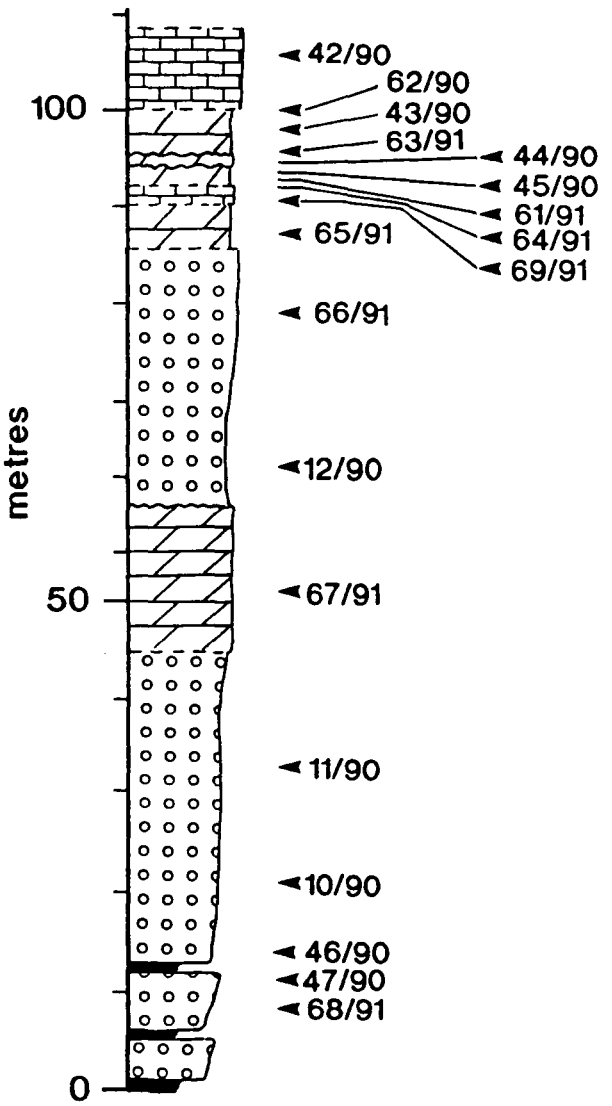

5 Pic de Oeillette

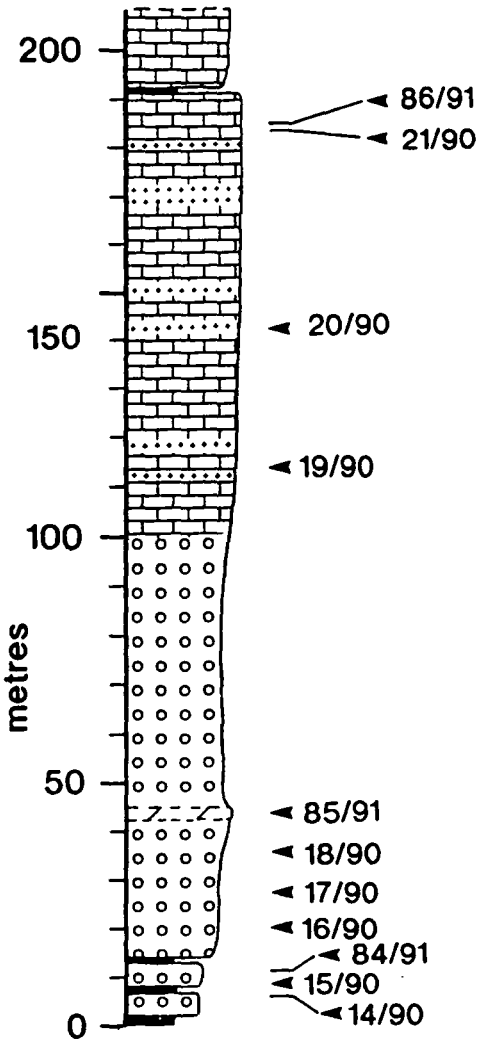

6 Gorge du Frou

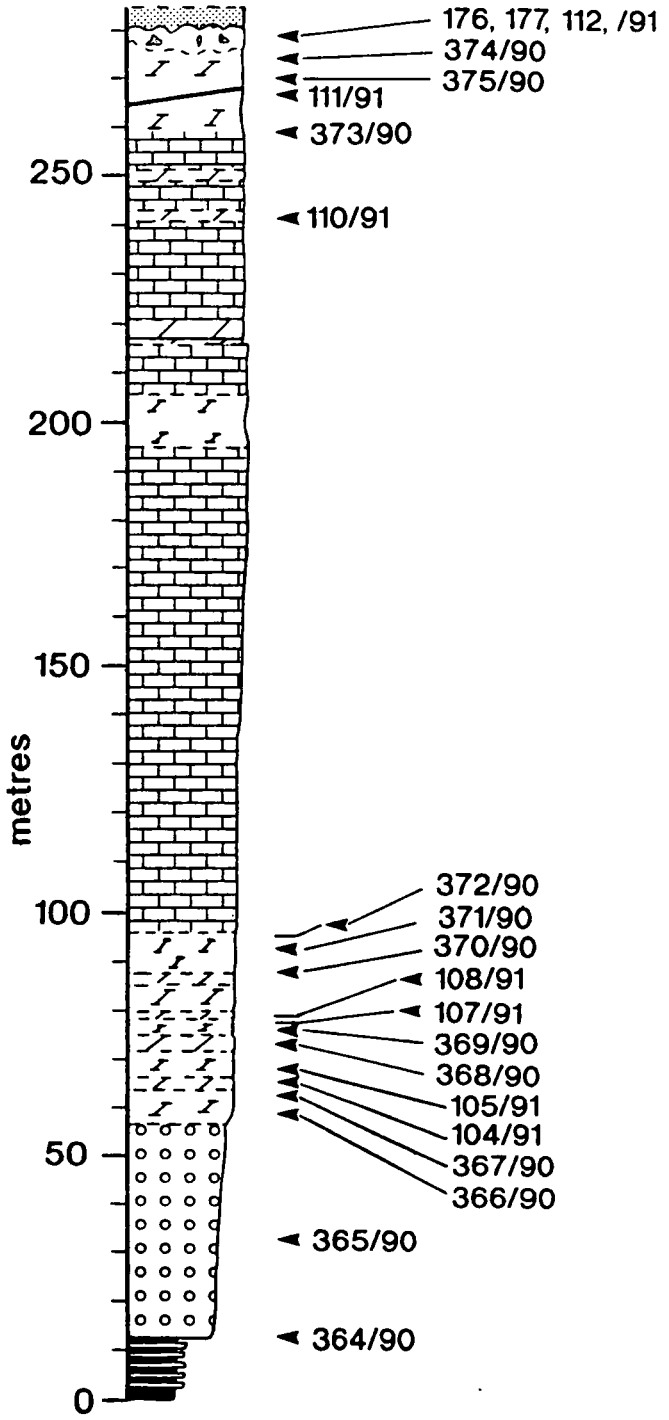

7 Dents d'Arclusaz

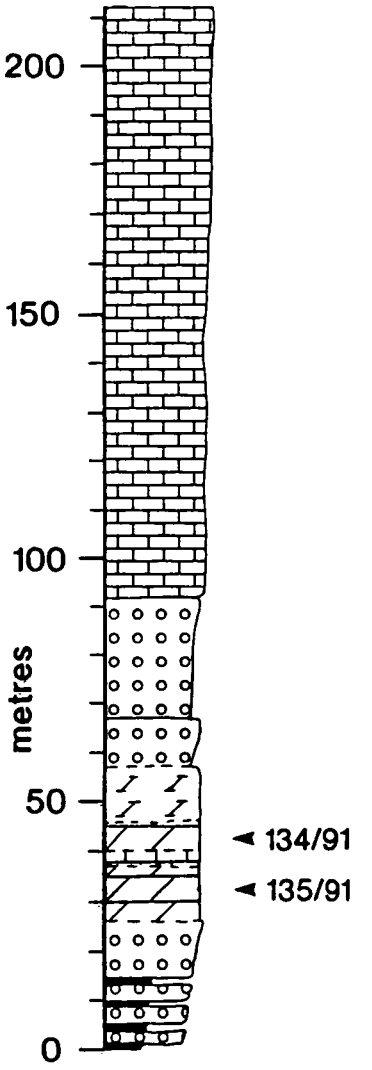

8 La Tournette

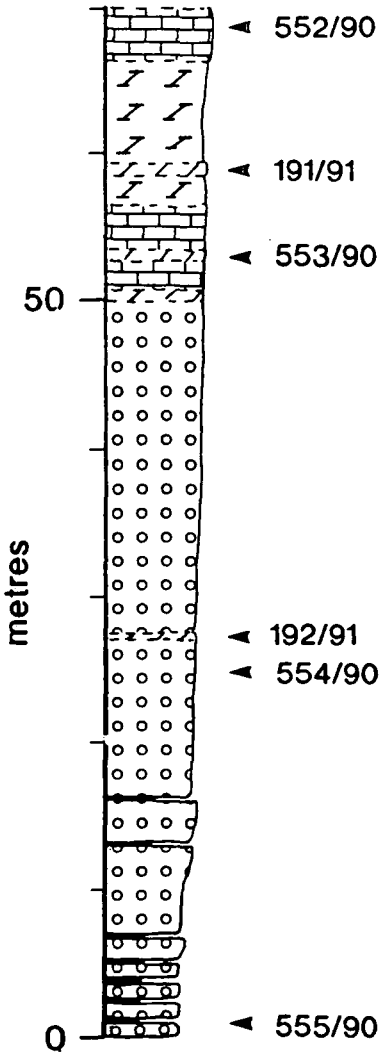

9 Pic de Jallouvre

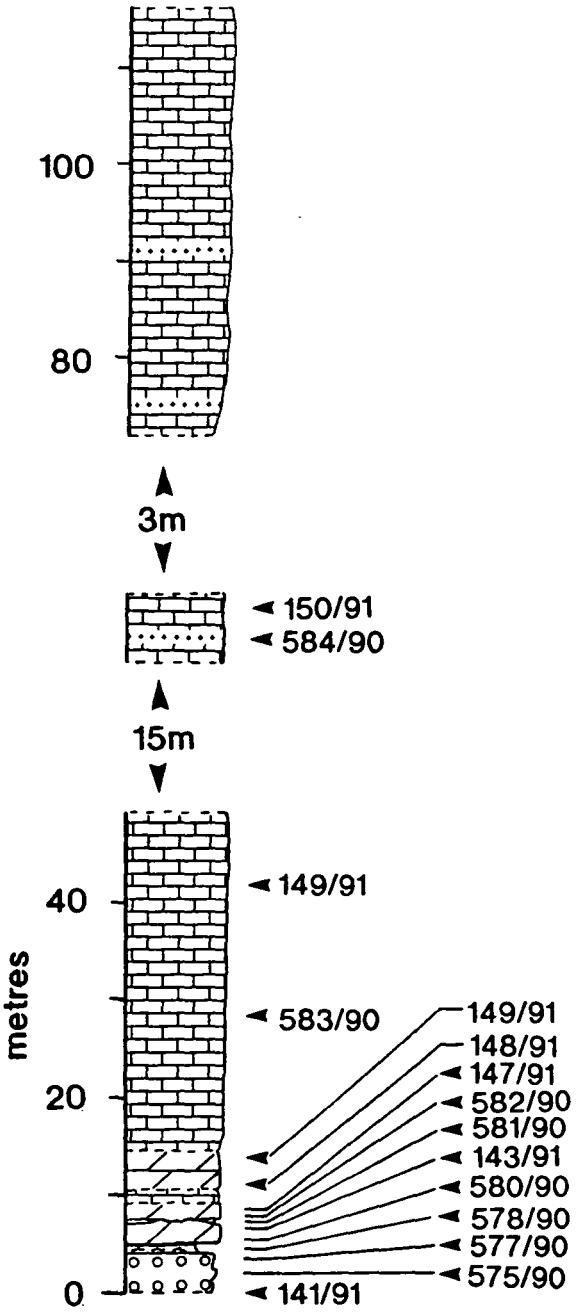

10 NW Termine road section (upper road)

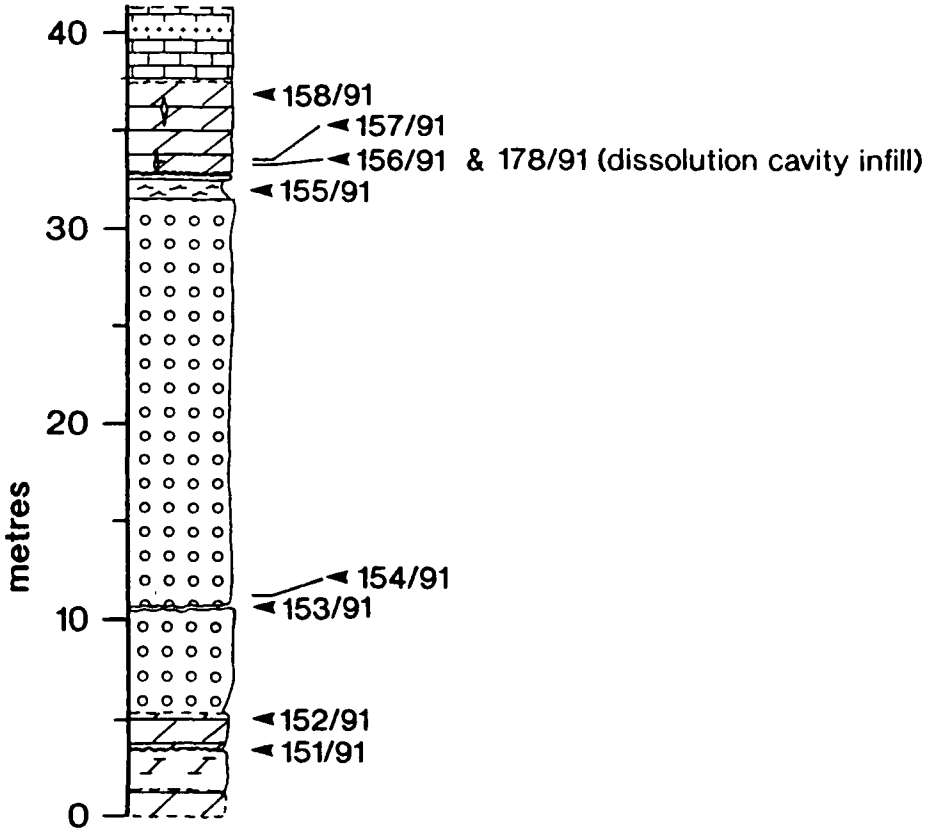

11 NW Termine road section (lower road)

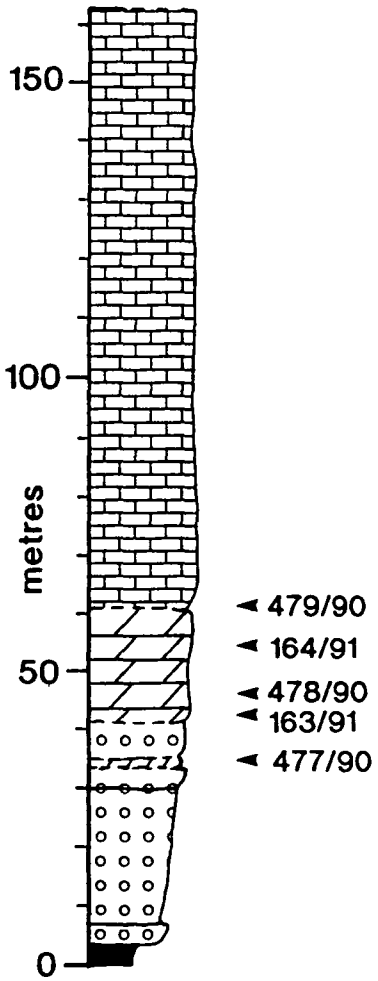

12 Upper Borne Valley

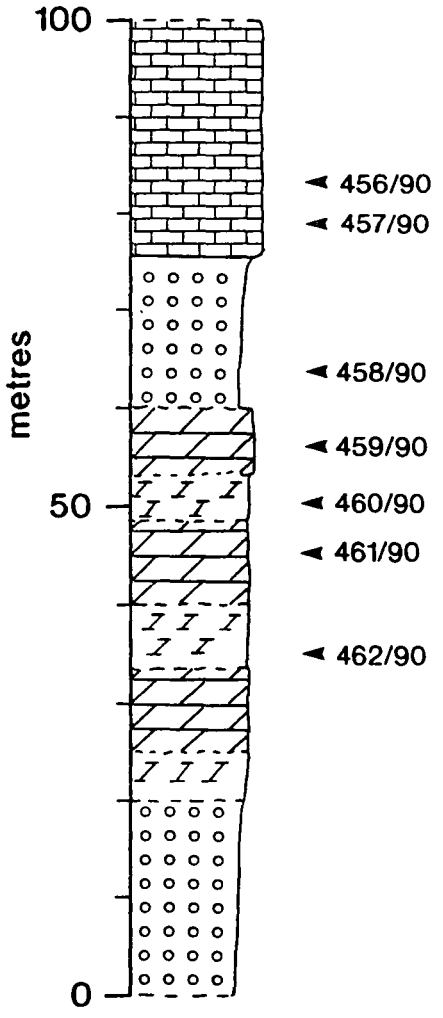

13 La Clusaz

Data Table A.2.1

Rudist isotopes

SAMPLE	O18	C13	Loc.n	Loc.n	Age	SAMPLE
21b-90	-4.8	-0.11	Chartreuse	Gorge de Frou	Ur	21b-90
42b-90	-4.02	1.56	Chartreuse	Pic d'Oillette	Ur	42b-90
128b-89	-5.45	-0.54	Chartreuse	Les Echelles	Ur	128b-89
134b-89	-4.29	-0.51	Chartreuse	Gorge de Frou	Ur	134b-89
243b2-90	-1.92	2.84	Chartreuse	Granier	Ur	243b2-90
243b-90	-2.42	2.88	Chartreuse	Granier	Ur	243b-90
226b1-90	-2.9	3	Vercors	Moucher	Ur	226b1-90
211b-90	-5.52	2.46	Vercors	Balcon Ecouges	Ur	211b-90
207b-90	-2.37	1.99	Vercors	Balcon Ecouges	Ur	207b-90
209-89	-4.47	0.69	Vercors	Bourne Gorge	Ur	209-89
374b-90	-3.89	2.12	Bauges	Arclusaz	Ur	374b-90
396b-90	-3.8	1.32	Bauges	Villaret Rouge	Ur	396b-90
410b-90	-6.3	-0.03	Bauges	Trelod	Ur	410b-90
424b-90	-4.6	0.7	Bauges	Mt Trelod	Ur	424b-90
441b-90	-3.26	2.36	Aravis	Grd Cret	Ur	441b-90
482b-90	-4.84	2.06	Aravis	Pointe Percee	Ur	482b-90
490b-90	-4.4	1.71	Aravis	Pointe Percee	Ur	490b-90
N =	17	17				
Mean =	-4.07	1.44				
Std. dev.	1.16	1.16				

Data Table A.2.2

Urgonian	rudist	shells															
sample	CaO	MgO	MAS	Fe-low	MN	SR	CAR	DOL	DoC	FE	Mn	Sr	SAMPLE	Des	Loc.n	O18	C13
21B-90	22.04	0.04	40.00	0.04	16.00	298.00	98.51	0.46	0.46	310.62	40.61	756.29	21B-90	U. rudist	Charteuse	-4.80	-0.11
42B-90	14.29	0.10	20.00	0.10	30.00	239.00	128.51	2.29	1.78	1387.78	116.72	929.87	42B-90	U. rudist	Charteuse	-4.02	1.56
128B-90	42.49	0.15	80.00	0.10	43.00	788.00	95.14	0.86	0.90	445.65	56.49	1035.26	128B-90	U. rudist	Charteuse		
14SA-89	24.44	0.16	40.00	0.01	11.00	415.00	109.84	1.83	1.67	55.72	25.04	944.56	14SA-89	U. rudist	Charteuse		
14A-89	23.81	0.23	40.00	0.01	12.00	222.00	107.40	2.63	2.45	73.26	27.93	516.78	14A-89	U.rudist	Charteuse		
14B-89T	23.71	0.18	40.00	0.01	11.00	326.00	106.69	2.06	1.93	73.75	25.78	763.91	14B-89	U. rudist	Charteuse		
67B-89	23.91	0.01	40.00	0.01	39.00	163.00	106.66	0.06	0.05	40.98	91.41	382.04	67B-89	U. rudist	Charteuse		
83B-89	23.26	0.11	40.00	0.01	9.00	278.00	104.31	1.26	1.21	108.95	21.57	666.25	83B-89	U. rudist	Charteuse		
115B-89T	22.28	0.17	40.00	0.01	15.00	206.00	100.26	1.94	1.94	113.36	37.40	513.68	115B-89T	U. rudist	Charteuse		
128B-89	23.13	0.06	40.00	0.01	7.00	410.00	103.47	0.69	0.66	59.14	16.91	990.59	128B-89	U. rudist	Charteuse	-5.45	-0.54
139B-89T	23.21	0.37	40.00	0.02	22.00	105.00	105.45	4.23	4.01	182.39	52.16	248.93	139B-89T	U. rudist	Charteuse		
243B-90	23.81	0.25	40.00	0.04	21.00	435.00	107.50	2.86	2.66	341.57	48.84	1011.63	243B-90	U. rudist	Charteuse	-2.42	2.88
sample	CaO	MgO	MAS	Fe-low	MN	SR	CAR	DOL	DoC	FE	Mn	Sr	SAMPLE	Des	Loc.n	O18	C13
172B-89	23.89	0.14	40.00	0.01	3.00	286.00	107.28	1.60	1.49	89.64	6.99	666.47	172B-89	U. rudist	Vercors		
175B-89T	23.78	0.16	40.00	0.01	3.00	448.00	106.90	1.83	1.71	57.25	7.02	1047.75	175B-89T	U. rudist	Vercors		
224B-89	23.19	0.13	40.00	0.01	25.00	119.00	104.11	1.49	1.43	100.77	60.03	285.76	224B-89	U. rudist	Vercors		
236B-89	23.91	0.03	40.00	0.01	8.00	117.00	106.80	0.34	0.32	81.86	18.73	273.89	236B-89	U. rudist	Vercors		
242B-89T	21.20	0.18	40.00	0.01	20.00	110.00	95.49	2.06	2.16	100.71	52.36	287.98	242B-89T	U. rudist	Vercors		
211B-90	15.47	0.16	40.00	0.27	79.00	170.00	69.83	1.83	2.62	3430.25	282.82	608.59	211B-90	U. rudist	Vercors	-5.52	2.46
226B1-90	21.50	0.09	40.00	0.12	45.00	400.00	96.36	1.03	1.07	1061.50	116.75	1037.77	226B1-90	U. rudist	Vercors	-2.90	3.00
sample	CaO	MgO	MAS	Fe-low	MN	SR	CAR	DOL	DoC	FE	Mn	Sr	SAMPLE	Des	Loc.n	O18	C13
374B-90	25.08	0.20	40.00	0.02	24.00	88.00	112.90	2.29	2.03	131.64	53.14	194.86	374B-90	U. rudist	Bauges	-3.89	2.12
410B-90	27.32	0.16	40.00	0.03	13.00	220.00	122.68	1.83	1.49	192.40	26.49	448.31	410B-90	U. rudist	Bauges	-6.30	-0.03
424B-90	25.38	0.09	40.00	0.05	22.00	423.00	113.67	1.03	0.91	361.50	48.39	930.36	424B-90	U. rudist	Bauges	-4.60	0.70
sample	CaO	MgO	MAS	Fe-low	MN	SR	CAR	DOL	DoC	FE	Mn	Sr	SAMPLE	Des	Loc.n	O18	C13
441B-90	22.14	0.14	40.00	0.01	3.00	453.00	99.48	1.60	1.61	61.52	7.54	1138.46	441B-90	U. rudist	Aravis	-3.26	2.36
482B-90	22.77	0.64	40.00	0.09	36.00	391.00	104.90	7.32	6.98	758.40	85.79	931.83	482B-90	U. rudist	Aravis	-4.84	2.06
490B-90	23.04	0.10	40.00	0.01	9.00	78.00	103.28	1.14	1.11	67.72	21.79	188.80	490B-90	U. rudist	Aravis	-4.40	1.71
271B-89T	24.24	0.22	40.00	0.01	3.00	315.00	109.26	2.52	2.30	56.01	6.86	720.75	271B-89	U. rudist	Aravis		
									N=	26							
									Mean	375	52	674					
									Std deviat.	692	55	305					
									Max.	3430	300	1140					
									Min.	60	7	200					

Data Table A.2.3

URGONIAN SPAR CEMENTS

Sample	O18	C13	Loc.n	Sample	Pore type	CL
21s-90	-9.58	-3.49	Gorge de Frou	21s-90	biomoldic	NL/DO
41s-90	-7.99	0.14	Pic d Oiellete	41s-90	biomoldic	NL
42s-90	-7.3	2.14	Pic d Oiellete	42s-90	biomoldic	NL
61s-90	-9.66	1.67	Pas Echel	61s-90	biomoldic	NL/DO
58s-89	-9.5	0.69	Grde Som	58s-89	biomoldic	NL/DO
67s-89	-8.85	1.01	Grde Som	67s-89	biomoldic	NL/DO
70s-89	-8.99	2.24	Pas d Echel	70s-89	biomoldic	NL/DO
128s-89	-7.04	-3.39	Les Echelle	128s-89	biomoldic	NL/DO
162s-89	-6.98	-0.4	Col Cachette	162s-89	biomoldic	NL/DO
134s-89	-8.97	2.3	St. Chris. Guiers	134s-89	biomoldic	NL/DO

North Chartreuse

Sample	O18	C13	Loc.n	Sample	Pore type	CL
243s-90	-7.57	3.16	Granier	243s-90	biomoldic	NL/DO

Vercors

Sample	O18	C13	Loc.n	Sample	Pore type	CL
134s-90	-6.26	0.07	Gorge de Nant	134s-90	biomoldic	NL/DO
130s-90	-8.33	1.39	Gorge de Nant	130s-90	biomoldic	NL
140s-90	-7.9	-4.8	Gorge de Nant	140s-90	biomoldic	NL/DO
141s-90	-7.68	-2.97	Gorge de Nant	141s-90	biomoldic	NL/DO
142s-90	-7.68	-3.49	Gorge de Nant	142s-90	biomoldic	NL/DO
163s-90	-8.92	2.36	Rimets	163s-90	coralline	NL/DO
163s2-90	-8.6	2.44	Rimets	163s2-90	coralline	NL/DO
193s-90	-8.69	0.1	Montbrand	193s-90	biomoldic	NL/DO
195s-90-	-7.88	1.29	Montbrand	195s-90-	biomoldic	NL/DO
195s2-90	-7.64	1.21	Montbrand	195s2-90	biomoldic	NL/DO
207s-90	-7.68	1.57	Balcon Ecouges	207s-90	biomoldic	NL/DO
211s2-90	-8.92	2.45	Balcon Ecouges	211s2-90	biomoldic	NL/DO
212s-90	-7.3	0	Balcon Ecouges	212s-90	biomoldic	NL/DO
219s-90	-10.72	0.32	Moucherolle	219s-90	biomoldic	NL/DO
226s-90	-10.9	1.15	Moucherolle	226s-90	biomoldic	NL
227s-90	-9.9	2.71	Moucherolle	227s-90	biomoldic	NL
237s-90	-6.29	1.75	Cote 2000	237-90	coralline	DO
236s-89	-6.49	-4.13	Naz.e Roy	236s-89	biomoldic	NL
253s-89	-6.14	2.91	G. Goulets	253s-89	biomoldic	NL/DO

Bauges

Sample	O18	C13	Loc.n	Sample	Pore type	CL
372s-90	-8.08	0.85	Arclusaz	372s-90	biomoldic	NL
400s-90	-12.12	-0.26	Villaret Rouge	400s-90	fenestral	NL/DO
411s-90	-5.59	1.31	Mt. Trelod	411s-90	biomoldic	NL
412s-90	-6.26	1.1	Mt. Trelod	412s-90	biomoldic	NL
412s2-90	-5.43	1.24	Mt. Trelod	412s2-90	biomoldic	NL
125s-91	-6.92	-0.2	Combe Orme	125s-91	biomoldic	NL/DO

Bornes

Sample	O18	C13	Loc.n	Sample	Pore type	CL
580s-90	-8.1	-2.54	Termine	580s-90	biomoldic	NL/DO
584s1-90	-6.31	-1.09	Termine	584s1-90	keystone	NL/DO
590s-90	-7.55	-0.22	Rumilly	590s-90	keystone	NL/DO

Aravis

Sample	O18	C13	Loc.n	Sample	Pore type	CL
348s-90	-9	2.87	Sallaz	348s-90	biomoldic	NL/DO

441s-90	-8.6	1.35	Grde Cret	441s-90	biomoldic	NL/DO
480sda-90	-7.67	-2.41	Pt. Percee	480sda-90	biomoldic	NL/DO
487s-90	-5.52	1.24	Pt. Percee	487s-90	biomoldic	NL
488s-90	-7.07	0.8	Pt. Percee	488s-90	Fenestral	DO
490s-90	-6.78	-0.14	Pt. Percee	490s-90	biomoldic	NL
	O18	C13				
Mean=	-7.94	0.36				
Std. Dev.=	1.44	2.03	N=	45		

Data Table

Chartreuse																
Sample	CaO	MgO	MAS	Fe-low	MN	SR	CAR	DOL	DoC	FE	Mn	Sr	Sample	Loc.n	O18	C13
27A-89	23.69	0.14	40.00	0.01	16.00	58.00	106.39	1.60	1.51	49.30	37.60	136.29	27A-89	Grde Vache		
27B-89T	23.94	0.18	40.00	0.02	18.00	125.00	107.71	2.06	1.91	129.86	41.78	290.12	27B-89T	Grde Vache		
58S-89	12.34	0.03	20.00	0.00	4.00	57.00	110.39	0.69	0.62	63.36	18.12	258.18	58S-89	Grde Sommet	-9.50	0.69
64S-89T	24.22	0.07	40.00	0.01	34.00	109.00	108.39	0.80	0.74	96.79	78.42	251.41	64S-89T	Grde Sommet		
67S-89	23.58	0.10	40.00	0.01	49.00	171.00	105.69	1.14	1.08	66.17	115.91	404.49	67S-89	Grde Sommet	-8.85	1.01
70S-89	23.23	0.14	40.00	0.02	82.00	77.00	104.34	1.60	1.53	125.69	196.48	184.50	70S-89	Pas de Echell	-8.99	2.24
115S-89T	24.02	0.16	40.00	0.01	22.00	140.00	107.97	1.83	1.69	97.17	50.94	324.18	115S-89T	Charmont		
128S-89T	24.47	0.03	40.00	0.01	17.00	33.00	109.29	0.34	0.31	95.99	38.89	75.49	128S-89T	Les Echelles	-7.04	-3.39
Sample	CaO	MgO	MAS	Fe-low	MN	SR	CAR	DOL	DoC	FE	Mn	Sr	Sample	Loc.n	O18	C13
21S-90	22.73	0.03	40.00	0.02	39.00	21.00	101.53	0.34	0.34	189.43	96.03	51.71	21S-90	Gorge de Frou	-9.58	-3.49
41S-90	21.54	0.03	40.00	0.08	29.00	25.00	96.23	0.34	0.36	699.58	75.34	64.95	41S-90	Pic d Oiellette	-7.99	0.14
42S-90	20.98	0.18	40.00	0.03	17.00	70.00	94.51	2.06	2.18	314.50	44.97	185.16	42S-90	Pic d Oiellette	-7.30	2.14
61S-90	23.00	0.08	40.00	0.04	15.00	89.00	103.00	0.92	0.89	322.54	36.41	216.02	61S-90	Pas Echel	-9.66	1.67
243S-90	23.17	0.18	40.00	0.17	101.00	71.00	104.28	2.06	1.97	1433.61	242.14	170.22	243S-90	Mt. Granier	-7.57	3.16
243S2-90	21.86	0.23	40.00	0.04	23.00	527.00	98.70	2.63	2.67	318.88	58.26	1334.87	243S2-90	Mt. Granier		
Vercors																
Sample	CaO	MgO	MAS	Fe-low	MN	SR	CAR	DOL	DoC	FE	Mn	Sr	Sample	Loc.n	O18	C13
172S-89T	24.36	0.13	40.00	0.01	4.00	168.00	109.33	1.49	1.36	103.96	9.15	384.17	172S-89T	Pic St. Michel		
175S-89T	24.29	0.20	40.00	0.01	8.00	134.00	109.38	2.29	2.09	111.90	18.28	306.27	175S-89T	Pic St. Michel		
198S-89T	23.57	0.12	40.00	0.03	43.00	77.00	105.75	1.37	1.30	206.68	101.66	182.03	198S-89T	u. Bourne gorge		
208S-89T	23.86	0.18	40.00	0.02	22.00	93.00	107.36	2.06	1.92	162.87	51.23	216.57	208S-89T	Bourne gorge		
224S-89	23.98	0.07	40.00	0.02	23.00	90.00	107.32	0.80	0.75	130.34	53.58	209.66	224S-89	l. Bourne gorge		
236SA-89	23.57	0.02	40.00	0.00	15.00	10.00	105.23	0.23	0.22	33.23	35.64	23.76	236SA-89	St. Naz en Roy	-6.49	-4.13
236S-89	24.26	0.03	40.00	0.00	4.00	10.00	108.36	0.34	0.32	16.14	9.23	23.07	236S-89	St. Naz en Roy	-6.49	-4.13
236S-89	22.53	0.03	40.00	0.03	17.00	10.00	100.64	0.34	0.34	260.61	42.23	24.84	236S-89	St. Naz en Roy	-6.49	-4.13
236s-89du	22.59	0.03	40.00	0.03	18.00	11.00	100.91	0.34	0.34	233.92	44.59	27.25	236s-89du	St. Naz en Roy	-6.49	-4.13
Sample	CaO	MgO	MAS	Fe-low	MN	SR	CAR	DOL	DoC	FE	Mn	Sr	Sample	Loc.n	O18	C13
134S-90	22.40	0.11	40.00	0.02	26.00	47.00	100.48	1.26	1.25	200.12	64.69	116.94	134S-90	Gorge de Nant	-6.26	0.07
140S-90	11.45	0.02	40.00	0.01	19.00	11.00	51.17	0.23	0.45	222.10	92.82	53.74	140S-90	Gorge de Nant	-7.9	-4.8
141S-90	27.99	0.06	40.00	0.02	16.00	36.00	125.15	0.69	0.55	125.74	31.96	71.91	141S-90	Gorge de Nant	-7.68	-2.97
142S-90	26.96	0.04	40.00	0.02	11.00	25.00	120.45	0.46	0.38	116.13	22.83	51.89	142S-90	Gorge de Nant	-7.68	-3.49
163S-90	22.54	0.08	40.00	0.06	90.00	113.00	100.95	0.92	0.91	502.31	222.89	279.85	163S-90	Rimets	-8.92	2.36
195S-90	25.11	0.07	40.00	0.05	31.00	76.00	112.36	0.80	0.71	350.15	68.98	169.10	195S-90	Montbrand	-7.88	1.29
195S2-90	22.18	0.05	40.00	0.05	28.00	72.00	99.18	0.57	0.58	414.28	70.58	181.48	195S2-90	Montbrand	-7.64	1.21
212S-90	21.68	0.03	40.00	0.02	10.00	21.00	96.85	0.34	0.35	153.46	25.81	54.21	212S-90	Balcon Ecouges	-7.3	0
219S-90	22.26	0.08	40.00	0.05	26.00	100.00	99.70	0.92	0.92	473.53	65.20	250.76	219S-90	Moucher	-10.72	0.32
227S-90	24.67	0.15	40.00	0.05	36.00	149.00	110.81	1.72	1.55	418.14	81.22	336.15	227S-90	Moucher	-9.9	2.71
Bauges																
Sample	CaO	MgO	MAS	Fe-low	MN	SR	CAR	DOL	DoC	FE	Mn	Sr	Sample	Loc.n	O18	C13
411S-90	26.08	0.09	40.00	0.02	8.00	95.00	116.79	1.03	0.88	119.77	17.13	203.36	411S-90	Trelod	-5.59	1.31
412S-90	24.13	0.28	40.00	0.02	12.00	100.00	109.08	3.20	2.94	160.29	27.50	229.18	412S-90	Trelod	-6.26	1.1
412S2-90	22.18	0.09	40.00	0.11	44.00	74.00	99.39	1.03	1.04	932.36	110.67	186.13	412S2-90	Trelod	-5.43	1.24
Aravis																
Sample	CaO	MgO	MAS	Fe-low	MN	SR	CAR	DOL	DoC	FE	Mn	Sr	Sample	Loc.n	O18	C13
480S-90	22.65	0.11	40.00	0.26	125.00	58.00	101.59	1.26	1.24	2263.20	307.60	142.72	480S-90	Pt. Percee	-7.67	-2.41
488S-90	22.07	0.09	40.00	0.11	63.00	116.00	98.90	1.03	1.04	936.98	159.25	293.22	488S-90	Pt. Percee	-7.07	0.8
271S-89	23.12	0.14	40.00	0.03	8.00	159.00	103.85	1.60	1.54	269.40	19.26	382.77	271S-89	Tardevant		
Bornes																

Sample	CaO	MgO	MAS	Fe-low	MN	SR	CAR	DOL	DoC	FE	Mn	Sr	Sample	Loc.n	O18	C13
580S-90	21.66	0.15	40.00	0.05	57.00	73.00	97.39	1.72	1.76	439.87	146.32	187.39	580S-90	w. of Termine	-8.1	-2.54
N=	40.00								Mean	334	92	213				
									Std. Dev.	418	67	209				

Data Table A.2.5

DOLOMITES					
Chartreuse					
SAMPLE	**O18**	**C13**	**Loc.n**	**Age**	**SAMPLE**
43wd-90	-4.23	2.27	Pic d Oiellette	Ur	43wd-90
44wd2-90	-5.08	-0.69	Pic d Oiellette	Ur	44wd2-90
44wd-90	-3.52	2.15	Pic d Oiellette	Ur	44wd-90
45wd-90	-3.57	1.65	Pic d Oiellette	Ur	45wd-90
13wd-89	-4.28	0.74	Dent de Crolles	Ur	13wd-89
Spar after dol.					
81sd-89	-14.04	-0.77	Pic d Oiellette	Ur	81sd-89
43sd-90	-9.95	0.84	Pic d Oiellette	Ur	43sd-90
44sda-90	-11.12	-1.35	Pic d Oiellette	Ur	44sda-90
45sd-90	-9.6	-1.7	Pic d Oiellette	Ur	45sd-90
93sad-91	-15.23	-0.03	Dent de Crolles	Ur	93sad-91
Vercors					
SAMPLE	**O18**	**C13**	**Loc.n**	**Age**	**SAMPLE**
205wd-89	-4.99	1.37	P. Valchevrie	Ur	205wd-89
215wd-89	-5.84	0.5	Rencurel	Ur	215wd-89
216wd-89	-4.1	1.6	Rencurel	Ur	216wd-89
255wd-89	-3.39	2.47	Grd Goulets	Ur	255wd-89
112wd-90	-4.19	-0.6	Foulliet	Ur	112wd-90
167wd-90	-3.71	2.5	Montagne	Ur	167wd-90
2wd-91	-3.8	2.58	Grd Goulets	Ur	2wd-91
28wd-91	-5.36	-0.7	Bourne Gorge	Ur	28wd-91
Spar after dol.					
255sd-89	-7.45	-4.69	Grd Goulets	Ur	255sd-89
144sd-90	-8.3	-4.2	Gorge de Nant	Ur	144sd-90
128sd-90	-7.66	-0.66	Gorge de Nant	Ur	128sd-90
DEDOLOMITE					
144wd-90	-7.2	-5.62	Gorge de Nant	Ur	144wd-90
144sd-90	-8.3	-4.2	Gorge de Nant	Ur	144sd-90
128sd-90	-7.66	-0.66	Gorge de Nant	Ur	128sd-90
128wd-90	-7.8	-2.31	Gorge de Nant	Ur	128wd-90
143wl-90	-7.45	-7.19	Gorge de Nant	Ur	143wl-90
143sd-90	-7.34	-6.86	Gorge de Nant	Ur	143sd-90
5dd-91	-7.49	-6.19	Grd Goulets	Ur	5dd-91
29dd-91	-9.35	-6.36	Bourne Gorge	Ur	29dd-91
AR12	-6.58	-2.9	S. Vercors	Ur	Ar12
Bauges					
SAMPLE	**O18**	**C13**	**Loc.n**	**Age**	**SAMPLE**
372wd-90	-5.04	1.82	Arclusaz	Ur	372wd-90
373wd-90	-5.09	2.76	Arclusaz	Ur	373wd-90
374wd-90	-5.43	2.84	Arclusaz	Ur	374wd-90
176wd-91	-5.94	1.8	Arclusaz	Ur	176wd-91
177wd-91	-5.4	3.05	Arclusaz	Ur	177wd-91
177bd-91	-5.27	2.81	Arclusaz	Ur	177bd-91
Spar after dol.					
373sda-90	-4.5	0.12	Arclusaz	Ur	373sda-90
177sabd/91	-4.79	2.23	Arclusaz	Ur	177sabd-91
Bornes					
477wd-90	-5.3	1.13	Borne valley	Ur	477wd-90
478wd-90	-6.12	-0.47	Borne valley	Ur	478wd-90
163wd1-91	-4.6	1.42	Borne valley	Ur	163wd1-91

163wd1-91	-5.89	-0.3	Borne valley	Ur	163wd2-91
562wd-90	-5.1	1.58	Termine	Ur	562wd-90
581wd-90	-3.76	1.88	U. Termine	Ur	581wd-90
152wd-91	-5.02	0.47	L. Termine	Ur	152wd-91
192wd-91	-3.34	1.52	Pic Jallouvre	Ur	192wd-91
Spar after dol.					
478sda-90	-9.23	-0.14	Borne valley	Ur	478sda-90
Dedolomite					
147dd-91	-7.5	-4.34	U. Termine	Ur	147dd-91
147sadd-91	-4.98	-1.59	U. Termine	Ur	147sadd-91
153dd-91	-3.81	-0.98	L. Termine	Ur	153dd-91
Aravis					
SAMPLE	**O18**	**C13**	**Loc.n**	**Age**	**SAMPLE**
441wd-90	-5.44	1.9	Grde Cret	Ur	441wd-90
448wd-90	-4.64	2	Paccauly	Ur	448wd-90
461wd-90	-3.47	2.2	La Clusaz	Ur	461wd-90
482wd-90	-6.86	1.7	Pt. Percee	Ur	482wd-90
489bd-90	-5.95	1.88	Pt. Percee	Ur	489bd-90
483bd-90	-5.82	0.54	Pt. Percee	Ur	483bd-90
562wd-90	-5.08	1.58	Tardevant	Ur	562wd-90
Spar after dol.					
461sda-90	-7.5	-0.14	La Clusaz	Ur	461sda-90
482sda-90	-5.73	1.43	Pt. Percee	Ur	482sda-90
489sda-90	-6.72	-0.91	Pt. Percee	Ur	489sda-90
489sd-90	-7.16	-1.35	Pt. Percee	Ur	489sd-90
483sd-90	-8.01	-2.62	Pt. Percee	Ur	483sd-90

	18O	13C	
Mosaic dol			N=35
Mean	-4.88	1.41	
Std. Dev.	0.92	1.10	
Baroque dol			N=3
Mean	-5.68	1.74	
Std. Dev.	0.29	0.93	
Spar after dol.			N=14
Mean	-8.65	-0.65	
Std. Dev.	3.06	1.66	
Dedolomite			N=12
mean	-7.12	-4.10	
Std. Dev.	1.40	2.26	
Karst dolomite			N=2
mean	-5.67	2.425	
Std. Dev.	0.27	0.625	

Data Table A.2.6

Dolomites Chartreuse																
Sample	CaO	MgO	MAS	Fe-low	MN	SR	CAR	DOL	DoC	Fe	Mn	Sr	SAMPLE	Location	18O	13C
13WD-89	14.03	5.82	40.00	0.32	38.00	59.00	93.01	66.57	71.57	2960.77	102.14	158.58	13WD-89	Dent d'Crolle	-9.76	0.74
81W-89	22.25	1.12	40	0.03	24	24	105.09	12.81	12.19	249.57	57.09	57.09	81W-89	Pic de Oiellete		
43WD-90	15.54	5.67	40.00	0.06	29.00	54.00	98.96	64.85	65.53	565.39	73.26	136.42	43WD-90	Pic de Oiellete	-4.23	2.27
44WD2-90	16.14	5.05	40.00	0.14	34.00	36.00	98.40	57.76	58.70	1199.48	86.39	91.47	44WD2-90	Pic de Oiellete	-5.08	-0.69
44WD-90	12.79	6.68	40.00	0.23	28.00	48.00	91.98	76.40	83.06	2195.61	76.10	130.46	44WD-90	Pic de Oiellete	-3.52	2.15
45WD-90	14.89	6.76	40.00	0.10	39.00	47.00	101.76	77.32	75.98	850.50	95.81	115.46	45WD-90	Pic de Oiellete	-3.57	1.65
Vercors																
Sample	CaO	MgO	MAS	Fe-low	MN	SR	CAR	DOL	DoC	Fe	Mn	Sr	SAMPLE	Location	18O	13C
205WD-89	13.22	7.49	40.00	0.12	57.00	37.00	98.13	85.67	87.30	1024.51	145.21	94.26	205WD-89	P. Valchevrie	-4.99	1.37
215WD-89	14.97	5.75	40.00	0.12	53.00	30.00	96.84	65.77	67.91	1056.26	136.83	77.45	215WD-89	Rencurel	-5.84	0.5
216WD-89	13.93	6.73	40.00	0.07	31.00	45.00	97.33	76.97	79.09	592.86	79.63	115.59	216WD-89	Rencurel	-4.99	1.37
255W-89	14.92	7.47	40	0.048	48	45	105.61	85.44	80.90	397.34	113.62	106.52	255W-89	Grde Goulet	-3.39	2.47
255WD-89	13.27	8.21	40.00	0.07	57.00	48.00	102.12	93.90	91.95	607.82	139.54	117.51	255WD-89	Grde Goulet	-3.39	2.47
112WD-90	6.60	4.27	20.00	0.03	17.00	21.00	103.54	97.68	94.34	472.86	82.10	101.41	112WD-90	Pas Fouillet	-4.19	-0.6
167WD-90	11.94	9.08	40.00	0.01	13.00	34.00	100.74	103.85	103.09	112.82	32.26	84.37	167WD-90	Montagnette	-3.71	2.5
Bauges																
Sample	CaO	MgO	MAS	Fe-low	MN	SR	CAR	DOL	DoC	Fe	Mn	Sr	SAMPLE	Location	18O	13C
372WD-90	13.70	7.20	40.00	0.01	12.00	61.00	98.76	82.35	83.39	115.08	30.38	154.42	372WD-90	Arclusaz	-5.04	1.82
373WD-90	13.03	8.03	40.00	0.20	58.00	61.00	100.11	91.84	91.74	1702.90	144.84	152.33	373WD-90	Arclusaz	-5.09	2.76
375WD-90	21.66	0.29	40.00	0.17	42.00	52.00	98.12	3.32	3.38	1479.06	107.01	132.49	375WD-90	Arclusaz	-10.12	-3.35
Aravis																
Sample	CaO	MgO	MAS	Fe-low	MN	SR	CAR	DOL	DoC	Fe	Mn	Sr	SAMPLE	Location	18O	13C
441WD-90	18.34	7.16	40.00	0.02	13.00	72.00	119.24	81.89	68.68	175.96	27.26	150.95	441WD-90	Grde Cret	-5.44	1.9
448WD-90	16.77	5.64	40.00	0.03	17.00	59.00	104.29	64.51	61.85	285.01	40.75	141.43	448WD-90	C. de Pacauley	-4.64	2
448WD-90r	12.67	7.45	40.00	0.04	18.00	51.00	95.47	85.21	89.25	366.29	47.13	133.55	448WD-90r	C. de Pacauley	-4.64	2
461WD-90	13.61	7.80	40.00	0.73	275.00	61.00	101.49	89.21	87.90	6288.04	677.38	150.25	461WD-90	La Clusaz	-3.47	2.2
482WD-90	16.62	4.60	40.00	0.04	18.00	58.00	98.18	52.61	53.59	338.36	45.83	147.68	482WD-90	Pt. Percee	-6.86	1.7
483BD-90	18.03	6.73	40.00	0.02	16.00	75.00	115.61	76.97	66.58	136.12	34.60	162.18	483BD-90	Pt. Percee	-5.82	0.54
489BD-90	13.77	6.64	40.00	0.05	20.00	59.00	96.14	75.95	78.99	491.04	52.01	153.42	489BD-90	Pt. Percee	-5.95	1.88
562WD-90	12.59	8.55	40.00	0.07	26.00	59.00	100.87	97.79	96.95	563.37	64.44	146.23	562WD-90	C. de Tardevant	-5.08	1.58
Bornes																
Sample	CaO	MgO	MAS	Fe-low	MN	SR	CAR	DOL	DoC	Fe	Mn	Sr	SAMPLE	Location	18O	13C
581WD-90	14.08	9.15	40.00	0.04	31.00	60.00	110.65	104.65	94.58	308.14	70.04	135.56	581WD-90	Termine	-3.78	1.88
477WD-90	13.10	7.73	40.00	0.05	19.00	56.00	98.85	88.41	89.44	451.04	48.05	141.62	477WD-90	Borne valley	-2.91	-2.09
478WD-90	14.48	8.93	40.00	0.02	10.00	58.00	111.28	102.14	91.78	125.70	22.46	130.30	478WD-90	Borne valley	-5.3	1.13
N=	27								Mean=	930	97	127				
									Std. Dev.=	1246	120	27				

Dedolomite

143SD-90	24.13	0.06	40.00	0.03	41.00	8.00	107.93	0.69	0.64	267.30	94.97	18.53	143SD-90	G. de Nant	-7.34	-6.86
143DD-90	22.21	0.23	40.00	0.54	63.00	9.00	100.26	2.63	2.62	4691.29	157.09	22.44	143DD-90	G.de Nant	-8.06	-5.62
128WD-90	24.22	0.39	40.00	0.74	136.00	21.00	110.06	4.46	4.05	5886.01	308.92	47.70	128WD-90	G. de Nant	-8.64	-2.31
N=	3								Mean=	3614.86	186.99	29.56				
									Std. Dev.=	2416.82	89.87	12.93				

Spar after dol.

Sample	CaO	MgO	MAS	Fe-low	MN	SR	CAR	DOL	DoC	Fe	Mn	Sr	SAMPLE	Location	18O	13C
43SD-90	21.73	0.09	40.00	0.05	10.00	57.00	97.39	1.03	1.06	457.83	25.67	146.32	43SD-90	Plc de Olellete	-9.95	0.84
375SD-90	24.85	0.18	40.00	0.04	19.00	274.00	111.77	2.06	1.84	297.22	42.50	612.85	375SD-90	Arclusaz	-4.95	2.61
482SDA-90	13.21	7.24	40.00	0.17	71.00	61.00	96.78	82.81	85.56	1526.61	183.40	157.57	482SDA-90	Pt. Percee	-5.73	1.43
489SDA-90	20.15	0.40	40.00	0.28	114.00	58.00	91.96	4.58	4.97	2623.86	309.91	157.68	489SDA-90	Pt. Percee	-6.72	-0.91
489SD-90	20.68	0.66	40.00	0.02	9.00	67.00	95.68	7.55	7.89	155.33	23.51	175.05	489SD-90	Pt. Percee	-7.16	-1.35
N=	5								Mean=	1012	117	250				
									Std. Dev.=	940	113	182				

VEIN FILLS

Chartreuse

Sample	O18	C13	Loc.n	Age	Sample	Desc.
1v1-90	-6.58	-1.29	Entremont	N1b	1v1-90	
1v2-90	-6.15	1.66	Entremont	N1b	1v2-90	
3v1-90	-6.81	-0.62	Entremont	Urg	3v1-90	TZ
3v2-90	-9.97	-2.39	Entremont	Urg	3v2-90	TZ
4v1-90	-10.34	-2.72	Entremont	Urg	4v1-90	TZ
4v2-90	-12.09	-1.62	Entremont	Urg	4v2-90	TZ
6v-90	-4.51	0.62	Entremont	Urg	6v-90	TZ
7v1-90	-4.75	0.63	Entremont	Ur	7v1-90	TZ
17v-90	-9.81	-6.51	Gorge du Frou	Ur	17v-90	BU
18v-90	-9.1	-7.67	Gorge du Frou	Ur	18v-90	BU
18v-90 2	-10.25	-0.72	Gorge du Frou	Ur	18v-90 2	BU
139v-89	-10.28	-0.63	Gorge du Frou	Ur	139v-89	BU
154v-89	-5.8	1.54	Epernay	Tith	154v-89	
156v1-89	0.18	2.19	Epernay	U. Kimm	156v1-89	
156v2-89	-10.53	2.14	Epernay	U. Kimm	156v2-89	
73v-90	-9.51	3.34	Epernay	J6b	73v-90	
150v-89	-1.93	0.54	Epernay	N1	150v-89	
81v-90	-5.28	0.8	Epernay	N1b	81v-90	
82v-90	-7.17	1.49	Epernay	N1b	82v-90	
75v-90	-6	2.03	Epernay	Ur	75v-90	TZ
83v-90	-4.83	1.57	Epernay	Ur	83v-90	TZ
94v-90	-12.46	-2.7	Chailles Gorge	N2S	94v-90	
98v-90	-6.41	-2.68	Chailles Gorge	Ti	98v-90	
64v-89	-7.8	-0.34	Grde Sommet	Ur	64v-89	TZ
67v-89	-7.79	-0.16	Grde Sommet	Ur	67v-89	TZ
38v-89	-5.64	2.16	Canaple	Sen	38v-89	
115v-89	-9.9	-0.93	Canaple	Ur	115v-89	TZ
40v-89	-10.62	-0.15	Canaple	N2	40v-89	
37v-90	-8.67	0.27	P.Pierre	N1	37v-90	
38v-90	-6.2	1.14	P.Pierre	Tith.	38v-90	
73v-89	-3.83	-0.59	w Pont Pierre	U. Kim.	73v-89	
39v-90	-7.97	-0.13	Pont Pierre	N2	39v-90	
75v-89	-6.92	-0.34	CSP Guier	N2	75v-89	
42v-90	-13.7	-0.17	Pic de Oiellete	Ur	42v-90	TU
78v-89	-12.72	0	Guiers Mort	Ur	78v-89	TU
162v-89	-12.3	-0.37	Col de Cachete	Ur	162v-89	TZ
163v-89	-10.73	-1.87	Col de Cachete	Ur	163v-89	TZ
121v-89	-12.92	-1.71	Fourvoire	Ti	121v-89	
124v1-89	-10.84	-0.07	Fourvoire	Ti	124v1-89	
124v2-89	-11.25	-0.2	Fourvoire	Ti	124v2-89	
125v-89	-7.48	-0.39	Fourvoire	Ur	125v-89	TZ
133v-89	-13.26	-0.03	St Chris.Guiers	Ur	133v-89	TZ
136v-89	-10.61	1.33	St Chris.Guiers	Ur	136v-89	TZ
146v-89	-6.93	-0.54	Corbel	Ur	146v-89	TZ

Vercors samples

Sample	O18	C13	Loc.n	Age	Sample	Desc.
117v-90	-7.55	-0.87	Pas de Fouillet	Ur	117v-90	TU
120v-90	-7.69	-1.32	Pas de Fouillet	Ur	120v-90	TU
160v-90	-6.79	-4.13	Mont noir	C6-7	160v-90	TU
174v-90	-8.32	-1.5	Montagnette	Ur(Bi1)	174v-90	TU
175v-90	-10.96	-4.7	Montagnette	Bi1 Ur	175v-90	TU
182v-90	-9.89	1.5	Pas d Montbrand	Ur	182v-90	TU
191v1-90	-8.89	-4.75	Pas d Montbrand	Ur	191v1-90	TU
192v1-90	-9.66	-4.06	Pas d Montbrand	Ur	192v1-90	BU
192v2-90	-9.25	-2.8	Pas d Montbrand	Ur	192v2-90	BU
230v-90	-5.79	2.13	Moucherolle	Sen.	230v-90	
236v-90	-11.36	-1.23	Arret d Gherbier	Ur	236v-90	TZ

238v-90	-9.1	2.24	Cote 2000	Ur	238v-90	TU
164v-89	-9.02	-1.59	Col Furron	Senonian	164v-89	
165v-89	-8.18	-3.87	Col Furron	Senonian	165v-89	
208v1-89	-8.71	-2.28	Bourne Gorge	Ur	208v1-89	TZ
208v2-89	-8.12	-1.49	Bourne Gorge	Ur	208v2-89	TZ
210v-89	-7.08	-1.4	Bourne Gorge	Ur	210v-89	TZ
216v-89	-10.67	-1.32	Rencurel	Ur	216v-89	TZ
240v1-89	-6.8	-2.62	Petit Goulets	Ur	240v1-89	TZ
240v2-89	-8.26	-3.9	Petit Goulets	Ur	240v2-89	TZ
243v-89	-6.43	-2.13	Petit Goulets	Ur	243v-89	TZ
Bauges samples						
Sample	**O18**	**C13**	**Loc.n**	**Age**	**Sample**	**Desc.**
255v1-90	-6.66	-2.88	Lac Aiguebellete	N2	255v1-90	
255v2-90	-6.54	-2.88	Lac Aiguebellete	N2	255v2-90	
256v-90	-5.42	0.23	Lac Aiguebellete	N2CO	256v-90	
276v-90	-15.88	1.56	Nivolet	N2	276v-90	
277v-90	-10.4	-6.84	Nivolet	Ur	277v-90	BU
277v(s)90	-6.49	-17.99	Nivolet	Ur	277v(s)90	BU
278v1-90	-4.94	-5.45	Nivolet	Ur	278v1-90	BU
278v2-90	-5.57	-5.42	Nivolet	Ur	278v2-90	BU
284v1-90	-4.55	1.48	Curienne	Ti	284v1-90	
287v-90	-7.56	2.28	Curienne	Ti	287v-90	
288g-90	-5.52	0.6	Curienne	N1	288g-90	
294v-90	-3.2	0.15	Galoppaz	N2	294v-90	
290v-90	-8.78	1.5	Galoppaz	Ur	290v-90	BU
360v-90	-1.02	2.4	La Place	Tith	360v-90	
374v1-90	-6.8	2.1	Arclusaz	Ur	374v1-90	TU
374v2-90	-4.44	2.15	Arclusaz	Ur	374v2-90	TU
374v-90A	-5.4	2.49	Arclusaz	Ur	374v-90A	TU
379v-90	-4.65	-1.67	Cheran Gorge	Ur	379v-90	TZ
380v1-90	-2.2	-11.5	Cheran Gorge	Ur	380v1-90	TZ
380v2-90	-11.37	-7.74	Cheran Gorge	Ur	380v2-90	TZ
381v1-90	-6.85	-0.67	Cheran Gorge	Ur	381v1-90	TZ
381v2-90	-9.35	-4.18	Cheran Gorge	Ur	381v2-90	TZ
385v-90	-5.99	0.71	Cheran	N2	385v-90	
396v-90	-3.8	1.32	Lescheraine	Ur	396v-90	TU
397v-90	-8.28	1.54	Villaret Rouge	Ur	397v-90	TU
399v-90	-13.86	-3.69	Villaret Rouge	Ur	399v-90	TU
401v-90	-7.79	0.13	Villaret Rouge	Ur	401v-90	TU
402v-90	-16.21	-1.42	Villaret Rouge	Ur	402v-90	TU
414v-90	-4.72	0.45	Mt Trelod	Sen	414v-90	
415v-90	-5.67	-0.27	Mt Trelod	M foram	415v-90	
423v-90	-12.6	-0.8	Mt Trelod	Sen	423v-90	
424v-90	-10.95	-0.55	Mt Trelod	Ur	424v-90	TU
Bornes samples						
Sample	**O18**	**C13**	**Loc.n**	**Age**	**Sample**	**Desc.**
297v-90	-8.2	-0.91	Encrenaz	e7	297v-90	
301v-90	-3.55	1.11	Encrenaz	Ur	301v-90	TZ
304v-90	-2.5	1.17	Encrenaz	Ur	304v-90	TZ
477v-90	-19.84	-1.15	Borne valley	Ur	477v-90	BU
541v-90	-5.52	-0.81	C Columbiere	e5-6	541v-90	
549v-90	-6.41	1.38	Col de Razoir	Ur	549v-90	BU
553vw-90	-1.6	0.99	Jallouvre	Ur	553vw-90	BU
553v-90	-1.65	0.83	Jallouvre	Ur	553v-90	BU
595v-90	-5.06	0.81	Petit Bornand	N1	595v-90	
600v-90	-5.06	2.29	Petit Bornand	Sen	600v-90	
Aravis samples						
Sample	**O18**	**C13**	**Loc.n**	**Age**	**Sample**	**Desc.**
342v90	-10.98	0.32	Sallaz	eN	342v90	
351v-90	-5.42	-6.72	Sallaz	eN	351v-90	

354v-90	-3.28	-1.01	Sallaz	Ur	354v-90	TZ
430v-90	-4.4	0	T d Chatel	N1	430v-90	
439v1-90	-11.68	2.26	Grde Cret	Ur	439v1-90	TU
439v2-90	-5.77	2.25	Grde Cret	Ur	439v2-90	TU
447v-90	-8.6	-0.48	Paccauly	Ur	447v-90	BU
464v-90	-5.24	1.32	La Clusaz	Ur	464v-90	BU
468v-90	-5.26	1.12	La Clusaz	Ur	468v-90	BU
495v-90	-5.42	0.6	Roulletaz	Ur	495v-90	TU
506v-90	-3.71	0.65	La Goenne	eN	506v-90	
562v-90	-4.64	1.57	Tardevant	Ur	562v-90	BU
570v-90	-8.99	-2.92	Tardevant	Gault	570v-90	

Platé samples

Sample	**O18**	**C13**	**Loc.n**	**Age**	**Sample**	**Desc.**
319v-90	-3.97	2.64	Flaine	e7	319v-90	
320v-90	-3.17	-0.26	G Plate	eN	320v-90	
324v-90	-3.99	0.87	Col Fete	Ur	324v-90	BU
325v-90	-4.18	-0.9	Col Fete	Ur	325v-90	BU
337v-90	-4.13	1.24	La Colonne	Ur	337v-90	TZ
636v-90	-4.17	0.48	HW Salles	Urg	636v-90	TZ
642v-90	-4.23	2.17	FW Salles	Sen.	642v-90	

Haut-Giffre samples

VEINS

Sample	**O18**	**C13**	**Loc.n**	**Age**	**Sample**	**Desc.**
607v-90	-4.86	-0.65	Folly	Gault	607v-90	
612v-90	-4.6	1.98	Folly	Sen	612v-90	
616v-90	-5.28	-1.27	Combe aux Paures	Sen	616v-90	
621v-90	-5.02	1.18	Vogealle	Tith	621v-90	
624v-90	-4.5	0.51	Vogealle	Sen	624v-90	
626v-90	-4.25	1.33	Chambres	Ur	626v-90	TZ

Non-Urgonian			**Urgonian**		
Mean	-6.76	0.11	**Mean**	-7.73	-1.19
Std dev.	3.17	1.92	**Std dev.**	3.34	3.23
N=	50		**N=**	83	

Desc=	description.	
TU=	upper and	mid- Urgonian.
BU=	basal Urgonian	
TZ=	thrust zone.	related.

Ages.

M.foram.= forminifera shales. Oligocene. e7 & e5-6= Val d'Illiez sst. Oligocene. eN= Nummulite lst. Sen., C6-7 & base Sen.= Senonian. Gault= Albian Urg., Ur & U. vein = Urgonian N1-N2= Berriasian/Valanginian. N2, N2f, N2S, N2Co & Val= Valanginian. N1b & Berri= Berriasian. u. Kimm= upper Kimmeridgian. Tith= Tithonian. J6b= upper Jurassic.

Data Table A.2.8

Sample	CaO	MgO	MAS	Fe-low	MN	SR	CAR	DOL	DoC	Fe	Mn	Sr	Sample	Age	Desc	Loc.n	O18	C13
14C-89	24.10	0.16	40.00	0.02	18.00	73.00	108.32	1.83	1.69	145.27	41.54	168.48	14C-89	U. vein	BU	Dent de Crolle		
14VC-89	22.92	0.18	40.00	0.01	15.00	126.00	103.16	2.06	2.00	76.27	36.35	305.34	14VC-89	U. vein	BU	Dent de Crolle		
17V-89	22.38	0.16	40.00	0.08	137.00	115.00	100.65	1.83	1.82	703.56	340.28	285.64	17V-89	Tith.		w. D. de Crolle	-2.52	2.20
38-89	23.35	0.16	40.00	0.06	46.00	222.00	104.98	1.83	1.74	474.69	109.55	528.68	38-89	Sen. vein		Canaple	-5.64	2.16
40-89	23.57	0.22	40.00	0.05	85.00	222.00	106.27	2.52	2.37	436.00	199.96	522.24	40-89	Val.		Canaple	-10.62	-0.15
48V-89	23.01	0.15	40.00	0.04	35.00	271.00	103.41	1.72	1.66	363.53	84.62	655.16	48V-89	U. vein	TZ	Port Enclos		
57V-89	23.66	0.04	40.00	0.00	2.00	18.00	105.73	0.46	0.43	33.07	4.73	42.56	57V-89	U. vein	TZ	e. Grde Somm		
58V-89	24.27	0.10	40.00	0.01	7.00	54.00	108.77	1.14	1.05	56.26	16.09	124.12	58V-89	U. vein	TZ	e. Grde Somm		
64V-89	23.50	0.09	40.00	0.02	45.00	182.00	105.28	1.03	0.98	132.86	106.86	432.18	64V-89	U. vein	TZ	w. Grde Somm	-7.80	-0.34
67V-89	23.72	0.08	40.00	0.01	22.00	39.00	106.21	0.92	0.86	65.85	51.78	91.80	67V-89	U. vein	TZ	w. Grde Somm	-7.79	-0.16
73V-89	22.12	0.12	40.00	0.05	41.00	127.00	99.28	1.37	1.38	431.48	103.24	319.79	73V-89	Tith.		CSP Guiers		
75V-89	21.31	0.21	40.00	0.02	17.00	167.00	96.14	2.40	2.50	154.59	44.21	434.26	75V-89	Tith.		CSP Guiers		
78V-89	23.38	0.07	40.00	0.04	7.00	36.00	104.64	0.80	0.77	292.42	16.72	86.01	78V-89	U. vein	TU	Guiers Mo	-12.72	0.00
83V-89	23.97	0.07	40.00	0.01	14.00	50.00	107.27	0.80	0.75	40.75	32.63	116.53	83V-89	U. vein	TU	Guiers Mo		
92V-89	24.06	0.12	40.00	0.01	31.00	81.00	107.94	1.37	1.27	81.00	71.80	187.61	92V-89	Val. vein		Pont St. Bruno		
115V-89	24.98	0.06	40.00	0.02	12.00	30.00	111.72	0.69	0.61	156.50	26.85	67.13	115V-89	Urg.	TZ	Canaple	-9.90	-0.93
121V-89	23.27	0.10	40.00	0.06	50.00	175.00	104.31	1.14	1.10	469.36	119.84	419.43	121V-89	Tith.		Fourvoire		
124V-89	23.22	0.15	40.00	0.06	68.00	80.00	104.35	1.72	1.64	502.70	162.92	191.67	124V-89	Berri. vein		Fourvoire	-10.84	-0.07
125V-89	22.21	0.08	40.00	0.04	43.00	80.00	99.48	0.92	0.92	316.39	108.07	201.06	125V-89	Urg.	TZ	Fourvoire	-7.48	-0.39
133v-89	21.96	0.14	40.00	0.07	18.00	55.00	98.67	1.60	1.62	629.06	45.60	139.35	133v-89	Urg.	TZ	St. Chris. G	-13.26	-0.03
139V-89	23.59	0.16	40.00	0.19	30.00	64.00	106.05	1.83	1.73	1574.58	70.72	150.87	139V-89	U. vein	BU	G. Frou	-10.28	-0.63
146V-89	22.81	0.13	40.00	0.28	142.00	54.00	102.41	1.49	1.45	2381.70	346.64	131.82	146V-89	Urg.	TZ	Corbel	-6.93	-0.54
1V1-90	21.94	0.08	40.00	0.02	28.00	1321.00	98.27	0.92	0.93	186.82	71.23	3360.61	1V1-90	N1b		Entremont	-6.58	-1.29
1V2-90	22.09	0.20	40.00	0.30	119.00	293.00	99.57	2.29	2.30	2651.71	298.79	735.68	1V2-90	N1b		Entremont	-6.15	1.66
3V1-90	22.07	0.15	40.00	0.05	50.00	199.00	99.22	1.72	1.73	449.39	125.99	501.43	3V1-90	N1b		Entremont	-6.81	-0.62
4V1-90	24.75	0.15	40.00	0.02	21.00	42.00	111.17	1.72	1.54	125.83	47.23	94.45	4V1-90	N2		Entremont	-10.34	-2.72
4V2-90	22.80	0.17	40.00	0.23	111.00	80.00	102.58	1.94	1.90	1977.30	270.53	194.98	4V2-90	N2		Entremont	-12.09	-1.62
6V-90	22.17	0.11	40.00	0.01	23.00	215.00	99.45	1.26	1.27	114.28	57.82	540.45	6V-90	N2f		Entremont	-4.51	0.62
7V1-90	24.01	0.11	40.00	0.02	25.00	179.00	107.66	1.26	1.17	162.41	58.05	415.66	7V1-90	Ur	TZ	Entremont	-4.75	0.63
18V-90	22.58	0.09	40.00	0.03	12.00	3.00	101.18	1.03	1.02	241.94	29.65	7.41	18V-90	Ur	BU	G. Frou	-9.10	-7.67
37V-90	23.75	0.12	40.00	0.05	145.00	229.00	106.55	1.37	1.29	385.63	340.21	537.29	37V-90	Berri		P. Pierre	-8.67	0.27
42V-90	22.14	0.08	40.00	0.12	46.00	40.00	99.16	0.92	0.92	1093.22	115.97	100.84	42V-90	Ur	TU	Pic de. O	-13.70	-0.17
73V-90	22.93	0.13	40.00	0.04	43.00	128.00	102.95	1.49	1.44	356.67	104.42	310.84	73V-90	J6b		Epernay	-9.51	3.34
75V-90	21.85	0.12	40.00	0.11	53.00	195.00	98.08	1.37	1.40	980.51	135.10	497.05	75V-90	Ur	TZ	Epernay	-6.00	2.03
83V-90	22.75	0.11	40.00	0.06	43.00	199.00	102.04	1.26	1.23	471.22	105.35	487.55	83V-90	Ur	TZ	Epernay	-4.83	1.57
154V-89	22.39	0.10	40.00	0.01	25.00	139.00	100.38	1.14	1.14	121.93	62.26	346.18	154V-89	Tith.		Epernay	-5.80	1.54
156V2-89	24.14	0.17	40.00	0.03	43.00	139.00	108.55	1.94	1.79	217.45	99.03	320.12	156V2-89	u. Kimm		Epernay	-10.53	2.14
Vercors	veins.																	
Sample	CaO	MgO	MAS	Fe-low	MN	SR	CAR	DOL	DoC	Fe	Mn	Sr	Sample	Age	Desc	Loc.n	O18	C13
208V1-89	23.17	0.20	40.00	0.03	29.00	34.00	104.38	2.29	2.19	209.38	69.45	81.43	208V1-89	U. vein	TZ	B. Gorge	-8.71	-2.28
208V2-89	23.56	0.12	40.00	0.04	34.00	51.00	105.71	1.37	1.30	289.47	80.41	120.62	208V2-89	U. vein	TZ	B. Gorge	-8.12	-1.49
210V-89	22.67	0.08	40.00	0.04	40.00	86.00	101.53	0.92	0.90	370.27	98.50	211.77	210V-89	Urg.	TZ	B. Gorge	-7.08	-1.40
216V-89	21.57	0.17	40.00	0.04	33.00	144.00	97.09	1.94	2.00	351.17	84.97	370.79	216V-89	Urg.	TZ	Rencurel	-10.67	-1.32
240V1-89	22.11	0.07	40.00	0.08	40.00	72.00	98.98	0.80	0.81	697.80	101.03	181.86	240V1-89	Urg.	TZ	Petit Goulets	-6.80	-2.62
240V2-89	24.81	0.16	40.00	0.03	31.00	35.00	111.49	1.83	1.64	227.41	69.51	78.48	240V2-89	Urg.	TZ	Petit Goulets	-8.26	-3.90
243V-89	22.17	0.08	40.00	0.24	102.00	66.00	99.30	0.92	0.92	2069.04	256.81	166.17	243V-89	Urg.	TZ	Petit Goulets	-6.43	-2.13
117V-90	22.19	0.11	40.00	0.08	56.00	136.00	99.54	1.26	1.26	728.96	140.64	341.56	117V-90	Urg.	TU	P. Foullet	-7.55	-0.87
182V-90	22.36	0.08	40.00	0.04	29.00	40.00	100.14	0.92	0.91	366.66	72.40	99.86	182V-90	Urg.	TU	P. de Montb	-9.89	1.50
192V1-90	22.45	0.12	40.00	0.02	6.00	11.00	100.75	1.37	1.36	130.16	14.89	27.29	192V1-90	Urg.	TU	P. de Montb	-9.66	-4.06

192V2-90	21.14	0.13	40.00	0.10	26.00	24.00	94.96	1.49	1.57	874.58	73.71	63.18	192V2-90	Urg.	TU	P. de Montb	-9.25	-2.80
230V-90	24.28	0.27	40.00	0.11	55.00	149.00	109.70	3.09	2.82	860.69	125.34	339.56	230V-90	Senonian		Moucher.	-5.79	2.13
236V-90	21.81	0.17	40.00	0.05	63.00	59.00	98.16	1.94	1.98	427.50	160.45	150.26	236V-90	Urg.	TZ	A. d Gherb	-11.36	-1.23
238V1-90	21.70	0.14	40.00	0.04	42.00	52.00	97.51	1.60	1.64	340.68	107.68	133.31	238V1-90	Urg.	TU	Cote 2000	-9.10	2.24
238V2-90	21.42	0.14	40.00	0.09	68.00	54.00	96.27	1.60	1.66	781.02	176.60	140.24	238V2-90	Urg.	TU	Cote 2000		
Bauges	**veins.**																	
Sample	**CaO**	**MgO**	**MAS**	**Fe-low**	**MN**	**SR**	**CAR**	**DOL**	**DoC**	**Fe**	**Mn**	**Sr**	**Sample**	**Age**	**Desc**	**Loc.n**	**O18**	**C13**
276V-90	22.27	0.13	40.00	0.06	34.00	229.00	100.00	1.49	1.49	480.82	85.00	572.48	276V-90	N2		Nivolet	-15.88	1.56
277V-90	22.21	0.03	40.00	0.10	57.00	26.00	99.21	0.34	0.35	872.37	143.63	65.52	277V-90	Urg.	BU	Nivolet	-6.49	-17.99
278V1-90	21.71	0.06	40.00	0.02	69.00	196.00	97.14	0.69	0.71	144.00	177.58	504.42	278V1-90	Urg.	BU	Nivolet	-4.94	-5.45
278V2-90	23.45	0.06	40.00	0.05	38.00	49.00	104.90	0.69	0.65	375.03	90.56	116.78	278V2-90	Urg.	BU	Nivolet	-5.57	-5.42
284V-90	22.13	0.25	40.00	0.17	79.00	180.00	100.01	2.86	2.86	1477.37	197.49	449.97	284V-90	Tith		Curienne	-4.55	1.48
287v-90spi	19.42	0.16	40.00	0.17	111.00	177.00	87.45	1.83	2.09	1679.52	317.32	506.00	287v-90spi	Tith		Curienne	-7.56	2.28
288G-90	21.92	0.17	40.00	0.15	59.00	765.00	98.65	1.94	1.97	1355.88	149.52	1938.63	288G-90	N1-2		Curienne	-5.52	0.60
294V-90	24.07	0.15	40.00	0.41	74.00	160.00	108.14	1.72	1.59	3290.46	171.08	369.90	294V-90	N1-2		Galoppaz	-3.20	0.15
374V1-90	21.71	0.21	40.00	0.05	20.00	91.00	97.92	2.40	2.45	401.75	51.06	232.32	374V1-90	Urg.	TU	Arclusaz	6.80	2.10
374V2-90	21.94	0.13	40.00	0.04	22.00	104.00	98.53	1.49	1.51	337.16	55.82	263.87	374V2-90	Urg.	TU	Arclusaz	-4.44	2.15
380V1-90	21.92	0.09	40.00	0.04	33.00	68.00	98.23	1.03	1.05	347.09	83.98	173.06	380V1-90	Urg.	TZ	Mt. Bange	-2.20	-11.50
381V1-90	21.86	0.05	40.00	0.06	48.00	97.00	97.76	0.57	0.58	554.47	122.75	248.06	381V1-90	Urg.	TZ	Mt. Bange	-6.85	-0.67
381V2-90	22.36	0.05	40.00	0.01	36.00	52.00	99.99	0.57	0.57	113.67	90.01	130.02	381V2-90	Urg.	TZ	Mt. Bange	-9.35	-4.18
385V-90	21.92	0.07	40.00	0.12	82.00	58.00	98.13	0.80	0.82	1042.37	208.91	147.76	385V-90	N2		Mt. Bange	-5.99	0.71
397V-90	23.21	0.09	40.00	0.01	9.00	110.00	103.99	1.03	0.99	92.48	21.64	264.46	397V-90	Urg.	TU	Mt. Bange	-8.28	1.54
400V-90	23.92	0.11	40.00	0.07	78.00	146.00	107.26	1.26	1.17	595.01	181.80	340.30	400V-90	Urg.	TU	V. Rouge	-12.12	-0.26
401V-90	21.61	0.11	40.00	0.22	100.00	305.00	96.96	1.26	1.30	1938.65	257.85	788.44	401V-90	Urg.	TU	V. Rouge	-7.79	0.13
415V-90	23.35	0.16	40.00	0.30	150.00	390.00	104.98	1.83	1.74	2490.06	357.22	928.77	415V-90	M Foram		Mt.Trelod	-5.67	-0.27
423V-90	22.19	0.07	40.00	0.11	63.00	167.00	99.33	0.80	0.81	932.92	158.56	420.30	423V-90	base Sen		Mt. trelod	-12.60	-0.80
424V-90	24.99	0.09	40.00	0.02	9.00	20.00	111.93	1.03	0.92	187.46	20.10	44.67	424V-90	Urg.	TU	Mt. Trelod	-10.95	-0.55
Bornes	**veins.**																	
Sample	**CaO**	**MgO**	**MAS**	**Fe-low**	**MN**	**SR**	**CAR**	**DOL**	**DoC**	**Fe**	**Mn**	**Sr**	**Sample**	**Age**	**Desc**	**Loc.n**	**O18**	**C13**
297V-90	21.15	0.10	40.00	0.18	329.00	518.00	94.85	1.14	1.21	1659.06	867.14	1365.28	297V-90	e7		Encrenaz	-8.20	-0.91
477V-90	23.02	0.29	40.00	0.05	19.00	61.00	104.19	3.32	3.18	377.61	45.59	146.37	477V-90	Urg.	BU	Borne V	-19.84	-1.15
541V-90	21.43	0.26	40.00	0.08	34.00	468.00	96.94	2.97	3.07	676.40	87.69	1206.96	541V-90	e5-6		C. Columbier	-5.52	-0.81
549V-90	23.34	0.17	40.00	0.05	22.00	136.00	104.99	1.94	1.85	433.02	52.39	323.85	549V-90	Urg.	BU	C. de Razor	-6.41	1.38
553V-90	21.75	0.16	40.00	0.03	11.00	165.00	97.84	1.83	1.87	223.38	28.11	421.60	553V-90	Urg.	BU	Jallouvre	-1.60	0.99
595V-90	21.30	0.29	40.00	0.25	114.00	712.00	96.51	3.32	3.44	2228.32	295.29	1844.28	595V-90	N1		P. Bornand	-5.06	0.81
600V-90	22.35	0.13	40.00	0.08	118.00	174.00	100.36	1.49	1.48	653.33	293.94	433.44	600V-90	Cs		P. Bornand	-5.06	2.29
Aravis	**veins**																	
Sample	**CaO**	**MgO**	**MAS**	**Fe-low**	**MN**	**SR**	**CAR**	**DOL**	**DoC**	**Fe**	**Mn**	**Sr**	**Sample**	**Age**	**Desc**	**Loc.n**	**O18**	**C13**
342V-90	23.02	0.11	40.00	0.24	92.00	476.00	103.24	1.26	1.22	1989.92	222.77	1152.60	342V-90	eN		Sallaz	-10.98	0.32
351V-90	21.65	0.14	40.00	0.18	49.00	265.00	97.29	1.60	1.65	1644.42	125.91	680.95	351V-90	eN		Sallaz	-5.42	-6.72
439V1-90	20.61	0.18	40.00	0.04	20.00	170.00	92.86	2.06	2.22	348.34	53.84	457.67	439V1-90	Urg.	TU	Grde Cret	-11.68	2.26
447V-90	24.99	0.20	40.00	0.04	23.00	336.00	112.50	2.29	2.03	326.38	51.11	746.66	447V-90	Urg.	BU	Paccauly	-8.60	-0.48
464V-90	43.50	0.54	40.00	0.19	73.00	445.00	196.83	6.18	3.14	861.66	92.72	565.20	464V-90	Urg.	BU	La Clusaz	-5.24	1.32
468V-90	21.91	0.22	40.00	0.04	13.00	252.00	98.87	2.52	2.55	318.33	32.87	637.21	468V-90	Urg.	BU	La Clusaz	-5.26	1.12
495V-90	21.56	0.15	40.00	0.06	39.00	126.00	96.94	1.72	1.77	523.06	100.58	324.94	495V-90	Urg.	TU	Roulletaz	-5.42	0.60
506V-90	21.96	0.17	40.00	0.04	11.00	389.00	98.83	1.94	1.97	336.15	27.83	984.01	506V-90	eN		La Goenne	-3.71	0.65
570V-90	10.35	0.04	20.00	0.16	38.00	78.00	92.74	0.92	0.99	3092.01	204.87	420.53	570V-90	Gault		Tardevant	-8.99	-2.92
Pisté	**veins**																	
Sample	**CaO**	**MgO**	**MAS**	**Fe-low**	**MN**	**SR**	**CAR**	**DOL**	**DoC**	**Fe**	**Mn**	**Sr**	**Sample**	**Age**	**Desc**	**Loc.n**	**O18**	**C13**
337V-90	21.72	0.22	40.00	0.07	23.00	664.00	98.02	2.52	2.57	624.33	58.66	1693.50	337V-90	Urg.	TZ	La Colonn	-4.13	1.24
642V-90	22.42	0.17	40.00	0.13	68.00	339.00	100.88	1.94	1.93	1126.59	168.51	840.09	642V-90	Senonian		FW Salles	-4.23	2.17

Haut-Giffre Sample	veine CaO	MgO	MAS	Fe-low	MN	SR	CAR	DOL	DoC	Fe	Mn	Sr	Sample	Age	Desc	Loc.n	O18	C13
612V-90	21.33	0.22	40.00	0.28	476.00	232.00	96.28	2.52	2.61	2497.02	1235.95	602.39	612V-90	Senonian		R. de Folly	-4.60	1.98
621V-90	25.16	0.19	40.00	0.04	26.00	1002.00	113.21	2.17	1.92	278.01	57.42	2212.75	621V-90	Tith.		Vogealle	-5.02	1.18
624V-90	22.23	0.11	40.00	0.04	41.00	122.00	99.72	1.26	1.26	350.68	102.79	305.85	624V-90	Senonian		Vogealle	-4.50	0.51
626V-90	23.83	0.32	40.00	0.03	30.00	226.00	107.96	3.66	3.39	259.14	69.47	523.36	626V-90	Urg.	TZ	Chambres	-4.25	1.33

	Urgonian			Non-Urgonian		
	Fe	Mn	Sr	Fe	Mn	Sr
Mean	499.2	91.9	285.1	1050.3	207.5	690.9
Std.Dev.	484.7	69.7	270.7	929.9	228.8	673.6
Max.	2381.7	346.6	1693.5	3290.5	1235.9	3360.6
Min.	33.1	4.7	7.4	81.0	27.8	94.5
N=	32			37		

Desc.=	Description		
TU=	upper &	mid- Urgonian	
BU=	basal	Urgonian	
TZ=	thrust	related	Urgonian

Ages.

M. foram.= foraminifera shales, Oligocene, e5-6 = Val d'Illiez sst, Oligocene,

eN= Nummulite lst, Eocene, Sen. & base Sen.= Senonian, Gault =Albian,

Urg. & U. vein= Urgonian, N1-2= Berrisian/Valanginian, N2, N2f & Val= Valanginian,

N1b & Berri= Berriasian, u. Kimm.= upper Kimmeridgian, Tith= Tithonian, J6B= upper Jurassic,

Data Table A.3.1

Sample #	Locality	Quartz	Calcite	Total Clay	Dolomite	Location
4/89	Pas de Rocheplane	66.5	30.5	3.1	0	Chartreuse
5/89	Pas de Rocheplane	51.7	40.1	1.8	6.4	Chartreuse
12/89	Dent de Crolles	59.9	36.4	1.9	1.9	Chartreuse
28/89	SW of Petite Vache	38.8	60	1.3	0	Chartreuse
29/89	NW of Petite Vache	29.4	68.8	1.8	0	Chartreuse
49/89	Guiers Mort gorge	53	43.9	3	0	Chartreuse
86/89	Guiers Mort gorge	30.4	68	1.6	0	Chartreuse
87/89	Guiers Morrt gorge	63	31.5	5.47	0	Chartreuse
138/89	Guiers Vif gorge	35.8	57.9	6.3	0	Chartreuse
147/89	HW Corbel TZ	45.7	51.7	2.5	0	Chartreuse
Sample #	**Locality**	**Quartz**	**Calcite**	**Total Clay**	**Dolomite**	**Location**
170/89	E. of Pic St. Michel	59.7	36.4	3.9	0	Vercors
186/89	E. of ColVert	13.5	86.5	0	0	Vercors
187/89	E. of Col Vert	59.7	36.4	3.9	0	Vercors
204/89	HW of Ferrriere TZ	9.2	86.8	4.1	0	Vercors
212a/89	Bourne gorge	21.4	72	7.2	0	Vercors
212b/89	Ist band, Bourne gorge	11.6	87.3	1.6	0	Vercors
213a/89	Chalimont thrust	57	38	5.3	0	Vercors
213b/89	Chalimont thrust	58.2	31	4	7.7	Vercors
214/89	Rencurel	13.5	82.6	1.6	2.4	Vercors
228/89	W. end of Bourne gorge	51.2	46.8	2	0	Vercors
230/89	S. of Les Drevets	37.3	61.4	1.3	0	Vercors
256/89	Grand Goulets	9.33	88	2.6	0	Vercors
Sample #	**Locality**	**Quartz**	**Calcite**	**Total Clay**	**Dolomite**	**Location**
267/89	Combe deTardevant	66.5	30.7	2.9	0	Aravis
	N=23					
	Mean =	**40.97**	**55.33**	**3.01**	**0.80**	
	Standard deviation =	**19.61**	**20.52**	**1.74**	**2.03**	

Data Table A.3.2

Sample #	Locality	Illite	I/S	Smectite	Chlorite	I/S Ordering	
4/89	Dent de Crolle	3	1	96	0	random	
5/89	Dent de Crolle	7.7	15.5	77	0	random	
12/89	Dent de Crolle	8.8	3.5	87.7	0	random	Chartreuse
28/89	Grande Vache	13.7	2.1	87.2	0	random	
29/89	Grande Vache	15.9	8.8	75.22	0	random	massif
49/89	Guiers Mort	8.8	5.3	85.8	0	random	
85/89	Guiers Mort	9.6	15.5	75	0	random	
86/89	Guiers Mort	6	12	82	0	random	
87/89	Guiers Mort	7	12	81	0	random	
138/89	Guiers vif	19.8	4.7	75.5	0	random	
147/89	Corbel	9.8	8	82	0	random	
Sample #	**Locality**	**Illite**	**I/S**	**Smectite**	**Chlorite**	**I/S Ordering**	
187/89	l'Embossu	8	78	13	0	random	
204/89	Bourne gorge	8.5	6.5	84.9	0	random	Vercors
214/89	Bourne gorge	14	21	65	0	random	
228/89	Bourne gorge	24	14.6	61	0	random	massif
230/89	Bourne gorge	8.3	15.5	76	0	random	
Sample #	**Locality**	**Illite**	**I/S**	**Smectite**	**Chlorite**	**I/S Ordering**	
376/90	Dents d'Arclusaz	60	16	15	10	allevardite	Bauges
Sample #	**Locality**	**Illite**	**I/S**	**Smectite**	**Chlorite**	**I/S Ordering**	
476/90	E. Bourne valley	64	10	17	10	allievardite	Bornes
589/90	nr. Haut-Rumilly	35	34	18	13	allevardite	massif
Sample #	**Locality**	**Illite**	**I/S**	**Smectite**	**Chlorite**	**I/S Ordering**	
267/89	Combe deTardevant	70	7.3	3.3	20	kalkberg	Aravis
357/90	Nancy-sur-Cluses	65	18.5	9.3	7.4	kalkberg	
446/90	Trou de la Mouche	42.5	13.8	34.5	9.5	kalkberg	massif
Sample #	**Locality**	**Illite**	**I/S**	**Smectite**	**Chlorite**	**I/S Ordering**	
339/90	La Colonne	70	8	1	21	kalkberg	Platé
Sample #	**Locality**	**Illite**	**I/S**	**Smectite**	**Chlorite**	**I/S Ordering**	
617/90	Combe aux Paures	75	5	1	19	kalkberg	Haut-Giffre

N=24

From Deconinck, 1984

Sample #	Locality	Illite	I/S	Smectite	Chlorite	I/S Ordering	
?	La Clusaz	58	17.5	7	17.5	?	Aravis
?	Aleves	20	10	70	0	?	Bauges

Data Table A.3.3

Miscellaneous **XRD Data**

1. Rudist shells.

Sample #	Location	Peak positions (°s 2 theta)	Composition
21B/90	Chartreuse	34.30, 46.12, 50.7	calcite
490B/90	Aravis	34.35, 46.2, 50.6	calcite
410B/90	Bauges	34.4, 46. 15, 50.8	calcite
236/89	Vercors	34.25, 46.12, 50.7	calcite

2. Karst infill.

Sample #	Location	Peak positions (°s 2 theta)	Composition
118/91	Villaret Rouge,	10.1, 20.6, 23.2, 40.9, 42.0	glauconite
118/91	Bornes	24.2, 31.1, 42.7, 46.1, 49.9	quartz
118/91		34.2, 46.1, 50.5	calcite
118/91		33.1, 38.5, 43.2, 47.6,	pyrite
178/91	Termine road	14.4, 21.8, 29.2	chlorite
178/91	lower road section	24.2, 31.0, 42.2, 46.1, 58.9	quartz

3. Fine grained, pore filling material.

Sample #	Location	Peak positions (°s 2 theta)	Composition
119/91	Villaret Rouge,	34.3, 46.1, 50.6	Calcite
119/91	Bornes	24.3, 31.1, 42.6	Quatrtz

Data Table A.3.4

MAJOR ELEMENTS SAMPLE #	Si02	AlO2	FeO2	MgO2	CaO2	NaO2	KO2	TiO2	MnO2	PO2	S	LOI	TOTALS	SAMPLE #	Location
4\89	43.41	5.97	2.11	1.10	24.39	0.10	1.10	0.41	0.02	0.06	0.04	21.28	100.00	**4\89**	Chartreuse
12\89	24.04	2.32	1.14	1.14	40.98	0.15	0.58	0.21	0.03	0.03	0.14	29.43	100.17	**12\89**	Chartreuse
49\89	45.47	5.14	1.81	1.09	24.43	0.11	0.91	0.63	0.02	0.05	0.40	20.23	100.00	**49\89**	Chartreuse
86\89	14.04	2.44	1.28	1.05	46.80	0.17	0.35	0.19	0.02	0.04	0.24	33.42	100.00	**86\89**	Chartreuse
138\89	19.36	2.74	1.35	0.83	43.91	0.14	0.41	0.21	0.03	0.03	0.18	30.83	100.00	**138\89**	Chartreuse
147\89	24.27	2.48	1.18	0.07	39.70	0.12	0.40	0.18	0.02	0.47	0.00	30.91	100.42	**147\89**	Chartreuse
187\89	45.39	4.99	2.09	0.98	25.20	0.12	0.87	0.35	0.02	0.06	0.32	19.64	100.00	**187\89**	Vercors
212A\89	15.42	4.48	1.28	1.28	41.90	0.14	0.49	0.24	0.01	0.05	0.31	34.34	99.93	**212A\89**	Vercors
228\89	35.12	3.92	1.69	0.85	32.40	0.16	0.68	0.29	0.02	0.06	0.49	24.23	99.91	**228\89**	Vercors
230\89	27.28	3.39	1.40	0.65	37.30	0.14	0.57	0.21	0.02	0.11	0.20	28.70	100.00	**230\89**	Vercors
256\89	8.44	2.45	0.74	1.54	47.10	0.16	0.26	0.12	0.01	0.03	0.14	39.04	100.25	**256\89**	Aravis
267\89	53.60	5.12	2.25	1.25	20.21	0.17	1.25	0.38	0.02	0.09	0.26	15.42	100.00	**267\89**	Aravis

Ro (%)	Std Dev	UV	Location	Age	Sample #
			Vercors massif		
0.44	0.03	orange/yellow	L'Embossu	Hauterivian	186/89
0.48	0.052	orange	L'Embossu	Hauterivian	187/89
0.7	0.029	orange	St. Loup	Tithonian	189/89
barren	-	dull orange	Uriol	Kimmeridgian	190/89
0.83	0.037	dull orange	St. Loup	Oxfordian	191/89
0.35	0.041	dull yellow	Pont Valchevrie	Hauterivian	204/89
0.35	0.021	yellow	W. of Pont de la Goule Noire	Hauterivian	212/89
0.32	0.042	yellow	W. of Pont de la Goule Noire	Hauterivian	213a/89
0.27	0.024	yellow	Rencurel	Hauterivian	214/89
barren	-	green	Rencurel	Miocene	220/89
0.21	0.06	greeny/yellow	Barrage de Choranche	Hauterivian	228/89
0.48	0.52	orange/yellow	W. Choranche	Valanginian	231/89
barren	-	yellow	E. Pont-en-Royan	Hauterivian	232/89
barren	-	yellow/green	Grand Goulets	upper Orbitolina	249/89
0.2	0.08	green	Lans-en-Vercor	Miocene	258/89
Ro (%)	**Std Dev**	**UV**	**Location**	**Age**	**Sample #**
			Chartreuse massif		
0.47	0.07	dull orange	Pas de Rocheplane	Valanginian	1/89
0.38	0.027	orange/yellow	Pas de Rocheplane	Hauterivian	4/89
barren	-	yellow	Dent de Crolle	Hauterivian	5/89
0.45	0.018	orange	Col du Coq	Berriasian	9/89
0.4	0.05	orange/yellow	Pas de Perraux	Hauterivian	12/89
0.3	0.041	yellow	Port d'Enclos	Hauterivian	49/89
0.4	0.04	dullyellow	Perequelin	Berriasian	16/89
0.5	0.038	orange	Perequelin	Kimmeridgian	17/89
barren	-	brown/orange	W. Grande Sure	Tithonian	22/89
0.8	0.03	orange	Trois Fontaines, Grande Sure	Tithonian	23/89
0.35	0.03	yellow	W. Grande Vache	Hauterivian	28/89
0.27	0.06	yellow	SW Charmont Sommet	Senonian	34/89
1.25	0.03	none	Corenc	Oxfordian	41/89
0.33	0.028	dull yellow	Pont St. Pierre	Berriasian	53/89
barren	-	dull orange	W. Pont St. Pierre	Tithonian	71/89
barren	-	dull orange	W. Pont St. Pierre	Tithonian	74/89
barren	-	dull yellow	Pic d'Oillette	Hauterivian	85/89
0.35	0.037	dull yellow	Pic d'Oillette	Hauterivian	86/89
barren	-	yellow	W. pont St. Bruno	Berrisian	101/89
0.43	0.043	orange/yellow	Fourvoire	Berriasian	104/89
0.47	0.073	orange/red	Fourvoire	Berriasian	105/89
0.87	0.037	orange/brown	La Perelle	Kimmeridgian	120/89
0.21	0.07	green	St. Laurent du Pont	Miocene	126/89
0.33	0.035	yellow	Pas du Frou	Hauterivian	138/89
0.46	0.021	orange/yellow	Corbel	Hauterivian	147/89
0.31	0.04	yellow	Les Moulins	Berriasian	141/89
0.38	0.041	orange/yellow	La Martinere	Valanginian	148/89
0.38	0.04	orange/yellow	Les Courriers	Berriasian	153/89
Ro (%)	**Std Dev**	**UV**	**Location**	**Age**	**Sample #**
			Bauges massif		
0.35	0.045	yellow/orange	Nivolet	Hauterivian	282/90
barren	-	dull orange	La Place	Kimmeridgian	358/90
barren	-	brown	Dents d'Arclusaz	Hauterivian	376/90
barren	-	orange/yellow	Gorge du Cheran	Hauterivian	380/90
barren	-	orange/yellow	W. Mt.Trelod	Valanginian	426/90
barren	-	none	Col de Frene	Bathonian	123/91
Ro (%)	**Std Dev**	**UV**	**Location**	**Age**	**Sample #**
			Bornes massif		
1.1	0.067	brown	Glieres Plateau	Hauterivian	133/91
0.73	0.051	orange	nr. Pointe d'Andey	Oligocene	173/91
barren	-	orange	S. Romme	Oligocene	297/90
barren	-	oranbe/brown	WSW Nancy-sur-Cluses	Hauterivian	335/90
barren	-	none	Nancy-sur-Cluses	Hauterivian	357/90
barren	-	none	la Giettaz	Malm	435/90
1.3	0.061	none	La Clusaz	Hauterivian	465/90
barren	-	orange	La Clusaz	Oligocene	470/90

0.54	0.33	orange	La Clusaz	Oligocene	471/90
1.13	0.059	none	upper Bourne valley	Hauterivian	474/90
1.2	0.06	none	upper Bourne valley	Hauterivian	476/90
1.34	0.073	none	La Clusaz	Hauterivian	465/90
0.6	0.041	orange	Les Nants	Oligocene	556/90
0.45	0.043	orange/yellow	Haut-Rumilly	Oligocene	592/90
Ro (%)	**Std Dev**	**UV**	**Location**	**Age**	**Sample #**
			Aravis massif		
1.75	0.034	none	Combe de Tardevant	Hauterivian	267/89
1.7	0.043	none	Combe de Grande Cret	Hauterivian	443/90
barren	-	none	Trou de la Mouche	Hauterivian	446/90
0.75	0.076	dull orange	W. Mt. Charvin	Eocene	265/89
barren	-	brown/orange	W. Mt. Charvin	Eocene	512/90
Ro (%)	**Std Dev**	**UV**	**Location**	**Age**	**Sample #**
			Platé massif		
barren	-	none	Col de la Fete	Hauterivian	328/90
barren	-	none	L Colonne	Hauterivian	339/90
1.23	0.055	none	Pointe Anterne	Oligocene	632/90
1.3	0.07	none	Pointe Anterne	Oligocene	633/90
2	0.047	none	Cascade de Salles	Hauterivian	204/91
barren	-	none	Cascade de Salles	Berriasian/?Val	205/91
Ro (%)	**Std Dev**	**UV**	**Location**	**Age**	**Sample #**
			Haut-Giffre massif		
barren	-	none	Combe aux Paures	Hauterivian	617/90
2.1	0.045	none	Col de Sageroux	Berriasian	623/90
2.7	0.021	none	Combe des Fonds	Oxfordian	622/90
1.49	0.056	none	Chambres lake	Eocene	207/91
barren	-	none	Col de Sageroux	Berriasian	208/91
barren	-	none	Col de Sageroux	Berriasian	209/91
barren	-	none	Col de Sageroux	Berriasian	210/91
barren	-	none	above Vogealle refuge	Berriasian	211/91
2.8	0.024	none	Combe des Fonds	Oxfordian	212/91
Ro (%)	**Std Dev**	**UV**	**Location**	**Age**	**Sample #**
			From Kübler et al. (1979)		
			Bornes massif		
0.88	not given	not given	Thuet	Oligocene	
0.78	not given	not given	Cenise	Oligocene	
0.61	not given	not given	Brison	Eo	
0.54	not given	not given	Bonneville	Oligocene	
0.58	not given	not given	St. Pierre	Oligocene	
0.42	not given	not given	Thorens	Oligocene	
0.43	not given	not given	La Roche	Oligocene	
0.8	not given	not given	Petit Bornand	Eo	
0.79	not given	not given	Thones	Oligocene	
Ro (%)	**Std Dev**	**UV**	**Location**	**Age**	**Sample #**
			Bauges massif		
0.72	not given	not given	Entrevernes	Eo	

Data Table A.4.2

Sample #	Unit	Age	Locality	Locality	TOC	Hydrogen Index	Kerogen type	Ro
592/90	Melatta shales	Oligocene	Haut-Rumilly	Bornes	1.85	176.9	III	0.45
632/90	Foramin. shales	Oligocene	nr. Tete l'Anne	Platé	1.03	9.8	IV	1.23
173/90	Val d'Illiez ssts	Oligocene	La Torche	Bornes	0.95	122.4	III	0.73
189/90	Taveyannaz ssts	Oligocene	Col d'Emnay	Haut-Giffre	0.78	7.68	IV	n.k.
196/90	Gault	Albian	Bossetan	Haut-Giffre	0.93	34.3	IV	n.k.
197/91	Callovian	Callovian	Lac d'Anterne	Platé	0.39	38.8	IV	n.k.
207/90	Diablerets beds	Eocene	Lac du Chambres	Haut-Giffre	2.38	118.5	III	1.49
211/90	Berriasian	Berriasian	Pas l'Ours	Haut-Giffre	2.17	9.68	IV	barren

Sample #	S1	S2	Tmax
592/90	0.17	3.27	443
632/90	0.01	0.09	559
173/90	0.09	1.16	446
189/90	0.02	0.1	553
196/90	0.01	0.23	550
197/91	0.01	0.15	447
207/90	0.02	0.52	557
211/90	0.03	0.21	557

Data Table A.5.1

UNIT	LITHOLOGICAL DATA	COMPUTED INITIAL POROSITY	COMPACTION FACTOR
Alpine Molasse	80% sst, 18% siltst., 2% shale	0.47%	1.84
Taveyanne Ssts	80% sst, 18% siltst., 2% shale	0.47%	1.84
Eocene-Olig. sands	98% sst, 2% shale	0.45%	1.76
Tertiary shales	15% siltst., 85% shale	0.59%	2.37
Nummulite lsts	2% sst, 20% silt. 3% shale, 75% lst	0.59%	1.67
Calcaire lithographique	15% shale, 85% lst	0.60%	1.64
Aravis Fm	55% sst, 1% silt, 40% silt, 4% lst	0.52%	2.00
Senonian	30% sst, 10% shale, 60 lst	0.56%	1.67
Lumachelle	7% sst, 93% lst	0.59%	1.52
Urgonian	100% lst	0.60%	1.50
Hauterivian	35% silt, 10% shale, 55% lst	0.58%	1.84
Valanginian	100% lst	0.60%	1.50
Berriasian	15% shale, 85% lst	0.60%	1.64
Tithonian	100% lst	0.60%	1.50

Journal of the Geological Society, London, Vol. **149**, 1992, pp. 503–515, 9 figs, 4 tables. Printed in Northern Ireland

Organic maturation in the French Subalpine Chains: regional differences in burial history and the size of tectonic loads

S. MOSS

Department of Geological Sciences, University of Durham, Durham, DH1 3LE, UK

Abstract: The French Subalpine Chains of southeastern France are the foreland fold/thrust belt of the Western Alps, formed in the mid- to late Tertiary as a result of the continental collision between the European and Italian–North African plates. With the change from passive margin to destructive margin, certain areas of the Subalpine Chains experienced enhanced temperatures through being buried to greater depths. Burial of these areas has been investigated using vitrinite reflectance (R_o).

Levels of organic maturity of Mesozoic and Tertiary horizons have been established using vitrinite reflectance (R_o) and spore fluorescence. In the southwestern part of the chain, values of R_o for Mesozoic units from the Vercors and Chartreuse massifs are generally low, with all Cretaceous units having values $<0.5\%$ R_o. Older Jurassic horizons have higher values, up to 1.25% for the mid-Jurassic (Oxfordian). When compared to values from the same horizons, and from younger Tertiary units (published data) from the northeastern part of the chain, it is clear that this part of the belt has encountered higher temperatures, produced by greater depth of burial. In the Haut-Giffre and Aravis massifs Mesozoic units have R_o values as high as 2.7% and, in terms of hydrocarbon generation, can be considered mature or overmature.

Two causes of greater depth of burial of the northeastern part of the belt are indicated by field studies and by burial history modelling of specific localities of the Subalpine Chains: first, the earlier initiation of the Tertiary foredeep in the northeast compared to the southwest; and second, differences in the size of tectonic loads emplaced onto the Subalpine Chains during the final stages of Alpine compression, with the greater structural deformation of the Subalpine Chains occurring in the northeast.

Vitrinite reflectance (hereafter referred to as R_o) and spore fluorescence are techniques which have been in use for several years as a means of estimating palaeotemperatures and geothermal gradients (Barker & Pawlewicz 1986; Tissot *et al.* 1987). Both are optical techniques for assessing the thermal maturity of sedimentary organic material. The reflectance of vitrinite macerals is most often used as a rank parameter which can be directly related to hydrocarbon maturation; for example 0.5% R_o and 1.3% R_o are the usually quoted values for the start and end of oil generation (Hood *et al.* 1975; Teichmüller 1987). Fluorescence of sporinite macerals can similarly be used to show maturity, but it is less precise, because it depends upon the judgement of the observer, unless more quantitative techniques are used such as the CEI colour system (Marshall 1991). The use of R_o and spore fluorescence in basin analysis and thermal modelling is reviewed by Teichmüller (1987), Robert (1988) and Barker (1989).

This paper describes the use of R_o to detail the differences in burial and thermal history that occur across and along strike of a foreland fold/thrust belt. The results obtained using this technique are then compared to the results of burial and thermal modelling of this foreland fold/thrust belt.

Geological background

The northern French Subalpine Chain is a roughly NE–SW-trending mountain chain, situated within the southeast corner of France (Fig. 1), flanking the cities of Annecy and Grenoble. Formed in the Tertiary, the Subalpine Chain represents the external part of Western Alps. As such, it is a classic example of a foreland fold/thrust belt. The orogenic hinterland, referred to as the Internal Zone (Debelmas & Kerckhove 1980), is the area immediately to the east of the Frontal Pennine thrust (FPT, see Fig. 1). The Internal Zone comprises rocks from the

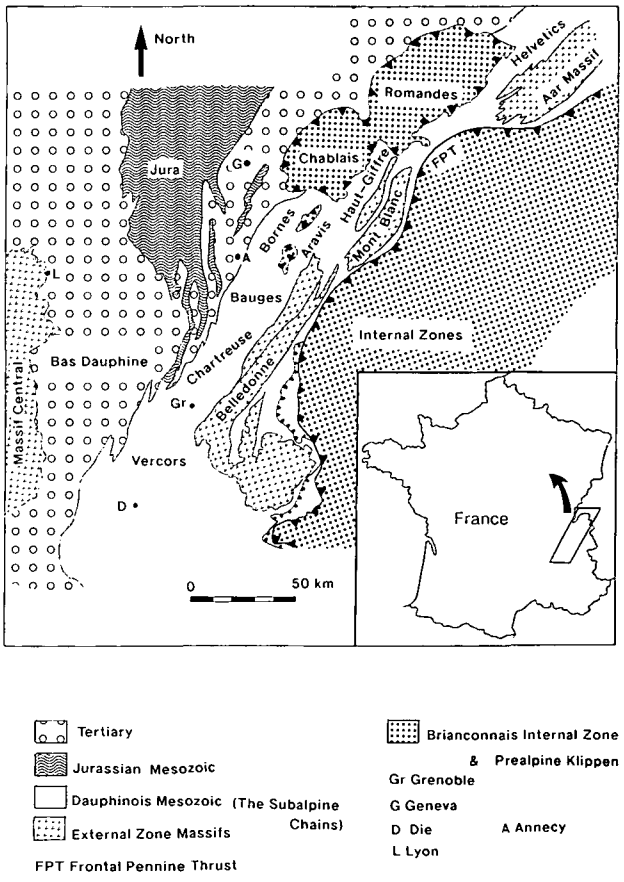

Fig. 1. Location of the Subalpine Chains within France and the Western Alps.

Penninic and Austroalpine palaeogeographic domains which are the remnants of a Tethyan ocean and the Adria/African plate margins (Dewey *et al.* 1973).

To the west of the Internal Zones (and the Frontal Pennine thrust) is the External Zone or Dauphinois zone, which is the lateral equivalent of the Helvetic zone in Switzerland. Basement massifs of the External Zone (such as the Belledonne and Mont Blanc Massifs) and Ultra-Helvetic sediments (now in their own nappe structures) are in the immediate footwall of the Frontal Pennine thrust. Mesozoic sedimentary cover rocks of the Subalpine Chains and the Tertiary Bas Dauphine and Swiss molasse basins occur farther to the west/northwest within the Dauphinois/Helvetic domain (see Fig. 1). Triassic continental rocks directly overlying peneplained basement units are followed by Jurassic and Cretaceous shales, argillaceous limestones and carbonate platform limestones deposited upon the European passive margin within the Dauphinois domain as part of the post-rift succession (Lemoine *et al.* 1986; Arnaud 1988).

Collision between Europe and the Adria/North African continent began approximately 62 Ma ago (Lemoine *et al.* 1986; Lemoine & Trümpy 1987) and resulted in the downward flexure of the European lithosphere in the Alpine region (Karner & Watts 1983), and the formation of a foredeep or foreland basin, which migrated north-westwards ahead of the main orogenic mountain belt (Homewood *et al.* 1986). Foredeep-related flexure did not commence in the area of the Subalpine Chains until the Eocene (46 Ma). Prior to flexural subsidence parts of the Subalpine Chains were eroded during the Palaeogene, in places as far down as the Lower Cretaceous, leading to the formation of karstic surfaces in some localities (Debrand-Passard *et al.* 1984). These were covered by syn-orogenic sediments later in the Tertiary. The duration and extent of this period of Palaeogene erosion vary along the strike of the Subalpine Chains, with more pronounced erosion taking place in the southwestern massifs of the Chartreuse and Vercors. Only localized pockets of thin (maximum 30 m thickness) continental clastics were deposited during the Eocene and Oligocene in these areas, and during foredeep formation in the Aquitanian. In the northeast part of the Subalpine Chains, in the Haut-Giffre, Platé, Aravis, Bornes and Bauges massifs, foredeep formation occurred much earlier in the Bartonian (46 Ma, Eocene, Pairis & Pairis 1975; Debelmas & Kerchkhove 1980; Debrand-Passard *et al.* 1984) with the deposition of the Nummulitic limestones, followed by the deeper water shales and volcaniclastic turbidites of the Taveyannaz and Val d'Illiez sandstones (Lateltin 1988). The Bas Dauphine and Swiss Molasse basins (collectively referred to as the Peri-Alpine Molasse Basin or 'sillon perialpine') represent the final position of the molasse basin.

Structural style within the Subalpine Chains likewise varies along the strike of the fold/thrust belt. The overall geometry of the the Western Alps is well constrained, both from geophysics (e.g. Bayer *et al.* 1987) and from structural studies (e.g. Debelmas *et al.* 1983; Butler 1986; Ramsay 1981, 1989). The southwestern massifs of Chartreuse, Vercors, Bauges and western Bornes are characterized by low displacement thrusts and open asymmetric folds (Mugnier *et al.* 1987; Butler *et al.* 1987). The northeastern Haut-Giffre, Platé and Aravis massifs, along with the northeastern part of the Bornes massif (referred to as the Massif du Bargy) represent the southern termination of the Helvetic nappes (Ramsay 1989; Butler *et al.* 1987). There are three stacked nappe units, which from bottom to top are the Morcles, Diablerets (or Samoens) and Wildhorn (or Sallanches) nappes. These nappes have their 'root zone' in the 'syncline de Chamonix', between the Mont Blanc and Aiguilles Rouges basement massifs, the latter of which has been overridden by this cover sequence nappe pile. The Helvetic nappe pile, prior to its formation was itself overridden by Ultra-Helvetic and Pennine nappes, containing sediments with affinities to those seen in the Internal zones (Kindler 1988) and tectonically linked to the Ultra-Helvetic thrust and the Frontal Pennine thrust, both of which are exposed to the east of the Mont Blanc massif (see Fig. 1). These more travelled nappes are represented today in the Subalpine Chains by erosional klippe, such as the Sulens, Annes, Chablais and Romandes klippen. Boyer & Elliot (1982) suggested that the Ultra-Helvetic and Frontal Pennine thrusts provided the roof thrust for the Helvetic nappes, forming a duplex structure.

There have been several previous studies of the thermal maturity and very low grade metamorphism of this part of the Alpine arc. Frey (1970; 1974), Monnier (1979), Kisch (1980), Frey *et al.* (1980) and Aprahamian (1988), have all described thermal maturity and low grade metamorphism of the Helvetic region of the Swiss Alps and the Swiss molasse basin. In a review paper Kübler *et al.* (1974) described low grade metamorphic minerals in Switzerland and the border region with France, particularly within the Taveyannaz sandstones. Aprahamian & Pairis (1981) detailed a reverse gradient in the very low grade metamorphism of the Arve Valley section on the edge of the Platé massif, suggesting the cause of an inverted metamorphic grade of illite crystallinity was due to frictional heating along the thrust plane of the pre-Alpine thrust sheets. Kübler *et al.* (1979) presented the results of a study on values of R_o in the area east of Geneva, in France and Switzerland, but only gave a brief explanation of increasing grade of metamorphism toward the Internal Zones to account for the variations in R_o they found. Levels of low grade metamorphism have been demonstrated to change with structural position within a traverse across the Morcles nappe in Switzerland (Goy-Eggenberger & Kübler 1990). Burkhard & Kalkreuth (1989) used R_o to show differences in the depth of burial due to tectonic loads in the Wildhorn nappe and surrounding units in the Kander valley region of western Switzerland. Chaplet (1989) and Deconinck (1984) investigated the clay mineralogy of the Upper Cretaceous, relating illite and chlorite-rich samples from east of the Dent d'Arclusaz fault (eastern Bauges) to greater depth of burial. Sawatzki (1975) studied the burial metamorphism of the Tertiary flysch units within the Thones syncline (which divides the Bornes and Aravis massifs), and from the presence of certain clay minerals (such as corrensite) he suggested that these flysch units had experienced burial temperatures in the region of 100°C to 200°C. Previous work carried out in the Western Alps has concentrated mainly on differences in the thermal history across strike of the regional structure instead of along strike, which is the major objective of this paper.

Analytical techniques

All samples for reflected light (R_o) and fluorescence (spores) microscopy (see Stach *et al.* 1982) were gently crushed by hand and set into epoxy resin blocks and polished. Mean vitrinite reflectances were calculated from the arithmetic mean of measurements made on random pieces of vitrinite within the sample block, using oil immersion. All values of R_o are quoted as mean vitrinite reflectance in oil. Spore fluorescences was estimated using a Zeiss UV microscope. All measurements of organic maturity were made at The University of

Newcastle-upon-Tyne (Newcastle Research Group in Fossil Fuels and Environmental Geochemistry). All values of R_o are reported as the arithmetic mean.

Levels and variation of vitrinite veflectance (R_o) within the Subalpine Chains

Readings of R_o are principally governed by the geothermal gradient and the length of exposure time to maximum burial temperatures experienced by the rocks in question. Geothermal gradients also encompass other variables such as thermal conductivity of each horizon and heat flow within the area. Differences in the hydrocarbon content of the total organic fraction and variations in the kinetic properties of the macerals involved are also important and should be considered. Various models of increases in R_o with temperature and/or time have been published and can be used to obtain a value for the temperature to which a series of rocks has been exposed. Published models vary greatly in their level of sophistication, partly because of the uncertainities concerning time in the maturation of vitrinite macerals and activation energies of different macerals. Consequently a number of different nomograms of R_o versus temperature and time have been presented, and some have taken kinetic considerations into account as well. Price (1983) and Barker & Pawlewicz (1986) suggest that temperature is the main control upon R_o, with time a much less important factor in determining the value of R_o. Both suggest that full organic matter thermal maturation is controlled principally by maximum temperature, with time showing little or no influence. It is thought that full maturation is achieved after an exposure time to maximum burial temperatures of only about 10 000 years' duration. In a recent review Barker (1989) states that there is evidence that only 10^6 to 10^7 years are required for kerogen to stabilize during thermal maturation via burial diagenesis. Barker concludes that models of organic maturation that consider both temperature and time, or just temperature alone, will predict palaeotemperatures with the same precision. Sweeney & Burnham (1990) have published the most recent model of vitrinite maturation. Their equation integrates chemical kinetic equations for activation energies of vitrinite over time and temperature. Their nomogram of R_o v. exposure time and maximum temperature for their equation is shown in Fig. 2, along with those for several other equations for R_o (Bostick *et al.* 1978; Middleton 1982; Hood *et al.* 1975). The Sweeney & Burnham equation is preferred, and used below to estimate temperatures, because it incorporates a distribution of activation energies for vitrinite as well as temperature and time. This models the maturation of vitrinite macerals more accurately than using a single activation energy.

Abundance and occurrence of organic material in the Subalpine Chains

Readings of R_o and spore fluorescence were made from samples prepared from fresh outcrop samples of argillaceous lime mudstones, shales and sandstones from Mesozoic and Tertiary units. Readings of R_o would ideally be made on more than 20 vitrinite particles; however, the average number of readings that could be obtained was generally less than this. This might be expected because the samples come mainly from carbonate rocks, which were deposited in oxygen-rich environments, in which organic material is readily oxidized. Vitrinite macerals derived from land plants are typically more common in continental–marginal marine facies rocks than fully marine rocks, where slightly anoxic to anoxic bottom conditions are common.

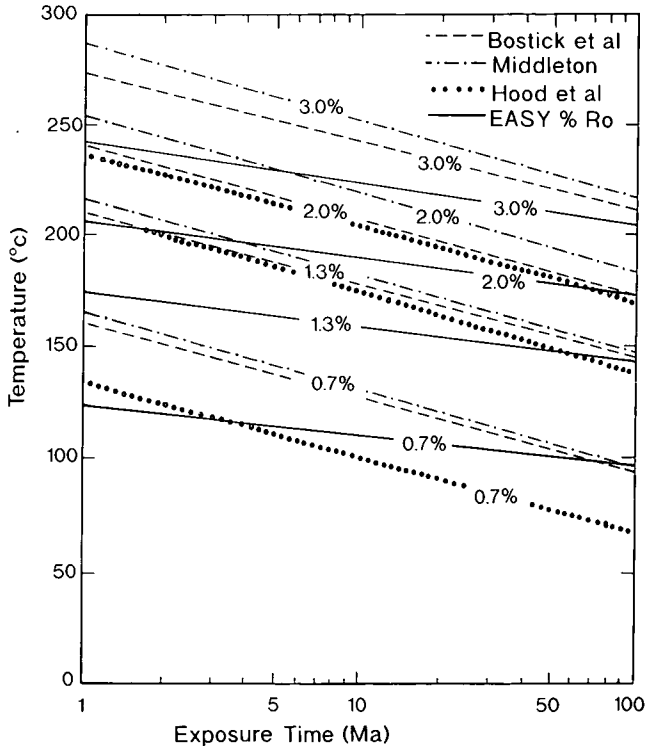

Fig. 2. Graph showing the relationship between R_o, temperature and time for Sweeney & Burnham's (1990) nomogram (referred to as EASY % R_o on the figure). The equations for the same relationship suggested by Bostick *et al.* (1978), Middleton (1982) and Hood *et al.* (1975) are also shown.

The results

Table 1 lists the recorded values for R_o and Figs 3 and 4 show distribution of these values within the study area.

SW part of the Subalpine Chains

In the Chartreuse and Vercors massifs (Table 1 and Fig. 3), Lower Cretaceous units such as the Berriasian and Valanginian have low values of R_o, generally in the region of 0.35% to 0.45%. Spores from these horizons are green/yellow to yellow, sometimes with a slightly orange fluorescence, which is consistent with the vitrinite values recorded for these horizons. Upper Jurassic to middle Jurassic units from these same areas of the Subalpine Chains have higher values of R_o, as would be expected since they come from 500 m to 900 m lower down in the stratigraphic column. Values of R_o range from 0.5% for the uppermost Jurassic (Kimmeridgian) to 1.25% for the middle Jurassic (Oxfordian) (see Table 1 and Fig. 3). Spores from the Jurassic show a range of fluorescence, from yellow/orange, to orange, to brown, to dark/non-fluorescent. Again the fluorescence matches the values obtained for R_o for each respective sample. Only one R_o value was recorded from the Upper Tertiary (Miocene) molasse deposits in this part of the chain. This was from the western edge of the Chartreuse massif and

Table 1. *R_o values, age and location of samples from the Subalpine Chains*

R_o (%)	Location	Age
	Vercors	
0.27	Rencurel	Ha
0.21	Barrage de Choranche	Ha
0.32	Pont de la Goule Noire	Ha
0.35	Pont Valchevrie	Ha
0.7	St Loup	Ti
0.83	St Loup	Ox
0.44	L'Embossu (Col Vert)	Ha
0.48	L'Embossu	Va
0.29	Choranche	Ha
	Chartreuse	
0.47	Pas de Rocheplane	Va
0.38	Pas de Rocheplane	Ha
0.45	Col du Coq	Be
0.4	Pas De Perraux	Ha
0.3	Port d'Enclos	Ha
0.4	Perequelin	Be
0.5	Perequelin	Ki
0.8	Trois Fontaines, Grande Sure	Ti
0.35	W. Grande Vache	Ha
1.25	Corenc	Ox
0.33	Pont St Pierre	Be
0.35	Pic d'Oillette	Ha
0.43	Fourvoire	Be
0.47	Fourvoire	Be
0.87	La Perelle	Ki
0.46	Corbel	Ha
0.31	Les Moulins	Be
0.38	La Martinere	Va
0.38	Les Courriers	Be
0.21	St Laurent du Pont	Mioc
	Bauges	
0.35	Nivolet	Ha
	Haut-Giffre	
2.1	Col du Sageroux	Va
2.7	Combe des Fonds	Ox
	Aravis	
1.75	Combe de Tardevant	Ha
0.75	Mt Charvin	Eo
1.7	Combe de Grande Cret	Ha
	Bornes	
0.45	Haut-Rumilly	Ol
0.54	La Clusaz	Ol
1.13	upper Bourne valley	Ha
1.2	upper Bourne valley	Ha
1.34	La Clusaz	Ha
0.6	Les Nants	Ol
	Platé	
1.23	Pointe Anterne	Ol
	From Kübler *et al.* 1979	
	Bornes	
0.89	Thuet	Ol
0.78	Cenise	Ol
0.61	Brison	Eo
0.54	Bonneville	Ol
0.58	St Pierre	Ol
0.42	Thorens	Ol
0.43	La Roche	Ol
0.8	Petit Bornand	Eo
0.79	Thones	Ol
	Bauges	
0.72	Entrevernes	Eo

See Figs 3 and 4 for explanation of age abbreviations.

gave a value of 0.21% R_o. Spores within this sample had a bright green fluorescence.

NE part of the Subalpine Chains

Further to the northeast, along strike of the Subalpine Chains, in the Haut-Giffre, Platé and Aravis massifs (Fig. 1), the Lower Cretaceous units of the Hauterivian and Berriasian have much higher R_o values than the areas to the southwest discussed above. Here, R_o values of 1.75% and 2.1% were recorded for the Hauterivian and Berriasian respectively, whilst the mid-Jurassic (Oxfordian) reaches an R_o value of 2.7% (see Table 1 and Fig. 4). Under fluorescent light, these samples appeared dark and non-fluorescent, which is typical for rocks which have R_o values greater than 1.0%.

R_o values reported by Kübler *et al.* (1979) for the Eocene and Oligocene 'flysch' units of the Bornes massif (to the northeast of Annecy, see Fig. 1) and two values recorded by the author for the Oligocene of the Aravis and the Eocene of the Platé massifs, are shown in Table 1 and Fig. 4. The Eocene–Oligocene of the Bornes massif has R_o values (0.42% to 0.43%) that are similar to, or higher (0.54% to 0.8%), than the R_o values for the Cretaceous of the Chartreuse and Vercors massifs to the southwest. Further to the east samples from the Eocene and Oligocene have R_o values of 0.74% and 1.25%, in the Aravis and Platé massifs respectively.

Interpretation

SW part of the Subalpine Chains

The R_o values recorded from the Chartreuse and Vercors massifs suggest that the Lower Cretaceous strata have experienced maximum temperatures considerably less than 100°C (see Fig. 2), if the nomogram of Sweeney & Burnham (1990) is used. Roberts (1990) obtained similar maximum burial temperatures (40°C to 80°C) for the Hauterivian of the Vercors massif. This suggests that neither the depth of burial nor the residence time at maximum depth of burial were sufficient to cause any significant heating (in terms of organic maturity). Periods of burial related to foredeep formation and deformation are likely to be short in comparision to other basinal areas, such as mid-continental basins. Only very short periods, of up to 10 Ma, for residence time at maximum burial depth (see discussion in basin modelling section) are likely within the area.

R_o values from Upper Jurassic to mid-Jurassic units suggest temperatures of between 100°C to 160°C (see Fig. 2) assuming a heating duration of up to 10 Ma (see burial history section for discussion).

Overall, the data for the level of organic maturity of Mesozoic and Tertiary units in the Chartreuse and Vercors massifs suggest that this part of the Subalpine Chains has been subjected only to shallow burial, short residence times or abnormally low geothermal gradients, or all three. Foreland areas are typified by low geotherms (Allen & Allen 1990) and it is also likely that maximum burial depths were slight for this part of the Subalpine Chains. Thus it is possible that a combination of these factors produced the low levels of thermal maturity in this region. Both geothermal gradients and maximum depths of burial are discussed in the section on burial history.

NE part of the Subalpine Chains

Using the nomogram shown in Fig. 2, the R_o values suggest that the Cretaceous to middle Jurassic rocks of the north-

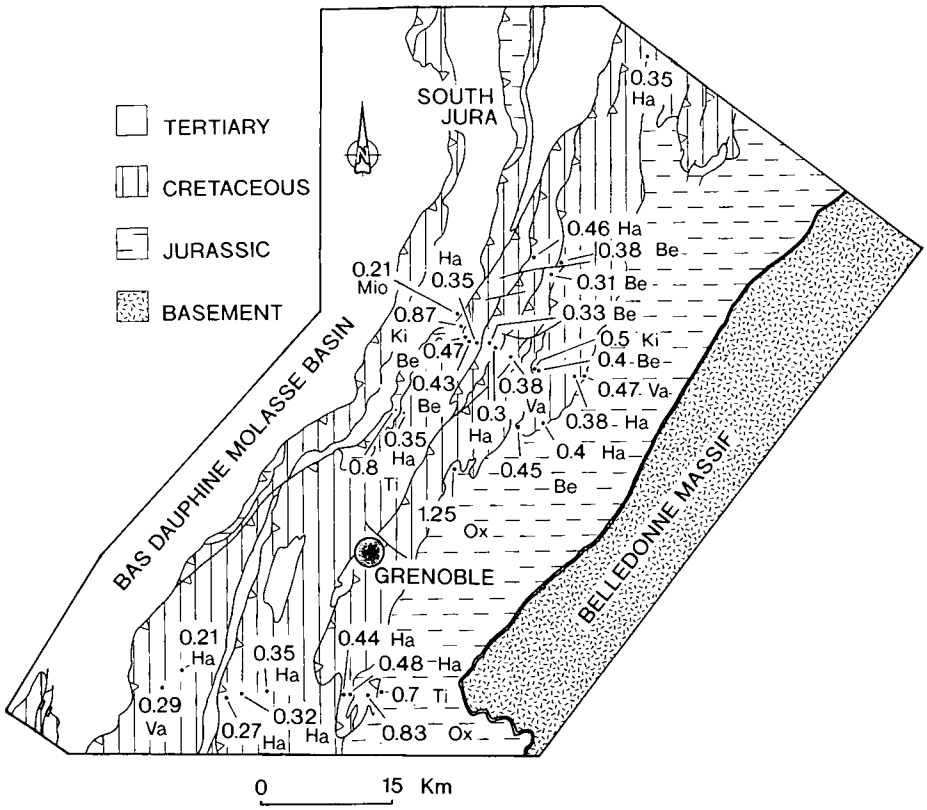

Fig. 3. Mean R_o (%) values for the southwest study area of the French Subalpine Chains. Stratigraphic ages of the samples used for the determinations are indicated by abbreviations: Mio, Miocene; Ha, Hauterivian; Va, Valangian; Be, Berriasian; Ki, Kimmeridgian; Ti, Tithonian; Ox, Oxfordian.

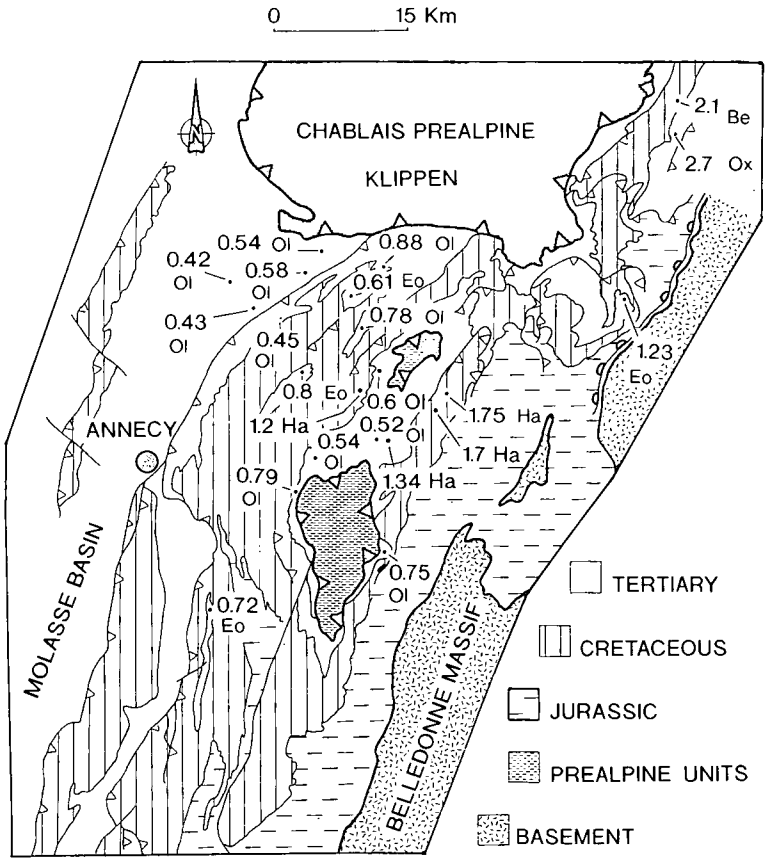

Fig. 4. Mean R_o (%) values for the northeast study area of the French Subalpine Chains. Stratigraphic ages of the samples used for the determinations are indicated by abbreviations: Ol, Oligocene; Eo, Eocene; Ha, Hauterivian; Be, Berriasian; Ox, Oxfordian.

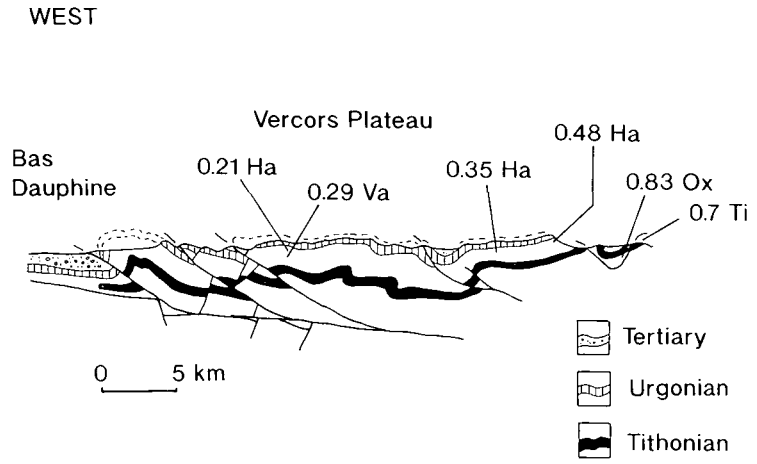

Fig. 5. Cross section through the Vercors massif, in the southwest part of the Subalpine Chains. R_0 values (%) for different horizons along the line of section are shown. A west to east increase in the level of R_0 for the Hauterivian can be seen. However, values of R_0 below 0.5 can be prone to scatter (Barker 1989). The section is based on Butler *et al.* (1987).

eastern part of the belt have experienced temperatures of around 175 °C to 225 °C, assuming that the length of exposure time to these maximum temperatures was up to 10 Ma. These temperatures indicate that the Cretaceous and Jurassic rocks of the northeastern part of the belt have been buried more deeply than their equivalent horizons to the southwest.

The R_0 values for Eocene and Oligocene units in the Bornes massif (up to 0.8) suggest that maximum burial temperatures of up to 135 °C were reached (see Fig. 2) for these horizons. Higher R_0 values for the sediments of the same age further to the east suggest slightly higher temperatures of 160 °C (assuming a heating time of up to 10 Ma). This indicates that the Tertiary rocks of the northeastern part of the Subalpine Chains has experienced greater burial temperatures than the older Cretaceous and Upper Jurassic rocks of the southwestern part of the belt, and reached levels of organic maturity similar to those of the middle Jurassic (Oxfordian) rocks of the southwestern part of the belt.

Using indicators of organic maturity in the Subalpine Chains gives evidence that the maximum burial depths and the time at those depths, and therefore the highest temperatures experienced, were in the northeast of the belt. The greatest variation in maximum burial temperatures is along strike of the fold/thrust belt, although temperatures do vary across the belt (see Figs 3, 4, 5 and 6), with higher temperatures experienced on the eastern side, closest to the orogenic hinterland. The values recorded for the southwest parts of the chain can be explained by sedimentary burial alone. Similar variations in temperature across strike of fold/thrust belts have been documented by Hoffman & Hower (1979), Kalkreuth & McMechan (1988), Underwood *et al.* (1988) and Guthrie *et al.* (1986).

Burial history modelling of the Subalpine Chains

Burial history diagrams (plots of time versus decompacted thickness of stratigaphic units) have become a common tool in basin analysis (van Hinte 1978; Falvey & Dieghton 1982; Guthrie *et al.* 1986). They are used here to model the thermal history of specific points of the Subalpine Chains. The results of this modelling are shown in Fig. 7. These should not be mistaken for subsidence history curves which would also consider depositional depths and eustatic sea-level corrections for each lithological unit. Wildi *et al.* (1989) have considered the Mesozoic subsidence history of the Helvetic, Swiss Plateau and Jura regions.

The plots were generated using the Basinmod™ program developed by the Platte River Associates (Modular Basin Modelling System. Version 2.80, October 1991), which is able to decompact the curves and to calculate the thermal maturity of the rocks involved. The basic lithological data for all the plots are shown in Table 2, along with the computed initial porosities of the units, which were checked by comparision with thin sections and reference to the porosities of similar recent sediments. Using these porosities the program calculated a

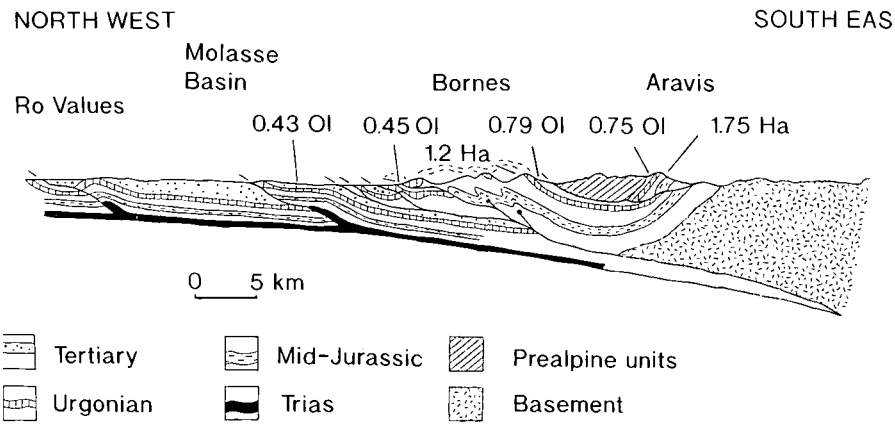

Fig. 6. Northwest to southeast cross section through the Bornes/Aravis massif, in the northeast part of the Subalpine Chains, showing R_0 values (%) for different horizons along the line of section. Notice the northwest to southeast increase in the level of R_0 in both the Oligocene and Hauterivian horizons. The section is based on Butler *et al.* (1987).

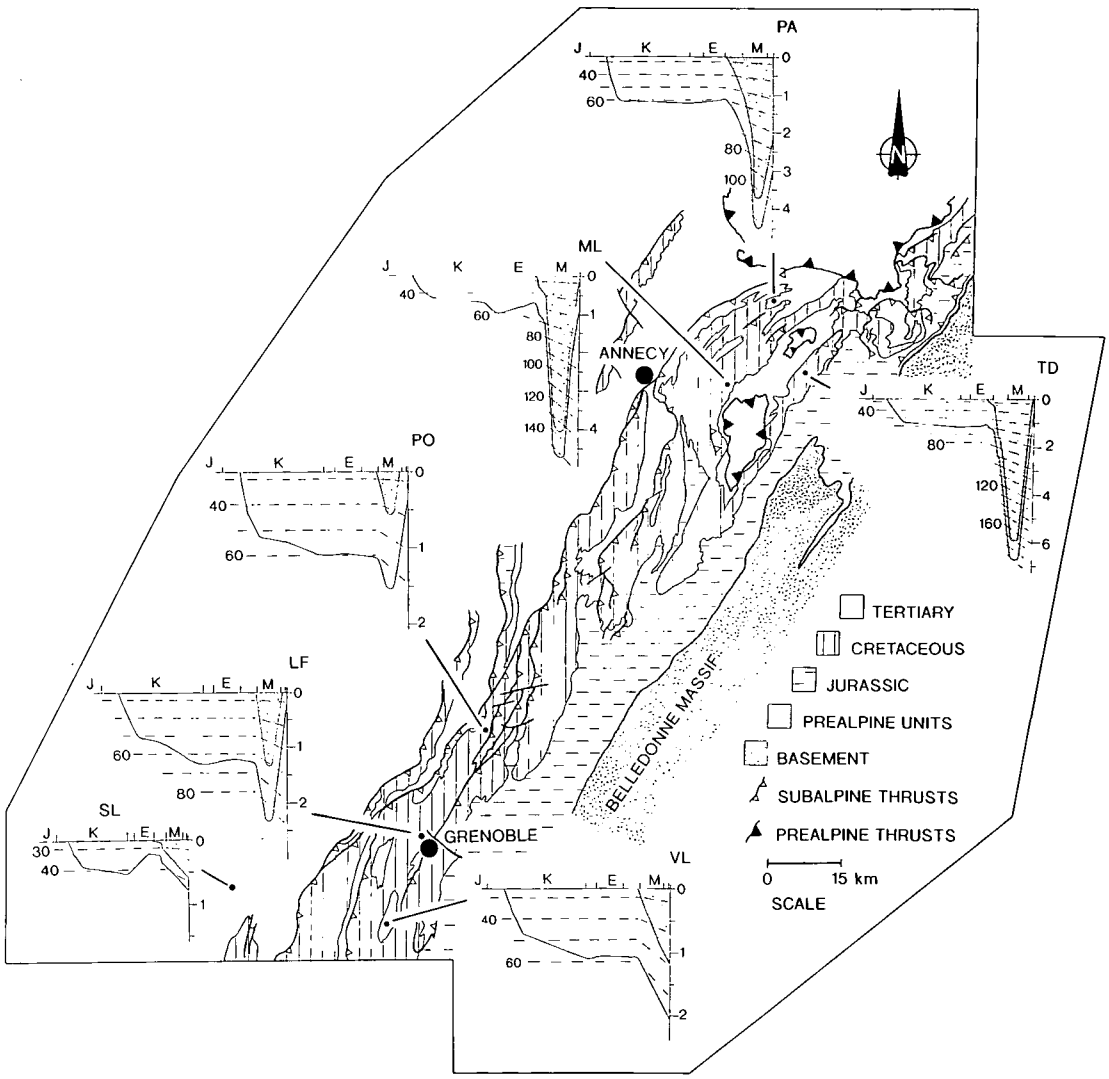

Fig. 7. Burial history models for several locations throughout the Subalpine Chains. The lower of the two horizons modelled (unornamented area) is the base of the Lower Cretaceous Hauterivian mudstones, and the upper horizon (stippled area) is the inferred Tertiary load (foredeep sediments and/or tectonic loads). Ages (horizontal axes) are as follows: J, Jurassic; K, Cretaceous; E, Eocene; M, Miocene; depths (vertical axes) are in kilometres. Temperature contours (dashed lines on the models) are shown in degrees centigrade. These were generated at the same time as the burial history models using the conditions shown in Table 3. Locations are as follows: TD, Combe de Tardevant, Aravis massif; PA, Plateau d'Andey, Bornes massif; ML, Mont Lachat, Bornes massif; PO, Pic d'Oeilette, Chartreuse massif; LF, La Fontanil, southern Chartreuse massif; SL, St Lattier borehole, Romans region, western Vercors massif; VL, Villard-de-Lans, Vercors massif. Timescale from Haq *et al.* (1987).

Table 2. *Lithological data and computed values for initial porosity and compaction factors using Falvey & Middleton's (1981) exponential equation*

Unit	Lithological Data	Computed initial porosity	Compaction factor
Alpine molasse	80% sst, 18% siltst., 2% shale	0.47%	1.84
Taveyannaz ssts	80% sst, 18% siltst., 2% shale	0.47%	1.84
Eocene–Olig. sands	98% sst, 2% shale	0.45%	1.76
Tertiary shales	15% siltst., 85% shale	0.59%	2.37
Nummulite lsts	2% sst, 20% silt, 3% shale, 75% lst	0.59%	1.67
Calcaire lithographique	15% shale, 85% lst	0.60%	1.64
Aravis Fm	55% sst, 1% silt, 40% silt, 4% lst	0.52%	2.00
Senonian	30% sst, 10% shale, 60% lst	0.56%	1.67
Lumachelle	7% sst, 93% lst	0.59%	1.52
Urgonian	100% lst	0.60%	1.50
Hauterivian	35% silt, 10% shale, 55% lst	0.58%	1.84
Valanginian	100% lst	0.60%	1.50
Berriasian	15% shale, 85% lst	0.60%	1.64
Tithonian	100% lst	0.60%	1.50

compaction factor for each horizon, using the compaction equation chosen, which in this case was the Falvey & Middleton (1981) equation. It should be noted that this approach neglects the timing of cementation, which has the potential to lesson the affects of compaction, especially if the cement phase is an early cement (Gallagher 1990). However, errors in the predicted burial history curve are likely to be quite small, in the region of ± 100 m (Gallagher 1990). Compaction factors for each horizon were calculated by the program, using the lithological data for each horizon and are shown in Table 2. Dating of sediments, always a possible source of error in burial history curve construction, was carried out principally using facies correlation because of the lack of good biostratigraphic or radiometric evidence, and the incomplete fossil record (similar problems are discussed by Wildi *et al.* 1989). Because of the known facies diachronism in the Helvetics, Wildi *et al.* (1989) speculated that errors upto 3 Ma could be introduced by using facies correlation. Thermal maturity is calculated by the program using kinetically-based equations of maturation with time and temperature, developed by the Lawrence Livermore National Laboratories, California. The modelling parameters used in the generation of the curves are shown in Table 3.

Foreland basins are typically cooler than other sedimentary basins (sometimes referred to as hypothermal), because they have not had the time to re-equilibrate thermally, and commonly large amounts of 'cold', low conductivity, sediments are deposited within them at very rapid rates (Kominz & Bond 1986). The low geothermal gradient, 20°C km^{-1} from 32 Ma to 0 Ma, was taken from recorded geothermal gradients in the North Alpine Foreland Basin (Teichmüller & Teichmüller 1986; Teichmüller 1987; Rybach & Bodmer 1980; Rybach *et al.* 1980). Teichmüller & Teichmüller (1986) and Teichmüller (1987) showed the geothermal gradient (based on R_0 measurements from borehole samples) at the front of the northern Alps (Helvetics) of Switzerland to be 20°C km^{-1}, and to increase away from the Alps to a figure of 23°C km^{-1} (see Teichmüller 1987, fig. 38). Rybach & Bodmer (1980) presented details of the present geothermal gradient from the Rhine Graben to the Swiss Alps; the geothermal gradient on the Alpine side of the traverse (near Lucerne) was recorded at <20°C km^{-1}. Rybach *et al.* (1980) also showed the results of R_0 measurements in the Swiss Molasse basin. Their data show that a low temperature geotherm has been in existence in this area since the deposition of the molasse and like today's geotherm in the area, the palaeogeotherm decreases towards the Alps. Similarly low present-day geothermal gradients have been recorded by Deming & Chapman (1989) in the Utah–Wyoming thrust belt using bottom-hole temperatures, and give gradients between 23°C km^{-1} and 24°C km^{-1}. Prior to foredeep formation the gradient is likely to have been higher, in the region of 25°C km^{-1} to 30°C km^{-1}, which is typical for old passive margins (Allen & Allen 1990). The European passive margin formed in Lower and Middle Jurassic times (200–165 Ma, Lemoine *et al.* 1986) and so can be considered as old.

The heat flow of 70 mW m^{-2} used in the model was taken from values for the heat flow density for the Western Alps shown in Della Vedova *et al.* (1990, see their fig. 2). Allen & Allen (1990, their fig. 9.18) give 70 mW m^{-2} as typical for collisional foldbelts. A similar value for heat flow of 60 (± 8) mW m^{-2}, has been recorded in the Utah–Wyoming thrust belt by Deming & Chapman (1989). Geophysical studies of the Western Alps indicate a crustal thickness of 35–40 km (Bayer *et al.* 1987). The typical heat flow through such a crustal thickness

Table 3. *Modelling conditions used in thermal model and in the burial history model*

Heat flow:	70 mW m^{-2}
Maturity Calculation:	LLNL kinetic equation
Geotherms:	65 Ma to 32 Ma = 30°C km^{-1}
	32 Ma to 0 Ma = 20°C km^{-1}
Decompaction:	Falvey & Middleton's (1981) exponential curve

LLNL, Lawrence Livermore National Laboratories.

is in the region of 80 to 60 mW m^{-2} (Teichmüller & Teichmüller 1986, their diagram 21), so the value chosen was assumed to be a good estimate of the likely value of heat flow in the study area.

The stratigraphic data used in the modelling are shown in Fig. 8. These data are based on fieldwork by the author, as well as information from numerous French works summarized in Debelmas & Kerckhove (1980), Debrand-Passard *et al.* (1984), Chaplet (1989), Deconinck (1984), Lateltin (1988) and Nicolet (1979).

The plots shown in Fig. 7 bring out several features of the burial history of the Subalpine Chains. In the southwest, after a period of uplift and erosion in the Palaeogene, the rate of burial increased with the onset of molasse-style deposition (plots for the St Lattier borehole, Villard-de-Lans and Pic d'Oeillette). However, this depositional event was not long enough to cause significant thermal maturation of the Mesozoic units of the Subalpine Chains, except for in stratigraphically deeper units such as the middle Jurassic (Oxfordian). In the St Lattier borehole on the western front of the Vercors massif, Miocene molasse sediments are only 590 m thick (BRGM 1975). To the east of this locality, actually within the Vercors massif, the Miocene deposits were probably much thicker, in the region of 1200 m (now preserved in synclinal cores, such as the one at Villard-de-Lans). This is deduced from the R_0 values which show that the Mesozoic rocks have experienced a slightly higher degree of thermal alteration than the same horizons farther to the west (see Fig. 5). Further to the northeast, hydrocarbon exploration boreholes to the west and southwest of Annecy, at Chapery, Poisy and Chavanod, show the Miocene to be up to 1950 m thick (Michel & Caillon 1957). This dramatic increase in the thickness of the molasse probably reflects the fact that the Pre-alpine thrust sheets, emplaced in the upper Oligocene on to the Subalpine Chains to the east/northeast of these localities, provided a far greater quantity of detritus to the molasse basin in front (i.e. to the west) of the northeast part of the Subalpine Chains (the Bornes, Aravis, Platé and Haut-Giffre massifs). This accounts for the higher values of R_0 within the Tertiary units of this area, when compared to R_0 values for older Mesozoic units further to the southwest. From burial history plots for the Aravis and Haut-Giffre massifs (see Fig. 7), it is apparent that the major cause of enhanced burial of this part of the chain was the emplacement of the Pre-alpine thrust sheets in the upper Oligocene. These contributed 5 km to the burial of the Mesozoic of the Subalpine Chains in this area. This Pre-alpine roof was then involved in the folding and thrusting of the Helvetic nappes over the basement massifs of the Aigulles Rouges and Aar Massif (Ramsay 1981). This deformation will have further increased the burial of certain areas of the northeast part of the Subalpine Chains (i.e. inverted limbs of recumbent folds, as reported by Goy-Eggenberger & Kübler 1990, and footwall locations).

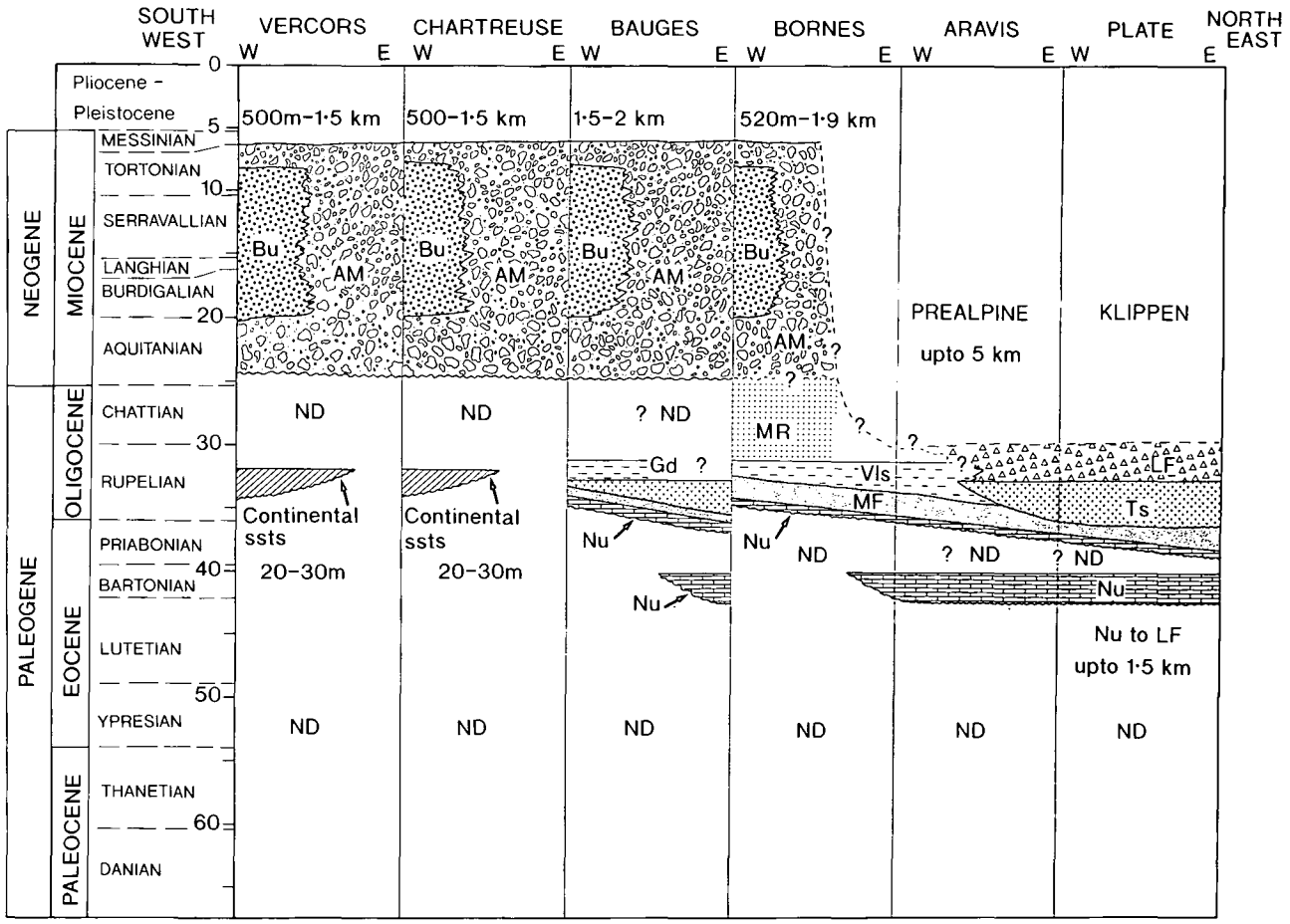

Fig. 8. Summary chart of facies and ages for Tertiary sediments from the massifs along the strike of the Subalpine Chains. Within the massifs in the northeast of the belt it can be seen that the foredeep sedimentation was initiated much earlier than the foredeep in the southwest of the belt (Early Eocene compared to Miocene). The thickness of the foredeep fill in the northeast is not thicker than its counterpart to the southwest. The Prealpine thrust sheets emplaced in the Upper Oligocene (Ramsay 1989) are of significantly greater thickness than the foredeep sediments in the southwest. Bu, Burdigalian molasse; AM, Alpine molasse, the 'Conglomerate toute de aures' of Debrand-Passard *et al.* (1984); MR, Molasse rouge; Gd, Gres de deserts; Vls, Val d'Illiez ssts; Ts, Taveyannaz ssts; MF, Marnes foraminifera; Nu, Nummulite lst; ND, non-deposition. Data are taken from the following sources: Lateltin (1988), Chaplet (1989), Nicolet (1979), Debrand-Passard *et al.* (1984), Charollais & Jamet (1990), Mugnier & Menard (1986), Homewood (1983), Wildi *et al.* (1989 and references therein) and fieldwork by the author. Timescale from Haq *et al.* (1987).

There are no data to suggest the possibilty of further molasse deposition above these thrust sheets, so they have been modelled here showing the thrust sheet emplacement as the final burial event in these areas.

Calculated thermal maturity vs depth profiles for each of the burial history models were plotted against R_o values vs depth for each respective area of the Subalpine Chains. Regression analysis was carried out on the plots of vitrinite data and compared to the vitrinite maturity profile calculated by the program using the appropiate burial history model. The match or mis-match between the data set and the thermal model was then used to check the accuracy of the burial history model. This was used to test the validity of each burial history curve and the thermal model. The results are shown in Fig. 9. A similar approach was used by Middleton & Falvey (1983) to test their thermal and burial history models of the Otway Basin on the southern Australian continental margin. Any difference between the calculated and the real thermal profile could be due to a number of factors, including mistakes in the decompaction and real depth of burial, error in the geothermal gradients used, error in the timing of deposition of certain units (Wildi *et al.* 1989; Homewood 1983) and in the timing of emplacement of orogenic loads (Mugnier *et al.* 1990; Ramsay 1981, 1989), and miscalculation of the R_o data. It should also be noted that the R_o data were obtained from samples solely from outcrops within the vicinity of the point being modelled and not from an individual borehole, as most commonly seen in the literature. All the values plotted, however, were from individual thrust sheets and not from a mix of units from hanging wall and footwall locations. The generally good first order agreement of the R_o data with the modelled maturity suggests that the values used in the thermal modelling are generally correct.

Hydrocarbon prospects in the French Subalpine Chains

Several occurrences of hydrocarbons in the northeast of the Subalpine Chains have been detailed in the literature. Michael & Caillon (1957) briefly mentioned oil shows within the

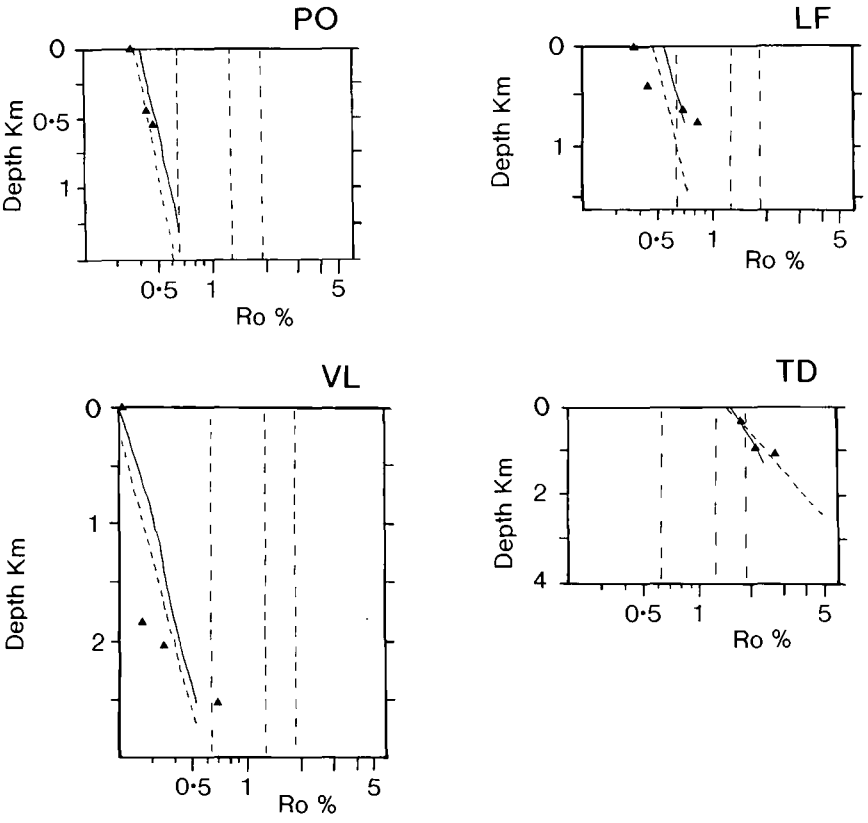

Fig. 9. Plots of maturity regression for measured R_0 v. calculated maturity regression from the modelling, plotted against depth for four of the burial history models shown in Fig. 7. Dashed lines are the maturity regression for the measured R_0 values; solid lines are the maturity regression lines calculated by the burial history models for each location and the thermal model used. Recorded R_0 are shown by the black triangles. Locations are given in the caption to Fig. 7. This shows the generally good agreement between measured R_0 readings and calculated maturity using the thermal model described in the text and the burial history model for each specific locality.

molasse, middle Cretaceous Urgonian limestones and lower Cretaceous Berriasian limestones in exploration wells drilled in the area immediately west of Annecy (see Fig. 1). Previously worked asphalt mines are also known to occur in the Annecy area (Butler 1991). Similar asphalt occurrences have been documented from the more external region of the Swiss Jura by Zweidler (1985). The Brizon # 1 well (BZN–1), drilled in 1987 to the southwest of Bonneville in the Bornes Massif, had gas shows (Charollais & Jamet 1990; their fig. 1), although the Faucigny # 1 well (FAY 1), drilled to the northeast, on the edge of the Chablais Pre-alpine Klippen in 1970 was a dry hole (Charollais & Jamet 1990). Possible hydrocarbon source rocks exist within the northeast part of the Subalpine Chains are summarized in Table 4 (see 'notice explicative' BRGM 1988 & Gorin *et al.* 1989). Within the Bornes/Aravis massifs the only possible source rocks known to date are coal beds, the upper Eocene Diablerets Formation, and shales of the lower to middle Oligocene Melatta shales Formation. The latter formation, in the east of the Bornes massif where it is mature, is probably responsible for local oil impregnation of the Val d'Illiez sandstones (Gorin *et al.* 1989).

Table 4. *Possible hydrocarbon source rocks in the Bornes Massif, northeast Subalpine Chains*

Horizon	Age	Total organic content	Kerogen type
Melatta shales	middle Oligocene	0.83–1.32	2
Diablerets beds	Upper Eocene	up to 7.42	3
Liassic shales	Toarcian	No data	No data
Coal beds	Carboniferous	No data	No data

After BRGM (1988) & Gorin *et al.* (1989).

Discussion

The results of this study of vitrinite reflectance show that variation in maximum burial temperature is more marked along strike of the Subalpine Chains than across strike. An across strike variation in the maximum temperatures experienced does exist (see Figs 3, 4, 5 and 6), but this variation is not as marked, especially in the Chartreuse and Vercors massifs where there is little difference in the recorded R_0 value from east to west. R_0 values in these two areas for Cretaceous and Tertiary rocks are low, less than 0.5%. At such low values, R_0 readings are generally prone to scatter and are generally less accurate than readings made from rocks which have reached higher levels of maturity (Barker 1989). However, the values recorded for the R_0 in these areas are consistent with the fluorescence of spores from the same samples.

The burial history modelling is based on the following assumptions: (1) similar geotherms affected the whole of the Subalpine Chains, although variations to a lower gradient occured at different times spatially; (2) uplift occurred soon after the final stages of thrusting; (3) uplift occurred at a constant rate. These assumptions are discussed in the following paragraphs.

Burial history modelling was performed using the premise that the geothermal gradient was the same throughout the whole of the Subalpine Chains. The sedimentary units of the northeastern massifs of the Haut-Giffre, Platé and Aravis originated further to the oceanic side of the continental margin (and are therefore more internal within the Alpine system) than

the southwestern massifs of the Vercors, Chartreuse, Bauges and western Bornes (more external). Thus it is possible that they experienced a different thermal history prior to the Alpine orogeny, as well as during the collisional event when they quite clearly experienced greater depth of burial. With no evidence to the contary, it is assumed that any pre-Alpine burial thermal anomalies were completely overprinted in the Tertiary.

No hard data are available on the timing and rate of uplift of the Subalpine Chains at the end of collisional events, which has uplifted sediments originally deposited below wave base (several hundred metres in the case of some of the flysch units) and near wave base (in the case of some of the molasse units) to heights of more than two thousand metres above sea level. This factor is important because it will have affected the residence time of any given unit at a certain temperature. All modelling was carried out using the assumption that uplift occurred instantaneously after the final episode of burial and thrusting. Following this assumption, episodes of thrusting can be roughly approximated by using shortening rates within the Alpine arc (Butler 1986, 1991), and the dating of the youngest sediments in footwall localities (Mugnier *et al.* 1990), to estimate the dates of deformational periods. For the northeast part of the chain deformation began during the Oligocene (Burkhard 1990), whilst more external areas, such as the southwest part of the chain, experienced deformation much later in the Tertiary (mid- to end- Miocene, Burkhard 1990 & Mugnier *et al* 1990). Deformation ended in the Late Miocene (see discussion in Burkhard 1990). Timing of the uplift and exhumation of the external crystalline massifs based on fission track and K-Ar isotope data (see Mugnier *et al.* 1990, for references and discussion) can also be used to constrain the timing and rate of uplift of the Subalpine Chains. Burkhard & Kalkreuth (1989) used the timing and rate of uplift of the crystalline Aar massif to estimate a rate of uplift of between 0.5 mm a^{-1} to 1 mm a^{-1}, starting at 12 Ma to 6 Ma respectively, for the Kander Valley region of the Swiss Helvetics. Subsidence history curves for Swiss Molasse Basin presented by Lemcke (1974), show an average net rise of 0.3–0.4 mm a^{-1} starting in the end Miocene.

There are some published data on the recent rate of rock uplift (as opposed to surface uplift, see England & Molnar 1990, for discussion) within the Subalpine Chains. From re-levelling studies, Fourniquet (1977) put the rate of present uplift of the St Pierre de Albigny area of the Bauges at 1 mm a^{-1} (1 km Ma^{-1}). This seems unrealistically fast. Vernet (1980), also from re-levelling studies, estimated values for the rate of uplift of the Cluse d'Iseran (around Grenoble) and the Arve valley (in the northeast of the chain) 0.3 mm a^{-1} (0.3 km Ma^{-1}) and 0.4 mm a^{-1} (0.4 km Ma^{-1}) respectively. These are considered to be more realistic values. Kaelin *et al.* (1991) used compaction trends derived from studying sonic and density logs to estimate missing stratigraphic thicknesses in the Swiss Molasse basin and so calculate the rate and starting date of uplift, which they put at 0.5 mm a^{-1}, starting at 12 Ma. This starting time of uplift for the Subalpine Chains is similar to the values suggested by Mugnier & Menard (1986), estimated by dating of the uplift and cooling of the external basement massifs, by Butler (1986, 1991), estimated from shortening rates across the Western Alps, and by Mugnier *et al.* (1990). Using the values quoted by Vernet (1980), uplift and erosion beginning at around 12–10 Ma could account for the present relief and level of erosion of the Subalpine Chains. This was the value used in the modelling, assuming the rate of uplift was constant throughout this period.

From the above discussion it is possible that periods of residence time at maximum burial depth are likely to be short, in the region of 5–6 Ma. Some authors, notably Lemcke (1974, fig. 5), show much shorter periods (roughly 1 Ma) at maximum burial depths. However, given the length of time between the onset of foredeep sedimentation and uplift, the slowness of Alpine convergence and the inertia of heating and cooling rocks, broader burial history curves are more realistic. Burkhard & Kalkreuth (1989) discuss this point at greater length.

Models of the thermal evolution of thin-skinned fold/thrust belts, such as the Subalpine Chains, typically include one or all three of the following as mechanisms of increased heat production: (1) normal burial heating via both tectonic and stratigraphic burial, (2) thermal inversion by emplacement of a hot thrust sheet, and (3) frictional heating next to thrust faults. Frictional heating is considered here to have only been important locally (as previously suggested by Bustin (1983) and Underwood *et al.* (1988), for other areas). The major factor against frictional heating being important on anything larger than a local scale, is that the high fluid content expected with the emplacement of the Pre-alpine sheets (Ramsay 1981) would quickly dissipate any frictionally-produced higher temperatures. This suggestion goes against the ideas of Aprahamian & Pairis (1981), who proposed that frictional heating was the cause of an inverse low grade metamorphic gradient in the Tertiary Taveyannaz sandstones of the Platé Massifs. As regards the second point, it is likely that the units forming the Pre-alpine thrust sheets were not significantly hotter than the Subalpine units they were thrust on to, although the base of the Prealpine sheets was probably hotter than the top of the Subalpine units at the time of thrusting. Thus it is suggested here that the major contribution to the greater burial temperatures experienced in the northeast of the Subalpine Chains was normal burial heating via tectonic and stratigraphic loading.

There are two possible causes of the along strike variation in burial temperature: (1) increasing stratigraphic burial in the northeast part of the belt due to the increased thickness of foredeep sediments; (2) increased burial via emplacement of allochthonous thrust sheets and increased intensity of deformation within some areas of the Subalpine units (i.e. Haut-Giffre, Platé and Aravis massifs, which represent the southwestern termination of the Helvetic nappes). The first point is considered to be less important because it appears there was little difference in the thickness of foredeep sediments in the northeast of the belt compared with the southwest part of the belt (see Fig. 8). Although it is impossible to ascertain the exact thickness of the foredeep succession in the northeast part of the belt because the emplacement of the Prealpine thrust sheets may have cut out the upper part of the succession, it is likely that it was not much greater than 1 km (Kübler *et al.* 1974). However, in the west/southwest of the chains there is at present 2 km of molasse sediments within the molasse basin in the Annecy region (Michel & Caillon 1957), resting unconformably on the middle Cretaceous 'Urgonian' limestone. This great thickness of molasse sediment thins to the southwest to a thickness of between 1.5 km and 0.5 km, suggesting that there was a less prolific source of detritus feeding the molasse basin in this direction, or that a depositional trench existed in the northeast part of the chain at this time. It is considered here that the main cause of the increased burial of the northeast part of the chain was the emplacement of the Prealpine thrust sheets on to this part of the belt in the upper Oligocene (see Fig. 8). This did not occur in the southwest part of the belt. Of lesser

importance is the fact that the northeast part of the study area has experienced a much higher degree of deformation, being the southwest termination of the Helvetic nappe pile, which thickens to 8 km further round the Alpine arc into Switzerland (Ramsay 1981). The importance of the Prealpine thrust sheets in increasing the overburden and thermal maturity in the northeast part of the chain has already been noted by Sawatzki (1975), Kübler *et al.* (1979) and Gorin *et al.* (1989).

Conclusions

(1) Organic maturity indicators demonstrate both across and along strike variations in the maximum depth of burial and burial temperatures within the French Subalpine Chains, with the greatest variation being along the strike of this foreland fold/thrust belt.

(2) The results of a comparative study of thermal data and thermal modelling suggest that the Haut-Giffre, Platé, Aravis and parts of the eastern Bornes and Bauges massifs have experienced up to 5 km greater depth of burial than the Chartreuse and Vercors massifs and the western parts of the Bauges and Bornes massifs.

(3) This greater depth of burial was produced by two factors, namely, the earlier initiation of foredeep sedimentation and marked differences in the structural style producing differences in the sizes of tectonic loads.

(4) It is suggested that the earlier initiation of the foredeep and its sedimentation (mid- to late Eocene compared to mid-Miocene) in the northeast, although producing a similar thickness of foredeep sediments as in the southwest, was the casuse of the earlier beginning of deeper burial in the northeast part of the chain. This was followed by the emplacement of Prealpine thrust sheets which are the main cause of burying this part of the chain to a greater depth than the massifs to the southwest.

This contribution is part of the author's PhD research into Tectonic Loading, Burial Diagenesis and Organic Maturation in the French Subalpine Chains. Associated with this research effort are G. Roberts, M. Tucker and R. Butler, who are all gratefully acknowledged. The author would like to thank D. Hunt for help with field logistics, J. M. Jones for his advice on organic maturation and R. E. Swarbrick for his advice on thermal and burial modelling. M. Burkhard (Neuchatel University) and H. Shaw (Imperial College, London) reviewed an earlier draft of this paper and made many useful comments. H. Sinclair is also thanked for his comments on an earlier draft. The author acknowledges the continued financial support of NERC grant GT4/89/GS/021 and his mother's purse.

References

ALLEN, P. A. & ALLEN, J. R. 1990. *Basin Analysis*. Blackwell Scientific Publications, Oxford.

APRAHAMIAN, J. 1988. Cartographie du métamorphisme faible à très faible dans les Alpes françaises externes par l'utilisation de la cristallinité de l'illite. *Geodinamica Acta (Paris)*, **2**, 1, 25–32.

—— & PAIRIS, J. L. 1981. Very low grade metamorphism with a reverse gradient induced by an overthrust in the Haute-Savoie (France). *In*: MCCLAY, K. R. & PRICE, N. J. (eds) *Thrust and Nappe Tectonics*. Geological Society, London, Special Publication, **9**, 159–165.

ARNAUD, H. 1988. Subsidence in certain domains of southeastern France during the Ligurian Tethys opening and spreading stages. *Bulletin Société géologique de France*, **8**, 725–732.

BARKER, C. E. 1989. Temperature and time in the thermal maturation of sedimentary organic matter. *In*: NAESER, N. D. & MCCULLOH, T. H. (eds) *Thermal History of Sedimentary Basins. Methods and Case Histories*. Springer-Verlag, New York, 73–98.

—— & PAWLEWISCZ, M. J. 1986. The correlation of vitrinite reflectance with maximum temperature in humic organic matter. *In*: BUNTEBARTH G. & STEGENA, L. (eds) *Paleogeothermics*. Springer-Verlag, New York, 79–93.

BAYER, R., CAZES, M., PIAZ, G. V., DAMOTTE, B., ELTER, G., GOSSO, G., HIRN, A., LANZA, R., LOMBARDO, B., MUGNIER, J-L., NICOLAS, A., POLINO, R., ROURE, F., SACCHI, R., SCARASCIA, S., TABACCO, I., TAPPONNIER, P., TARDY, M., TAYLOR, M., THOUVENOT, F., TORREILLES, G. & VILLIEN, A. 1987. Premiers résultats de la traversée des Alpes occidentales par sismique reflexion verticale (Programme ECORS-CROP). *Comptes Rendus Académie Sciences, Paris*, **305**, Serie II, 1461–1470.

BOSTICK, N. H., CASHMAN, S. M., MCCOLLUH, T. H. & WADDEL, C. T. 1978. Gradients of vitrinite reflectance and present temperature in the Los Angeles and Ventura basins, California. *In*: OLTZ, D. F. (ed.) *Low Temperature Metamorphism of Kerogen and Clay Minerals*. Pacific section of the Society of Economic Paleontologists & Mineralogists, special symposium, 65–96.

BOYER, S. E. & ELLIOT, D. 1982. Thrust systems, *American Association Petroleum Geologists Bulletin*, **66**, 1196–1230.

BRGM, 1988. *Carte Géologique à 1/50000. Annecy-Bonneville.*

—— 1975. *Carte Géologique à, 1/50000, Romans-sur-Isère.*

BURKHARD, M. 1990. Aspects of the large-scale deformation in the most external part of the Swiss Alps (Subalpine Molasse to Jura fold belt). *Eclogae géologicae Helveticae*, **83/3**, 559–583.

—— & KALKREUTH, W. 1989. Coalification in the northern Wildhorn nappe and adjacent units, western Switzerland. Implications for tectonic burial histories. *International Journal of Coal Geology*, **11**, 47–64.

BUSTIN, R. M. 1983. Heating during thrust faulting in the Rocky Mountains: friction or fiction? *Tectonophysics*, **95**, 309–328.

BUTLER, R. W. H. 1986. The geometry of crustal shortening in the Western Alps. *In*: SENGOR, A. M. C. (ed.) *Tectonic evolution of the Tethyan region*. Kluwar Academic Publication, 43–76.

—— 1991. Hydrocarbon maturation, migration and thrust sheet loading in the Western Alpine foreland thrust belt. *In*: ENGLAND, W. A. & FLEET, A. S. (eds) *Petroleum Migration*. Geological Society, London. Special Publication, **59**, 227–244.

——, WELBORN, A., GILLCRIST, R. & COWARD, M. P. 1987. *The external Western Alpine thrust belt*. Tectonic Studies Group Field excursion guide.

CHAPLET, M. 1989. *Etude géologique du Massif Subalpin des Bornes (Haute-Savoie)*. PhD thesis, Univ. de Savoie, Chambery, Travaux du Dépt. des Sciences de la Terre, **11**.

CHAROLLAIS, J. & JAMET, M. 1990. Principaux résultats géologiques du forage Brizon 1 (BZN 1), Haute-Savoie, France. *In*: ROURE, F., HEITZMANN, P. & POLINO, R. *Deep Structure of the Alps*. Memoire Société géologique de France, Paris, **156**.

DEBELMAS, J. & KERCKHOVE, CL. 1980. Les Alpes franco-Italiennes. *Géologie Alpine*, **50**, 22–90.

——, ESCHER, A. & TRÜMPY, R. 1983. Profiles through the Western Alps. *In*: RAST, N & DELANEY, F. M. (eds) *Profiles of Orogenic Belts*. American Geophysical Union & the Geological Society of America, Geodynamic Series, **10**.

DEBRAND-PASSARD, S., COURBOULEIX, S. & LIENHARDT, M-J. 1984. *Synthèse géologique du Sud-Est de la France. Volume 1– Stratigraphy*. Mémoire de Bureau Recherches Géologiques et Minieres, **125**.

DECONINCK, J-F. 1984. *Sédimentation et diagenese des minéraux argileux du Jurassique supérieur-Cretacé dans le Jura meridional et le domaine subalpin (France-Sud-est). Comparaison avec le domaine atlantique Nord*. PhD thésis, 3è. Univ. des Sciences et Techniques de Lille, France.

DELLA VEDOVA, B., LUCAZEAU, F., PELLIS, G. & PASQUALE, V. 1990. Heat flow and tectonics along the EGT southern segment. *In*: FREEMAN, R. & MUELLER, ST. (eds) *Proceedings VIth EGT project workshop—data compilations and synoptic interpretation*. March, 1990, 431–440.

DEMING, D. & CHAPMAN, D. S. 1989. Thermal histories and hydrocarbon generation: An example from the Utah–Wyoming thrust belt. *American Association Petroleum Geologists Bulletin*, **73**, 1455–1471.

DEWEY, J. F., PITMAN, W. C., RYAN, W. & BONIN, J. 1973. Plate tectonics and the evolution of the Alpine system. *Geological Society America Bulletin*, **84**, 3137–3180.

ENGLAND, P. & MOLNAR, P. 1990. Surface uplift, uplift of rocks, and exhumation of rocks. *Geology*, **18**, 1173–1177.

FALVEY, D. A. & DEIGHTON, I. 1982. Recent advances in burial and thermal geohistory analysis. *Australian Petroleum Explorationists Association Journal*, **22**, 65–81.

FALVEY, D. G. & MIDDLETON, M. F. 1981. Passive continental margins: evidence for prebreakup deep crustal metamorphic subsidence mechanism. *Oceanologica Acta*, **4**, 103–114.

FREY, M. 1970. The step from diagenesis to metamorphism in pelitic rocks during Alpine orogenesis. *Sedimentology*, **15**, 261–279.

—— 1974. Alpine metamorphism of pelitic and marly rocks of the Central Alps. *Schweizerische Mineralogische und Petrographische Mitteilungen*, **54**, 489–506.

——, TEICHMÜLLER, M., TEICHMÜLLER, R., MULLIS, J., KÜNZI, B., BREITSCHMID,

A., GRUNER, U. & SCHWIZER, B. 1980. Very low grade metamorphism in the external parts of the Central Alps. Illite crystallinity, coal rank, and fluid inclusion data. *Eclogae géologicae Helveticae*, **73**, 173–203.

FOURNIQUET, J. 1977. Mise en évidence de mouvements actuels, verticaux, dans le Sud-Est de al France par comparision de nivellements successifs. *Comptes Rendus Sommaires Société géologique de France*. Fasc. **5**, 266–268.

GALLAGHER, K. 1990. An examination of some uncertainties associated with estimates of sedimentation rates and tectonic subsidence. *Basin Research*, **2**, 97–114.

GORIN, G., GÜLAÇAR, F. & CORNIOLEY, Y. 1989. Organic geochemistry, maturity, palynofacies and palaeoenvironments of Upper Kimmeridgian and Lower Tertiary organic-rich samples in the southern Jura (Ain, France) and Subalpine massifs (Haute-Savoie, France). *Eclogae géologicae Helveticae*, **82**, 491–515.

GOY-EGGENBERGER, D. & KÜBLER, B. 1990. Résultats préliminaires d'un saaai de zonéographie métamorphique à travers les formations calcaires de la Nappe de Morcles. *Schweizerische Mineralogische und Petrographische Mitteilungen*, **70**, 83–88.

GUTHRIE, J. M., HOUSEKNECHT, D. W. & JOHNS, W. D. 1986. Relationships among vitrinte reflectance, illite crystallinity and organic geochemistry in Carboniferous strata, Ouchita Mountains, Oklahoma and Arkansas. *American Association Petroleum Geologists Bulletin*, **70**, 26–38.

HAQ, B. U., HARDENBOL, J. & VAIL, P. R. 1987. Chronology of fluctuating sea-levels since the Triassic. *Science*, **235**, 1165–1167.

HOFFMAN, J. & HOWER, J. 1979. Clay mineral assemblages as low grade metamorphic geothermometers: application to the thrust faulted disturbed belt of Montana, USA. *In*: SCHOLLE, P. A. & SCHLUGER, P. R. (eds) *Aspects of Diagenesis*. Society of Economic Paleontologists and Mineralogists Special Publication, **26**, 55–79.

HOMEWOOD, P. 1983. Palaeogeography of Alpine flysch. *Palaeogeography, Palaeoclimatology, Palaeoecology*, **44**, 169–184.

——, ALLAN, P. A. & WILLIAMS, G. D. 1986. Dynamics of the Molasse Basin of western Switzerland. *In*: ALLAN, P. A. & HOMEWOOD, P. (eds) *Foreland Basins*. International Association of Sedimentologists, Special Publication, **8**. Blackwell Scientific Publications, Oxford, 199–217.

HOOD, A., GUTJAHR, C. M. & PEACOCK, R. L. 1975. Organic metamorphism and the generation of petroleum. *American Association Petroleum Geologists Bulletin*, **59**, 986–996.

KAELIN, B., RYBACH, L. & KEMPTER, E. H. K. 1991. Deposition, uplift and erosion in the Swiss molasse basin, estimated from sonic and density logs. *Terra Abstracts*, **3**, # 1, 370, VI[th]EUG, Strasbourg, 24–28 March, 1991.

KALKREUTH, W. & MCMECHAN, M. 1988. Burial history and thermal maturity, Rocky Mountain Front Ranges, Foothills, and Foreland, East Central British Columbia and adjacent Alberta, Canada. *American Association Petroleum Geologists Bulletin*, **72**, 1395–1410.

KARNER, G. D. & WATTS, A. B. 1983. Gravity anomalies and flexure of the lithosphere at mountain ranges. *Journal of Geophysical Research*, **88**, 10449–10477.

KINDLER, P. 1988. *Géologie des wildflyschs entre Arve et Giffre (Haute-savoie, France)*. Publ. Dépt. de Géologie et de Paléontologie de l'université de Genève, **6**.

KISCH, H. J. 1980. Illite crystallinity and coal rank associated with lowest-grade metamorphism of the Taveyanne greywacke in the helvetic zone of the Swiss Alps. *Eclogae géologicae Helveticae*, **73**, 753–777.

KOMINZ, M. A. & BOND, G. C. 1986. Geophysical modelling of the thermal history of foreland basins. *Nature*, **320**, 252–256.

KÜBLER, B., MARTINI, J. & VUAGNAT, M. 1974. Very low grade meatmorphism in the Western Alps. *Schweizerische Mineralogische und Petrographische Mitteilungen*, **54**, parts 2–3, 461–469.

——, PITTION, J-L., HEROUX, Y., CHAROLLAIS, J. & WEIDMANN, M. 1979. Sur le pouvoir réflecteur de la vitrinite dans quelques roches du Jura, de la Molasse et des Nappes préalpines, helvétiques et penniques. *Eclogae géologicae Helveticae*, **72**, 347–373.

LATELTIN, O. 1988. *Les dépôts turbiditiques oligocènes d'avant-pays entre Annecy (Haute-Savoie et le Sanetsch, Suisse). Grès de Taveyannaz et du d'Illiez*. PhD Thèse Faculté des Sciences de l'Université de Fribourg (Suisse).

LEMCKE, M. 1974. Vertikalbewegungen des vormesozoisch Sockels im nördlichin Alpenvorland vom Perm bis zur Gegenwart. *Eclogae géologicae Helveticae*, **67**, 121–133.

LEMOINE, M., BAS, T., ARNAUD-VANNEAU, A., ARNAUD, H., DUMONT, T., GIDON, M., BOURBON, M., DE GRACIANSKY, P-C., RUDKIEWICZ, J-L., MÉGARD-GALLI, J. & TRICART, P. 1986. The continental margin of Mesozoic Tethys in the Western Alps. *Marine and Petroleum Geology*, **3**, 179–199.

—— & TRÜMPY, R. 1987. Pre-oceanic rifting in the Alps. *Tectonophysics*, **133**, 305–320.

MARSHALL, J. E. A. 1991. Quantative spore colour. *Journal of the Geological Society, London*, **148**, 223–233.

MICHEL, P. & CAILLON, G. 1957. Quelques résultats des sondages exécutés en Savoie par la Regie autonome des Petroles. *Bulletin société Géologique de France*, **7**, série 6, 995–1008.

MIDDLETON, M. F. 1982. Tectonic history from vitrinite reflectance. *Geophysical Journal of the Royal Astronomical Society*, **68**, 121–132.

—— & FALVEY, D. A. 1983. Maturation modelling in the Otway Basin, Australia. *American Association Petroleum Geologists Bulletin*, **67**, 271–279.

MONNIER, F. 1979. Thermal diagenesis in the Swiss Molasse basin: implications for oil generation. *Canadian Journal Earth Sciences*, **19**, 328–342.

MUGNIER, J-L. & MÉNARD, G. 1986. The development of the Swiss molasse basin and the evolution of the external Alps: A kinematic model. *Bulletin Centres Recherches Exploration-Production, Elf Aquitaine*, 167–180.

——, ARPIN, R. & THOUVENOT, F. 1987. Coupes equilibrées à travers le massif subalpin de la Chartreuse. *Geodinamica Acta (Paris)*, **1**, 125–137.

——, GUELLEC, S., MÉNARD, G., ROURE, F., TARDY., M. & VIALON, P. 1990. A crustal scale balanced cross-section through the external Alps deduced from the ECORS profile. *In*: ROURE, F., HEITZMANN, P. & POLINO, R. (eds) *Deep Structure of the Alps*. Memoire Société géologique de France, Paris, **156**.

NICOLET, C. 1979. *Le Bas-Dauphine Septentrional étude stratigraphiqué et sedimentologiqué*. These 3è cycle, Univ. Grenoble.

PAIRIS, B. & PAIRIS, J-L. 1975. Précisions nouvelles sur le Tertiare du Massif de Platé (Haute-Savoie). *Géologie Alpine*. **51**, 83–127.

PRICE, L. C. 1983. Geologic time as a parameter in organic metamorphism and vitrinite reflectance as an absolute paleogeothermometer. *Journal of Petroleum Geology*, **6**, 5–38.

RAMSAY, J. G. 1981. Tectonics of the Helvetic nappes. *In*: MCCLAY, K. R. & PRICE, N. J. (eds) *Thrust and Nappe Tectonics*, Geological Society, London, Special Publication, **9**, 293–309.

—— 1989. Fold and fault geometry in the western Helvetic nappes of Switzerland and France and its implication for the evolution of the arc of the Western Alps. *In*: COWARD, M. P., DIETRICH, D. & PARK, R. G. (eds) *Alpine Tectonics*, Geological Society, London, Special Publication, **45**, 33–45.

ROBERT, P. 1988. *Organic Metamorphism and Geothermal History*. Elf-Aquitaine and Reidel Publ. Co.

ROBERTS, G. P. 1990. *Deformation and diagenetic histories around foreland thrust faults*. PhD thesis, Univ. Durham.

RYBACH, V. L. & BODMER, P. 1980. Die goethermischen Verhältnisse der Schweizer Geotraverse im Abschnitt Basel-Luzern. *Eclogae géologicae Helveticae*, **73**, 501–512.

——, BÜCHI, U. P., BODMER, P. & KRÜSI, H. R. 1980. Die Tiefengrundwässer des schweizerischen Mittellandes aus geothermischer Sicht. *Eclogae géologicae Helveticae*, **73**, 293–310.

SAWATZKI, G. G. 1975. *Etude Géologique et Minéralogique des flyschs a grauwackes volcaniques du synclinal de Thônes (Haute-Savoie, France)*. Thèse # 1643, Université de Genève.

STACH, E., MACKOWSKY, M., TEICHMÜLLER, M., TAYLOR, G. H., CHANDRA, D. & TEICHMÜLLER, R. 1982. *Textbook of Coal Petrology (3rd Ed.)*. Berlin Gebruder Borntraeger.

SWEENEY, J. J. & BURNHAM, A. K. 1990. Evaluation of a simple model of vitrinite reflectance based on chemical kinetics. *American Association Petroleum Geologists Bulletin*, **74**, 1559–1570.

TEICHMÜLLER, M. 1987. Recent advances in coalification studies and their application to geology. *In*: SCOTT, A. C. (ed.) *Coal and Coal Bearing Strata: Recent advances*. Geological Society, London, Special Publication, **32**, 127–169.

TEICHMÜLLER, R. & TEICHMÜLLER, M. 1986. Relations between coalification and palaeogeothermics in Variscan and Alpidic foredeeps of Western Europe. *In*: BUNTEBARTH, G. & STEGENA, L. (eds) *Paleogeothermics*, Lecture notes in Earth Sciences, **5**. Springer-Verlag, New York, 53–78.

TISSOT, B. P., PELET, R. & UNGERER, PH. 1987. Thermal history of sedimentary basins, maturation indices and kinetics of oil and gas generation. *American Association Petroleum Geologists Bulletin*, **71**, 1445–1466.

UNDERWOOD, M. B., FULTON, D. A. & MCDONALD, K. W. 1988. Thrust control on thermal maturity of the frontal Ouachita Mountains, central Arkansas, USA. *Journal of Petroleum Geology*, **II** (3), 325–339.

VAN HINTE, J. E. 1978. Geohistory analysis—application of micropaleontology in exploration geology. *American Association Petroleum Geologists Bulletin*, **62**, 201–222.

VERNET, J. 1980. Mise en évidence d'une orogenèse et d'une tectonique alpines actuelles par les mesures de nivellement. *Comptes Rendues sommaires géologie de France*, Fasc. **6**, 246–249.

WILDI, W., FUNK, H., LOUP, B., AMATO, E. & HUGGENBERGER, P. 1989. Mesozoic subsidence history of the European marginal shelves of the Alpine Tethys (Helvetic realm, Swiss Plateau and Jura). *Eclogae géologicae Helveticae*, **82**, 817–840.

ZWEIDLER, D. 1985. *Genesé des Gisements d'Asphalte des Formations de la Pierre Jaune de Neuchâtel et Calcaire Urgoniens du Jura (Jura Neuchâtelois et Nord Vaudois)*. PhD Thèse Faculté des Sciences Université de Neuchâtel.

Received 24 April 1991; revised typescript accepted 10 December 1991.